RESISTANCE MECHANISMS DURING ENDOCRINE TREATMENT IN BREAST CANCER.

Benyamin Ertefai

A thesis presented for the degree of Doctor of Philosophy

at Cardiff University

March 2016

Breast Cancer Molecular Pharmacology Group

School of Pharmacy and Pharmaceutical Sciences

Redwood Building

Cardiff University

King Edward VII Avenue

Cardiff, CF10 3NB

Statement of contribution

I confirm that I designed and carried out all the work presented in this thesis with the following exceptions.

MCF7 derived endocrine resistant models were developed by the Breast Cancer Molecular Pharmacology Group prior to this project.

Cell lysis, RNA isolation for Affymetrix genechip human WT 1.0ST array was performed by Mr. Richard McClelland prior to this project.

The Affymetrix GeneChip® gene expression profiling of breast cancer models was performed by Cardiff University Centre of Biotechnology Services (CBS).

Proteomic dataset using SysQuant mass spectrometry and bioinformatics investigation of spectra was performed by Dr David Britton at Proteome Sciences (Kings College, London).

Acknowledgements

I would first and foremost like to thank my supervisors Dr Julia M W Gee and Professor Robert I Nicholson for providing me with the opportunity to conduct this research and for their unwavering guidance, support and patience in practical work, writing and completion of this thesis.

I would also like to acknowledge members of Breast Cancer Molecular Pharmacology Group for their help during last 4 years particularly, Richard McClelland and Carol Dutkowski for their technical advice and proof-reading skills.

Many thanks to Dr David Britton at Proteome Sciences (Kings College, London) who provided access to the Proteomics data.

A special thanks to Breast Cancer NOW for funding the gene expression microarraying. Also, funding from School of Pharmacy and Pharmaceutical Sciences for experimental work and attending conference was gratefully acknowledged. I'm also grateful to Dr Emma Kidd and Dr William Ford for insightful and constructive comments through this study.

I would like to express my gratitude to my wonderful colleagues: Dr James Blaxland, Leonam Vieira Goncalves, Dmitry Malyshev, Shayda Maleki-Toysrkani, Hannah Bundy, Melissa Fallon, Helene Herault and Evans Ahortor for their support during writing the thesis.

Last, but certainly not least, I would like to express my deepest thanks to my sister, Mum and Dad for their amazing support and encouragement for the whole of my life. Everything I have achieved I owe to you all.

''Science is adventure, discovery, new horizons, insight into our world, a means of predicting the future and enormous power to help others.''

Mahlon Hoagland (1921- 2009), MD. Director, Worcester Foundation for Experimental Biology

Summary

Prolonged endocrine therapy is the mainstay of treatment for ER+ breast cancer patients. However, resistance develops in many patients which leads to more aggressive disease. Understanding the mechanisms of acquired resistance that emerge as a consequence of prolonged endocrine treatment remains critical. This study aimed to use gene expression profiling to discover induced mechanisms shared by a panel of MCF7-derived acquired resistant cells that underpin endocrine resistant growth. The in vitro panel represents resistance to oestrogen deprivation, tamoxifen or fulvestrant and includes long-term (3year) models to better-mimic clinical endocrine exposure.

Affymetrix 1.0ST microarrays detected 572 genes induced in all resistant models versus MCF7. Over-represented ontologies, pathways and functional classification for these genes revealed induction of oxidative phosphorylation (OxPhos) and TCA cycle enzymes in the resistant models, a finding further confirmed by mass spectrometry. Increased oxygen consumption, NADH dehydrogenase and/or cytochrome C oxidase activity was detected in resistant cells, and targeting with OxPhos inhibitors Metformin or Antimycin A confirmed growth-dependency on OxPhos. Western blotting for AMPK (energy sensor) activity and its downstream anabolic targets (ACC, mTOR/P70S6K) showed Metformin reduced fatty acid and protein synthesis in growth-sensitive endocrine resistant cells. In silico analysis inferred clinical relevance since many TCA/OxPhos genes associated with earlier relapse in ER+ and/or tamoxifen treated patients. Monitoring basal glycolysis (extracellular lactate) and growth impact of 2DG or glutamine restriction demonstrated glycolysis and glutaminolysis also contribute to endocrine resistance. The microarrays furthermore revealed that metabolic kinases PCK2, ALDH18A1 and PFKFB2, and components of cell response to Zn were commonly-induced which may additionally help endocrine resistant growth.

This study has revealed increased OxPhos arises as a consequence of prolonged endocrine treatment and is a key bioenergetic pathway sustaining resistance. Since resistant growth is Metformin-sensitive, such targeting of this energy pathway (alongside further antihormones or glycolysis/glutaminolysis inhibitors) could help treat resistance.

Presentations

Ertefai B, Taylor KM, Gee JMW (2012). Role of zinc transporters in breast cancer. 7th ZINC -UK meeting, UCL Institute of Ophthalmology, London, UK (Oral presentation)

Ertefai B, McClelland R, Dutkowski C, Mottram H, Nicholson RI, Gee JMW (2014). Targeting metabolic pathway in endocrine resistant breast cancer cells. NCRI Cancer Conference, Liverpool, UK (Poster presentation)

Ertefai B, McClelland R, Nicholson RI, Gee JMW (2014). Metabolic switch in endocrine resistant breast cancer cells. BACR meeting, Development of Cancer Medicines from target to disease: modelling stratified approaches in oncology, The Royal Society of Medicine, London, UK (Poster presentation)

Ertefai B, McClelland R, Nicholson RI, Gee JMW (2015). Targeting energy pathway in endocrine resistant breast cancer cells. BACR meeting, Breast Cancer: Bridging gaps in our knowledge to improve patient outcome, Newcastle, UK (Poster presentation)

Ertefai B, McClelland R, Nicholson RI, Gee JMW (2016). Repurposing the antidiabetic drug metformin for treatment of endocrine resistance in breast cancer cells. BACR and ECMC joint meeting, Therapeutic interventions for cancer prevention – the way forward, Bristol University, Bristol, UK (Oral presentation)

Table of content

Abbreviations

1,3-BPG	1, 3-bisphosphoglycerate
2DG	2-deoxy glucose
α-KG	α-ketoglutarate
µM	micro molar
AA	Antimycin A
AASS	Aminoadipate-Semialdehyde Synthase
ACAA1	Acetyl-CoA Acyltransferase 1
ACAA2	Acetyl-CoA Acyltransferase 2
ACACB	Acetyl-CoA Carboxylase Beta
ACAT1	Acetyl-CoA Acetyltransferase 1
ACAT2	Acetyl-CoA Acetyltransferase 2
ACC1	Acetyl CoA carboxylase 1
ACC2	Acetyl CoA carboxylase 2
ACHE	Acetylcholinesterase
ACLY	ATP citrate lyase
ACO2	Aconitase 2
ACSM3	Acyl-CoA Synthetase Medium-Chain Family Member 3
ACSS2	Acyl-CoA Synthetase Short-Chain Family Member 2
ADCK3	AarF Domain Containing Kinase 3
ADP	Adenosine diphosphate
AF1	activation function 1
AF2	activation function 2
AGPAT6	1-Acylglycerol-3-Phosphate O-Acyltransferase 6
AH	Anti-hormone
AI	Aromatase Inhibitor
ALDH18A1	Aldehyde Dehydrogenase 18 Family, Member A1
ALDH1A3	Aldehyde Dehydrogenase 1 Family, Member A3
ALDH3A2	Aldehyde Dehydrogenase 3 Family, Member A2
ALDH4A1	Aldehyde Dehydrogenase 4 Family, Member A1
ALDH6A1	Aldehyde Dehydrogenase 6 Family, Member A1

ALDH7A1	Aldehyde Dehydrogenase 7 Family, Member A1
ALDH9A1	Aldehyde Dehydrogenase 9 Family, Member A1
ALG3	ALG3, Alpha-1,3- Mannosyltransferase
AMP	Adenosine monophosphate
AMPK	AMP kinase
AOX1	Aldehyde Oxidase 1
AP-1	activator protein 1
APIP	APAF1 Interacting Protein
APS	Ammonium Persulfate
AR	androgen receptor
ARG2	Arginase 2
ASNS	Asparagine Synthetase
ASS1	Argininosuccinate Synthase 1
ATP	Adenosine triphosphate
ATP5J2	ATP Synthase, H+ Transporting, Mitochondrial Fo Complex, Subunit F2
B4GALT7	Xylosylprotein Beta 1,4-Galactosyltransferase, Polypeptide 7
BCKDHB	Branched Chain Keto Acid Dehydrogenase E1, Beta Polypeptide
BCL-2	B-Cell CLL/Lymphoma 2
BRCA1	Breast Cancer 1
BRCA2	Breast Cancer 2
CAB 39	Calcium Binding Protein 39
CAF	cancer-associated fibroblast
CARS	Cysteinyl-TRNA Synthetase
CBS	Centre of Biotechnology Services
CCD	charge-coupled device
CDH18	Cadherin 18
CDH3	Cadherin 3
CDS2	CDP-Diacylglycerol Synthase
CERK	Ceramide Kinase
CHPT1	Choline Phosphotransferase 1
CK17	Cytokeratin-17

CK18	Cytokeratin-18
CK5	Cytokeratin-5
CK8	Cytokeratin-8
COASY	CoA Synthase
COMT	Catechol-O-Methyltransferase
CONFIRM	Comparison of Fulvestrant in Recurrent or Metastatic Breast Cancer
COX	cytochrome c oxidase
COX7B	Cytochrome C Oxidase Subunit VIIb
CREB	cAMP response element-binding protein
CS	Citrate Synthase
Cu	Copper
DAB	diaminobenzidine
DAVID	Database for Annotation, Visualization and Integrated Discovery
DLAT	dihydrolipoamide acetyltransferase
DLD	lipoamide dehydrogenase
DLST	Dihydrolipoamide S-Succinyltransferase
DSC2	Desmocollin 2
DTT	1,4-Dithiothreitol
E2	Oestradiol
EC	effective concentration
ECA	extracellular acidification
ECHS1	enoyl-CoA hydratase, Short Chain, 1
EFNA4	Ephrin-A4
EFNA5	Ephrin-A5
EFNB2	Ephrin-B2
EGFR	Epidermal Growth Factor Receptor
ELOVL1	ELOVL Fatty Acid Elongase 1
ELOVL4	ELOVL Fatty Acid Elongase 4
EPT1	Ethanolaminephosphotransferase 1
ER	Oestrogen Receptor
ERE	oestrogen response element

ERR	oestrogen-related receptor α
ETC	electron transport chain
ETFP	electron-transferring flavoprotein
EXT2	Ethanolaminephosphotransferase 1
FADH2	Flavin adenine dinucleotide
FasR	short-term fulvestrant resistant (27 mo)
FasRLT	long-term fulvestrant resistant (36 mo)
FCS	Foetal Calf Serum
FDG	fluoro-2-deoxy-d-glucose
FDR	False Discovery Rate
FECH	Ferrochelatase
FH	Fumarate hydratase
FXN	Frataxin
G6PD	Glucose 6-phosphate dehydrogenase
GALNT12	Polypeptide N-Acetylgalactosaminyltransferase 12
GALNT14	Polypeptide N-Acetylgalactosaminyltransferase 14
GALNT6	Polypeptide N-Acetylgalactosaminyltransferase 6
GCDH	Glutaryl-CoA Dehydrogenase
GLS	Glutaminase
GLS2	Glutaminase 2
GLUD1	glutamate dehydrogenase 1
GLUD2	glutamate dehydrogenase 2
GLUL	Glutamate-Ammonia Ligase
GO	Gene Ontology
GOT1	Glutamic-Oxaloacetic Transaminase 1
GOT2	Glutamic-Oxaloacetic Transaminase 2
GPD1	glycerol-3- phosphate dehydrogenase 1
GPD2	glycerol-3- phosphate dehydrogenase 2
GPNA	γ-L-glutamyl p-nitroanilide
GS	glutamine synthetase
GSS	Glutathione Synthetase

GSTA4	Glutathione S-Transferase Alpha 4
GSTO1	Glutathione S-Transferase Omega 1
HADH	Hydroxyacyl-CoA Dehydrogenase
HADH	Hydroxyacyl-CoA Dehydrogenase
HADHA	Hydroxyacyl-CoA Dehydrogenase/3-Ketoacyl-CoA Thiolase/Enoyl-CoA Hydratase (Trifunctional Protein), Alpha Subunit
HADHB	Hydroxyacyl-CoA Dehydrogenase/3-Ketoacyl-CoA Thiolase/Enoyl-CoA Hydratase (Trifunctional Protein), Beta Subunit
HARS	Histidyl-TRNA Synthetase
HCO3	hydrogen carbonate
HER2	Human Epidermal Growth Factor Receptor 2
HK	hexokinase
HMGCS2	3-Hydroxy-3-Methylglutaryl-CoA Synthase 2
HR	Hazard Ratio
HRT	Hormone replacement therapy
HSFCS	Heat deactivated Stripped Foetal Calf Serum
IARS	Isoleucyl-TRNA Synthetase
ICK	Intestinal Cell (MAK-Like) Kinase
IDH1	Isocitrate Dehydrogenase 1 (NADP+)
IDH3B	Isocitrate Dehydrogenase 3 (NAD+) Beta
IGF-1	insulin-like growth factor 1
IGF1R	Insulin-Like Growth Factor 1 Receptor
IMAC	Immobilized metal affinity chromatography
INPP4A	Inositol Polyphosphate-4-Phosphatase Type I A
INPP5A	Inositol Polyphosphate-5-Phosphatase Type I A
ISP	iron-sulfur protein
ITGB1	Integrin, Beta 1
ITGB4	Integrin, Beta 4
ITGB6	Integrin, Beta 6
KEGG	Kyoto Encyclopedia of Genes and Genomes
KMO	Kynurenine 3-Monooxygenase
LARS	Leucyl-TRNA Synthetase

LDH	lactate dehydrogenase
LDHB	lactate dehydrogenase B
LKB1	liver kinase B1
LONP1	Lon Peptidase 1
LTED	Long Term Oestrogen Deprived
MARK1	MAP/Microtubule Affinity-Regulating Kinase 1
MARS	Methionyl-TRNA Synthetase
MATE	multidrug and toxin extrusion proteins
MCF7	Michigan Cancer Foundation-7
MCF7(X)	short-term oestrogen-deprived resistant (25 mo)
MCF7(X)LT	long -term oestrogen-deprived resistant (36 mo)
MDH1	malate dehydrogenase 1
MDH2	Malate dehydrogenase 2
ME1	malic enzyme
MGST1	Microsomal Glutathione S-Transferase 1
mM	milimolar
MMP	mitochondrial membrane potential
MRPL 15	Mitochondrial Ribosomal Protein L15
MRPL 17	Mitochondrial Ribosomal Protein L17
MRPL 2	Mitochondrial Ribosomal Protein L2
MRPL 20	Mitochondrial Ribosomal Protein L20
MRPL 21	Mitochondrial Ribosomal Protein L21
MRPL 34	Mitochondrial Ribosomal Protein L34
MRPL 37	Mitochondrial Ribosomal Protein L37
MRPL 40	Mitochondrial Ribosomal Protein L40
MRPL 47	Mitochondrial Ribosomal Protein L47
MRPL15	Mitochondrial Ribosomal Protein L15
MRPL17	Mitochondrial Ribosomal Protein L17
MRPL2	Mitochondrial Ribosomal Protein L2
MRPL21	Mitochondrial Ribosomal Protein L21
MRPL34	Mitochondrial Ribosomal Protein L34

MRPL37	Mitochondrial Ribosomal Protein L37
MRPL40	Mitochondrial Ribosomal Protein L40
MRPL47	Mitochondrial Ribosomal Protein L47
MRPS 15	Mitochondrial Ribosomal Protein S15
MRPS 18A	Mitochondrial Ribosomal Protein S18A
MRPS 18B	Mitochondrial Ribosomal Protein S18B
MRPS 34	Mitochondrial Ribosomal Protein S34
MRPS15	Mitochondrial Ribosomal Protein S15
MRPS18A	Mitochondrial Ribosomal Protein S18A
MRPS18B	Mitochondrial Ribosomal Protein S18B
MRPS24	Mitochondrial Ribosomal Protein S24
MRPS34	Mitochondrial Ribosomal Protein S34
MRPS5	Mitochondrial Ribosomal Protein S5
MRPS5	Mitochondrial Ribosomal Protein S5
MT1E	Metallothionein 1E
MT1F	Metallothionein 1F
MT1G	Metallothionein 1G
MT1H	Metallothionein 1H
MT1X	Metallothionein 1X
MT2A	Metallothionein 2A
MT-ATP6	Mitochondrially Encoded ATP Synthase 6
MT-CO3	Mitochondrially Encoded Cytochrome C Oxidase III
MT-ND1	Mitochondrially Encoded NADH Dehydrogenase 1
MT-ND2	Mitochondrially Encoded NADH Dehydrogenase 2
MT-ND3	Mitochondrially Encoded NADH Dehydrogenase 3
MT-ND4	Mitochondrially Encoded NADH Dehydrogenase 4
MT-ND4L	Mitochondrially Encoded NADH Dehydrogenase 4L
MT-ND5	Mitochondrially Encoded NADH Dehydrogenase 5
MT-ND6	Mitochondrially Encoded NADH Dehydrogenase 6
mTOR	mammalian Target Of Rapamycin
NADH	Nicotinamide adenine dinucleotide

NADPH	Nicotinamide adenine dinucleotide phosphate
NCOA3 (AIB1)	Nuclear Receptor Coactivator 3
NCoR	Nuclear Receptor Corepressor
NCoR1	Nuclear Receptor Corepressor 1
NCOR2 (SMRT)	Nuclear Receptor Corepressor 2
NCoR2	Nuclear Receptor Corepressor 2
NDUB10	NADH Dehydrogenase (Ubiquinone) 1 Beta Subcomplex, 10
NDUFA3	NADH Dehydrogenase (Ubiquinone) 1 Alpha Subcomplex, 3
NDUFA7	NADH Dehydrogenase (Ubiquinone) 1 Alpha Subcomplex, 7
NDUFA8	NADH Dehydrogenase (Ubiquinone) 1 Alpha Subcomplex, 8
NDUFA9	NADH Dehydrogenase (Ubiquinone) 1 Alpha Subcomplex, 9
NDUFAF2	NADH Dehydrogenase (Ubiquinone) Fe-S Protein 2
NDUFAF4	NADH Dehydrogenase (Ubiquinone) Fe-S Protein 4
NDUFB10	NADH Dehydrogenase (Ubiquinone) 1 Beta Subcomplex, 10
NDUFB5	NADH Dehydrogenase (Ubiquinone) 1 Beta Subcomplex, 5
NDUFB9	NADH Dehydrogenase (Ubiquinone) 1 Beta Subcomplex, 9
NDUFS1	NADH Dehydrogenase (Ubiquinone) Fe-S Protein 1, 75kDa (NADH-Coenzyme Q Reductase)
NDUFS2	NADH Dehydrogenase (Ubiquinone) Fe-S Protein 2, 49kDa (NADH-Coenzyme Q Reductase)
NDUFS3	NADH Dehydrogenase (Ubiquinone) Fe-S Protein 3
NDUFS7	NADH Dehydrogenase (Ubiquinone) Fe-S Protein 7, 20kDa (NADH-Coenzyme Q Reductase)
NDUFS8	NADH Dehydrogenase (Ubiquinone) Fe-S Protein 8, 23kDa (NADH-Coenzyme Q Reductase)
NDUFV1	NADH Dehydrogenase (Ubiquinone) Flavoprotein 1, 51kDa
NDUFV2	NADH Dehydrogenase (Ubiquinone) Flavoprotein 2, 24kDa
NEU1	Sialidase 1
nM	nanomolar
NRP1	Neuropilin 1
OAA	Oxaloacetate
OC	oxygen consumption
OCT	Organic Cation Transporter

OGDHL	Oxoglutarate Dehydrogenase-Like
OMIM	Online Mendelian Inheritance in Man
ORA-O	Over Represented Analysis- Ontology
ORA-P	Over Represented Analysis-Pathway
OS	overall survival
OxPhos	Oxidative phosphorylation
p53	Tumor Protein P53
P70S6K	Ribosomal Protein S6 Kinase, 70kDa, Polypeptide 1
PBS	phosphate buffer saline
PC	pyruvate carboxylase
PCDH9	Protocadherin 9
PCK2	Phosphoenolpyruvate Carboxykinase 2
PDHA1	Pyruvate Dehydrogenase (Lipoamide) Alpha 1
PDHB	Pyruvate dehydrogenase B
PDK1	pyruvate dehydrogenase kinase
PEP	phosphoenolpyruvate
PET	positron emission tomography
PFKFB2	6-Phosphofructo-2-Kinase/Fructose-2,6-Biphosphatase 2
PGM1	Phosphoglucomutase 1
PGS1	Phosphatidylglycerophosphate Synthase 1
PI3K	Phosphatidylinositol 3-Kinase
PIGO	Phosphatidylinositol Glycan Anchor Biosynthesis, Class O
PLEC	Plectin
PMAT	plasma membrane monoamine transporters
PNP	Purine Nucleoside Phosphorylase
POLR2C	Polymerase (RNA) II (DNA Directed) Polypeptide C
POLR2H	Polymerase (RNA) II (DNA Directed) Polypeptide H
POLR2I	Polymerase (RNA) II (DNA Directed) Polypeptide I
POLR3D	Polymerase (RNA) III (DNA Directed) Polypeptide D
PPA2	Pyrophosphatase (Inorganic) 2
PPP	pentose phosphate pathway

PR	progesterone receptor
PRKAA1	Protein Kinase, AMP-Activated, Alpha 1 Catalytic Subunit
PRKAA2	Protein Kinase, AMP-Activated, Alpha 2 Catalytic Subunit
PRKAB1	Protein Kinase, AMP-Activated, Beta 1 Non-Catalytic Subunit
PRKAB2	Protein Kinase, AMP-Activated, Beta 2 Non-Catalytic Subunit
PRKAG1	Protein Kinase, AMP-Activated, Gamma 1 Non-Catalytic Subunit
PRKAG2	Protein Kinase, AMP-Activated, Gamma 2 Non-Catalytic Subunit
PRKAG3	Protein Kinase, AMP-Activated, Gamma 3 Non-Catalytic Subunit
PRKD3	Protein Kinase D3
PRPS1	Phosphoribosyl Pyrophosphate Synthetase 1
PRSS3	Phosphoribosyl Pyrophosphate Synthetase 3
PSMA1	Proteasome Subunit Alpha 1
PSMA6	Proteasome Subunit Alpha 6
PSMB6	Proteasome Subunit Beta 6
PSMC4	Proteasome 26S Subunit, ATPase 4
PSMD2	Proteasome 26S Subunit, Non-ATPase 2
PSMD8	Proteasome 26S Subunit, Non-ATPase 8
PSME1	Proteasome Activator Subunit 1
PSME3	Proteasome Activator Subunit 3
PSPH	Phosphoserine Phosphatase
PTDSS1	Phosphatidylserine Synthase 1
PTEN	Phosphatase And Tensin Homolog
Q	ubiquinone
Raptor	Regulatory Associated Protein of MTOR
RFS	relapse free survival
RIOK1	RIO Kinase 1
ROBO1	Roundabout Guidance Receptor 1
RPMI	Roswell Park Memorial Institute
RUNX2	Runt related transcription factor
SCX-HPLC	strong cation exchange chromatography
SDHB	Succinate dehydrogenase B

SDS-PAGE	Sodium dodecyl sulphate polyacrylamide gel electrophoresis
SEM	standard error of the mean
SEMA3A	Semaphorin 3A
SEMA3C	Semaphorin 3C
Ser	Serine
SERD	selective oestrogen receptor down-regulators
SERM	selective oestrogen receptor modulator
SFCS	Stripped Foetal Calf Serum
SGPL1	Sphingosine-1-Phosphate Lyase 1
SHMT2	Serine Hydroxymethyltransferase 2
SLC1A5	Solute Carrier Family 1 (Neutral Amino Acid Transporter), Member 5
SLC1A5	Solute Carrier Family 1 (Neutral Amino Acid Transporter), Member 5
SLC22A1	Solute Carrier Family 22 (Organic Cation Transporter), Member 1
SLC22A2	Solute Carrier Family 22 (Organic Cation Transporter), Member 2
SLC22A3	Solute Carrier Family 22 (Organic Cation Transporter), Member 3
SLC25A11 11	Solute Carrier Family 25 (Mitochondrial Carrier; Oxoglutarate Carrier), Member
SLC25A13	Solute Carrier Family 25 (Aspartate/Glutamate Carrier), Member 13
SLC25A20 2	Solute Carrier Family 25 (Mitochondrial Carrier; Ornithine Transporter) Member
SLC25A3	Solute Carrier Family 25 (Mitochondrial Carrier; Phosphate Carrier), Member 3
SLC25A31 Member 31	Solute Carrier Family 25 (Mitochondrial Carrier; Adenine Nucleotide Translocator),
SLC25A33	Solute Carrier Family 25 (Pyrimidine Nucleotide Carrier), Member 33
SLC25A4 Member 4	Solute Carrier Family 25 (Mitochondrial Carrier; Adenine Nucleotide Translocator),
SLC25A5 Member 5	Solute Carrier Family 25 (Mitochondrial Carrier; Adenine Nucleotide Translocator),
SLC25A5 Member 5	Solute Carrier Family 25 (Mitochondrial Carrier; Adenine Nucleotide Translocator),
SLC25A6 Member 6	Solute Carrier Family 25 (Mitochondrial Carrier; Adenine Nucleotide Translocator),
SLC29A4	Solute Carrier Family 29 (Equilibrative Nucleoside Transporter), Member 4
SLC2A1	Solute Carrier Family 2 (Facilitated Glucose Transporter), Member 1

SLC2A2	Solute Carrier Family 2 (Facilitated Glucose Transporter), Member 2
SLC2A3	Solute Carrier Family 2 (Facilitated Glucose Transporter), Member 3
SLC2A4	Solute Carrier Family 2 (Facilitated Glucose Transporter), Member 4
SLC39A7	Solute Carrier Family 39 (Zinc Transporter), Member 7
SLC47A1	Solute Carrier Family 47 (Multidrug And Toxin Extrusion), Member 1
SLC47A2	Solute Carrier Family 47 (Multidrug And Toxin Extrusion), Member 2
SLC7A5	Solute Carrier Family 7 (Amino Acid Transporter Light Chain, L System), Member 5
SLC7A6	Solute Carrier Family 7 (Amino Acid Transporter Light Chain, Y+L System), Member 6
SMPD1	Sphingomyelin Phosphodiesterase 1
SP-1	Specificity Protein 1
SRC-1	Steroid Receptor Coactivator-1
SRC-2	Steroid Receptor Coactivator-2
SRC-3	Steroid Receptor Coactivator-3
STK11	Serine/Threonine Kinase 11
STK35	Serine/Threonine Kinase 35
STOML2	Stomatin (EPB72)-Like 2
STR	Short Tandem Repeat
STRADA	STE20-Related Kinase Adaptor Alpha
STRADB	STE20-Related Kinase Adaptor Beta
STT3A	Subunit of the Oligosaccharyltransferase Complex
TALDO1	Transaldolase 1
TamR	short-term tamoxifen resistant (18 mo)
TamRLT	long-term tamoxifen resistant (36 mo)
TBST	Tris-buffered saline with Tween 20
TCA	tricarboxylic acid
TdT	terminal deoxynucleotidyl transferase
TEK	Tec Protein Tyrosine Kinase
TEMED	Tetramethylethylenediamine
TFF1	Trefoil Factor 1
Thr	Threonine

TIMM	Translocase Inner Mitochondrial Membrane
TIMM17A	Translocase Of Inner Mitochondrial Membrane 17 Homolog A
TIMM44	Translocase Of Inner Mitochondrial Membrane 44
TIMM8A	Translocase Of Inner Mitochondrial Membrane 8 Homolog A
TIMM9	Translocase Of Inner Mitochondrial Membrane 9
TiO2	titanium dioxide
TMT	Tandem Mass Tag
TOMM	Translocase Outer Mitochondrial Membrane
TOMM20	Translocase Of Outer Mitochondrial Membrane 20
TSC2	Tuberous Sclerosis 2
UDG	uracil DNA glycosylase
UniProt	Universal Protein Resource
UQCRFS1	Ubiquinol-Cytochrome C Reductase, Rieske Iron-Sulfur Polypeptide 1
UQH2	Ubiquinol
UST	Uronyl-2-Sulfotransferase
VDAC	voltage dependent anionic channels
VRK3	Vaccinia Related Kinase 3
WARS	Tryptophanyl-TRNA Synthetase
XSFCS	charcoal stripped foetal calf serum
XYLB	Xylulokinase Homolog
YARS	Tyrosyl-TRNA Synthetase
Zn	Zinc

CHAPTER 1

Introduction

1.1 Breast cancer incidence

Breast cancer is the most common cancer among women in the UK accounting for 30% of newly diagnosed cancer in women. Breast cancer incidence is higher in older women, where 80% of breast cancer cases were in the over 50s as reported from 2010 to 2012 in the UK. Age-specific incidence rises in women aged 34 to 69 and subsequently drops for women aged 70-74 (Office of National Statistics 2014).

1.2 Breast cancer survival and mortality

Statistical analysis in England and Wales has reported 96% survival for at least one year, 87% survival for five years or more and 78% survival for 10 years or more in women with breast cancer (Cancer research UK 2014). However, although many patients now survive their disease, breast cancer is the 3rd most common cause of cancer death (after lung cancer and colorectal cancer) and the 2nd cause of cancer death (after lung cancer) among women in the UK. Breast cancer mortality is associated with increasing age: 46% of breast cancer deaths in women aged ≥75, and 76% of such deaths in women aged ≥60 was reported between 2010 and 2012 in the UK (Office of National Statistics 2014).

1.3 The aetiology of breast cancer

Breast cancer is the most common cancer in adult females and along with age, risk factors such as gender, genetics, diet and obesity all associate with breast cancer development (Aguas et al. 2005). Endocrine factors such as exposure to exogenous oestrogen also increase the risk of breast cancer in women (Ali et al. 2002).

1.3.1 Gender

The female hormone oestrogen is strongly implicated in breast cancer development because less than 1% of breast cancer patients are males. Furthermore, oestrogen, progesterone and androgen receptors (ER, PR and AR respectively) are expressed in male breast tumours, and the main driver of male breast cancer is thought to be the local oestrogen secretion (Murphy et al. 2006). The ER+ profile common in male breast cancer is similar to breast tumours in women that frequently express this receptor.

1.3.2 Genetics

A meta-analysis of 52 separate epidemiological studies has suggested that 12% of breast cancer patients have one family member with breast cancer. Also, the risk of breast cancer in women with one or more first degree relatives who are affected with breast cancer is higher than those who do not have a first degree relative with breast cancer (Dumitrescu and Cotarla. 2005).

Moreover, germline mutation of BRCA1, BRCA2, p53 and PTEN genes have been associated with 5-10% of hereditary breast cancer cases (Dumitrescu and. Cotarla, 2005). However, the vast majority of breast cancers are sporadic.

1.3.3 Alcohol consumption and diet

The study by Dumitrescu and Cotarla. (2005) also showed an association between increased risk of breast cancer and alcohol intake in a dose dependent manner. Based on this study, 0.75-1 L alcohol consumption per day appeared to increase the risk by 9%. Moreover, high fat diets (40% fat in calories, and seen in western diets) enriched with cholesterol (a precursor for steroid hormones including oestrogen) can drive development of breast cancer (Aguas et al. 2005). Interestingly, high fibre diets (35-45g per day) have an inhibitory role on intestinal resorption of oestrogens and reducing breast cancer incidence in African, Asian and South American women (Aguas et al. 2005).

1.3.4 Obesity

Obesity in postmenopausal women has been associated with increased risk of breast cancer development. The excess fat increases aromatization of androstenedione to oestrone and thus increases the plasma level of oestrogen (android obesity) (Aguas et al. 2005). The study by Dumitrescu and Cotarla (2005) showed each 5 kg of weight gain increases risk of breast cancer by 8% in obese women, supporting the idea that increased fat (cholesterol) plays an important role in synthesis of oestrogen in adipose tissue, promoting breast cancer.

1.3.5 Age and steroid hormones

Breast cancer incidence is associated with age, and the disease is rare before age 20 but increases gradually according to age. This is believed to be due to oestrogen secretion from the ovaries during the female reproductive period. Furthermore, the age at menarche and menopause (i.e. exposure time to oestrogen) contributes to breast cancer pathogenesis (Abdulkareem et al. 2013). A longer exposure time to endogenous oestrogen (early menarche or delayed menopause) in combination with genetic and life style factors all serve to increase the risk of breast cancer in women (Aguas et al 2005).

1.3.6 Exogenous oestrogen

Hormone replacement therapy (HRT) in postmenopausal women for >5 years has also been associated with increased breast cancer incidence (Aguas et al 2005). The meta-analysis study by Dumitrescu and Cotarla (2005) showed long term HRT is correlated with excess breast tumours in women aged 50-70. A large meta-analysis study involving 150,000 women also showed a modest adverse effect of oral contraceptives (containing oestrogen) on breast cancer incidence for those who start taking contraception before age 20 (Aguas et al 2005).

1.4 Oestrogen and ER signalling

Overall, many of the above risk factors evidence a central importance for the steroid hormone oestrogen in driving breast cancer development. In premenopausal women, ovaries are the main source for oestrogen secretion which circulates in the blood to act on distal target tissues (Simpson et al. 2003). Local oestrogen production also occurs in both pre and postmenopausal women in the breast fibroblasts (Miller et al. 1976), while in postmenopausal women oestrogens are derived predominantly in adipose tissue and muscle by aromatization of androgens (Johnston et al. 2003). A high proportion of breast cancers are positive for the expression of the oestrogen receptor (ER, found in approximately 70%), and consequently patients with such tumours often benefit from endocrine measures which target the ER. ER signalling, however, is complex, as are the myriad of treatments which seek to deprive tumour cells of oestrogen.

1.4.1 Genomic ER signalling

Oestrogen receptor alpha (ER) is a nuclear receptor coded by ESR1 and is the principle receptor for oestrogen in breast cancers. ER has two transactivation domains: one at the amino-terminal (activation function (AF)-1) and the other at the carboxy-terminal (AF2) (Kumar et al. 1987). Growth factors and their associated kinases regulate the AF1 domain (Kato et al. 1995), while oestrogen binding to the receptor activates the AF2 domain (Kumar et al. 1987). Synergistic activity of both domains is required for maximal ER transcriptional activity.

In ER+ breast tumours, oestrogen from the plasma or from breast tissue (fibroblasts) diffuses into the cancer cells and physically binds to the ligand binding domain in its receptor protein. This causes a conformational change allowing the helix 12 region to retain the hormone in its ER binding pocket and the ER to dissociate from its protective heat shock proteins, dimerise and enter the nucleus. ER interactions can occur with coactivators (such as steroid receptor coactivators SRC-1, SRC-2, and SRC-3) or corepressor (such as nuclear receptor corepressor NCoR1 and NCoR2) proteins in a tissue specific pattern (Klinge et al. 2000), and when oestrogen is bound coactivator recruitment enhances ER transcriptional activity. The oestrogen-bound ER can also suppress gene expression but this involves corepressor recruitment. The E2/ER complex subsequently associates via the ER DNA binding domain with oestrogen response element (ERE) sequences within the promoter of genes to exert transcriptional control (Johnston et al. 2003). In parallel to its classical genomic mechanism, the E2/ ER complex can bind additionally to AP-1/SP-1 sites in gene promoters via tethering to other transcription factors to influence transcriptional events (Heldring et al. 2007). Critically, gene transcription promoted by oestrogen involves the upregulation of cell survival proteins (such as cyclins, survivin, growth

factors and growth factor receptors) and the downregulation of apoptosis proteins (such as caspase9) (Frasor et al. 2003), thereby promoting breast cancer growth.

Importantly, ERs are heavily phosphorylated and this often involves growth factors and their signalling kinases which phosphorylate ER at multiple sites to aid the transcription of ER regulated genes (Anbalagan and Rowan 2015). Phosphorylation sites in the AF1 domain (S102, S106, S118 and S167), DNA binding domain (S236) and ligand binding AF2 domain (S305, T311 and Y537) of ER have been characterised (Williams et al. 2009). ER can be phosphorylated at S118 via MAPK, CDK7 and mTOR. Epidermal growth factor (EGF) mediated ER phosphorylation at S118 via the MAPK pathway (Chen et al. 2002) is associated with recruitment of coactivators to ER and thus transcription of ER regulated genes (Dutertre and Smith, 2003). In clinical studies, S118 ER activation has in some instances been associated with better prognosis and response to adjuvant tamoxifen treatment (Bergqvist et al. 2006, Jiang et al. 2007, Kok et al. 2009). ER phosphorylation at S167 is mediated via ERK1/2/MAPK, AKT, mTOR/P70S6K and P90RSK. Phosphorylation at S167 induces recruitment of coactivator SRC3 to the ER (in the presence of oestrogen) and thus increases transcription of ER regulated genes (Riggins et al. 2007). Although a study by Kirkegaard et al. (2005) showed AKT overexpression correlated with ER phosphorylation at S167 and reduced sensitivity to adjuvant tamoxifen treatment, ER phosphorylation at S167 has also been reported as a predictive marker of benefit from adjuvant treatment when accompanied by ER/PR positivity (Yamashati et al. 2005, 2008). Similarly, Jiang et al, (2007) showed an association between S167 phosphorylation of ER and tamoxifen response.

1.4.2 Non-genomic ER signalling

Interestingly, while genomic ER signalling is thought to initiate long term transcriptional events which mediate cell signalling over days and weeks, additional plasma membrane associated ER can produce rapid cytoplasmic signalling within seconds. In such circumstances, ER acts as a G protein –coupled receptor (Levin et al. 2009) to facilitate further crosstalk between ER and growth factor receptor signalling pathways. This coupling promotes cell survival and proliferation (Segars et al. 2002) and is convergent with the genomic ER mechanism since several downstream signalling elements of growth factors, as described above, can subsequently phosphorylate nuclear ERs to promote genomic ER signalling (Heldring et al. 2007).

1.5 Molecular subtypes of breast tumours and ER

Breast cancer is considered to be a highly heterogeneous disease and this is reflected in its diverse clinical presentation, behaviour and patient prognosis. Molecular analysis of breast cancer has revealed gene expression profiles which further evidence heterogeneity. A study by

Perou et al. (2000) which analysed gene expression (using cDNA microarrays) of normal and malignant breast tissues, including ductal carcinoma in situ, lobular carcinoma, infiltrating ductal carcinoma, fibroadenoma and normal breast tissue, employing a hierarchical clustering analysis of 1,753 genes has enabled the molecular subtyping of breast cancers. This study identified four molecularly-defined subgroups comprising luminal (ER+), basal, HER-2 positive and normal. Molecular classification based on expression of specific subsets of genes has revealed variation in signalling pathways, cellular composition and growth rate between such breast tumours. Similarly, Sorlie et al. (2001) using hierarchical clustering of 427 genes in malignant and non-malignant breast samples have classified breast tumours into 4 main groups involving luminal (termed A, B and C; characterized by different expression of the ER and oestrogen-regulated genes), basal, HER-2 positive and normal. Furthermore, in this study survival analyses (overall survival (OS) and relapse free survival (RFS)) of breast tumours from 49 patients with locally-advanced disease and with no distant metastases was determined vs. molecular subtype. Basal-like and HER2+ tumours which were characterized with distinct gene expression from the luminal tumours were associated with the shortest OS and RFS (Sorlie et al. 2001). Building further on these expression studies, breast tumours have been classified as follows, with two of the subtypes (luminal A and B) hallmarked by ER expression:

1.5.1 Luminal A tumours

Luminal A breast cancer is characterised by ER, oestrogen regulated genes PR and Bcl-2, and cytokeratin CK8/18 expression, an absence of HER2 overexpression, and a low proliferation rate, as measured by Ki67 staining (Perou et al. 2000 and Sorlie et al. 2001). This subtype accounts for 50-60% of breast tumours. Breast cancer patients with luminal A subtype disease have a better prognosis, with a 27.8% relapse rate and median 2.2 years survival from the time of relapse, as compared to other subtypes (Kennecke et al. 2010). Bone metastases incidence (18.7%) is higher in luminal A subtype patients, as compared to central nervous system, lung and liver metastases which account for 10%. Many Luminal A tumours show growth dependency on oestrogen/ER signalling since they commonly respond to endocrine treatment such as tamoxifen and aromatase inhibitors (AIs) (Guarneri et al. 2009).

1.5.2 Luminal B tumours

The Luminal B subtype is again characterised by ER expression but has a more aggressive phenotype, higher proliferative index and worse clinical outcome as compared to luminal A tumours. It accounts for 10-20% of breast tumours. Luminal B tumours are associated with 30% bone metastases and 13.8% recurrence in other organs such as liver. A median 1.6 year survival has been estimated for breast cancer patients with luminal B tumours (Kennecke et al. 2010).

Luminal B tumours are more likely to be ER+/HER-2+ and thus can be treated with endocrine agents targeting oestrogen/ER signalling (Guarneri et al. 2009) alongside HER2-targeted agents. However, these tumours are less responsive to endocrine treatment (Paik et al. 2004) compared with their luminal A counterparts and thus may benefit from chemotherapy alongside endocrine agents (Parker et al. 2009).

1.5.3 HER-2 enriched tumours

HER-2+ tumours show an amplification of the HER-2 gene and typically have a highly invasive phenotype and a relatively poor clinical outcome, as compared to the luminal subtypes described above. They account for 15-20% of breast tumours. Such tumours are often highly sensitive to anti-HER-2 targeted signalling agents, including trastuzumab (Herceptin®; monoclonal antibody against HER2), Pertuzumab (Perjeta® a HER2 and HER3 dimerisation inhibitor) and Lapatinib (Tykerb®; tyrosine kinase inhibitor). In this context, Trastuzumab treatment has been shown to improve survival in both early stage and advanced HER2+ metastatic breast cancer (Bartsch et al. 2007). Many HER-2+ tumours are ER negative and so independent of oestrogen/ER signalling. However, since almost half of HER-2 positive tumours are ER+/PR+, endocrine therapy is often given alongside anti-HER-2 targeted therapy for ER+/HER2+ patients (see 1.4.2).

1.5.4 Basal-like tumours

Basal-like tumours are characterised by the expression of cytokeratins CK5/CK17, P-cadherin, caveolin 1/2, nestin, CD44 and EGFR (Epidermal Growth Factor Receptor) genes. These tumours are often referred to as triple negative tumours because of their absence of ER, PR and HER2 expression and this tumour subtype accounts for 10–20% of breast tumours. Triple negative tumours have higher relapse incidence as compared to the luminal subtype in the first 3 years (Dent et al. 2007). Basal tumours are more likely to be associated with central nervous system, lung and lymph node metastases (Smid et al. 2008 and Kennecke et al. 2010). Lacking ER, they are inappropriate for endocrine therapy. Furthermore, although patients with these tumours can show responsiveness to adjuvant chemotherapy, they often have a poor prognosis relative to the other subtypes (Rouzier et al. 2005). Interestingly, recent studies by Barton et al. (2015a, b) suggested a role for androgen receptor (AR) signalling in the development of triple negative tumours and thus the targeting of ARs may benefit such patients.

In general, such molecular classification of breast tumours aims to also predict prognosis and to aid making decisions for type of treatment. However, hierarchical cluster analysis of breast tumours to define tumour subtypes is not statistically robust and shows only modest inter observer reproducibility. Genomic, transcriptomic and proteomic data with global functional

analysis from genome-wide RNA interference screens will be required for more accurate breast tumour taxonomy (Mackay et al. 2011). In addition to these molecular subtype studies, some successful molecular prognosis tools have been developed from gene expression signatures to predict recurrence risk (for 10 years) in cancer patients. Oncotype DX (Genomic Health) and Prosigna (NanoString Technologies) can help screen ER+ tumours for additional chemotherapy in patients treated with endocrine agents. Mammaprint (Agendia) predicts risk of distant recurrence and again screens patients for chemotherapy. These tools can help predict if a patient would get benefit from chemotherapy. However, in the clinic the most useful selection criteria for further breast cancer patient treatments remains those based only on ER status, together with PR and HER2. ER+ (as well as PR+) predicts increased likelihood of response to endocrine therapy, HER2+ predicts increased likelihood of response to HER-2 targeted therapy (e.g. trastuzumab) and a triple negative tumour status predicts possible response to chemotherapy (Clarke et al. 2015).

1.6 Types of endocrine therapies available to treat ER+ breast cancer patients

In 1896 George Beatson showed oophorectomy in an advanced breast cancer patient was able to reduce the size of her metastatic tumour and thus established, for the first time, a link between ovarian secretions (subsequently shown to be oestrogens) and breast cancer progression. Since that time, multiple endocrine therapies have been developed to either inhibit oestrogen synthesis within the body or block its capacity to activate oestrogen signalling within breast cancer cells (Miller et al. 2007). Characteristically, all such endocrine agents exert a cytostatic effect on tumours by causing a cell cycle arrest at G1/S phase (Doisneau-Sixou et al. 2003) to reduce their rate of proliferation (Dowsett et al. 2005). ER+ tumours (i.e. luminal A and B subtypes) comprise the target patient group. The management of such tumours can include targeting ER activity/expression (antioestrogens: tamoxifen/fulvestrant) or inhibiting oestrogen production (with zoladex in premenopausal women and AIs in postmenopausal women). 75% of both ER+/PR+, and 50% of ER+ tumours, respond to one or more endocrine agents.

1.6.1 Oestrogen receptor blockers: Antioestrogens

The non-steroidal drug Tamoxifen was found to competitively bind to ER and to cause conformational changes involving a shift of helix 12 into the AF2 site (Wakeling et al. 2000). This blocks coactivator binding and reduces the transcription of oestrogen regulated genes (Wakeling et al. 2000 and Dowsett et al. 2006). Significantly, tamoxifen only blocks ER signalling through the AF2 site, while the AF1 site remains active to exert variable partial oestrogen (agonist) activity (Wakeling et al. 2000) in a tissue and species manner (Jordan et al. 1987). Because of this property, tamoxifen is categorised as a selective oestrogen receptor modulator (SERM).

While it is growth-inhibitory in breast cancer, in the endometrium tamoxifen exerts a high level of agonist activity and this modestly increases the incidence of endometrial cancer in breast cancer patients who are treated with this drug (Hu et al. 2015).

In contrast to tamoxifen, a newer class of steroidal anti-oestrogens, called selective oestrogen receptor down-regulators (SERDs), have been developed which lack oestrogen like activity (Thompson et al. 1989). Such drugs, including the pure anti-oestrogen fulvestrant (fulvestrant), while binding to the ER receptor, not only inactivate both activation function domains (AF1 and AF2) of the receptor by inhibiting recruitment of coactivators to EREs (Wakeling et al. 2000) but also cause rapid ER degradation via the ubiquitin-proteasome pathway to generate much lower levels of ER within breast cancer cells (Klinge et al. 2001).

Tamoxifen is effective in pre- and post-menopausal women with ER+ breast cancer, although in premenopausal women, it can be combined with ovarian ablation (surgical or medical oestrogen deprivation with zoladex) to reduce circulating oestrogen levels (Bartsch et al. 2012). The first Oxford EBCTCG meta-analysis of adjuvant tamoxifen treatment in 30,000 breast cancer patients (from 28 trials) for 5 years showed reduced mortality by 20% during the first 5 years of treatment and also reduced death in women at least 50 years of age (Early Breast Cancer Trialists' Collaborative Group, 1988). The most recent meta-analysis (13 years follow-up) showed tamoxifen treatment (for 5 years) in ER+ breast cancer patients reduced yearly mortality by a third and a 39% reduced recurrence rate was also reported (Early Breast Cancer Trialists' Collaborative Group, 2011).

Fulvestrant can be used during the management of ER+ breast cancer in postmenopausal women following prior endocrine agent failure. The recent phase III dose Comparison of Fulvestrant in Recurrent or Metastatic Breast Cancer (CONFIRM) trial (250mg every 28 days vs. 500mg every 28 days plus an additional 500mg on day 14 of the first month only) significantly increased progression-free survival (PFS) without increased toxicity in postmenopausal women with locally advanced or metastatic ER+ breast cancer who had previously relapsed on endocrine therapy. In this study, 500mg fulvestrant is associated with reduced mortality by 19% and improved overall survival by 4.1 months as compared to 250mg fulvestrant treatment (Di Leo et al. 2014).

1.6.2 Aromatase inhibitors

Gold standard endocrine therapies currently available for ER+ postmenopausal women comprise the third generation of aromatase inhibitors (AIs) which target the aromatase enzyme which is key to the synthesis of oestrogens within the body, as well as within breast tumours

(Howell et al, 2004). Such drugs which cause severe oestrogen deprivation can be subdivided into two categories: Reversible (competitive) non-steroidal inhibitors (anastrazole and letrozole) and irreversible steroidal inhibitors (e.g. exemestane) (Johnston et al. 2003). In each instance, these drugs have proved highly effective at delaying the recurrence of primary breast cancer and promoting tumour remissions in women with recurrent disease (Doughty et al. 2011). Indeed, when used as a neoadjuvant endocrine treatment they are able to shrink the size of tumours in postmenopausal women with large and inoperable cancers (Larionov et al. 2009).

1.7 Resistance to endocrine treatment

Endocrine therapy is an effective treatment in ER+ breast cancer patients. However, resistance can be present de novo, which involves lack of response to first line endocrine therapy, and can also occur as acquired resistance after initial response to the treatment via tumour recurrence. Inherent resistance in the neoadjuvant setting can be observed in 30-50% of patients (Colleoni et al. 2012). In the adjuvant setting, approximately 40-50% of initial responders eventually relapse during or after completion of adjuvant treatment with acquired resistance (Ma et al. 2009). Clinical studies showed 10-15% of early stage breast cancer relapse within 5 years (Dowsett et al. 2010) and 30% recurrence was observed by 15 years (Early Breast Cancer Trialists' Collaborative Group: EBCTCG, 2005). In addition, virtually all advanced disease patients ultimately progress on endocrine therapy with acquired resistance.

In vitro mechanistic studies of acquired resistance to endocrine treatment have involved ER+ breast cancer cells continuously treated with anti-oestrogens (tamoxifen or fulvestrant), or by oestrogen depleting culture media, for various time points from 6-18months to investigate molecular changes in response to endocrine treatment and on acquisition of resistance (Knowlden et al. 2003, Staka et al. 2005, Nicholson et al. 2007). Moreover, breast cancer cells transfected with aromatase genes (CYP19) have aimed to model tumour response to AIs in postmenopausal women (Masri et al. 2008) and in vivo study of xenograft models by Brodie et al. (2010) has investigated the mechanism of acquired resistance to AIs.

Clinical studies to investigate response and resistance mechanisms can involve study of tumour samples taken from either the neoadjuvant or adjuvant setting. In the neoadjuvant setting, the tumour remains in place during the treatment course and thus mammography or 3D ultrasound (measuring tumour size) can be used to determine clinical tumour response to the neoadjuvant endocrine treatment. Sequential biopsies can thus be used to investigate molecular changes (both gene expression and protein expression) in responsive and inherently resistant tumours during treatment (Miller et al. 2007 and 2009). The effect of endocrine treatment in the adjuvant setting can be monitored when the primary tumour has been surgically removed, by analysing

patient survival and recurrence over long term follow up. Samples can be taken at surgery for mechanistic study and this can be related to subsequent time to recurrence. Two issues are associated with this type of study in relation to recurrence in the adjuvant setting: first, patient sample group size should be large enough for statistical analysis of recurrence rate after endocrine treatment (Larinov et al. 2009) and the second is related to tumour assessment to determine if the recurrence has been acquired during the course of endocrine treatment (rather than due to inherent tumour aggressiveness) (Dixon et al. 2014). Furthermore, it is usually not possible to study mechanisms within clinical acquired endocrine resistant samples because relapsed, metastatic tissue remains scarce as it often occurs in life-threatening, inaccessible sites. Consequently, cell models have proved an important research tool in understanding mechanisms underpinning acquired endocrine resistance in breast cancer.

1.8 Previously-studied resistant mechanisms to endocrine treatment

1.8.1 ER status

ER negative breast cancers are de novo resistant to endocrine treatment and Brouckaert et al. (2013) showed tumours with low ER expression also can respond poorly to endocrine therapy but may benefit from adjuvant chemotherapy. Approximately 40-60% of tumours with enriched ER expression respond to endocrine treatment. The response rate and clinical benefit is up to 75% in tumours when ER expression is accompanied with PR expression (Brouckaert et al. 2013). PR expression (an oestrogen regulated gene) can indicate ER activity in tumour cells, and in addition a recent study showed PR can also dictate ER chromatin binding events and thus regulates gene expression profile associated with better clinical outcome (Mohammed et al. 2015). Most tumours which recur on endocrine treatment with acquired resistance remain ER+ and thus ER signalling is the main driver of proliferation. Therefore, such tumours can be treated with sequential endocrine therapy (Carlson and Henderson, 2003). Up to 20% ER loss has been reported by some researchers (Drury et al., 2011), although a study by Ellis et al. (2008) showed less than 10% of tumours lose ER+ and become ER-. Epigenetic events (e.g. methylation of the ER promoter and chromatin remodelling), ER proteolysis, and also growth factor pathway hyperactivity have all been implicated in driving loss of ER (Brinkman and El-Ashry, 2009). During the course of adjuvant therapy, a further hypothesis is that ER loss occurs in heterogeneous tumours (with both ER+ and ER- cell populations) that have small numbers of ER+ clones, and thus continued treatment eliminates these remaining ER+ cells and leads to tumour recurrence when the ER- clones dominate over ER+ clones.

1.8.2 Coregulators

ER associated coregulator proteins including coactivators (AIB1) and corepressors (NCoR and SMRT) increase and decrease transcription of ER regulated genes respectively. A study by Osborne et al. (2003) revealed an association between induced coactivator expression and increased agonist activity of tamoxifen which contributes to endocrine resistance. Another study showed an association between reduced corepressor expression and resistance to tamoxifen treatment in xenograft models (Lavinsky et al. 1998). Based on these studies the coactivator/corepressor ratio appears to play an important role for response or resistance to endocrine treatment (Osborne et al. 2003). A study by Naughton et al. (2007) suggested a progressive loss of coregulator recruitment (NCoR and SMRT) from responsive cells through to tamoxifen resistant cells which contributes to cell proliferation and survival.

1.8.3 ER mutation

ER mutation (codons 537 and 538) within the ligand binding domain of ER has been implicated in acquired endocrine resistance clinically, particularly with AIs. It has been exclusively reported in at least 12% of ER+ metastatic lesions, while ER mutation was not detected in primary tumours (Jeselsohn et al. 2014). In tumours, hypersensitivity of the mutated ER to oestrogen and the presence of constitutively active mutant ER protein may explain resistance to endocrine treatment in some patients (Fuqua et al. 2014).

1.8.4 Pharmacokinetics and pharmacodynamics of tamoxifen

Tamoxifen metabolism involves production of both antioestrogenic and oestrogenic metabolites (Clarke et al. 2001). Different forms of CYP2D6 gene (P450 cytochrome) were detected in the liver and breast tissue which metabolize tamoxifen to endoxifen, 4-OH tamoxifen and N-desmethyltamoxifen (Coller et al. 2002). Endoxifen is the main metabolite and the two other metabolites are present at relatively higher concentrations in the serum as compared to the tumour tissue (Clarke et al. 2001). CYP2D6 alleles can be inactivated in breast cancer. In patients with functional CYP2D6 the serum concentration of endoxifen is 10 times higher than 4-OH tamoxifen. A relatively higher intratumour concentration of 4-OH tamoxifen is detected which can compete with oestrogen for binding to the ER (Clarke et al. 2001). Based on CYP2D6 genotype, breast cancer patients have been divided into three groups; extensive metabolizer, intermediate metabolizer and poor metabolizer in response to tamoxifen treatment, and some reports have indicated patients with the poor metabolizer genotype may get less benefit from adjuvant tamoxifen treatment. An ongoing study by International Tamoxifen Pharmacogenetics is examining the effect of CYP2D6 genotype on tamoxifen responsiveness. A study by Province et al. (2014) suggested a possible link between tamoxifen metabolism and response to adjuvant endocrine treatment. However, this remains a controversial area.

1.8.5 Growth factor signalling and ER activation

Development of resistance can be associated with changes in ER function and growth factor pathways which drive cell survival and proliferation (Clarke et al. 2015). ER phosphorylation can be mediated in a ligand dependent manner (via oestrogen at AF2) or ligand independent manner (via growth factors at AF1 sites). Ligand independent ER activity involves growth factors and their receptor kinases which phosphorylate ER at multiple AF-1 sites and thus mediate transcription of ER regulated genes (Anbalagan and Rowan 2015). Increased growth factor receptor signalling and its cross talk with ER phosphorylation (Britton et al.2006), as well as further growth factor cross-talk to enhance the non-genomic ER mechanism (Massarweh and Schiff 2006), have been heavily-implicated by several laboratories in endocrine resistant cell models grown in vitro or as xenografts. Interestingly, EGFR and HER2 show evidence of being oestrogen-repressed in ER+ endocrine responsive cell lines, and so increases in these receptors occur following initial antihormone treatment providing a compensatory growth and cell survival mechanism that culminates in development of resistance (Gee et al. 2003). Such signalling appears able to enhance the agonistic qualities of tamoxifen driving resistance, or to promote hypersensitivity to residual oestrogens affording resistance to oestrogen deprivation. As examples of this considerable field, “compensatory” adaptive increases in expression and activity of the ERBB receptors EGFR and HER2 (Knowlden et al. 2003) with subsequent, phosphorylation of downstream kinases PI3K/AKT and mTOR (Jordan et al. 2014) and MAPK (Britton et al. 2006), and interplay with further receptors including IGF-1R which cross-talks with EGFR via activation of Src kinase (Knowlden et al. 2005), have all been implicated in driving acquired tamoxifen resistance experimentally in an MCF7-derived cell line TamR. In this model, the deregulated growth factor pathway signalling ultimately cross-talks with ER through AF-1 phosphorylation which re-activates this receptor and thereby cell growth. EGFR signalling was shown to increase MAPK- promoted Ser118 phosphorylation of ER, production of ER-regulated growth factor ligands (e.g. amphiregulin) and thereby promotion of an EGFR/ER autocrine growth signalling loop (Britton et al. 2006). The most well characterized of such signalling involves a crosstalk between EGFR/HER2 and ER and in clinical studies, association between HER2 overexpression and recurrence on endocrine treatment (either tamoxifen or AIs) has been documented in some instances (Mehta et al. 2014) while further studies have demonstrated changes in downstream kinases and ER activity in clinical resistance samples (Gutierrez et al. 2005). Moreover, further mechanisms such as cyclin D1 and its cyclin dependent kinases (CDKs) that contribute to cell cycle (Jirstrom et al. 2005), and histone deacetylases (HDACs) that can repress ER (Brinkman and El Ashry 2009), can also promote emergence of growth that is resistant to endocrine treatment.

1.9 Cotargeting ER and growth factor signalling in pre-clinical models

Based on the considerable evidence that induced growth factor signalling after endocrine therapy leads to acquired endocrine resistance in breast cancer cells in the laboratory, cotargeting with signal transduction inhibitors against growth factor receptor and their signalling molecules has been substantially studied in pre-clinical models. For example, Knowlden et al. (2003) showed, elevation of EGFR/HER2 phosphorylation in the tamoxifen resistant compared to responsive MCF7 control cells. Targeting such molecules with gefitinib (EGFR inhibitor), trastuzumab (HER-2 inhibitor), and their downstream signalling with PD098059 (MAPK inhibitor) reduced ERK1/2 activity, ER phosphorylation and ER-regulated genes including decreasing amphiregulin, and inhibited growth in the TamR cells. Another study by Gee et al (2003) revealed cotargeting MCF7 cells by tamoxifen and gefitinib reduced cell growth by inhibiting downstream MAPK and AKT phosphorylation. Also, such treatment cotargeting delayed acquired resistance in MCF7 cells by 5 weeks compared to tamoxifen treatment alone. An in vivo study of stably transfected HER2-positive MCF-7 xenografts similarly showed cotargeting gefitinib with tamoxifen delayed tumour growth and overcame tamoxifen agonist activity in vivo (Shou et al. 2004). There are also examples of targeting further growth factor receptors and kinases alongside antihormonal agents in pre-clinical studies. For example, cotargeting insulin-like growth factor I receptor (IGF1R) with ER signalling via IGF1R antagonists (a-IR3, AG1024) and antihormone (tamoxifen or fulvestrant) drastically inhibited growth in MCF7 and BT474 as compared to the single agents (Chakraborty et al. 2010). A study by Larsen et al. 2015 showed increased Src kinase in both tamoxifen and fulvestrant resistant models compared to responsive T47D control cells. In this study combined treatment with dasatinib and fulvestrant effectively reduced growth in the tamoxifen resistant T47D cells compared to dasatinib alone, although combined dasatinib with tamoxifen did not show additional effects compared to single agent treatment in the fulvestrant resistant cells. Finally, cotargeting of either tamoxifen resistant cells (TamR) or oestrogen deprived resistant cells (MCF7(X)) with an mTOR inhibitor (AZD8055) and fulvestrant provided superior growth inhibition as compared to either agent alone (Jordan et al. 2014).

1.10 Cotargeting ER and growth factor signalling in clinical breast cancer

The considerable successes in the laboratory for co-targeting growth factor pathways alongside ER have provided strong support for evaluation of cotargeting strategies with antihormones and various anti-growth factors to overcome resistance in breast cancer patients (Fig 1.1). Successful clinical cotargeting of ER and growth factor receptor signalling could potentially delay progression in advanced disease and perhaps reduce the risk of recurrence to adjuvant

endocrine treatment. The following provide details of some of the clinical trials examining such strategies:

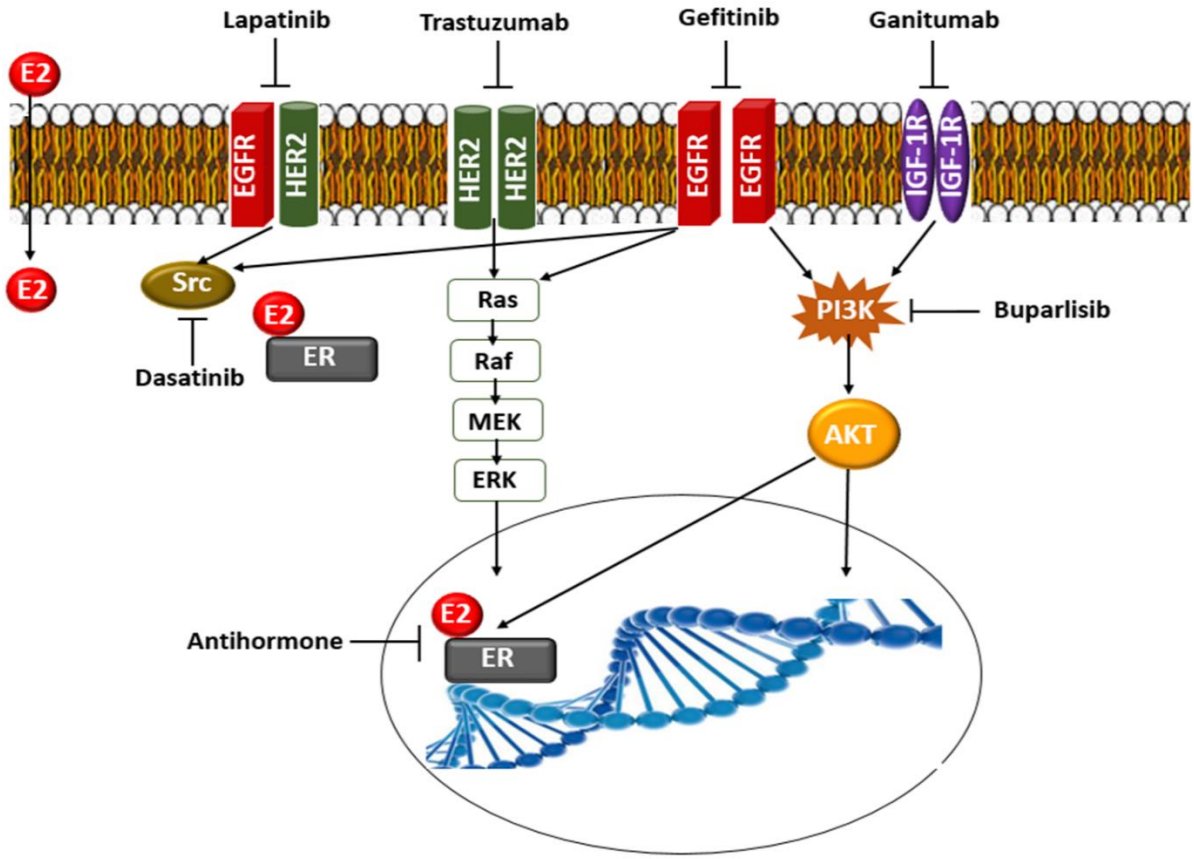

Fig 1.1. Targeting both ER signalling and growth factor signalling in breast cancer cells.

1.10.1 Cotargeting ER and EGFR

Targeting EGFR activity via small molecule inhibitors (gefitinib) in combination with endocrine therapy has been studied in two randomized phase II trials that showed modestly-improved outcome with the gefitinib/antihormone co-treatment in ER+ patients:

1. The effect of gefitinib in combination with anastrazole vs. anastrazole in postmenopausal metastatic breast cancer was studied by Cristofanilli et al. (2010). Median free survival was 14.7 months for the gefitinib co-treated patients vs. 8.4 months for the anastrazole plus placebo arm.

2. The gefitinib effect in combination with tamoxifen was studied by Osborne et al. (2011) in ER+ metastatic breast cancer (regardless of HER-2 status). Median progression free

survival (PFS) was 10.9 months for the gefitinib co-treated patients vs. 8.8 months for the tamoxifen plus placebo group of patients.

However, these successes remain controversial, since no clear benefit was apparent in further clinical co-treatment studies including those from Carlson et al. (2012).

1.10.2 Cotargeting ER and HER-2

Trastuzumab (Herceptin®) a recombinant humanized monoclonal antibody against HER-2 is used in breast cancer patients with HER2 positive (HER2 overexpressing) tumours. Clinical trials (phase III) have studied combination treatment of trastuzumab alongside AIs and some successes have been seen in the ER+/HER2+ patient cohort, for example:

1. A clinical study in breast cancer patients with HER2+ locally advanced tumours or metastatic disease (TAnDEM trial) showed trastuzumab in combination with anastrazole improved PFS to 4.8 months as compared to 2.4 months in the anastrazole alone arm (Kaufman et al. 2009).
2. The eLEcTRA trial recruited patients with HER2+ locally advanced tumours or metastatic disease to receive letrozole plus trastuzumab or letrozole alone. Patients in the letrozole arm had more previous treatment with tamoxifen as compared to the combination arm and the combination arm had more patients with liver metastases, so the two studied arms were not well matched. Nevertheless, time to progression (TTP) of disease was 14.1 months in the combination arm vs. 3.3 months in the letrozole alone arm. In this study TTP did not reach significance due to the small number of patients (Huober et al. 2012).

1.10.3 Cotargeting ER, EGFR and HER-2

A dual tyrosine kinase inhibitor against EGFR and HER2 activity (lapatinib) was used in combination with letrozole in a phase III clinical trial. Postmenopausal women with ER+/PR+ tumours were recruited for this trial. 17% of patients in either the combination arm or letrozole arm were HER2+. Median PFS for the combination arm in the intention to treat ER+ cohort was 11.9 months vs. 10.8 months for the letrozole arm. However, median PFS in patients with HER2+ tumour was 8.2 months in the combination treatment arm vs. 3 months in letrozole alone (Johnston et al. 2009), showing benefit in ER+/HER2+ disease as seen with trastuzumab (1.10.2).

These co-treatment findings are promising, as are the findings with trastuzumab described above, but it is apparent that resistant disease still emerges using strategies for HER2 blockade. Various resistance mechanisms have been proposed for resistance to agents such as lapatinib, herceptin and also gefitinib, including compensatory increases in alternative receptor activity

(e.g. further ERBB receptors or IGF1R, Hutcheson et al. 2006). Moreover, such co-treatment (aiming to target any antihormone-promoted HER2) appears largely ineffective for most HER2- tumours which comprise the majority of ER+ disease (Johnston 2015).

1.10.4 Cotargeting ER and PI3K

Buparlisib (BKM120) is a pan-PI3K inhibitor which targets all isoforms of this protein including catalytic subunit p110α (encoded by the PIK3CA gene). A phase I clinical trial of this drug in combination with letrozole was evaluated. 30% clinical benefit rate (CBR) was observed in patients regardless of treatment schedule. Tumour evaluation revealed 50% of patients who did not have disease progression for 12 months had PIK3CA mutation. In such tumours, changes in PI3K pathway may be associated with response to buparlisib treatment. However, downstream signalling of PI3K such as mTOR does not respond to this treatment and thus may contribute subsequently to disease progression (Mayor et al. 2014).

1.10.5 Cotargeting ER and mTOR

Two mTOR inhibitors, everolimus and temsirolimus (which bind and inhibit mTORC1 in the mTOR complex) were evaluated in clinical trials in combination with endocrine treatment:

1. A Phase III clinical trial (BOLERO-2) recruited postmenopausal women with advanced HER-2 negative tumours who had recurred on either letrozole or anastrazole for everolimus in combination with exemestane vs. exemestane alone. Median PFS for the combination arm was 6.9 months vs. 2.8 months in placebo arm (Baselga et al. 2012).

2. A Phase II clinical trial (TAMRAD) studied the impact of everolimus in combination with tamoxifen as compared to tamoxifen alone in ER+/HER2 negative metastatic breast cancers previously treated with AIs. CBR for duration of 6 months was 61% for the combination arm vs. 42% for tamoxifen treated arm (Bachelot et al. 2012).

3. A Phase III clinical trial (HORIZON) studied the combination of temsirolimus plus letrozole vs. letrozole alone on ER+ locally advanced or metastatic breast cancer with no prior endocrine treatment. 23% and 18% HER2+ patients in the combination arm and letrozole arm were recruited respectively. PFS was 8.9 months for combination arm vs. 9 months for letrozole alone (Wolff et al. 2013), suggesting that most benefit is derived in endocrine resistant patients (as in BOLERO-2 and TAMRAD) rather than in endocrine naive disease.

The BOLERO-2 and TAMRAD trials are promising for such cotreatment in controlling endocrine resistant disease, but again it is notable from such trials that patients soon progress and there is little further survival benefit compared with antihormone alone, while further patients are insensitive to such mTOR inhibitor/antihormone cotreatment. Feedback signalling loops

following mTOR blockade have been reported, including those that maintain AKT activity which may contribute to emergence of everolimus resistance (Jordan et al., 2014).

1.10.6 Cotargeting ER and IGF-1R

A human monoclonal antibody against IGF-1R (ganitumab) blocks binding of IGF-1 and IGF-2 to the receptor. A phase II clinical trial evaluated treatment of ganitumab in combination with either fulvestrant or exemestane vs. endocrine agent alone in ER+ postmenopausal patients with locally advanced or metastatic breast cancer. Disappointingly, median PFS was only 3.9 months for combination treatment vs. 5.7 months for the placebo arm (Robertson et al. 2013).

1.10.7 Cotargeting ER and Src

Dasatinib is an oral Bcr-Abl tyrosine kinase inhibitor and Src family kinase inhibitor. A phase II clinical trial of dasatinib plus letrozole was studied on ER+/HER2 negative metastatic breast cancer. PFS was 20.1 months in the combination arm vs. 9.9 months in letrozole alone. However, CBR was not different between the two arms (71% for combination arm vs. 66% for letrozole arm). Additional studies with dasatinib and another Src inhibitor, saracatinib, are ongoing. However, a further phase II clinical trial evaluated efficiency of dual Src/Abl inhibitor (bosutinib) in combination with either letrozole or exemestane in ER+/HER2 negative locally advanced or metastatic breast cancer. This trial was terminated due to high toxicity and poor clinical benefits (Moy et al. 2014 a and b).

1.10.8 Cotargeting ER and CDKs

CDK4/6 inhibitor (Palbociclib) is a cytostatic agent which causes cell cycle arrest at G1. Clinical trials have evaluated efficacy of Palbociclib in combination with endocrine treatment:

1. A phase II clinical trial (PALOMA-1/TRIO-18) studied the combination effect of palbociclib plus letrozole vs. letrozole alone in ER+/HER2 negative postmenopausal women with advanced breast cancer. Median PFS was 20.2 months for the combination arm vs. 10.2 months for letrozole alone (Finn et al. 2015).
2. Based on these interesting data, an ongoing phase III trial (PALOMA-2) is comparing the combination of letrozole plus palbociclib vs. letrozole plus placebo in ER+/HER2 negative pre or perimenopausal patients (who are taking zoladex) with metastatic breast cancer who have not been previously treated with endocrine agents (Finn et al. 2013), and further co-treatment trials are also ongoing with palbociclib including examining whether it is valuable in endocrine resistant patients.

1.10.9 Cotargeting ER and HDAC

Both histone acetyltransferases (HATs) and histone deacetylases (HDACs) affect histone acetylation. HATs regulate gene transcription while HDAC mediate gene silencing, and have been implicated in epigenetic loss of ER expression (Brinkman and El Ashry 2009). HDAC inhibitors such as vorinostat and entinostat are in clinical trials alongside endocrine treatment in ER+ breast cancer patients.

1. A phase II trial studied the combination of vorinostat and tamoxifen in ER+/PR+ pre and postmenopausal women with metastatic cancer who recurred on endocrine therapy. CBR was 40% and median response duration was 10.3 months in patients who received combination treatment (Munster et al. 2011).
2. A phase II clinical trial examined the effect of entinostat in combination with exemestane vs. exemestane alone in either ER+ postmenopausal women who relapsed after 12 months on nonsterodial AIs or postmenopausal women with metastatic disease who relapsed on nonsterodial AIs after 3 months. Median PFS was 4.3 months for combination arm vs. 2.3 months for exemestane alone (Yardley et al. 2013). Further studies are underway.

In summary, although endocrine therapy is the mainstay of treatment for ER+ breast cancer patients, both de novo and acquired resistance remain a clinical challenge. Most clinical trials cotargeting ER and growth factor signalling aim to delay or treat resistance. Although there have been some positive studies, in further instances targeting growth factor signalling has proved quite disappointing in the clinic (particularly for growth factor receptors), with non-responders and also responses of limited duration. This contrasts the considerable promise of co-treatments seen pre-clinically. One contributory mechanism appears to be that targeting of growth factor signalling can promote other compensatory mechanisms to drive proliferation in cancer cells, which in turn limits co-treatment impact. Targeting downstream mTOR, CDK4/6-driven proliferation or epigenetic mechanisms have promise, but further clinical studies are needed and it seems probable that responses with these approaches will again be of finite duration. Gutierrez et al. (2005) have also reported that HER2 overexpression or amplification emerges on tamoxifen relapse in only ~11% of HER2-negative tumours, which infers the existence of as yet unknown mechanisms underpinning antihormone relapse. Hence, further resistance research remains needed to discover new drug targets better able to control endocrine resistance.

1.11 New cell model panel to represent clinical antihormone relapse

In vitro study of endocrine resistance that develops during treatment of ER+ breast cancer cells (MCF7, T47D, BT-474 and ZR-75-1) can help to mimic ER+ subgroups of breast tumours which develop resistance in patients. Most laboratories have used MCF7, which is an ER+/HER2- (luminal A) breast cancer cell model (Neve et al., 2006), to study acquired resistance to antioestrogen therapy. Initially, the MCF7 cell line was derived from the pleural effusion of a 69-year-old breast cancer patient who was diagnosed with adenocarcinoma (Soule et al. 1973). MCF7 cells have been shown to form xenograft tumours in response to oestrogen administration in vivo (Soule and McGrath 1980). MCF7 is ER+ and thus proliferates in the presence of oestradiol. Moreover, tamoxifen competitively binds to ER and inhibits DNA synthesis in MCF7 (Levenson and Jordan, 1997) while further antihormonal measures, such as using oestrogen depleted media conditions or fulvestrant treatment, are also initially growth inhibitory in such cells (Gee et al. 2003).

Continuous antihormone treatment can be used to generate in vitro and in vivo models from MCF7 cells for acquired resistance. There are many examples of researchers using this strategy to provide acquired resistant models for study, which are cultured for 6-18months in the presence of antihormone and so represent relatively short-term resistance. Previous studies on such endocrine resistance models by our group have revealed evidence for crosstalk between ER and growth factor signalling pathways in cell proliferation and survival in the model systems although the nature of this cross talk differs; for example, hyperactivation of EGFR/HER2 signalling and AF-1 ER activation was detected in the tamoxifen resistance model (TamR) (Knowlden et al. 2003). In a fulvestrant resistant FasR model an importance for EGFR was also detected (McClelland et al. 2001, Nicholson et al. 2007), and PI3K/AKT signalling crosstalk with ER was found to be a significant mechanism of resistance to acquired oestrogen deprivation in the MCF7(X) model (Staka et al. 2005). Clarke's laboratory generated an MCF7:LCC1 subclone by inoculating MCF7 into ovariectomized athymic mice to generate an oestrogen independent model. MCF7:LCC2 was then generated by culturing MCF7:LCC1 in the presence of tamoxifen until resistance to tamoxifen developed. This model is ER+ and thus responds to fulvestrant treatment; however, a further model MCF7:LCC9 was generated in vitro from MCF7:LCC1 which is resistant to both tamoxifen and fulvestrant (Clarke et al. 1989, Brunner et al. 1993a and b, 1997). Santen's laboratory generated an oestrogen deprivation resistant (oestrogen hypersensitive) model by culturing MCF7 in oestrogen deprived media conditions for 1-6 months (Song et al. 2001).

However, longer term oestrogen deprived resistant MCF7 (MCF7: LTED) cells were also generated by Santen's group by continuous culturing of these oestrogen deprived cells.

Interestingly, this model was growth inhibited in the presence of oestradiol (Song et al. 2001) suggesting there may be further changes in resistance mechanisms that develop during more prolonged endocrine exposure. MCF7 derived acquired tamoxifen resistant models serially re-transplanted long-term in vivo have also been described by the Jordan group that are sensitive to oestrogen-induced apoptosis (Osipo et al. 2003), providing further proof of principle that mechanistic pathways can indeed be further altered in long-term resistance. Since pathway targeting of EGFR/HER2 receptors, implicated from shorter term models, has proved inadequate for many patients in the clinic, it is possible that including models to also consider more prolonged duration of endocrine exposure in vitro may better reflect resistance mechanisms emerging during adjuvant treatment timeframes in the clinic.

For this purpose, our Breast Cancer Molecular Pharmacology group has developed a small panel of acquired resistant models which encompasses shorter and longer-term continuous endocrine treatment in vitro. Various strategies were taken to develop multiple endocrine resistant models in the research group. ER + breast cancer cells (MCF7) were exposed to endocrine agents for up to 3 years aiming to more fully mimic clinical acquired endocrine resistance in breast cancer patients. Two resistant models were developed for each major endocrine strategy that differed from each other with regards to duration of resistance (shorter and also longer- term), comprising acquired tamoxifen resistance models (TamR/TamRLT), fulvestrant resistance models (FasR/FasRLT) and oestrogen deprived resistant models (MCF7(X)/MCF7(X)LT). The earlier resistant models TamR, FasR and MCF7(X) represented 18 months-2 years exposure to endocrine agents (Knowlden et al. 2003, Staka et al. 2005, Nicholson et al., 2007), whereas the longer term resistant models (TamRLT, FasRLT and MCF7(X)LT) were developed by maintaining these shorter term resistant models for up to 36 months with endocrine agent (Gee et al. 2011). Using the panel of acquired endocrine resistance breast cancer models for this thesis gives an opportunity to study whether there are resistance mechanisms that span multiple endocrine agents and earlier/later resistance. As potentially key resistance mechanisms, their targeting might provide new ways to control antihormone resistance

1.12 Large scale genomic/bioinformatics approach to investigate mechanisms of endocrine resistance in the new endocrine resistant breast cancer cell panel

Screening large numbers of genes for biomarker discovery and determination of induced cellular pathways in breast cancer samples can be achieved through gene microarray studies for expression profiling (Perou et al. 2000 and Sorlie et al. 2001) and can also be applied to cell model studies in some instances yielding relevant pathways. Bioinformatics tools for gene analysis can provide users with gene profiles, ontological data and functional clustering for

uploaded genes that (based on statistical approaches) can determine the enriched association of expressed genes with significant cellular pathways. Gene microarray analysis using Affymetrix's GeneChip™ Human Gene 1.0 ST platform and subsequent bioinformatics approaches have been applied in the current study to search for mechanisms of endocrine resistance shared across the MCF7 derived, acquired resistant breast cancer cell model panel.

1.13 Aims and objectives

ER+ breast cancer accounts for approximately 70% of breast tumours and blockade of oestrogen/ER signalling through endocrine therapy is the mainstay of treatment in ER+ disease. Despite initial response to endocrine treatment, many patients eventually relapse having acquired resistance which represents a significant clinical issue in breast cancer management urgently requiring mechanistic study. The hypothesis of this thesis is that interrogation of the unique panel of MCF7 derived acquired resistant breast cancer cells will yield new mechanisms of resistance. This project aims to use gene microarray expression profiling to specifically focus on discovering from the models if there are shared mechanisms of resistance to endocrine treatment. Since the model panel encompasses breast cancer cells treated with different endocrine agents and at different time points, it is envisaged that subsequent targeting of the shared mechanism may be important in helping to overcome resistance in breast cancer cells.

To investigate this hypothesis, the following principle objectives were set:

- ✓ To determine significantly deregulated genes in potentially proliferative pathways that are shared across all the endocrine resistant models vs. endocrine responsive MCF7 cells.

  Gene microarray analysis in the models will extend to the "whole genome" accompanied by statistical approaches, focussing on identifying robustly-induced elements. For whole genome analysis, genes with similar functional annotation will be clustered to assist in identifying deregulated pathways from the gene lists. Ontological information and pathway elements will be further interrogated to evaluate the biological and functional role of deregulated genes and gauge whether they may contribute to resistant cell growth. Promising deregulated genes will be examined in relation to time to relapse using publically-available ER+ and tamoxifen treated breast cancer expression databases so that any potential adverse function in promoting clinical resistance can be determined, and further MCF7 arrays will be interrogated to determine the resistant gene profiles in relation to initial antihormone treatment.

- ✓ To pharmacologically target the shared resistant model pathway with the most significant associations from the whole genome analysis. This will further verify if the pathway is functional and contributes to growth and proliferation in endocrine resistant breast cancer models versus responsive models. Activity of the pathway before and after application of inhibitor needs to be determined across the panel to help evaluate mechanism. Pharmacological manipulation will also provide an indication of whether such targeting might have future value in controlling endocrine resistance.
- ✓ To investigate if further shared genes with kinase activity (or their potential regulators) can be identified from the endocrine resistant models vs. MCF7. The gene microarray analysis will extend to the ‘’whole kinome’’and ontological study and expression evaluation in the clinical datasets will again be used to interrogate the kinases to determine those with potential impact on resistant growth. This will provide further mechanistic insight into endocrine resistance, and may yield additional therapeutic approaches.

Chapter 2

Materials and Methods

2.1 Cell culture

2.1.1 Routine cell maintenance

The parental MCF-7 cell line (a gift from AstraZeneca, Cheshire, UK) was routinely maintained in phenol red-containing RPMI-1640 medium ((+) L-glutamine, Life Technologies, UK) supplemented with 5% FCS (foetal calf serum), penicillin-streptomycin (10iU/ml-100µg/ml) and fungizone (2.5 µg/ml). MCF-7 derived acquired tamoxifen resistant (TamR/TamRLT) and Fulvestrant resistant (FasR/FasRLT) cells were routinely grown in phenol red-free RPMI-1640 medium ((-) L-glutamine, Life Technologies, UK) supplemented with 5% charcoal stripped (i.e. steroid-depleted) foetal calf serum (SFCS), penicillin-streptomycin (10iU/ml-100µg/ml), fungizone (2.5 µg/ml) and glutamine (4mM), together with either 4-OH-Tamoxifen at 10^{-7} M (Sigma-Aldrich, UK) or Fulvestrant at 10^{-7} M (a gift from AstraZeneca, Cheshire, UK) respectively. MCF-7 derived cells with acquired resistance to oestrogen deprivation (MCF7(X)/MCF7(X)LT) were routinely grown in phenol-red free RPMI-1640 medium containing 5% heat-inactivated (65°C, 40 min) charcoal stripped foetal calf serum (XSFCS), penicillin-streptomycin (10iU/ml-100µg/ml), fungizone (2.5 µg/ml) and glutamine (4mM). All the antihormone resistant cell lines comprising the model panel used in this thesis were developed prior to this project by the Breast Cancer Molecular Pharmacology (BCMP) group by continuous culture of MCF-7 cells in the presence of 4-OH tamoxifen (10^{-7}M), fulvestrant (10^{-7}M) or severe oestrogen deprivation (XSFCS medium). Authenticity of the cell lines was verified by STR profiling through collaboration with Dr Walther Parson (University of Innsbruck). The resistant TAMR (Knowlden et al. 2003), MCF7(X) (Staka et al. 2005) and FASR lines (Nicholson et al. 2005) were studied after 18, 25 and 27 months culture respectively, and maintained in antihormone up to 3 years to generate the longer-term TamRLT, FasRLT and MCF7(X)LT acquired resistant lines. All cells were cultured under sterile conditions at 37°C in a humidified incubator (Sanyo MCO-17AIC, Sanyo Gallenkamp, Loughborough, UK) supplied with 5% CO2. The media was changed every 3 days and cells were passaged during log-phase on day 7 with a seeding ratio of 1:10 for MCF-7, TamR, FasR, MCF7(X) and MCF7(X)LT, and at 1:20 for FasRLT and 1:40 for TamRLT cells. For passaging, 70% confluent monolayers of each model were disrupted by addition of 3ml trypsin/EDTA (0.05%/0.02%w/v) for 3 minutes, followed by addition of an equal volume of the respective routine media and centrifugation (Mistral 3000i centrifuge Sanyo Gallenkamp, Loughborough, UK) at 1000rpm for 5 minutes. The supernatant was discarded and cell pellets was suspended in 5-10ml of fresh

routine medium. Cells were seeded in a flask and the media was replaced every 3 days until further passaging was required. All cell culture reagents and FCS were purchased from Life Technologies (Paisley, UK). Cell culture plasticware was purchased from Nunc (Roskilde, Denmark), supplied by Fisher Scientific (Loughborough, UK).

2.1.2 Experimental cell culture

For microarray and basal growth studies, experimental medium for all breast cancer models was the same as their respective routine culture medium, except for MCF-7 cells which were grown for 7 days in experimental media comprising phenol-red free RPMI 1640 ((-) L-glutamine) supplemented with 5% SFCS, penicillin-streptomycin (10iU/ml-100µg/ml), fungizone (2.5 µg/ml) and glutamine (4mM). Further experiments were performed using MCF7 cells grown for 10 days using the alternative 5% heat-inactivated SFCS to match the oestrogen deprivation strategy used for the oestrogen deprived resistant models. Endocrine response microarray studies also utilised MCF7 cells grown for 10 days in the presence of 4-OH-Tamoxifen or Fulvestrant (10^{-7}M), or with 17-β oestradiol supplementation (10^{-9}M).

2.1.3 Growth assays

Monolayers of cells were trypsinized and resuspended in fresh medium. Cells were seeded overnight at 20,000 cells/well (using 48 well plates) in their respective medium as described for routine cell culture. After 24 hours, the media was replaced by fresh medium which contained experimental treatment (e.g. TAMR/TAMRLT in experimental medium plus 4-OH Tamoxifen 10^{-7}M, FASR/FASRLT in experimental medium plus Fulvestrant 10^{-7}M, antimycin A (5-100nM, Sigma-Aldrich, UK), metformin (0.5-7mM, Sigma-Aldrich, UK), +/- glutamine (4mM or 10mM, Life Technologies, UK), or with oestrogen deprivation (MCF7(X)/(X)LT in XSFSC media). The experimental medium was replaced every 4 days. Cell growth was evaluated at day 3, 5 and 7 by trypsin dispersion followed by cell number counting using a Coulter™ Multisizer II (Beckman Coulter UK Ltd, High Wycombe, UK). Mean number of cells/well (from triplicate wells) were determined. All experiments were performed in three independent experiments and every cell line was used within a window of 20 passages. Basal growth and treatment data were used to plot growth curves, to evaluate growth at day 7 in relation to control, and to calculate EC_{50} values for treatments. To calculate mean of half-maximum response (EC_{50}), cell number for each treatment (including untreated control) were normalized against number of cells for maximum response (highest dose). Percentage of maximum response for each dose was uploaded on GraphPad Prism 5 (range between 0-100) and then log transformed for further analysis. Non-linear regression followed by dose response inhibition equation (log (agonist) versus normalized response-variable slope) and sigmoidal dose response curve were determined using GraphPad Prism 5 software.

2.2 Gene microarray study

Prior to the thesis, mRNA samples of each breast cancer cell model (MCF-7, TamR, TamRLT, FasR, FasRLT, MCF7(X) and MCF7(X)LT) were isolated in experimental triplicate by the BCMP group and used to generate gene microarrays for the subsequent expression studies that have been performed in this thesis, as follows:

2.2.1 Cell lysis

All breast cancer cell models (MCF7 and the 6 derived resistant lines) were seeded at 3,000,000 cells per 150mm diameter dishes in triplicate. For basal profiling, cell lysis was performed at day 7 (within log-phase of growth) at room temperature in a fume cupboard. Medium was poured off from dishes and drained briefly. 10ml tissue culture grade Dulbecco's phosphate buffer saline 1X (PBS) was added onto each dish and dishes were left for 10 seconds before pouring off the buffer followed by further draining of the dishes for 5 seconds. This was repeated for 3 times before addition of 1.5ml Tri-Reagent (T9424, Sigma Aldrich, UK) onto the surface of each dish. Dishes were covered with a lid and gently rocked for 1 minute to ensure full coverage of cells with the lysis solution. Each cell lysate was collected by using a sterile disposable cell scraper and half of the lysate was transferred to each of two 1.5ml micro-centrifuge tubes (i.e. >750µl/tube). The lids were closed and tubes containing the lysate were inverted twice before being placed into dry ice.

2.2.2 Total RNA isolation from Tri-Reagent-lysed samples

Sample volume was adjusted to 1ml by addition of Tri-reagent and mixed thoroughly by inversion. 200µl chloroform was added to each tube and rapidly vortexed for 20 seconds. This was repeated 3 times and tubes were left at room temperature for 10 minutes. Tubes were then spun in a pre-cooled centrifuge (4°C, Labofuge 400R, Heraeus, Germany) at 13000rpm (16000g) for 10 minutes. At this point samples separated into 3 phases; the upper aqueous phase which contained the RNA, the middle phase (clear and less obvious layer) containing DNA and the lower phenolic phase containing protein. The upper phase was carefully removed and transferred to a clean micro-centrifuge tube. 500µl of isopropanol (propan-2-ol) was added to the supernatant to precipitate the RNA. Samples were vortexed briefly and left to stand at room temperature for 10 minutes. Samples were then spun again in the pre-cooled centrifuge at 13000rpm for 10 minutes. The supernatant was discarded and the RNA was left as a white pellet at or near the base of tube. 1ml 70% ethanol was added to wash the RNA before spinning in the pre-cooled centrifuge at 13000rpm for a further 10 minutes. The ethanol was discarded and tubes were inverted on clean tissue paper. The RNA pellet was then air dried for 10 minutes before resuspending in 25µl RNase-free water. The RNA concentration and purity was determined by using a Biomate3S UV-visible spectrophotometer (Fisher Scientific,

Loughborough, UK) at 260/280 nm and RNA integrity was evaluated via gel electrophoresis (2% agarose gel, BioLine, UK) followed by detection of 18s and 28s ribosomal RNA in all triplicate samples. All RNA samples were stored at -80° C for further analysis.

2.2.3 DNase treatment of isolated RNA

RNase-free DNase reagents from RNeasy Micro kit (Qiagen, UK) were used for this procedure to remove any trace of DNA contamination. In the sterile micro-centrifuge tube, 45µg RNA (<87.5µl of the stock RNA) from each sample was mixed with 10µl of kit buffer ("RDD") and 25µl of DNase I solution, and the volume was adjusted to 100µl by addition of RNase free water (Sigma-Aldrich, UK). The mixture was left at room temperature for 10 minutes before proceeding to the RNA clean-up step.

2.2.4 RNase treatment of isolated RNA

RNeasy Micro kit (Qiagen, UK) reagents were also used for this protocol. 350µl of kit "RLT" buffer supplemented with 6µl β-mercaptoethanol was mixed thoroughly with each of the 100µl RNA samples to inactivate RNases and other proteins which may degrade RNA. 250µl 100% ethanol was added to each tube and mixed well. An RNeasy MinElute spin column (Qiagen, UK) was inserted into a 2ml kit collection tube and the entire content of each RNA sample tube (700µl) was transferred into the spin column followed by centrifugation at 13000rpm (10000g) for 15 seconds in a benchtop microcentrifuge (Biofuge, Heraeus, Germany). The through-flow was discarded and 700µl of kit "RW1" buffer was added to each column and spun again for 15 seconds at 13000rpm.The through-flow and collection tube were discarded and the column was inserted into a new 2ml collection tube. 500µl kit "RPE" buffer was added to each tube and spun for 15 seconds at 13000rpm. Again through-flow was discarded and 500µl of 80% ethanol was added to each column. The columns were spun for 15 seconds at 13000rpm followed by discarding through-flow and collection tubes. The columns were inserted into new 2ml collection tubes and left open and spun for 4 minutes at 13000rpm to dry the columns thoroughly. Columns were then inserted into sterile 1.5ml Eppendorf-type microcentrifuge tubes and 14µl of RNase-free sterile water was added to the centre of each column membrane. The column lids were closed and the columns were spun for 1 minute at 13000rpm to elute the RNA. Columns were discarded and microcentrifuge tubes containing 12µl eluted RNA were placed on ice. RNA concentration and integrity of each sample was again determined by spectrophotometry and gel electrophoresis respectively. RNA samples were aliquoted (1µg RNA/7µl H_2O) before storage at -80°C.

2.2.5 Affymetrix genechip human WT 1.0ST array study

All three independent RNA samples from each cell model were sent by the BCMP group to Cardiff University Centre of Biotechnology Services (CBS) Affymetrix GeneChip® profiling service to perform microarraying using an Affymetrix-recommended procedure and associated kits. All samples passed an initial quality control assessment by CBS using an Agilent analyser to check for any RNA degradation and DNA contamination. In brief, for the subsequent arraying 100ng RNA of each sample was subjected to a ribosomal RNA (rRNA) reduction procedure where the 28S and 18S rRNA was depleted from the total RNA samples to minimize background and enhance sensitivity of detection of gene expression. Double stranded cDNA was then synthesized with random hexamer tagged with a T7 promoter sequence and it was used as a template for synthesis of cRNA via T7 RNA polymerase. In the second cycle, single stranded DNA in the sense orientation was synthesized from cRNA and dUTP was incorporated into DNA during first-strand reverse transcription reaction. A combination of uracil DNA glycosylase (UDG) and apurinic/apyrimidinic endonuclease 1(APE 1) was added to single stranded DNA to detect unusual dUTP residues and break the DNA strand. DNA was then labelled by terminal deoxynucleotidyl transferase (TdT) which is covalently linked to biotin (Affymetrix GeneChip WT terminal labelling kit). By this procedure, sufficient target was generated to hybridize to a single Affymetrix array GeneChip (WT human 1.0ST microarray, Table 2.1) for every sample analysed. Arrays were incubated at 45°C for 17 hours followed by washing and staining for detection, prior to CBS scanning the chip using an Affymetrix GeneChip Scanner for the expression of exons for all genes in the samples. CBS subsequently performed pre-processing of the Gene Chip scan data which included background correction, data normalisation, and summarisation of gene expression level using RMA. These gene expression data in triplicate for the breast cancer models were provided to the BCMP group as CHP files and displayed following file upload into Genesifter for further investigation.

Transcript coverage of the array	Human gene 1.0ST Array
Total RefSeq transcript covered	36,079
NM RefSeq coding transcript (well established annotation)	32,020
NR RefSeq non-coding transcript (well established annotation)	2,967
XM RefSeq coding transcript (provisional annotation)	579
XR RefSeq non-coding transcript (provisional annotation)	513
lincRNA transcripts	466
RefSeq (Entrez) gene count	21,014

Table 2.1. Transcript coverage and gene count from RefSeq on the Affymetrix Human gene 1.0ST microarray platform.

2.2.6 Genesifter analysis for microarray data

All Gene expression data for three independent samples for each breast cancer model were uploaded into the Genesifter online bioinformatics analysis tool (www.genesifter.net), where expression of all the gene probes was log transformed before detailed profile analysis. Expression level of each probe was then displayed either by (i) heatmap (with the parental MCF7 cells set as control) or (ii) using $\log_2$ intensity plots. Fold change comparison was tabulated for each resistant model in relation to control MCF7 cells using the software.

Given this array platform does not provide an presence/absence expression "call", a cut-point for detectable expression was estimated based on the $\log_2$ intensity detected for a known ER-model in the panel (FASR cells; ESR1 gene $\log_2$ intensity=8) and also according to the array's standard negative control probes. This was considered to be a mean value of approximately 8 on the $\log_2$ intensity plot. An initial evaluation of profiling of basic expression features across the models e.g. for ESR1 (ER) gene, ER-regulated gene TFF1 (pS2), and HER2 (ERBB2) from the array data was then performed that also served to verify microarray performance, since the expression profile of ER in TAMR, FASR and MCF7(X) cells is already known (Knowlden et al. 2003, Staka et al. 2005).

Subsequently a total of 11 "projects" using the 1.0ST arrays were created in Genesifter to determine genes with down/upregulated expression changes that were greater than ≥ 1.2 fold versus MCF7 (To allow enough genes for further analysis). These projects were (i) for each of

the six endocrine resistant breast cancer model as compared to the parental MCF-7 line, (ii) in relation to duration of resistance by considering the earlier resistant lines (TAMR, FASR and MCF7(X)) or the later resistant lines (TAMRLT, FASRLT and MCF7(X)LT) versus MCF7 and (iii) according to antihormone resistant type by considering tamoxifen resistant (TamR and TamRLT), fulvestrant resistant (FasR and FasRLT) or oestrogen deprived resistant cells (MCF7(X) and MCF7(X)LT) versus MCF7. Generation of these gene lists was followed by statistical analysis for each project using ANOVA statistical testing with Benjamini Hochberg correction in order to determine "shared" genes that were induced or suppressed in all the resistant models in the panel versus MCF7. The resultant Affymetrix probe IDs for all shared deregulated genes from each analysis were extracted for further cluster, ontological and pathway investigation.

In addition to the resistance arrays, further microarray data (median normalised, log2 transformed from three independent experiments) previously accumulated by the BCMP group from commercially-analysed HGU133A chips were made available for Genesifter interrogation of the resistance genes of interest in relation to initial treatment with oestrogen or anti-hormones. This "endocrine response" analysis project comprised gene microarray data from hormone responsive MCF7 cells treated for 10 days with 10^{-9} M 17-β oestradiol, oestrogen deprivation (using 2 strategies i.e. 5% SFCS or heat inactivated SFCS to parallel the MCF7(X)/(X)LT resistant model treatment), fulvestrant or 4-OH tamoxifen (10^{-7} M). The array data for the antihormone treatments were then analysed in Genesifter to construct gene lists with ≥1.2 fold change, in this instance compared to the MCF7+E2-treated cells.

2.2.7 ID conversion and cluster analysis of microarray data

Gene IDs from Genesifter projects were uploaded into DAVID bioinformatic online software (www.DAVID.abcc.ncif.crf.gov). These IDs were converted in DAVID to ENSEMBL gene IDs to permit subsequent pathway analysis using Innatedb data base. In addition, for genes implicated in metabolic pathways resultant from such pathway analysis, ontological clustering of those upregulated >1.2 fold in the endocrine resistant models was performed within DAVID using a functional classification tool to see if there was enrichment of particular metabolic pathways (using kappa calculation in the software for enrichment score (www. david.ncifcrf.gov/helps/functional classification). Such clusters were again displayed using heatmaps, noting those clusters with the highest enrichment score.

2.2.8 Ontology and pathway analysis of microarray data

Extracted ENSEMBL IDs from DAVID for the shared deregulated genes identified from projects were uploaded into Innatedb online (www.Innatedb.ca) to perform ontology and pathway analysis using associated databases. ENSEMBL IDs from each project were run through the gene ontology (Go terms) analysis tool ("Gene Ontology" database) in Innatedb followed by the software applying a hypergeometric algorithm with Benjamini and Hochberg correction (i.e. overrepresented gene ontology analysis or "ORA-O" in relation to associated biological process, molecular function and cellular compartment) to display significant enriched ontologies for the uploaded genes (p value <0.05). The same uploaded ENSEMBL IDs were then used by Innatedb to perform an overrepresented pathway analysis ("ORA-P") using the affiliated KEGG pathway database, again applying a hypergeometric algorithm with Benjamini and Hochberg correction (p value <0.05). Innatedb ORA-O and ORA-P analysis was also applied to the "endocrine response" HGU133A-derived gene lists to identify over-represented ontologies and pathways during initial endocrine treatment of MCF7 cells. In addition, a list of significantly upregulated kinases shared by all endocrine resistant models was extracted from the resistance arrays (comparing list of shared upregulated genes with list of Human Kinome using www.Human Kinome - Kinase.com) and ontological interrogation of the resultant induced kinase list was again performed using Innatedb. This was used (together with clinical profile: see Methods section 2.9) to prioritise 3 resistance kinases for further study in the thesis.

Further ontological investigation was made for genes/enzymes in the most significant pathways using either KEGG (www.KEGG.jp) or Genecards (www.genecards.org) resources, as well as using Pubmed for the genes of interest in relation to function and any association with breast cancer or therapeutic resistance.

2.3 RT-PCR profile verification

RT-PCR was performed to verify the microarray gene expression profiles of ER, pS2 and ERBB2, three promising deregulated kinases from pathway analysis, and two induced zinc related genes SLC39A7 and MT2A in the model panel. Experimental triplicate RNA samples for each of the breast cancer models (prepared as in section 2.2.2) were reverse transcribed and subjected to RT-PCR to detect expression of the genes of interest across the cell model panel (compared with the parental MCF7 line) as follows:

2.3.1 Reverse transcription

The triplicate RNA samples were subjected to reverse transcription to generate complementary DNA molecules (cDNA) prior to performing PCR. The RT reaction master mix was composed of 5µl deoxy nucleotide tri-phosphates (dNTP, 2.5mM, Invitrogen, UK), 2µl PCR 10X buffer (10mM tris-HCl, pH.8.3, 50mM NH_4, 0.001% w/v gelatin, BIOLINE, UK), 2µl DTT (0.1M, Invitrogen, UK), 2µl random hexamers (RH, 100µM, BIOLINE, UK) and 0.5µl $MgCl_2$ (50mM, BIOLINE, UK) which was added to each 1µg RNA sample (in a total 7µl RNAse-free Water (Sigma-Aldrich, UK)). The resulting 11.5µl RT-reaction solution for each model was denatured at 95°C for 5 minutes in a PTC-100™ programmable thermocycler machine (MJ Research Inc, USA) followed by rapid cooling on ice for 5 minutes. The RT-solutions were pulse spun in a microfuge (Biofuge, Heraeus, Germany) and placed on ice. 1µl MMLV (200U/µl, Invitrogen, UK) and 0.5µl ribonuclease inhibitor (RNAse inhibitor, Promega, UK) were added to each sample, adjusting the final volume to 20µl prior to reverse transcription. Samples were placed in the PTC-100™programmable thermocycler machine and then reverse transcribed under the following conditions:

Annealing at 22°C for 10 minutes,

RT extension at 42°C for 40 minutes

Denaturing at 95°C for 5 minutes

The resulting cDNA samples were collected and stored at -20°C until needed for PCR.

2.3.2 Polymerase chain reaction (PCR)

PCR was performed to amplify cDNA using specific primers for the genes of interest. In summary, cDNA molecules were denatured and polymerization was initiated via DNA polymerase which adds deoxy ribonucleotides to the 3'-OH group of complementary oligonucleotide sequences (forward/reverse primers). The reaction was repeated several times to yield copy numbers desirable for optimal detection for the genes of interest:

2.3.3 Primer design

To verify the mRNA expression profiles of genes of interest from the microarray data (e.g. ER, pS2, ERBB2; also 3 resistance-associated kinases (PCK2, ALDH18A1, PFKFB2), SLC39A7 and MT2A, and also β-actin for normalisation purposes), primers were designed to detect similar sequences to those recognized by the microarray gene probes. To do this, multiple isoforms of the genes of interest were identified using the PubMed Gene database (www.ncbi.nlm.nih.gov/gene) and compared with available exons for the gene on the Affymetrix GeneChip 1.0ST array. Nucleotide sequences of multiple isoforms were aligned on the NCBCI nucleotide blast online tool (www.ncbi.nlm.nih.gov/Blast) and sequences with high alignment scores were selected for designing primers. The highly matched sequences were uploaded on the online primer design tool (www.ncbi.nlm.nih.gov/tools/primer-blast) and the following

parameters were selected to design optimum primers for genes of interest: PCR product size 100-500bp, Homo sapiens organism, primer size 15-25 -mers and primer GC content between 40%-60%. Final primer sequences were checked using the primer-blast online tool to check specificity of designed primers only for the gene of interest. The primers utilised in the thesis are detailed in Table 2.2.

Gene	Forward primer	Reverse primer	Cycle Number	Product size
ERBB2 (HER-2)	5′ CCT CTG ACG TCC ATC ATC TC 3′	5′ ATC TTC TGC TGC CGT TT 3′	29	98bp
ESR1 (ER)	5′ GGA GAC ATG AGA GCT GCC ACC 3′	5′ CCA GCA GCA TGT CGA AGA TC 3′	33	432bp
TFF1 (pS2)	5′ CAT GGA GAA CAA GGA GAT CTG 3′	5′ CAG AAG CGT GTC TGA GGT GTC 3′	27	336bp
ALDH18A1	5′ TAG CCT TTG GCA AAC AAC GC 3′	5′ AAT AAC CCC CTG CAG GTC AC 3′	26	359bp
PCK2	5′ TCA TGC CGT AGC ATC CAG AC 3′	5′ ATG CAG CCT GGA AAC CTC TC 3′	24	389bp
PFKFB2	5′ GAC TGC TGA ATC TCT CGG GG 3′	5′ AGC TCA TCT GCG CCC TTA TC 3′	29	303bp
SLC39A7	5′ TGC TTG GCT TAT GGA GAA CC 3′	5′ GAG ATG ACG GTC ACA CAG AGG 3′	25	392bp
MT2A	5′ ACC TGT CCC GAC TCT AGC CGC 3′	5′ GGC GCA GGT GCA GGA GTC AC 3′	25	83bp
β-actin	5′GGA GCA ATG ATC TTG ATC TT 3′	5′ CCT TCC TGG GCA TGG ACT CCT 3′	____	204bp

Table 2.2. Primer sequences (forward and reverse) and cycle numbers used in the RT-PCR verification experiments, together with the predicted product size. β-actin was co-amplified in each RT-PCR experiments as a loading control for the normalization.

2.3.4 PCR procedure

The PCR reaction mixture was composed of 37.25µl sterile RNA/DNAse free water (Sigma-aldrich, UK), 5µl 10X PCR buffer, 4µl dNTPs, 1.25µl forward/reverse primers (20µM, Invitrogen, UK), 0.2µl TAQ DNA polymerase (5 units/µl, BIOLINE, UK) for each cDNA sample. 0.5µl of cDNA was added to this PCR reaction mixture followed by pulse spinning and addition of 2 drops mineral oil (Sigma-aldrich, UK) on top of each PCR tube to avoid evaporation of the reaction mixture. PCR samples were then placed in a PCT-100 programmable thermal cycler and the following conditions were used to amplify the gene of interest. For the first cycle, cDNA samples were denatured at 95°C for 2 minutes followed by cooling at 55°C for 1 minute to allow primers to anneal to cDNA and TAQ enzyme to initiate polymerization. In the last step, samples were heated at 72°C for 5 minutes to extend primer polymerization and PCR product formation.

Between the first and last cycle, further cycles were repeated between 20-40 cycles. Cycle numbers were optimized for each gene of interest (Table 2) For these repeated cycles, samples were heated to 94°C for 30 seconds, followed by cooling to 55°C for 1 minute, and then they were heated to 72°C for 1 minute, with a final cycle carried out by heating samples to 94°C for 1 minute, cooling them to 55°C for 1 minute and then heating them to 60°C for 10 minutes.

2.3.5 Visualizing PCR products via agarose gel electrophoresis

2% molecular biology grade agarose (BIOLINE, UK) was added in 100ml tris acetate buffer 1X (TAE, pH 8.3) and microwaved for 2 min until dissolved. The agarose solution was cooled and 1µl ethidium bromide (EtBr, 5mg/ml (Sigma Aldrich, UK)) was added prior to pouring the solution into a wide mini-sub cell GT apparatus (Biorad, UK) with a comb used to create wells, and this was left for 20 minutes at room temperature to solidify. 10µl of each PCR product per sample was mixed with Crystal DNA loading buffer 5X (BIOLINE, UK) and loaded into the wells on the gel. 5µl hyperladder 100bp marker (BIOLINE, UK) was also loaded into the first well and an electric field was applied at 70V for 45 minutes to separate the DNA molecules by their size. The gel was visualized and photographed using a ChemiDoc™ XRS system (Biorad, UK). Associated Image Lab™ software was used to determine density of the specific band on the gel for each sample, which related to the amount of expressed RNA. All PCR reactions were coamplified with β-actin and the final PCR results for expression of the test genes were normalized against β-actin expression for each sample, displaying mean normalized volume across the three independent experiments for each model in the cell panel (+/- SEM).

2.4 LC-MS/MS

To further verify key findings from the microarrays, a proteomic approach based on Liquid chromatography tandem mass spectrometry (LC-MS/MS) was used to identify and quantify proteins (considering both total and phosphorylated peptides) in an antihormone resistant model versus MCF7 cells. This was achieved by accessing a proteomic dataset previously generated by Dr. David Britton and his further collaborators at Proteome Sciences (Kings College, London) on these cells.

To initially generate the protein samples for analysis, TamR and MCF7 cells were seeded (500,000 cells/dish) in 2x75mm diameter dishes (three independent experiments) and grown in their respective experimental media until 70% confluency (7 days). The media was removed and cells were washed with 1X phosphate buffered saline (PBS) twice. Lysis buffer containing a protease inhibitor cocktail (inhibits protein degradation and dephosphorylation, (Sigma Aldrich, UK)) was added and cells were scraped and collected into Eppendorf tubes which were kept on ice for 5 minutes. Samples were then centrifuged at 12,000rpm in 4°C for 15 minutes and

supernatants before shipping on dry ice for LC-MS/MS at Proteome Sciences. At the Proteome Sciences Lab, protein samples were trypsin digested and resulting peptides were labelled with isobaric Tandem Mass Tag® eight-plex reagents (TMT8). Samples were split into three aliquots and separated by strong cation exchange chromatography (SCX-HPLC).

Each chromatography run resulted in 12 fractions to maximize phosphorylation site coverage and to provide unmodified peptides for total protein quantification. Three arms including non-enriched, TiO2 and IMAC phosphopeptide enrichment were added and thus 12 crude SCX fractions plus 12 x TiO2 and 12 x IMAC enriched phosphopeptide fractions were analyzed each three times by LC-MS/MS. Spectra were collected in data dependent mode with a top 10 HCD method (LTQ-Orbitrap Velos, Thermo Scientific, Germany) in the first and second runs. A time dependent rejection list for all peptide precursor ions identified in the first and second runs were used with top 10 HCD for the third run.

Dr Britton subsequently used SEQUEST and MASCOT tools (and Phospho-RS for phospho-sites) via Proteome Discoverer to search the mass spectrometry data against the human UniProtKB database, including both total and non-phosphorylated peptides. The TMT reporter intensity which correlates with peptide abundance was assessed to quantify proteins in the samples. All identified peptides were filtered for ≤5% false discovery rate (FDR) and ≥75% phosphorylation site confidence for further analysis (Britton et al. 2014). The data were passed through Proteome Sciences bioinformatics pipeline to generate a list of peptides significantly changed in TamR versus MCF7 cells, considering the 3 replicates per cell line. Significant change was indicated by a $\log_2$ change ≥0.7 (1.63 fold change) and p≤0.05 significance. The significantly-induced protein list was then provided for analysis in this thesis. This involved ontology and pathway interrogation using Innatedb data base ($p \leq 0.05$) including examining if there was any evidence for metabolic pathway change.

2.5 Immunocytochemistry

This method was used to assess expression and localization in the model panel of TOMM20 protein using a specific antibody, and also to monitor proliferation by immunostaining for Ki67. In brief, for these studies the models were grown in their routine experimental culture medium until cells were in log phase (7 days). For TOMM20, models were grown in experimental triplicate prior to pelleting, paraffin embedding and immunostaining for the protein of interest. For Ki67, cells were grown on coverslips in experimental triplicate under basal conditions or in the presence of metformin and subsequently fixed prior to assay.

2.5.1 Cell pelleting for TOMM20 immunostaining

All breast cancer models in the panel were grown in 150mm dishes in their experimental media until log phase prior to cell pelleting. Spent media was removed from the dishes and 10ml fresh RPMI 1640 was added to each dish followed by scraping the cells and collecting them into Falcon tubes. The cells were centrifuged (Juan C312 centrifuge, UK) at 1000rpm for 5 minutes to pellet. The medium was removed and the cell pellets fixed in 15ml 3.7% formaldehyde (made by dilution of 37-40% formaldehyde, Fisher, UK) in Dulbecco's phosphate buffer saline ((-) $MgCl_2$, (-) $CaCl_2$; Lifescience, UK) at 40°C for 70 minutes. The fixative was removed and fixed cells (approximately 1ml) were transferred to a graduated Eppendorf followed by incubation at 40°C for 50 minutes with same the fixative. Residual fixative was removed and an equal volume of nobel agar (12%, dissolved in distilled water, Sigma-Aldrich, UK) was mixed with the cells. The mixture of nobel agar and fixed cells was immediately transferred to a 1ml syringe with a cut end (BD Plastipak, Spain) and left in an upright position for 30 minutes to settle. Syringes were kept in a fridge at 4C overnight. The Agar embedded fixed cells were then sliced into 3-4mm discs and placed in plastic embedding cassettes which were transferred into further fixative (again 3.7% formaldehyde in PBS) in a glass jar for 2 hours at room temperature. The agar-embedded cells were then gradually dehydrated through graded ethanol (10%-60%) for 45 minutes and left in 70% ethanol overnight. The following day, the cells were continued their dehydration in graded ethanol up to 100% ethanol for 45 minutes. The cells were then transferred into 100% xylene in a glass jar, replacing the xylene every 30 minutes for three times prior to a 1 hour soak in a final xylene bath. Paraplast Plus (M.P 56°C, Sigma-aldrich) paraffin wax was melted in a wax dispenser apparatus and poured in three jars into embedding chambers (Hearson, UK). The cells were transferred into these embedding chambers and incubated in the paraplast in each at 56°C for 30 minutes. Embedding moulds were then half filled with paraplast. The cell discs were removed from the embedding cassettes and placed in these moulds which were covered by plastic embedding cassettes and left to solidify.

The embedded cells were subsequently sectioned (4µm thick) using a microtome (Spencers microtome). Cell sections were flattened by floating in a 37C water bath (Thermo scientific, UK) and placed on X-tra™ adhesive coated glass slides (Leica, UK). Slides were then dried overnight at 40°C in an incubator (Heraeus, Germany) ready for TOMM20 immunocytochemistry on the sections.

2.5.2 Dewaxing and Rehydration of cell pellet sections

The slides containing the paraffin-embedded cell pellet sections were dewaxed in two xylene baths each for 5 minutes followed by rehydration through graded ethanol (100%, 90% and 70% each twice for 2 minutes) and transfer to distilled water for 5 minutes.

2.5.3 Blocking endogenous peroxidase activity

Use of horseradish peroxidase (HRP)-conjugated antibodies in immunocyochemistry may be associated with non-specific background staining due to any endogenous peroxidase activity present in cells. Therefore, 3% aqueous hydrogen peroxide solution (Fisher, UK) was initially applied on each section for 5 minutes in order to quench this unwanted activity, and sections were then rinsed with distilled water for 5 minutes.

2.5.4 Heat-induced epitope retrieval (HIER) for TOMM20

Heat-mediated antigen retrieval has previously been recommended for use with the TOMM20 antibody (Sotgio et al. 2012*b*) 2 litres of 0.01M pH 6 sodium citrate tribasic dihydrate buffer (5.88g sodium citrate in 2L distilled water, Sigma-aldrich) was prepared and subsequently used for pressure cooker antigen retrieval of the sections. Slides were placed in the sodium citrate buffer and full pressure applied in the pressure cooker for 2 minutes, followed by 10 minutes cooling of the slides under running tap water.

2.5.5 Blocking background staining

Blocking sections with serum is essential to avoid background staining due to either non-specific antibody binding to endogenous Fc receptors or due to unwanted ionic and hydrophobic interactions. To achieve this, 20% Normal Human Serum (NHS, Golden West Biologicals Inc, US) was applied to each section for 10 minutes. Excess blocking agent was then removed prior to incubating sections with the primary antibody.

2.5.6 Immunostaining of cell pellets from the model panel for TOMM20

PBS/Tween buffer (pH 7.2, Sigma-Aldrich, UK) was applied to each section prior to incubation with TOMM20 primary antibody for 5 minutes. Mouse anti-human TOMM20 antibody (Santa Cruz Biotechnology, US) at 1:500 dilution (prepared in PBS buffer) was applied to the cell pellet sections for all models and incubated overnight at 4^{o}C in a humidity chamber. The next day all slides were washed with PBS and were incubated with the secondary mouse EnVision+ HRP labelled polymer system (DAKO, UK) for 1 hour at 25^{o}C. Following buffer washing, immunoreactivity was revealed using 3 3'-diaminobenzidine solution (DAB, DAKO, UK; comprising 10µl chromogen mixed thoroughly with 500µl substrate). The sections were then counterstained with methyl green (Sigma-Aldrich, UK) for 15 minutes, washed in water, and air-dried before slide mounting using DPX mountant (a mixture of Distyrene, a plasticizer, and xylene, Sigma-Aldrich, UK). Cytoplasmic staining was evaluated for each slide by light microscopy from three fields by viewing at 40X magnification using H-Scoring, considering both percentage positivity and staining Intensity (negative staining cells=0, weak staining cells= 1+, moderate staining cells=2+ and high staining cells =3+). H-Score was calculated on a 0-300 scale as: (% of

1+)x1 + (% of 2)x2 + (% of 3+)x3. H-Score was presented as a mean for each of the cell models for statistical analysis.

2.5.7 Immunostaining of breast cancer cells for Ki-67

The cell lines were seeded onto sterile 3-aminopropyltriethoxysilane (TESPA) coated glass coverslips (100,000 cells/coverslip) in 35mm diameter dishes for 24hrs prior to metformin administration (0.5-2mM) for 7 days in their respective experimental media. Basal coverslips were also prepared for analysis of Ki67 by growing the models to day 7 in log phase. Fresh media was replaced after 4 days culture. To fix the cells before immunostaining, coverslips were immersed in 3.7% formal saline for 10 minutes at room temperature. The coverslips were then immersed in 70% ethanol for 5 minutes followed by two times PBS wash (each for 10 minutes). Coverslips were kept in sucrose storage media (42.8g sucrose, 0.33g magnesium chloride, 250ml glycerol and 250ml PBS) at -20°C. On the day of Ki-67 assay, the storage media was discarded and fixed cells on cells on the coverslips were washed with PBS (3 times). Coverslips were then washed with PBS/Tween for 30 seconds prior to incubation with Ki67 primary antibody (Dako Ltd Species: mouse anti human, 1:150 in PBS) in a humidity chamber for an hour at room temperature. This antibody dilution had previously been optimised for coverslip work in the BCMP group. Coverslips were then washed with PBS (3 minutes) followed by PBS/Tween incubation (0.02%) for 2x5 minutes. Coverslips were then incubated with the secondary detection system (Dako Envision+ system-HRP labelled polymer antimouse, Dako, K4001) in a humidity chamber for 75 minutes at room temperature. After incubation, the coverslips were washed with PBS (3 minutes) followed by PBS/Tween incubation (0.02%) for 2x5 minutes. The coverslips then were each incubated with 50µl of Dako's diaminobenzidine (DAB)/substrate chromagen system solution (Dako Ltd, K3468) for 10 minutes and rinsed with distilled water. Cells were then counterstained with 0.05% Methyl green for 1 minute and washed with distilled water before mounting onto microscope slides (FB58628, Fisher Scientific, UK) by applying DPX mountant. The percentage of cells with nuclear staining positivity for Ki-67 was evaluated by light microscopy (obtaining an average from 3 fields/coverslip by viewing at 40X magnification, and also involving 3 independent experiments), for each cell model and after metformin treatment.

2.6 Enzyme histochemistry to evaluate electron transport chain (ETC) component activity

Enzyme histochemical staining serves as a link between biochemistry and morphology and is based on the metabolization of a substrate provided to a tissue enzyme in its orthotopic localization. The end product for enzyme activity is detectable as an insoluble dye. This method is quite sensitive and has been shown to detect minor metabolic defects in pathological conditions (Meier-Ruge et al. 2007).

2.6.1 NADH dehydrogenase enzyme cytochemistry

Activity of the NADH dehydrogenase enzyme (complex I of ETC) is detectable in living cells because the enzyme transfers hydrogen from nicotinamide dinucleotide (NADH) to the nitrotetrazolium blue chloride stain (Sigma-Aldrich). The final product of this reaction is a water-insoluble formazan blue pigment which marks the site of enzyme activity. Cells from the model panel were seeded at 100,000 cells per coverslips (TESPA-coated) and grown in their respective basal experimental medium with/without the NADH dehydrogenase inhibitor (complex I inhibitor) metformin (0.5-2mM) for 24hrs. The NADH staining solution consisted of 6mg NADH, 38mM $CoCl_2$, and 1.2mg Nitrotetrazolium blue in 3ml Tris-buffer (50mM, pH.7.6). The cell coverslips were washed with Tris-buffer for 5 minutes and incubated with this NADH solution for 2hours at 37^{o}C., and then visualised for cytoplasmic staining and photographed under a light microscope at 40X magnification. Magnitude of metformin impact on staining was subsequently assessed (in 3 independent experiments) as a weak (+), moderate (++), high (+++) or very high reduction in the staining signal (++++).

2.6.2 Cytochrome c oxidase enzyme cytochemistry

Activity of cytochrome oxidase (COX, complex IV) was evaluated using a technique that centres on the ability of this enzyme in living cells to transfer electrons to cytochrome c from an electron donor substrate such as DAB, generating a brown formazan pigment marking the site of enzyme activity. Cells from the model panel were seeded at 100,000 cells per coverslip and grown on TESPA-coated coverslips in both their respective basal experimental medium and in the presence of the NADH dehydrogenase inhibitor (metformin; 0.5-2mM) for 24hrs. Briefly, coverslips were washed with PBS and incubated in pre-incubation media consisting of 50mM Tris-HCl (pH.7.6), 10g sucrose and 28mg cobalt chloride for 15 minutes at 25^{o}C. Coverslips were then washed with 0.1M sodium phosphate buffer (pH.7.6) and incubated with COX activity-detecting solution for 3.30 hours at 37^{o}C. This was composed of 10mg cytochrome c (Sigma-

aldrich), 10mg DAB (Sigma-aldrich) and 2mg catalase (Sigma-aldrich) in 10ml sodium phosphate buffer. Coverslips were counterstained with methyl green and then visualised for cytoplasmic staining and photographed under a light microscope at 40X magnification. Magnitude of metformin impact on staining was again assessed (in 3 independent experiments) as a weak (+), moderate (++), high (+++) or very high reduction in the staining signal (++++).

2.7 SDS-PAGE and Western Blotting

Immunoblotting with chemiluminescence detection was used to monitor several signalling elements in cell lysates from each model in the presence and absence of metformin treatment. AMPK phosphorylation (Thr172), ACC phosphorylation (Ser79), and phosphorylation of mTORC1 (Ser2448) and Ribosomal Protein S6 Kinase (P70S6K, Thr389) were all examined by Western blotting. In addition, Western blotting was used to monitor expression profile of the zinc transporter SLC39A7 across the panel at log phase. To achieve this, the proteins in the cell lysates were first separated via SDS-polyacrylamide gel electrophoresis and immobilized onto a nitrocellulose membrane:

2.7.1. Cell lysis for protein extraction

Cells were seeded in 35mm diameter dishes (500,000 cells/dish) where they allowed to grow for 72hrs prior to ± metformin treatment (0.5-2mM) for 2, 12 and 24 hrs in their respective experimental media before cell lysis. Further cells were grown to day 7 in the experimental media for SLC39A7 profiling. Three independent experiments were performed in all instances. The media was removed and cells were washed with ice cold PBS (twice) prior to lysis buffer addition (pH 7.6, 50mM trizma base, 150mM NaCl, 5mM EGTA, 1% Triton-X-100, Sigma-Aldrich, UK) containing protease inhibitors (Sigma-Aldrich, UK). Cells were scraped from the dishes, collected into an Eppendorf for each model, and placed on ice for 5 minutes. Cell lysates then were centrifuged at 12,000rpm for 15 minutes at 4°C. Subsequently, the supernatant from cells (containing protein) was used for further analysis.

2.7.2 Protein quantitation

The BioRad protein assay (Bradford et al. 1976) was used to determine concentration of solubilized protein in the lysates via addition of acidic dye to protein solution and measurement at 595nm with a spectrophotometer.

Six dilutions of a protein standard (BSA, Sigma-Aldrich, UK) were prepared (0, 5, 10, 15, 20 and 25 µl/ml). Test samples were then prepared (in duplicate) at 1:200 dilution for each lysate. To

both the protein standards and lysate samples, 200 µl BioRad dye (BioRad, UK) was added and incubated for 5 minutes before measure the absorbance at 595nm. Protein standards were measured and a standard curve was created which was used to estimate protein concentration of the lysate samples.

2.7.3 Sodium dodecyl sulphate polyacrylamide gel electrophoresis (SDS-PAGE)

An appropriate amount (for 40ug protein) of each lysate was mixed with Laemmli sample loading buffer (BioRad, UK, Laemmli et al. 1970) and 24mg/ml DTT followed by protein denaturing at 90°C for 5 minutes. DTT addition denatures tertiary structure of the proteins by breaking disulphide bridges in the protein structure.

SDS-polyacrylamide gels were prepared using gel stacking apparatus (Mini Protean 3, BioRad, UK). A 1.5mm glass plate was used to cast a resolving polyacrylamide gel (8%) using reagents as detailed in Table 3. A 5% stacking gel (Table 2.3) was then poured on top of the resolving gel and a 15 wells comb was inserted. After setting, the gel was transferred to an electrophoresis running tank (BioRad, UK) containing running buffer (comprising 192mM glycine, 25mM Tris, 0.1% w/v SDS, Sima-Aldrich, UK). An equal amount of sample protein (40 µg) and Precision Plus Protein All Blue marker (BioRad) were then loaded for each model and treatment into the wells of the SDS-PAGE gel. A voltage of 120V was applied for 90 minutes to separate the proteins by electrophoresis.

Reagents	Resolving gel (8%)	Stacking gel (5%)
d.H2O	7 ml	2.28 ml
Tris-HCl	3.75 ml, pH 8.8	937 µl, pH 6.8
30% acrylamide	4 ml	480 µl
10% SDS	150 µl	37.5 µl
10% APS	75 µl	18.7 µl
TEMED	15 µl	5 µl

Table 2.3. SDS polyacrylamide gel constituents for resolving and stacking gels. All reagents used in the gels were sourced from Sigma-Aldrich, UK.

Separated proteins on the gel were then transferred to a nitrocellulose membrane (GE Healthcare, UK) in the presence of transfer buffer (0.25M TRIS base, 1.92M Glycine (Sigma-Aldrich, UK), and 20 % methanol (Fisher Scientific, UK)) by applying a voltage of 120V for 60 minutes. The membrane was stained with Ponceau-S (Sigma-Aldrich, UK) to visualize the proteins and thus ensure adequate transfer efficiency before Western blotting. The membrane was then blocked with 5% non-fat milk (Marvel, Premier International Foods, UK) prepared in TBS Tween-20 (0.05%) (TBST) for 1 hour at room temperature. The membrane was then washed with TBST three times (each time for 10 minutes) prior to incubation with primary antibody (Table 4) at 4°C overnight (on a roller bed) with a further 1 hour incubation at room temperature the following morning. The membrane was then washed with TBST (three times) and incubated with an appropriate Horseradish peroxidise (HRP)-conjugated secondary antibody (Table 2.4) for 1 hour at room temperature. Membranes were then washed with TBST prior to chemiliminescent detection.

Antibody	Dilution	MW (KDa)	Source of purchase
Phospho-AMPKα (Thr172)	1:1000	62	Cell Signalling, US
Phospho-Acetyl-CoA Carboxylase (Ser79)	1:1000	280	Cell Signalling, US
Phospho-mTOR (Ser2448)	1:1000	289	Cell Signalling, US
Phospho-p70 S6 Kinase (Thr389)	1:1000	70	Cell Signalling, US
Total SLC39A7	1:2000	50	In house
β-actin	1:100,000	45	Cell Signalling, US
Anti-rabbit IgG, HRP-linked Antibody	1:5000		Cell Signalling, US

Table 2.4. List of primary antibodies used for Western blotting analysis with their corresponding dilution, molecular weight (MW) (kDa) and source of purchase.

2.7.4 Chemiluminescence detection

To visualize proteins after immunoblotting, a chemiluminescence detection system was applied. The HRP enzyme in the HRP-conjugated antibody catalyses a reaction where the chemiluminescence substrate (containing luminol) produces a light signal which is detectable with a charge-coupled device (CCD) imager such as the ChemiDoc™ XRS+ system (BioRad, UK). This system enables blot exposure for imaging for an optimal time (5 seconds to 5 minutes) since the system is able to determine when signals are overexposed. For signal visualization and automated image analysis, each blot was first photographed using ChemiDoc™ automated image capture and the associated Image Lab™ software was used to perform volume of the protein signals on the blot. All protein activity/expression were subsequently normalised to the loading protein control (β-actin). Data were used to calculate mean volume score from three independent Western blotting experiments and were presented as % of the relevant control for each model (+/- SEM).

2.7.5 Stripping and reprobing membranes

For some of the signalling elements examined, membranes were re-probed with a further primary antibody to detect other proteins in the same lysate. To achieve this, membranes were soaked in Restore™ Plus Western Blot Stripping Buffer (Fisher, UK) for 15 minutes at room temperature to remove any bound primary and secondary antibodies. The blot was then washed with TBST (three times) prior to blocking (with 5% non-fat milk for an hour) and re-probing with a further primary antibody.

2.8 Oxygen consumption/glycolysis dual assay

A Cayman's oxygen consumption/glycolysis dual kit (Cayman, US) assay was used to measure both cellular oxygen consumption (OC) and glycolysis (extracellular acidification; ECA) in live cells representing the model panel.

A phosphorescent oxygen probe, MitoXpress®-Xtra, was used to analyse oxygen consumption in the breast cancer cell lines as an indication of oxidative phosphorylation. This probe is a porphryin based water soluble (cell impermeable) which is quenched by oxygen, and thus the phosphorescent signal measured is inversely proportional to the extracellular oxygen level. Cell respiration depletes oxygen in the media (extracellular environment) which is seen as an increase in phosphorescent signal. The assay is non-chemical and reversible and gas exchange with the surrounding environment is avoided by addition of mineral oil. Therefore, the phosphorescent signal is proportional to the intracellular oxygen consumption during oxidative

phosphorylation. The probe is excitable between 360-400nM and emits at 360-680nM. A BMG LABTECH CLARIOstar plate reader (BMG LABTECH, UK) was adjusted to 380nM (maximum excitation peak)/ 650nM (maximum emission peak) to optimally detect the phosphorescent signal.

The extracellular lactate level is proportionally correlated with intracellular glycolysis, and the lactate released from cells into their cell culture media can be measured by addition of lactate dehydrogenase which converts the extracellular lactate to pyruvate. In this reaction, the formed NADH reduces a tetrazolium substrate to give a highly coloured formazan which can be detected (absorbed) at 490-520nM.

For these assays, cells for each model were seeded at 80,000 cells/ well in their respective basal experimental medium for 24hrs prior to addition of the inhibitors 2-deoxy glucose (glycolysis inhibitor 0.5mM-5mM), metformin (complex I inhibitor 0.5-2mM) and antimycin A (complex III inhibitor 5nM and 10 nM). OC and ECA was measured 24hrs after administration of inhibitors, as well as under untreated conditions to evaluate basal oxygen consumption and glycolysis respectively. Three independent experiments were performed for all measurements to calculate mean OC and ECA, and data were then presented as % of respective control (+/-SEM).

2.9 Analysis of genes of interest in publically-available clinical breast cancer transcriptome datasets using KMplotter

Clinical datasets from antihormone relapse material are not publically available to examine clinical prevalence of genes of interest in acquired resistance. However, it is possible to use publically-available transcriptome datasets to explore relation between the intrinsic expression of a gene at diagnosis and subsequent outcome in ER+ breast cancer patients. To achieve this, the online tool KMplotter can be used. This tool is furthermore able to interrogate the publically available Affymetrix microarray gene expression datasets (www.kmplot.com) to determine associations of the gene of interest with endocrine outcome in such breast cancer patients. The datasets interrogated in this thesis include mRNA expression data from ER+ breast cancer patients prior to subsequent tamoxifen treatment to analyse relation to relapse free survival (RFS). Kaplan Meier Survival plots are generated by the tool that splits patients into two groups according to expression level of the particular gene (i.e. higher or lower expression; with the software optimising this cutpoint). This gauges how gene expression links to clinical outcome in the breast cancer patients (Györffy et al., 2010). For the Kaplan-Meier survival analysis in this thesis, the optimal Jetset gene probe was used (Li et al. 2011). Hazard ratio (HR) and log rank value (p<0.05) for each analysis was automatically calculated using the tool. Such gene

expression analysis was performed in two subsets of breast cancer patients: ER+ (unselected ER+ patient cohort, comprising 1802 patients, for 16.5 years followup) and ER+ tamoxifen treated comprising 712 patients, with 20 years followup to gauge any adverse relation to shortened response duration in patients with increased gene expression.

2.10 Statistical analysis

Graph pad prism 5 was used for the statistical analysis of data. One-way analysis of variance tests (ANOVA) with posthoc test was used for multiple comparisons (to compare the means of more than two groups of data). Significance was determined as $p \leq 0.05$. Error bars were expressed as mean ± SEM.

CHAPTER 3

Microarray gene expression profiling of endocrine resistant breast cancer cells

3.1 Introduction

Gene microarray analysis monitors transcriptional activity of genes and for the human can track 20,000-25,000 protein coding genes (International Human Genome Sequencing Consortium, Lander et al. 2001). Gene expression profiling via gene microarray studies has revealed breast cancer is a complex disease with multiple subtypes. This approach was first described for molecular taxonomy of breast cancer by Sorlie et al. (2001), classifying the disease into 4 subtypes, with more recent expression studies further expanding on subtype number. Since that time, gene microarrays have been widely used for discovery of reliable prognostic biomarker signatures that can assist stratification of breast cancer patients who may or may not require more stringent adjuvant treatment. Clinical microarray-based gene expression profiling signatures, such as MammaPrint® (70 genes signature), have been developed (van de Vijver et al 2002) to estimate risk of recurrence in early stage breast cancer patients. Mammaprint and also PCR-based expression signatures such as the 21-gene Oncotype DX test (Sparano et al. 2015) can help to determine whether a patient is at high risk of recurrence necessitating chemotherapy alongside adjuvant endocrine treatment.

Efficacy of individual breast cancer biomarkers in predicting ER+ response or failure with treatment has been limited. At the mRNA level, it has become clear that use of large scale gene expression profiling to discover predictive multi-gene signatures may perform better than single biomarker discovery (Hartwell et al. 2006). Multiple-gene signature analysis and network interaction studies were postulated by several researchers to have potential to predict clinical outcome in breast cancer patients (van de Vijver et al. 2002 and Pawitan et al. 2005). In this regard, there is some evidence for potential of such microarray analysis in the context of predicting response to endocrine treatment. For example, Jansen et al (2005) used gene expression profiling (81 discriminatory genes) to categorise oestrogen receptor positive (ER+) breast cancer tumours based on sensitivity/resistance to tamoxifen treatment. A similar approach has been applied by Miller et al. (2007) to determine a gene signature (143 genes) of response to Letrozole treatment. Both studies revealed involvement of deregulated genes in diverse molecular pathways in response to endocrine treatments.

Gene signatures derived from large scale genomic analysis can thus be used to stratify breast cancer subtypes and prognosis and are of emerging value in predicting adjuvant treatment outcome. However, the majority of them are not based around genes within specific biological pathways whose molecular function might feasibly contribute to acquisition of endocrine resistance and relapse. One important factor contributory towards this limitation is that pathways ultimately relevant following acquisition of resistance at relapse may not be adequately represented in samples prior to treatment. Such predictive signatures therefore have not generally yielded targets in the context of endocrine resistance.

To achieve such target discovery, high-throughput gene analysis must first determine differential expression between appropriate biological sample sets (such as from patients during treatment through to relapse, or from cell models reflecting endocrine response versus acquired resistance). Robust computational and statistical analysis of over-represented genes is then required to cluster genes based on biological association with cellular pathways and subcellular compartments. Many annotation analysis tools for exploring genes in cancer research have been launched (such as InnateDB, DAVID bioinformatics and GO). InnateDB uses gene ontology (GO) terms for ontological analysis and is supplemented with multiple cellular pathway databases (such as KEGG, REACTOME, BIOCARTA and NETPATH) for pathway analysis. This database is suitable for large gene expression analysis to determine associated interaction networks (with more than 98,760 interaction databases) and pathways (from 2500 pathways) within the list of uploaded genes. The over-representation tool associated using this database is able to identify particular pathway or ontology terms that are enriched in uploaded data sets and is strengthened by a hypergeometrical distribution test (with Benjamini and Hochberg post hoc correction) for the false discovery rate. Additionally, the Database for Annotation, Visualization and Integrated discovery (DAVID) bioinformatics tool includes a biological analysis tool to condense gene data sets (no more than 400 genes) into functional clusters (Jiao et al. 2012).

This Chapter aimed to use GeneChip® gene 1.0ST microarrays to discover deregulated gene expression and perform such pathway analysis using a panel of acquired endocrine resistant models as compared to their ER+/HER2-, endocrine responsive parental line MCF7. The model panel not only reflects acquired resistance to multiple types of antihormones but also shorter and longer-term (~3 yr) endocrine treatment in vitro. This potentially allows discrimination of key pathways that are deregulated and may drive acquired resistance irrespective of treatment duration or type. Such study could potentially provide novel targets amenable to diverse endocrine resistant states. In this project an initial basic growth characterisation of the models

was performed to evaluate resistance to the respective endocrine treatment along with establishing key gene profiles (ER, HER2 and an oestrogen/ER-regulated gene TFF1 (pS2)) and verifying these by RT-PCR to ensure adequate microarray performance for subsequent exploratory profiling. Subsequently, microarray analysis was performed in independent experiments and the expression of either significantly induced genes (≥1.2 fold changes) or reduced genes (≥1.2 fold changes) was assessed. The fold change 1.2 was chosen to allow enough genes for entry into the pathway analysis. Over-represented ontologies, over-represented pathways and functional classification of deregulated genes in the endocrine resistant models were obtained using InnateDB database and DAVID bioinformatics respectively, allowing pathway prioritisation for further study in the thesis.

3.2 Results

3.2.1 Basic characterisation of endocrine resistant cell lines

3.2.1.1 Growth analysis of endocrine resistant cells

For growth curve analysis, cells were seeded at 20,000 cells/well, maintaining the respective antihormone for each resistant line. Cell number for each model was then determined after day 3, 5 and 7 via Coulter counting. A line graph was drawn (Fig.3.1A) and statistical analysis (ANOVA with Dunnett *post hoc* correction) ($p \leq 0.05$) was then carried out to compare growth of resistant models vs. MCF7 (Fig 3.1B) at day 7. All models grew well despite the presence of antihormone over the 7 day period, compared with growth of the MCF7 in the basal media. Analysis revealed modest (2.28-3.79 fold changes) increases in TamR, FasR and MCF7(X) versus MCF7 (Fig 3.1B). The growth was further significantly induced in TamRLT ($p<0.0001$), FasRLT ($p<0.001$) and MCF7(X) LT ($p<0.001$), cells (all longer-term endocrine resistant models), by 7.85, 5.81 and 5 fold changes respectively, as compared to MCF7 (Table 3.1). Thus, acquired resistant cells were clearly capable of growing in presence of AHs, with the highest growth rate in long-term resistant cells.

A

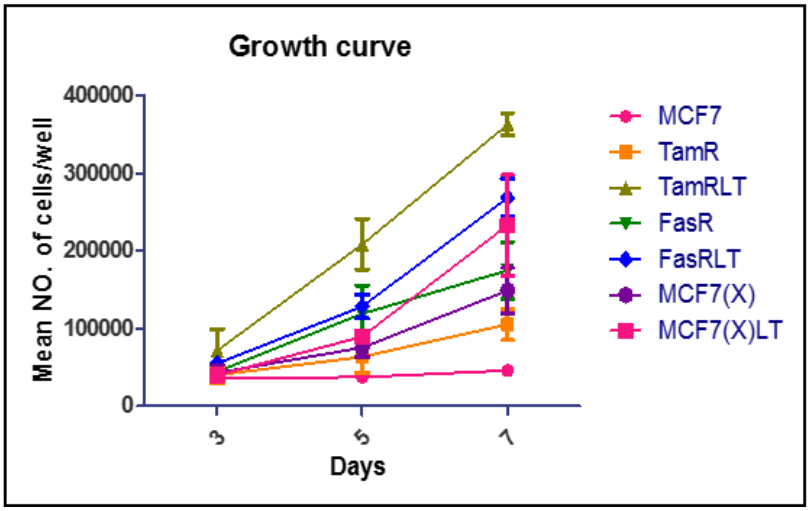

B

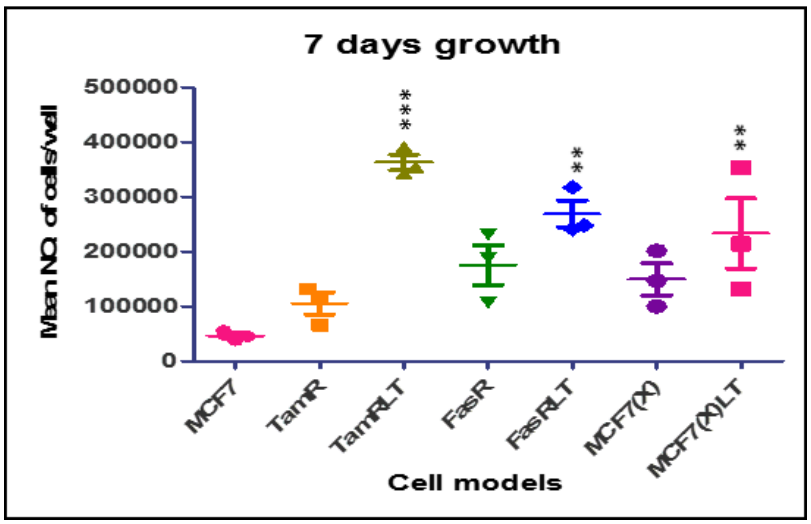

Fig 3.1. (A) Growth curve represents mean number of cells for endocrine resistant models in comparison with MCF7 up to 7 days for three independent experiments ± SEM (B) Growth of endocrine resistant models vs. MCF7 compared at day 7. Statistical analysis (ANOVA with *Dunnett post hoc* correction) was done using GraphPad Prism 5 (** p<0.01, *** p<0.001).

Fold change	TamR	TamRLT	FasR	FasRLT	MCF7(X)	MCF7(X)LT
MCF7	2.28	7.85	3.79	5.81	3.23	5.04

Table 3.1. Fold changes for growth of endocrine resistant models vs. MCF7 at day 7

3.2.1.2 Proliferative capacity of endocrine resistant cells

Ki-67 immunohistochemical analysis using MIB1 antibody, a routinely used biomarker to evaluate tumour proliferative activity in clinical samples (Yerushalmi et al. 2010), was performed in the model panel at 7 days to compare resistant lines versus baseline (stripped serum) MCF7 control (Fig 3.2). Percentage of positively stained nuclei for Ki-67 expression was calculated over n=3 fields for each model in three independent experiments (Table 3.2). Proliferation was high in the MCF7 under baseline conditions and in all the resistant lines, with Ki67 staining seen irrespective of type of antihormone treatment (Fig 3.2). Ki-67 expression was significantly ($p \leq 0.05$) increased in long-term tamoxifen and fulvestrant resistant models (TamRLT and FasRLT) with over 90% positivity while only modestly increased in TamR and FasR with 80% positivity versus MCF7 cells (Fig 3.3).

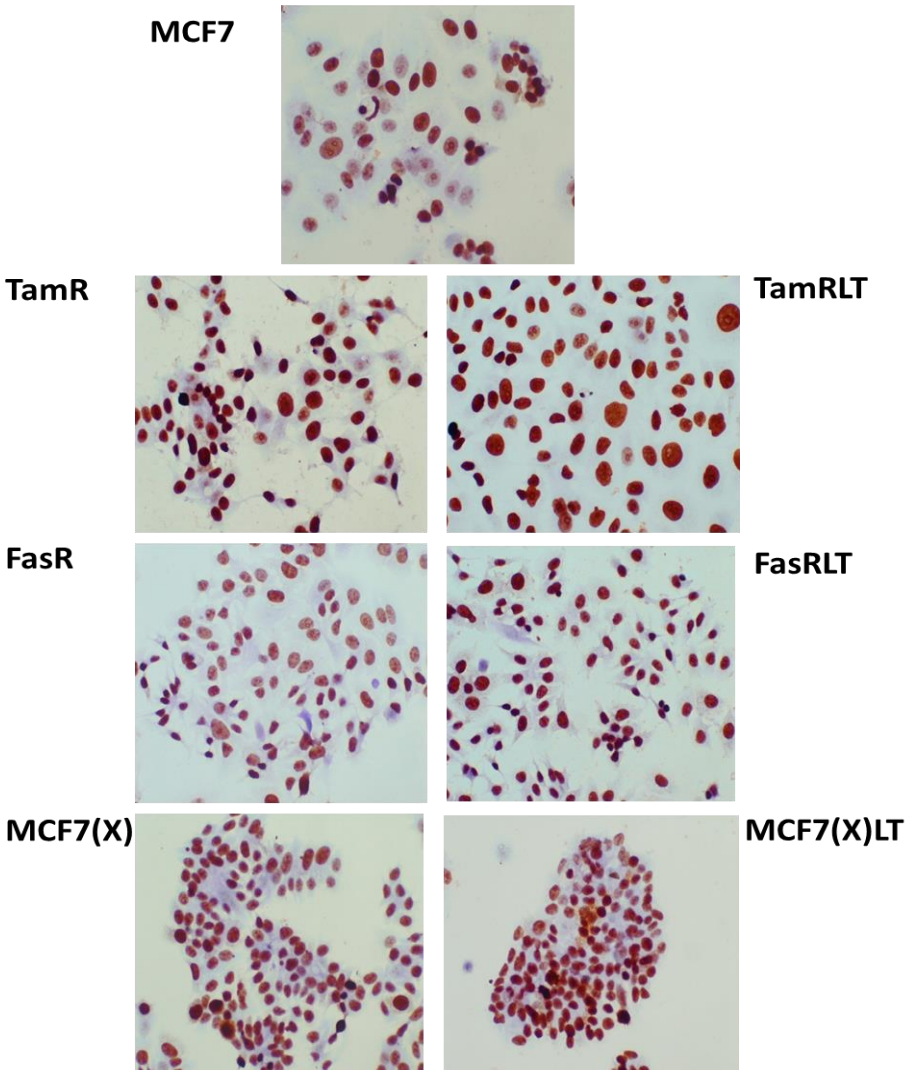

Fig 3.2. Immunocytochemistry for proliferative marker (Ki-67) expression across the model panel after 7 days growth. Original magnification was 40X.

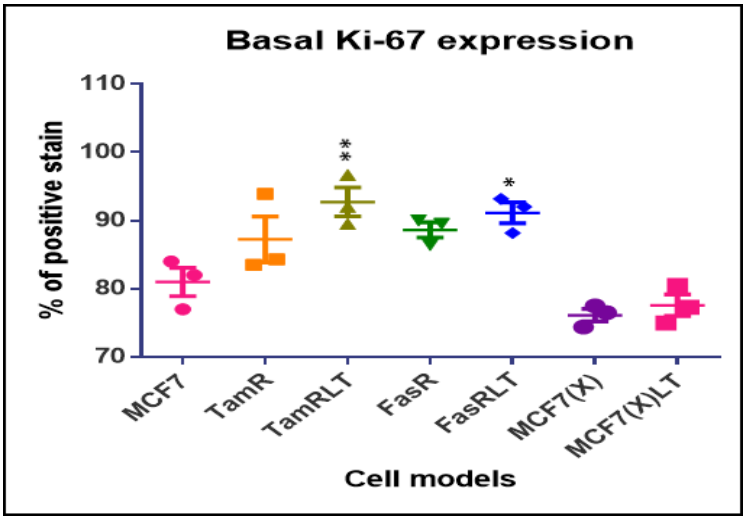

Fig 3.3. Graph represents percentage of positive Ki-67 staining in endocrine resistant models vs. MCF7 for three independent samples per cell line (N=3). Statistical analysis (ANOVA with *Dunnett post hoc* correction) was carried out (* p≤0.05, ** p≤0.01).

3.2.1.3 mRNA expression of ER, HER2 and pS2

To establish any changes in basic features of resistant models with respect to oestrogen receptor (ER) signalling and Human Epidermal Growth Factor Receptor 2 (HER2) status versus the ER+/HER2- parental MCF7 cell line in baseline media, Affymetrix 1.0ST arrays were used to determine mRNA expression of HER2 (erbB2 gene), ER (ESR1 gene) and the oestrogen-regulated gene Trefoil Factor 1 (pS2 or TFF1 gene) in the panel of MCF7 derived endocrine resistant models (three experimental replicates, Fig 3.4). The Genesifter analysis tool was used to generate heatmaps, $\log_2$ intensity plots fold changes and to perform statistical testing (one-way ANOVA with *Tukey post hoc* correction, $p \leq 0.05$ for gene expression in each resistant model versus MCF7). RT-PCR was then used to verify mRNA expression profile obtained using the microarrays for HER2, ER and pS2 in the panel of MCF7 derived endocrine resistant models. The Primer blast tool on NCBI data base was used to design forward and reverse primers for the gene of interest for the PCR studies (Chapter 2, Table 2.2). The RT-PCR results were normalized against β-actin expression as an internal control (Fig 3.5). GraphPad Prism 5 was then used to generate graphs and perform statistical tests (one-way ANOVA with *Dunnett post hoc* correction, $p \leq 0.05$) for three independent experiments (N=3) to compare expression of genes in resistant models versus MCF7 cells.

3.2.1.3.1 HER2

In keeping with reported modest expression but lack of HER2 gene amplification (HER2 negative) in the parental line (MCF7) (Soule et al. 1973), HER2 (erbB2) was moderately expressed in the parental line and across the resistant model panel (log_2 >8) (Fig 3.4). Changes in expression were small in the resistant lines, but HER2 expression was significantly reduced in TamRLT, FasR and FasRLT by more than 1.2 fold and it was induced in MCF7(X) by 1.36 fold as compared to MCF7 (control) (Fig 3.4). RT-PCR broadly verified this HER2 expression profile, again with a slight fall in expression in FASR and FASRLT and slight increase in MCF7(X), but no significant differential change was detected across the panel (Fig 3.5).

3.2.1.3.2 ER

MCF7 cells are oestrogen receptor positive (ER+) and ESR1 gene expression was detected in this model using microarray analysis (log_2 ≥8) (Fig 3.4). While ER expression was significantly reduced in TamR (2.7 fold change), it reduced prominently in TamRLT, FasR and FasRLT cells by 4.5, 5.3 and 7.8 fold changes versus control (Fig 3.4), with levels in the latter line almost at the limit of detection. Thus the greatest falls in ER were seen for acquired antioestrogen resistance. In contrast, its expression was maintained in the oestrogen deprivation resistant MCF7(X) cells and modestly induced in MCF7(X) LT by 1.3 fold changes versus MCF7 (Fig 3.4). RT-PCR broadly verified the ER expression profile across the panel (Fig 3.5). Similar to the array data, ER expression was reduced in the antioestrogen resistant lines TamRLT, FasR and FasRLT, in this instance by 1.2, 2.5 and 2.9 fold changes respectively versus control (Fig 3.5). The fall was significant in the fulvestrant resistant lines. In contrast, ER expression was retained in the oestrogen deprivation resistant models by RT-PCR.

3.2.1.3.3 pS2

pS2 (an oestrogen (E2)/ER regulated gene; TFF1 gene) was also expressed on the microarrays across the model panel (log_2 >8) (Fig 3.4). However, its expression was significantly reduced in the antioestrogen resistant models with reduced ER expression i.e. in TamR and particularly TamRLT, FasR and FasRLT by 1.8, 9.7, 5.6 and 8 fold changes respectively as compared to MCF7 (Fig 3.4). In contrast, pS2 expression was retained in both oestrogen deprivation resistant lines with a modest induction in MCF7(X) by 1.2 fold change versus control (Fig 3.4). RT-PCR again broadly verified the pS2 expression profile across the panel (Fig 3.5). Similar to the array data, pS2 expression was most reduced in TamRLT, FasR and FasRLT by 1.37, 1.39 and 2 fold changes respectively as compared to MCF7 (Fig 3.5) while being retained in the oestrogen deprivation resistant lines.

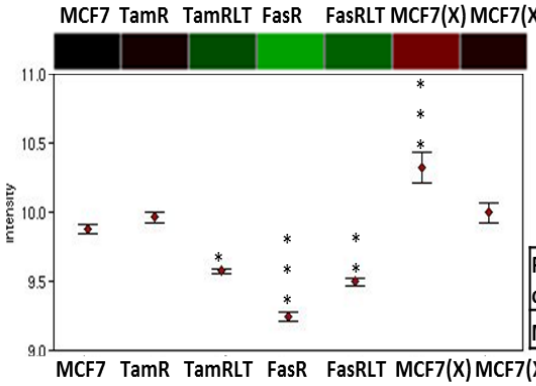

Fold change	TamR	TamRLT	FasR	FasRLT	MCF7(X)	MCF7(X)LT
MCF7	1.06	1.23	1.55	1.3	1.36	1.09

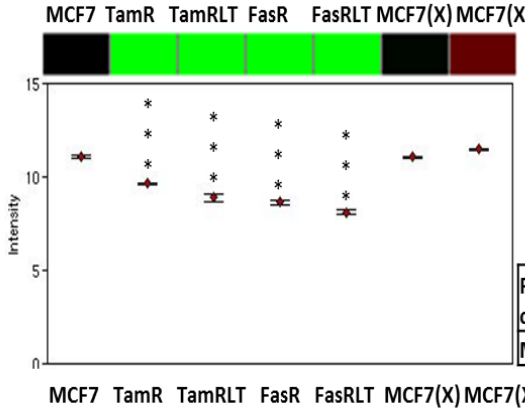

Fold change	TamR	TamRLT	FasR	FasRLT	MCF7(X)	MCF7(X)LT
MCF7	2.73	4.5	5.35	7.85	1.02	1.32

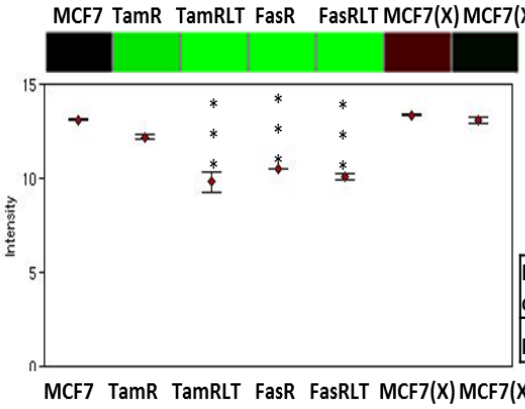

Fold change	TamR	TamRLT	FasR	FasRLT	MCF7(X)	MCF7(X)LT
MCF7	1.85	9.72	5.96	8.12	1.21	1.03

Fig 3.4. Log 2 intensity plots generated using Genesifter displaying mean (+/-SEM) of three independent microarray experiments (N=3) for HER2, ER and pS2 mRNA expression in the model panel. Statistical analysis (ANOVA with *Tukey post hoc* correction) was performed to compare gene expression in each resistant model vs. MCF7 (*p<0.05, ** p<0.01 & *** p<0.001). Heatmaps represent gene expression in resistant models vs. MCF7 (Green: reduced gene expression, Red: induced gene expression and Black: no changes in gene expression as compared to MCF7). Fold changes for gene expression in resistant models vs. MCF7 are also tabulated.

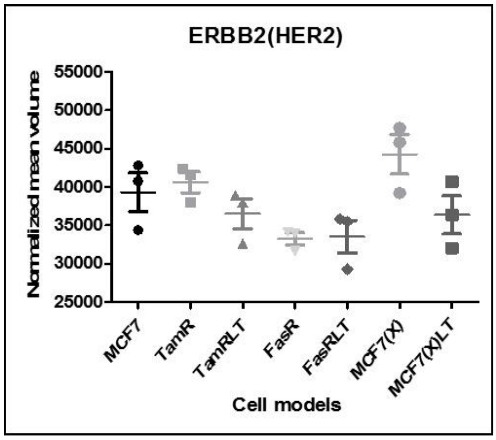

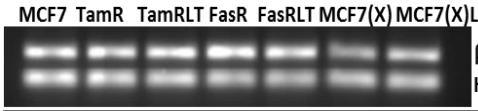

Fold change	TamR	TamRLT	FasR	FasRLT	MCF7(X)	MCF7(X)LT
MCF7	1.03	1.07	1.18	1.17	1.12	1.08

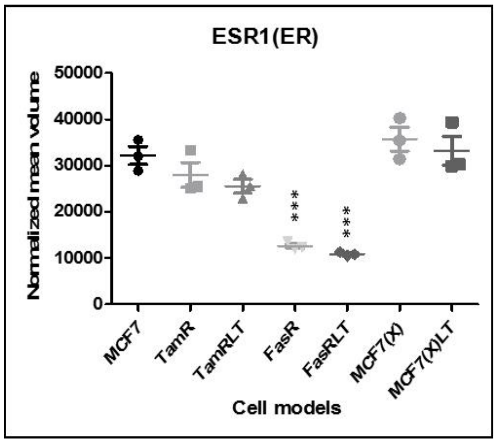

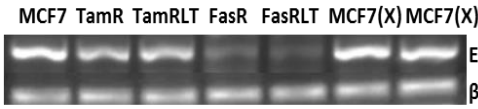

Fold change	TamR	TamRLT	FasR	FasRLT	MCF7(X)	MCF7(X)LT
MCF7	1.14	1.26	2.54	2.95	1.10	1.03

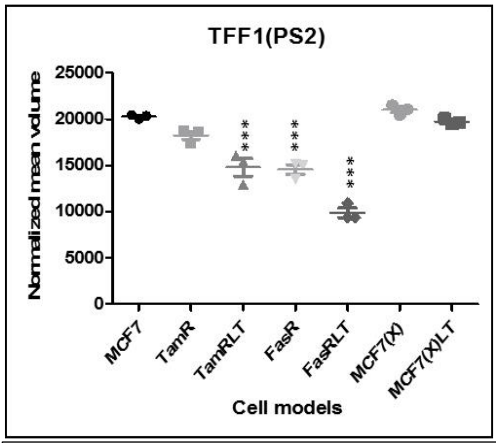

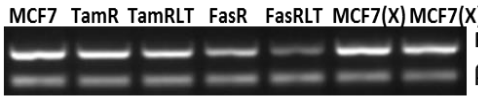

Fold change	TamR	TamRLT	FasR	FasRLT	MCF7(X)	MCF7(X)LT
MCF7	1.11	1.37	1.39	2.05	1.03	1.02

Fig 3.5. Representative gels following RT-PCR and graphs display normalized mean volume of HER2, ER and pS2 expression signals across the model panel (Mean of three independent experiments, +/- SEM for each cell line). Statistical analysis (ANOVA with Dunnett *post hoc* correction) was performed to compare gene expression in each model vs. MCF7 (*** $p<0.001$). Fold changes for gene expression in resistant models vs. MCF7 are tabulated.

3.2.2 Using the Gene 1.0ST microarrays to identify deregulated genes in the panel of endocrine resistant models

A key project goal was to determine those gene probes whose upregulation or downregulation was common to all resistant models and thus may include genes within regulatory pathways shared by multiple forms of resistance irrespective of treatment type or duration. To achieve this, the pattern navigation tool on the Genesifter web page was enabled to compare the expression patterns of gene probes in the endocrine resistant models versus the responsive MCF7 model in baseline media. Two strategies were used to initially determine deregulated gene probes across the model panel; first, determining upregulated gene probes by using a cut-point of ≥1.2 fold expression increase and second, determining downregulated gene probes again using ≥1.2 fold expression fall in each endocrine resistant model versus the responsive model. Control probes (background probes, Affymetrix array controls, intron-exon controls as well as unmapped human mRNAs) were excluded from both the upregulated and downregulated gene analysis for each model. The resultant deregulated gene probes were statistically tested (using ANOVA with *Benjamini and Hochberg post hoc* correction ($p \leq 0.05$) across the model panel). Subsequent bioinformatics analysis of the significant downregulated gene probe lists is shown in Table 3.2-3.8 (Appendix 1-6) and for upregulated gene probes in Tables 3.9-3.15 (Appendix 7-18) as detailed below.

Using this approach to discriminate significant deregulated gene probes, 6 lists for downregulated gene probes (based on type and duration of antihormone treatment, Table 3.2) and 12 lists for upregulated gene probes (comparing each resistant models versus MCF7 and also comparing type and duration of antihormone treatment versus MCF7, Table 3.9) were generated in total for the TAMR, TAMRLT, FASR, FASRLT, MCF7(X) and MCF7(X)LT models. When considering individual resistant models, the highest number of upregulated probes was seen with the fulvestrant resistant lines, particularly for the long term FASRLT model. Lists of upregulated gene probes were then compared with each other to extract those “shared” gene probes that were upregulated in the resistant models either for a particular type or according to duration of antihormone. These were subsequently used to extract gene probes shared by all types of resistant models versus control. The same strategy was used to generate a further list for all “shared” downregulated gene probes in the resistant models versus the responsive model so as to potentially enrich for common mechanisms in antihormone resistance. This resulted in N=407 downregulated gene probes and N=572 upregulated gene probes that were shared by all resistant models (Table 3.2 and 3.9; see Appendix 6 and 18 for detailed lists). It was noted that more downregulated gene probes were shared by the tamoxifen resistant (TamR and TamRLT)

or the oestrogen deprived resistant models (MCF7(X) and MCF7(X)LT) (Table 3.2). In contrast, more upregulated gene probes were shared by the fulvestrant resistant models (FasR and FasRLT) and again by the oestrogen deprived resistant models (MCF7(X) and MCF7(X)LT) (Table 3.9). It was also noted that there was a slightly larger number of down- or upregulated gene probes shared by all longer-term resistant models (TamRLT, FasRLT and MCF7(X)LT) compared with their shorter- term resistant counterparts (Tables 3.2 and 3.9).

Heatmaps for both the downregulated (Fig 3.6A-3.6D) and upregulated (Fig 3.7A-3.7F) shared gene probes across the model panel were then generated by Genesifter with corresponding gene ID to confirm shared profile. In this instance, red on the heatmap indicates upregulated expression and green shows downregulated expression of shared genes versus the parental endocrine responsive MCF7 line (black). While magnitude of expression change could clearly vary substantially according to the particular resistant model, nevertheless the heatmaps confirmed a shared downregulated or upregulated profile for the 407 and 572 probes respectively.

3.2.2.1 Ontology analysis of shared down-regulated genes in endocrine resistant models

Following brief checking of the heatmap profiles of the significantly reduced gene probes (≥1.2 fold decrease versus MCF7) (Fig 3.6A-3.6D), probe IDs for the significantly reduced genes in the endocrine resistant models were converted to ENSEMBL gene IDs via the ID conversion tool on the DAVID bioinformatics site (www.david.abcc.ncifcrf.gov) (Table 3.2). ENSEMBL gene IDs were then uploaded on to the Innatedb ontology analysis tool (www.Innatedb.com) (Breuer et al. 2013).

This mining tool is based on Gene Ontology Consortium (GO: WWW. Gneontology.org) and provides information about associations of genes and their encoded proteins with cellular component (localisation), biological process and molecular function in the cell. Ontological analysis was performed by monitoring over represented gene ontology (ORA-O) via the Innatedb hypergeometric algorithm with *Benjamini and Hochberg post hoc* correction ($p \leq 0.05$) to robustly-determine significant occurrence of more prevalent GO annotations. The final gene list utilised for this GO annotation analysis represented significant reduced genes shared between all resistant lines versus MCF7. Accordingly, ENSEMBL gene IDs for the 407 shared reduced genes (n= 559 Table 3.2) from the model panel were uploaded into the Innatedb tool t*o discover 53 significantly over represented ontology terms (Table 3.2) versus cellular component, molecular function and biological process* (Tables 3.3-3.5). *In total, 559* ENSEMBL gene IDs were detected

for 407 probe IDs using ID conversion tool on DAVID bioinformatics since there was more than one ENSEMBL gene IDs detected for some gene probe IDs. GO terms identified from ORA-O analysis associated with extracellular vesicular exosome (such as ITGB1, ITGB4, ITGB6, PLEC, DSC2 and DSG2; *p=4.89E-07)*, with the molecular function calcium ion binding (such as CDH3, CDH18, DSC2, DSG2 and PCDH9; *p=2.51E-05)* and with the biological process cell junction assembly (such as CDH3, CDH18, ITGB1, ITGB4 and PLEC; *p=0.000868)* were the most significantly enriched GO terms for reduced genes shared across the resistant model panel (Tables 3-5). Further significant GO terms including plasma membrane and desmosome for cellular components, the biological processes of cell adhesion, cell-cell junction organization and also signal transduction (including receptor complexes such as IGF1R) and negative regulation of multicellular organism growth were reduced across the resistant models versus MCF7 (Table 3.3 and 3.5). Therefore, reduction in cell adhesion and decreases in pathways negatively regulating growth contribute to the aggressive phenotypes of resistant models versus MCF7.

Tamoxifen resistant models with 1504 significantly reduced probe IDs (3465 ENSEMBL IDs) were involved in Go terms associated with protein binding and the transcription DNA-binding template in the nucleus. Fulvestrant resistant models with 462 significantly reduced probe IDs (560 ENSEMBL IDs) were related to GO terms associated with calcium ion binding, cell junction assembly and extracellular vesicular exosome. Oestrogen deprived resistant models with 1626 significantly reduced probe IDs (4820 ENSEMBL IDs) were involved in Go terms associated with protein binding, axon guidance and again extracellular vesicular exosome. Shorter-term resistant models with 592 significantly reduced probe IDs (746 ENSEMBL IDs) were related to Go terms associated with calcium ion binding, signal transduction and extracellular vesicular exosome, while longer-term resistant models with 640 significantly reduced probe IDs (3529 ENSEMBL IDs) were involved in calcium ion binding but also genes linked to homophilic cell adhesion and cell-cell adherens junction. Finally, 407 significantly shared reduced probe IDs (559 ENSEMBL IDs) were related to GO terms associated with calcium ion binding, cell junction assembly and extracellular vesicular exosome (Table 3.2 and 3.6).

3.2.2.2 Pathway analysis of shared reduced genes in endocrine resistant models

Following the gene ontology analysis, ENSEMBL gene IDs for significantly reduced genes (Appendix 6) in the endocrine resistant models were also uploaded into the Innatedb online tool to determine the biological pathways (ORA-P analysis) which were significantly over represented in the resistant models. Associations of the uploaded genes with biological pathways from KEGG databases (www.genome.jp/kegg) were determined via ORA-P and enrichment of genes in the most significant pathways was revealed via Innatedb's hypergeometric algorithm with *Benjamini*

and Hochberg post hoc correction ($p \leq 0.05$) (Table 3.7). Based on this analysis, axon guidance (including the downregulated genes EFNA4, EFNA5, EFNB2, ITGB1, NRP1, SEMA3A, SEMA3C & ROBO1) was the most significant (p =0.00199) reduced shared pathway across the model panel (Table 3.7).

Axon guidance had also proved significant on the GO analysis of biological process for shared reduced genes (Table 3.5), and appeared a particularly prominent biological process for downregulated genes in oestrogen deprivation resistant cells (Table 3.6). A summary of the ORA-P pathways obtained for reduced genes based on type/duration of endocrine resistance is also illustrated on Table 3.8. This again indicates the most significant pathway for down regulated genes is axon guidance in all types of antihormone resistance, and is also most significant for longer-term resistant models.

Comparison Categories	Probe ID	Ensembl gene ID	ORA Ontology Terms (p<0.05)	ORA Pathways (p<0.05)
TamR & TamRLT vs. MCF7	1504	3465	18	4
FasR & FasRLT vs. MCF7	462	560	64	9
MCF7(X) & MCF7(X)LT vs. MCF7	1626	4820	63	23
TamR, FasR & MCF7(X) vs. MCF7	592	746	58	12
TamRLT, FasRLT & MCF7(X)LT vs. MCF7	640	3529	51	3
TamR, TamRLT, FasR, FasRLT, MCF7(X) & MCF7(X)LT vs. MCF7	407	559	53	9

Table 3.2. Number of significantly reduced gene probe IDs from the microarrays, corresponding ENSEMBL gene IDs after conversion in DAVID bioinformatics, ORA ontology terms and ORA pathways obtained using Innatedb for all cell model comparisons.

A

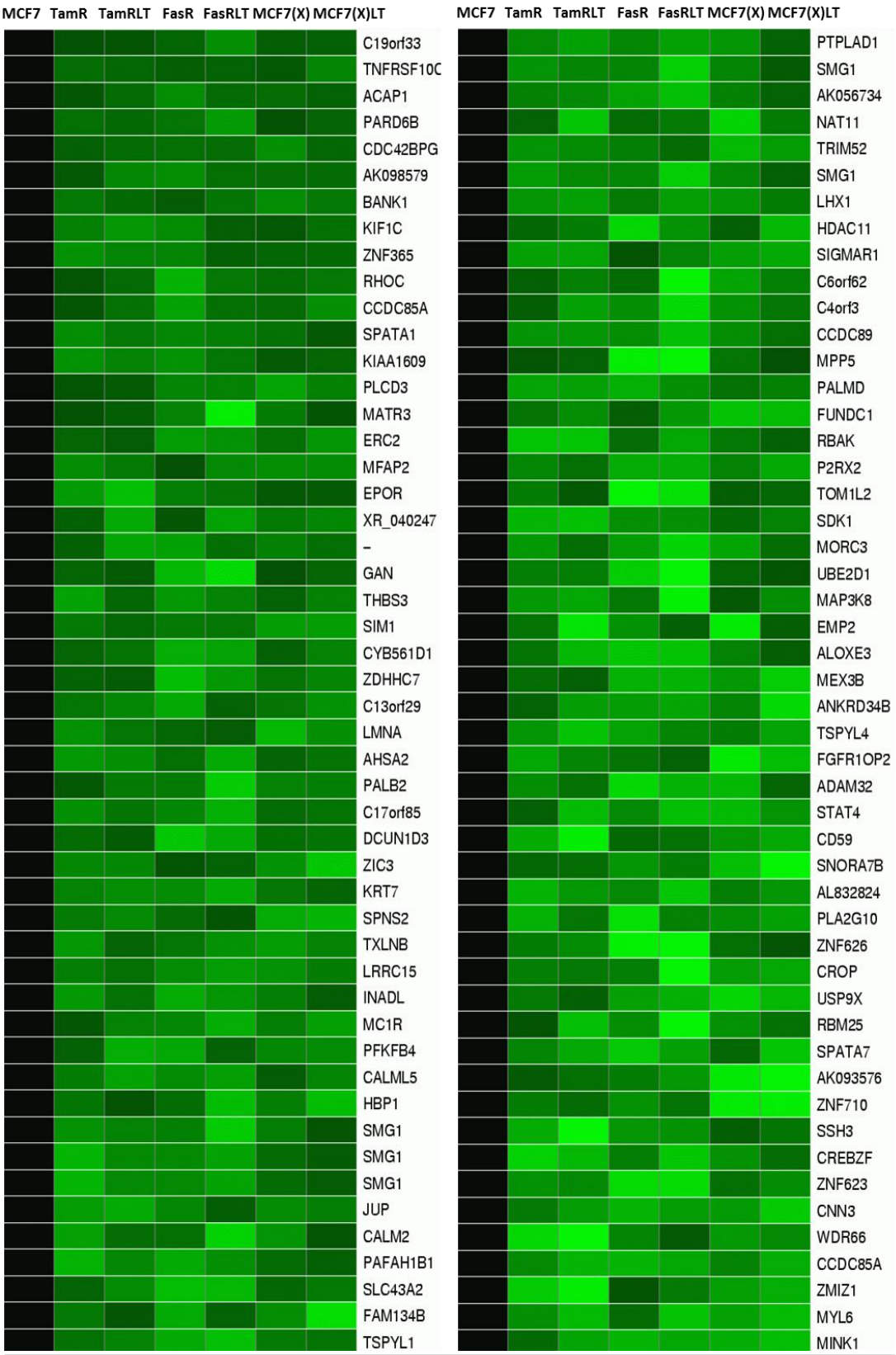

Fig 3.6. (A) Heatmap displays first 100 shared downregulated gene probes listed according to gene (≥1.2 fold changes) identified by comparing microarrays from endocrine resistant and the endocrine responsive models. Expression of these genes in the resistant models vs. MCF7 was statistically tested (ANOVA with *Benjamini and Hochberg post hoc* correction) and all were $p \leq 0.05$.

B

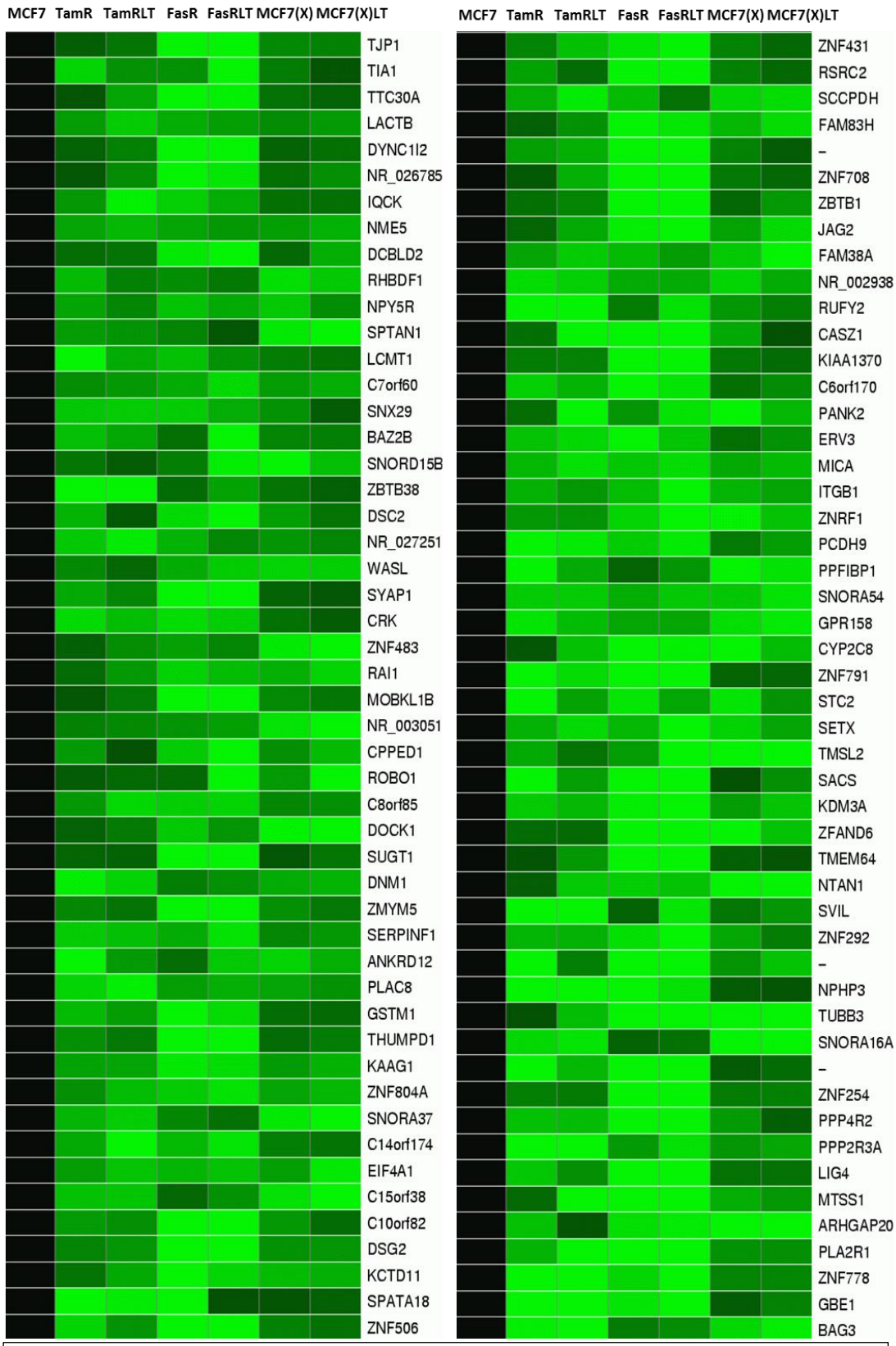

Fig 3.6. (B) Heatmap displays second 100 shared downregulated gene probes listed according to gene (≥1.2 fold changes) identified by comparing microarrays from endocrine resistant and the endocrine responsive models. Expression of these genes in the resistant models vs. MCF7 was statistically tested (ANOVA with *Benjamini and Hochberg post hoc* correction) and all were $p \leq 0.05$.

C

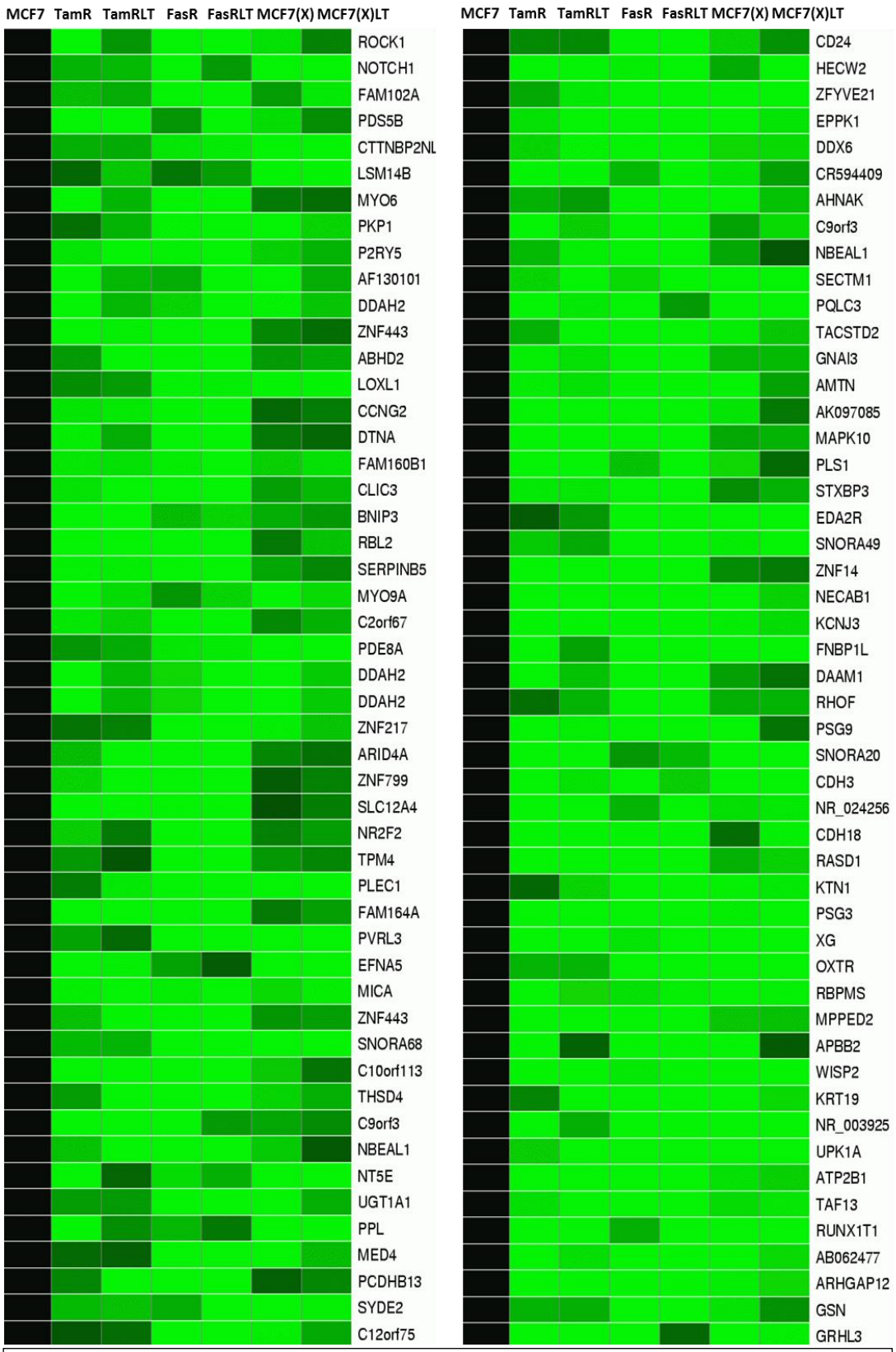

Fig 3.6. (C) Heatmap displays third 100 shared downregulated gene probes listed according to gene (≥1.2 fold changes) identified by comparing microarrays from endocrine resistant and the endocrine responsive models. Expression of these genes in the resistant models vs. MCF7 was statistically tested (ANOVA with *Benjamini and Hochberg post hoc* correction) and all were $p \leq 0.05$.

D

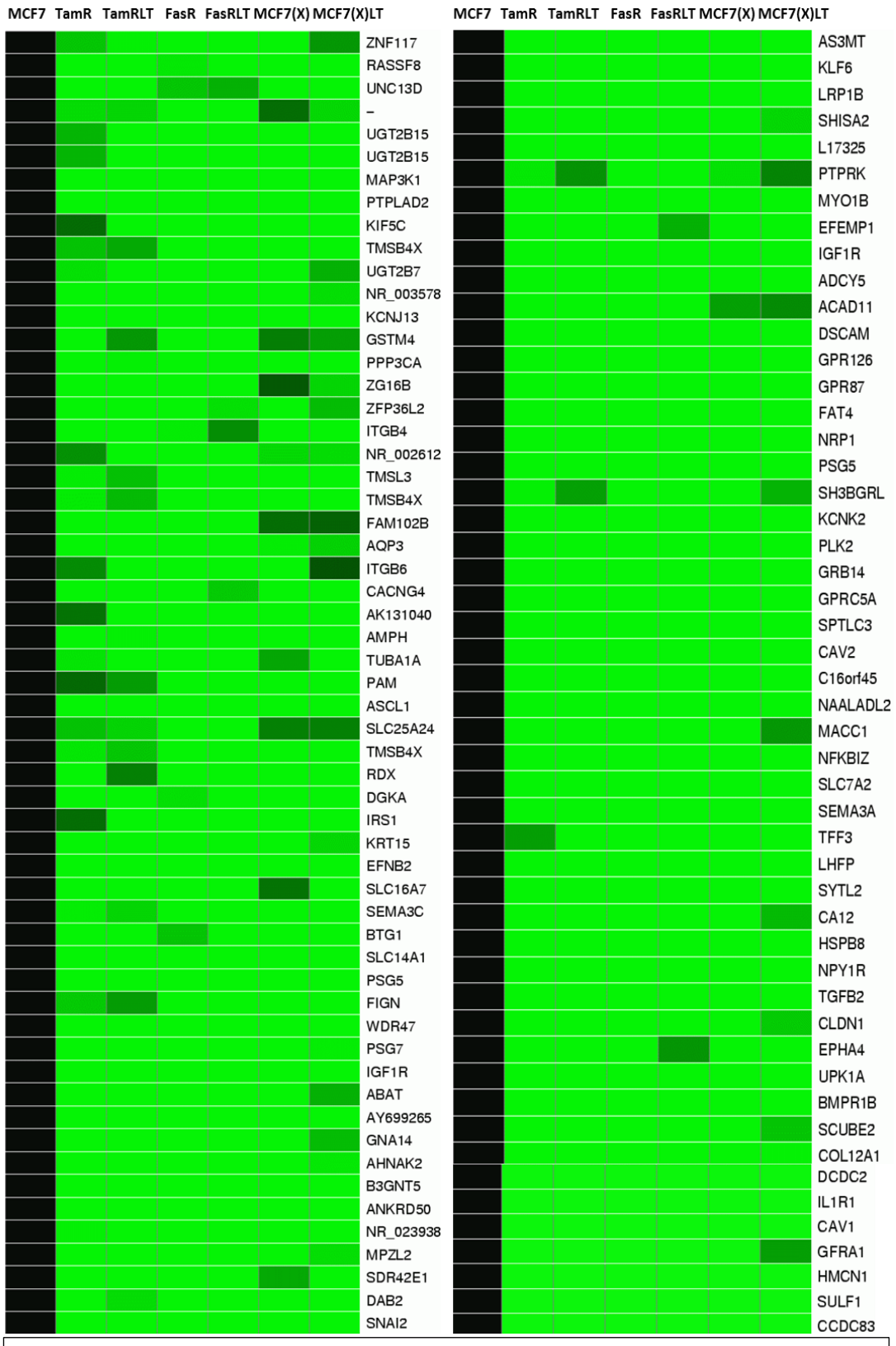

Fig 3.6. (D) Heatmap displays last 107 shared downregulated gene probes listed according to gene (≥1.2 fold changes) identified by comparing microarrays from endocrine resistant and the endocrine responsive models. Expression of these genes in the resistant models vs. MCF7 was statistically tested (ANOVA with *Benjamini and Hochberg post hoc* correction) and all were $p \leq 0.05$.

GO term name (Cellular-component)	GO term p-value (corrected)	Gene Symbols
extracellular vesicular exosome	5.31E-04	ABAT; AHNAK; ATP2B1; CALM1; CALM2; CALM3; CALML5; CD59; CLIC3; COL12A1; CPPED1; CRK; DAB2; DDAH2; DDX5; DSC2; DSG2; EFEMP1; FAT4; FNBP1L; GBE1; GDI2; GFRA1; GNAI3; GPRC5A; GSN; HDAC11; HMCN1; HNRNPK; INADL; ITGB1; ITGB4; ITGB6; JUP; KRT15; KRT19; LRRC15; MINK1; MOB1A; MPP5; MYL6; MYO1B; MYO6; NT5E; PAFAH1B1; PAM; PARD6B; PDE8A; PKP1; PLA2R1; PLEC; PLS1; PPL; RBL2; RDX; RHOC; RHOF; SDK1; SECTM1; SERPINB5; SERPINF1; SH3BGRL; SNX29; SPTAN1; STXBP3; TACSTD2; TFF3; THSD4; TOM1L2; TPM4; TUBA1A; UGT1A6; UPK1A; WASL; WISP2; ZG16B;
plasma membrane	0.001452	ADCY5; AHNAK2; AHNAK; AQP3; ATP2B1; BAG3; BMPR1B; CA12; CACNG4; CALM1; CALM2; CALM3; CAV1; CAV2; CD59; CDH18; CDH3; CLDN1; CRK; DAAM1; DAB2; DGKA; DSC2; DSCAM; DSG2; DTNA; EFNA5; EFNB2; EPHA4; FAT4; FNBP1L; GFRA1; GNA14; GNAI3; GPR126; GPR158; GPR87; GPRC5A; GRB14; HDAC11; IGF1R; IL1R1; INADL; IRS1; ITGB1; ITGB4; ITGB6; JAG2; JUP; KCNJ3; KCNK2; LIG4; LPAR6; MAPK10; MICB; MPP5; MPZL2; MYO1B; MYO6; NOTCH1; NPY1R; NPY5R; NRP1; NT5E; OXTR; P2RX2; PARD6B; PCDH9; PCDHB13; PIEZO1; PKP1; PLA2R1; PLCD3; PLEC; PPFIBP1; PPL; PVRL3; RASD1; RDX; RHOC; RHOF; ROBO1; ROCK1; SECTM1; SLC12A4; SLC14A1; SLC16A7; SLC43A2; SLC7A2; STXBP3; SULF1; SVIL; SYTL2; TACSTD2; TJP1; UPK1A; WASL; WISP2;
desmosome	0.004086	DSC2; DSG2; JUP; PKP1; PPL;
costamere	0.004119	AHNAK2; AHNAK; KRT19; PLEC; SVIL;
receptor complex	0.00426	BMPR1B; IGF1R; ITGB1; ITGB4; ITGB6; LRP1B; NOTCH1; NRP1; P2RX2; PLA2R1;
cell-cell adherens junction	0.004585	CDH3; DSC2; JUP; OXTR; PVRL3; TJP1;
sarcolemma	0.005136	AHNAK2; AHNAK; CD59; DTNA; ITGB1; KRT19; PLEC; PPP3CA;
growth cone	0.005709	APBB2; CALM3; DSCAM; ERC2; NRP1; PAFAH1B1; PCDH9; SIGMAR1; USP9X;
unconventional myosin complex	0.012201	MYL6; MYO6; MYO9A;
hemidesmosome	0.017615	ITGB1; ITGB4; PLEC;
axon	0.027683	DSCAM; DTNA; EPHA4; MINK1; MYO6; NRP1; PAFAH1B1; PTPRK; SACS; SEMA3A; SERPINF1; TGFB2;
apical part of cell	0.049247	FAT4; INADL; MYO6; PARD6B; RDX; TJP1; USP9X;

Table 3.3. Table displays significant ORA-O GO terms for the shared genes (after ENSEMBL ID conversion) that were decreased in all resistant models vs. MCF7 (≥1.2 fold changes & $p \leq 0.05$), based on cellular compartment ontologies. Significance of the Go term after Innatedb analysis (Hypergeometric algorithm with *Benjamini & Hochberg post hoc* correction) and associated gene IDs for each GO term are provided.

GO term name (Molecular-Function)	GO term p-value (corrected)	Gene Symbols
calcium ion binding	1.23E-04	CALM1; CALM2; CALM3; CALML5; CDH18; CDH3; DGKA; DSC2; DSG2; DTNA; EFEMP1; FAT4; GSN; HMCN1; JAG2; LRP1B; MEX3B; MYL6; NECAB1; NOTCH1; PCDH9; PCDHB13; PLA2G10; PLCD3; PLS1; PPP2R3A; PPP3CA; SCUBE2; SLC25A24; SPTAN1; STAT4; SULF1; THBS3; TPM4; WDR66;
N-terminal myristoylation domain binding	0.001176	CALM1; CALM2; CALM3;
protein phosphatase activator activity	0.001176	CALM1; CALM2; CALM3;
phospholipase binding	0.001689	CALM1; CALM2; CALM3; PAFAH1B1; PLA2R1;
protein binding	0.004932	ADAM32; ADCY5; AHNAK2; AHNAK; ALOXE3; AMPH; ANKRD12; ANKRD34B; ANKRD50; APBB2; ARHGAP12; ASCL1; ATP2B1; BAG3; BANK1; BAZ2B; BMPR1B; BNIP3; BTG1; C16orf45; C6orf170; CALM1; CALM2; CALM3; CAV1; CAV2; CCDC89; CD59; CDC42BPG; CLDN1; CLIC3; COL12A1; CREBZF; CRK; CTTNBP2NL; DAAM1; DAB2; DCBLD2; DDAH2; DDX5; DDX6; DNM1; DOCK1; DSC2; DSCAM; DTNA; DYNC1I2; EDA2R; EFEMP1; EFNA5; EFNB2; EPHA4; EPOR; ERC2; FAT4; FNBP1L; FUNDC1; GDI2; GNAI3; GPR158; GRB14; GRHL3; GSN; GSTM1; GSTM4; HBP1; HDAC11; HECW2; HMCN1; HNRNPK; HSPB8; IGF1R; IL1R1; INADL; IRS1; ITGB1; ITGB4; JAG2; JUP; KCNJ3; KCNK2; KDM3A; KHDRBS1; KIAA1609; KIF1C; KIF5C; KRT15; KRT19; KTN1; LCMT1; LIG4; LMNA; LOXL1; LRP1B; LRRC15; MAP3K1; MAP3K8; MAPK10; MATR3; MED4; MEX3B; MFAP2; MICB; MINK1; MOB1A; MPP5; MPZL2; MTSS1; MYL6; MYO1B; MYO6; MYO9A; NBEAL1; NFKBIZ; NOTCH1; NPHP3; NPY1R; NR2F2; NRP1; OXTR; P2RX2; PAFAH1B1; PALB2; PALMD; PAM; PARD6B; PCDH9; PDS5B; PKP1; PLAC8; PLCD3; PLEC; PLK2; PLS1; PPFIBP1; PPL; PPP2R3A; PPP3CA; PPP4R2; PSG3; PSG5; PSG8; PSG9; PTPLAD1; PTPRK; PVRL3; RAI1; RASD1; RBL2; RBM25; RBPMS; RDX; RHOC; ROBO1; ROCK1; RUNX1T1; SACS; SAMD15; SCUBE2; SDK1; SEMA3A; SEMA3C; SERPINB5; SETX; SIGMAR1; SIM1; SNAI2; SPATA18; SPTAN1; STC2; STXBP3; SUGT1; SVIL; SYDE2; SYTL2; TACSTD2; TAF13; TFF3; TGFB2; THBS3; THSD4; TIA1; TJP1; TMEM64; TMSB4X; TNFRSF10C; TOM1L2; TTC30A; TUBA1A; TXLNB; UBE2D1; UNC13D; UPK1A; USP9X; WASL; WDR47; WDR66; WISP2; ZBTB1; ZBTB38; ZFAND6; ZIC3; ZNF217; ZNF365; ZNRF1;
actin binding	0.017075	DAAM1; GSN; INF2; ITGB1; MTSS1; MYO6; MYO9A; PLEC; PLS1; RDX; SPTAN1; SSH3; SVIL; TMSB4X; TPM4; WASL;
pancreatic polypeptide receptor activity	0.03619	NPY1R; NPY5R;
poly(A) binding	0.038306	KHDRBS1; RBPMS; TIA1;
nitric-oxide synthase binding	0.04681	CALM3; CAV1; DNM1;

Table 3.4. Table displays significant ORA-O GO terms for the shared genes (after ENSEMBL ID conversion) that were decreased in all resistant models vs. MCF7 (≥1.2 fold changes & $p \leq 0.05$), based on molecular function ontologies. Significance of the Go term after Innatedb analysis (Hypergeometric algorithm with *Benjamini & Hochberg post hoc* correction) and associated gene IDs for each GO term are provided.

GO term name (Biological-Process)	GO term p-value (corrected)	Gene Symbols
cell junction assembly	5.47E-04	CDH18; CDH3; INADL; ITGB1; ITGB4; JUP; MPP5; PARD6B; PLEC; PVRL3;
cell adhesion	9.30E-04	AMTN; CDH3; CLDN1; COL12A1; DCBLD2; DSC2; DSCAM; DSG2; EFNB2; EPHA4; ITGB1; ITGB4; ITGB6; JUP; MTSS1; NRP1; PKP1; PPFIBP1; PTPRK; PVRL3; ROBO1; SDK1; THBS3; WISP2;
cellular component disassembly involved in execution phase of apoptosis	9.46E-04	DSG2; GSN; LMNA; PKP1; PLEC; ROCK1; SPTAN1; TJP1;
cell-cell junction organization	9.75E-04	CDH18; CDH3; CLDN1; INADL; JUP; MPP5; PARD6B; PVRL3; TGFB2;
positive regulation of cyclic nucleotide metabolic process	0.001176	CALM1; CALM2; CALM3;
regulation of nitric-oxide synthase activity	0.004086	CALM1; CALM2; CALM3; CAV1; WASL;
nitric oxide metabolic process	0.004119	CALM1; CALM2; CALM3; CAV1; WASL;
axon guidance	0.00453	APBB2; DOCK1; EFNA5; EFNB2; EPHA4; GFRA1; ITGB1; MYL6; NRP1; PLA2G10; RHOC; ROBO1; ROCK1; SEMA3A; SEMA3C; SPTAN1; TGFB2; WASL;
vesicle organization	0.004783	CAV1; CAV2; FNBP1L; WASL;
dichotomous subdivision of terminal units involved in salivary gland branching	0.004979	NRP1; SEMA3A; SEMA3C;
positive regulation of cyclic-nucleotide phosphodiesterase activity	0.004979	CALM1; CALM2; CALM3;
regulation of cell communication by electrical coupling involved in cardiac conduction	0.004979	CALM1; CALM2; CALM3;
homophilic cell adhesion	0.005101	CDH18; CDH3; DSC2; DSG2; FAT4; ITGB1; MPZL2; PCDH9; PCDHB13; PVRL3; ROBO1;
signal transduction	0.006222	ADCY5; ARHGAP12; ARHGAP20; CALM1; CALM2; CALM3; CALML5; CLIC3; DOCK1; DTNA; EPOR; FNBP1L; GDI2; GNA14; GNAI3; GPRC5A; GRB14; HNRNPK; IGF1R; IL1R1; IRS1; KHDRBS1; MAPK10; MTSS1; MYO9A; NR2F2; NRP1; PDE8A; PKP1; PLCD3; PLS1; PTPRK; RASD1; RASSF8; RHOC; RHOF; ROCK1; SECTM1; SIM1; STAT4; SYDE2; TNFRSF10C; TOM1L2; WISP2;
cell migration involved in sprouting angiogenesis	0.008287	EFNB2; ITGB1; NRP1; ROBO1;
regulation of Rho GTPase activity	0.008287	CRK; EFNA5; EPHA4; PAFAH1B1;
negative regulation of anoikis	0.010533	CAV1; ITGB1; NOTCH1; SNAI2;
sympathetic ganglion development	0.012201	ASCL1; NRP1; SEMA3A;
bundle of His cell to Purkinje myocyte communication	0.017615	DSC2; DSG2; JUP;
cellular response to cobalt ion	0.018144	BNIP3; SERPINF1;
vesicle transport along actin filament	0.018144	FNBP1L; WASL;
positive regulation of ryanodine-sensitive calcium-release channel activity	0.024019	CALM1; CALM2; CALM3;

Table 3.5 continue…

GO term name (Biological-Process)	GO term p-value (corrected)	Gene Symbols
cell migration	0.024113	BTG1; DOCK1; ITGB1; JUP; NRP1; PAFAH1B1; PTPRK; RHBDF1; SNAI2; TGFB2;
response to calcium ion	0.028326	AQP3; CALM1; CALM2; CALM3; CAV1; PPP3CA;
negative regulation of keratinocyte proliferation	0.029928	EFNB2; PTPRK; SNAI2;
somatic stem cell division	0.029928	NOTCH1; TGFB2; ZFP36L2;
neuron migration	0.032166	APBB2; ASCL1; DCDC2; NR2F2; NRP1; PAFAH1B1; SEMA3A; USP9X;
synaptic transmission	0.034877	ABAT; ADCY5; AMPH; CACNG4; CALM1; CALM2; CALM3; DTNA; GNAI3; KCNJ3; KCNK2; MINK1; MYO6; NPY5R; P2RX2; PAFAH1B1; PCDHB13;
auditory receptor cell fate commitment	0.03619	JAG2; NOTCH1;
cell migration involved in endocardial cushion formation	0.03619	NOTCH1; SNAI2;
gonadotrophin-releasing hormone neuronal migration to the hypothalamus	0.03619	NRP1; SEMA3A;
mitochondrial protein catabolic process	0.03619	BNIP3; SPATA18;
neural crest cell migration involved in autonomic nervous system development	0.03619	NRP1; SEMA3A;
positive regulation of clathrin-mediated endocytosis	0.03619	DAB2; WASL;
regulation of axon extension involved in axon guidance	0.03619	NRP1; SEMA3A;
negative regulation of ryanodine-sensitive calcium-release channel activity	0.037159	CALM1; CALM2; CALM3;
positive regulation of phosphoprotein phosphatase activity	0.037159	CALM1; CALM2; CALM3;
regulation of cell migration	0.038183	JAG2; LMNA; MAP3K1; MINK1; NOTCH1; PARD6B;
negative regulation of multicellular organism growth	0.038306	PLAC8; RAI1; STC2;
regulation of epithelial cell proliferation	0.038306	NOTCH1; SERPINB5; TACSTD2;
wound healing	0.040282	CDH3; DCBLD2; FGFR1OP2; GRHL3; GSN; MAP3K1; TGFB2;
negative regulation of endothelial cell proliferation	0.042872	CAV1; CAV2; NR2F2; SULF1;
regulation of cytokinesis	0.04681	CALM1; CALM2; CALM3;

Table 3.5. Table displays significant ORA-O GO terms for the shared genes (after ENSEMBL ID conversion) that were decreased in all resistant models vs. MCF7 (≥1.2 fold changes & $p \leq 0.05$), based on biological process ontologies. Significance of the Go term after Innatedb analysis (Hypergeometric algorithm with *Benjamini & Hochberg post hoc* correction) and associated gene IDs for each GO term are provided.

Categories	ORA Cellular components	P value	ORA Molecular Function	P value	ORA Biological Process	P value
TamR & TamRLT vs. MCF7	nucleus	1.56E-05	Protein binding	2.72E-06	Transcription, DNA-template	3.71E-05
FasR & FasRLT vs. MCF7	Extracellular vesicular exosome	5.31E-04	Calcium ion binding	1.23E-04	Cell junction assembly	5.47E-04
MCF7(X) & MCF7(X)LT vs. MCF7	Extracellular vesicular exosome	8.27E-14	Protein binding	2.90E-25	axon guidance	5.69E-10
TamR, FasR & MCF7(X) vs. MCF7	Extracellular vesicular exosome	5.24E-04	Calcium ion binding	5.17E-04	Signal transduction	7.57E-05
TamRLT, FasRLT & MCF7(X)LT vs. MCF7	Cell-cell adherens junction	0.007964	Calcium ion binding	2.22E-05	Homophilic cell adhesion	2.91E-04

Table 3.6. Summary of most significant ORA-O GO terms from Innatedb for reduced genes (≥1.2 fold changes & $p \leq 0.05$) based on type/duration of endocrine resistance across resistant models.

Pathway Name	Pathway p-value (corrected)	Gene Symbols
Axon guidance	0.00199	EFNA5 ; EFNB2 ; EPHA4 ; GNAI3 ; ITGB1 ; NRP1 ; PPP3CA ; ROBO1 ; ROCK1 ; SEMA3A ; SEMA3C ;
Arrhythmogenic right ventricular cardiomyopathy (ARVC)	0.00386	CACNG4 ; DSC2 ; DSG2 ; ITGB1 ; ITGB4 ; ITGB6 ; JUP ; LMNA ;
Dilated cardiomyopathy	0.01035	ADCY5 ; CACNG4 ; ITGB1 ; ITGB4 ; ITGB6 ; LMNA ; TGFB2 ; TPM4 ;
Bacterial invasion of epithelial cells	0.0107	CAV1 ; CAV2 ; CRK ; DNM1 ; DOCK1 ; ITGB1 ; WASL ;
Shigellosis	0.02527	CRK ; DOCK1 ; ITGB1 ; MAPK10 ; ROCK1 ; WASL ;
Hypertrophic cardiomyopathy (HCM)	0.02353	CACNG4 ; ITGB1 ; ITGB4 ; ITGB6 ; LMNA ; TGFB2 ; TPM4 ;
Focal adhesion	0.02226	CAV1 ; CAV2 ; CRK ; DOCK1 ; IGF1R ; ITGB1 ; ITGB4 ; ITGB6 ; MAPK10 ; ROCK1 ; THBS3 ;
Regulation of actin cytoskeleton	0.03189	CRK ; DOCK1 ; GSN ; ITGB1 ; ITGB4 ; ITGB6 ; RDX ; ROCK1 ; SSH3 ; TMSB4X ; WASL ;
Pathogenic Escherichia coli infection	0.04085	CLDN1 ; ITGB1 ; ROCK1 ; TUBA1A ; WASL ;

Table 3.7. ORP-P pathways for genes reduced in all the resistant models (≥1.2 fold changes & $p \leq 0.05$) identified as significant using Innatedb analysis. Significance of the pathway after Innatedb analysis (Hypergeometric algorithm with *Benjamini & Hochberg post hoc* correction) and associated gene IDs for each pathway are provided.

Categories	ORA pathway	P value
TamR & TamRLT vs. MCF7	Axon guidance	0.00724
FasR & FasRLT vs. MCF7	Axon guidance	0.00199
MCF7(X) & MCF7(X)LT vs. MCF7	Axon guidance	4E-08
TamR, FasR & MCF7(X) vs. MCF7	Bacterial invasion of epithelial cells	0.00296
TamRLT, FasRLT & MCF7(X)LT vs. MCF7	Axon guidance	0.00575

Table 3.8. Summary of ORA-P pathways identified as significant using Innatedb analysis for genes reduced (≥1.2 fold changes & $p \leq 0.05$) according to type/duration of endocrine resistance and shared across resistant models is represented.

3.2.2.3 Ontology analysis of shared induced genes in endocrine resistant models

ENSEMBL gene IDs for the 572 shared induced gene probes (n=636 ENSEMBLE gene IDs Table 3.9, see full list in Appendix 18) (Fig 3.7A-3.7F, Table 3.9) were uploaded on Innatedb data base t*o discover 123 significantly over represented ontology terms versus cellular component, molecular function and biological process using ORA-O analysis* (Table 3.9). According to this analysis, genes that were associated with the following cellular components were the most frequently occurring induced genes shared in all resistant models (Table 3.10):

1) Mitochondrion (*p*=1.53E-23) including genes for pyruvate metabolism (PDHA1), TCA cycle (ACO2, IDH3B, SDHB, FH and MDH2), oxidative phosphorylation (NDUFA3/8, NDUFAF2/4, NDUFB5/9/10, NDUFS3, SDHB, UQCRFS1, COX7B, PPA2 and MT-ATP6) and mitochondrial ribosomal subunits (MRPL15, MRPL17, MRPL2, MRPL21, MRPL34, MRPL37, MRPL40, MRPL47, MRPS15, MRPS18A, MRPS18B, MRPS24, MRPS34 and MRPS5).

2) Mitochondrial inner membrane (*p*=2.3E-14) including genes which were associated with regulation of mitochondrial biogenesis (STOML2; plays a role in cell proliferation and migration), oxidative phosphorylation (NDUFA3, NDUFA7, NDUFA8, NDUFA9, NDUFB10, NDUFB5, NDUFB9, NDUFS3, SDHB & UQCRFS1), pyruvate carrier (BRP44), pyrimidine transporter (SLC25A33), ADP/ATP carrier (SLC25A5) and translocase inner mitochondrial membrane (TIMM44, TIMM8A & TIMM9).

3) Mitochondrial matrix (*p*=2.7E-8) including genes in TCA cycle (ACO2 and IDH3B), β-oxidation of fatty acids (HADH), ketogenesis (HMGCS2), integrity of mitochondrial genome (LONP1), glutamate and α-ketoglutarate metabolism (GOT1 & GOT2), butrate

metabolism (ACSM3), heme biosynthesis (FECH), repair and assembly of iron-sulphur cluster (FXN) and biosynthesis of amino acids (SHMT2).

For molecular function, aminoacyl-tRNA ligase activity (such as CARS, HARS, IARS, LARS, MARS, WARS and YARS; *p*=7.2E-5) was the most frequently occurring induced genes shared in all resistant models (Table 3.11).

For biological process, small molecule metabolic process (*p*=1.8E-14) which generate low molecular weight, monomeric, non-encoded metabolites via amino acid synthesis (ACAT1, ALDH9A1, APIP, ASNS, ASS1, GOT1, GOT2, KMO and PSPH), acetyl CoA synthesis (ACSS2 and COASY), lipid biosynthesis (AGPAT6, CHPT7, EPT1 and PTDSS1), glycosamino glycan biosynthesis (B4GALT7 and EXT2), fatty acid elongation process (ELOVL1 and ELOVL4), phosphate pentose pathway (G6PD), glutathine metabolism (GSS, GSTA4, GSTO1 and MGST1), β-oxidation of fatty acids (HADH), ketogenesis (HMGCS2), nucleotide sugar/amino sugar metabolism (PFKFB2), glycolysis (PGM1), purine metabolism (PNP), proteasome (PSMA1, PSMA6, PSMB6, PSMC4, PSMD2, PSMD8, PSME1, PSME3 and PSME3), pyruvate metabolism (PDHA1), TCA cycle (ACO2, IDH1, IDH3B, SDHB, FH and MDH2) and oxidative phosphorylation (NDUFA3, NDUFA7, NDUFA8, NDUFA9, NDUFB5, NDUFB9, NDUFB10, NDUFS3, COX7B and UQCRFS1) were the most frequently occurring induced genes shared in all resistant models (Tables 3.12). Moreover, genes that were associated to cellular response to zinc ion (MT1E, MT1F, MT1G, MT1H, MT1X and MT2A; *p*=1.6E-06) for biological process were also shared in all resistant models (which is further studied in Chapter 5).

The same approach was used to compare endocrine resistant models based on type/duration of endocrine resistance for significantly induced GO terms (Table 3.13). In total, 636 ENSEMBL gene IDs were detected for 572 probe IDs using the ID conversion tool in the DAVID bioinformatics resource, since there was more than one ENSEMBL gene ID detected for some gene probe IDs. According to ENSEMBL gene IDs, more upregulated genes were shared by the fulvestrant resistant models (FasR and FasRLT) and by the oestrogen deprived resistant models (MCF7(X) and MCF7(X)LT) (Table 3.9). Also, more upregulated genes were shared by long-term resistant models (TamRLT, FasRLT and MCF7(X)LT) as compared with shorter-term resistant counterparts (Table 3.9).

Tamoxifen resistant models had 1835 significantly induced probe IDs (2419 ENSEMBL IDs) that were involved in Go terms associated with electron carrier activity, small molecule metabolic process and mitochondrion. Fulvestrant resistant models had 2897 significantly induced probe IDs (3107 ENSEMBL IDs) that were related to GO terms associated with poly (A) RNA binding,

and again small molecule metabolic process and mitochondrion. Oestrogen deprived models had 2312 significantly induced probe IDs (4430 ENSEMBL IDs) that were involved in Go terms associated with aminoacyl tRNA ligase activity, gene expression and similarly mitochondrion. The shorter-term resistant models had 877 significantly induced probe IDs (1079 ENSEMBL IDs) related to Go terms associated with aminoacyl tRNA ligase activity, and also small molecule metabolic process and mitochondrion. Long-term resistant models had957 significantly induced probe IDs (1079 ENSEMBL IDs) that were involved in aminoacyl tRNA ligase activity, gene expression and mitochondrion. Finally, there were 572 significantly shared induced probe IDs (636 ENSEMBL IDs) and these were related to GO terms associated with aminoacyl tRNA ligase activity, small molecule metabolic process and mitochondrion (Table 3.9 and 3.13).

3.2.2.4 Pathway analysis of shared induced genes in endocrine resistant models

The same list of shared induced genes (N=572) (Appendix 18) was used to analyse ORA-P pathways shared across resistant models. ENSEMBL gene IDs for the shared significantly induced genes in endocrine resistant models were uploaded into the Innatedb online tool to determine biological pathways (ORA-P) which are significantly over represented in the resistant models. (Table 3.15, Appendix 18). Of the 28 resultant significant pathways, the most significant over represented pathway for the genes induced across all the endocrine resistant models was defined as “metabolic pathways” (p=4.16E-16) (Table 3.15). This comprised 89 genes deregulated in all endocrine resistant lines which participate in particular metabolic pathways including TCA cycle, glutathione metabolism, oxidative phosphorylation (OxPhos), arginine & proline metabolism, pyruvate metabolism, one carbon pool by folate, butanoate metabolism, alanine/aspartate and glutamate metabolism, amino sugar/nucleotide sugar metabolism, valine/leucine and isoleucine metabolism, cysteine and methionine metabolism, tryptophan metabolism, phenylalanine, tyrosine & tryptophan biosynthesis, pyrimidine metabolism, terpenoid backbone biosynthesis, glycolysis/gluconeogenesis, glycine/serine and threonine metabolism and glyoxylate/decarcoxylate metabolism were also represented in the list (Table 3.15). These metabolic pathways were also implicated from the ORP-O analysis for biological process (Table 3.12).

Aminoacyl tRNA biosynthesis was the second most prominent pathway whose induction was shared by the resistant lines (*p*=3.5E-05) and this had again been implicated from molecular function analysis (Table 3.11). The same approach was used to compare endocrine resistant models based on type/duration of endocrine resistance for the most significant induced pathway (Table 3.14, Appendix 7-17), again indicating that enrichment of “metabolic pathways”

was significant and the most prominent pathway in the gene lists from the resistant models irrespective of endocrine strategy.

Categories	Probe ID	Ensembl gene ID	ORA Ontology Terms (p<0.05)	ORA Pathways (p<0.05)
TamR vs. MCF7	2212	3811	96	21
TamRLT vs. MCF7	1813	2877	24	11
FasR vs. MCF7	2719	4497	137	17
FasRLT vs. MCF7	3630	5436	137	21
MCF7(X) vs. MCF7	2620	5602	82	14
MCF7(X)LT vs. MCF7	2445	6849	90	15
TamR & TamRLT vs. MCF7	1835	2419	77	9
FasR & FasRLT vs. MCF7	2897	3107	157	67
MCF7(X) & MCF7(X)LT vs. MCF7	2312	4430	99	14
TamR, FasR & MCF7(X) vs. MCF7	877	1069	146	17
TamRLT, FasRLT & MCF7(X)LT vs. MCF7	957	1079	152	12
TamR, TamRLT, FasR, FasRLT, MCF7(X) & MCF7(X)LT vs. MCF7	572	636	123	28

Table 3.9. Number of significantly induced gene probe IDs from the microarrays, corresponding ENSEMBL gene IDs after conversion in DAVID bioinformatics, ORA ontology terms and ORA pathways obtained using Innatedb for all cell model comparisons.

A

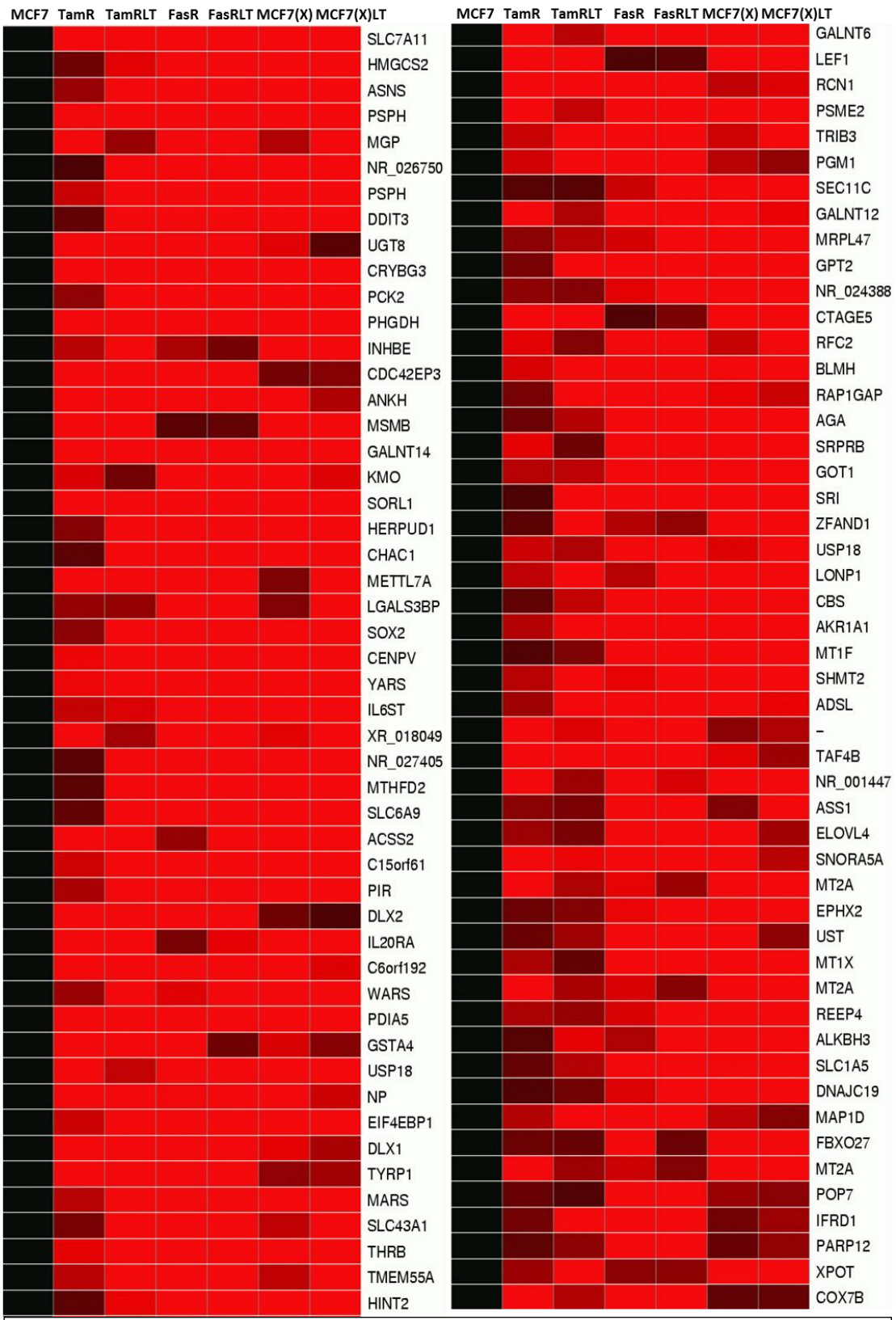

Fig 3.7. (A) Heatmap displays first 100 shared upregulated gene probes listed according to gene (≥1.2 fold changes) identified by comparing microarrays from endocrine resistant and the endocrine responsive models. Expression of these genes in the resistant models vs. MCF7 was statistically tested (ANOVA with *Benjamini and Hochberg post hoc* correction) and all were $p \leq 0.05$.

B

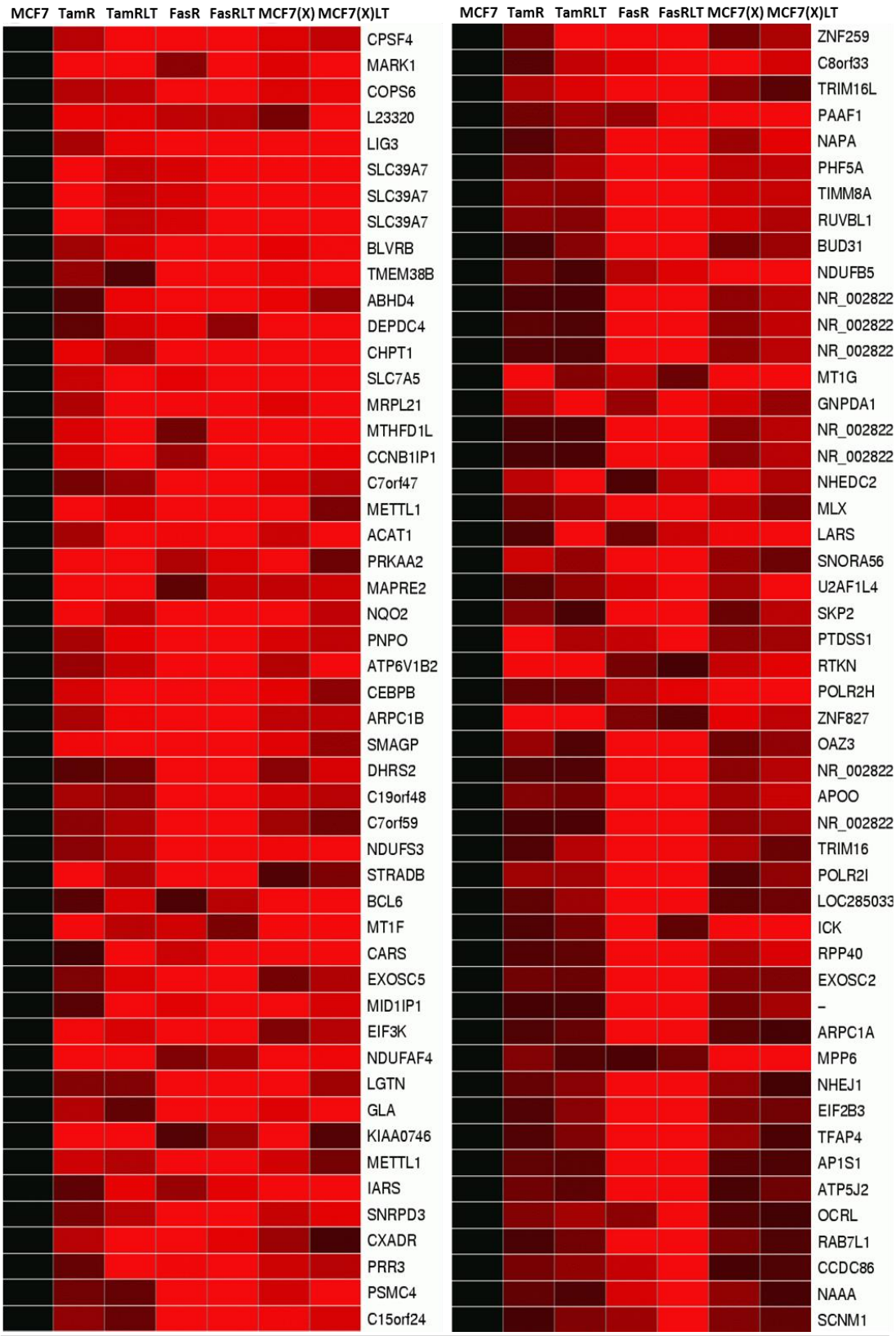

Fig 3.7. (B) Heatmap displays second 100 shared upregulated gene probes listed according to gene (≥1.2 fold changes) identified by comparing microarrays from endocrine resistant and the endocrine responsive models. Expression of these genes in the resistant models vs. MCF7 was statistically tested (ANOVA with *Benjamini and Hochberg post hoc* correction) and all were $p \leq 0.05$.

C

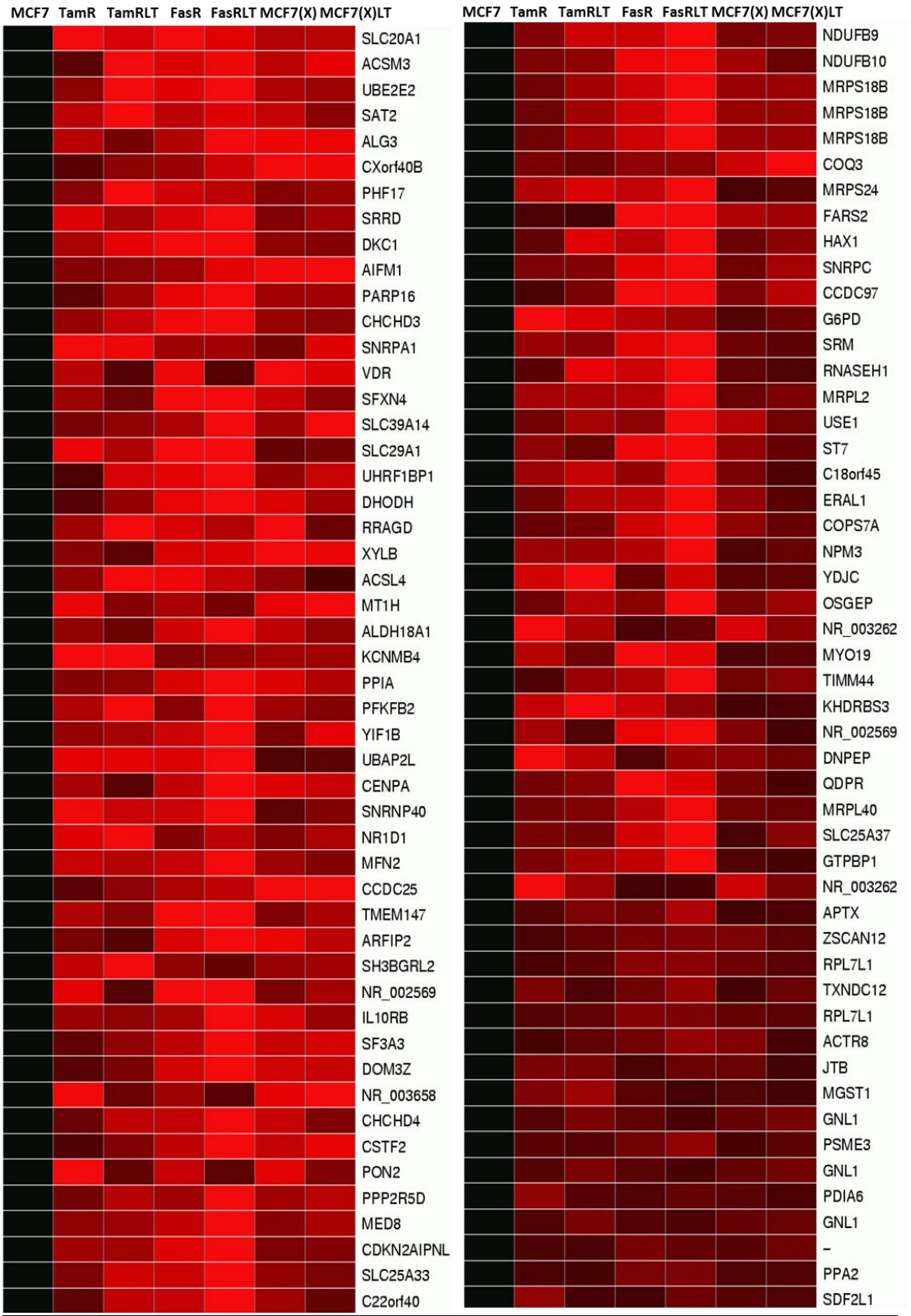

Fig 3.7. (C) Heatmap displays third 100 shared upregulated gene probes listed according to gene (≥1.2 fold changes) identified by comparing microarrays from endocrine resistant and the endocrine responsive models. Expression of these genes in the resistant models vs. MCF7 was statistically tested (ANOVA with *Benjamini and Hochberg post hoc* correction) and all were $p \leq 0.05$.

D

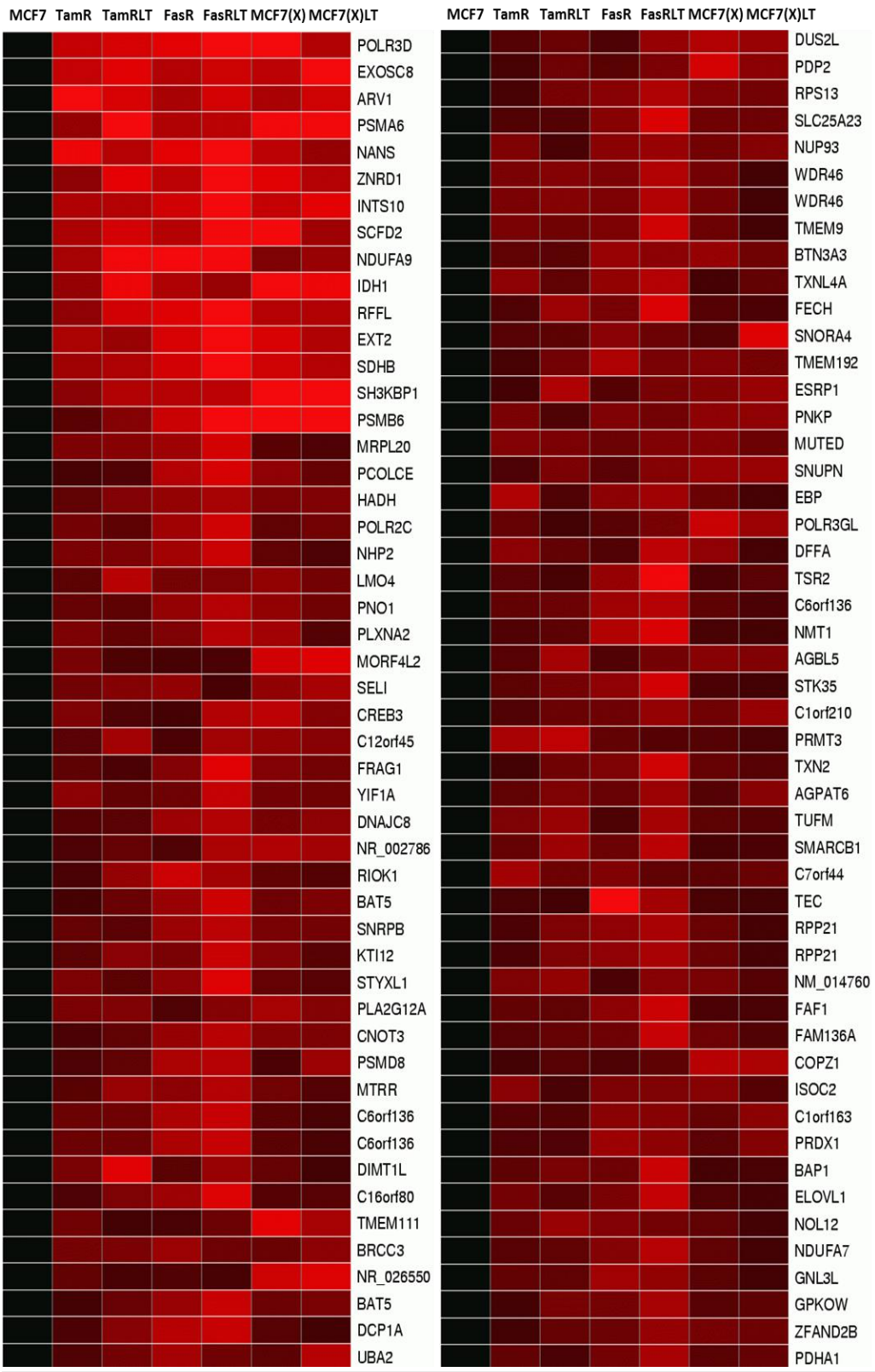

Fig 3.7. (D) Heatmap displays fourth 100 shared upregulated gene probes listed according to gene (≥1.2 fold changes) identified by comparing microarrays from endocrine resistant and the endocrine responsive models. Expression of these genes in the resistant models vs. MCF7 was statistically tested (ANOVA with *Benjamini and Hochberg post hoc* correction) and all were $p \leq 0.05$.

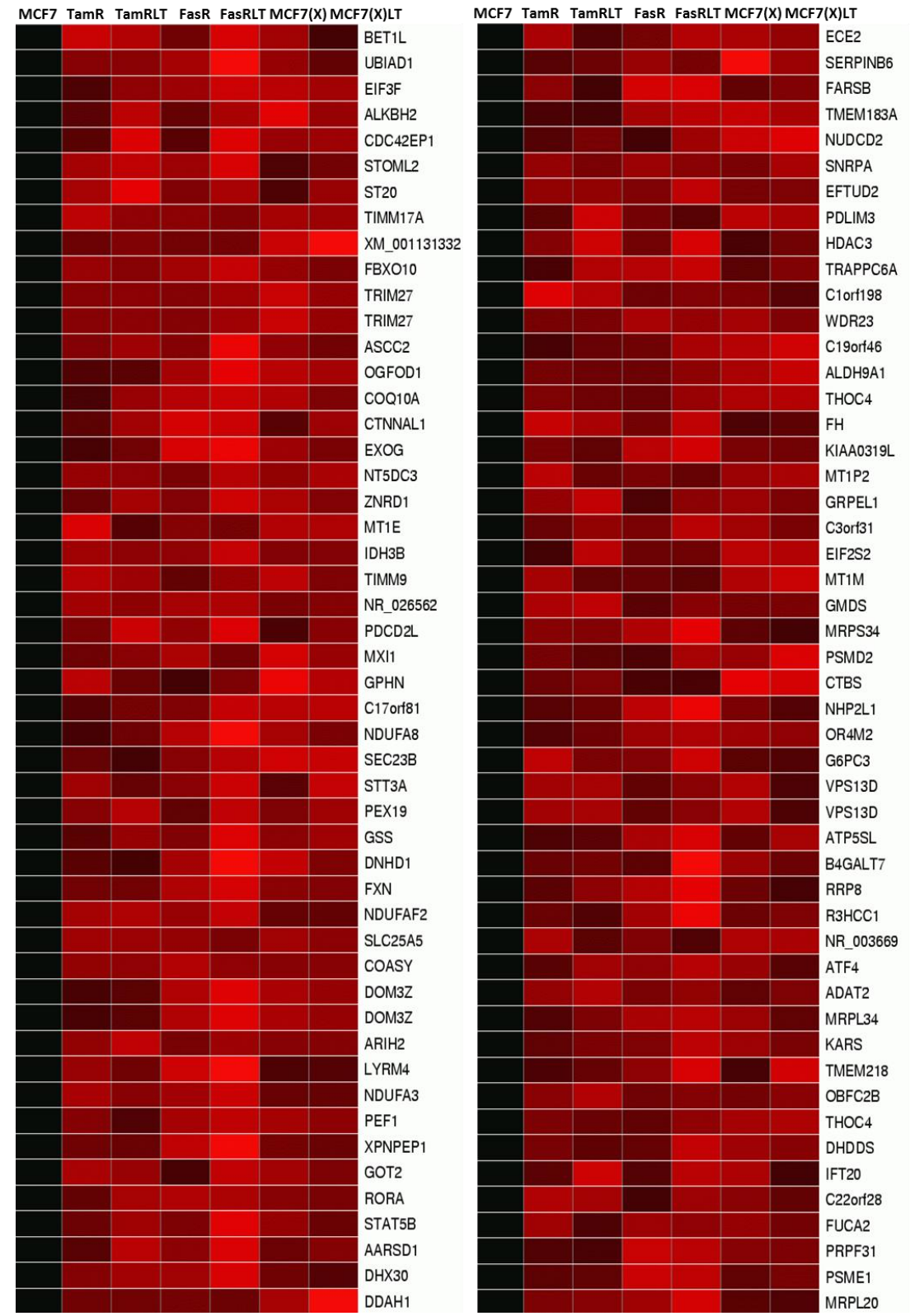

Fig 3.7. (E) Heatmap displays fifth 100 shared upregulated gene probes listed according to gene (≥1.2 fold changes) identified by comparing microarrays from endocrine resistant and the endocrine responsive models. Expression of these genes in the resistant models vs. MCF7 was statistically tested (ANOVA with *Benjamini and Hochberg post hoc* correction) and all were $p \leq 0.05$.

F

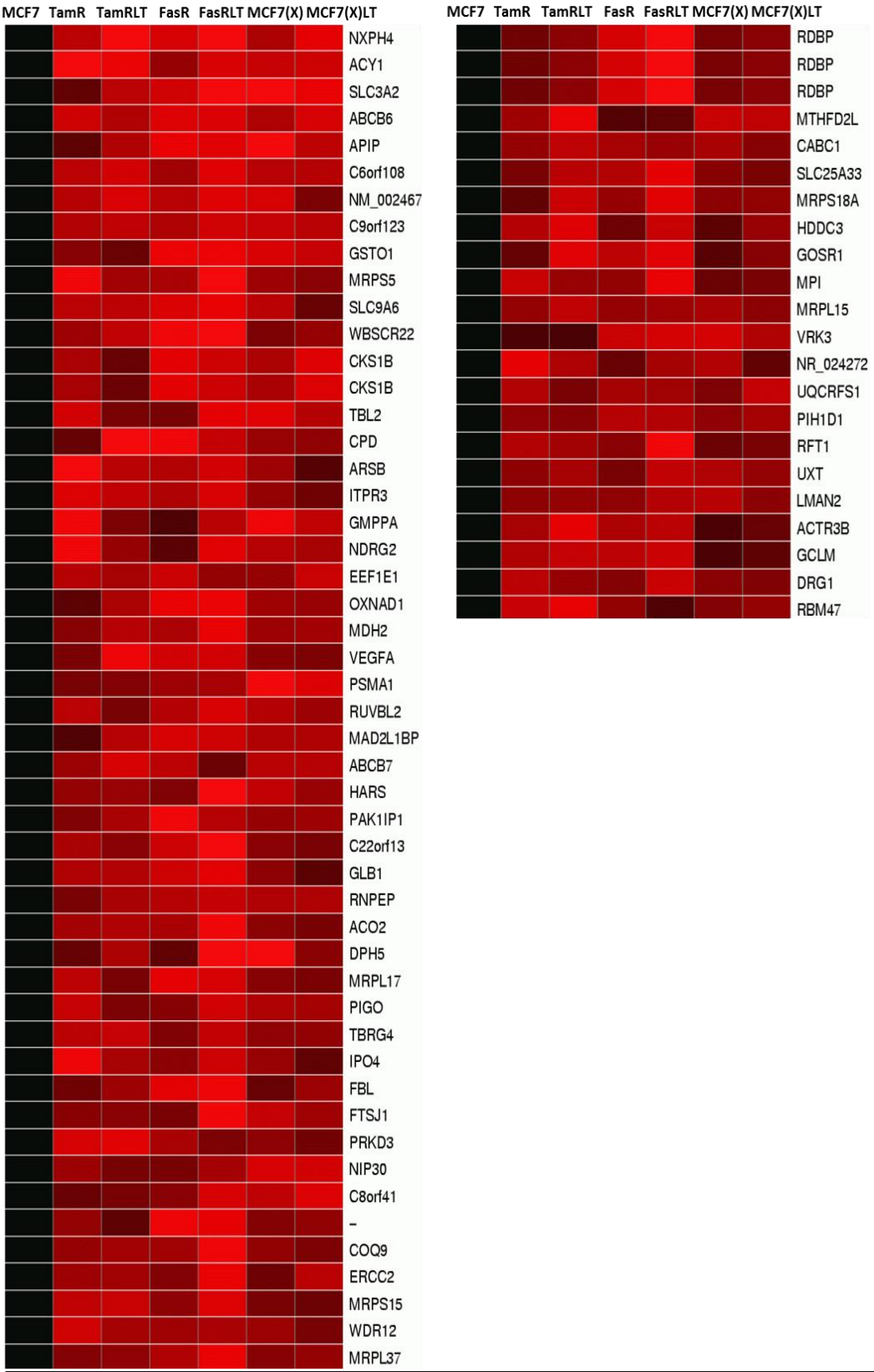

Fig 3.7. (F) Heatmap displays last 72 shared upregulated gene probes listed according to gene (≥1.2 fold changes) identified by comparing microarrays from endocrine resistant and the endocrine responsive models. Expression of these genes in the resistant models vs. MCF7 was statistically tested (ANOVA with *Benjamini and Hochberg post hoc* correction) and all were $p \leq 0.05$.

GO term name (Cellular-Components)	GO term p-value (corrected)	Gene Symbols
mitochondrion [cellular_component]	1.53E-23	ABCB6 ; ABCB7 ; ACAT1 ; ACO2 ; ACSL4 ; ACSM3 ; ADCK3 ; AIFM1 ; ALDH18A1 ; ALDH9A1 ; ALKBH3 ; ARSB ; ATP5SL ; BRP44 ; C6orf136 ; CHCHD3 ; CHCHD4 ; COQ3 ; COQ9 ; COX7B ; CPSF4 ; DDAH1 ; DHODH ; DHRS2 ; DHX30 ; DNAJC19 ; DUS2L ; EXOG ; FAM136A ; FARS2 ; FECH ; FH ; FXN ; GNL3L ; GOT2 ; GPT2 ; GRPEL1 ; HADH ; HAX1 ; HINT2 ; HMGCS2 ; IDH1 ; IDH3B ; ISOC2 ; JTB ; KARS ; KMO ; LIG3 ; LONP1 ; LYRM4 ; MARS ; MDH2 ; METAP1D ; MFN2 ; MGST1 ; MRPL15 ; MRPL17 ; MRPL2 ; MRPL21 ; MRPL34 ; MRPL37 ; MRPL40 ; MRPL47 ; MRPS15 ; MRPS18A ; MRPS18B ; MRPS24 ; MRPS34 ; MRPS5 ; MT-ATP6 ; MTHFD1L ; MTHFD2 ; NDUFA3 ; NDUFA8 ; NDUFAF2 ; NDUFAF4 ; NDUFB10 ; NDUFB5 ; NDUFB9 ; NDUFS3 ; NT5DC3 ; OXNAD1 ; PCK2 ; PDHA1 ; PDP2 ; PHF17 ; PON2 ; PPA2 ; PRDX1 ; PSMA6 ; PSMC4 ; QDPR ; RDBP ; RNASEH1 ; SDHB ; SHMT2 ; SLC25A23 ; SLC25A33 ; SLC25A37 ; SLC25A5 ; SLC9A6 ; STOML2 ; TAMM41 ; TBRG4 ; TIMM17A ; TIMM44 ; TIMM8A ; TIMM9 ; TUFM ; TXN2 ; UBIAD1 ; UQCRFS1 ;
mitochondrial inner membrane [cellular_component]	2.3E-14	ABCB7 ; ACAT1 ; AIFM1 ; ALDH18A1 ; BRP44 ; CHCHD3 ; COQ10A ; COX7B ; DHODH ; DNAJC19 ; ERAL1 ; EXOG ; FECH ; FXC1 ; GOT2 ; HADH ; HMGCS2 ; KMO ; MDH2 ; MGST1 ; MRPL17 ; MT-ATP6 ; MT-CO3 ; MTHFD2L ; NDUFA3 ; NDUFA7 ; NDUFA8 ; NDUFA9 ; NDUFB10 ; NDUFB5 ; NDUFB9 ; NDUFS3 ; SDHB ; SHMT2 ; SLC25A23 ; SLC25A33 ; SLC25A37 ; SLC25A5 ; STOML2 ; TIMM44 ; TIMM8A ; TIMM9 ; UQCRFS1 ;
mitochondrial matrix [cellular_component]	2.7E-08	ACAT1 ; ACO2 ; ACSM3 ; COQ3 ; ERAL1 ; FARS2 ; FECH ; FH ; FXN ; GOT2 ; GPT2 ; GRPEL1 ; HADH ; HMGCS2 ; IDH3B ; KARS ; LONP1 ; MDH2 ; NDUFA9 ; PCK2 ; PDHA1 ; PDP2 ; PPA2 ; PRDX1 ; SHMT2 ; TIMM44 ;
nucleoplasm [cellular_component]	1.4E-06	ALKBH2 ; ALKBH3 ; ALYREF ; APTX ; ATF4 ; CENPA ; CKS1B ; CPSF4 ; CSTF2 ; DDIT3 ; DFFA ; DKC1 ; DNAJC8 ; EFTUD2 ; ERCC2 ; HDAC3 ; ITPR3 ; LIG3 ; MED8 ; MYC ; NHP2L1 ; NR1D1 ; PHF5A ; POLR2C ; POLR2H ; POLR2I ; POLR3D ; POLR3GL ; PRKAA2 ; PSMA1 ; PSMA6 ; PSMB6 ; PSMC4 ; PSMD2 ; PSMD8 ; PSME1 ; PSME2 ; PSME3 ; RDBP ; RFC2 ; RORA ; RUVBL1 ; SF3A3 ; SKP2 ; SMARCB1 ; SNRNP40 ; SNRPA ; SNRPB ; SNRPD3 ; STAT5B ; TAF4B ; TATDN2 ; THRB ; TRIM27 ; TXNL4A ; VDR ; WDR12 ; XPOT ;
cytosol [cellular_component]	5.3E-06	ACSS2 ; AGBL5 ; AIFM1 ; AKR1A1 ; ALDH9A1 ; ALYREF ; AP1S1 ; APIP ; ASNS ; ASS1 ; ATP6V1B2 ; BLMH ; BLVRB ; CARS ; CBS ; CENPA ; CHAC1 ; CNOT3 ; COPZ1 ; CREB3 ; CTNNAL1 ; DFFA ; EEF1E1 ; EIF2B3 ; EIF2S2 ; EIF3F ; EIF3K ; EIF4EBP1 ; EPHX2 ; EXOSC2 ; EXOSC5 ; EXOSC8 ; FAF1 ; FARSB ; FXN ; G6PD ; GCLM ; GMPPA ; GNL1 ; GOT1 ; GSS ; GSTA4 ; GSTO1 ; GTPBP1 ; HARS ; IARS ; ICK ; IDH1 ; KARS ; KMO ; LARS ; MARS ; MFN2 ; MID1IP1 ; MPI ; MT2A ; MTRR ; NANS ; NAPA ; NDRG2 ; NMT1 ; NT5DC3 ; OAZ3 ; OCRL ; PEX19 ; PFKFB2 ; PGM1 ; PHGDH ; PNP ; PNPO ; PPIA ; PRDX1 ; PRKAA2 ; PRMT3 ; PSMA1 ; PSMA6 ; PSMB6 ; PSMC4 ; PSMD2 ; PSMD8 ; PSME1 ; PSME2 ; PSME3 ; PSPH ; QDPR ; RAP1GAP ; RPS13 ; SEC13 ; SERPINB6 ; SH3KBP1 ; SKP2 ; SLC7A5 ; SNRPB ; SNRPD3 ; SNUPN ; SOX2 ; SRM ; STAT5B ; STRADB ; TEC ; TRIB3 ; USP18 ; VDR ; WARS ; XPNPEP1 ; YARS ;

Table 3.10 continue…

GO term name (Cellular-Component)	GO term p-value (corrected)	Gene Symbols
cytoplasm [cellular_component]	0.00071	AARSD1 ; ABCB7 ; ABHD14A-ACY1 ; ACSL4 ; ACSS2 ; ACTR3B ; AGBL5 ; AIFM1 ; ALDH18A1 ; ALDH9A1 ; ALKBH3 ; APIP ; APTX ; ARFIP2 ; ARIH2 ; ARPC1B ; ASS1 ; ATF4 ; ATP6V1B2 ; BAP1 ; BLMH ; BLVRB ; C1orf198 ; C22orf28 ; C6orf108 ; CARS ; CBS ; CDC42EP1 ; CDC42EP3 ; CEBPB ; CENPV ; CHCHD3 ; CNOT3 ; COASY ; COPS6 ; COPS7A ; COQ3 ; CREB3 ; DDAH1 ; DDIT3 ; DFFA ; DHRS2 ; DHX30 ; DKC1 ; DNPEP ; DRG1 ; DUS2L ; EEF1E1 ; EFTUD2 ; EIF1 ; EIF2B3 ; EIF2D ; EIF4EBP1 ; ELP5 ; EMC7 ; EPHX2 ; ERCC2 ; EXOSC2 ; EXOSC5 ; EXOSC8 ; FAF1 ; FAM136A ; FARS2 ; FARSB ; FH ; G6PD ; GLA ; GMDS ; GNPDA1 ; GOT1 ; GPHN ; GSTO1 ; HADH ; HARS ; HAX1 ; HDAC3 ; IARS ; IDH1 ; INTS10 ; IPO4 ; ISOC2 ; ITPR3 ; JTB ; KARS ; LARS ; LEF1 ; LONP1 ; MAD2L1BP ; MAPRE2 ; MARK1 ; MARS ; METTL1 ; MID1IP1 ; MLX ; MPI ; MT1E ; MT1F ; MT1G ; MT1H ; MT1M ; MT1X ; MT2A ; MTRR ; MYO19 ; NAAA ; NANS ; NDRG2 ; NMT1 ; NQO2 ; OAZ3 ; OGFOD1 ; PCK2 ; PDCD2L ; PEF1 ; PEX19 ; PFKFB2 ; PGM1 ; PHF17 ; PIR ; PNP ; POLR2C ; POLR2H ; PPA2 ; PPP2R5D ; PRDX1 ; PRKD3 ; PRMT3 ; PSMA1 ; PSMA6 ; PSMC4 ; PSMD8 ; PSME1 ; PSPH ; QDPR ; RAB7L1 ; RRAGD ; RRP8 ; RUVBL1 ; RUVBL2 ; SAT2 ; SERPINB6 ; SNRNP40 ; SNRPB ; SNRPD3 ; SNUPN ; SOX2 ; SRI ; SRPRB ; STAT5B ; STK35 ; STRADB ; TAF4B ; TEC ; TRIM16L ; TRIM27 ; TXNL4A ; UBIAD1 ; UXT ; VEGFA ; WARS ; XPNPEP1 ; XPOT ; YARS ; ZNF259 ;
proteasome activator complex [cellular_component]	0.00146	PSME1 ; PSME2 ; PSME3 ;
mitochondrial respiratory chain complex I [cellular_component]	0.00199	NDUFA3 ; NDUFA7 ; NDUFA8 ; NDUFA9 ; NDUFB10 ; NDUFB5 ; NDUFB9 ; NDUFS3 ;
proteasome complex [cellular_component]	0.00638	PAAF1 ; PSMA1 ; PSMC4 ; PSMD2 ; PSMD8 ; PSME1 ; PSME2 ; PSME3 ;
mitochondrial intermembrane space [cellular_component]	0.00662	AIFM1 ; CHCHD4 ; FXC1 ; NDUFA8 ; SHMT2 ; TIMM8A ; TIMM9 ;
mitochondrial intermembrane space protein transporter complex [cellular_component]	0.01779	FXC1 ; TIMM8A ; TIMM9 ;
nucleolus [cellular_component]	0.02031	APTX ; BAP1 ; CBS ; CCDC86 ; DIMT1 ; DKC1 ; EPHX2 ; EXOSC2 ; EXOSC5 ; EXOSC8 ; FBL ; GNL3L ; ITPR3 ; MORF4L2 ; MYC ; NHP2 ; NHP2L1 ; NPM3 ; PNKP ; PNO1 ; POLR2H ; PRDX1 ; RPS13 ; RRP8 ; SMARCB1 ; STK35 ; TAF4B ; TXN2 ; WDR12 ; ZNF259 ; ZNRD1 ;
endoplasmic reticulum membrane [cellular_component]	0.02639	ACSL4 ; AGPAT6 ; ALG3 ; CREB3 ; DHDDS ; EBP ; ELOVL1 ; EPT1 ; EXT2 ; G6PC3 ; HERPUD1 ; ITPR3 ; LMAN2 ; MGST1 ; PARP16 ; PDIA5 ; PDIA6 ; PGAP2 ; PIGO ; PTDSS1 ; SEC11C ; SEC13 ; SEC23B ; SLC39A7 ; SLC9A6 ; SRPRB ; STT3A ; TMEM147 ; UBIAD1 ; USE1 ; YIF1A ;
ribosome [cellular_component]	0.02762	MRPL17 ; MRPL2 ; MRPL21 ; MRPL34 ; MRPL37 ; MRPS15 ; MRPS18A ; MRPS18B ; MRPS34 ; MRPS5 ; PRMT3 ; RPL7L1 ; RPS13 ;
Cajal body [cellular_component]	0.03345	DKC1 ; EFTUD2 ; FBL ; NHP2 ; PRPF31 ; SNRPC ;
mitochondrial membrane [cellular_component]	0.03746	ACSL4 ; COA1 ; NDUFA9 ; NDUFAF4 ; NDUFS3 ; SFXN4 ; SLC9B2 ; UQCRFS1 ;
spliceosomal complex [cellular_component]	0.03966	EFTUD2 ; NHP2L1 ; SF3A3 ; SNRPA ; SNRPB ; SNRPD3 ; TXNL4A ; U2AF1L4 ;
mitochondrial ribosome [cellular_component]	0.04604	MRPL34 ; MRPL37 ; MRPL40 ; MRPL47 ;
mitochondrial nucleoid [cellular_component]	0.04538	DHX30 ; LONP1 ; SHMT2 ; SLC25A5 ; TUFM ;

Table 3.10. Table displays significant ORA-O GO terms for the shared genes (after ENSEMBL ID conversion) that were increased in all resistant models vs. MCF7 (≥1.2 fold changes & $p \leq 0.05$), based on cellular compartment ontologies. Significance of the Go term after Innatedb analysis (Hypergeometric algorithm with *Benjamini & Hochberg post hoc* correction) and associated gene IDs for each GO term are provided.

GO term name (Molecular –Function)	GO term p-value (corrected)	Gene Symbols
aminoacyl-tRNA ligase activity [molecular_function]	7.2E-05	CARS ; FARS2 ; HARS ; IARS ; KARS ; LARS ; MARS ; WARS ; YARS ;
metal ion binding [molecular_function]	0.00066	AARSD1 ; ACAT1 ; ACSM3 ; APIP ; ARSB ; B4GALT7 ; BRCC3 ; C22orf28 ; CARS ; CBS ; CCNB1IP1 ; CHPT1 ; DDAH1 ; DOM3Z ; ECE2 ; EIF2S2 ; EPT1 ; ERCC2 ; EXOG ; FXC1 ; GPHN ; HDDC3 ; KARS ; LMAN2 ; METAP1D ; MT1E ; MT1F ; MT1G ; MT1H ; MT1M ; MT1X ; MT2A ; NQO2 ; NT5DC3 ; OSGEP ; PCK2 ; PDP2 ; PIGO ; PIR ; PON2 ; PRKAA2 ; PRKD3 ; SCNM1 ; SDHB ; TATDN2 ; TEC ; TIMM8A ; TIMM9 ; TRIM27 ; UBA2 ; UQCRFS1 ; XPNPEP1 ;
tRNA binding [molecular_function]	0.00156	CARS ; FARS2 ; KARS ; MARS ; METTL1 ; XPOT ; YARS ;
nucleotide binding [molecular_function]	0.00288	AARSD1 ; ABCB6 ; ABCB7 ; ALYREF ; BLVRB ; CARS ; CSTF2 ; DHRS2 ; DOM3Z ; ESRP1 ; FARS2 ; FARSB ; GMDS ; HADH ; HARS ; IARS ; KARS ; LARS ; LONP1 ; MARS ; MDH2 ; MTHFD1L ; MTHFD2 ; MTHFD2L ; NDUFA9 ; PSMC4 ; QDPR ; R3HCC1 ; RBM47 ; RDBP ; RFC2 ; RUVBL1 ; RUVBL2 ; SLC9B2 ; SNRPA ; U2AF1L4 ; WARS ; YARS ;
transferase activity [molecular_function]	0.00341	CBS ; DIMT1 ; EIF2B3 ; ELOVL4 ; GMPPA ; GPHN ; GSTO1 ; MGST1 ; PIGO ; PRMT3 ; PTDSS1 ;
methylenetetrahydrofolate dehydrogenase (NADP+) activity [molecular_function]	0.00361	MTHFD1L ; MTHFD2 ; MTHFD2L ;
catalytic activity [molecular_function]	0.00501	ACAT1 ; ACSL4 ; ACSM3 ; ACSS2 ; ADAT2 ; ALDH18A1 ; APTX ; ARSB ; BLVRB ; DDAH1 ; EPHX2 ; FH ; G6PC3 ; GLA ; GMDS ; GPT2 ; HDDC3 ; HINT2 ; HMGCS2 ; ISOC2 ; MDH2 ; MTHFD1L ; MTHFD2 ; MTHFD2L ; NANS ; NDUFA9 ; NMT1 ; PDP2 ; PIGO ; PNP ; PSPH ; RIOK1 ; SLC3A2 ; SRM ; UBA2 ;
neutral amino acid transmembrane transporter activity [molecular_function]	0.00586	SLC1A5 ; SLC3A2 ; SLC43A1 ; SLC7A5 ;
protein homodimerization activity [molecular_function]	0.00696	ACAT1 ; ALDH9A1 ; ASNS ; CARS ; CBS ; CEBPB ; CREB3 ; EPHX2 ; EXT2 ; G6PD ; GLA ; GRPEL1 ; GSS ; GSTA4 ; IDH1 ; IL6ST ; MGST1 ; MLX ; MTHFD1L ; PRDX1 ; PSPH ; QDPR ; RAP1GAP ; RNASEH1 ; SNRPC ; SRM ; TFAP4 ; TIMM9 ; TYRP1 ; VEGFA ; XPNPEP1 ;
oxidoreductase activity, acting on the CH-OH group of donors, NAD or NADP as acceptor [molecular_function]	0.0088	BLVRB ; HADH ; IDH1 ; IDH3B ; MDH2 ; NDUFA9 ; PHGDH ;
methyltransferase activity [molecular_function]	0.01152	COQ3 ; DIMT1 ; DPH5 ; ECE2 ; FBL ; FTSJ1 ; METTL7A ; PRMT3 ; RRP8 ; SHMT2 ; WBSCR22 ;
ferrous iron binding [molecular_function]	0.01288	ALKBH2 ; ALKBH3 ; FECH ; FXN ;
electron carrier activity [molecular_function]	0.01422	AIFM1 ; AKR1A1 ; IDH3B ; NDUFAF2 ; NDUFS3 ; NQO2 ; PDIA5 ; PDIA6 ; PHGDH ; QDPR ; SDHB ; SH3BGRL2 ; TXN2 ;
structural constituent of ribosome [molecular_function]	0.01666	MRPL15 ; MRPL17 ; MRPL2 ; MRPL21 ; MRPL34 ; MRPL37 ; MRPL47 ; MRPS15 ; MRPS18A ; MRPS18B ; MRPS24 ; MRPS5 ; RPS13 ;
3 iron, 4 sulfur cluster binding [molecular_function]	0.01733	ACO2 ; SDHB ;
L-aspartate:2-oxoglutarate aminotransferase activity [molecular_function]	0.01733	GOT1 ; GOT2 ;
cytosine C-5 DNA demethylase activity [molecular_function]	0.01733	ALKBH2 ; ALKBH3 ;
methylenetetrahydrofolate dehydrogenase (NAD+) activity [molecular_function]	0.01733	MTHFD2 ; MTHFD2L ;

Table 3.11. Table displays significant ORA-O GO terms for the shared genes (after ENSEMBL ID conversion) that were increased in all resistant models vs. MCF7 (≥1.2 fold changes & $p \leq 0.05$), based on molecular function ontologies. Significance of the Go term after Innatedb analysis (Hypergeometric algorithm with *Benjamini & Hochberg post hoc* correction) and associated gene IDs for each GO term are provided.

GO term name (Biological-Process)	GO term p-value (corrected)	Gene Symbols
small molecule metabolic process [biological_process]	1.8E-14	ACAT1 ; ACO2 ; ACSL4 ; ACSS2 ; AGPAT6 ; ALDH18A1 ; ALDH9A1 ; APIP ; ARSB ; ASNS ; ASS1 ; B4GALT7 ; BLVRB ; CBS ; CHPT1 ; COASY ; COX7B ; DHODH ; EBP ; ELOVL1 ; ELOVL4 ; EPT1 ; EXT2 ; FECH ; FH ; G6PC3 ; G6PD ; GCLM ; GLA ; GLB1 ; GOT1 ; GOT2 ; GPHN ; GPT2 ; GSS ; GSTA4 ; GSTO1 ; HADH ; HDAC3 ; HMGCS2 ; IDH1 ; IDH3B ; ITPR3 ; KMO ; MDH2 ; MGST1 ; MLX ; MT-ATP6 ; MT-CO3 ; NDUFA3 ; NDUFA7 ; NDUFA8 ; NDUFA9 ; NDUFB10 ; NDUFB5 ; NDUFB9 ; NDUFS3 ; NUP93 ; OAZ3 ; OCRL ; PCK2 ; PDHA1 ; PDP2 ; PFKFB2 ; PGM1 ; PHGDH ; PLA2G12A ; PNP ; PNPO ; PRKAA2 ; PSMA1 ; PSMA6 ; PSMB6 ; PSMC4 ; PSMD2 ; PSMD8 ; PSME1 ; PSME2 ; PSME3 ; PSPH ; PTDSS1 ; QDPR ; SDHB ; SEC11C ; SLC25A5 ; SRM ; TRIB3 ; UQCRFS1 ; UST ;
gene expression [biological_process]	4.8E-14	ALYREF ; CARS ; CNOT3 ; CSTF2 ; DNAJC8 ; EEF1E1 ; EFTUD2 ; EIF2B3 ; EIF2S2 ; EIF3F ; EIF3K ; EIF4EBP1 ; ERCC2 ; EXOSC2 ; EXOSC5 ; EXOSC8 ; FARS2 ; FARSB ; HARS ; IARS ; KARS ; LARS ; MARS ; MED8 ; MYC ; NHP2L1 ; NR1D1 ; PHF5A ; POLR2C ; POLR2H ; POLR2I ; POLR3D ; POLR3GL ; PPA2 ; PSMA1 ; PSMA6 ; PSMB6 ; PSMC4 ; PSMD2 ; PSMD8 ; PSME1 ; PSME2 ; PSME3 ; RDBP ; RORA ; RPS13 ; SEC11C ; SF3A3 ; SNRNP40 ; SNRPA ; SNRPB ; SNRPD3 ; SNUPN ; SRPRB ; TAF4B ; THRB ; TXNL4A ; VDR ; WARS ; YARS ;
cellular nitrogen compound metabolic process [biological_process]	6E-09	ACAT1 ; ALDH18A1 ; ALDH9A1 ; APIP ; ASNS ; ASS1 ; CBS ; GCLM ; GOT1 ; GOT2 ; GPT2 ; KMO ; OAZ3 ; PHGDH ; PSMA1 ; PSMA6 ; PSMB6 ; PSMC4 ; PSMD2 ; PSMD8 ; PSME1 ; PSME2 ; PSME3 ; PSPH ; QDPR ; SRM ;
tRNA aminoacylation for protein translation [biological_process]	4.3E-07	CARS ; EEF1E1 ; FARS2 ; FARSB ; HARS ; IARS ; KARS ; LARS ; MARS ; PPA2 ; WARS ; YARS ;
cellular response to zinc ion [biological_process]	1.6E-06	MT1E ; MT1F ; MT1G ; MT1H ; MT1M ; MT1X ; MT2A ;
negative regulation of growth [biological_process]	4.5E-05	MT1E ; MT1F ; MT1G ; MT1H ; MT1M ; MT1X ; MT2A ;
cellular amino acid biosynthetic process [biological_process]	8.8E-05	ALDH18A1 ; ASNS ; GOT1 ; GOT2 ; GPT2 ; PHGDH ; PSPH ;
regulation of cellular amino acid metabolic process [biological_process]	0.00015	OAZ3 ; PSMA1 ; PSMA6 ; PSMB6 ; PSMC4 ; PSMD2 ; PSMD8 ; PSME1 ; PSME2 ; PSME3 ;
translation [biological_process]	0.00014	EIF2B3 ; EIF2S2 ; EIF3F ; EIF3K ; EIF4EBP1 ; FARSB ; HARS ; MRPL15 ; MRPL17 ; MRPL2 ; MRPL21 ; MRPL34 ; MRPL37 ; MRPL47 ; MRPS15 ; MRPS18A ; MRPS18B ; MRPS24 ; MRPS5 ; RPS13 ; SEC11C ; SRPRB ; WARS ;
mRNA splicing, via spliceosome [biological_process]	0.00031	ALYREF ; CSTF2 ; DNAJC8 ; EFTUD2 ; NHP2L1 ; PHF5A ; POLR2C ; POLR2H ; POLR2I ; PRPF31 ; SF3A3 ; SNRNP40 ; SNRPA ; SNRPB ; SNRPC ; SNRPD3 ; TXNL4A ;
respiratory electron transport chain [biological_process]	0.00043	COX7B ; MT-ATP6 ; MT-CO3 ; NDUFA3 ; NDUFA7 ; NDUFA8 ; NDUFA9 ; NDUFB10 ; NDUFB5 ; NDUFB9 ; NDUFS3 ; SDHB ; UQCRFS1 ;
NADH dehydrogenase (ubiquinone) activity [molecular_function]	0.00042	NDUFA3 ; NDUFA7 ; NDUFA8 ; NDUFA9 ; NDUFAF2 ; NDUFB10 ; NDUFB5 ; NDUFB9 ; NDUFS3 ;
oxaloacetate metabolic process [biological_process]	0.00062	GOT1 ; GOT2 ; MDH2 ; PCK2 ; STAT5B ;
protein targeting to mitochondrion [biological_process]	0.00069	CHCHD4 ; DNAJC19 ; FXC1 ; GRPEL1 ; MFN2 ; TIMM17A ; TIMM44 ; TIMM8A ; TIMM9 ;

Table 3.12 continue…

GO term name (Biological-Process)	GO term p-value (corrected)	Gene Symbols
L-serine metabolic process [biological_process]	0.0007	CBS ; PHGDH ; PSPH ; SHMT2 ;
oxidation-reduction process [biological_process]	0.00085	AIFM1 ; ALDH18A1 ; ALDH9A1 ; ALKBH2 ; ALKBH3 ; BLVRB ; DHODH ; DHRS2 ; DUS2L ; FXN ; G6PD ; HADH ; IDH1 ; IDH3B ; MDH2 ; MGST1 ; MTHFD1L ; MTHFD2 ; MTHFD2L ; MTRR ; NDUFA9 ; NDUFS3 ; OGFOD1 ; OXNAD1 ; PDHA1 ; PDIA5 ; PHGDH ; PNPO ; PRDX1 ; SDHB ; UQCRFS1 ;
2-oxoglutarate metabolic process [biological_process]	0.00086	GOT1 ; GOT2 ; GPT2 ; IDH1 ; IDH3B ; STAT5B ;
metabolic process [biological_process]	0.00112	ABHD14A-ACY1 ; ACAT1 ; ACO2 ; ACSL4 ; ACSM3 ; ACSS2 ; AGPAT6 ; ALDH18A1 ; ALDH9A1 ; ARSB ; ASNS ; CENPV ; COQ3 ; DHRS2 ; DIMT1 ; DPH5 ; ECE2 ; EPHX2 ; HMGCS2 ; ISOC2 ; METTL7A ; PDHA1 ; PHGDH ; PIGO ; PRMT3 ; PSPH ; QDPR ; RRP8 ; TYRP1 ; UGT8 ; WBSCR22 ;
lipid biosynthetic process [biological_process]	0.00112	ACSL4 ; ACSS2 ; AGPAT6 ; COQ3 ; PRKAA2 ;
cellular response to cadmium ion [biological_process]	0.00154	MT1E ; MT1F ; MT1G ; MT1H ; MT1X ;
mitochondrial electron transport, NADH to ubiquinone [biological_process]	0.00174	NDUFA3 ; NDUFA7 ; NDUFA8 ; NDUFA9 ; NDUFB10 ; NDUFB5 ; NDUFB9 ; NDUFS3 ;
antigen processing and presentation of peptide antigen via MHC class I [biological_process]	0.0028	BLMH ; PSMA1 ; PSMA6 ; PSMB6 ; PSMC4 ; PSMD2 ; PSMD8 ; PSME1 ; PSME2 ; PSME3 ; SEC13 ;
anaphase-promoting complex-dependent proteasomal ubiquitin-dependent protein catabolic process [biological_process]	0.00339	PSMA1 ; PSMA6 ; PSMB6 ; PSMC4 ; PSMD2 ; PSMD8 ; PSME1 ; PSME2 ; PSME3 ; SKP2 ;
S phase of mitotic cell cycle [biological_process]	0.00321	CKS1B ; PSMA1 ; PSMA6 ; PSMB6 ; PSMC4 ; PSMD2 ; PSMD8 ; PSME1 ; PSME2 ; PSME3 ; RFC2 ; SKP2 ;
protein polyubiquitination [biological_process]	0.00321	ARIH2 ; BLMH ; PSMA1 ; PSMA6 ; PSMB6 ; PSMC4 ; PSMD2 ; PSMD8 ; PSME1 ; PSME2 ; PSME3 ; SKP2 ;
activation of signaling protein activity involved in unfolded protein response [biological_process]	0.00326	ASNS ; ATF4 ; DDIT3 ; HERPUD1 ; PDIA5 ; PDIA6 ; SRPRB ; TATDN2 ; YIF1A ;
negative regulation of ubiquitin-protein ligase activity involved in mitotic cell cycle [biological_process]	0.00326	PSMA1 ; PSMA6 ; PSMB6 ; PSMC4 ; PSMD2 ; PSMD8 ; PSME1 ; PSME2 ; PSME3 ;
tricarboxylic acid cycle [biological_process]	0.00334	ACO2 ; FH ; IDH1 ; IDH3B ; MDH2 ; SDHB ;
RNA splicing [biological_process]	0.00353	ALYREF ; CSTF2 ; DNAJC8 ; EFTUD2 ; ESRP1 ; NHP2L1 ; PHF5A ; POLR2C ; POLR2H ; POLR2I ; SCNM1 ; SF3A3 ; SNRNP40 ; SNRPA ; SNRPB ; SNRPD3 ; TXNL4A ; U2AF1L4 ;
DNA damage response, signal transduction by p53 class mediator resulting in cell cycle arrest [biological_process]	0.00377	PSMA1 ; PSMA6 ; PSMB6 ; PSMC4 ; PSMD2 ; PSMD8 ; PSME1 ; PSME2 ; PSME3 ;
L-serine biosynthetic process [biological_process]	0.00361	PHGDH ; PSPH ; SHMT2 ;
cellular amino acid metabolic process [biological_process]	0.00492	ABHD14A-ACY1 ; ASNS ; ATF4 ; GOT1 ; GOT2 ; GSS ; QDPR ; SLC7A5 ;
carbohydrate metabolic process [biological_process]	0.00486	ARSB ; B4GALT7 ; CTBS ; EXT2 ; FUCA2 ; G6PC3 ; G6PD ; GALNT14 ; GLA ; GLB1 ; GNPDA1 ; GOT1 ; GOT2 ; MDH2 ; MPI ; NUP93 ; PCK2 ; PFKFB2 ; PGM1 ; SLC3A2 ; UGT8 ; UST ; XYLB ; YDJC ;

Table 3.12 continue…

GO term name (Biological-Process)-	GO term p-value (corrected)	Gene Symbols
positive regulation of ubiquitin-protein ligase activity involved in mitotic cell cycle [biological_process]	0.00511	PSMA1 ; PSMA6 ; PSMB6 ; PSMC4 ; PSMD2 ; PSMD8 ; PSME1 ; PSME2 ; PSME3 ;
viral reproduction [biological_process]	0.00557	AP1S1 ; ERCC2 ; NMT1 ; NUP93 ; POLR2C ; POLR2H ; POLR2I ; PPIA ; PSMA1 ; PSMA6 ; PSMB6 ; PSMC4 ; PSMD2 ; PSMD8 ; PSME1 ; PSME2 ; PSME3 ; RDBP ; RPS13 ; SLC25A5 ; TAF4B ; ZSCAN12 ;
forebrain neuron differentiation [biological_process]	0.00586	DLX1 ; DLX2 ; LEF1 ; SOX2 ;
antigen processing and presentation of exogenous peptide antigen via MHC class I, TAP-dependent [biological_process]	0.00641	PSMA1 ; PSMA6 ; PSMB6 ; PSMC4 ; PSMD2 ; PSMD8 ; PSME1 ; PSME2 ; PSME3 ;
regulation of ubiquitin-protein ligase activity involved in mitotic cell cycle [biological_process]	0.00686	PSMA1 ; PSMA6 ; PSMB6 ; PSMC4 ; PSMD2 ; PSMD8 ; PSME1 ; PSME2 ; PSME3 ;
rRNA processing [biological_process]	0.00721	DIMT1 ; DKC1 ; EXOSC2 ; EXOSC5 ; EXOSC8 ; FBL ; FTSJ1 ; NPM3 ; RRP8 ; TSR2 ;
cell redox homeostasis [biological_process]	0.00819	AIFM1 ; DDIT3 ; PDIA5 ; PDIA6 ; SH3BGRL2 ; TXN2 ; TXNDC12 ; TXNL4A ;
regulation of M/G1 transition of mitotic cell cycle [biological_process]	0.0085	PSMA1 ; PSMA6 ; PSMB6 ; PSMC4 ; PSMD2 ; PSMD8 ; PSME1 ; PSME2 ; PSME3 ;
antigen processing and presentation of exogenous peptide antigen via MHC class I [biological_process]	0.0085	PSMA1 ; PSMA6 ; PSMB6 ; PSMC4 ; PSMD2 ; PSMD8 ; PSME1 ; PSME2 ; PSME3 ;
tRNA processing [biological_process]	0.00873	ADAT2 ; DUS2L ; FARS2 ; FBL ; KARS ; OSGEP ; POP7 ; RPP40 ;
glutamate metabolic process [biological_process]	0.00981	ALDH18A1 ; GCLM ; GOT1 ; GOT2 ;
neutral amino acid transport [biological_process]	0.00981	SLC1A5 ; SLC3A2 ; SLC43A1 ; SLC7A5 ;
isocitrate metabolic process [biological_process]	0.01157	ACO2 ; IDH1 ; IDH3B ;
endoplasmic reticulum unfolded protein response [biological_process]	0.01313	ASNS ; ATF4 ; DDIT3 ; HERPUD1 ; PDIA5 ; PDIA6 ; SRPRB ; TATDN2 ; YIF1A ;
response to endoplasmic reticulum stress [biological_process]	0.01387	ATF4 ; CEBPB ; CREB3 ; DDIT3 ; TRIB3 ;
chaperone-mediated protein transport [biological_process]	0.01779	PEX19 ; TIMM8A ; TIMM9 ;
tetrahydrofolate interconversion [biological_process]	0.01779	MTHFD1L ; MTHFD2L ; SHMT2 ;
L-ascorbic acid biosynthetic process [biological_process]	0.01733	AKR1A1 ; GSTO1 ;
NADPH regeneration [biological_process]	0.01733	G6PD ; IDH1 ;
aspartate biosynthetic process [biological_process]	0.01733	GOT1 ; GOT2 ;
cellular response to erythropoietin [biological_process]	0.01733	MT1X ; MT2A ;
cerebral cortex GABAergic interneuron fate commitment [biological_process]	0.01733	DLX1 ; DLX2 ;

Table 3.12 continue…

GO term name (Biological-Process)-	GO term p-value (corrected)	Gene Symbols
glutamate catabolic process to 2-oxoglutarate [biological_process]	0.01733	GOT1 ; GOT2 ;
glutamate catabolic process to aspartate [biological_process]	0.01733	GOT1 ; GOT2 ;
protein import into mitochondrial matrix [biological_process]	0.01733	GRPEL1 ; TAMM41 ;
regulation of transcription from RNA polymerase II promoter involved in forebrain neuron fate commitment [biological_process]	0.01733	DLX1 ; DLX2 ;
RNA metabolic process [biological_process]	0.01758	CNOT3 ; EXOSC2 ; EXOSC5 ; EXOSC8 ; PSMA1 ; PSMA6 ; PSMB6 ; PSMC4 ; PSMD2 ; PSMD8 ; PSME1 ; PSME2 ; PSME3 ; RPS13 ; SNRPB ; SNRPD3 ; SNUPN ;
cell cycle checkpoint [biological_process]	0.01741	ERCC2 ; PSMA1 ; PSMA6 ; PSMB6 ; PSMC4 ; PSMD2 ; PSMD8 ; PSME1 ; PSME2 ; PSME3 ; RFC2 ;
G1/S transition of mitotic cell cycle [biological_process]	0.01742	CKS1B ; EIF4EBP1 ; PSMA1 ; PSMA6 ; PSMB6 ; PSMC4 ; PSMD2 ; PSMD8 ; PSME1 ; PSME2 ; PSME3 ; SKP2 ;
protein import into mitochondrial inner membrane [biological_process]	0.02193	FXC1 ; TIMM8A ; TIMM9 ;
gluconeogenesis [biological_process]	0.02315	ATF4 ; G6PC3 ; GOT1 ; GOT2 ; MDH2 ; PCK2 ;
ferrous iron transport [biological_process]	0.02508	DRG1 ; ERAL1 ; GNL3L ; SLC39A14 ;
lactation [biological_process]	0.0277	AGPAT6 ; DHODH ; SLC29A1 ; STAT5B ; VDR ; VEGFA ;
folic acid-containing compound biosynthetic process [biological_process]	0.02953	MTHFD1L ; MTHFD2 ; MTHFD2L ;
cellular lipid metabolic process [biological_process]	0.03326	ACAT1 ; ACSL4 ; AGPAT6 ; ELOVL1 ; ELOVL4 ; HADH ; HDAC3 ; HMGCS2 ; IDH1 ; PRKAA2 ; TRIB3 ;
mitochondrial small ribosomal subunit [cellular_component]	0.03466	MRPS15 ; MRPS18A ; MRPS18B ; MRPS24 ;
positive regulation by host of viral transcription [biological_process]	0.03917	LEF1 ; SMARCB1 ; TFAP4 ;
positive regulation of ligase activity [biological_process]	0.03958	MID1IP1 ; NHEJ1 ;
response to interleukin-15 [biological_process]	0.03958	ACSL4 ; STAT5B ;
amino acid transport [biological_process]	0.04538	SLC1A5 ; SLC3A2 ; SLC43A1 ; SLC7A11 ; SLC7A5 ;

Table 3.12. Table displays significant ORA-O GO terms for the shared genes (after ENSEMBL ID conversion) that were increased in all resistant models vs. MCF7 (≥1.2 fold changes & $p \leq 0.05$), based on biological process ontologies. Significance of the Go term after Innatedb analysis (Hypergeometric algorithm with *Benjamini & Hochberg post hoc* correction) and associated gene IDs for each GO term are provided.

Categories	ORA Cellular components	P value	ORA Molecular Function	P value	ORA Biological Process	P value
TamR vs. MCF7	mitochondrion	4.74E-22	Metal ion binding	7.61E-05	small molecule metabolic process	1.35E-18
TamRLT vs. MCF7	mitochondrion	8.50E-29	Metal ion binding	8.58E-05	small molecule metabolic process	1.39E-08
FasR vs. MCF7	mitochondrion	9.09E-42	DNA_ directed RNA polymerase activity	0.000195	small molecule metabolic process	1.4E-14
FasRLT vs. MCF7	mitochondrion	6.43E-61	Structural constituent of ribosome	1.72E-08	Gene expression	2.99E-18
MCF7(X) vs. MCF7	mitochondrion	1.05E-30	Metal ion binding	6.32E-07	Gene expression	5.91E-09
MCF7(X)LT vs. MCF7	mitochondrion	5.29E-32	Nucleotide binding	3.7E-05	Gene expression	2.27E-11
TamR & TamRLT vs. MCF7	mitochondrion	7.33E-32	Electron carrier activity	5.3E-05	small molecule metabolic process	2.44E-17
FasR & FasRLT vs. MCF7	mitochondrion	3.50E-48	Poly (A) RNA binding	2.76E-013	small molecule metabolic process	3.64E-24
MCF7(X) & MCF7(X)LT vs. MCF7	mitochondrion	2.54E-33	Aminoacyl tRNA ligase activity	1.09E-06	Gene expression	1.77E-09
TamR, FasR & MCF7(X) vs. MCF7	mitochondrion	4.30E-26	Aminoacyl_tRNA ligase activity	1.82E-06	Small molecule metabolic process	2.09E-16
TamRLT, FasRLT & MCF7(X)LT vs. MCF7	mitochondrion	5.35E-37	Aminoacyl tRNA ligase activity	7.26E-12	Gene expression	1.45E-18
TamR, TamRLT, FasR, FasRLT, MCF7(X) & MCF7(X)LT vs. MCF7	mitochondrion	1.53E-23	Aminoacyl-tRNA ligase activity	7.19859E-05	small molecule metabolic process	1.81993E-14

Table 3.13. Summary of most significant ORA-O GO terms from Innatedb for induced genes (≥1.2 fold changes & $p \leq 0.05$) based on type/duration of endocrine resistance across resistant models.

Categories	ORA pathway	P value
TamR vs. MCF7	Metabolic pathways	5.64E-18
TamRLT vs. MCF7	Metabolic pathways	2.4E-12
FasR vs. MCF7	Metabolic pathways	3E-07
FasRLT vs. MCF7	Metabolic pathways	6.85E-14
MCF7(X) vs. MCF7	Metabolic pathways	9.08E-12
MCF7(X)LT vs. MCF7	Metabolic pathways	1.05E-06
TamR & TamRLT vs. MCF7	Metabolic pathways	3.52151E-15
FasR & FasRLT vs. MCF7	Metabolic pathways	8.48E-215
MCF7(X) & MCF7(X)LT vs. MCF7	Metabolic pathways	9.64E-160
TamR, FasR & MCF7(X) vs. MCF7	Metabolic pathways	4.47E-105
TamRLT, FasRLT & MCF7(X)LT vs. MCF7	Metabolic pathways	3.51E-24
TamR, TamRLT, FasR, FasRLT, MCF7(X) & MCF7(X)LT vs. MCF7	Metabolic pathways	4.16E-16

Table 3.14. Summary of ORA-P pathways identified as significant using Innatedb analysis for genes induced (≥1.2 fold changes & $p \leq 0.05$) according to type/duration of endocrine resistance and shared across resistant models

Pathway Name	Pathway p-value (corrected)	Gene Symbols
Metabolic pathways	4.16E-16	ACAT1 ; ACO2 ; ACSL4 ; ACSM3 ; ACSS2 ; AGPAT6 ; AKR1A1 ; ALDH18A1 ; ALDH9A1 ; ALG3 ; APIP ; ARSB ; ASNS ; ASS1 ; ATP6V1B2 ; B4GALT7 ; CBS ; CHPT1 ; COASY ; COQ3 ; COX7B ; DHODH ; EBP ; EPHX2 ; EPT1 ; EXT2 ; FECH ; FH ; G6PD ; GALNT12 ; GALNT14 ; GALNT6 ; GCLM ; GLB1 ; GMDS ; GMPPA ; GNPDA1 ; GOT1 ; GOT2 ; GPT2 ; GSS ; HADH ; HMGCS2 ; IDH1 ; IDH3B ; KMO ; MDH2 ; MPI ; MT-ATP6 ; MT-CO3 ; MTHFD1L ; MTHFD2 ; MTHFD2L ; NANS ; NDUFA3 ; NDUFA8 ; NDUFA9 ; NDUFB10 ; NDUFB5 ; NDUFB9 ; NDUFS3 ; OCRL ; PCK2 ; PDHA1 ; PGM1 ; PHGDH ; PIGO ; PLA2G12A ; PNP ; PNPO ; POLR2C ; POLR2H ; POLR2I ; POLR3D ; POLR3GL ; PON2 ; PSPH ; PTDSS1 ; QDPR ; SAT2 ; SDHB ; SHMT2 ; SRM ; STT3A ; TYRP1 ; UGT8 ; UQCRFS1 ; XYLB ; ZNRD1 ;
Aminoacyl-tRNA biosynthesis	3.5E-05	CARS ; FARS2 ; FARSB ; HARS ; IARS ; KARS ; LARS ; MARS ; WARS ; YARS ;
Citrate cycle (TCA cycle)	0.00011	ACO2 ; FH ; IDH1 ; IDH3B ; MDH2 ; PCK2 ; PDHA1 ; SDHB ;
Huntington`s disease	0.00027	COX7B ; CREB3 ; MT-ATP6 ; MT-CO3 ; NDUFA3 ; NDUFA8 ; NDUFA9 ; NDUFB10 ; NDUFB5 ; NDUFB9 ; NDUFS3 ; POLR2C ; POLR2H ; POLR2I ; SDHB ; SLC25A5 ; TAF4B ; UQCRFS1 ;
Glutathione metabolism	0.00029	G6PD ; GCLM ; GSS ; GSTA4 ; GSTO1 ; IDH1 ; MGST1 ; SRM ; TXNDC12 ;
Proteasome	0.00052	PSMA6 ; PSMB6 ; PSMC4 ; PSMD2 ; PSMD8 ; PSME1 ; PSME2 ; PSME3 ;
Oxidative phosphorylation	0.00054	COX7B ; MT-ATP6 ; MT-CO3 ; NDUFA3 ; NDUFA8 ; NDUFA9 ; NDUFB10 ; NDUFB5 ; NDUFB9 ; NDUFS3 ; PPA2 ; SDHB ; UQCRFS1 ;
Spliceosome	0.001	ALYREF ; BUD31 ; EFTUD2 ; NHP2L1 ; PHF5A ; PRPF31 ; SF3A3 ; SNRNP40 ; SNRPA ; SNRPB ; SNRPC ; SNRPD3 ; TXNL4A ;
Parkinson`s disease	0.00127	COX7B ; MT-ATP6 ; MT-CO3 ; NDUFA3 ; NDUFA8 ; NDUFA9 ; NDUFB10 ; NDUFB5 ; NDUFB9 ; NDUFS3 ; SDHB ; SLC25A5 ; UQCRFS1 ;
RNA polymerase	0.00149	POLR2C ; POLR2H ; POLR2I ; POLR3D ; POLR3GL ; ZNRD1 ;
RNA transport	0.00164	ALYREF ; DKC1 ; EIF1 ; EIF2B3 ; EIF2S2 ; EIF3F ; EIF4EBP1 ; NHP2 ; NUP93 ; POP7 ; RPP40 ; SEC13 ; SNUPN ; XPOT ;
Arginine and proline metabolism	0.00769	ALDH18A1 ; ALDH9A1 ; ASS1 ; GOT1 ; GOT2 ; SAT2 ; SRM ;
Pyruvate metabolism	0.00867	ACAT1 ; ACSS2 ; ALDH9A1 ; MDH2 ; PCK2 ; PDHA1 ;
Alzheimer`s disease	0.01002	COX7B ; ITPR3 ; MT-ATP6 ; MT-CO3 ; NDUFA3 ; NDUFA8 ; NDUFA9 ; NDUFB10 ; NDUFB5 ; NDUFB9 ; NDUFS3 ; SDHB ; UQCRFS1 ;

Table 3.15 continue…

Pathway Name	Pathway p-value (corrected)	Gene Symbols
One carbon pool by folate	0.01218	MTHFD1L ; MTHFD2 ; MTHFD2L ; SHMT2 ;
Butanoate metabolism	0.01241	ACAT1 ; ACSM3 ; HADH ; HMGCS2 ; PDHA1 ;
Alanine, aspartate and glutamate metabolism	0.01555	ASNS ; ASS1 ; GOT1 ; GOT2 ; GPT2 ;
Amino sugar and nucleotide sugar metabolism	0.0185	GMDS ; GMPPA ; GNPDA1 ; MPI ; NANS ; PGM1 ;
Valine, leucine and isoleucine biosynthesis	0.02122	IARS ; LARS ; PDHA1 ;
Cysteine and methionine metabolism	0.0239	APIP ; CBS ; GOT1 ; GOT2 ; SRM ;
Tryptophan metabolism	0.03246	ACAT1 ; ALDH9A1 ; HADH ; KMO ; WARS ;
Phenylalanine, tyrosine and tryptophan biosynthesis	0.03288	GOT1 ; GOT2 ;
Pyrimidine metabolism	0.03355	DHODH ; PNP ; POLR2C ; POLR2H ; POLR2I ; POLR3D ; POLR3GL ; ZNRD1 ;
Terpenoid backbone biosynthesis	0.03542	ACAT1 ; DHDDS ; HMGCS2 ;
Glycolysis / Gluconeogenesis	0.04286	ACSS2 ; AKR1A1 ; ALDH9A1 ; PCK2 ; PDHA1 ; PGM1
Other glycan degradation	0.04369	AGA ; FUCA2 ; GLB1 ;
Glycine, serine and threonine metabolism	0.04749	CBS ; PHGDH ; PSPH ; SHMT2 ;
Glyoxylate and dicarboxylate metabolism	0.04861	ACAT1 ; ACO2 ; MDH2 ;

Table 3.15. ORP-P pathways for genes induced in all the resistant models (≥1.2 fold changes & $p \leq 0.05$) identified as significant using Innatedb analysis. Significance of the pathway after Innatedb analysis (Hypergeometric algorithm with *Benjamini & Hochberg post hoc* correction) and associated gene IDs for each pathway are provided.

3.2.2.5 Functional classification of the shared induced metabolic genes (N=89) derived from the model panel indicates mitochondrial TCA and oxidiative phosphorylation pathway enrichment in resistance

Since it may have a bearing on proliferation of the resistant models, the most significant pathway comprising shared induced genes, metabolic pathways, was further investigated for detailed biological functions using the functional classification tool in DAVID bioinformatics. ENSEMBL gene IDs for the 89 induced metabolic probe IDs (gene set from metabolic pathway, Table 3.15) shared by all resistant lines were subsequently uploaded into the DAVID functional classification tool to categorize functionally-similar genes in the same cluster. This generated an enrichment score for each cluster in order to begin to better- define if there was enrichment of particular metabolic pathways. For this approach, a medium stringency classification was applied in the tool to allow enough genes to pass the functional classification

algorithm. The clustering algorithm was based on kappa calculation www.david.ncifcrf.gov/helps/functional_classification). Similarity term overlap which shows the minimum number of annotation overlaps between two genes was adjusted in the tool to 4 in order to qualify for the kappa calculation. Similarity threshold value, which determines the minimum kappa value with significant biological function, was set in the tool to 0.35 and multi-linkage threshold was considered as 50% so as to control how groups merge each other (higher percentage gives sharper separation between genes in each group OR it results in more tightly associated genes in each group).

Six gene clusters ("gene groups") were thus generated from the induced metabolic gene list (Table 3.15). Heatmaps for all six functional clusters were then generated within DAVID (Fig.3.8A-F). In this instance, green on the heatmap indicated a positive association of gene term with the reported biological function, whereas black indicated there was as yet no available data for association between a gene and a particular functional annotation (GO term).

The first gene cluster which had the highest enrichment score (7.8) contained N=11 ENSEMBL gene IDs coding for NADH dehydrogenase (NDUFA3, NDUFA8, NDUFA9, NDUFB5, NDUFB9, NDUFB10 and NDUFS3), ubiquinol-cytochrome c reductase (UQCRFS1), cytochrome c oxidase (MT-CO3 and COX7B) and ATP synthase subunits (MT-ATP6). Scanning the GO ontologies used to cluster these genes (Fig 3.8A) revealed such genes are associated with electron transport chain and oxidative phosphorylation in the mitochondrial inner membrane which are key for ATP synthesis (Fig 3.8A, Table 3.16). Deregulation of genes in oxidative phosphorylation were also associated with Alzheimer's, Parkinson's and Huntington diseases.

The second cluster with a 6.5 enrichment score contained N=4 ENSEMBL gene IDs coding for TCA cycle enzymes (ACO2, IDH3B, MDH2 and FH) which cumulatively are associated with generation of precursor metabolites and energy, acetyl CoA catabolic process, TCA cycle in the mitochondrial matrix (Fig 3.8B, Table 3.16).

The third cluster had a much smaller 2.2 enrichment score and contained N=4 ENSEMBL gene IDs coding for choline phosphotransferase 1 (CHPT1), 1-acylglycerol-3-phosphate O-acyltransferase 6(AGPAT6), selenoprotein 1 (EPT1; SELI) and phosphatidyl serine synthase 1 (PTDSS1) which cumulatively are associated with the lipid/phospholipid biosynthesis process and the organophosphate metabolic process for membrane biosynthesis (Fig 3.8C, Table 3.16).

The fourth cluster was also more minor, with a 1.7 enrichment score, again contained N=4 ENSEMBL gene IDs coding for phosphatidylinositol glycan anchor biosynthesis class O (PIGO), STT3 subunit of oligosaccharyl transferase complex (STT3A), exostoses (EXT2) and asparagine-

linked glycosylation 3 (ALG3) which are associated with glycan biosynthesis on the smooth endoplasmic reticulum and glycoprotein synthesis for the membrane (Fig 3.8D, Table 3.16).

The fifth cluster with a modest 1.6 enrichment score contained N=4 ENSEMBL gene IDs coding for RNA polymerase polypeptides (POLR2C, POLR3D, POLR2H and POLR2I). RNA polymerase is associated with RNA polymerization in the nucleus (Fig 3.8E, Table 3.16). The last cluster with a lower 1.5 enrichment score contained N=4 ENSEMBL gene IDs coding for GalNAc-T6/12/14 and galactosyltransferase 1 (GALNT6, GALNT12, GALNT14 & B4GALT7) which are associated with cation/ion binding, glycan biosynthesis and carbohydrate binding in the Golgi apparatus for membrane biosynthesis (Fig 3.8F, Table.3.16).

The functional clustering results (Table 3.16) and superior enrichment scores for the induced genes as well as the ORA-O (small molecule metabolic process for biological process (Table 3.12) and mitochondrion for cellular components (Table 3.10)) and ORA-P pathway (Table 3.15) data described above show oxidative phosphorylation and also TCA cycle as being particularly prominent metabolic pathways induced in all endocrine resistant models and so worthy of further study in the thesis.

Gene Group 1 Enrichment Score: 7.775500074815822
NADH dehydrogenase (ubiquinone) 1 alpha subcomplex, 9, 39kDa, NDUFA9
NADH dehydrogenase (ubiquinone) 1 beta subcomplex, 10, 22kDa, NDUFB10
cytochrome c oxidase subunit VIIb, COX7B
Cytochrome c oxidase subunit 3; ATP synthase protein 6, MT-CO3/MT-ATP6
ubiquinol-cytochrome c reductase, Rieske iron-sulfur polypeptide-like 1; ubiquinol-cytochrome c reductase, Rieske iron-sulfur polypeptide 1, UQCRFS1
NADH dehydrogenase (ubiquinone) Fe-S protein 3, 30kDa (NADH-coenzyme Q reductase), NDUFS3
NADH dehydrogenase (ubiquinone) 1 beta subcomplex, 5, 16kDa,NDUFB5
NADH dehydrogenase (ubiquinone) 1 alpha subcomplex, 3, 9kDa, NDUFA3
NADH dehydrogenase (ubiquinone) 1 alpha subcomplex, 8, 19kDa, NDUFA8
NADH dehydrogenase (ubiquinone) 1 beta subcomplex, 9, 22kDa, NDUFB9

Gene Group 2 Enrichment Score: 6.4840484090748545
aconitase 2, mitochondrial, ACO2
isocitrate dehydrogenase 3 (NAD+) beta, IDH3B
malate dehydrogenase 2, NAD (mitochondrial), MDH2
fumarate hydratase, FH

Gene Group 3 Enrichment Score: 2.1816262647358857
choline phosphotransferase 1, CHPT1
1-acylglycerol-3-phosphate O-acyltransferase 6 (lysophosphatidic acid acyltransferase, zeta), AGPAT6
selenoprotein I (EPT1; SELI)
phosphatidylserine synthase 1 (PTDSS1)

Gene Group 4 Enrichment Score: 1.729008004783438
phosphatidylinositol glycan anchor biosynthesis, class O, PIGO
STT3 subunit of the oligosaccharyltransferase complex, homolog A (S. cerevisiae), STT3A
exostoses (multiple) 2, EXT2
asparagine-linked glycosylation 3, alpha-1,3-mannosyltransferase homolog (S. cerevisiae), ALG3

Gene Group 5 Enrichment Score: 1.6230681621948058
polymerase (RNA) III (DNA directed) polypeptide D, 44kDa, POLR3D
polymerase (RNA) II (DNA directed) polypeptide C, 33kDa, PLR2C
polymerase (RNA) II (DNA directed) polypeptide H, POLR2H
polymerase (RNA) II (DNA directed) polypeptide I, 14.5kDa, POLR2I

Gene Group 6 Enrichment Score: 1.5881664068745822
UDP-N-acetyl-alpha-D-galactosamine:polypeptide N-acetylgalactosaminyltransferase 6 (GalNAc-T6), GALNT6
UDP-N-acetyl-alpha-D-galactosamine:polypeptide N-acetylgalactosaminyltransferase 12 (GalNAc-T12), GALNT12
xylosylprotein beta 1,4-galactosyltransferase, polypeptide 7 (galactosyltransferase I), B4GALT7
UDP-N-acetyl-alpha-D-galactosamine:polypeptide N-acetylgalactosaminyltransferase 14 (GalNAc-T14), GALNT14

Table 3.16. Functional classification and associated enrichment scores were generated using the functional classification tool within the DAVID bioinformatics resource for shared induced metabolic genes in resistant models.

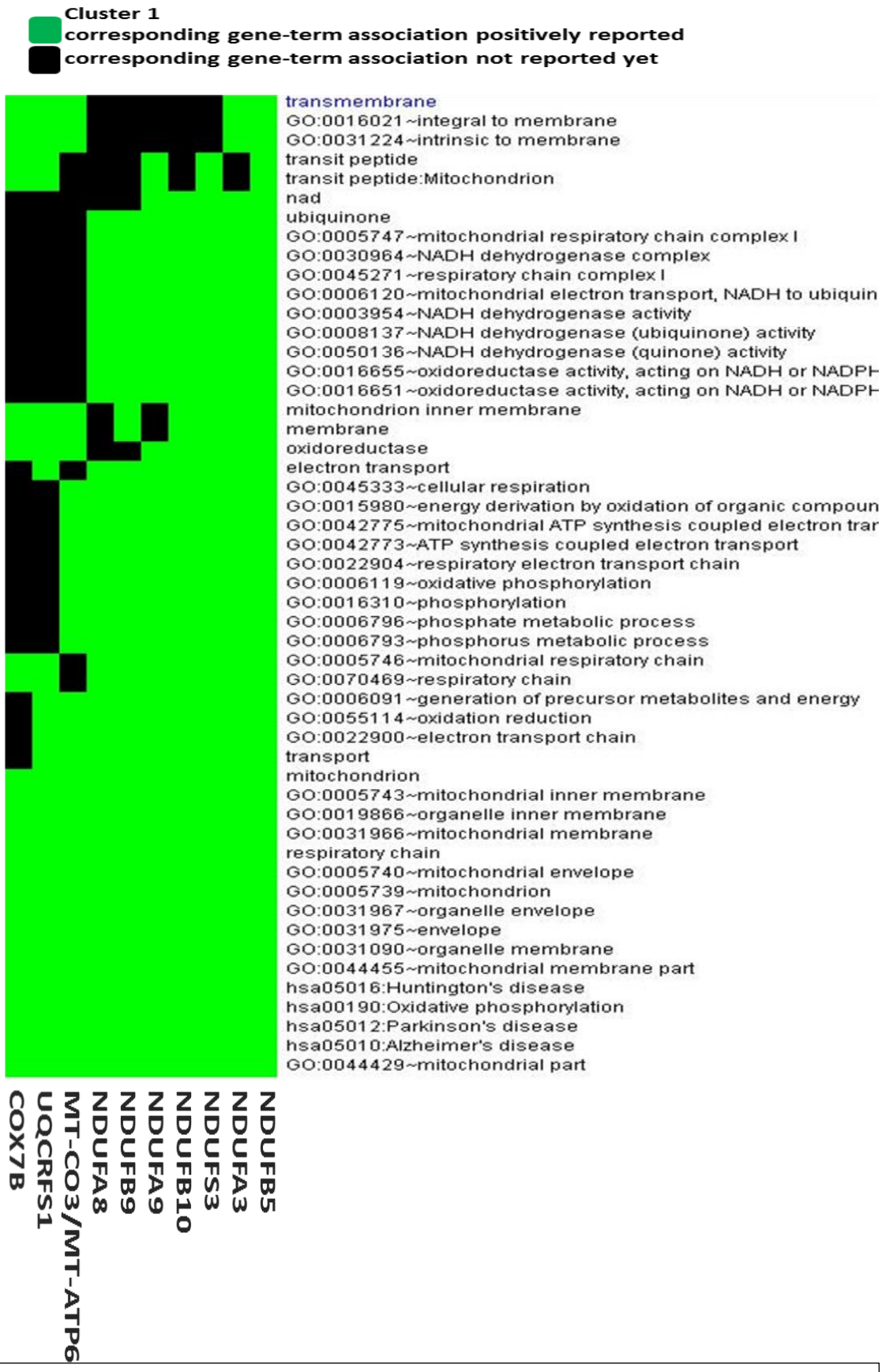

Fig 3.8. (A) Heatmap representing cluster 1 following functional classification analysis using DAVID bioinformatics tool. The cluster had an enrichment score of 7.8 and includes genes associated with electron transport chain and oxidative phosphorylation in the mitochondria as indicated by the gene ontology (GO) terms.

Fig 3.8. (B) Heatmap representing cluster 2 following functional classification analysis using DAVID bioinformatics tool. The cluster had an enrichment score of 6.5 and includes genes associated with TCA cycle, acetyl CoA catabolic process, generation of precursor metabolites and energy in the mitochondria as indicated by the GO terms.

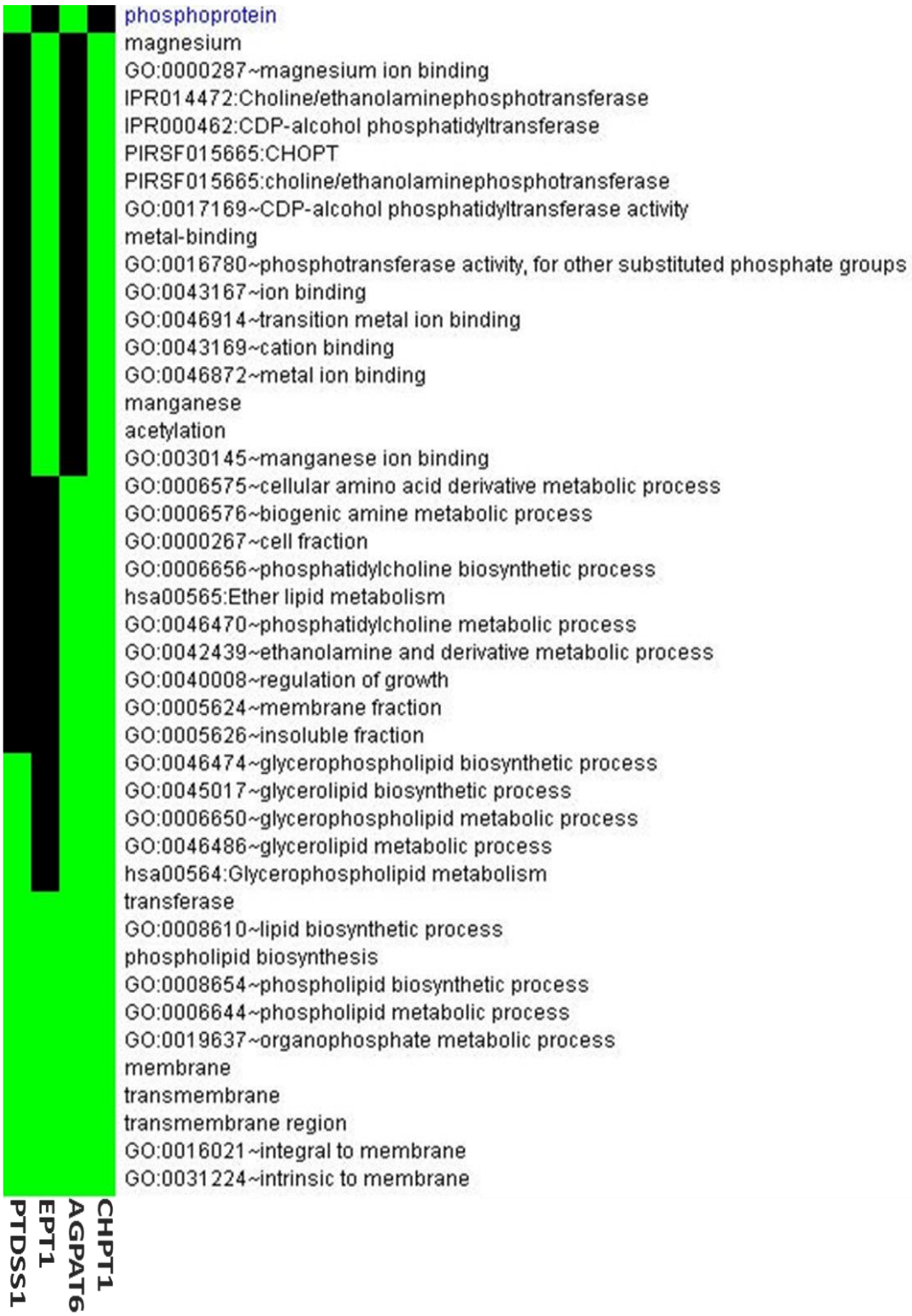

Fig 3.8. (C) Heatmap representing cluster 3 following functional classification analysis using DAVID bioinformatics tool. The cluster had an enrichment score of 2.2 and includes genes associated with lipid/phospholipid biosynthesis process and organophosphate metabolic process integral to the membrane as indicated by the GO terms.

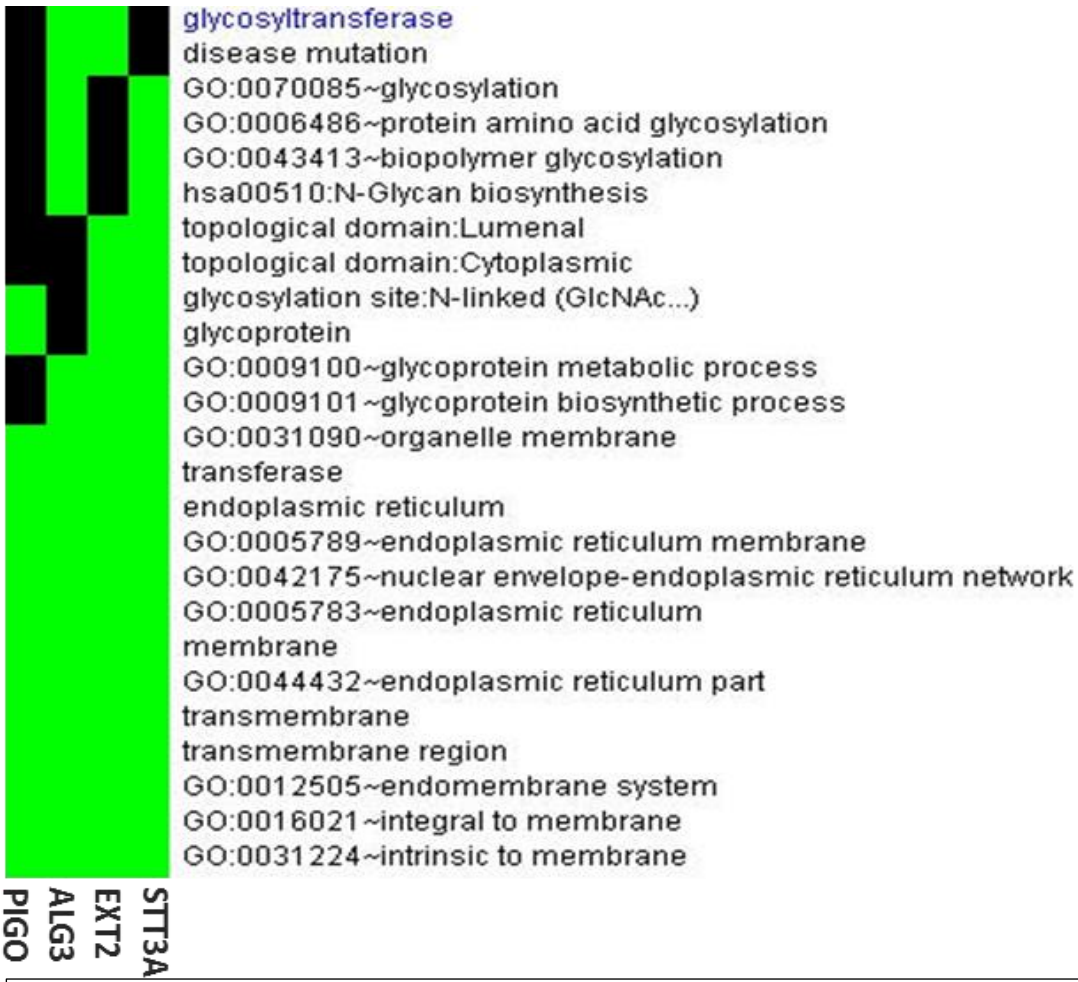

Fig 3.8. (D) Heatmap representing cluster 4 following functional classification analysis using DAVID bioinformatics tool. The cluster had an enrichment score of 1.7 and includes genes associated with glycan biosynthesis and glycoprotein synthesis on the endoplasmic reticulum membrane as indicated by the GO terms

Fig 3.8. (E) Heatmap representing cluster 5 following functional classification analysis using DAVID bioinformatics tool. The cluster had an enrichment score of 1.6 and includes genes associated with RNA biosynthesis and transcription process in the nucleus as indicated by the GO terms

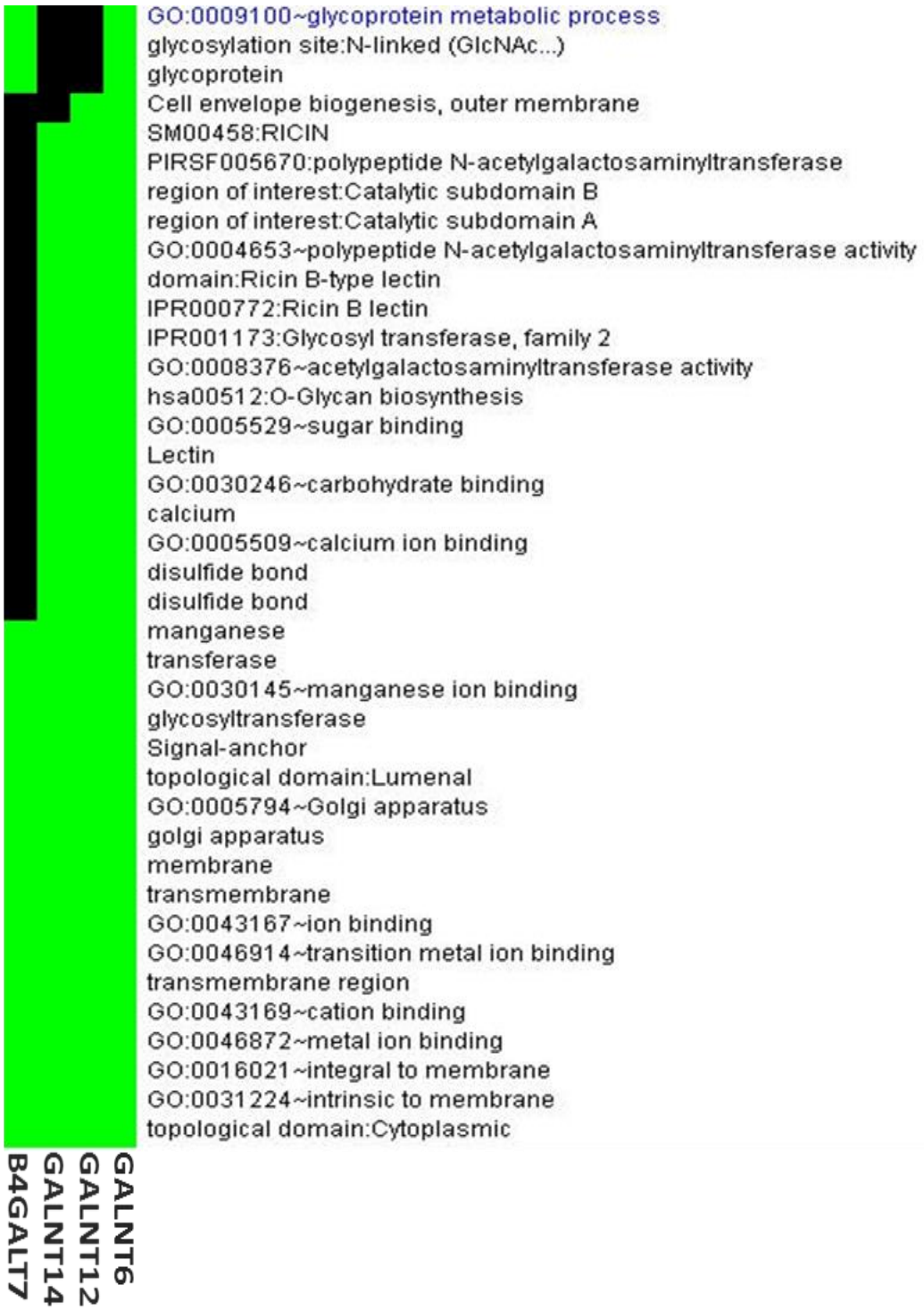

Fig 3.8. (F) Heatmap representing cluster 6 following functional classification analysis using DAVID bioinformatics tool. The cluster had an enrichment score of 1.5 and includes genes associated with glycan biosynthesis and carbohydrate binding in the Golgi apparatus as indicated by the GO terms

3.2.3 Ontology and pathway analysis of induced genes following initial endocrine treatment compared with resistance using U133A arrays

A series of Affymetrix U133A gene arrays was subsequently examined to address whether early endocrine treatment of MCF7 cells induced gene changes that are then retained in the AH resistant panel, with a particular focus being the candidate resistance pathways TCA/OxPhos, or whether such induced gene events are only found once acquired resistance developed in the model panel. This was achieved by (i) cataloguing the over-represented ontologies and pathways during initial endocrine treatment of MCF7 cells; (ii) comprehensively-detailing whether cellular metabolic pathways with induced genes, including TCA and OxPhos, are different in the resistant lines compared with those induced by initial endocrine treatment of MCF7 cells.

For these studies, the control for the endocrine treated panel comprised MCF7 cells grown in phenol red-free RPMI1640 supplemented with 4mM glutamine, 5% charcoal-stripped foetal calf serum (SFCS) and 10^{-9}M oestradiol (E2) treatment. Endocrine treatments which are growth inhibitory in responsive MCF7 cells then comprised (i) removal of E2 using SFCS or using heat deactivated SFCS (HSFCS, the condition used to deprive E2 for the MCF7(X) and MCF7(X)LT lines), (ii) treating with either tamoxifen (10^{-7}M) or (iii) treating with fulvestrant (10^{-7}M). All cells were grown for 10 days in treatment prior to mRNA extraction for microarray analysis. This response array data were then subjected to transcriptional analysis (using Genesifter) to identify significantly induced genes (≥1.2 fold change) as compared to the control cells (MCF7+E2).

3.2.3.1 Over-represented ontologies and pathways during initial endocrine treatment

In total 551 shared genes were significantly induced across the four endocrine treatments as compared to the control cells. “Lysosome pathway” was the only significantly induced pathway (p=0.031) shared by the endocrine-treated cells (Table 3.17). Based on ontology analysis of the shared induced genes, extracellular vesicular exosome (for cellular component ontology), aldehyde dehydrogenase (NAD) activity (for molecular function ontology) and small molecule metabolic process (for biological process ontology) were significantly induced across the panel (Table 3.18-3.20). Small molecule metabolic process (for biological process ontology) for the endocrine treated panel were associated with lipid metabolism (ACAA1, ACACB, CERK, NEU1, SGPL1, SMPD1, ACHE, CDS2, PGS1, ALDH7A1 and ALDH9A1), amino acid metabolism (ALDH4A1, ALDH6A1, ALDH7A1, ALDH9A1, ALDH1A3, AOX1, BCKDHB, AASS, GCDH, ARG2 and COMT), phosphate pentose pathway (PRPS1 and PRSS3) and inositolphosphate metabolism (INPP4A and INPP5A) (Table 3.19). However, the induced small molecule metabolic process in the resistant panel was broadly associated with mitochondrial metabolic processes including pyruvate

metabolism (PDHA1), TCA cycle (ACO2, IDH1, IDH3B, SDHB, FH and MDH2) and oxidative phosphorylation (NDUFA3, NDUFA7, NDUFA8, NDUFA9, NDUFB5, NDUFB9, NDUFB10, NDUFS3, COX7B and UQCRFS1) (Table 3.12). For biological processes in the endocrine treated panel, positive regulation of intrinsic apoptotic signalling pathway was also significant (*p*=0.038), which may be associated with the initial growth inhibitory effect of endocrine treatment in ER+ cells such as MCF7. In conclusion, induced mitochondrial pathways (TCA cycle and OxPhos) did not appear to be implicated during endocrine response from ORP-O ontology and pathway analysis.

Pathway Name	Pathway p-value (corrected)	Gene Symbols
Lysosome	0.031079	CTNS; CTSH; CTSL1; CTSZ; ENTPD4; FUCA1; GUSB; LIPA; NEU1; NPC2; PPT1; SLC11A2; SMPD1;

Table 3.17. Over-represented pathway analysis for shared induced genes (≥1.2 fold changes) across the MCF7 panel treated with endocrine agents for 10 days. Lysosome pathway was the only significantly induced pathway in the endocrine treated cells as compared to oestradiol treated control (Innatedb/KEGG).

GO term Name (Molecular_Function)	GO term p-value (corrected)	Gene Symbols
aldehyde dehydrogenase (NAD) activity	0.027018	ALDH1A3; ALDH4A1; ALDH7A1; ALDH9A1;
protein heterodimerization activity	0.027215	ABCG1; ARNT2; BCL2L1; BDKRB2; BIK; EPAS1; ERBB2; FZD4; HIST1H4C; HIST1H4H; HIST1H4J; HIST4H4; LIMK2; MID1; MID2; NR4A1; NR4A2; PBX1; PEF1; PPP3CA; RRAGA; RXRA; SIM1; TYR; UGT1A6; ZHX2;
oxidoreductase activity	0.041686	AASS; ADI1; AKR1C3; ALDH1A3; ALDH3B1; ALDH4A1; ALDH6A1; ALDH7A1; ALDH9A1; AOX1; BDH2; DCXR; DHCR24; DHRS3; GFOD2; GSR; NDOR1; NQO1; TYR; WWOX;

Table 3.18. Over represented ontology analysis for shared induced genes (≥1.2 fold changes) across the MCF7 panel treated with endocrine agents. GO term associated with aldehyde dehydrogenase (NAD) activity was the most significantly induced molecular function in endocrine responsive cells as compared to oestradiol treated control (Innatedb).

GO term Name (Cellular_component)	GO term p-value (corrected)	Gene Symbols
extracellular vesicular exosome	0.000117	ACOT2; AKR1C3; ALAD; ALDH3B1; ALDH6A1; ALDH7A1; ALDH9A1; ANXA9; AOX1; APLP2; BASP1; BDH2; BID; CADM4; CAMK4; CAPN5; CLU; COMT; CPQ; CST6; CTDSP1; CTNS; CTSH; CTSL1; CTSZ; CXCR4; CYB5A; CYFIP2; DAB2; DAG1; DCXR; DDR1; DOCK2; DOPEY2; DSTN; DUSP3; EFNA1; EPN3; ERAP1; FAM125B; FBP1; FN1; FUCA1; FZD4; GALNT2; GLG1; GPRC5A; GPRC5C; GSR; GUSB; GYG1; HEBP2; HIST1H4C; HIST1H4H; HIST1H4J; HIST4H4; HLA-DRB1; IGFBP3; INPP5A; LIN7A; LIPA; LXN; MARCKSL1; MID2; MYO1B; NEU1; NPC2; NQO1; PDCD2; PDGFC; PEBP1; PEF1; PEPD; PFN2; PITPNA; PLXNB2; PPL; PPT1; PRKCD; PRSS3; PTPRG; RAB15; REEP5; RFTN1; RND3; SH3BGRL; SH3BP4; SHROOM2; SLC12A2; SLC20A2; SLIT2; SMPD1; SORL1; SRP14; ST3GAL4; TAX1BP3; TMEM59; TMPRSS2; TSPAN6; UGT1A6; UPK1A; UPK2; UPK3A; URM1; UXS1; VAMP8;
lysosome	0.002273	CPQ; CTNS; CTSH; CTSL1; CTSZ; CXCR4; DRAM1; FUCA1; GUSB; LIPA; NEU1; NPC2; PLBD1; PPT1; RRAGA; SLC11A2; TMEM59; TMEM97; TYR;
Golgi apparatus	0.019156	ABCG1; ACHE; ADI1; ATP8A2; B4GALT7; BACE2; CPQ; CTGF; DUSP10; FGFR2; FUT9; GABARAPL1; GALNT2; GLG1; GLYR1; GORASP1; GPR143; IMPAD1; JAKMIP2; KIF1C; LMAN2L; MLANA; MPPE1; MTUS1; NEDD9; OBSL1; PMEL; PPT1; PSEN1; RAB20; RRAGA; SORL1; ST3GAL4; TFAP2A; TGOLN2; UNC13B; UST; WDR77; WWOX; ZDHHC7;
cytoplasm	0.033399	ADI1; AGAP1; AKR1C3; ALDH1A3; ALDH3B1; ALDH7A1; ALDH9A1; AMPH; ARHGEF10L; ARHGEF11; ARHGEF40; ARL14; ARNT2; BAG1; BAMBI; BASP1; BATF; BBS1; BCAS3; BCL2L1; BCL3; BDH2; BID; C7orf49; CAMK1; CAMK4; CAPN5; CASP9; CDH3; CITED2; CLMN; CLU; CPQ; CTNND2; CXCR4; CYFIP2; DAB2; DAG1; DHCR24; DRAM1; DSTN; DUSP10; EHD3; EIF2C1; ELF3; ELF5; ENSA; EPAS1; ERAP1; ERBB2; ERC1; ERCC2; FAM110B; FARP1; FBP1; FBXL15; FGF13; FGFR2; FUCA1; FZD2; FZD4; GABARAPL1; GABBR2; GLYR1; GPR143; HCFC1R1; HEBP2; HES1; HEXIM1; HOXC11; IER2; ITPR1; KANK1; KIAA0513; KPNA6; LANCL2; LARP4B; LIMA1; LIMK2; LMCD1; LXN; MARCKSL1; MECP2; MID1; MID2; MOAP1; MPRIP; MYO16; MYO1B; NDOR1; NEDD9; NFATC3; NPAS2; NQO1; NR1I3; NR3C1; NR4A1; NR4A2; NREP; NUAK1; OBSL1; PAK2; PBX1; PDCD2; PDGFC; PEBP1; PEF1; PFDN4; PFN2; PITPNA; PLEKHB1; PLEKHO1; PPP3CA; PRKCD; PRKCQ; PRUNE; PXN; RAB15; RABEP2; RAP1GAP2; RBM19; RFTN1; RIPK4; RPRM; RRAGA; SGCG; SH3BGRL; SH3BP4; SH3BP5; SHROOM2; SIK1; SIPA1L1; SIVA1; SLC11A2; SLIT2; SMAD6; SMYD2; SNRNP25; SRP14; SSH1; STXBP6; TACC1; TAX1BP3; TCF7L2; TFAP2A; TLE1; TNS3; TRIM16L; TRIM3; TSC22D3; TUFT1; TYR; UNC13B; UPP1; URM1; WDR77; WWC1; WWOX; ZFHX3; ZFP36L2; ZHX2; ZMIZ1; ZNF394;
transcription factor complex	0.034433	ARNT2; EPAS1; GATA6; HOXD12; MSX2; MTA2; NPAS2; NR4A1; PARP1; PBX1; PMF1; SMAD6; TBX2; TCF7L2; TLE1; ZFHX3;

Table 3.19. Over represented ontology analysis for shared induced genes (≥1.2 fold changes) across the MCF7 panel treated with endocrine agents. GO term associated with extracellular vesicular exosome was the most significantly induced cellular component in endocrine responsive cells as compared to oestradiol treated control (Innatedb).

GO term Name (Biological_Process)	GO term p-value (corrected)	Gene Symbols
small molecule metabolic process	0.000115	AASS; ABCC5; ABCG1; ABCG2; ACAA1; ACACB; ACHE; ADI1; AKR1C3; ALAD; ALDH4A1; ALDH6A1; ALDH7A1; ALDH9A1; AOX1; ARG2; B4GALT7; BCKDHB; CDS2; CERK; CIAO1; COMT; COQ2; COX7C; CPT1A; CSGALNACT1; CTGF; CYB5A; CYP3A7; CYP4B1; DHCR24; DIO1; ERCC2; FBP1; GCDH; GSR; GUSB; GYG1; HK2; HS3ST1; INPP4A; INPP5A; ITPR1; LPIN2; MTMR4; NAT1; NDOR1; NDST1; NDUFB2; NEU1; NPAS2; NQO1; NUDT4; PGS1; PIK3C2B; PIK3R3; PLBD1; PPP1R3C; PRPS1; PRSS3; RXRA; SGPL1; SLC19A3; SLC25A4; SLC5A6; SMPD1; ST3GAL4; TPK1; UGT1A6; UPP1; UROS; UST;
epithelial cell differentiation	0.01689	BDH2; CBFA2T2; CPT1A; ELF3; FGFR2; FZD2; GATA6; UPK1A; UPK2; UPK3A;
outflow tract morphogenesis	0.026938	CITED2; DHRS3; FZD2; HES1; MSX2; TBX2; TFAP2A;
metabolic process	0.027704	ABHD4; ACAA1; ACACB; ACHE; ALDH1A3; ALDH3B1; ALDH4A1; ALDH6A1; ALDH7A1; ALDH9A1; ATP2A3; ATP6V0E1; ATP6V0E2; ATP8A2; BCKDHB; BDH2; BDKRB2; CERK; COQ2; CPQ; CPT1A; DCXR; DHRS3; ENTPD3; ENTPD4; GALNT10; GCAT; GCDH; GYG1; KIF1C; KIF3C; LANCL2; MID1; MPPE1; MYO16; MYO1B; NAT1; NDST1; NEU1; NUAK1; NUDT4; OXSM; PEPD; PGS1; PIGG; PRUNE; SGPL1; SMARCE1; SMPD1; TYR; UBE2D4; UGT1A6; WWOX;
membrane protein ectodomain proteolysis	0.02882	BACE2; DAG1; ERAP1; PRKCQ; PSEN1;
post-embryonic development	0.030233	ERCC2; FGFR2; IMPAD1; ITPR1; MECP2; NR4A2; PLAGL2; PSEN1; SGPL1; TCF7L2;
negative regulation of transcription, DNA-templated	0.032937	AC005280; BASP1; BCL3; CBFA2T2; CITED2; DAB2; ELF3; GATA6; HES1; HEXIM1; LANCL2; MECP2; MSX2; MTA2; NKX3-1; NR1I3; NR2F2; OVOL2; SMARCE1; TBX2; TCF7L2; TFAP2A; TLE1; TLE2; TLE4; ZFHX3; ZHX2; ZNF12;
negative regulation of actin filament polymerization	0.035197	KANK1; PFN2; PRKCD; SLIT2;
negative regulation of organ growth	0.035197	CGA; TCF7L2; WWC1; WWC3;
positive regulation of intrinsic apoptotic signaling pathway	0.03863	BCL2L1; BID; CLU; EI24; NKX3-1; PLAGL2;
bone morphogenesis	0.038779	CITED2; DHRS3; FGFR2; GLG1; MSX2; TFAP2A;

Table 3.20. Over represented ontology analysis for shared induced genes (≥1.2 fold changes) across the MCF7 panel treated with endocrine agents. GO term associated with small molecule metabolic process was the most significantly induced biological process in endocrine responsive cells as compared to oestradiol treated control (Innatedb).

3.2.3.2 Cellular metabolic pathways with induced genes in resistance compared with initial endocrine treatment

The project then focussed on more specifically-evaluating whether any shared induced metabolic genes in endocrine resistance were also commonly-induced by initial endocrine treatment. Those genes that were induced on the arrays by all the 10 day endocrine treatments in MCF7 which encode genes in metabolic pathways were identified using Innatedb database. These were compared to shared induced metabolic genes identified from the resistant panel (Table 3.15). For this detailed study, metabolic pathways were broadly subdivided to carbohydrate metabolism, energy metabolism, lipid metabolism, nucleotide metabolism, amino acid metabolism, glycan metabolism, cofactors and vitamin metabolism, xenobiotic metabolism and terpenoids/polyketides metabolism pathways to enable the comparison. Induced metabolic genes shared by all resistant cell lines and during endocrine treatment were ALDH9A1 (implicated in carbohydrate, lipid and amino acid metabolism indicated in red, Tables 3.21B, 3.23B, 3.25B and 3.26), B4GALT7, UST and GALNT12 (implicated in glycan biosynthesis indicated in red, Table 3.27B). Although further genes in some metabolic pathways were also induced in the AH treated panel they were not significant (Appendix 19). Furthermore, there was evidence that the various metabolic pathways that contained induced genes differed between the endocrine resistant and responding panel (Table 3.21-3.30). Various carbohydrate metabolic pathways were examined in resistant and AH treated panels. TCA cycle, butanoate metabolism, glyoxylate and dicarboxylate metabolism were only induced across the resistant panel but not in the AH treated panel (Table 3.21A versus Table 3.21B).

TCA cycle	Glycolysis/Gluconeogenesis	Pyruvate metabolism	Amino sugar and nucleotide sugar metabolism	Fructose and Mannose metabolism	Galactose metabolism
ACO2	ACSS2	ACAT1	GMDS	GMDS	G6PC3
FH	AKR1A1	ACSS2	GMPPA	GMPPA	GLA
IDH1	ALDH9A1	ALDH9A1	GNPDA1	MPI	GLB1
IDH3B	G6PC3	FH	MPI	PFKFB2	PGM1
MDH2	PCK2	MDH2	NANS		
PCK2	PDHA1	PCK2	PGM1		
PDHA1	PGM1	PDHA1			
SDHB					

Glyoxylate and Dicarboxylate metabolism	Butanoate metabolism	Propanoate metabolism	Pentose phosphate pathway	Pentose and Glucuronate interconversion
ACAT1	ACAT1	ACAT1	G6PD	AKR1A1
ACO2	ACSM3	ACSS2	PGM1	XYLB
MDH2	HADH			
SHMT2	HMGCS2			

Table 3.21A. Shared induced genes in the resistant panel which take part in carbohydrate metabolism pathways.

Glycolysis/Gluconeogenesis	Pyruvate metabolism	Amino sugar and nucleotide sugar metabolism	Fructose and Mannose metabolism
ALDH1A3	ACACB	HK2	FBP1
ALDH7A1	ALDH7A1	UXS1	HK2
ALDH9A1	ALDH9A1		
BPGM			
FBP1			
HK2			

Propanoate metabolism	Pentose and Glucuronate interconversion	Pentose phosphate pathway
ACACB	DCXR	FBP1
ALDH6A1	GUSB	PRPS1
ALDH7A1	UGT1A6	
ALDH9A1		

Table 3.21B. Shared induced genes in endocrine treated MCF7 cells which take part in particular carbohydrate metabolism pathways. ALDH9A1 (highlighted in red) induced in this category that overlaps with resistance (see Table 3.21A). Of note there was no evidence of TCA cycle gene induction in the endocrine treated cells.

While some components of oxidative phosphorylation for energy metabolism were induced in the AH treated and resistant panels, the gene identities were always non-overlapping. Of note, only 2 OxPhos genes were induced in AH treated cells compared to 13 in resistant lines (Table. 3.22).

Several genes which were related to ether lipid metabolism, arachidonic acid metabolism, synthesis and degradation of ketone bodies, fatty acid degradation and fatty acid elongation in metabolism of fatty acids were only induced across the resistant panel but not the AH treated panel (Table. 3.23A), with fewer overall changes in such pathways during initial treatment (Table 3.23B). Some components of nucleotide metabolism including purine/pyrimidine metabolism were induced in both responsive and AH treated panels but again the gene identities were not overlapped and there were fewer changes in the endocrine treated MCF7 cells (Table 3.24).

Oxidative Phosphorylation	Oxidative Phosphorylation
NDUFA3	NDUFS3
NDUFA7	SDHB
NDUFA8	COX7B
NDUFA9	UQCRFS1
NDUFB5	ATP5J2
NDUFB9	PPA2
NDUFB10	

Oxidative Phosphorylation
NDUFB2
COX7C

Table 3.22. Shared induced genes in the resistant lines (left table) compared with those shared in endocrine treated MCF7 cells (right table) which take part in mitochondrial energy metabolism. Note: NDUFA3 and ATP5J2 are manually curated shared induced genes in all resistant cells.

Glycerophospholipid metabolism	Glycerolipid metabolism	Fatty acids degradation	Fatty acids elongation	Ether lipid metabolism	Sphingolipid metabolism	synthesis and degradation of ketone bodies	Arachidonic acid metabolism
AGPAT6	AGPAT6	ACAT1	ELOVL1	CHPT1	GLA	ACAT1	EPHX2
CHPT1	AKR1A1	ACSL4	ELOVL4	EPT1	GLB1	HMGCS2	PLA2G12A
EPT1	ALDH9A1	ALDH9A1	HADH	PLA2G12A	UGT8		
PLA2G12A	GLA	HADH					
PTDSS1							

Table 3.23A. Shared induced genes in the resistant panel which take part in lipid metabolism.

Sphingolipid metabolism	Glycerophospholipid metabolism	Glycerolipid metabolism
CERK	ACHE	ALDH7A1
NEU1	CDS2	ALDH9A1
SGPL1	PGS1	
SMPD1		

Table 3.23B. Shared induced genes in endocrine treated MCF7 cells which take part in lipid metabolism. ALDH9A1 (highlighted in red) is induced in this category and overlaps with resistance (see Table 3.23A)

Purine metabolism	Pyrimidine metabolism
HDDC3	DHODH
PGM1	PNP
PNP	POLR2C
POLR2C	POLR2H
POLR2H	POLR2I
POLR2I	POLR3D
POLR3D	POLR3GL
POLR3GL	ZNRD1
ZNRD1	

Purine metabolism	Pyrimidine metabolism
ENTPD3	ENTPD3
ENTPD4	ENTPD4
PRPS1	UPP1
PRUNE	

Table 3.24. Shared induced genes in the resistant lines (left table) compared with those shared in endocrine treated MCF7 cells (right table) which take part in nucleotide metabolism.

Expression of different genes involved in amino acid metabolism was also induced in both the resistant and AH treated cells. Thus, genes in tryptophan metabolism, cysteine and methionine metabolism, alanine, aspartate and glutamate metabolism, and phenylalanine metabolism were only induced across the resistant panel (Table 3.25A) compared with responding cells (Table 3.25B). Expression of different genes for valine, leucine and isoleucine degradation, arginine and proline metabolism, lysine degradation, tyrosine metabolism, glycine, serine and threonine metabolism were induced in resistant and AH treated models (Fig 3.25A-3.25B), with only ALDH9A1 implicated as a shared gene in many of these metabolic pathways. Moreover, gene expression for metabolism of other amino acids including beta-alanine metabolism (which again included ALDH9A1) were induced in both resistant and AH treated panels but induced glutathione metabolism genes were only detected in the resistant lines (Table 3.26).

Arginine and proline metabolism	Cystein and methionine metabolism	Alanine, asparate and glutamate metabolism	Glycine, serine and threonine metabolism	Tryptophan metabolism
ALDH18A1	APIP	ASNS	CBS	ACAT1
ALDH9A1	CBS	ASS1	PHGDH	ALDH9A1
ASS1	GOT1	GOT1	PSPH	HADH
GOT1	GOT2	GOT2	SHMT2	KMO
GOT2	MDH2	GPT2		
SAT2	SRM			
SRM				

Valine, leucine and isoleucine degradation	Lysine degradation	Tyrosine metabolism	Phenylalanine metabolism	Phenylalanine, tyrosine and tryptophan biosynthesis
ACAT1	ACAT1	GOT1	GOT1	GOT1
ALDH9A1	ALDH9A1	GOT2	GOT2	GOT2
HADH	HADH	TYRP1		
HMGCS2				

Table 3.25A. Shared induced genes in the resistant panel which take part in amino acid metabolism.

Valine, leucine and isoleucine degradation	Arginine and proline metabolism	Lysine degradation	Tyrosine metabolism	Glycine, serine and threonine metabolism	Tryptophan metabolism
ACAA1	ALDH4A1	AASS	ALDH1A3	ALDH7A1	ALDH7A1
ALDH6A1	ALDH7A1	ALDH7A1	AOX1	GCAT	ALDH9A1
ALDH7A1	ALDH9A1	ALDH9A1	COMT		AOX1
ALDH9A1	ARG2	GCDH	TYR		GCDH
AOX1					
BCKDHB					

Table 3.25B. Shared induced genes in the endocrine treated MCF7 panel which take part in amino acid metabolism. ALDH9A1 (highlighted in red) induced in this category that overlaps with resistance (see Table 23A).

Glutathione metabolism	beta-alanine metabolism
G6PD	ALDH9A1
GCLM	SRM
GSS	
GSTA4	
GSTO1	
IDH1	
MGST1	
SRM	
TXNDC12	

beta-alanine metabolism
ALDH7A1
ALDH9A1

Table 3.26. Shared induced genes in the resistant (left table) compared with those shared in endocrine treated MCF7 cells (right table) which take part in metabolism of other amino acids.

Components of glycan biosynthesis and metabolism including mucin type O-glycan biosynthesis, glycosaminoglycan biosynthesis and other glycan degradation were induced in both resistant and AH treated models but in general had differing identities (Table 3.27A and 3.27B). However, the expression of B4GALT7, UST and GALNT12 within such pathways was induced in both resistant and AH treated panels (Table. 3.27A and 3.27B). Genes which participate in glycosaminoglycan degradation and N-glycan biosynthesis were only induced in the resistant panel (Table 3.27A). The expression of different genes for metabolism of cofactors and vitamins including porphyrin metabolism were induced in both resistant and AH treated panels (Table. 3.28). Moreover the expression of some genes in one carbon pool by folate metabolism was only induced in the resistant panel (Table 3.28). Some components of drug/ xenobiotic metabolism (CYT P450) within xenobiotic biodegradation and metabolism pathway were induced in both resistant and AH treated panels (Table 3.29). The induction of differing genes for metabolism of terpenoids and polyketides was only seen in the resistant panel (Table 3.30).

Other glycan degradation	Mucin type O-glycan biosynthesis	Glycosaminoglycan degradation	Glycosaminoglycan biosynthesis	N-glycan biosynthesis
AGA	GALNT12	ARSB	B4GALT7	ALG3
FUCA2	GALNT14	GLB1	UST	STT3A
GLB1	GALNT6		EXT2	

Table 3.27A. Shared induced genes in the resistant panel which take part in glycan synthesis and metabolism.

Glycosaminoglycan biosynthesis	Mucin type O-glycan biosynthesis	Other glycan degradation
B4GALT7	GALNT10	FUCA1
CSGALNACT1	GALNT12	NEU1
UST	GALNT2	
HS3ST1		
NDST1		
FUT9		
ST3GAL4		

Table 3.27B. Shared induced genes in the endocrine responding MCF7 cells which take part in glycan synthesis and metabolism. Genes in red also induced in resistance.

One carbon pool by folate	Porphirin and chlorophyll metabolism
MTHFD1L	BLVRB
MTHFD2	FECH
MTHFD2L	
SHMT2	

Porphirin and chlorophyll metabolism
ALAD
GUSB
HCCS
UGT1A6
UROS

Table 3.28. Shared induced genes in the resistant lines (left table) compared with those shared in endocrine treated MCF7 cells (right table) which take part in metabolism of cofactors and vitamins.

Drug metabolism(CYT P450)	Metabolism of xenobiotics by CYT P450
GSTA4	GSTA4
GSTO1	GSTO1
MGST1	MGST1

Drug metabolism(CYT P450)	Metabolism of xenobiotics by CYT P450
ALDH1A3	AKR1C3
AOX1	ALDH1A3
CYP3A7	CYP3A7
UGT1A6	UGT1A6

Table 3.29. Shared induced genes in the resistant lines (left table) compared with those shared in endocrine treated MCF7 cells (right table) which take part in xenobiotic biodegradation and metabolism.

Terpenoid backone biosynthesis
ACAT1
DHDDS
HMGCS2

Table 3.30. Shared induced genes in the resistant panel which take part in metabolism of terpenoids and polyketides.

3.2.3.3 Profiling of the induced genes in TCA cycle and OxPhos pathways in endocrine resistance models and comparison with initial endocrine treatment of MCF7 cells

It was apparent that TCA cycle and oxidative phosphorylation were deregulated in all the acquired endocrine resistant models. In contrast, there was no evidence for induction of these pathways as a common event shared by all initial endocrine treatments in MCF7 cells. Expression of each shared induced gene (n=20) from the resistant panel involved in the TCA cycle (PDHA1, ACO2, IDH1, IDH3B, SDHB, FH, MDH2 and PCK2) and OxPhos pathways (NDUFA3, NDUFA7, NDUFA8, NDUFA9, NDUFB5, NDUFB9, NDUFB10, NDUFS3, COX7B, UQCRFS1, ATP5J2 and PPA2) (Fig 3.9-3.10, Table 3.31-3.32), was therefore detailed in the resistant lines using heatmap profiles and examining fold change. Comparison was also made for these gene profiles with endocrine-treated MCF7 cells (Fig 3.9-3.10, Table 3.32).

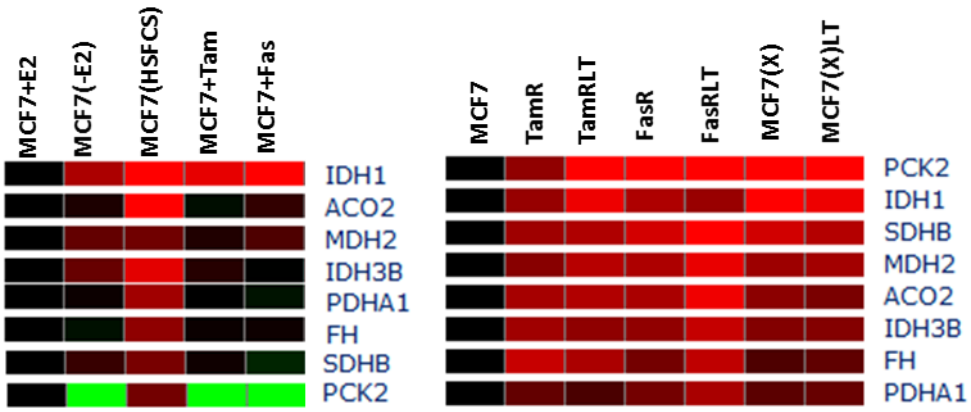

Fig 3.9. The 8 shared induced genes for the TCA cycle profiled by heatmaps in endocrine treated MCF7 (-E2 or oestrogen deprivation in HSFCS; 10^{-7}M Tamoxifen or Fulvestrant for 10 d) (left panel) and endocrine resistant cells (right panel). On the heatmap, red, green & black indicate induced, reduced & no change in gene expression respectively as compared to the E2-treated MCF7 for the AH treatment panel and control MCF7 cells for the resistant panel.

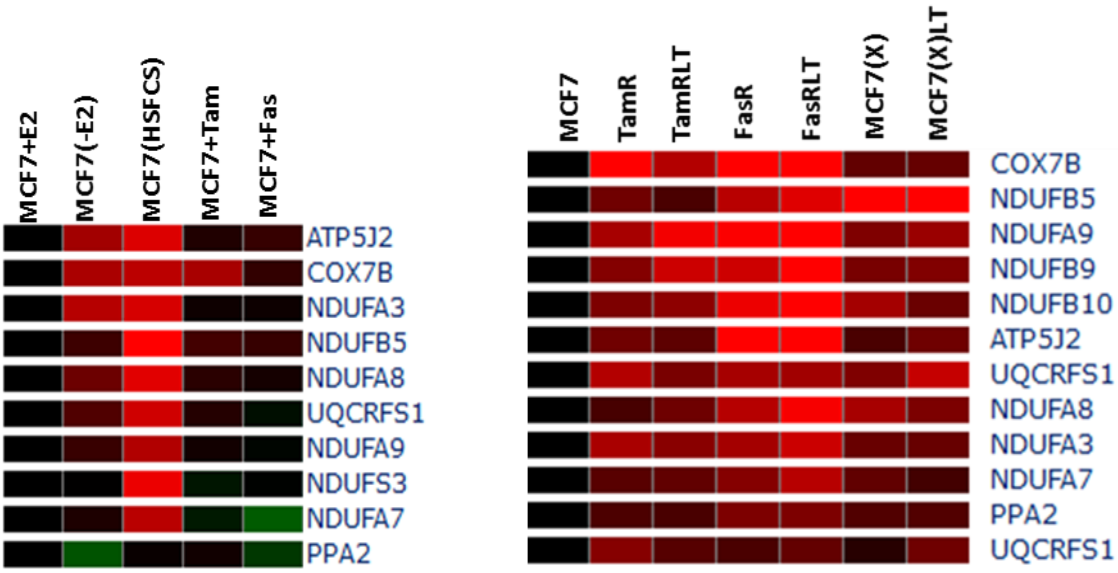

Fig 3.10. The 11 shared induced genes for the OxPhos pathway profiled by heatmaps in endocrine treated MCF7 (-E2 or oestrogen deprivation in HSFCS; 10^{-7}M Tamoxifen or Fulvestrant for 10 d) (left panel) and endocrine resistant cells (right panel). On the heatmap, red, green & black indicate induced, reduced & no change in gene expression respectively as compared to the E2-treated for the AH treatment panel and MCF7 cells for the resistant panel. Probe IDs for NDUFB9 & NDUFB10 were not found on the U133A array for the AH treated panel. Note: NDUFA3 and ATP5J2 are manually curated shared induced genes in all resistant cells.

Gene symbols	MCF7(-E2)	MCF7 (HSFCS)	MCF7 (TAM)	MCF7 (FAS)
PDHA1	1.04	1.66	1	1.06
ACO2	1.09	2.92	1.04	1.17
IDH1	1.72	2.51	2.07	2.65
IDH3B	1.38	2.04	1.13	1
SDHB	1.09	1.55	1.06	1.19
FH	1.05	1.57	1.04	1.05
MDH2	1.36	1.42	1.11	1.28
PCK2	2.41	1.44	2.91	3.91
NDUFA3	1.78	1.96	1.05	1.04
NDUFA7	1.10	1.79	1.08	1.33
NDUFA8	1.41	2.03	1.14	1.07
NDUFA9	1.19	1.75	1.06	1.02
NDUFB5	1.21	2.39	1.24	1.19
NDUFB9	———	———	———	———
NDUFB10	———	———	———	———
NDUFS3	1	2.10	1.07	1.01
COX7B	1.71	1.80	1.70	1.17
UQCRFS1	1.29	1.92	1.12	1.05
ATP5J2	1.67	1.99	1.11	1.18
PPA2	1.30	1.03	1.06	1.19

Table 3.31. Fold changes for the shared induced TCA cycle and OxPhos resistant model genes with the panel of endocrine treatments in MCF7 vs. MCF7+E2. Reduced fold changes (≤1.2) are indicated in green and induced fold changes (≥1.2) are indicated in red. Probe IDs for NDUFS3, NDUFB9 & NDUFB10 were not found on U133A microarrays.

Gene symbols	TamR	TamRLT	FasR	FasRLT	MCF7(X)	MCF7(X)LT
PDHA1	1.31	1.22	1.37	1.59	1.28	1.33
ACO2	1.57	1.62	1.59	1.92	1.47	1.4
IDH1	1.51	1.91	1.61	1.52	2.10	1.91
IDH3B	1.55	1.48	1.49	1.71	1.43	1.43
SDHB	1.54	1.61	1.78	2.06	1.77	1.63
FH	1.72	1.6	1.37	1.68	1.24	1.3
MDH2	1.45	1.65	1.6	1.89	1.53	1.56
PCK2	1.48	3.51	2.98	4.22	5.08	5.89
NDUFA3	1.58	1.45	1.56	1.74	1.33	1.32
NDUFA7	1.27	1.30	1.44	1.65	1.30	1.40
NDUFA8	1.21	1.35	1.64	1.96	1.58	1.4
NDUFA9	1.58	1.94	1.99	2.18	1.41	1.52
NDUFB5	1.36	1.23	1.65	1.83	2.25	2.56
NDUFB9	1.44	1.74	1.75	2.02	1.39	1.42
NDUFB10	1.4	1.47	1.91	2.11	1.56	1.34
NDUFS3	1.46	1.63	2.2	2.31	1.92	2
COX7B	2.3	1.63	2.23	2.02	1.31	1.32
UQCRFS1	1.63	1.39	1.57	1.55	1.42	1.71
ATP5J2	1.36	1.29	2.12	2.25	1.23	1.35
PPA2	1.23	1.22	1.41	1.41	1.25	1.25

Table 3.32. Fold changes for the shared induced TCA cycle and OxPhos genes with in resistant models vs. MCF7. Induced fold changes (≥1.2) are indicated in red. Note: NDUFA3 and ATP5J2 are manually curated shared induced genes in all resistant cells.

Table 3.31 confirms that there were very few induced (≥1.2fold) changes in expression of the TCA and OxPhos genes (n=19) during initial treatment of MCF7 cells that were shared by the multiple endocrine approaches. Only IDH1 (involved in the TCA cycle) expression appeared to be induced with all initial endocrine treatments, although increased expression of this gene did not reach significance (Table 3.31). Expression of genes in TCA cycle (PDHA1, ACO2, IDH1, IDH3B, SDHB, FH, MDH2 and PCK2) and OxPhos (NDUFA3, NDUFA7, NDUFA8, NDUFA9, NDUFB5, NDUFS3, COX7B, UQCRFS1 and ATP5J2) were induced (by ≥1.2 fold changes) with the E2-deprivation approaches (SFCS or HSFCS medium) as compared to E2 treated control MCF7 cells (Fig 3.9-3.10, Table 3.31). There were few changes in the panel that occurred with either tamoxifen (IDH1, NDUFB5 and COX7B) or fulvestrant treatment (IDH1 and MDH2) as compared to E2 treated control MCF7 cells (Fig 3.9-3.10, Table 3.31). Thus, many TCA cycle and OxPhos genes had some evidence for being oestrogen-suppressed genes (Fig 3.9-3.10, Table 3.31), and this induction was further increased on resistance development to oestrogen deprivation, since the MCF7 experimental control for the resistance panel was also maintained in charcoal stripped SFCS (Fig 3.10). Significant induction with tamoxifen and fulvestrant appeared to only occur in acquired resistance for the vast majority of TCA cycle and OxPhos pathway genes. A final further interesting observation from the U133A arrays was that the TCA cycle gene PCK2 was induced in all forms of resistance but was a suppressed gene in E2 deprived (-E2), tamoxifen and fulvestrant treated MCF7 compared with the E2-treated control (Fig 3.10, Table 3.31), indicating this gene is positively E2-regulated.

Induced genes (≥1.2 fold change) in the TCA cycle (*PDHA1, ACO2, IDH1, IDH3B, SDHB, FH, MDH2 and PCK2) and* OxPhos *p*athway (NDUFA3, NDUFA7, NDUFA8, NDUFA9, NDUFB5, NDUFS3, COX7B, UQCRFS1 and ATP5J2) were common mechanism in all resistant models, but further increased fold changes were observed in fulvestrant resistant models as compared to tamoxifen and oestrogen deprived models. Also, induced TCA cycle and OxPhos genes with higher fold changes were observed in long-term resistant models as compared to short term resistant models in each AH resistant pairs (Fig 3.9-3.10, Table 3.32).

3.3 Discussion

Targeting oestrogen/ER signalling is an effective strategy to inhibit growth of ER+ breast cancer cells, and is particularly beneficial in ER+/HER2- (luminal A) disease (Howell et al. 2008). This can be achieved by either competitively inhibiting oestrogen-promoted ER activity (tamoxifen/ fulvestrant treatment) or by suppressing oestrogen production in the body so reduced ligand is available (aromatase Inhibitor or zoladex treatment). Unfortunately, many ER+ patients who are treated with such antihormonal strategies eventually relapse at some point during or subsequent to the treatment, having acquired resistance. This can lead to more aggressive disease behaviour. Therefore, resistance to endocrine treatment remains a clinical problem (Johnston et al.2015). It is important that underlying resistance mechanisms are uncovered as this may lead to new targets for therapeutic strategies to control resistance. This chapter has described use of high throughput 1.0ST gene microarrays to discover deregulated gene expression and thereby associated pathways whose induction or suppression is shared irrespective of endocrine treatment type or duration of treatment. This has been achieved using a panel of acquired endocrine resistant models versus responsive control cells (MCF7, an established model for ER+, HER2- breast cancer). It is feasible that the identified shared pathways may comprise key resistance mechanisms.

Analysis of Coulter counting and proliferation (Ki-67) data revealed significant growth of TAMR, TAMRLT, FASR, FASRLT, MCF7(X) and MCF7(X)XLT cells despite being maintained under antihormone-treated conditions, indicating resistance had been acquired. Indeed, such studies revealed growth of all the resistant models was induced as compared to the MCF7 baseline control. Moreover, growth and proliferative capacity (Ki-67 expression) of the longer term resistant models (TamRLT and FasRLT) was further induced. Both these data indicate alternative mechanisms must have been acquired to substantially drive growth of resistant models as compared to MCF7.

Analysis of deregulated gene expression (both down/upregulated) was performed via 1.0ST gene array analysis after first testing the array performance with RT-PCR verification for HER2, ER and oestrogen/ER regulated pS2 gene expression. This profiling also served to characterise the baseline expression of key elements reflective of the luminal A (ER+/HER2-) phenotype and to gauge any marked change in ER or HER2 signalling at the mRNA level. In general, RT-PCR profiles for HER2, ER and pS2 broadly followed microarray and thus verified their appropriateness for further exploratory gene analysis. There was no substantial HER2 expression observed in the resistant models, although modest HER2 expression was detected in MCF7(X)

versus MCF7 which is compatible with a study by Martin et al. (2011) showing some induced expression of HER2 protein in long term oestrogen deprived breast cancer cells (LTED). Indeed, HER2 reduction was detected in some of the long term resistant models (TamRLT, FasRLT and MCF7(X)LT). Similarly, HER2 overexpression is not common in breast cancer patients who recur on endocrine treatment (Drury et al. 2011). These data imply relevance of the model panel for understanding mechanisms of acquired resistance from ER+/HER2- disease in this thesis. The pattern of ER expression in the models also reflects the breadth of acquired resistance clinically, since some patients retain ER, while a small proportion lose ER at relapse (Drury et al. 2011), further indicating the model panel is appropriate to define unifying novel mechanisms in acquired resistance using the 1.0ST arrays. Interestingly, ER loss appears more prevalent in the models treated with antioestrogens, particularly for fulvestrant resistance. It is feasible that the ER mRNA may perhaps be lost particularly effectively as the fulvestrant mechanism is primarily to deplete ER protein level (Osborne et al. 2004). Also, ER loss appears to be more substantial with more prolonged antioestrogen treatment (TAMRLT versus TAMR) (Bensmail et al. 2008)**.** Of note, however, ER is retained in short-term oestrogen deprived resistance (MCF7(X) (Staka et al. 2005) and increased in the long-term oestrogen deprived model (MCF7(X)LT), which is compatible with a study by Chan et al. (2002) in LTED cells. It does seem likely from these profiles that some role for ER interacting with further contributory resistance pathways will be retained where there is also some ER expression MCF7(X) (Staka et al. 2005), while in other forms of resistance where there is profound ER loss there will be a complete shift to alternative signalling mechanisms (FasR and FasRLT). pS2 profile broadly follows that of ER expression, in that it declines in all the antioestrogen resistant models, most particularly those with ER loss, which is in accordance with its reported E2/ER regulation (Osborne et al. 2004). In turn, it remains significantly expressed in the highly ER+ oestrogen deprived resistant model (Staka et al. 2005).

Having established the appropriateness of the models and the microarrays to study contributory pathways in acquired resistance, lists of statistically significant shared down/upregulated genes (by ≥1.2 fold changes, Appendix 6 and 18) obtained by the microarray analysis were used for ontology and pathway analysis. In total, 407 downregulated gene probes and 572 upregulated gene probes were shared by all resistant models (Table 3.2 and 3.9, Appendix 6 and 18). More downregulated gene probes were shared by tamoxifen and oestrogen deprived resistant models. In contrast, more upregulated gene probes were shared by fulvestrant and oestrogen deprived resistant models. This suggests that while there may be universal shared induced or suppressed mechanisms across all resistant models, there are also likely to be further genes whose changes may also be contributory according to particular antihormone type. Moreover,

there was a slightly larger number of down or upregulated gene probes shared by long-term resistant models as compared to short-term resistant models suggesting further gene changes may accumulate as the disease progresses (Table 3.2 and 3.9). Ontological analysis (ORA-O) of the shared downregulated genes revealed significant reduction of genes whose encoded proteins are associated with cell junction assembly such as cadherins (CDH3 and CDH18), integrins (ITGB1 and ITGB4) and plectin (PLEC) (Table 3.7). Cell junctions mediate passage of small molecules such as Ca^{2+}, cyclic nucleotides and inositol phosphates through cells (Donahue et al. 2003). On the arrays, expression of several cell junction-related genes which encode proteins binding to calcium ions including cadherins (CDH3 and CDH18), desmosome glycoprotein (DSC2), desmoglein (DSG2) and protocadherin (PCDH9) were significantly reduced across the resistant models (Table 3.6). Loss of cell junctions and cell-cell adhesion is also associated with breast cancer progression (Locke et al. 1998). Moreover, loss of cell adhesion has previously been reported for the TAMR cell line along with gained migratory and invasive capacity compared with the parental MCF7 model (Hiscox et al. 2006a), while the FASR line is also highly aggressive (Hiscox et al. 2006b). Reduction in expression of cell junction assembly genes may thus be an important underlying event contributing towards progression associated with endocrine resistance. According to further ontology of the shared downregulated genes, genes encoding extracellular vesicular exosome-related proteins, including integrins (ITGB1/4/6), plectin (PLEC) desmosome glycoprotein (DSC2) and desmoglein (DSG2), were also significantly reduced in the resistant models (Table 3.3). Extracellular exosome vesicles are lipid bilayer structures containing mRNAs, microRNAs, non-coding RNAs, proteins and bioactive lipids (Sato-Kuwabara et al. 2015, Valadi et al 2007 and Kim et al. 2002). Interestingly, proteomic analysis of colorectal cancer cells has recently revealed their exosomal vesicles are enriched with cell adhesion molecules, suggesting a role for reduction in exosomal vesicles in facilitating metastasis of cancer cells (Choi et al.2012). Based on the downregulated gene ontology, such events may also be important during progression in endocrine resistance. Loss of extracellular vesicular exosome related genes was more prominent in earlier resistant models, and loss of cell-cell adherens junction genes was more prominent in longer term models suggesting there may be temporal pattern of changes in genes and their associated mechanisms during progression. Also signal transduction was enriched for downregulated genes in the short term models, while cell adhesion was the most enriched downregulated category for the longer-term models: this further backs up concept of aggressive disease progression over time in endocrine resistance. Moreover, further ontologies associated with the shared downregualted genes could be relevant to resistance such as loss of certain receptor complexes (loss of IGF1R: an ER regulated gene that is an important pathway interactive with ER signalling to drive endocrine

responsive cells such as MCF7 (Dupont et al. 2001) and loss of negative regulators of growth may all reflect preferential gain of alternative signalling in resistance and mechanisms to promote resistant cell growth. Subsequent over-represented pathway analysis (ORA-P) of the shared reduced genes revealed decline in axon guidance pathway elements, including ephrins (EFNA4/5 and EFNB2), integrin (ITGB1), neuropilin (NRP1), semaphorins (SEMA3A and SEMA3C) and slit receptor (ROBO1), could also in some way comprise an important mechanism in resistant models (Table 3.7). This pathway was overrepresented for decreased genes for all antihormone resistance types, and also particularly in longer term resistant lines. Axon guidance molecules (AGMs) have been reported to not only maintain proliferation but also adhesion of cells during mammary gland development (Strickland et al. 2006), and so again loss of molecules such as EFNB2, NRP1, SEMA3A, SEMA3C and ROBO1 may contribute to loss of adhesion and thereby progression in resistance.

In contrast, over-represented ontological analysis of shared induced genes (and indeed in all resistant models) revealed genes associated with the mitochondrion including TCA cycle enzymes (ACO2, IDH3B, SDHB, FH and MDH2), components of oxidative phosphorylation (NDUFA3/8, NDUFAF2/4, NDUFB5/9/10, NDUFS3, SDHB, UQCRFS1, COX7B, PPA2 and MT-ATP6), translocase inner mitochondrial membrane (TIMM8A, TIMM9, TIMM17A and TIMM44), mitochondrial ribosomal subunits (MRPL15, MRPL17, MRPL2, MRPL21, MRPL34, MRPL37, MRPL40, MRPL47, MRPS15, MRPS18A, MRPS18B, MRPS24, MRPS34 and MRPS5) and mitochondrial ADP/ATP carriers (SLC25A5) were induced in resistant models versus MCF7 (Table 3.10). Mitochondrion play a critical role in biogenesis via TCA cycle and bioenergetics via oxidative phosphorylation in proliferative cells (Ahn and Metalo, 2015). Elevated mitochondrial biogenesis, translation and translocase machinery have also been reported in epithelial breast cancer cells as compared to the adjacent glycolytic fibroblast compartment in clinical tumours (Sotgia et al. 2012). In the panel of endocrine resistant models, the GO term associated with aminoacyl-tRNA ligase activity (CARS, HARS, FARS2, IARS, LARS, MARS, WARS and YARS) was also significantly enriched for the induced genes (Table 3.11). Aminoacyl tRNA synthases (ARSs) mediate ligation of amino acids to their corresponding tRNA for synthesis of polypeptides, thus deregulated ARS function may have a potential effect on protein synthesis machinery which may contribute to proliferation of the resistant cells. ARS expression was correlated with proliferative and mesenchymal prognostic signatures in glioblastoma patients (Kim et al. 2012). Moreover, association of elevated tRNA expression was reported in breast cancer cells and tumours versus normal cells (Pavon-Ethernod et al. 2009). The Go term associated with small molecule metabolic process was also enriched in all endocrine resistant models (Table 3.12). This Go term

encompasses genes which encode enzymes for amino acid synthesis (ACAT1, ALDH9A1, APIP, ASNS, ASS1, GOT1, GOT2, KMO and PSPH), acetyl CoA synthesis (ACSS2 and COASY), lipid biosynthesis (AGPAT6, CHPT7, EPT1 and PTDSS1), glycosaminoglycan biosynthesis (B4GALT7 and EXT2), fatty acid elongation process (ELOVL1 and ELOVL4), phosphate pentose pathway (G6PD), glutathione metabolism (GSS, GSTA4, GSTO1 and MGST1), β-oxidation of fatty acids (HADH), ketogenesis (HMGCS2), nucleotide sugar/amino sugar metabolism (PFKFB2), glycolysis (PGM1), purine metabolism (PNP), proteasome (PSMA1, PSMA6, PSMB6, PSMC4, PSMD2, PSMD8, PSME1, PSME3 and PSME3), pyruvate metabolism (PDHA1), TCA cycle (ACO2, IDH1, IDH3B, SDHB, FH and MDH2) and oxidative phosphorylation (NDUFA3, NDUFA7, NDUFA8, NDUFA9, NDUFB5, NDUFB9, NDUFB10, NDUFS3, COX7B and UQCRFS1). It has been reported that approximately 500-2000 mitochondrion per cell are in charge of converting available nutrients into fundamental building blocks including fatty acids and amino acids for growth and proliferation of rapidly dividing cells (Ralph et al. 2009). Moreover, mitochondria oxidise intermediates of the TCA cycle to generate high energy compounds in the form of ATP molecules which are consumed during energy demanding processes such as protein synthesis, nucleotide synthesis and Na^{+}/Ca^{2+} ATPase (Wieser et al. 2001). Based on the GO term enrichment, it appears that such mitochondrial metabolic processes are enhanced in endocrine resistant cells, potentially driving their growth. This appeared particularly prominent in models resistant to tamoxifen, fulvestrant resistance, and in shorter term-resistant models as compared to long-term resistant cells (Table 3.13).

Two anaplerotic processes, glycolysis and glutaminolysis are known to feed carbon into the TCA cycle. Pyruvate dehydrogenase (PDHA1/ PDHB) converts the end product of glycolysis (pyruvate) to acetyl CoA which is a precursor in the TCA cycle. Acetyl CoA condenses with oxaloacetate (OAA) via citrate synthase (CS) to form citrate which either converts to isocitrate in the TCA cycle (via ACO2) or diffuses into the cytosol to restore oxaloacetate (OAA) and acetyl CoA via ATP citrate lyase (ACLY). Furthermore, acetyl CoA serves as a precursor for de novo fatty acid synthesis and OAA converts to malate via malate dehydrogenase (MDH) where malic enzyme (ME) converts malate into pyruvate (Icard et al 2012). Glutamine enters into the TCA cycle by converting into glutamate via glutaminase (GLS/GLS2) and then glutamate is converted to the TCA precursor α-ketoglutarate (α-KG) via glutamate dehydrogenase (GLUD1/GLUD2). α-KG also plays a role in amino acid metabolism by accepting the amino group of α-amino acids to form α-keto acids which further act as precursors for synthesis of amino acids such as proline, threonine and lysine. Also, α-KG participates in ammonia metabolism through transformation of nicotinamide adenine dinucleotide (phosphate) (NAD(P)+) and reduced nicotinamide adenine

dinucleotide (phosphate) (NAD(P)H) molecules (Icard et al 2012). In resistant models, expression of ACO2 (converts citrate to isocitrate), IDH3B (converts isocitrate to α-KG), SDHB (converts succinate to fumarate), FH (converts fumarate to malate) and MDH2 (converts malate to OAA) were induced and thus may contribute in enhanced anaplerotic processes via converting precursors of the TCA cycle.

The TCA cycle harvests energy from carbon sources (TCA cycle precursors) to generate high energy compounds in the form of NADH (from isocitrate, α-KG and malate) and FADH2 (from succinate). Finally, oxidation of NADH and FADH2 in complex I and complex II of the electron transport chain respectively causes transfer of electrons from these compounds through the chain while hydrogen is pumped into the intracellular membrane space and the proton gradient flows through ATP synthase to generate ATP molecules (Berg et al. 2002). Induced activity of electron transport chain complexes such as NADH dehydrogenase (complex I), succinate dehydrogenase (complex II) and cytochrome C oxidase (complex IV) have been reported in epithelial breast cancer cells as compared to fibroblast compartments (Whitaker-Menezes et al. 2011). In the endocrine resistant models, expression of subunits for complex I (NADH dehydrogenase: NDUFA3, NDUFA7, NDUFA8, NDUFA9, NDUFB5, NDUFB9, NDUFB10, NDUFS3), complex II (succinate dehydrogenase: SDHB), complex III (cytochrome c reductase: UQCRFS1), complex IV (cytochrome c oxidase: COX7B) and ATP synthase (ATP5J2) were induced and thus may contribute towards enhanced ATP synthesis via oxidative phosphorylation in these resistant cells.

In addition to ORP-O ontology of shared induced genes, ORP-P pathway analysis revealed “metabolic pathways” (N=89 genes) as a potential shared induced mechanism in resistance, with this being the most significantly enriched pathway (and that also occurred irrespective of endocrine strategy) in the resistant models (Table 3.14). Functional classification of the 89 shared induced genes in metabolic pathways using DAVID bioinformatics revealed two clusters of oxidative phosphorylation (OxPhos) and TCA cycle enzymes as the most enriched shared genes across the resistant models (Fig. 3.8A-3.8B, Table 3.16). As mentioned earlier these two pathways (OxPhos and TCA cycle) play an important role for energy generation and synthesis of building blocks in the cell. Based on ontology and pathway analysis it can be concluded that proliferative endocrine resistant breast cancer cells are most prominently enriched with expression of mitochondrial biogenesis (TCA cycle, ribosomal sub units and TIMMs) and bioenergetics (OxPhos sub units) genes which may permit their resistant proliferation and growth. Although induced TCA cycle and OxPhos genes occurred in all resistant models and thus

likely to contribute in all endocrine resistant states, it was notable that the increased fold changes were particularly marked in in long-term resistant as compared to short term resistant models. This expression profile cumulatively re-enforces the concept that these metabolic gene changes are likely to be important in aiding disease progression during endocrine treatment. Furthermore, the observation that their increases are also more prominent in ER- fulvestrant resistant models as compared to ER+ tamoxifen or oestrogen deprived models is in keeping with a contribution to aggressive tumour growth, since ER negative tumours have a particularly poor prognosis in the clinic (Putti et al. 2004).

Further investigation was subsequently carried out to determine whether the expression of genes in the TCA cycle and OxPhos pathway were enhanced during initial AH treatment or gained only during acquisition of resistance. Study of AH treated MCF7 cells revealed that the induced gene cohort (n=551) shared by all AH treatments (10 days) had a significantly overrepresented lysosome pathway (Table 3.17). Induction of some genes (n=72) which were associated with small molecule metabolic process were discovered in ORP-O ontology analysis of these AH-treated MCF7 cells (Table 3.20), but they appeared to participate in lipid metabolism, amino acid metabolism, phosphate pentose pathway and inositolphosphate metabolism. This clearly differed from the enrichment of induced metabolic genes involved in TCA cycle and OxPhos seen in the resistant models. Indeed, only 2 OxPhos pathway genes (NDUFB2 and COX7C) were induced in AH treated cells. Further assessment confirmed there were virtually no TCA and OxPhos genes induced by initial treatment with all AHs , although expression of many TCA cycle (PDHA1, ACO2, IDH1, IDH3B, SDHB, FH, MDH2 and PCK2) and OxPhos genes (NDUFA3, NDUFA7, NDUFA8, NDUFA9, NDUFB5, NDUFB9, NDUFB10, NDUFS3, UQCRFS1, COX7B, ATP5J2 and PPA2) were induced in E2-deprived MCF7 cells after 10 days treatment (-E2/ HSFCS), with further induction of such genes after acquisition of resistance to oestrogen deprivation emerged. This indicates such OxPhos/TCA genes are commonly E2-suppressed, a regulation that has been described for further gene species including growth factor receptors previously implicated in endocrine resistance (Gee et al. 2011). In summary, based on ontology and pathway analysis it can be concluded that proliferative endocrine resistant breast cancer cells are most prominently enriched with expression of mitochondrion biogenesis (TCA cycle, ribosomal sub units and TIMMs) and bioenergetics (OxPhos sub units) genes which may permit their resistant proliferation and growth. Thus, the mechanism of TCA cycle and OxPhos pathways comprised a key focus of this project, and further investigations into the role of induced TCA cycle and OxPhos genes in endocrine resistant cells are carried out in Chapter 4. Finally, a Go term associated with biological process for cellular response to zinc ion

(MT1E, MT1F, MT1G, MT1H, MT1X and MT2A) was overrepresented in all resistant cells which suggest an evidence for zinc deregulation in such cells. Metallothionein (MTs) expression was reported in proliferative epithelial cells of breast tumours (Cherian et al. 2003) and induced expression of a zinc influx transporter (SLC39A7) has been previously detected in tamoxifen resistance cells (TamR) (Taylor et al. 2008). Thus, further investigation for induced expression of genes related to response to zinc was carried out in Chapter 5.

CHAPTER 4

Contribution of energy metabolism pathways to the panel of endocrine resistant breast cancer cells

4.1 Introduction

Two energy producing mechanisms operate to fuel normal and proliferative cancer cells in the form of high energy ATP molecules: glycolysis that occurs in the cytoplasm and oxidative phosphorylation (OxPhos) which takes place in the mitochondria. Based on the transcriptional profile analysis in Chapter 3, components of mitochondrial biogenesis and bioenergetics are commonly enriched in endocrine resistant breast cancer models versus their endocrine responsive control cells. The glycolysis pathway in the cytosol includes conversion of one molecule of glucose to two pyruvate molecules. While the first part of glycolysis involves consuming two ATP molecules to phosphorylate glucose and fructose-6-phosphate generating glucose-6-phosphate and fructose-1, 6-biphosphate respectively, the second part of glycolysis includes energy-producing reactions. These comprise conversion of 1, 3-bisphosphoglycerate (1,3-BPG) to 3-phosphoglycerate (producing 2 ATP molecules) and phosphoenolpyruvate (PEP) to pyruvate (producing 2 ATP molecules). Therefore, the net energy yield in conversion of glucose into pyruvate is 2 ATP molecules (Appendix, Fig A).

Pyruvate dehydrogenase in the mitochondrial matrix can oxidize such pyruvate to acetyl CoA which enters the TCA (citric acid) cycle by donating its acetyl group to oxaloacetate (OAA). The TCA cycle in turn provides substrates for the further energy-producing mechanism via OxPhos. The TCA cycle is a general pathway for oxidation not only of carbohydrates but also fatty acids and amino acids in the cell. Fatty acid oxidation (β-oxidation) involves successive removal of two carbon units from the carboxyl end of fatty acids generating nicotinamide adenine dinucleotide (NADH) and flavin adenine dinucleotide (FADH2) (substrates for OxPhos) via β-hydroxyacyl-CoA dehydrogenase and acyl-CoA dehydrogenase respectively and acetyl CoA to replenish the TCA cycle. Amino acids also can be used as fuel in energy metabolism through transamination and deamination reactions. Transamination involves conversion of amino acids to their respective α-ketoacids via aminotransferase and deamination includes removal of amino group from amino acids in the form of ammonia. Amino acid degradation replenishes the TCA cycle intermediates such as acetyl CoA (leucine, isoleucine and tryptophan degradation), α-ketoglutarate (arginine, proline, histidine, glutamine and glutamate degradation), succinyl CoA (isoleucine, methionine, threonine and valine degradation), fumarate (asparate, phenylalanine and tyrosine degradation) and oxaloacetate (aspartate and asparagine). Induced glutaminolysis (glutamine addiction) in proliferative cancer cells efficiently replenish the TCA cycle as it involves transamination of

glutamine to glutamate (via GLS and GLS2 enzymes) and deamination of glutamate to α-ketoglutarate (α-KG) (via GLUD1 and GLUD2 enzymes). Hence, glutamine degradation provides ATP (Fan et al. 2013), anapleurotic carbon (Yin et al. 2015) and nitrogen (Meng et al. 2010) for macromolecule biosynthesis in proliferative cancer cells.

The end product of glucose, fatty acid and some of amino acid catabolism is that acetyl CoA is oxidized to CO_2 in the TCA cycle. The first reaction of the TCA cycle involves condensation of two carbon acetyl groups of acetyl CoA with four carbons of oxaloacetate to form six carbon citrate. The TCA cycle then involves several oxidation reactions (isocitrate to oxalosuccinate, α-ketoglutarate to succinyl CoA, succinate to fumarate and malate to oxaloacetate) which regenerate oxaloacetate and also conserve energy by generating NADH and FADH2. Succinate dehydrogenase (by reducing FAD to FADH2), isocitrate dehydrogenase, glutarate dehydrogenase and malate dehydrogenase (by reducing NAD^+ to NADH) are involved in these oxidation-reduction reactions of the TCA cycle (Appendix, Fig B).

OxPhos involves oxidation of high energy compounds such as NADH and FADH2 formed during glycolysis, TCA cycle and β-oxidation of fatty acids. This is accompanied by transfer of electrons through the electron transport chain which comprises protein complexes called NADH dehydrogenase (complex I), cytochrome c oxidoreductase (complex III) and cytochrome c oxidase (complex IV) plus two mobile electron carriers (ubiquinone and cytochrome C) between protein complexes to reduce O_2 to H_2O. The electron carrier in this process, which is located in the inner mitochondrial membrane, contains Flavin, iron-sulfur, copper and heme to accept/donate electrons pump (complex I, III and IV) protons (H^+) from the mitochondrial matrix to the mitochondrial inner membrane. The proton electrochemical gradient (i.e. the pH differential between membranes plus membrane potential) drives an ATP synthase complex to phosphorylate ADP to ATP.

At complex II of the electron transport chain, succinate dehydrogenase (from the TCA cycle), acyl CoA dehydrogenase (from β-oxidation of fatty acids) and also glycerol 3-phosphate dehydrogenase (from the glycerol phosphate shuttle; see below) reduce FAD to $FADH_2$ and transfer electrons via complex III and IV to O_2.

NADH oxidation in the cell involves two catalytic redox carriers which are integral proteins of the inner mitochondrial membrane: The Malate-Asparate shuttle and the glycerol phosphate shuttle. The primary source of NADH is the glycolysis pathway. Reduction of OAA to malate by cytoplasmic malate dehydrogenase (MDH) is accompanied by oxidation of this NADH to NAD^+ and malate then enters the mitochondria where mitochondrial MDH (from the TCA cycle)

reverses the reaction to re-generate OAA and NADH. The NADH dehydrogenase (complex I) oxidises NADH to NAD^+ and thus transfers electrons to generate 3ATP molecules. Mitochondrial transaminase transfers the amino group from glutamate to convert impermeable OAA to aspartate and α-KG both of which products leave the mitochondria into the cytoplasm. As stated above, the glycerol phosphate shuttle is linked to complex II of the electron transport chain and involves cytosolic and mitochondrial glycerol 3-phosphate dehydrogenase, GPD1 (which has NADH as its substrate) and GPD2 (which has FAD^+ as it substrate) respectively. In this shuttle, oxidation of cytosolic NADH to NAD^+ is accompanied by reduction of mitochondrial FAD to FADH2 where 2ATP molecules will be generated. In general, for 1 mole of cytosolic NADH, 3ATP molecules and 2ATP molecules will generated via the Malate-Aspartate and glycerol phosphate shuttles respectively.

Given the promising transcriptional data showing TCA cycle and OxPhos enzymes as enriched shared genes across resistant models, the current Chapter focuses on further establishing the biological role of the induced TCA cycle/ OxPhos enzymes in endocrine resistant versus responsive cells using the model panel, and also explores the clinical impact of their increased expression on relapse free survival of ER+/tamoxifen treated breast cancer patients using publically-available gene expression datasets. During these studies, pharmacological targeting of substrate/energy metabolism and its impact on extracellular oxygen consumption/extracellular acidification, cell signalling pathways and growth has been evaluated.

4.2 Results

4.2.1 Analysis of induced proteome in TamR versus MCF7 using SysQuant mass spectrometry for evidence of deregulated TCA cycle and OxPhos pathway

Through collaboration with Dr D Britton at Proteome Sciences (Kings College, London), a large-scale proteomics dataset (comprising total and phosphorylated proteins) was investigated during this project for TamR versus MCF7 control cells. This allowed comparison of profile with gene microarray analysis, focussing on TCA cycle and OxPhos pathway elements, to investigate to what extent genomic changes have a proteomic output and therefore potentially the ability to influence resistant cell proliferation. To quantify total and phosphorylated proteins comprising the proteome of TamR and MCF7, the cells had initially been grown (three independent experiments N=3) to 70% confluency prior to protein extraction by the BCMP group. These samples had then been shipped to Proteome Sciences for trypsin digestion and

labelling with isobaric Tandom Mass Tag® eight-plex reagents (TMT8) followed by strong cation exchange chromatography prior to mass spectrometry. Three methodological approaches were taken i.e. non-enriched (total and phospho-peptides), TiO_2 and IMAC (phospho-peptides), to maximally-detect peptides in each sample. Spectra from each arm was searched using SEQUEST, MASCOT and Phospho-RS for phosphorylation sites and passed through SysQuant bioinformatics pipeline for expression analysis in TAMR versus MCF7 samples by Dr Britton. All identified peptides were then filtered for ≤5% false discovery rate (FDR) and ≥75% phosphorylation site confidence for further analysis. In total 74% of the phospho-peptides were detected by TiO_2 and 24% using IMAC. The TMT reporter intensity which correlates with peptide abundance in the sample was assessed to quantify proteins in the compared samples. Using this method, 2,106 (382 phospho-peptides plus 1,724 non-phospho-peptides) significantly induced UniProt IDs (using Proteome Sciences-recommended $\log_2 \geq 0.7$: 1.62 fold change and $P \leq 0.05$ significance filtering conditions) were detected in TamR versus MCF7.

In this project, pathway analysis for the induced phospho and non-phospho peptides was then carried out in Innatedb where ORP-P-significant pathways were determined (Table 4.1). While the most significant induced pathway encompassing both phospho and non-phospho peptides was the ribosome pathway (*P*=1.26E-25, Table 4.1, Appendix 20), protein processing in endoplasmic reticulum, TCA cycle, pyruvate metabolism, OxPhos, glutathione metabolism and amino sugar/nucleotide sugar metabolism were also found to be significantly induced in TamR cells versus MCF7 (Table 4.1), a finding compatible with the shared induced pathways revealed in resistant models from the microarray data (Appendix 18) (including pathway analysis data at a transcriptional level specifically in TamR cells, Appendix 7). Also, the induced peptide profile was examined for overlap with induced genes in metabolic pathways including carbohydrate metabolism, energy metabolism, lipid metabolism and amino acid metabolism in TamR versus MCF7 cells. Induced genes in TamR cells at both the gene/peptide level in each metabolic pathway were identified (indicated in blue in Table 4.2-4.5), and it was found that components of the TCA cycle, OxPhos and also pyruvate metabolism, aminosugar/ nucleotidesugar metabolism and glutathione metabolism were significantly induced at both transcriptional and translational level (Table 4.2-4.5). Furthermore, significant ORP of pathways such as aminoacyl-tRNA biosynthesis, Parkinson's disease, glyoxylate and dicarboxylate metabolism, Huntington's disease and also alanine, aspartate and glutamate metabolism in TamR versus MCF7 at translational level were overlapped with shared pathways in all resistant models versus MCF7 at the transcriptional level (Appendix 18).

Pathway Name	Pathway p-value (corrected)	Gene Symbols
Ribosome	1.26E-25	MRPL19; MRPL28; MRPL3; MRPL4; RPL10; RPL10A; RPL11; RPL12; RPL13; RPL13A; RPL14; RPL15; RPL18A; RPL19; RPL21; RPL22; RPL23A; RPL24; RPL27A; RPL28; RPL31; RPL32; RPL35; RPL35A; RPL36; RPL36AL; RPL37; RPL37A; RPL3; RPL38; RPL4; RPL5; RPL6; RPL7; RPL7A; RPL8; RPLP0; RPLP1; RPLP2; RPS10; RPS11; RPS16; RPS23; RPS24; RPS2; RPS3; RPS3A; RPS5; RPS6; RPS7; RPS8; RPS9;
Protein processing in endoplasmic reticulum	9.21E-16	BCAP31; CALR; CANX; CAPN2; CKAP4; DNAJA1; DNAJB11; DNAJC10; DNAJC1; DNAJC3; ERO1L; ERP29; GANAB; HSP90AA1; HSP90AB1; HSP90B1; HSPA1A; HSPA1B; HSPA5; HSPA8; HSPH1; LMAN1; LMAN2; MOGS; P4HB; PDIA3; PDIA4; PDIA6; PRKCSH; RPN1; RRBP1; SAR1A; SAR1B; SEC23A; SEC24A; SEC24B; SEC31A; SEC61B; SSR1; SSR3; SSR4; STT3A; TRAM1; UBE2D2; UGGT1; VCP;
Citrate cycle (TCA cycle)	9.43E-12	ACLY; ACO2; CS; DLD; DLST; FH; IDH1; IDH3A; IDH3G; MDH1; MDH2; OGDH; PCK2; PDHA1; PDHA2; SUCLA2; SUCLG2;
Aminoacyl-tRNA biosynthesis	2.68E-11	AARS; DARS2; DARS; EPRS; FARSB; GARS; HARS2; HARS; IARS2; IARS; LARS; MARS; NARS; RARS; SARS; TARS; TARS2; VARS; WARS; YARS;
RNA transport	1.79E-08	ACIN1; DDX39B; EEF1A1; EEF1A2; EIF2S3; EIF3A; EIF3B; EIF3C; EIF3CL; EIF4A1; EIF4A2; EIF4B; EIF4E; EIF4G3; EIF5; EIF5B; KPNB1; NUP107; NUP188; NUP88; NUP98; PABPC1; PABPC4; PNN; RAN; RANBP2; RPP30; SRRM1; SUMO2; SUMO3; TPR; TRNT1; XPO1; XPO5; XPOT;
Pyruvate metabolism	1.64E-06	ACAT1; ALDH3A2; DLD; FH; GRHPR; LDHB; MDH1; MDH2; ME1; ME2; PCK2; PDHA1; PDHA2; PKM2;
Pentose phosphate pathway	1.07E-04	ALDOA; G6PD; GPI; PFKL; PFKM; PGD; PRPS1; PRPS2; TALDO1; TKT;
Parkinson's disease	4.38E-04	ATP5A1; ATP5B; ATP5C1; ATP5D; ATP5F1; ATP5H; ATP5J; COX6B1; CYC1; NDUFA2; NDUFS1; PARK7; PPIF; SLC25A4; SLC25A5; SLC25A6; UBA1; UBE2L3; UQCRB; UQCRC1; UQCRFS1; UQCRH; UQCRQ; VDAC1;
Glyoxylate and dicarboxylate metabolism	0.001519	ACAT1; ACO2; CAT; CS; GRHPR; MDH1; MDH2; SHMT2;
Pathogenic Escherichia coli infection	0.002253	ARHGEF2; ARPC2; CTNNB1; CTTN; NCL; TUBA1A; TUBA1C; TUBA4A; TUBB2A; TUBB4B; TUBB; YWHAZ;
Glycolysis / Gluconeogenesis	0.003289	ALDH3A2; ALDOA; DLD; ENO1; GPI; LDHB; PCK2; PDHA1; PDHA2; PFKL; PFKM; PKM2; TPI1;
Fatty acid degradation	0.004011	ACAA1; ACAA2; ACADVL; ACAT1; ACSL1; ACSL3; ALDH3A2; CPT2; HADH; HADHB;
Oxidative phosphorylation	0.004767	ATP4A; ATP5A1; ATP5B; ATP5C1; ATP5D; ATP5F1; ATP5H; ATP5J; ATP6V0A2; ATP6V1G1; COX6B1; CYC1; NDUFA2; NDUFS1; PPA2; UQCRB; UQCRC1; UQCRFS1; UQCRH; UQCRQ;

Continue Table 4.1…

Pathway Name	Pathway p-value (corrected)	Gene Symbols
Proteasome	0.006371	PSMC2; PSMC3; PSMC4; PSMC5; PSMD12; PSMD1; PSMD2; PSMD6; PSME1; PSME2;
Huntington's disease	0.007846	ATP5A1; ATP5B; ATP5C1; ATP5D; ATP5F1; ATP5H; ATP5J; CLTC; COX6B1; CYC1; DNAH17; NDUFA2; NDUFS1; PPIF; SLC25A4; SLC25A5; SLC25A6; SOD1; TFAM; UQCRB; UQCRC1; UQCRFS1; UQCRH; UQCRQ; VDAC1;
Valine, leucine and isoleucine degradation	0.011165	ACAA1; ACAA2; ACAT1; ALDH3A2; DLD; HADH; HADHB; HIBCH; OXCT1;
Antigen processing and presentation	0.011719	CALR; CANX; HSP90AA1; HSP90AB1; HSPA1A; HSPA1B; HSPA4; HSPA5; HSPA8; PDIA3; PSME1; PSME2;
Spliceosome	0.012286	ACIN1; DDX39B; DDX5; DHX15; HNRNPA1; HNRNPU; HSPA1A; HSPA1B; HSPA8; LSM5; PPIH; SF3B2; SNRPA; SRSF1; SRSF2; SRSF6; TRA2A; TRA2B;
Protein export	0.014763	HSPA5; SEC61B; SRP19; SRP54; SRP68; SRPRB;
Glutathione metabolism	0.018427	G6PD; GCLC; GSR; GSTO1; IDH1; LAP3; PGD; RRM1; TXNDC12;
Alanine, aspartate and glutamate metabolism	0.027228	ALDH5A1; ASS1; CAD; GFPT1; GOT1; GOT2; PPAT;
Amino sugar and nucleotide sugar metabolism	0.039587	GALE; GFPT1; GMPPA; GNPNAT1; GPI; HEXB; NANS; UGDH;
PPAR signaling pathway	0.049182	ACAA1; ACSL1; ACSL3; CPT2; DBI; FABP5; ME1; PCK2; SCD; SLC27A2;

Table 4.1. ORP-P pathway analysis for all induced peptides/ phospho-peptides (≥1.6 fold changes) in TamR vs. MCF7 cells performed using Innatedb. "Ribosome pathway" was the most significantly induced pathway in TamR vs. MCF7. Metabolic pathways including TCA cycle, pyruvate metabolism, OxPhos, glutathione metabolism & aminosugar/nucleotide sugar metabolism pathways were also significantly induced. Additionally, other pathways such as aminoacyl-tRNA biosynthesis, glyoxylate & decarboxylate metabolism and alanine, aspartate & glutamate metabolism were also significantly induced in TamR vs. MCF7.

TCA cycle	Glycolysis/ Gluconeogenesis	Pyruvate metabolism	Pentose phosphate pathway	Aminosugar & nucleotidesugar metabolism	Glyoxylate & decarboxylate metabolism
ACLY	ALDH3A2	ACAT1	ALDOA	GALE	ACAT1
ACO2	ALDOA	ALDH3A2	G6PD	GFPT1	ACO2
CS	DLD	DLD	GPI	GMPPA	CAT
DLD	ENO1	FH	PFKL	GNPNAT1	CS
DLST	GPI	GRHPR	PFKM	GPI	GRHPR
FH	LDHB	LDHB	PGD	HEXB	MDH1
IDH1	PCK2	MDH1	PRPS1	NANS	
IDH3A	PDHA1	MDH2	PRPS2	UGDH	
IDH3G	PDHA2	ME1	TALDO1		
MDH1	PFKL	ME2	TKT		
MDH2	PFKM	PCK2			
OGDH	PKM2	PDHA1			
PCK2	TPI1	PDHA2			
PDHA1					
PDHA2					
SUCLA2					
SUCLG2					

Table 4.2. Induced peptides (≥1.6 fold changes) representing various carbohydrate metabolism pathways in TamR vs. MCF7. Blue indicates peptides whose corresponding gene was also induced at a transcriptional level in TamR vs. MCF7 cells. Black indicates peptides which their increased expression has only been detected at translational level.

Oxidative Phosphorylation	Oxidative Phosphorylation
ATP4A	COX6B1
ATP5A1	CYC1
ATP5B	NDUFA2
ATP5C1	NDUFS1
ATP5D	PPA2
ATP5F1	UQCRB
ATP5H	UQCRC1
ATP5J	UQCRFS1
ATP5O	UQCRH
ATP6V0A2	UQCRQ
ATP6V1G1	

Table 4.3. Induced peptides (≥1.6 fold changes) representing the OxPhos energy metabolism pathway in TamR vs. MCF7 cells. Blue indicates peptides whose corresponding gene was also induced at transcriptional level in TamR vs. MCF7 cells.

Fatty acid degradation
ACAA1
ACAA2
ACADVL
ACAT1
ACSL1
ACSL3
ALDH3A2
CPT2
HADH
HADHB

Table 4.4. Induced peptides (≥1.6 fold changes) representing lipid metabolism in TamR vs. MCF7 cells. Blue indicates peptides whose corresponding gene was also induced at transcriptional level in TamR vs. MCF7 cells.

Valine, Leucine & isoleucine degradation	Alanine, Asparate & glutamate metabolism	Glutathione metabolism	Glutathione metabolism
ACAA1	ALDH5A1		
ACAA2	ASS1		
ACAT1	CAD		
ALDH3A2	GFPT1		
DLD	GOT1	G6PD	LAP3
HADH	GOT2	GCLC	PGD
HADHB	PPAT	GSR	RRM1
HIBCH		GSTO1	TXNDC12
OXCT1		IDH1	

Table 4.5. Induced peptides (≥1.6 fold changes) representing amino acids metabolism pathways in TamR vs. MCF7 cells. Blue indicates peptides whose corresponding gene was also induced at transcriptional level in TamR vs. MCF7 cells.

4.2.2 Ontology studies of the induced TCA cycle and OxPhos genes and their expression analysis versus outcome of tamoxifen treated breast cancer patients using publically-available datasets

Ontological data for the n=20 TCA cycle/OxPhos genes induced in resistance were obtained using Genecard, KEGG (Kyoto Encyclopedia of Genes and Genomes) and OMIM (Online Mendelian Inheritance in Man), as well as from a laser-capture micro-dissected breast cancer dataset (Bonuccelli et al. 2010) and cancer EST (expressed sequences tags) libraries (Poliakov et al.2014). To determine if intrinsic increased gene expression at diagnosis was related to subsequent ER+ patient outcome, relapse free survival analysis was analysed in relation to expression of the candidate TCA/OxPhos genes using two publically-available Affymetrix microarray transcriptome clinical datasets. These comprise all ER+ breast cancer patients (250 months follow up available, N=1802) and tamoxifen treated ER+ breast cancer patient cohorts (200 months follow up available, N=712), with analysis performed using the online tool KMplotter.

ACO2 (aconitase 2)

ACO2 is encoded by the nuclear genome and functions in the mitochondria. This enzyme catalyses overall conversion of citrate to isocitrate in the second TCA cycle reaction. ACO2 homozygous mutation has been associated with infantile cerebellar-retinal degeneration, with induced glutaminolysis by 63% reported in these patients. However, their lactate production and OxPhos rate did not change as compared to normal individuals (Spiegel et al. 2012). Study of breast tumours has revealed ACO2 expression is induced in epithelial cancer cells as compared to adjacent stromal cells (cancer associated fibroblasts: CAFs) (Bonuccelli et al. 2010). While not reaching significance in ER+ breast cancer patients, survival analysis in KMplotter revealed higher ACO2 mRNA expression was significantly associated with a shortened relapse free survival (RFS) and increased risk of relapse in tamoxifen treated ER+ patients (HR=1.64, *P*=0.0014; Fig 4.1, Table 4.6).

citrate → isocitrate (overall reaction);

(1a) citrate → cis-aconitate + H2O;

(1b) cis-aconitate + H2O → isocitrate

Gene symbols	RFS, Tamoxifen treated N=712	RFS, ER+ N=1802
ACO2	HR=1.64, P=0.0014	HR=1.16, P=0.098
FH	HR=1.69, P=0.012	HR=1.36, P=0.00065
IDH1	HR=0.8, P=0.21	HR=1.09, P=0.37
IDH3B	HR=1.35, P=0.056	HR=1.3, P=0.0065
MDH2	HR=1.52, P=0.0057	HR=1.17, P=0.078
PCK2	HR=1.59, P=0.007	HR=1.46, P=2.5E-05
PDHA1	HR=1.28, P=0.13	HR=1.5, P=4.2E-6
SDHB	HR=1.23, P=0.19	HR=1.28, P=0.005

Table 4.6. Summary of RFS analysis using KMplotter for the induced pyruvate metabolism and TCA cycle genes in tamoxifen treated ER+ and all ER+ breast cancer patient cohorts. Hazard ratio (HR) >1 is associated with increased risk of relapse & log rank *P*≤0.05 was considered to be significant.

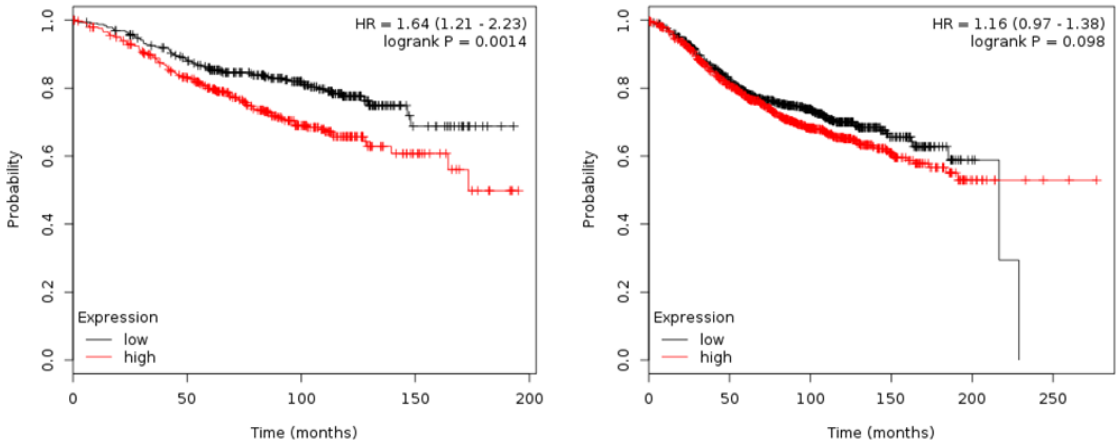

Fig 4.1. Kaplan Meier survival curves using KM plotter showing higher ACO2 mRNA expression (in red) was significantly associated with shortened relapse free survival in tamoxifen treated ER+ patients (left graph) but not in all ER+ patients (right graph).

FH (fumarate hydratase)

Nuclear encoded FH catalyses conversion of fumarate to malate in the TCA cycle. Two FH enzymes have been described: a cytosolic isoform and an N-terminal extended mitochondrial isoform. Fumarate accumulation in FH deficient cells in patients with leiomyomas and renal cell cancer has been reported to stabilize HIF1α and lead to tumour progression in pseudohypoxic condition (Pollard et al. 2005). Moreover, heterozygous germline mutation of FH was reported to be increased in cancer patients (Lehtonen et al. 2006). However, increased expression of FH was discovered in epithelial cancer cells as compared to CAFs in breast tumours (Bonuccelli et al. 2010). Also, using the cancer EST libraries (Brentani et al. 2003) induced FH expression was detected across multiple tumour cells as compared to normal tissues (Poliakov et al. 2014). Higher expression of FH was associated with shortened relapse free survival and increased risk of relapse in both tamoxifen treated ER+ (HR=1.69, *P*=0.012) and all ER+ (HR=1.36, *P*=0.00065) breast cancer patient cohorts (Fig 4.2, Table 4.6).

malate → fumarate + H2O

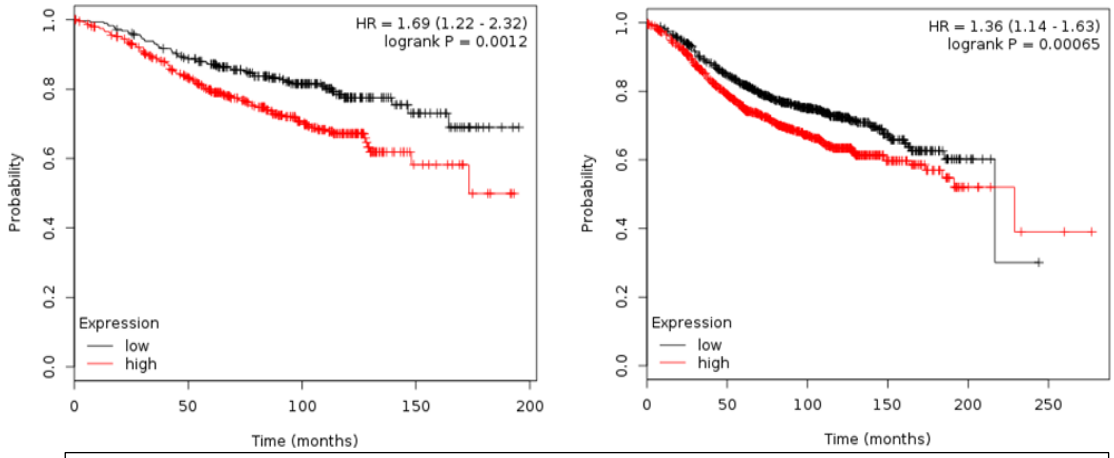

Fig 4.2. Kaplan Meier survival curves using KM plotter showing higher FH mRNA expression was significantly associated with shortened relapse free survival in ER+ patients (right graph) and tamoxifen treated ER+ patients (left graph).

IDH1 (isocitrate dehydrogenase 1 ($NADP^+$))

Five isocitrate dehydrogenases have been discovered: three mitochondrial NAD^+ dependent, one mitochondrial $NADP^+$ dependent and one cytosolic $NADP^+$ dependent form. The IDH1 encoded enzyme catalyses oxidative carboxylation of isocitrate to 2-αKG in the TCA cycle ($NADP^+$ dependent: mitochondrial). IDH1 mutation was detected in advanced ER+ breast adenocarcinomas (Fathi et al. 2014). However, induced IDH1 transcription was also detected in breast cancer cells as compared to CAFs (Bonuccelli et al 2010). RFS analysis in relation to IDH1 mRNA expression did not reach significance in both tamoxifen treated ER+ (HR=0.8, *P*=0.21) and all ER+ (HR=1.09, *P*=0.37) breast cancer patient cohorts (Fig 4.3, Table 4.6).

isocitrate + NADP+ → 2-αKG + CO_2 + NADPH + H+ (overall reaction)

(1a) isocitrate + NADP+ → oxalosuccinate + NADPH + H^+

(1b) oxalosuccinate → 2-αKG + CO_2

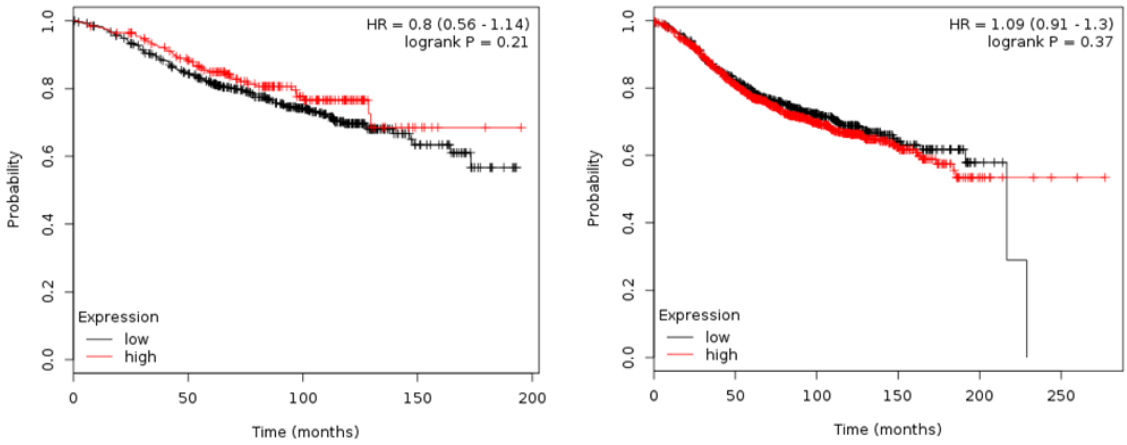

Fig 4.3. Kaplan Meier survival curves using KM plotter showing no significant association between IDH1 expression and RFS in either tamoxifen treated ER+ patients (left graph) or in all ER+ patients (right graph).

IDH3B (isocitrate dehydrogenase 3 β (NAD^+))

This is an NAD^+-dependent isocitrate dehydrogenase that catalyses the allosterically regulated rate-limiting reaction of the TCA cycle to convert isocitrate to 2-αKG. IDH3B homozygous mutation was described in retinitis pigmentosa by Hartong et al. (2008) where the enzyme expression is reduced in the retina of patients but remains unchanged in other tissues. Reduced IDH3B expression has been reported in metastatic nasopharyngeal cancer as compared to non-metastatic carcinoma (Liu et al. 2012). However, induced expression of this gene was reported by Bonuccelli et al. (2010) in epithelial breast cancer cells as compared to CAFs. Higher expression of this gene was significantly associated with shortened relapse free survival and increased risk of relapse in ER+ breast cancer patients (HR=1.3, *P*=0.0065) (Fig 4.4, Table 4.6), with a comparable but non-significant trend in tamoxifen treated ER+ patients (HR=1.35, *P*=0.056).

isocitrate + NAD^+ → 2- αKG + CO_2 + NADH

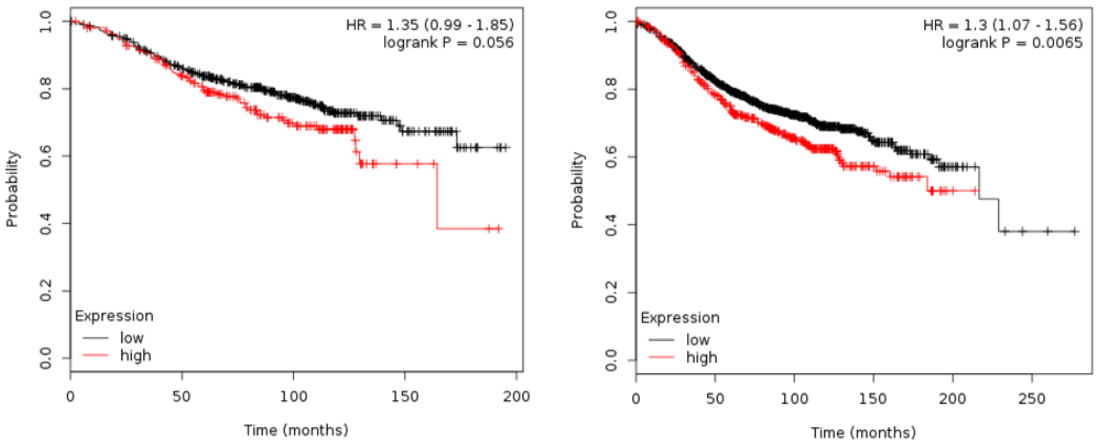

Fig 4.4. Kaplan Meier survival curves using KM plotter showing higher IDH3B mRNA expression was significantly associated with shortened relapse free survival in ER+ patients (right graph) and there was a also a non-significant trend in tamoxifen treated ER+ patients (left graph).

MDH2 (malate dehydrogenase (NAD^+))

MDH2 catalyses malate to oxaloacetate (OAA) (using NAD^+) in the final reaction of the TCA cycle. This enzyme is encoded by the nuclear genome and functions in the mitochondrial matrix. Cytosolic malate dehydrogenase and mitochondrial MDH2 regulate Malate-Asparate shuttle to supply the mitochondria with NADH. Association of MDH2 mutation (low expression) with HIF1α stabilization (pseudohypoxia) was reported in paraganglioma tumours (Jochmanova et al. 2015 and Cascon et al. 2015). However, induced MDH2 expression was discovered in epithelial breast cancer cells as compared to CAFs (Bonuccelli et al .2010). Also, MDH2 overexpression (using EST libraries) was reported in tumour cells as compared to normal tissues (Poliakov et al .2014). Higher expression of this gene was associated with shortened relapse free survival and increased risk of relapse in tamoxifen treated ER+ breast cancer patients (HR=1.52, *P*=0.0057) but there was only a trend in the all ER+ patient cohort (HR=1.17, *P*=0.078) (Fig 4.5, Table 4.6).

Malate + NAD^+ → oxaloacetate + NADH + H^+

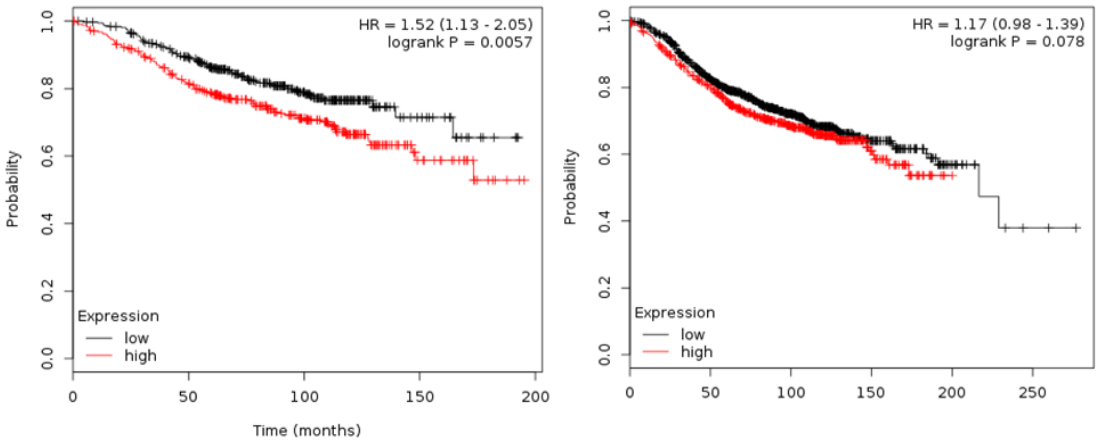

Fig 4.5. Kaplan Meier survival curves using KM plotter showing higher_MDH2 mRNA expression was significantly associated with shortened relapse free survival in tamoxifen ER+ treated patients (left graph) and there was also a trend in the all ER+ patient cohort (right graph).

PCK2 (**Phosphoenolpyruvate Carboxykinase 2)** PCK2 is encoded by the nuclear genome and functions in mitochondrion. This enzyme catalyses the conversion of OAA to phosphoenol pyruvate (PEP) using GTP. The cytosolic form of this enzyme catalyses the rate limiting step of gluconeogenesis in the liver by converting OAA (TCA cycle intermediate) to PEP (glycolysis/gluconeogenesis intermediate). Induced PCK2 expression was reported in lung cancer cell lines and non-small lung tumours (Leithner et al. 2015). Moreover, induced expression of PCK2 was detected in epithelial breast cancer cells versus CAFs by Bonuccelli et al. (2010). Higher expression of PCK2 was associated with shortened relapse free survival and increased risk of relapse in both tamoxifen treated ER+ (HR=1.59, *P*=0.007) and all ER+ (HR=1.46, *P*=2.5E-05) breast cancer patient cohorts (Fig 4.6, Table 4.6).

GTP + oxaloacetate → GDP + phosphoenolpyruvate + CO_2

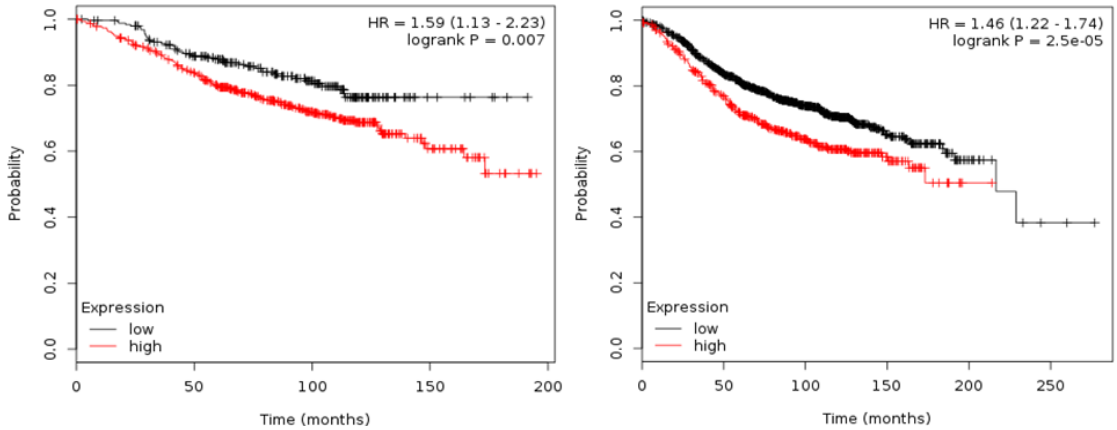

Fig 4.6. Kaplan Meier survival curves using KM plotter showing higher PCK2 mRNA expression was significantly associated with shortened relapse free survival in both tamoxifen treated ER+ (left graph) and all ER+ patient cohorts (right graph).

PDHA1 (Pyruvate Dehydrogenase (Lipoamide) Alpha 1)

Pyruvate dehydrogenase is a multienzyme complex which catalyses the overall conversion of pyruvate to acetyl CoA. This complex is composed of pyruvate dehydrogenase (PDHA/B), dihydrolipoamide acetyltransferase (DLAT) and lipoamide dehydrogenase (DLD). PDHA1 is a nuclear encoded subunit and the active site of pyruvate dehydrogenase. It converts pyruvate to acetyl CoA and thus drive the TCA cycle. In melanoma cell lines, induced PDH activity was reported in response to BRAF mediated suppression of pyruvate dehydrogenase kinase (PDK1) which induced OxPhos, redox stress and senescence in cells (Kaplon et al. 2013). In MCF7 reduced expression of Runt related transcription factor RUNX2 has been associated with PDK1 repression and activation of PDHA1 which induces OxPhos in cells (Choe et al. 2015). Moreover, induced PDHA1 expression was reported in epithelial breast cancer cells as compared to CAFs (Bonuccelli et al. 2010). Further interrogation of the gene microarrays revealed PDHB expression was induced in the fulvestrant resistant and oestrogen deprived resistant models (Fig 4.7A, Table 4.7). RUNX2 expression was reduced in fulvestrant resistant (FasR and FasRLT) and oestrogen deprived (MCF7(X) and MCF7(X)LT) models (Fig 4.7A, Table 4.7) and PDK1 expression was significantly reduced in TamRLT, FasR, FasRLT, MCF7(X) and MCF7(X)LT models (Fig 4.7A, Table 4.7). PDHA2 was not expressed in the model panel (Fig 4.7A, Table 4.7). Therefore, reduced RUNX2/PDK1 expression in fulvestrant resistant and oestrogen deprived models appears associated with induced PDHA1/PDHB expression in these lines (in accordance with association findings from Choe et al., 2015). Higher expression of PDHA1 was significantly associated with shortened relapse free survival and increased risk of relapse in the all ER+ (HR=1.5, *P*=4.2E-06) breast cancer patient cohort but its association in tamoxifen treated ER+ patients did not reach significance (HR=1.28, *P*=0.13) (Fig 4.7B, Table 4.6).

pyruvate + [dihydrolipoyllysine-residue acetyltransferase] lipoyllysine → [dihydrolipoyllysine-residue acetyltransferase] S-acetyldihydrolipoyllysine + CO_2

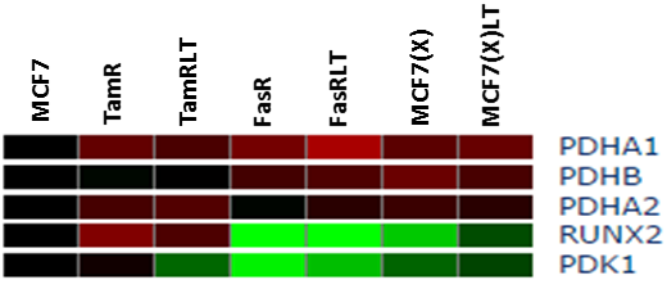

Fig 4.7A. mRNA expression of PDHA1, PDHA2, PDHB, RUNX2 & PDK1 across the panel of resistant models from the gene microarrays. On the heatmap, red, green & black indicate induced, reduced & no change in gene expression respectively as compared to the control MCF7 cells.

Gene symbols	TamR	TamRLT	FasR	FasRLT	MCF7(X)	MCF7(X)LT
RUNX2	1.42	1.23	2.02	2.08	1.73	1.23
PDK1	1.05	1.32	1.93	1.68	1.31	1.21
PDHA1	1.31	1.22	1.37	1.59	1.28	1.33
PDHA2	———	———	———	———	———	———
PDHB	1.02	1	1.20	1.24	1.33	1.22

Table 4.7. Fold changes for RUNX2, PDK1, PDHA1 & PDHB mRNA expression in endocrine resistant models vs. MCF7 control. Fold changes (≤1.2) for reduction of expression are indicated blue and fold changes for induction (≥1.2) are indicated red. PDHA2 was not expressed across the resistant panel despite a weakly-induced heatmap profile in some of the resistant lines.

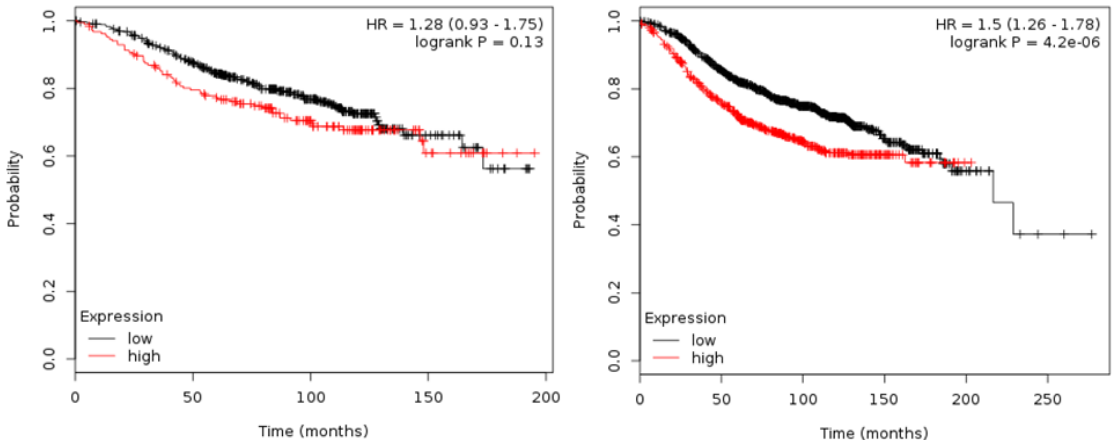

Fig 4.7B. Kaplan Meier survival curves using KM plotter showing higher PDHA1 mRNA expression was significantly associated with shorter relapse free survival in all ER+ patients (right graph) but no significant association was found in the tamoxifen treated ER+ patient cohort (left graph).

SDHB (succinate dehydrogenase B)

SDHB is encoded by the nuclear genome and catalyses the conversion of succinate to fumarate in the TCA cycle. It also participates in complex II of OxPhos where it oxidates succinate and transfers electrons from FADH2 to ubiquinone. Accumulation of succinate and HIF1α stabilization (pseudohypoxia) was again detected in paragangliomas due to SDHB mutation (Pollard et al. 2005). However, in breast cancer tumours SDHB expression was associated with higher grade tumours and its expression was not associated with either nuclear or cytoplasmic HIF1α expression (Kim et al. 2013). Also, induced SDHB expression was detected in epithelial breast cancer cells as compared to CAFs (Bonuccelli et al 2010). Higher expression of SDHB was significantly associated with shortened relapse free survival and increased risk of relapse in the all ER+ (HR=1.28, *P*=0.005) breast cancer patient cohort but its association in tamoxifen treated ER+ patients did not reach significance (HR=1.23, *P*=0.19) (Fig 4.8, Table 4.6).

Succinate + a quinone → fumarate + a quinol

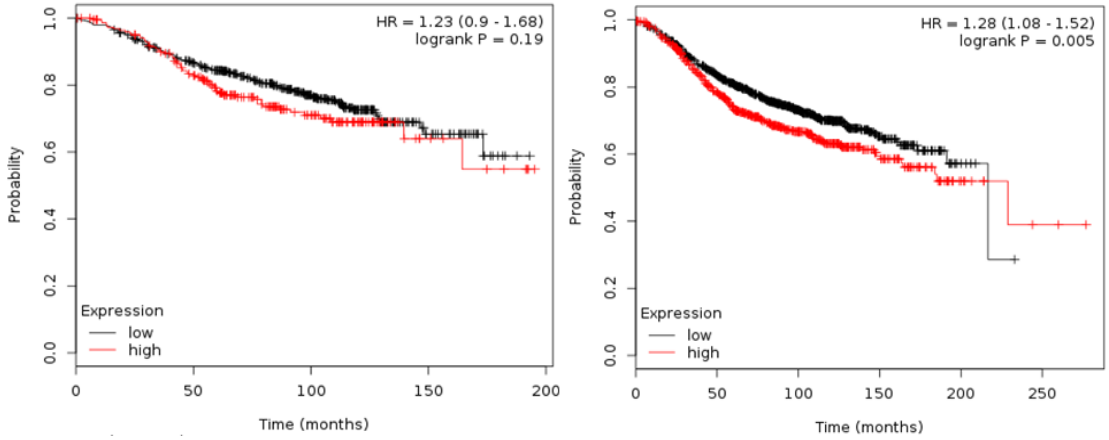

Fig 4.8. Kaplan Meier survival curves using KM plotter showing higher SDHB mRNA expression was significantly associated with shorter relapse free survival in all ER+ patients (right graph) but no significant association was found in the tamoxifen treated ER+ patient cohort (left graph).

ATP5J2 (ATP Synthase, H+ Transporting, Mitochondrial Fo Complex, Subunit F2)

Mitochondrial ATP synthase uses the proton electrochemical gradient across the inner mitochondrial membrane to catalyse ATP synthesis and thus involves in OxPhos. It consists of two multi subunit complexes. The membrane spanning complex (F0: proton channel) has nine subunits (a, b, c, d, e, f, g, F6 and F8) and the catalytic core (F1) has nine subunits (3α, 3β, 1γ, 1δ and 1ε). ATP5J2 encodes subunit f from the F0 complex. Induced ATP5J2 expression was detected in uterine leiomyomas as compared to myometrium (Tuncal et al. 2014). Also, induced expression of this gene was reported by Bonuccelli et al. (2010) in epithelial breast cancer cells as compared to CAFs. Higher ATP5J2 expression was associated with shorter relapse free survival and increased risk of relapse in both tamoxifen treated ER+ (HR=1.74, *P*=0.0022) and all ER+ (HR=1.36, *P*=0.0011) breast cancer patients (Fig 4.11, Table 4.22).

Gene symbols	RFS, Tamoxifen treated N=712	RFS, ER+ N=1802
COX7B	HR=1.21, P=0.24	HR=1.29, P=0.012
NDUFA3	HR=1.54, P=0.011	HR=1.27 ,P=0.0061
NDUFA7	HR=1.51 ,P=0.0098	HR=1.4 ,P=0.00012
NDUFA8	HR=1.98 ,P=1.7E-05	HR=1.59 ,P=2.2E-07
NDUFA9	HR=1.82 ,P=8.8E-05	HR=1.5 ,P=1.2E-05
NDUFB5	HR=1.42 ,P=0.019	HR=1.42 ,P=7.2E-05
NDUFS3	HR=1.73, P=0.00058	HR=1.42, P=9.5E-05
PPA2	HR=1.34, P=0.057	HR=1.17, P=0.079
UQCRFS1	HR=1.42, P=0.021	HR=1.31, P=0.0019
ATP5J2	HR=1.74, P=0.0022	HR=1.36, P=0.011

Table 4.8. Summary of RFS analysis using KM plotter for the induced OxPhos genes in tamoxifen treated ER+ and all ER+ breast cancer patient cohorts. HR>1 is associated with increased risk of relapse & logrank *P*≤0.05 was considered to be significant.

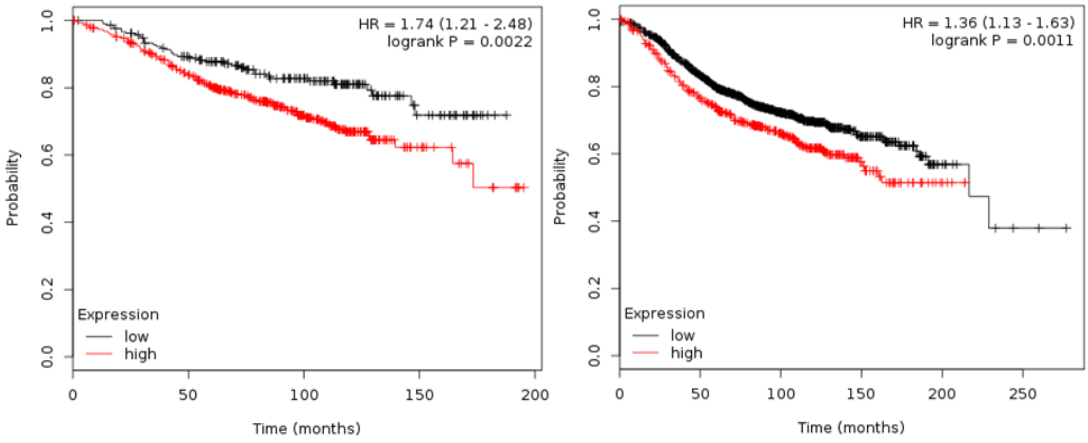

Fig 4.9. Kaplan Meier survival curves using KM plotter showing higher ATP5J2 mRNA expression was significantly associated with shorter relapse free survival in both tamoxifen treated ER+ (left graph) and all ER+ patients (right graph).

COX7B (Cytochrome C Oxidase Subunit VIIb)

The fourth complex of OxPhos consists of core catalytic subunits (cytochrome c oxidase: COX 1, COX2 and COX3) which catalyse the electron transfer from reduced cytochrome c to O_2. COX7B is a nuclear coded gene and regulatory subunit of complex IV. Induced COX7B expression was reported in advanced chemotherapy resistant ovarian cancer (L'Esperance et al. 2006). Moreover, induced expression of this gene was detected in epithelial breast cancer cells as compared to CAFs (Bonuccelli et al 2010). Association between relapse free survival and COX7B expression did not reach significance in tamoxifen treated ER+ patients (HR=1.21, *P*=0.24) but increased expression was significantly associated with shorter relapse free survival and increased risk of relapse in ER+ patients (HR=1.29, *P*=0.012) (Fig 4.10, Table 4.8).

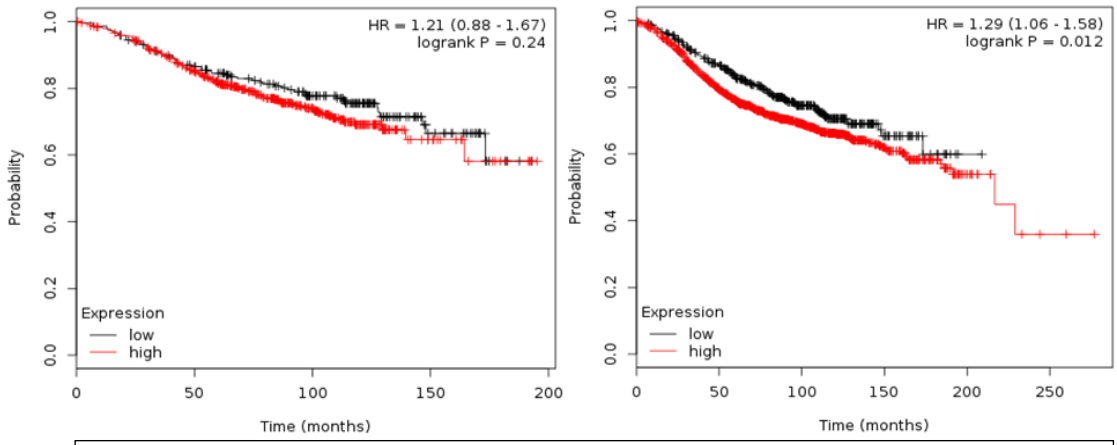

Fig 4.10. Kaplan Meier survival curves using KM plotter showing higher COX7B mRNA expression was significantly associated with shorter relapse free survival in ER+ patients (right graph) but did not reach significant in tamoxifen treated ER+ patients (left graph).

NDUFA3 (NADH Dehydrogenase (Ubiquinone) 1 Alpha Subcomplex, 3)

Eukaryotic complex I of OxPhos is composed of 45 subunits. This complex has 7 catalytic subunits (ND1, ND2, ND3, ND4, ND4L, ND5 and ND6) with NADH dehydrogenase and oxidoreductase activities to transfer electrons from NADH to ubiquinone. This nuclear coded gene (NDUFA3) is an accessory subunit of complex I which is not involved in catalysis. Induced expression of NDUFA3 was reported in epithelial breast cancer cells as compared to CAFs (Bonuccelli et al 2010). Increased expression of this gene was significantly associated with shorter relapse free survival and increased risk of relapse in both tamoxifen treated ER+ (HR=1.54, *P*=0.011) and all ER+ breast cancer patients (HR=1.27, *P*=0.0061) (Fig 4.11, Table 4.8).

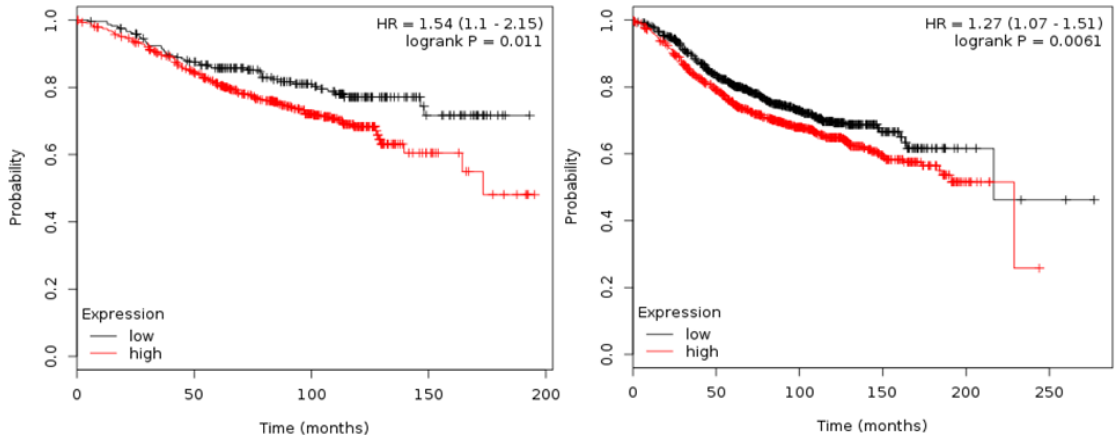

Fig 4.11. Kaplan Meier survival curves using KM plotter showing higher NDUFA3 expression was significantly associated with shorter relapse free survival in both tamoxifen treated ER+ (left graph) and ER+ patients (right graph).

NDUFA7 (NADH Dehydrogenase (Ubiquinone) 1 Alpha Subcomplex, 7)

This nuclear encoded gene is an accessory subunit of complex I which is not involved in the catalysis. Induced expression of this gene was detected in breast cancer epithelial cells as compared to CAFs (Bonuccelli et al 2010). Moreover, using EST libraries NDUFA7 overexpression was detected in tumours as compared to normal tissues (Poliakov et al 2014). Increased expression of this gene was significantly associated with shorter relapse free survival and increased risk of relapse in both tamoxifen treated ER+ (HR=1.51, *P*=0.0098) and ER+ breast cancer patients (HR=1.4, *P*=0.00012) (Fig 4.12, Table 4.8).

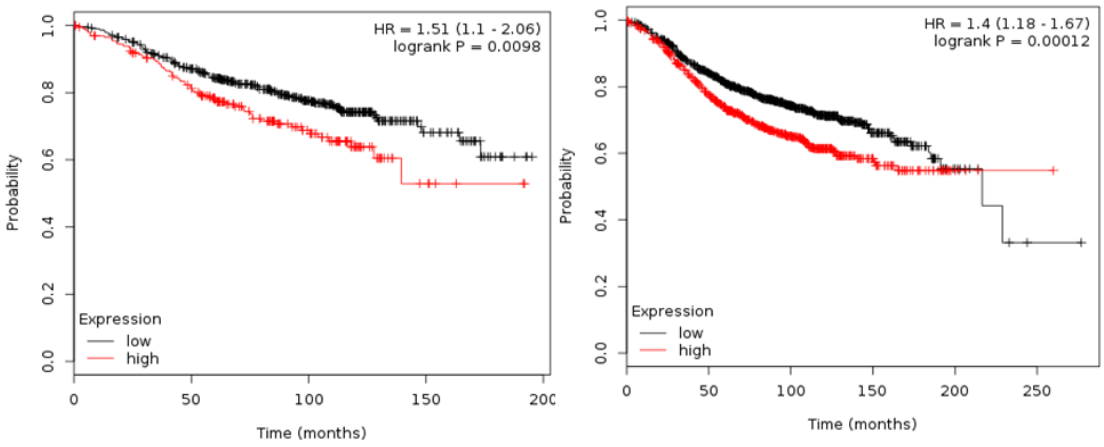

Fig 4.12. Kaplan Meier survival curves using KM plotter showing higher NDUFA7 expression was significantly associated with shorter relapse free survival in both tamoxifen treated ER+ (left graph) and all ER+ patients (right graph).

NDUFA8 (NADH Dehydrogenase (Ubiquinone) 1 Alpha Subcomplex, 8)

This nuclear encoded gene is an accessory subunit of complex I which is not involved in the catalysis. A transition mutation (325G-A) of NDUFA8 was determined in patients with neonatal dismorphic features, epilepsy, high plasma lactate and decreased complex I activity in skeletal muscles (Bugiani et al. 2004). Induced expression of this gene was reported in the breast cancer epithelial cells as compared to CAFs (Bonuccelli et al. 2010). Increased expression of NDUFA8 was significantly associated with shorter relapse free survival and increased risk of relapse in both tamoxifen treated ER+ (HR=1.98, *P*=1.7E-05) and all ER+ breast cancer patients (HR=1.59, *P*=2.2E-07) (Fig 4.13, Table 4.8).

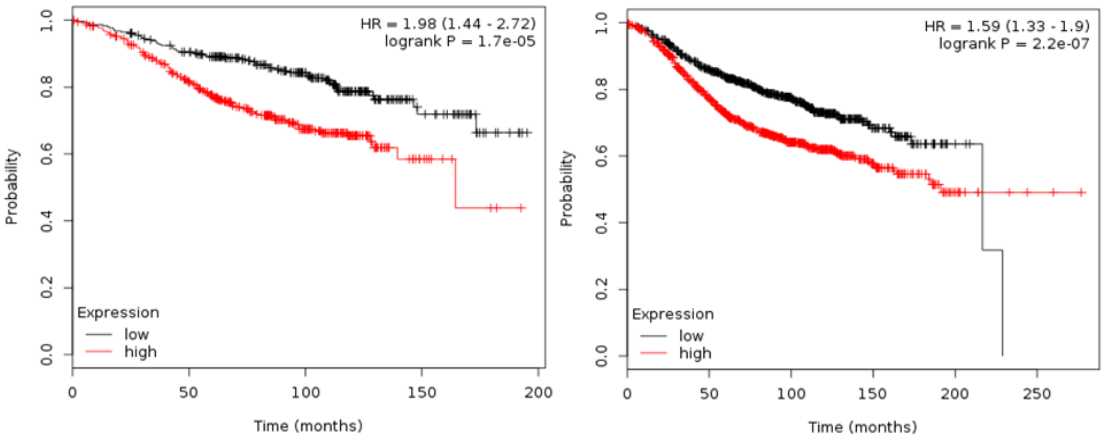

Fig 4.13. Kaplan Meier survival curves using KM plotter showing higher NDUFA8 mRNA expression was significantly associated with shorter relapse free survival in both tamoxifen treated ER+ (left graph) and ER+ patients (right graph).

NDUFA9 (NADH Dehydrogenase (Ubiquinone) 1 Alpha Subcomplex, 9)

This nuclear encoded gene is an accessory subunit of complex I which is not involved in the catalysis. The role for NDUFA9 in complex I stability was determined by van den Bosche et al. (2012) where the homozygous mutation of NDUFA9 caused neonatal Leigh syndrome due to complex I deficiency in muscle and fibroblasts of patients. Induced NDUFA9 expression was reported in breast cancer epithelial cells as compared to adjacent CAFs (Bonuccelli et al. 2010). Increased expression of NDUFA9 was significantly associated with shorter relapse free survival and increased risk of relapse in both tamoxifen treated ER+ (HR=1.82, *P*=8.8E-05) and ER+ breast cancer patients (HR=1.5, *P*=1.2E-05) (Fig 4.14, Table 4.8).

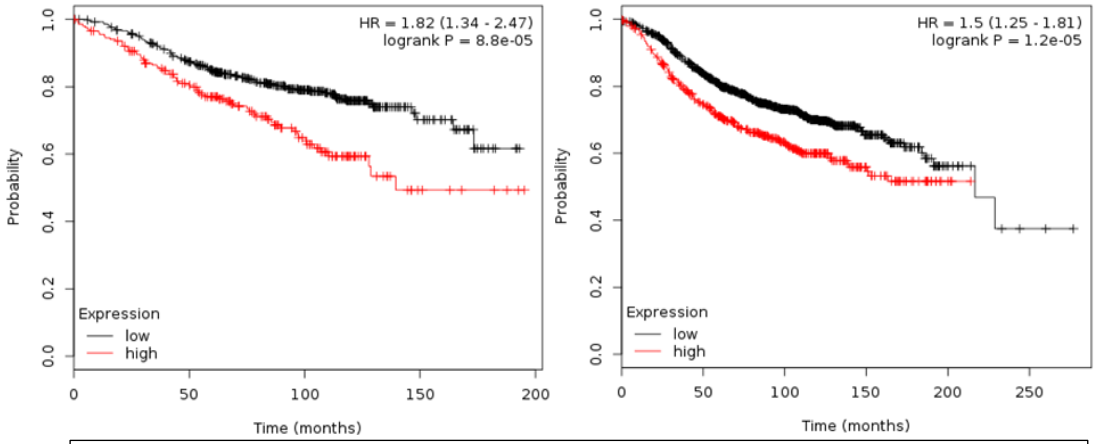

Fig 4.14. Kaplan Meier survival curves using KM plotter showing higher NDUFA9 mRNA expression was significantly associated with shorter relapse free survival in both tamoxifen treated ER+ (left graph) and all ER+ patients (right graph).

NDUFB5 (NADH Dehydrogenase (Ubiquinone) 1 Beta Subcomplex, 5)

This nuclear encoded gene is an accessory subunit of complex I which is not involved in the catalysis. Reduced NDUFB5 expression was detected in chemotherapy resistant versus responsive breast cancer tumours (Millour et al.2006). However, induced expression of this gene was determined in epithelial breast cancer cells as compared to CAFs (Bonuccelli et al. 2010). Using cancer EST libraries overexpression of NDUFB5 was revealed in tumours as compared to normal tissues (Poliakov et al 2014). Increased expression of NDUFB5 was significantly associated with shorter relapse free survival and increased risk of relapse in both tamoxifen treated ER+ (HR=1.42, *P*=0.019) and all ER+ breast cancer patients (HR=1.42, *P*=7.2E-05) (Fig 4.15, Table 4.8).

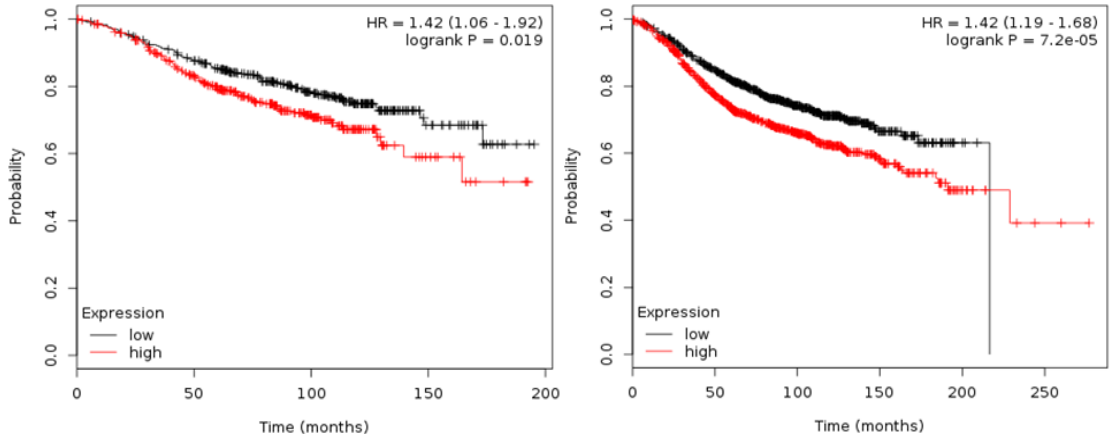

Fig 4.15. Kaplan Meier survival curves using KM plotter showing higher NDUFB5 mRNA expression was significantly associated with shorter relapse free survival in both tamoxifen treated ER+ (left graph) and all ER+ patients (right graph).

NDUFB9 (NADH Dehydrogenase (Ubiquinone) 1 Beta Subcomplex, 9)

This nuclear encoded gene is an accessory subunit of complex I which is not involved in the catalysis. Homozygous mutation and low expression of NDUFB9 was discovered in patients with complex I deficiency. NADH dehydrogenase activity in fibroblasts of such patients was reduced by 61% compared to normal cells (Hack et al. 2012). Increased NDUFB9 expression was detected in oesophageal tumours with lymph node metastasis compared to normal tissues (Uchikado et al. 2006). Moreover, overexpression of NDUFB9 was detected in the cancer EST libraries of tumours as compared to normal tissues (Poliakov et al. 2014). Since KMplotter relied on probe IDs from Affymetrix U133A arrays, there was unfortunately no available data for expression of this gene in either tamoxifen treated or ER+ breast cancer patients.

NDUFB10 (NADH Dehydrogenase (Ubiquinone) 1 Beta Subcomplex, 10)

This nuclear encoded gene is an accessory subunit of complex I which is not involved in the catalysis. There was again no data available on KMplotter for RFS analysis of NDUFB10 in the clinical breast cancer cohorts.

NDUFS3 (NADH Dehydrogenase (Ubiquinone) Fe-S Protein 3)

This nuclear encoded gene expresses one of the iron-sulfur core subunits of complex I which is essential for minimal assembly and catalytic activity of complex I. Mutation in NDUFS3 was associated with complex I deficiency in patients with Leigh syndrome (Benit et al. 2004). Induced expression of this gene was reported in epithelial breast cancer cells as compared to CAFs (Bonuccelli et al 2010). Increased expression of NDUFS3 was significantly associated with shorter

relapse free survival and increased risk of relapse in both tamoxifen treated ER+ (HR=1.73, *P*=0.00058) and all ER+ breast cancer patients (HR=1.42, *P*=9.5E-05) (Fig 4.16, Table 4.8).

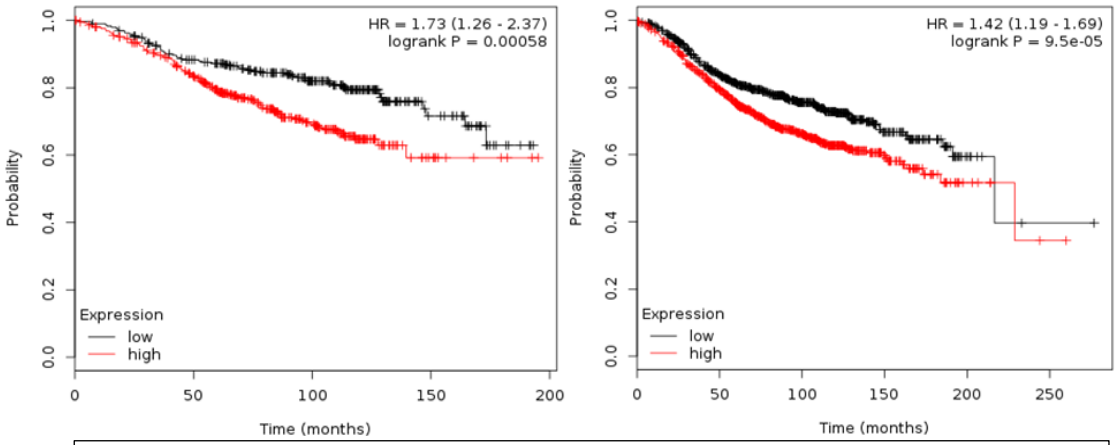

Fig 4.16. Kaplan Meier survival curves using KM plotter showing higher NDUFS3 expression was significantly associated with shorter relapse free survival in both tamoxifen treated ER+ (left graph) and all ER+ patients (right graph).

PPA2 (Pyrophosphatase (Inorganic) 2)

This nuclear coded gene plays an important role in phosphate metabolism by catalysing the hydrolysis of pyrophosphate to inorganic phosphate for the ATP synthesis in the OxPhos. There was a trend for increased expression of PPA2 to be associated with shorter relapse free survival and increased risk of relapse in both tamoxifen treated ER+ (HR=1.34, *P*=0.057) and all ER+ (HR=1.17, *P*=0.079) patients (Fig 4.17, Table 4.8).

Diphosphate + H_2O → 2 phosphate

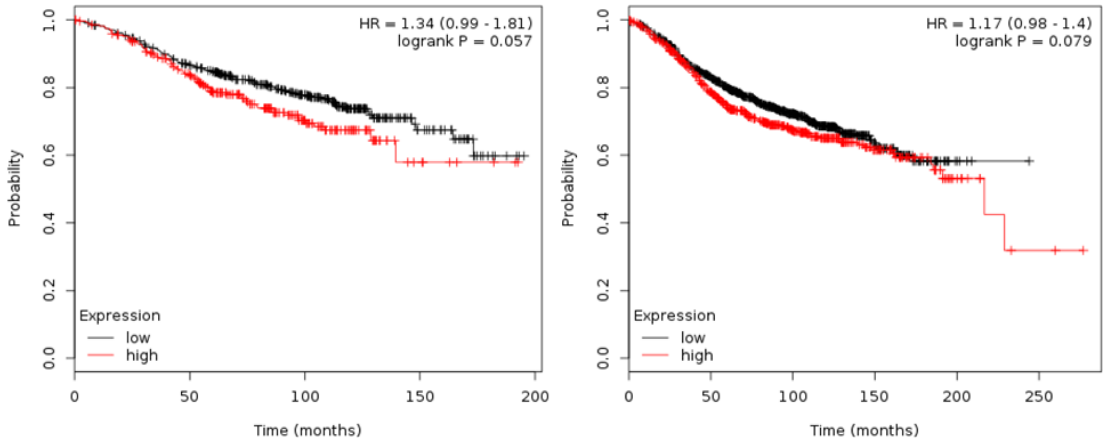

Fig 4.17. Kaplan Meier survival curves using KM plotter showing a trend for higher PPA2 mRNA expression to be associated with shorter relapse free survival in both tamoxifen treated ER+ (left graph) and all ER+ patients (right graph).

UQCRFS1 (Ubiquinol-Cytochrome C Reductase, Rieske Iron-Sulfur Polypeptide 1)

This nuclear encoded gene expresses the Rieske protein (11th subunit) of cytochrome b-c1 (complex III). Amplification of this gene was reported in ovarian cancer (Kaneko et al. 2002) and in primary breast cancer (Ohashi et al. 2004). Increased expression of this gene was significantly associated with shorter relapse free survival and increased risk of relapse n both tamoxifen treated ER+ (HR=1.42, *P*=0.021) and ER+ breast cancer patients (HR=1.31, *P*=0.0019) (Fig 4.18, Table 4.8).

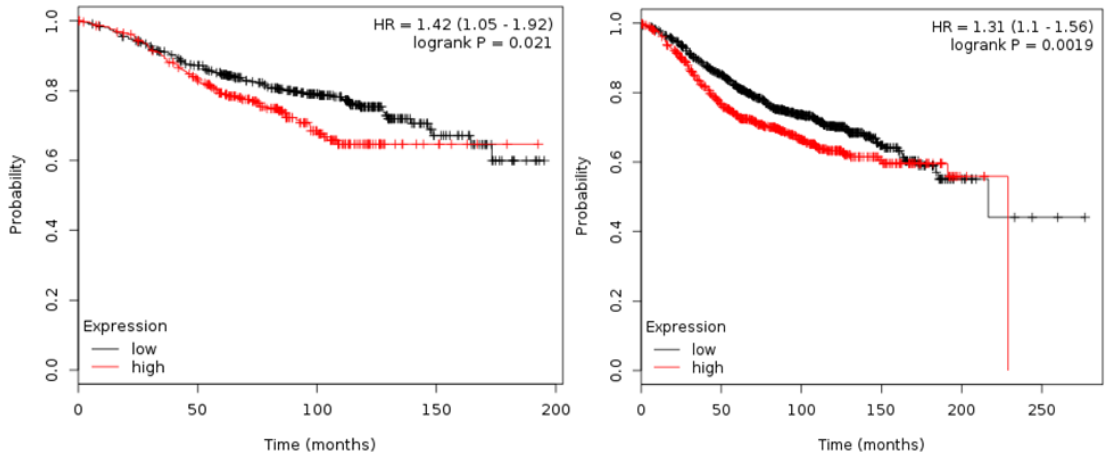

Fig 4.18. Kaplan Meier survival curves using KM plotter showing higher UQCRFS1 mRNA associates with shorter relapse free survival in both tamoxifen treated ER+ (left graph) and ER+ patients (right graph).

4.2.3 Interrogating the carbon source fuelling proliferation of breast cancer cells

Proliferation of cancer cells depends on availability of oxygen and also a carbon source for ATP generation, balance of intracellular redox status, and as building blocks of protein synthesis, fatty acid synthesis and carbohydrate biosynthesis. Carbohydrates and amino acids can be used as the carbon source in the cell. Glycolysis and glutaminolysis are two pathways that utilize a carbon source (glucose/glutamine). Glycolysis is an energy pathway that can also potentially feed the TCA cycle, and thereby OxPhos, after pyruvate conversion to Acetyl CoA, while glutaminolysis fuels TCA directly via α-KG, and so both act to maintain growth of proliferative cells. In this project endocrine resistant breast cancer cells were maintained in culture media which includes 11.11mM glucose, 4mM glutamine and non-dialyzed serum which contains further carbon sources (again glucose and glutamine). To study the importance of these carbon sources in resistant cell proliferation (potentially by fuelling the TCA/OxPhos pathway), glycolysis and glutaminolysis were manipulated across the resistant panel.

4.2.3.1 Role for glycolysis: impact of 2-deoxy glucose (glucose analogue) on glycolysis rate in endocrine resistant breast cancer cells

Aerobic glycolysis is well established as a hallmark of advanced cancers (Hanahan et al. 2011). Therefore, targeting the glycolysis pathway is a potential strategy to inhibit growth of tumour cells. 2-deoxyglucose (2DG) is a monosaccharide compound (glucose analogue) which inhibits glycolysis and ATP production. Hexokinase (HK) catalyses phosphorylation of 2DG to 2DG-P, which is trapped in the cell reducing glycolysis and ATP production (Pelicano et al.2006). To gauge the impact of 2DG on glycolysis in the resistant cells in the current study, a surrogate marker of glycolysis (extracellular lactate) was quantified after 24hrs 2DG treatment (0.5, 1, 3 and 5mM) of the panel of resistant models. Pyruvate is the end product of glycolysis which converts to lactate and releases into the extracellular environment via monocarboxylic transporters (MCT1-4) and thus is proportional to intracellular glycolysis (Griffin et al. 2004). L-lactate concentration can be experimentally-determined via monitoring basal extracellular acidification (ECA) through addition of lactate dehydrogenase enzyme (LDH) to catalyse the oxidation of extracellular lactate to pyruvate where NADH product reduces a tetrazolium substrate to a highly coloured formazan which is detectable at 490-520nm. Prior to monitoring 2DG impact, the basal extracellular L-lactate level was determined by monitoring ECA in this study across the model panel (Fig 4.19A). The ECA, and thus extracellular L-lactate level was induced in tamoxifen resistant and oestrogen deprived models (≥1.4 fold changes), reaching significance in TAMRLT cells, but in contrast remained unchanged in fulvestrant resistant models

as compared to MCF7 control cells (Fig 19A). Interestingly, this L-lactate profile also mirrored the expression of endogenous lactate dehydrogenase B (LDHB) in the resistant panel which was induced (≥1.5 fold changes) in tamoxifen resistant and oestrogen deprived models (Fig 4.19B, Table 4.9) but again remained unchanged in fulvestrant resistant models compared to MCF7 (Fig 4.19B, Table 4.9). These basal ECA and expression profile findings suggest increased glycolysis fuels tamoxifen resistant (particularly the TAMRLT cells) and oestrogen deprived resistant models in relation to the endocrine responsive cells.

L-lactate + NAD^+ → pyruvate + NADH + H+

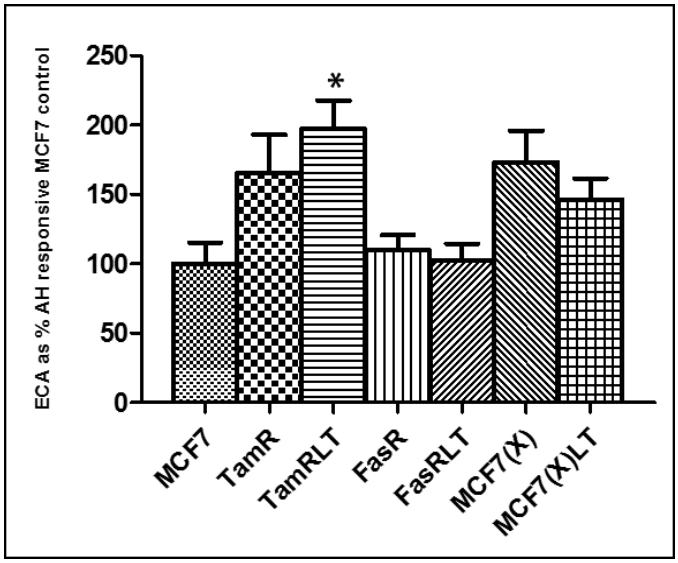

Fig 4.19A. Basal extracellular acidification (ECA) was determined via lactate measurement in the resistant breast cancer cell panel vs. their antihormone responsive (AH) parental cell control MCF7 (grown in SFCS). Data were represented as mean of 3 independent experiments (N=3). The error bar indicates SEM &* (*P*<0.05) following ANOVA with Dunnett post hoc correction.

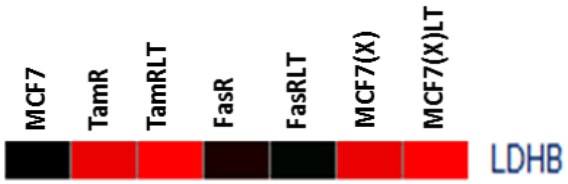

Fig 4.19B. Gene microarray **e**xpression of LDHB across the resistant panel. On the heatmap, red & black indicate induced & no change in gene expression respectively as compared to the control MCF7 cells.

Fold change	TamR	TamRLT	FasR	FasRLT	MCF7(X)	MCF7(X)LT
MCF7	1.58	2.65	1.07	1.01	1.66	1.41

Table 4.9. Fold change comparison of LDHB expression in resistant models vs. MCF7.

To further explore contribution of glycolysis to the resistant cells, the L-lactate level was determined after 24hrs of 2DG (0.5, 1, 3 and 5mM) treatment to inhibit glycolysis across the panel of resistant models and the parental MCF7 line (Fig 4.20A-D and 4.21A-C). In MCF7, the impact of 2DG was modest, with ECA significantly reduced by 43% after 5mM 2DG treatment (P<0.05) as compared to untreated control (Fig 4.20A). ECA was more significantly reduced by 2DG in TamR by 30%, 44%, 50% and 70% after 0.5mM (P<0.05), 1mM (P<0.01), 3mM (P<0.001) and 5mM (P<0.001) 2DG treatment respectively as compared to untreated control (Fig 4.20B). Moreover, ECA was significantly further reduced by 5mM treatment as compared to 0.5mM (P<0.01) and 1mM (P<0.05) treatment in such cells (Fig 4.20B). TamRLT showed substantial 2DG sensitivity in a dose dependent manner. ECA was reduced by 50%, 60% and 70% after 0.5mM, 1mM, 3mM 2DG treatment (Fig 4.20C) and thereafter was significantly reduced by 75% after 5mM (P<0.05) 2DG treatment respectively as compared to untreated control (Fig 4.20C). Also, in this model 2DG significantly reduced ECA by 5mM (P<0.05) as compared to 0.5mM treatment (Fig 4.20C). In FasR, while not reaching significance at 0.5mM, ECA was significantly reduced in a dose dependent manner thereafter by 40%, 50% and 60% after 1mM (P<0.05), 3mM (P<0.05) and 5mM (P<0.01) 2DG treatment respectively as compared to untreated control (Fig 4.20D). Similarly, the ECA was significantly reduced in FasRLT by 30%, 40% and 60% after 1mM (P<0.05), 3mM (P<0.001) and 5mM (P<0.001) 2DG treatment respectively as compared to untreated control (Fig 4.21A). Also, in this model 2DG significantly reduced ECA by 3mM (P<0.05) and 5mM (P<0.001) treatment as compared to 0.5mM treatment and by 5mM (P<0.01) as compared to 1mM 2DG treatment (Fig 4.21A). In the MCF7(X) resistant line, ECA was again significantly reduced by 25%, 35%, 40% and 60% after 0.5mM (P<0.05) 1mM (P<0.01), 3mM (P<0.001) and 5mM (P<0.001) 2DG treatment respectively as compared to untreated control (Fig 4.21B). Also, ECA was significantly reduced by 5mM as compared to 0.5mM (P<0.01) and 1mM (P<0.05) 2DG treatment (Fig 4.21B). While not reaching significance at 0.5mM, ECA was also significantly reduced in MCF7(X)LT by 35%, 40% and 50% after 1mM (P<0.05) 3mM (P<0.01) and 5mM

(*P*<0.001) 2DG treatment as compared to untreated control (Fig 4.21C). Again ECAR was significantly reduced (*P*<0.01) by 5mM as compared to 0.5mM treatment (Fig 4.21C).

In summary, 24hrs 2DG treatment reduced ECA (quantified by L-lactate production) in a dose dependent manner in the model panel, with apparent increased sensitivity in the resistant lines versus the parental MCF7 control. Of note, TamRLT was the most sensitive resistant model with 50% L-lactate reduction after treatment with the lowest 2DG dose (0.5mM) and at least 70% inhibition from 3mM (Fig 4.20A), with the MCF7 control being the least sensitive model with 45% L-lactate reduction in the highest dose of 2DG treatment (5mM) (Fig 4.20A). These ECA profiles with 2DG again suggest there is an increased importance for glycolysis in driving resistant cells, particularly TAMRLT, in relation to endocrine responsive cells.

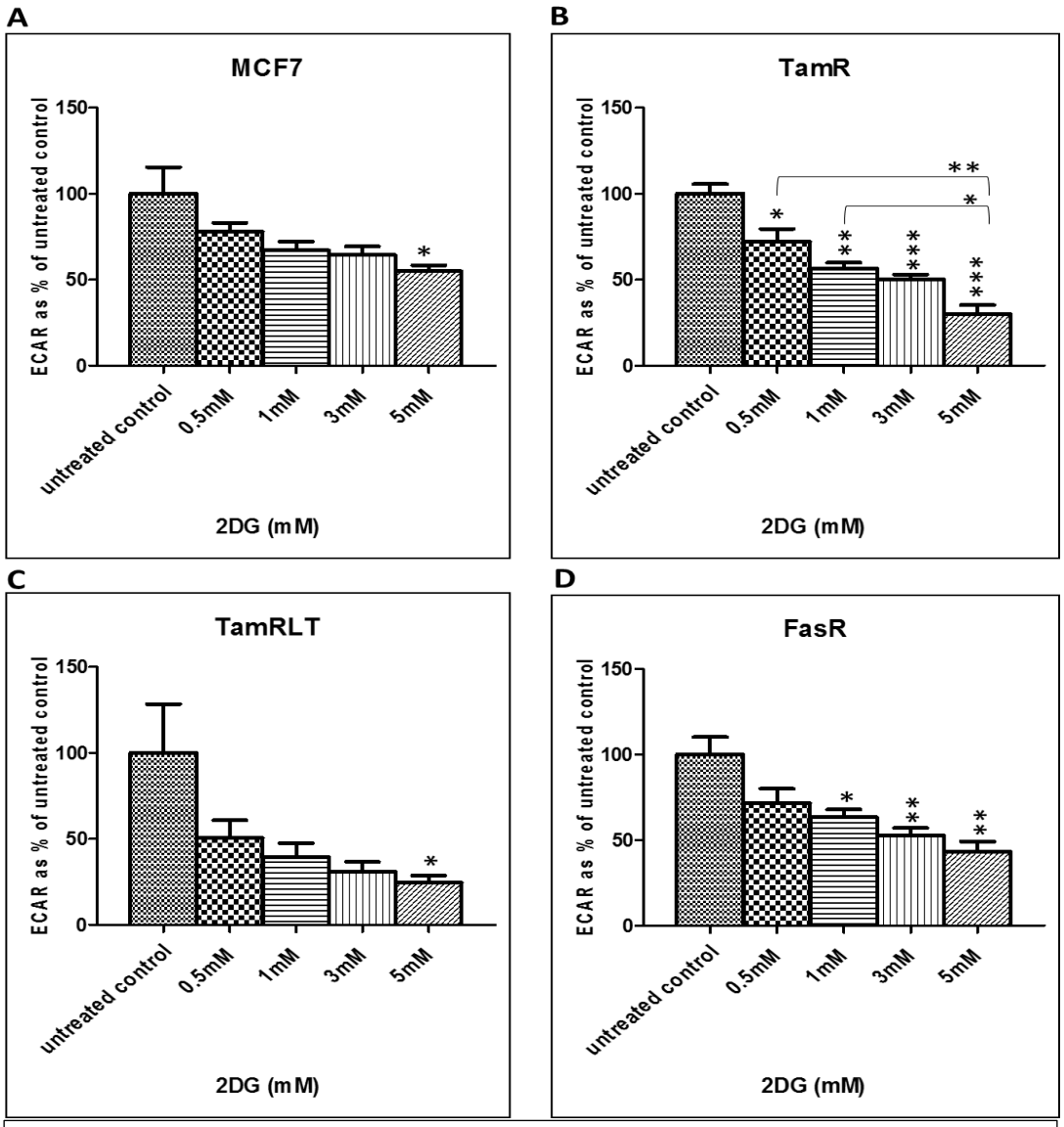

Fig 4.20A-D. ECAR quantification after 24hrs 2DG treatment in MCF7, TamR, TamRLT & FasR. Data were represented as mean of 3 independent experiments (N=3). The error bar indicates SEM. * (*P*<0.05), ** (*P*<0.01) & *** (*P*<0.001) following ANOVA with Bonferroni post hoc

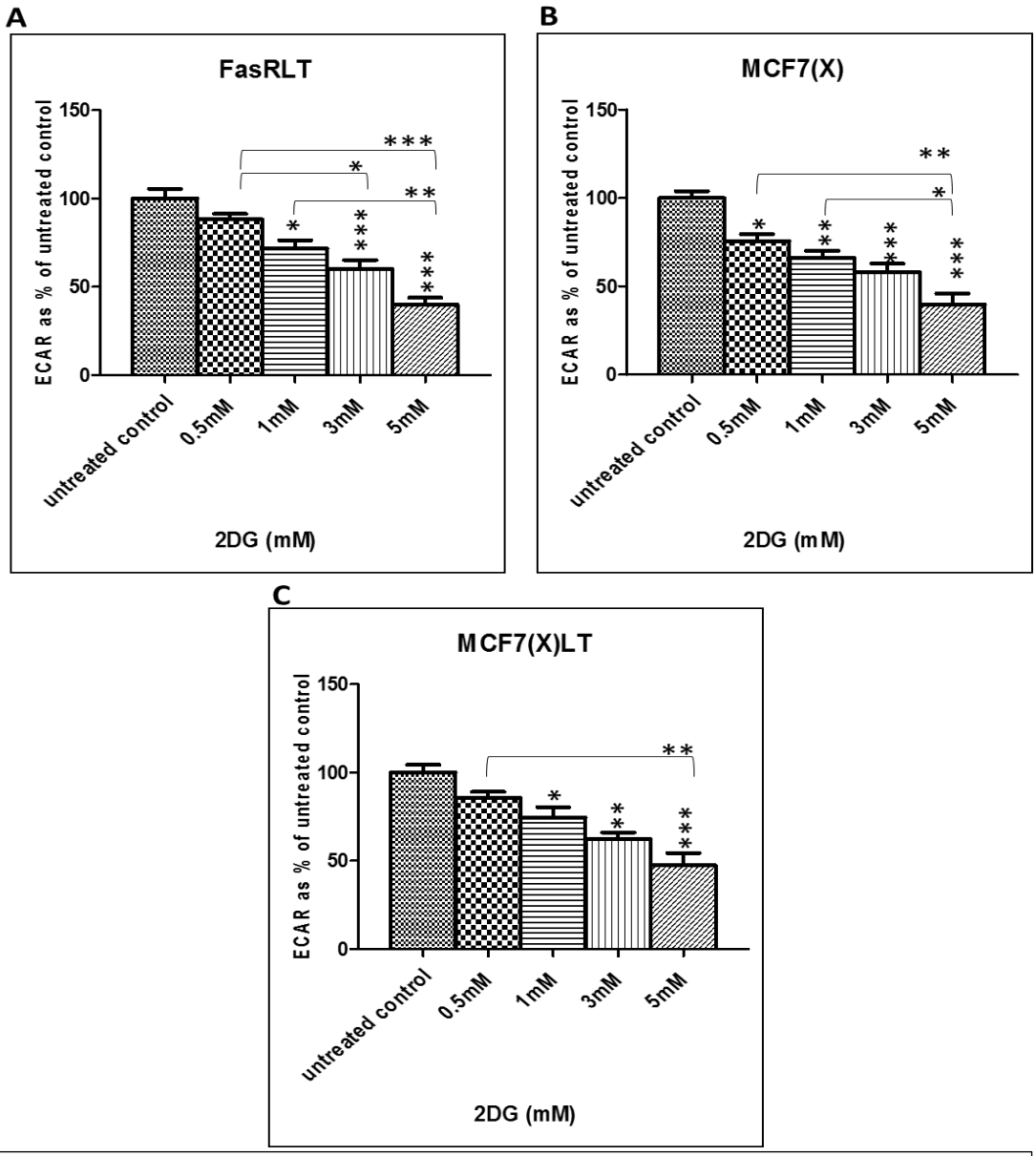

Fig 4.21B. ECAR quantification after 24hrs 2DG treatment in FasRLT, MCF7(X) & MCF7(X)LT. Data were represented as mean of 3 independent experiments (N=3). The error bar indicates SEM. * (*P*<0.05), ** (*P*<0.01) & *** (*P*<0.001) following ANOVA with Bonferroni post hoc correction.

4.2.3.2 Role for glycolysis: impact of 2-deoxy glucose on growth rate in endocrine resistant breast cancer cells

The growth inhibitory effect of 2DG treatment was determined in culture over day 3, 5 and 7 in the panel of resistant models (Fig 4.22-4.28) using Coulter counting. Cells were seeded at 20,000 cells/well for 24hrs prior to 2DG administration, and the corresponding EC_{50} for growth inhibitory effect of the drug on day 7 was calculated for each model as summarised in Table 4.10 (Appendix 21).

Monitoring of the growth curves generated for MCF7 showed that by day 7 growth rate was reduced by 50% after treatment with 5mM 2DG treatment as compared to untreated control (Fig 4.22A-B). Cell numbers fell below the seeding density at 5mM treatment on day 7 (Fig 4.22A). In general, growth of MCF7 was reduced in a 2DG-dose dependent manner but this did not reach significance in this model compared with untreated control (Figure 4.22B). Mean of half-maximum response (EC_{50}) for 2DG treatment in MCF7 was 1mM (Table 4.10). In TamR, growth was reduced in a dose dependent manner compared with untreated control, and reduced by more than 50% after 3mM and 5mM treatment by day 7 (Fig 4.23A-B). However, the reduction of growth was not significant (Fig. 4.23B). Mean of half-maximum response (EC50) for 2DG treatment in TamR was 1mM (Table 4.10). In TamRLT, growth rate was significantly and substantially reduced in a dose dependent manner by 60%, 87% and 90% after 1mM (P<0.001), 3mM (P<0.001) and 5mM (P<0.001) 2DG treatment by day 7 as compared to untreated control (Fig 4.24A-B). Moreover, the growth was significantly further reduced after 1mM (P<0.01), 3mM (P<0.001) and 5mM (P<0.001) treatment as compared to 0.5mM treatment and after 5mM treatment as compared to 1mM (P<0.05) and 3mM (P<0.05) treatment (Fig 4.24B). Mean of half-maximum response (EC_{50}) for 2DG treatment in TamRLT was 0.8mM (Table 4.10). The growth rate in FasR was reduced in a dose dependent manner with this inhibition significant and more than 60% after 3mM (P<0.05) and 5mM (P<0.01) 2DG treatment by day 7 as compared to untreated control (Fig 4.25A-B). Mean of EC_{50} for 2DG treatment in FasR was 0.39mM (Table 4.10). In FasRLT, the growth impact was again dose dependent and significantly reduced by >60% after 1mM (P<0.05), 3mM (P<0.05) and 5mM (P<0.01) treatment as compared to untreated control (Fig 4.26A-B). Mean of EC_{50} for 2DG treatment in FasRLT was 0.43mM (Table 4.10). In MCF7(X), the growth rate was reduced in a dose dependent manner, up to 50% with 3mM and 65% after 5mM 2DG treatment by day 7 as compared to untreated control (Fig 4.27A-B). However, this growth rate reduction did not reach significance after 2DG treatment as compared to untreated control (Fig 4.27B). Mean of EC_{50} after 2DG treatment in MCF7(X) was 1mM (Table 4.10). The growth rate of MCF7(X)LT was also similarly reduced in a dose dependent manner (Fig

4.28A-B), with significant growth reduction by 50% observed after 5mM 2DG treatment as compared to untreated control by day 7 (Fig 4.28B). Mean of EC50 for 2DG treatment in MCF7(X)LT was 0.9mM (Table 4.10).

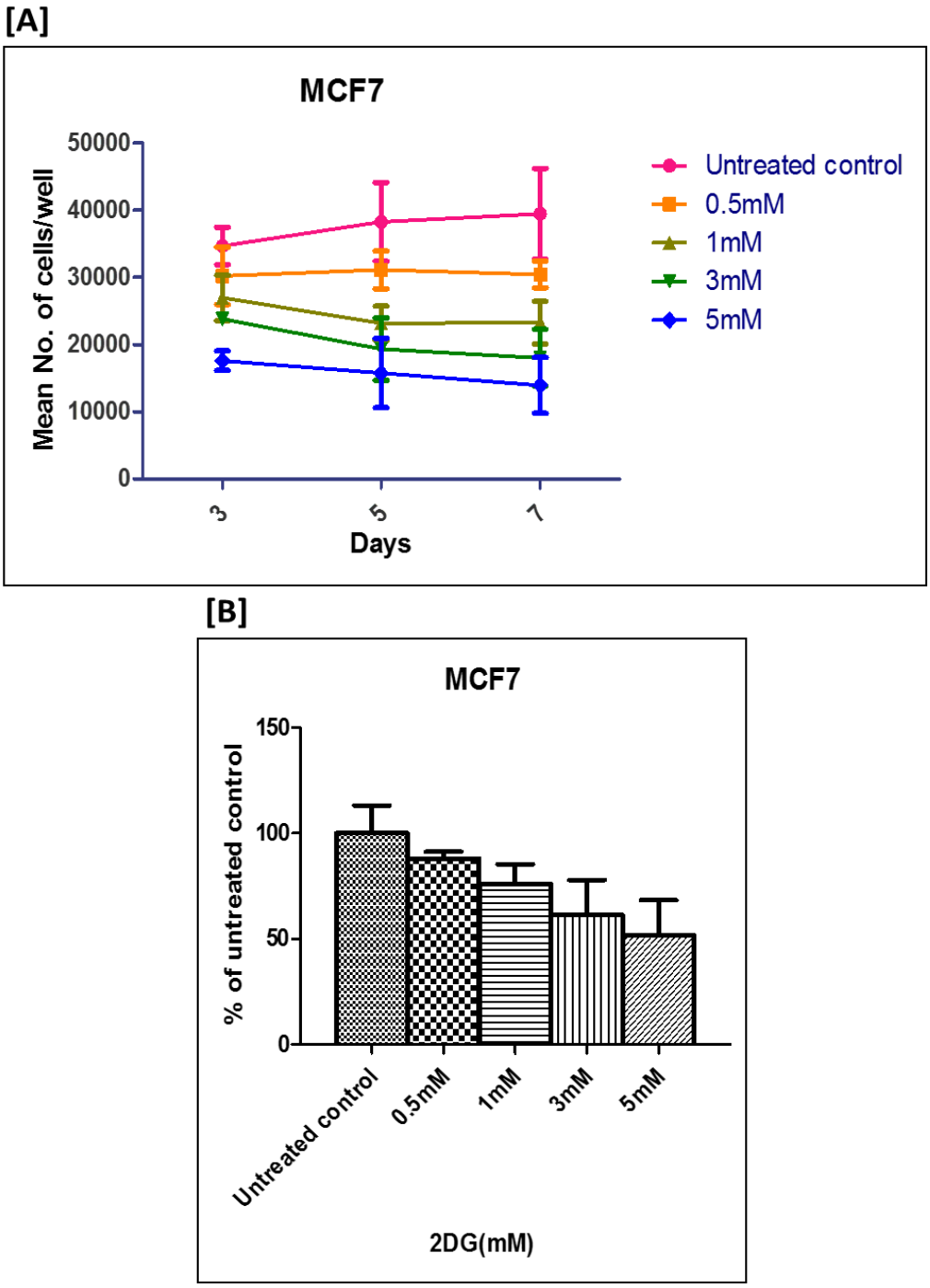

Fig 4.22. MCF7 were seeded at 20,000 cells/well and the growth rate was determined by Coulter counting after 0.5-5mM 2DG treatment on day 3, 5 & 7. (A) Shows growth curve profiles and (B) % of untreated control growth at day 7 (Data were represented as mean of 3 independent experiments (N=3)). The error bar indicates SEM.

[A]

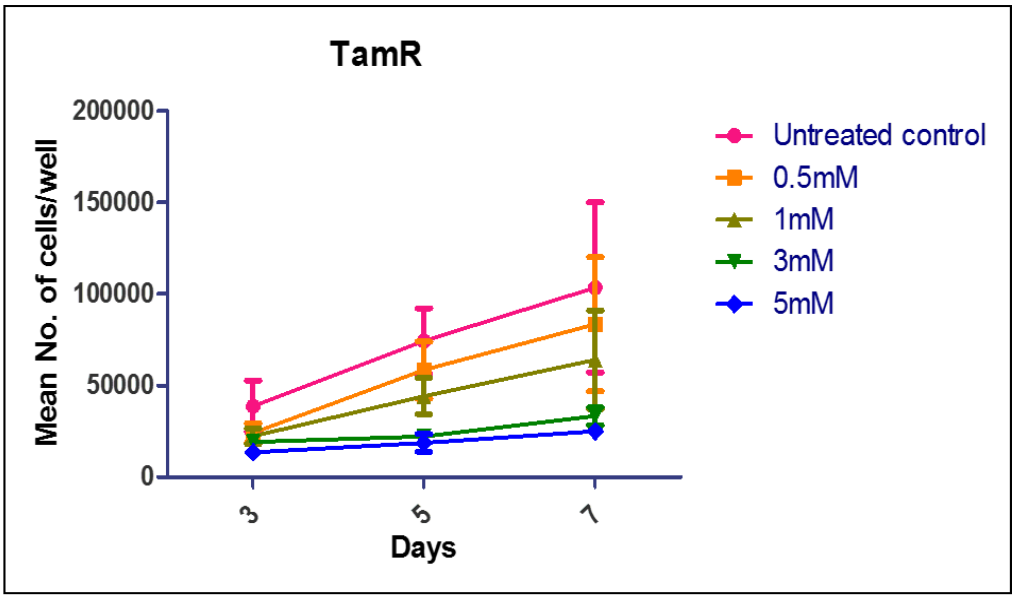

[B]

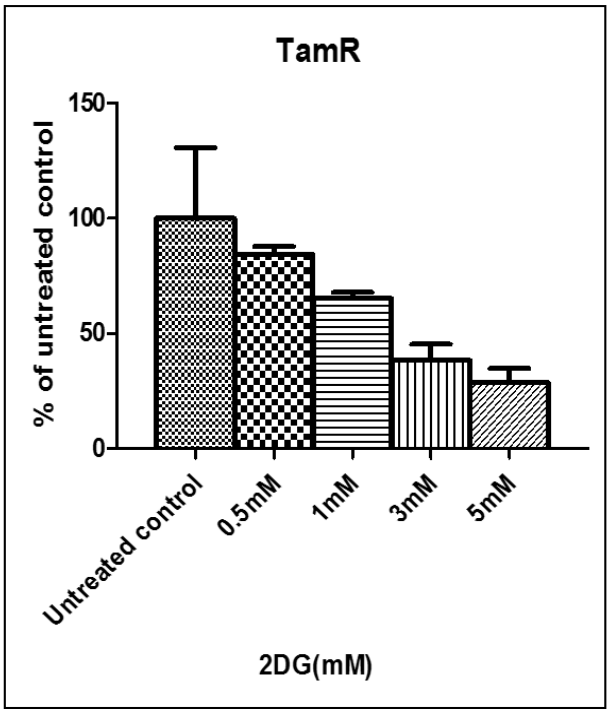

Fig 4.23. TamR were seeded at 20,000 cells/well and the growth rate was determined by Coulter counting after 0.5-5mM 2DG treatment on day 3, 5 & 7. (A) Shows growth curve profiles and (B) % of untreated control growth at day 7 (Data were represented as mean of 3 independent experiments (N=3)). The error bar indicates SEM.

[A]

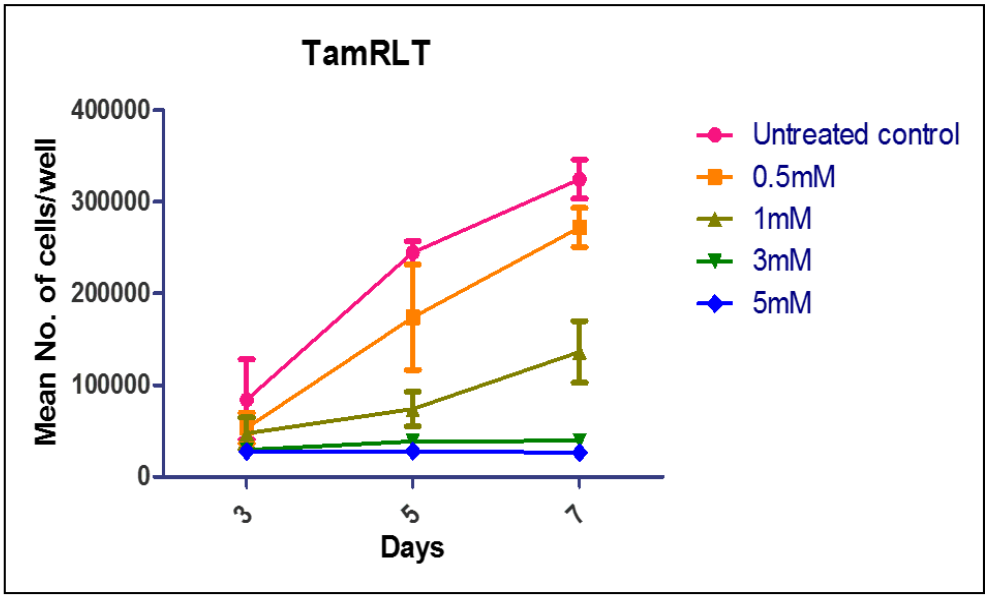

[B]

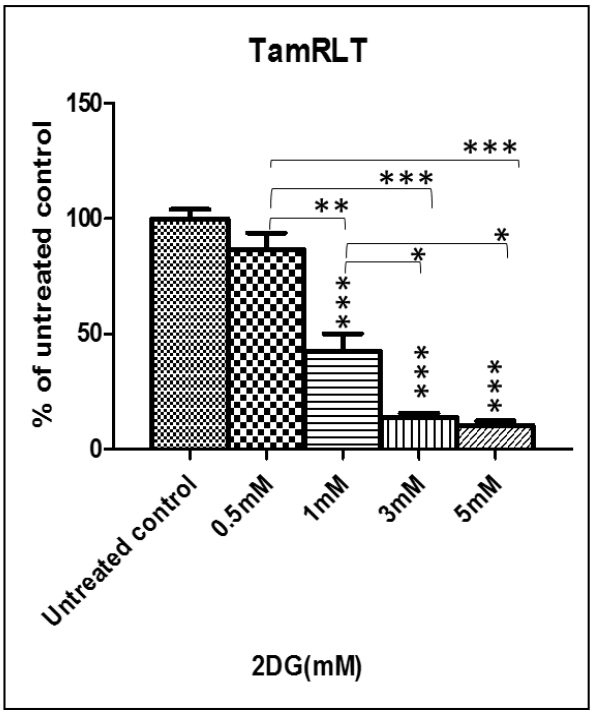

Fig 4.24. TamRLT were seeded at 20,000 cells/well and the growth rate was determined by Coulter counting after 0.5-5mM 2DG treatment on day 3, 5 & 7. (A) Shows growth curve profiles and (B) % of untreated control growth at day 7 (Data were represented as mean of 3 independent experiments (N=3)). The error bar indicates SEM. *(P<0.05), ** (P<0.01) & *** (P<0.001) following ANOVA with Bonferroni post hoc correction.

[A]

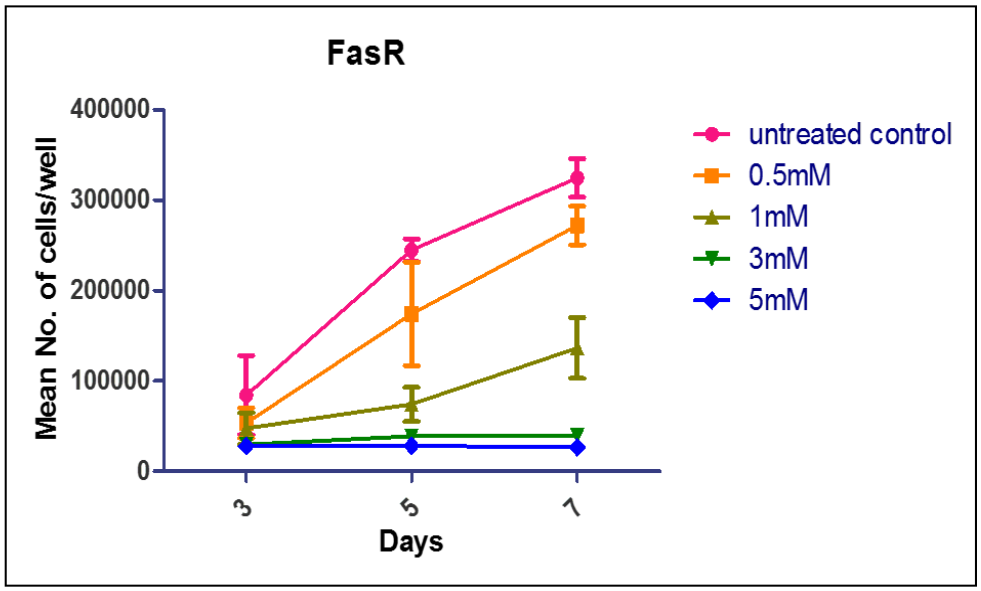

[B]

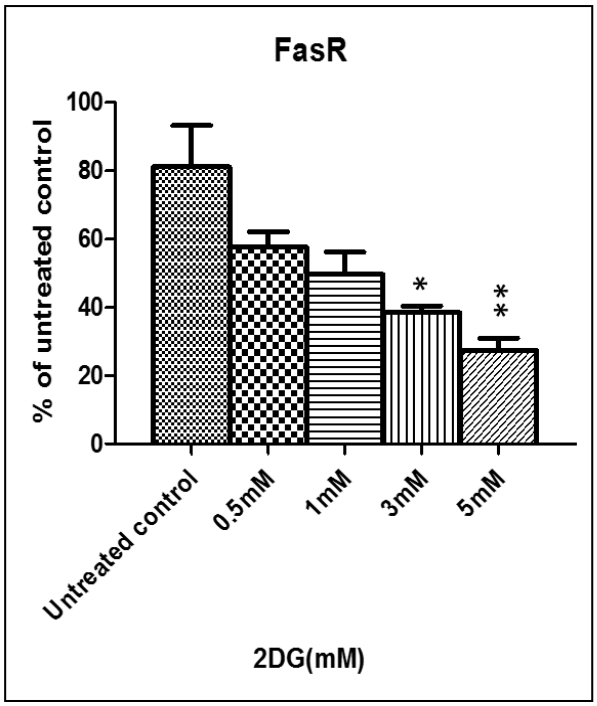

Fig 4.25. FasR were seeded at 20,000 cells/well and the growth rate was determined by Coulter counting after 0.5-5mM 2DG treatment on day 3, 5 & 7. (A) Shows growth curve profiles and (B) % of untreated control growth at day 7 (Data were represented as mean of 3 independent experiments (N=3)). The error bar indicates SEM. *(P<0.05) & ** (P<0.01) following ANOVA with Bonferroni post hoc correction.

[A]

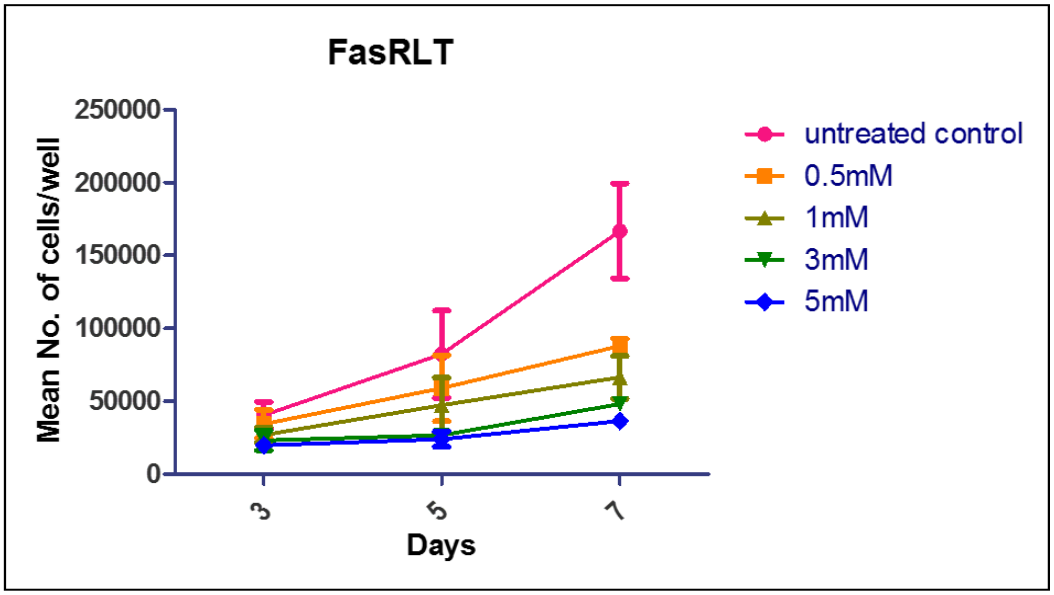

[B]

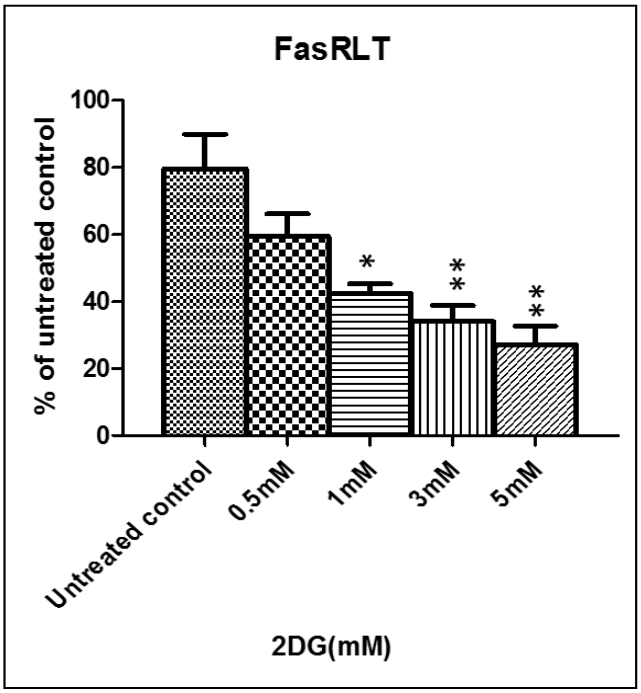

Fig 4.26. FasRLT were seeded at 20,000 cells/well and the growth rate was determined by Coulter counting after 0.5-5mM 2DG treatment on day 3, 5 & 7. (A) Shows growth curve profiles and (B) % of untreated control growth at day 7 (Data were represented as mean of 3 independent experiments (N=3)). The error bar indicates SEM. *(P<0.05) & ** (P<0.01) following ANOVA with Bonferroni post hoc correction.

[A]

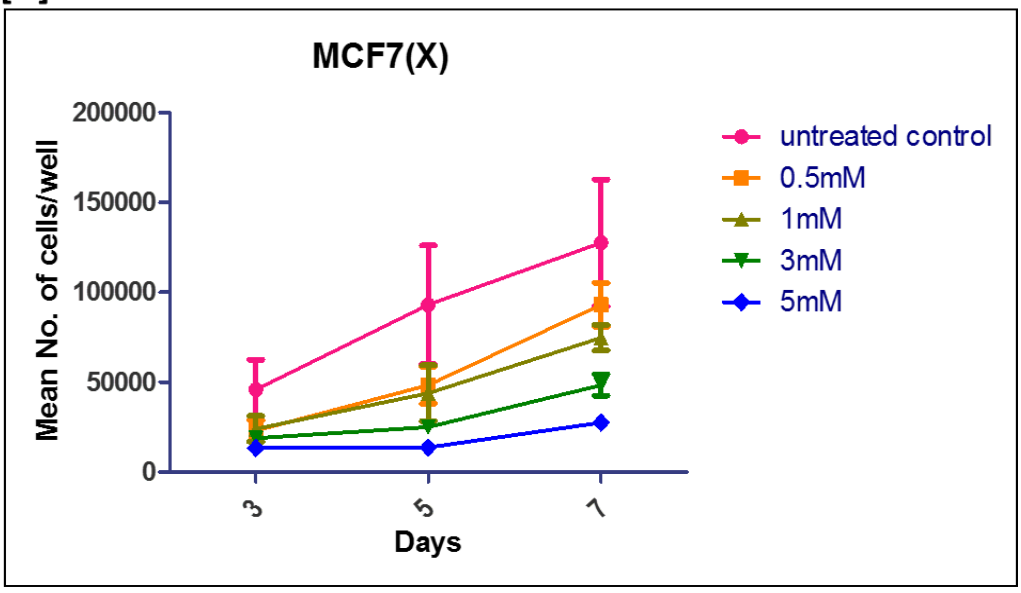

[B]

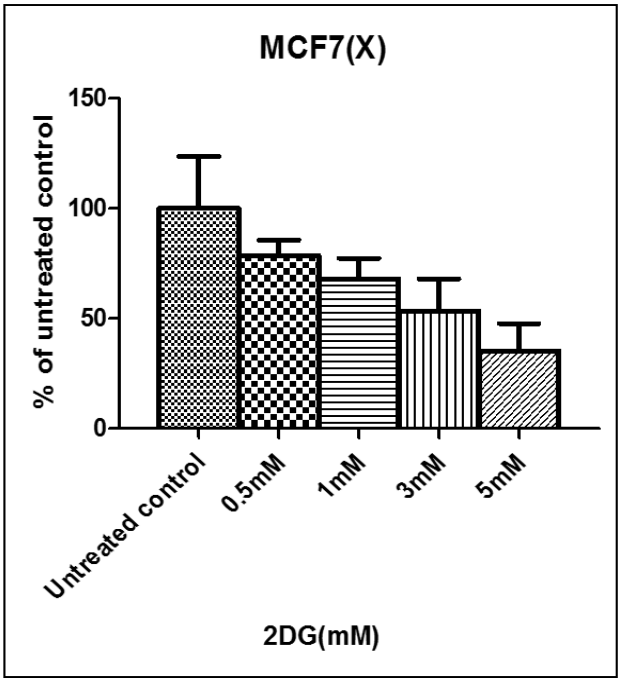

Fig 4.27. MCF7(X) were seeded at 20,000 cells/well and the growth rate was determined by Coulter counting after 0.5-5mM 2DG treatment on day 3, 5 & 7. (A) Shows growth curve profiles and (B) % of untreated control growth at day 7 (Data were represented as mean of 3 independent experiments (N=3)). The error bar indicates SEM.

[A]

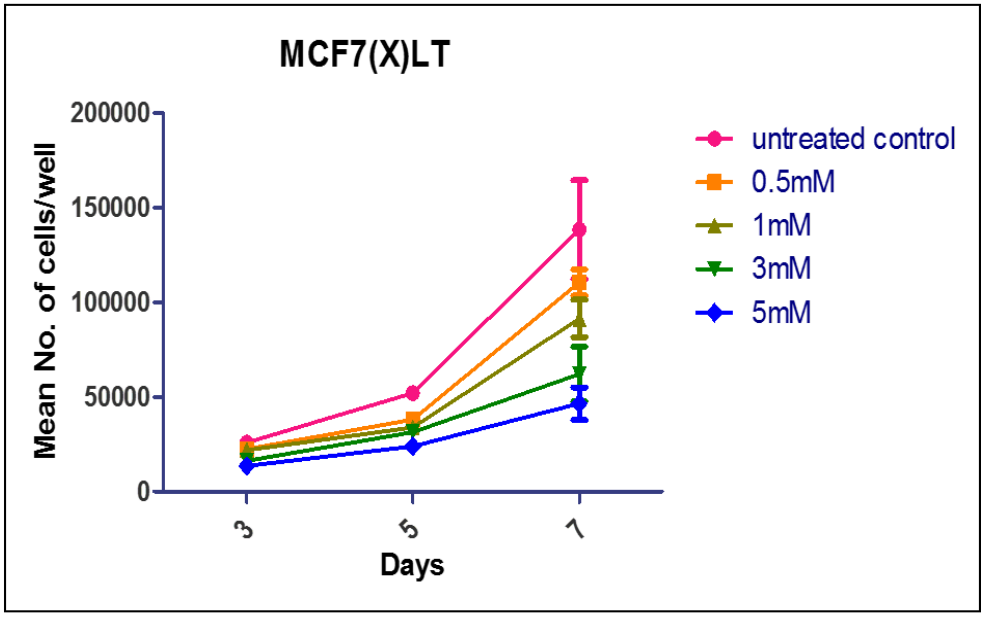

[B]

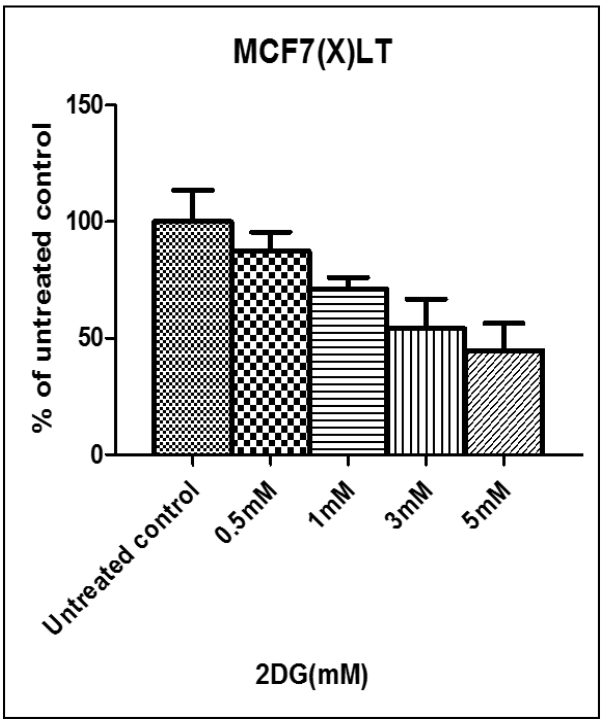

Fig 4.28. MCF7(X)LT were seeded at 20,000 cells/well and the growth rate was determined by Coulter counting after 0.5-5mM 2DG treatment on day 3, 5 & 7. (A) Shows growth curve profiles and (B) % of untreated control growth at day 7 (Data were represented as mean of 3 independent experiments (N=3)). The error bar indicates SEM.

Cell models	EC50 (mM) 2DG
MCF7	1.05±0.092
TamR	1±0.18
TamRLT	0.84±0.17
FasR	0.39±0.15
FasRLT	0.43±0.10
MCF7(X)	1.05±0.37
MCF7(X)LT	0.99±0.19

Table 4.10. EC50 calculated based on Coulter counter growth data on day 7 for the model panel. EC50 data are represented here as mean of 3 independent experiments (N=3) ± SD.

In conclusion, MCF7, TamR, MCF7(X) and MCF7(X)LT were the least sensitive models to 2DG treatment if considering EC_{50}, which approximated 1mM (Table 4.10). Fulvestrant resistant cells were the most sensitive models to 2DG treatment according to EC_{50}, which approximated 0.4mM (Table 4.10).

To help interpret sensitivity to growth inhibition by 2DG, the project also interrogated glucose transporter and hexokinase (HK) expression in the model panel. Using the 1.0ST gene microarray, expression of various glucose transporters (SLC2A1-4) and HKs (1-3) were studied in the resistant panel (Fig 4.29-4.30). SLC2A2, SLC2A4 and HK3 were not expressed across the panel (log_2 intensity values were all ≤8). The expression of SLC2A1 was reduced by ≥1.3 fold in TamRLT, FasR and FasRLT as compared to MCF7 (Fig 4.29, Table 4.11). Interestingly, the expression of SLC2A3 was markedly induced by >7 fold in fulvestrant resistant models versus MCF7. Moreover, HK1 and HK2 expression were induced (>1.2 fold changes) in FasR and FasRLT as compared to MCF7 (Fig 4.30, Table 4.12). Therefore, when interpreting the significant growth sensitivity to 2DG treatment in the fulvestrant resistant models one must also take into account that there may be a contribution for induced 2DG uptake by SLC2A3 and induced 2DG phosphorylation by HK. Similarly, expression of the further glucose transporter SLC2A1 was reduced by 1.5 fold in TamRLT (Fig 4.29, Table 4.11) and while HK1 was unchanged, HK2 was also reduced in tamoxifen resistant models by up to 1.8 fold as compared to MCF7(Fig 4.30, Table 4.12). There was also modest induction of 1.42 fold SLC2A1 in MCF7(X) (Fig 4.29, Table 4.11). These further

observations may contribute towards the apparent lower growth sensitivity according to EC_{50} in tamoxifen and oestrogen deprived resistant models versus their fulvestrant resistant counterparts.

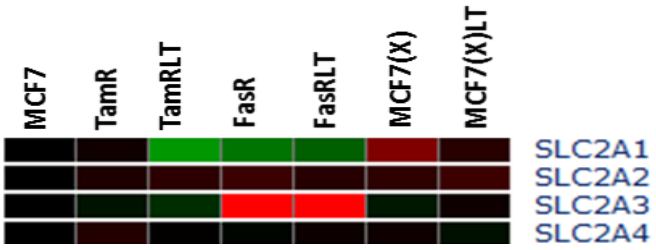

Fig 4.29. Microarray expression of glucose transporters across the panel of resistant models. SLC2A3 was induced by >7 fold in fulvestrant resistant models. SLC2A2 & SLC2A4 were not reliably-expressed across the panel (log_2intensity <7). On the heatmap, red, green & black indicate induced, reduced & no change in gene expression respectively as compared to the control MCF7 cells.

Gene symbols	TamR	TamRLT	FasR	FasRLT	MCF7(X)	MCF7(X)LT
SLC2A1	1.05	1.51	1.37	1.30	1.42	1.12
SLC2A2	———	———	———	———	———	———
SLC2A3	1.05	1.13	7.51	7.27	1.07	1.14
SLC2A4	———	———	———	———	———	———

Table 4.11. Fold changes for microarray expression of glucose transporters in endocrine resistant models vs. MCF7. Reduced fold changes (≤1.2) are indicated in green and induced fold changes (≥1.2) are indicated in red.

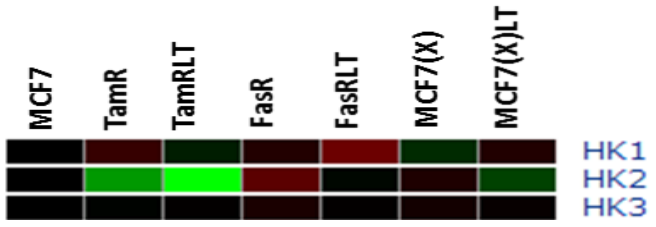

Fig 4.30. Microarray expression of hexokinases across the panel of resistant models. HK3 was not expressed across the panel. HK2 was induced in FasR & HK1 was induced in FasRLT. On the heatmap, red, green & black indicate induced, reduced & no change in gene expression respectively as compared to the control cell.

Gene symbols	TamR	TamRLT	FasR	FasRLT	MCF7(X)	MCF7(X)LT
HK1	1.12	1.06	1.08	1.25	1.09	1.07
HK2	1.39	1.82	1.21	1.02	1.07	1.15
HK3	———	———	———	———	———	———

Table 4.12. Fold changes for microarray expression of hexokinases in endocrine resistant models vs. MCF7. HK3 was not expressed (log_2 intensity <7). Reduced fold changes (≥1.2) are indicated in green & induced fold changes (≥1.2) indicated in red.

Higher growth sensitivity of fulvestrant resistant models to 2DG treatment implies an increased glucose consumption (glycolysis) as a main carbon source in these models. In contrast, other mechanisms such as amino acid degradation (lysine, valine, leucine and isoleucine) and glutaminolysis may replenish the TCA cycle by acetyl CoA, succinyl CoA and α-KG to drive growth in tamoxifen resistant and oestrogen deprived models after 2DG treatment. Increased expression of genes for lysine, valine, leucine and isoleucine degradation in tamoxifen resistant and oestrogen deprived models was compared (Table 4.13). Increased expression of Acetyl-CoA Acyltransferase 2 (ACAA2, in tamoxifen resistant and oestrogen deprived models) and Oxoglutarate Dehydrogenase-Like (OGDHL, in tamoxifen resistant and long term oestrogen deprived model) drive acetyl CoA synthesis (Table 4.13). Increased expression of Aldehyde Dehydrogenase 3 Family, Member A2 (ALDH3A2, in tamoxifen resistant and short term oestrogen deprived model) and Dihydrolipoamide S-Succinyltransferase (DLST, in TamR and MCF7(X)) drive succinyl CoA synthesis and thus feed into the TCA cycle (Table 4.13). The effect of glutamine consumption as an alternative carbon source on growth of resistant models and sensitivity to glutamine deprivation is investigated in section 4.2.4.3. Interestingly, basal ECA was higher in TamRLT as compared to other resistant models and MCF7 control (Fig 4.19A). This suggests an additional pathway is operating to maintain the glycolysis intermediate in TamRLT. Study of pentose phosphate pathway (PPP) suggest a possible role for Transaldolase 1 (TALDO1) enzyme in this model. TALDO1 plays a role in the non-oxidative pentose phosphate pathway to balance the metabolite in the PPP and thus regulates glycolysis intermediates such as fructose 6-phosphate and glyceraldehyde 3-phosphate.

Sedoheptulose 7-phosphate + D-glyceraldehyde 3-phosphate → D-erythrose 4-phosphate + D-fructose 6-phosphate

Glucose 6-phosphate is a precursor for PPP and 2DG treatment inhibits phosphorylation of glucose to glucose 6-phosphate (via inhibition of HK/ ADP-dependent glucokinase). Therefore, 2DG treatment can potentially disrupt the PPP and interrupt regulatory mechanism of glycolysis

intermediates via TALDO1. This may explain a sudden ECA fall after 1mM 2DG treatment (for 24hrs) in TamRLT (Fig 4.20C). Although, other compensatory mechanisms such as glutaminolysis and amino acid degradation somehow masked the growth inhibitory effect of 0.5mM 2DG treatment in this model (Fig 4.23), despite a substantial growth inhibitory effect was observed after 1mM 2DG treatment in TamRLT (Fig 4.24).

TamR	TamRLT	MCF7(X)	MCF7(X)LT
ACAA2	ACAA1	ACAT2	ACAD8
ACAT1	ACAA2	ACAA2	ACAA2
ALDH1B1	ACADM	HIBADH	ACADM
ALDH3A2	ACADS	ACAT1	HIBADH
HMGCS1	ACAT1	ALDH1B1	ACAT1
AASS	ALDH1B1	ALDH3A2	ALDH9A1
OGDHL	ALDH3A2	HMGCL	BCAT1
POLD1	HMGCL	PCCB	HMGCL
POLD3	PCCB	BCAT2	PCCB
GLT25D1	AASS	HMGCS2	OXCT1
DLST	OGDHL	HMGCS1	HMGCS2
		EHHADH	EHHADH
		MCCC1	MCCC1
		POLD1	AADAT
		SETD8	SETD8
		SETD7	OGDHL
		AADAT	TMLHE
		TMLHE	WHSC1L1
		DLST	

Table 4.13. Induced probe IDs (≥1.2 fold changes) representing either valine, leucin & isoleucin degradation or lysine degradation in TamR, TamRLT, MCF7(X) & MCF7(X)LT vs. MCF7. Red indicates probe IDs whose activity is associated with acetyl CoA (ACAA2 & OGDHL) and succinyl CoA (ALDH3A2 & DLST) generation in these models.

4.2.4. Role for glutaminolysis: impact of exogenous glutamine and glutamine deprivation on growth of endocrine resistant breast cancer cells

Although glucose is the main fuel source for energy pathways in many proliferative tumours, it accounts for insufficient energy production through glycolysis (2ATP molecules). Instead, glutamine catabolism (glutaminolysis) is the more efficient pathway to replenish the TCA cycle intermediates (anaplerosis) and so produce ATP via oxidative phosphorylation (Fan et al. 2013). Glutaminolysis is mediated by two mitochondrial enzymes (glutaminases; GLS and GLS2) to generate glutamate which participates in synthesis of glutathione and a key TCA pathway substrate, α-KG, via transaminases (GLUD1 and GLUD2).

There is evidence that glutaminolysis can be important to fuel cancer cell proliferation. In some cancer cells including HeLa and MCF7, it has been reported that exchange of glutamine with essential amino acids activates serine/threonine kinase mTOR and thus regulates cell proliferation (Nicklin et al.2009). Moreover, monitoring glutaminolysis provides a diagnostic and prognostic tool to trace glutamine consumption in proliferative tumour cells. On this basis 18F-(2S,4R)4-fluoroglutamine PET imaging is able to detect proliferating tumours which had induced glutaminolysis (Leiberman et al.2011). Glutamine dependency for growth (glutamine addiction) is variable among tumour cells, evidenced by a study of lung cancer cells which displayed variable growth-dependency to glutamine deprivation. In this regard, lung cancer cells with a higher glutaminolysis rate were more dependent on glutamine consumption for proliferation (van den Heuvel et al.2012). Interestingly, study of breast cancer subtypes has also revealed higher sensitivity to glutamine deprivation in basal as compared to luminal subtypes. De novo glutamine synthesis via glutamine synthetase (GS: encoded by the GLUL gene) occurred in the basal subtype to sustain the growth and proliferation of such breast cancer cells (Kung et al. 2011). However, the importance of glutamine in fuelling endocrine resistant cells has not been addressed.

To achieve this, therefore, glutamine dependency was assessed in two extreme glutamine conditions in the project, exploring impact of exogenous L-glutamine (10mM versus basal concentration in the model maintenance media of 4mM) and glutamine deprivation across the panel of endocrine resistant models versus the parental MCF7 line. Impact on growth rate was determined after 7 days treatment versus basal growth conditions (containing 4mM glutamine) for each model (Fig 4.31A-B).

These experiments showed that the growth of MCF7 was only very slightly increased (by 9.6%) by 10mM exogenous glutamine and also remained unchanged in glutamine deprived conditions as compared to basal growth conditions (4mM glutamine supplementation) for MCF7 (Fig 4.31A) implying limited contribution for glutaminolysis and minimal glutamine dependency in this endocrine responsive model. Similarly, a study by Kung et al. (2001) revealed glucose depletion had more effect on MCF7 growth compared to glutamine deprivation in such cells. TamR cell growth was also only slightly increased (by 10.8%) under excess glutamine conditions as compared to basal growth (Fig 4.31B). However, the growth of TamR cells in glutamine deprived conditions was significantly reduced as compared to basal growth by 46.2% (P <0.01) and it also reduced as compared to excess glutamine conditions by 57% (Fig 4.31B). The growth of TamRLT was again only slightly increased by 10.4% in excess glutamine conditions as compared to the basal growth (Fig 4.31C). However, growth of this model was significantly and substantially reduced after glutamine deprivation by 67.6% (P <0.001) as compared to basal growth and it also reduced by 78% in glutamine deprived condition as compared to excess glutamine conditions (Fig 4.31C). The growth of FasR was also only slightly increased by 13% in excess glutamine conditions as compared to basal growth conditions (Fig 4.31D). However, FasR growth was modestly reduced by 22.3% (P <0.05) in glutamine deprived conditions as compared to basal growth and it further reduced by 35.3% as compared to excess glutamine conditions (Fig 4.31D). The growth of FasRLT was again only slightly increased by 12.4% in excess glutamine conditions as compared to basal growth conditions (Fig 4.32A). However, the growth of FasRLT was significantly reduced (P<0.01) by 36.6% in glutamine deprived condition as compared to basal growth conditions and further reduction was observed by 49% in glutamine deprived conditions as compared to excess glutamine conditions (Fig 4.32A). The growth of MCF7(X) was slightly induced by 24% in excess glutamine conditions as compared to basal growth (Fig 4.32B). However, the growth of MCF7(X) was significantly reduced by 23.5% in glutamine deprived conditions as compared to basal growth condition and further growth reduction (47.5%) was detected in glutamine deprived conditions as compared to excess glutamine conditions (Fig 4.32B). The growth of MCF7(X)LT was similarly slightly increased in excess glutamine conditions as compared to basal growth by 9.4% (Fig 4.32C). However, the growth of this model was significantly reduced by 36.9% (P<0.01) in glutamine deprived condition as compared to basal growth and further reduction was observed by 46.3% in glutamine deprived condition as compared to excess glutamine conditions (Fig 4.32C).

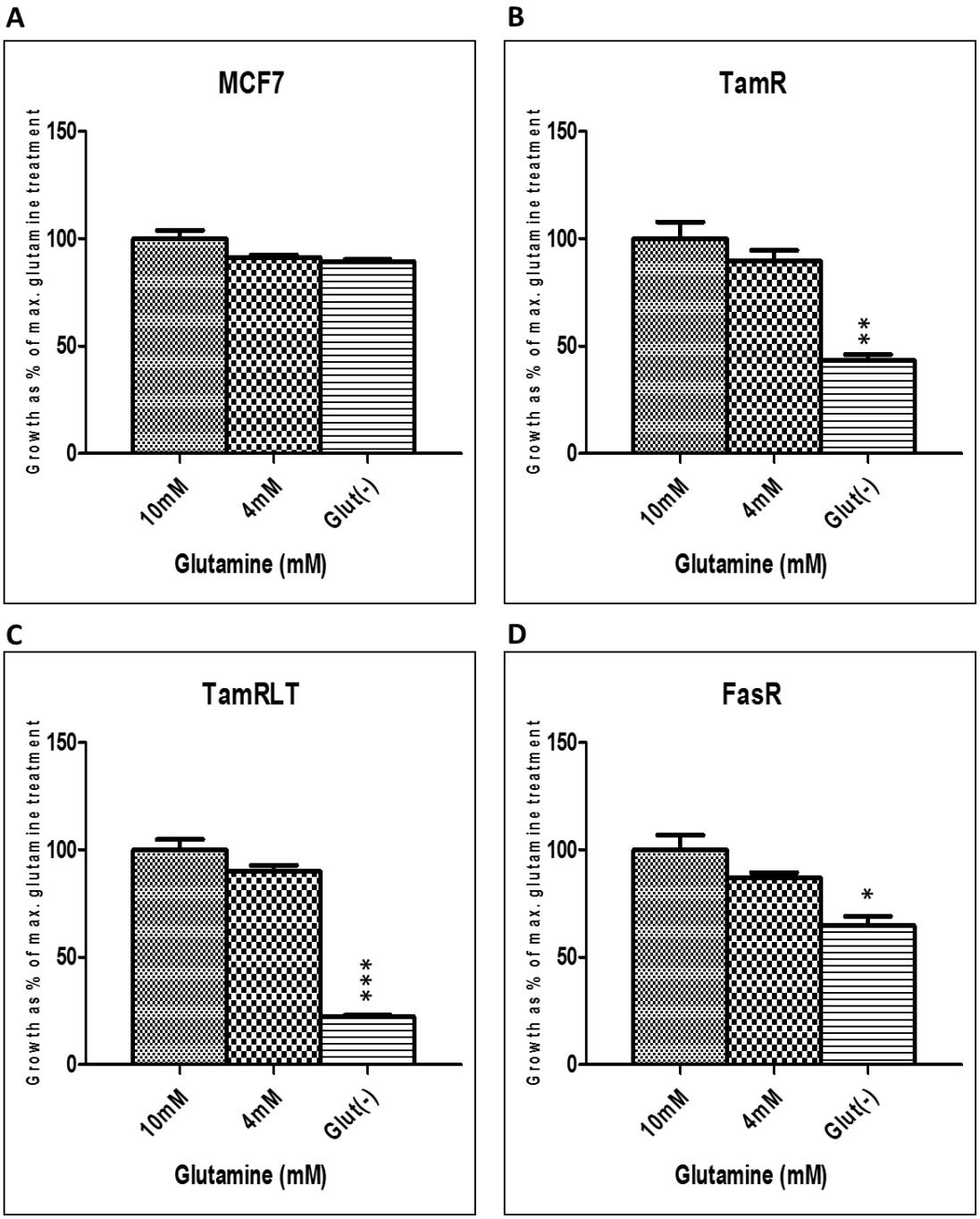

Fig 4.31A-D. Growth rate of MCF7, TamR, TamRLT & FasR after 7d treatment with excess glutamine (10mM), basal glutamine (4mM) & glutamine deprived conditions. Data were represented as mean of 3 independent experiments (N=3). The error bar indicates SEM. * (P<0.05), ** (P<0.01) & *** (P<0.001) following ANOVA with Dunnett's post hoc correction.

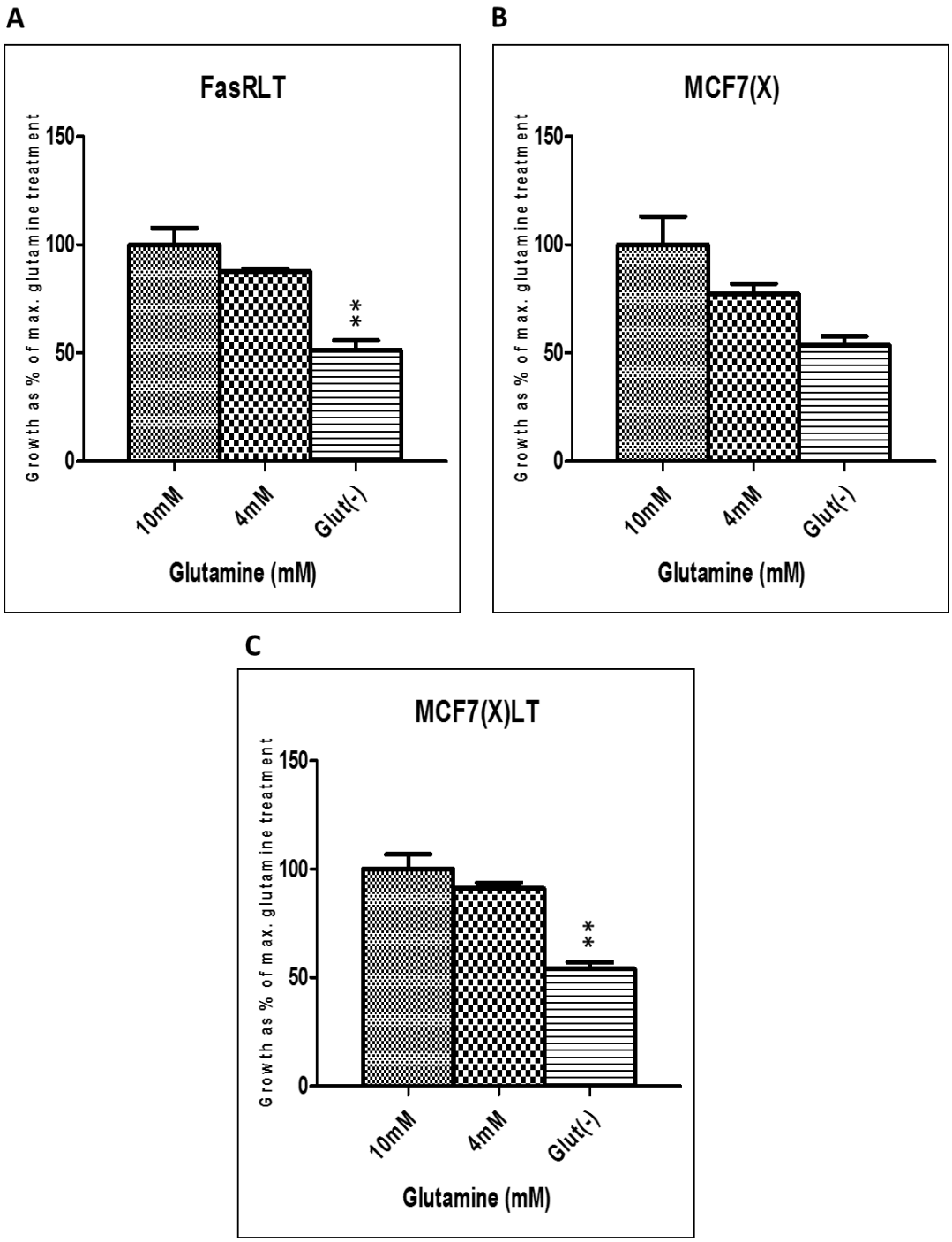

Fig 4.32A-C. Growth rate of FasRLT, MCF7(X) & MCF7(X)LT after 7d treatment with excess glutamine (10mM), basal glutamine (4mM) & glutamine deprived conditions. Data were represented as mean of 3 independent experiments (N=3). The error bar indicates SEM. ** (P<0.01) following ANOVA with Dunnett's post hoc correction.

In general, excess exogenous glutamine appeared to have little impact but all resistant lines showed some sensitivity to glutamine deprivation and thus evidence of significant growth dependency on glutaminolysis. However, tamoxifen resistant models were the most sensitive of the resistant models cells to glutamine deprivation (>40% growth reduction), contrasting with the largely-refractory MCF7 model (Fig 4.31A-C). To further help interpret these findings, expression of various glutamine transporters, glutaminolysis and de novo glutamine synthesis enzymes were profiled using the 1.0ST gene microarray in the model panel (Fig 4.33).

The expression of SLC1A5 (a glutamine influx transporter) and SLC7A5 (a glutamine efflux transporter) was induced across the whole resistant panel as compared to MCF7 (Fig 4.33, Table 4.14). Expression of SLC7A6 (a further glutamine influx transporter) was also induced in fulvestrant resistant models, oestrogen deprived models and TamR as compared to MCF7 (Fig 4.33, Table 4.14). Such expression changes must in total ensure efficient delivery of glutamine for glutaminolysis in the resistant models, and perhaps explain why there was little further growth impact of exposing the cells to excess exogenous glutamine at 10mM.

Glutaminases GLS and GLS2 are involved during glutaminolysis to generate glutamate as follows: GLS/GLS2: L-glutamine + H_2O → L-glutamate + NH_3. The expression of GLS and GLS2 was reduced in oestrogen deprived and fulvestrant resistant models as compared to MCF7 (Fig 4.33, Table 4.14). This reduced expression may have dampened the ability of these models to use glutaminolysis compared with the more highly glutamine deprivation-sensitive tamoxifen resistant lines. Indeed, fulvestrant sensitivity to glycolysis inhibitor (2DG; EC50: 0.4mM) is supportive of the concept that they may use glucose as the main carbon source for growth and proliferation.

While the transaminase GLUD2 was not expressed across the resistant panel (log_2 <8) (Fig 4.33, Table 4.14), GLUD1, a further glutaminolysis enzyme involved in synthesis of glutathione and α-KG, was induced in the oestrogen deprived resistant cells and also FasRLT as compared to MCF7 (Fig 4.33, Table 4.14).

GLUD1: L-glutamate + H_2O + $NAD(P)^+$ = 2-oxoglutarate (α-KG) + NH_3 + NAD(P)H + H^+

This enzyme enables use of L-glutamic acid in the growth media (0.13mM in RPMI1640) as an alternative carbon source to generate α-KG and ultimately promote some growth despite glutamine deprivation in these models.

Growth sensitivity to glutamine deprivation has been reported to be associated with de novo glutamine synthesis via GLUL expression in luminal breast cancer cells (Kung et al. 2011) or with

use of alternative anaplerotic pathways via pyruvate carboxylase (PC; converts pyruvate to OAA) as seen in glioblastoma cells (Cheng et al. 2011): PC: ATP + pyruvate + HCO_3^- → ADP + phosphate + oxaloacetate (OAA). However, there was no convincing evidence for the GLUL or PC mechanism in the panel of resistant models, since (i) although GLUL expression was induced in MCF7(X) cells, it was reduced in glutamine deprivation-sensitive tamoxifen and fulvestrant resistant models (Fig 4.33, Table 4.14) and (ii) PC expression was reduced in several of the glutamine deprivation-sensitive resistant models versus MCF7 (Fig 4.33, Table 4.14).

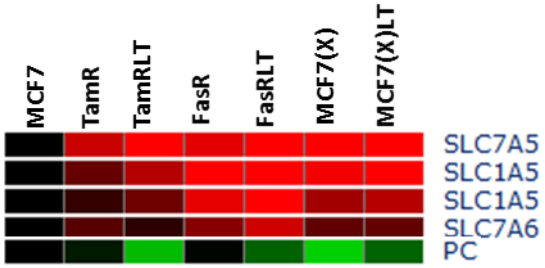

Fig 4.33. Microarray expression of glutamine transporters and pyruvate carboxylase across the panel of resistant models. On the heatmap, red, green & black indicate induced, reduced & no change in gene expression respectively as compared to the control MCF7 cells.

Gene symbols	TamR	TamRLT	FasR	FasRLT	MCF7(X)	MCF7(X)LT
SLC1A5	1.32	1.64	2.23	2.49	1.94	2.23
SLC1A5	1.15	1.35	1.87	2.08	1.55	1.64
SLC7A5	1.73	2.28	1.87	2.29	1.99	2.08
SLC7A6	1.27	1.13	1.44	1.76	1.31	1.31
PC	1.07	1.66	1.02	1.31	1.76	1.32

Table 4.14. Fold changes for glutamine transporters and pyruvate carboxylase in endocrine resistant models vs. MCF7. Reduced expression with fold changes ≥1.2 is indicated in green & induced expression with fold changes ≥1.2 are indicated in red.

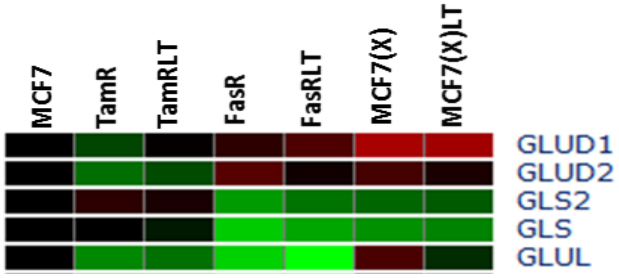

Fig 4.34. Microarray expression of glutaminase (GLS & GLS2), glutamate dehydrogenase (GLUD1 & GLUD2) and glutamine synthase (GLUL) across the panel of resistant models. On the heatmap, red, green & black indicate induced, reduced & no change in gene expression respectively as compared to the control MCF7 cells.

Gene symbols	TamR	TamRLT	FasR	FasRLT	MCF7(X)	MCF7(X)LT
GLS	1.01	1.07	1.74	1.57	1.48	1.43
GLS2	1.13	1.07	1.53	1.37	1.33	1.28
GLUD1	1.21	1.02	1.13	1.24	1.58	1.55
GLUD2	———	———	———	———	———	———
GLUL	1.45	1.36	1.77	2.17	1.23	1.13

Table 4.15. Fold changes for GLS, GLS2, GLUD1, GLUD2 & GLUL in endocrine resistant models vs. MCF7. GLUD2 was not expressed (log_2 intensity< 7). Reduced expression with fold changes ≥1.2 are indicated in green & induced expression with fold changes ≥1.2 are indicated in red.

4.2.5 The contribution of mitochondrial bioenergetics (OxPhos) in endocrine resistant breast cancer cells

There is considerable evidence supportive of deregulation of the energy-associated oxidative phosphorylation pathway in cancer epithelial cells. Thus, induced expression of OxPhos components was reported by Bonuccelli et al. (2010) in breast cancer epithelial cells as compared to adjacent cancer-associated fibroblasts (CAFs). Furthermore, increased activity of OXPhos components including NADH dehydrogenase, SDH and cytochrome c oxidase was also detected in breast cancer epithelial cells from >2000 patients as compared to CAFs (Whitaker-Menezes et al. 2011). Induced mitochondrial fatty acids oxidation and therefore induced OxPhos activity has similarly been reported in ovarian cancer cells (Nieman et al. 2011). In situ metabolic control analysis of locally-advanced breast tumours (from women aged 50-71) has confirmed upregulation of mitochondrial respiration in breast cancer cells as compared to matched normal tissue, with induced activity of the OxPhos components such as complex I, II, III, IV, ATP synthase, ATP/ ADP carrier and Pi carrier (Kaambre et al. 2013). Based on induced respiration in some cancer cells, therapeutic strategies focused on targeting OxPhos components to reduce growth of tumour cells. In the current study induced expression of several OxPhos components was detected in endocrine resistant models as compared to MCF7 (Fig 4.10, Table 4.32). Based on functional annotation analysis (Chapter 3, Fig 3.8A, Table 3.16), components of complex I (NDUFA3, NDUFA8, NDUFA9, NDUFB5, NDUFB9, NDUFB10 and NDUFS3) and complex III (UQCRFS1) got the highest enrichment score for the shared induced metabolic genes in resistant models versus MCF7. Thus metformin and antimycin A were used to pharmacologically-inhibit complex I and III of OxPhos respectively to gauge whether OxPhos has an enhanced role in resistant cells. Oxygen consumption (a surrogate marker of OxPhos) and growth were determined after each treatment in the resistant panel.

4.2.5.1 The inhibitory effect of antimycin A on oxygen consumption rate in endocrine resistant breast cancer cells

Complex III (ubiquinol:cytochrome c oxidoreductase) of the electron transport chain catalyses reversible transfer of two electrons from UQH2 to cytochrome c and generates a proton gradient across the inner mitochondrial membrane. This complex contains three redox subunits comprising cytochrome b, cytochrome c1, and the iron-sulfur protein (ISP), which contain two hemes B (BH and BL), heme C and a Rieske iron-sulfur protein [2Fe-2S] respectively. Hydroquinone oxidation which occurs via the Q cycle involves bifurcation of electrons at the Q_0 position of the cytochrome b so one electron transfers to ISP, cytochrome c1 and then on to cytochrome c (the mobile carrier). The other electron transfers to the heme bL and then on to the heme bH near the quinone reduction site of cytochrome b (Q_i). During the Q cycle two protons are consumed from the matrix and four protons are pumped into the intermembrane space (Iwata et al. 1998). Antimycin A (AA) is an antibiotic which is produced by Streptomyces Kitazawensis (Nakayama et al. 1956). AA is the most potent inhibitor of OxPhos and so comprises a useful tool to help determine OxPhos contribution in the resistant models. Its mechanism of action is to bind to the quinone reduction site (Q_i) of cytochrome b and thus disrupts the Q cycle. AA inhibits reoxidation of cytochrome b and partially blocks reduction of cytochrome c via cytochrome bc1 of complex III (Muller 2002).

In the current study, a surrogate marker of OxPhos activity (oxygen consumption) was determined across the panel of endocrine resistant models under basal growth conditions and after 24hrs AA treatment (Fig 4.35-4.37). MitoXpress® Xtra probe (a cell impermeable oxygen sensing fluorophore) was used to measure extracellular oxygen consumption (OC) across the resistant panel. This probe is quenched by O_2 and thus, the fluorescence signal is inversely correlated with the extracellular O_2. While the fluorescence signal is proportional to OC or OxPhos in the cell. Cells were seeded (80,000 cells/well) to measure OC under basal condition and after 24hrs AA treatment (at 5nM and 10nM).

Under basal conditions, OC was significantly increased in TamRLT (P<0.05), FasR (P<0.01), FasRLT (P<0.001), MCF7(X) (P<0.001) and MCF7(X)LT models (P<0.001) as compared to MCF7 cells (Fig 4.35), providing evidence for increased OxPhos in most endocrine resistant states. While more modestly-increased in tamoxifen resistance, OC increased by ≥2 fold in fulvestrant resistant and oestrogen deprived resistant models as compared to MCF7 (Fig 4.35).

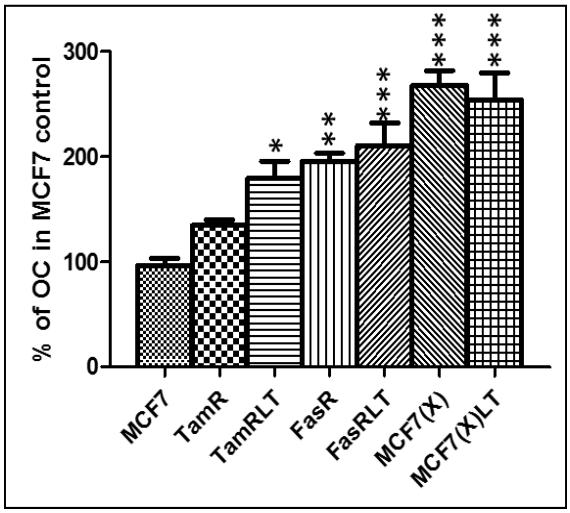

Fig 4.35. Basal oxygen consumption (OC) was determined in endocrine resistant cells vs. MCF7 control. Data are represented as mean of 3 independent experiments (N=3). The error bar indicates SEM. * (P<0.05), ** (P<0.01) & *** (P<0.05) following ANOVA with Dunnett's post hoc correction.

In MCF7, the OC was significantly reduced by 40% and 67% after 5nM (P<0.001) and 10nM (P<0.001) AA treatment respectively as compared to untreated control (Fig 4.36A). The OC was also significantly reduced in TamR cells by 51% and 69% after 5nM (P<0.01) and 10nM (P<0.001) AA treatment respectively as compared to untreated control (Fig 4.36B). In TamRLT, the OC was more substantially reduced by 77% and 83% after 5nM (P<0.001) and 10nM (P<0.001) AA treatment respectively (Fig 4.36C). The OC in FasR was significantly reduced by 60% and 69% after 5nM (P<0.001) and 10nM (P<0.001) AA treatment respectively as compared to untreated control (Fig 4.36D). Comparable reduction was seen in FasRLT, with the OC significantly reduced by 61% and 69% after 5nM (P<0.01) and 10nM (P<0.01) AA treatment respectively as compared to untreated control (Fig 4.37A). In MCF7(X), the OC was more reduced by 36% and 52% after 5nM (P<0.01) and 10nM (P<0.01) AA treatment respectively as compared to untreated control (Fig 4.37B) while in MCF7(X)LT, OC was reduced by 53% and 59% after 5nM (P<0.05) and 10nM (P<0.01) AA treatment as compared to untreated control (Fig 4.37C).

In summary, the OC was reduced by ≥60% in the most AA-sensitive models (TamRLT, FasR and FasRLT) and by ≤50% in the least sensitive models examined (MCF7, TamR, MCF7(X) and MCF7(X)LT) after 5nM AA treatment for 24hrs (Fig 4.36-4.37). All resistant lines (except MCF7(X)) appeared to show somewhat increased sensitivity of their OC to AA compared with the endocrine responsive MCF7 cells at the 5nM concentration. These findings are in keeping with

increased importance for Complex III-driven OxPhos in resistance, most prominently for TAMRLT cells.

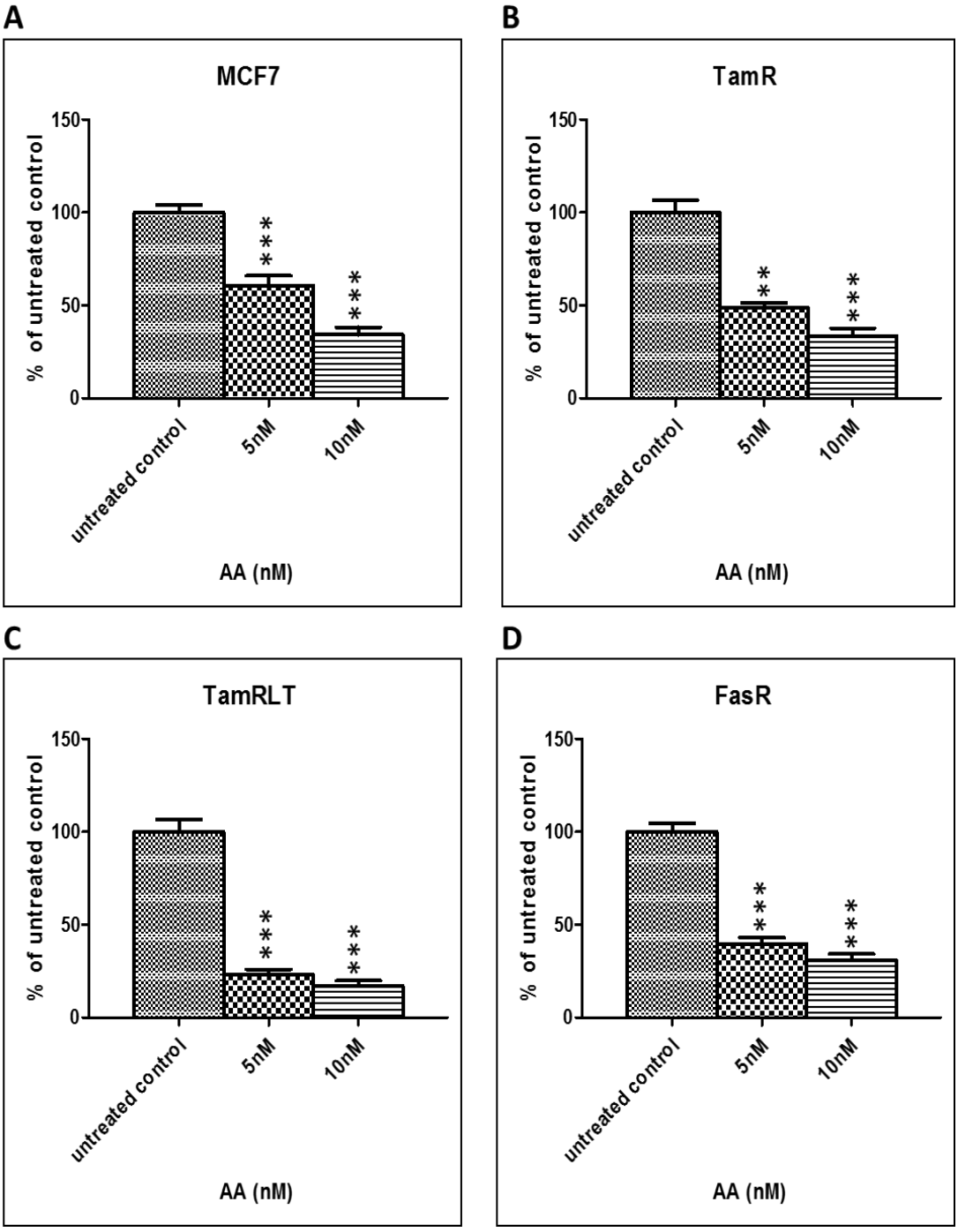

Fig 4.36A-D. OC quantified in MCF7, TamR, TamRLT & FasR cells after 24hrs antimycin A (AA) treatment. Data are expressed as % of untreated control and comprise a mean of 3 independent experiments (N=3). The error bar indicates SEM. ** (P<0.01) & *** (P<0.001) following ANOVA with Bonferroni post hoc correction.

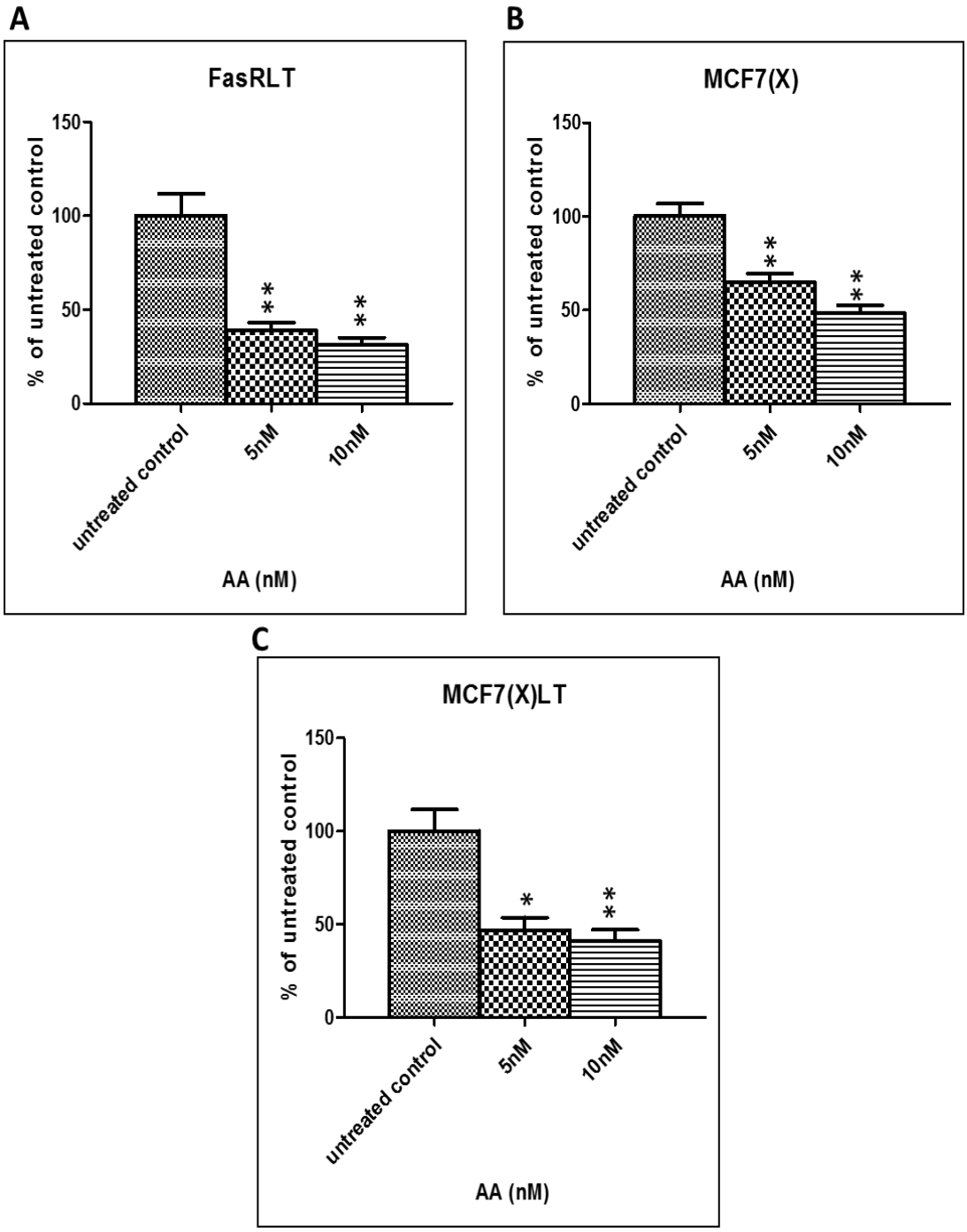

Fig 4.37A-C. OC quantified in FasRLT, MCF7(X) & MCF7(X)LT cells after 24hrs antimycin A (AA) treatment. Data are expressed as % of untreated control and comprise a mean of 3 independent experiments (N=3). The error bar indicates SEM. * (P<0.05) & ** (P<0.01) following ANOVA with Bonferroni post hoc correction.

4.2.5.2 The inhibitory effect of antimycin A on growth of endocrine resistant breast cancer cells

To study the inhibitory effect of AA treatment on growth and so further gauge importance of OxPhos in resistance, the breast cancer models were seeded (at 20,000 cells/well) for 24hrs prior to AA administration over 5, 10, 20, 30, 40, 50 and 100nM concentration range. Cell growth was then determined by Coulter counting on day 3, 5 and 7 for the panel of endocrine resistant models (Fig 4.38-4.43). Mean of half-maximum response (EC_{50}) for AA treatment was calculated based on growth on day 7 for individual models (Table 4.16, Appendix 21).

Cell models	EC50 (nM) AA
MCF7	10.57±.5.56
TamR	3.41±0.212
TamRLT	0.72±0.35
FasR	3.88±0.35
FasRLT	1.30±0.71
MCF7(X)	4.02±2.37
MCF7(X)LT	4.69±1.25

Table 4.16. EC_{50} calculated based on Coulter counter growth data on day 7 for the model panel. EC_{50} data are represented here as mean of 3 independent experiments (N=3) ± SD.

The growth of the endocrine responsive MCF7 cells was significantly reduced, by approximately 40% versus untreated control at 7 days, with either 40nM (P<0.05), 50nM (P<0.05) or 100nM (P<0.01) AA treatment (Fig 4.38B). Indeed, the cell number had also dropped below the initial seeding density (20,000 cells/well) after 30-100nM AA treatment by day 7 (Fig 4.38A). The mean half-maximum response (EC_{50}) for AA treatment in MCF7 was 10.5nM (Table 4.16). TamR growth was significantly reduced by ≥65% after 10nM (P<0.01), 20nM (P<0.01), 30nM (P<0.01), 40nM (P<0.01), 50nM (P<0.001) and 100nM (P<0.001) AA treatment as compared to untreated control (Fig 4.39B). The cell number dropped below the seeding density after 40-100nM AA treatment on day 7 (Fig 4.39A). The mean EC_{50} for AA treatment in TamR was 3.4nM (Table 4.16). TamRLT growth was particularly sensitive to AA, significantly reducing (P<0.0001) by ≥80% from 5nM through to 100nM AA treatment (Fig 4.40B). The cell number dropped below the seeding density by 100nM AA treatment on day 7 (Fig 4.40A). The mean EC_{50} for such treatment in TamRLT was

0.7nM (Table 4.16). Fulvestrant resistant cells also showed increased sensitivity to AA compared with the MCF7 model. The growth of FasR was significantly reduced by ≥44% after 5nM (P<0.01), 10nM (P<0.001), 20nM (P<0.001), 30nM (P<0.0001), 40nM (P<0.0001), 50nM (P<0.0001) and 100nM (P<0.0001) AA treatment as compared to untreated control (Fig 4.41A-B). The mean EC_{50} for AA treatment in FasR was 3.8nM (Table 4.16). Although some variation was seen so significance was not reached, mean FasRLT growth was reduced by ≥57% after 10nM (Fig 4.42A-B) while the mean EC_{50} for AA treatment was 1.3nM (Table 4.16). Oestrogen deprivation resistant cells also showed significant growth-sensitivity to AA. The growth of MCF7(X) was significantly reduced by ≥55% after 5nM (P<0.05), 10nM (P<0.01), 20nM (P<0.01), 30nM (P<0.001), 40nM (P<0.001), 50nM (P<0.001) and 100nM (P<0.001) AA treatment as compared to untreated control (Fig 4.43A-B). The mean EC_{50} for AA treatment in MCF7(X) was 4nM (Table 4.16). The growth of MCF7(X)LT was also significantly reduced by ≥62% after 10nM (P<0.01), 20nM (P<0.01), 30nM (P<0.001), 40nM (P<0.001), 50nM (P<0.001) and 100nM (P<0.001) AA treatment (Fig 44A-B), with a mean EC_{50} of 4.6nM (Table 4.16).

In summary, all the resistant models showed increased sensitivity to AA treatment compared with MCF7 cells suggesting increased growth dependency on complex III in OxPhos in resistant cells. Based on EC_{50} data, TamRLT and FasRLT were the most sensitive models to AA treatment (Table 16), although the FasRLT findings remain equivocal due to lack of significance.

[A]

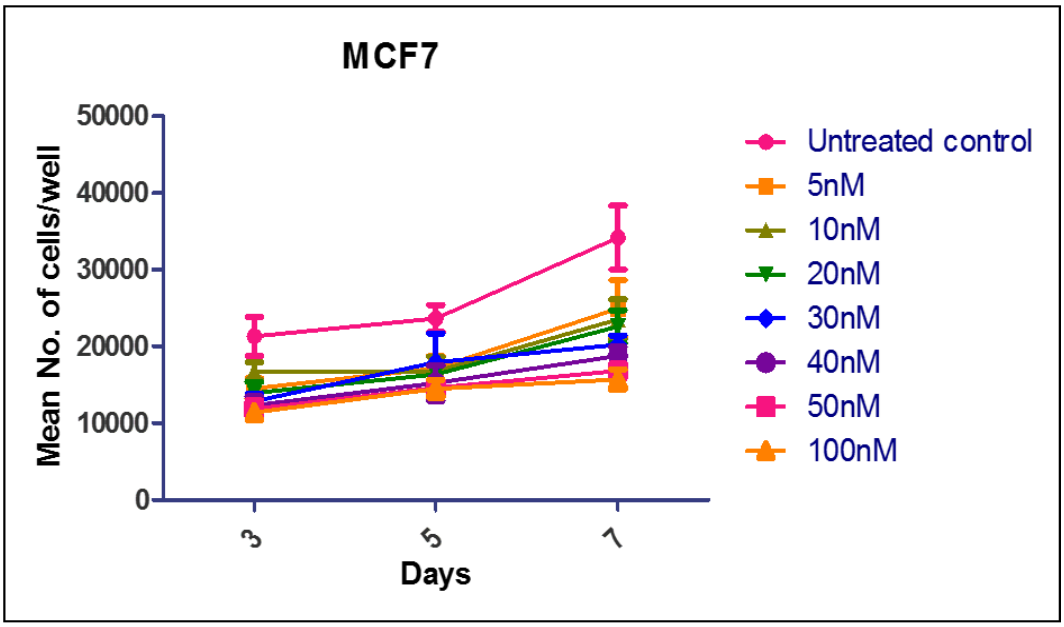

[B]

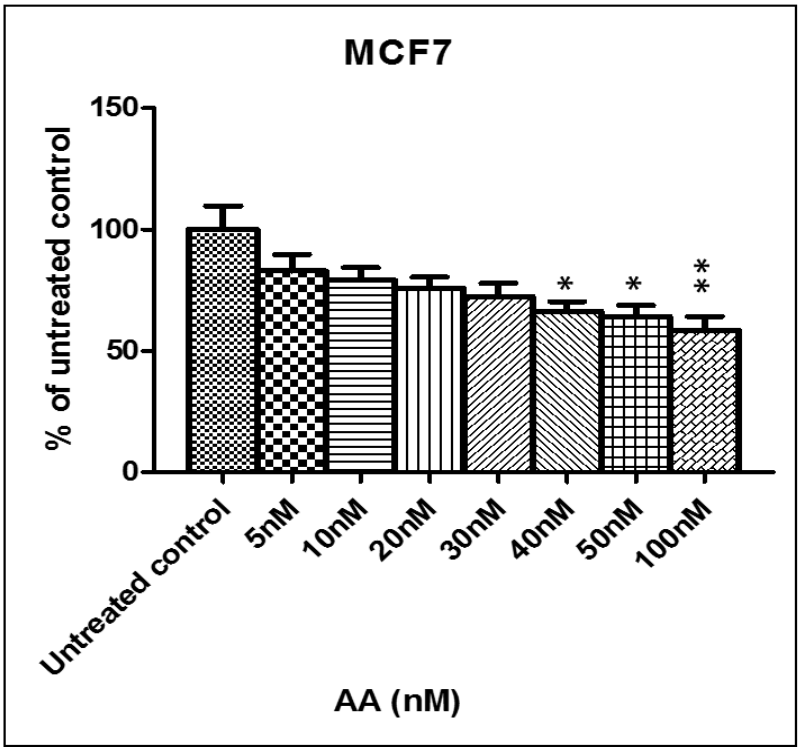

Fig 4.38. MCF7 cells were seeded at 20,000 cells/well and the growth was determined by Coulter counting after 5-100nM antimycin A (AA) treatment on day 3, 5 & 7. (A) Shows growth curve profiles and (B) % untreated control growth at day 7. Data were represented as mean of 3 independent experiments (N=3). The error bar indicates SEM. *(P<0.05) & ** (P<0.01) following ANOVA with Bonferroni post hoc correction.

[A]

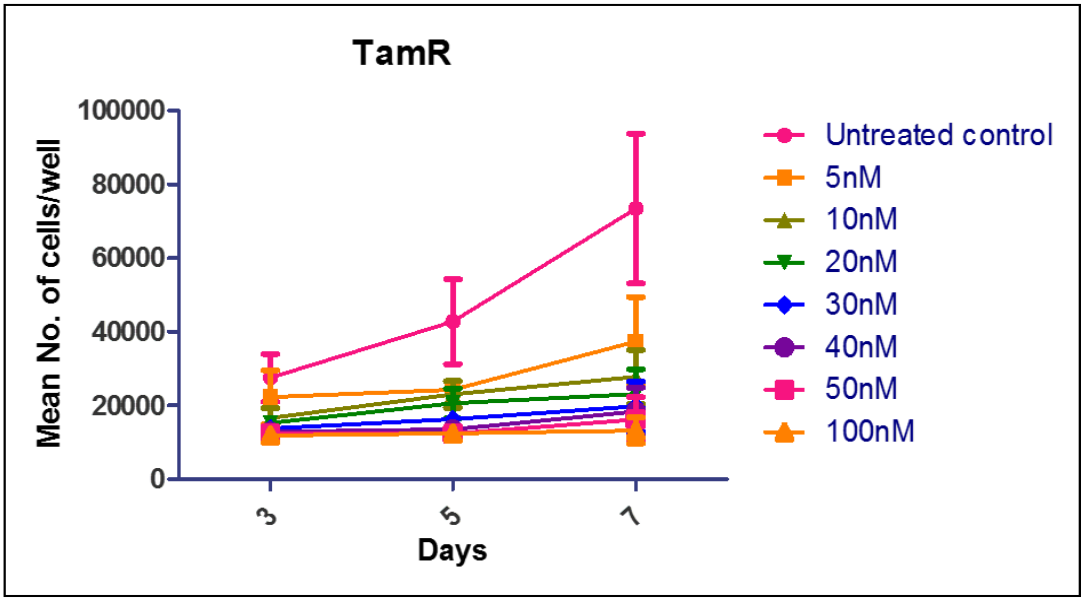

[B]

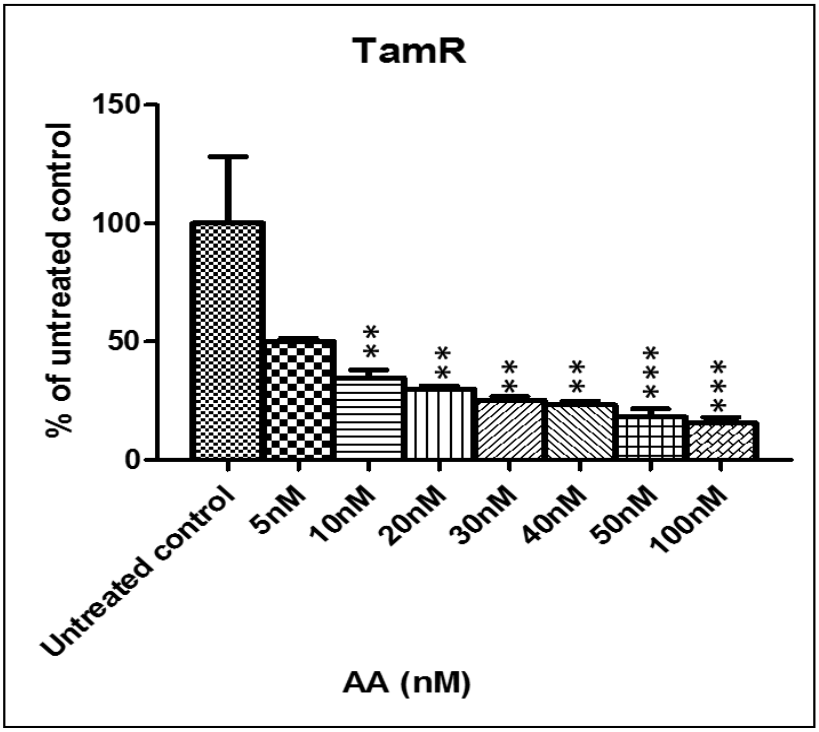

Fig 4.39. TamR cells were seeded at 20,000 cells/well and the growth was determined by Coulter counting after 5-100nM antimycin A (AA) treatment on day 3, 5 & 7. (A) Shows growth curve profiles and (B) % untreated control growth at day 7. Data were represented as mean of 3 independent experiments (N=3). The error bar indicates SEM. ** (*P*<0.01) & *** (*P*<0.001) following ANOVA with Bonferroni post hoc correction.

[A]

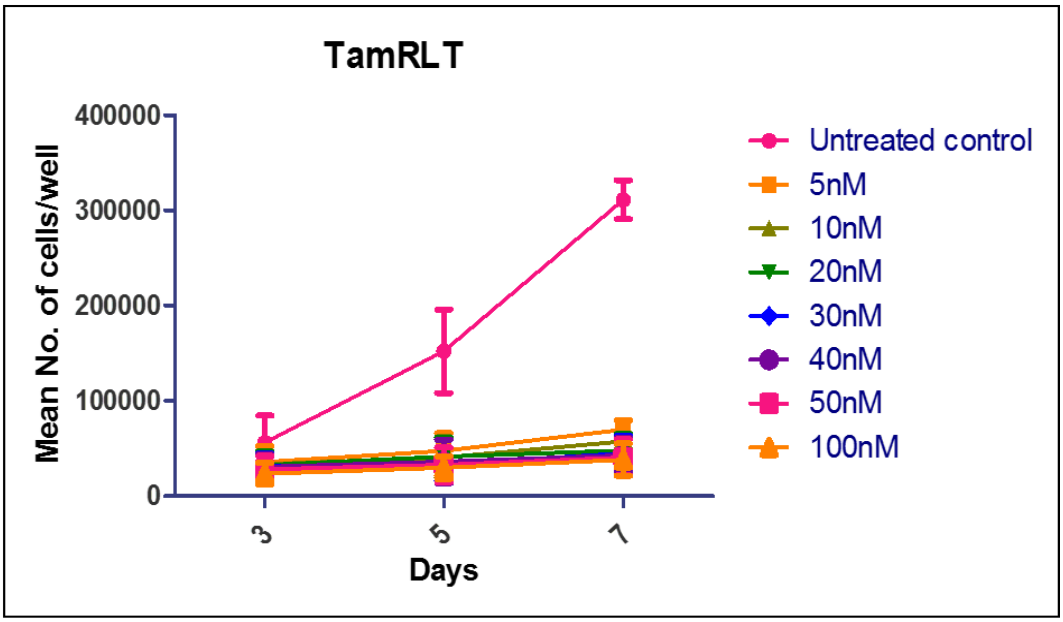

[B]

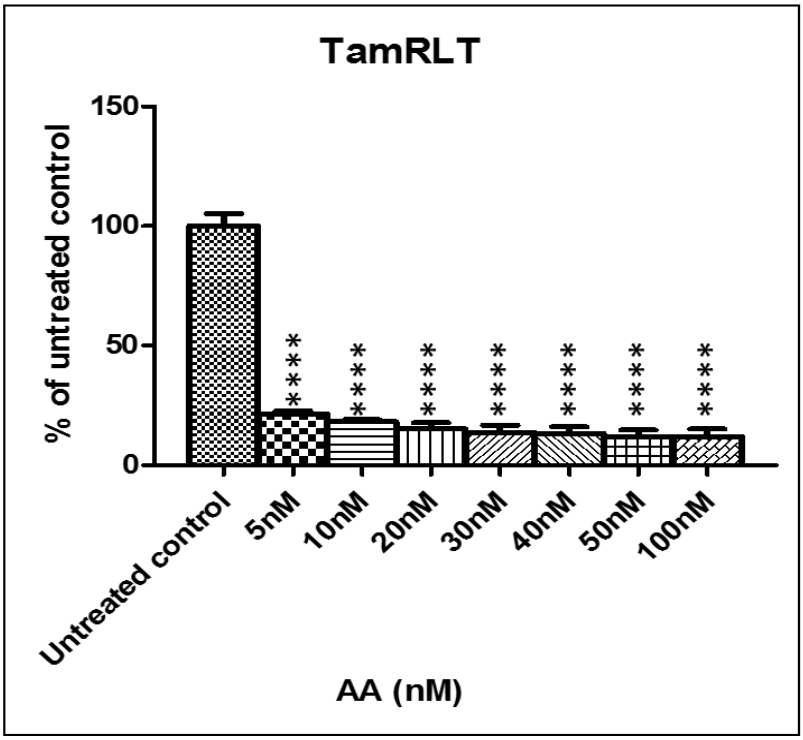

Fig 4.40. TamRLT cells were seeded at 20,000 cells/well and the growth was determined by Coulter counting after 5-100nM antimycin A (AA) treatment on day 3, 5 & 7. (A) Shows growth curve profiles and (B) % untreated control growth at day 7. Data were represented as mean of 3 independent experiments (N=3). The error bar indicates SEM. **** (P<0.0001) following ANOVA with Bonferroni post hoc correction.

[A]

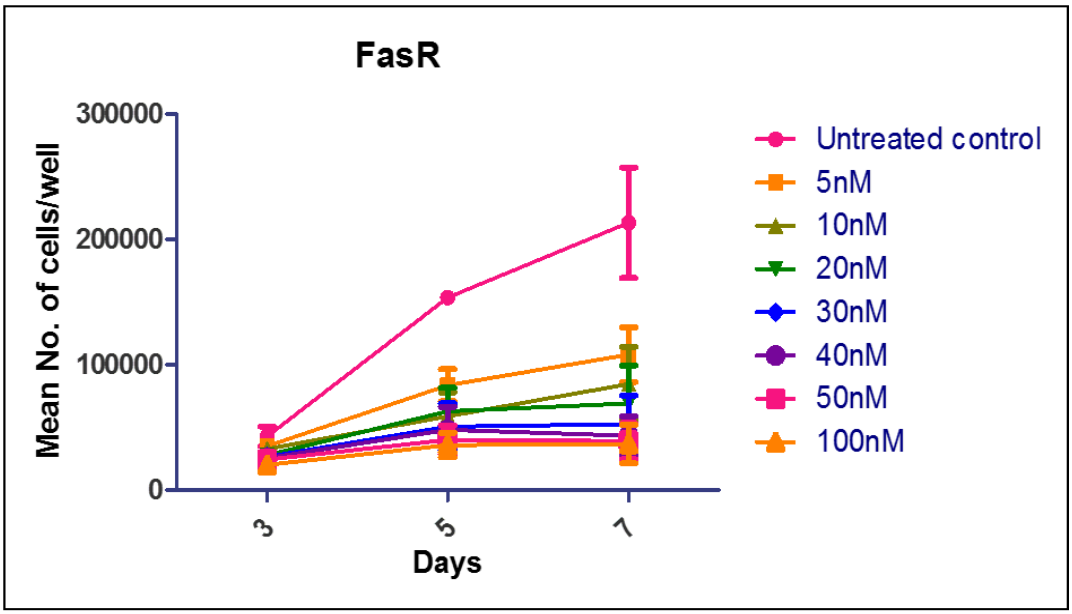

[B]

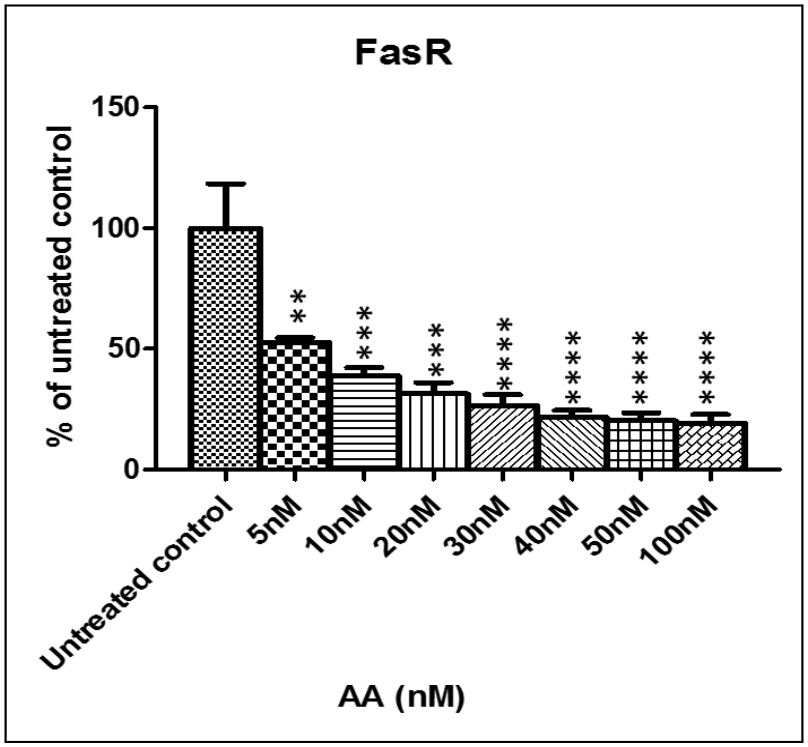

Fig 4.41. FasR cells were seeded at 20,000 cells/well and the growth was determined by Coulter counting after 5-100nM antimycin A (AA) treatment on day 3, 5 & 7. (A) Shows growth curve profiles and (B) % untreated control growth at day 7. Data were represented as mean of 3 independent experiments (N=3). The error bar indicates SEM. ** (*P*<0.01), *** (*P*<0.001) & **** (*P*<0.0001) following ANOVA with Bonferroni post hoc correction.

[A]

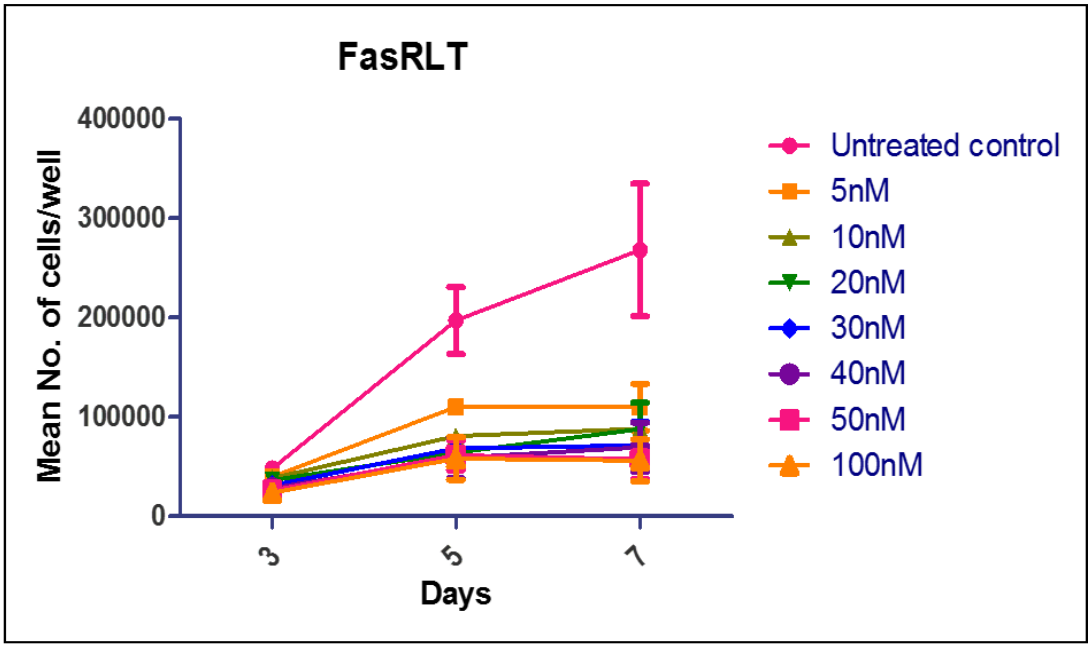

[B]

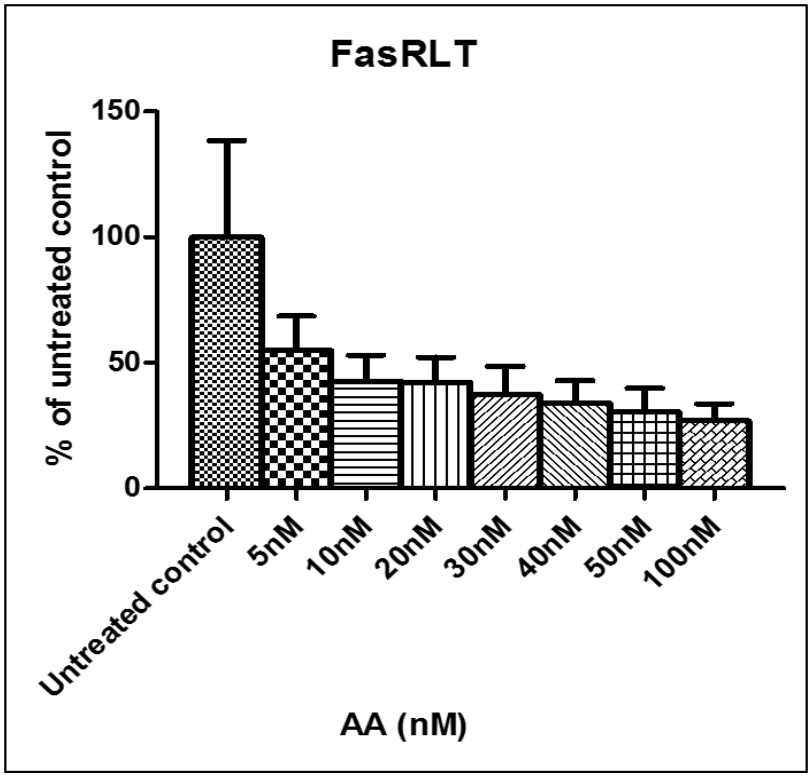

Fig 4.43. FasRLT cells were seeded at 20,000 cells/well and the growth was determined by Coulter counting after 5-100nM antimycin A (AA) treatment on day 3, 5 & 7. (A) Shows growth curve profiles and (B) % untreated control growth at day 7. Data were represented as mean of 3 independent experiments (N=3). The error bar indicates SEM.

[A]

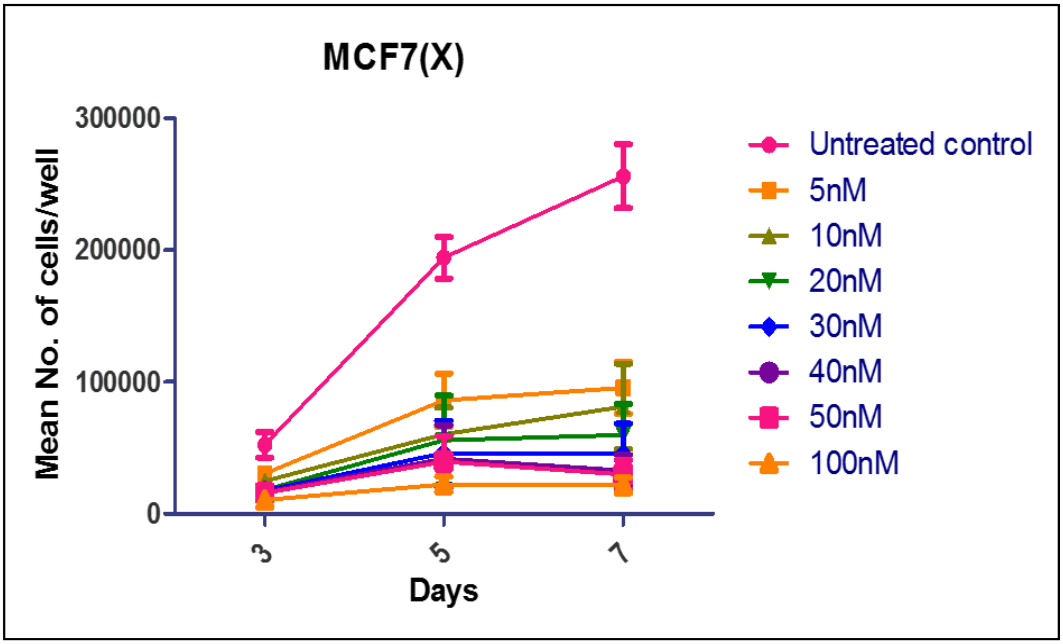

[B]

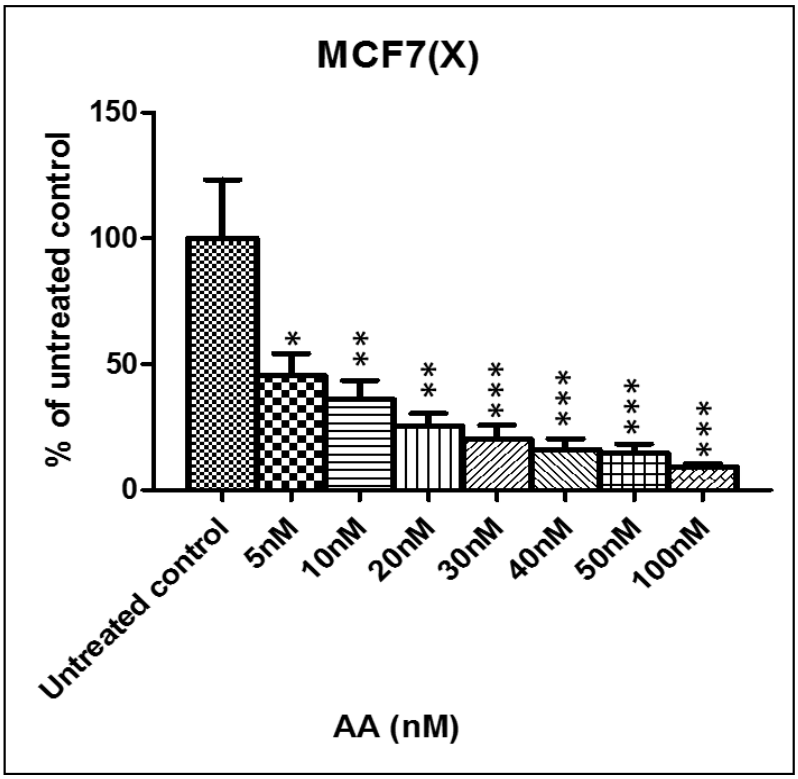

Fig 4.42. MCF7(X) cells were seeded at 20,000 cells/well and the growth was determined by Coulter counting after 5-100nM antimycin A (AA) treatment on day 3, 5 & 7. (A) Shows growth curve profiles and (B) % untreated control growth at day 7. Data were represented as mean of 3 independent experiments (N=3). The error bar indicates SEM. * (P<0.05), ** (P<0.01) & *** (P<0.001) following ANOVA with Bonferroni post hoc correction.

[A]

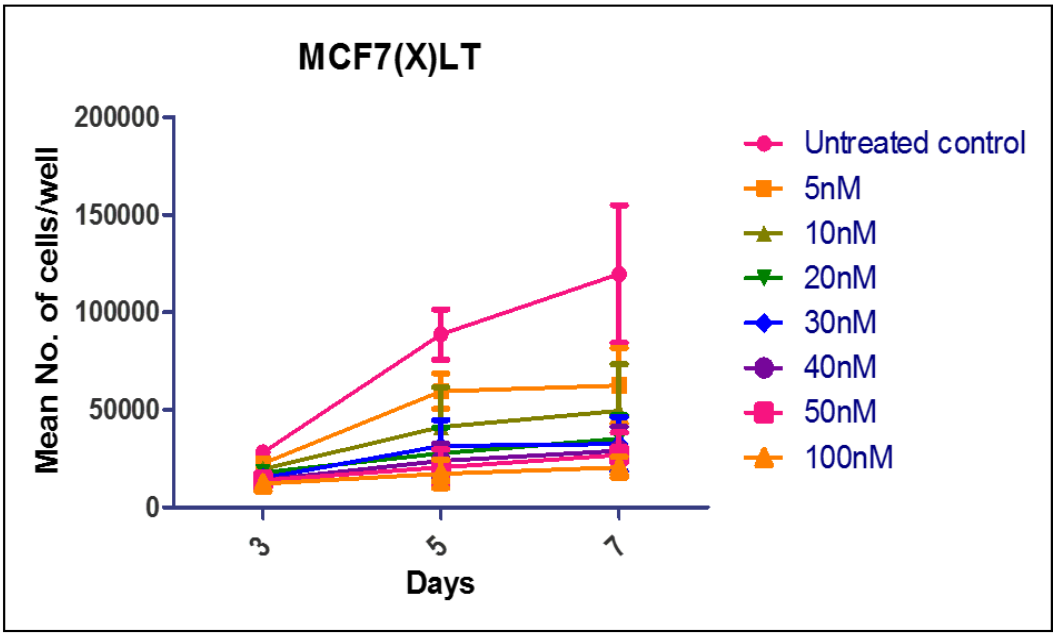

[B]

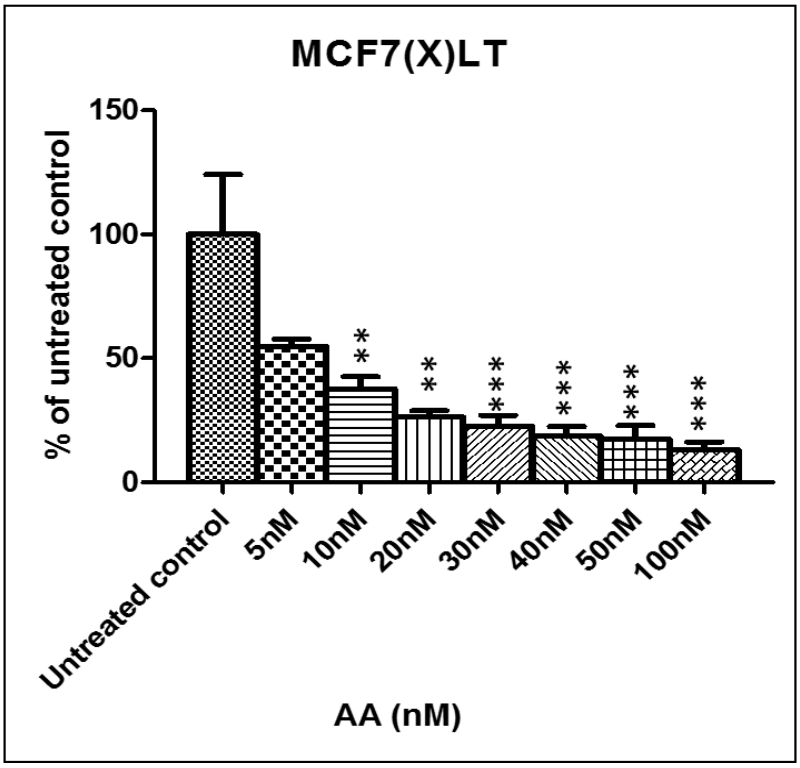

Fig 4.43. MCF7(X)LT cells were seeded at 20,000 cells/well and the growth was determined by Coulter counting after 5-100nM antimycin A (AA) treatment on day 3, 5 & 7. (A) Shows growth curve profiles and (B) % untreated control growth at day 7. Data were represented as mean of 3 independent experiments (N=3). The error bar indicates SEM. ** (P<0.01) & *** (P<0.001) following ANOVA with Bonferroni post hoc correction.

4.2.5.3. The inhibitory effect of metformin treatment on NADH dehydrogenase and cytochrome c oxidase activity in endocrine resistant cells

Based on the functional classification of the shared induced metabolic genes (Chapter 3, 3.2.2.5, Table 3.16), the highest enrichment score (7.8) belongs to subunits of complex I, III and IV associated with OxPhos, and according to gene ontology, 8 components of complex I (NADH dehydrogenase) were significantly induced in all resistant models (Chapter 3, Fig 3.10). NADH dehydrogenase is an enzyme complex located within the inner mitochondrial membrane, and transfers electrons from NADH to ubiquinone (Q). To further explore the contribution of OxPhos (in particular complex I activity) to the models, the current study investigated the impact of targeting complex I activity on NADH dehydrogenase activity, cytochrome c oxidase which lies downstream in the electron transport chain, OC as a surrogate for OxPhos activity in cells, key cell signalling pathways potentially influenced by OxPhos and also cell growth in the panel of resistant models.

The agent chosen to inhibit complex I in this study was metformin, which is also of emerging clinical interest in breast cancer (Goodwin et al. 2008 and Hadad et al. 2015). Biguanides such as phenformin and metformin are capable of exerting anti-tumour effects through inhibition of mitochondrial complex I activity (Birsoy et al. 2014). This alters cellular ATP balance, which in turn is reported to activate AMPK, inhibit mTOR signalling, and inhibit growth (Dowling et al. 2007). This is the direct cellular mechanism for metformin, but an additional indirect systemic mechanism has also been defined (Viollet et al. 2012). Clinically, metformin hydrochloride (N, N-dimethylimidodicarbonimidic diamide hydrochloride) is used for type II diabetic patients and reduces glucose production by suppressing gluconeogenesis in the liver while increasing glucose uptake in peripheral tissues (Viollet et al. 2012). Also, metformin reduces level of circulating insulin and insulin-like growth factor 1 (IGF-1). Both Insulin and IGF-1 play a role in insulin receptor and IGF receptor signalling pathways respectively and thus elimination of those factors via metformin treatment exert anticancer effect on tumour growth (Pollak et al. 2010).

In the current study, the ability of metformin treatment (0.5-2mM) to target complex I activity was firstly assessed on NADH dehydrogenase activity after 24hrs incubation time. The metformin concentration used is in a range utilized in diabetes studies to test the effect of the drug on hepatocytes (Stephenne et al. 2011: ex vivo). A mM concentration range has also been explored in further breast cancer cell line growth studies (Hadad et al. 2014). To determine NADH dehydrogenase activity before and after metformin treatment, an enzyme histochemistry approach was used across the panel of endocrine resistant models. This technique is based on

metabolizing a substrate by tissue enzyme in its orthotopic localization to generate an insoluble dye product which provides insights into pathobiological condition and vitality of cells. For NADH dehydrogenase assay, the enzyme substrate β-nicotinamide adenine dinucelotide is oxidized and a colour indicator (nitrotetrazolium blue chloride) is reduced to blue formazan. The formazan binds to local proteins and so reveals localization of NADH dehydrogenase enzyme in a particular cell compartment when viewed by light microscopy (Balan et al. 2010 and Whitaker-Menezes et al. 2011). This technique is semiquantitative, since it lacks reliable quantification of the enzyme activity.

In oncology, dehydrogenase activity of a tumour reveals vitality of cells and efficiency of cytostatic treatment (Meier-Ruge et al. 2007). Under untreated conditions, the NADH dehydrogenase enzyme activity was detected in the cytoplasm in all cell models, reflecting where mitochondria are located (Fig 4.44). NADH dehydrogenase activity was only slightly induced in TamR, TamRLT and FasR when compared to MCF7 under untreated conditions, but this enzyme activity was induced more substantially in FasRLT, MCF7(X) and MCF7(X)LT cells (Fig 4.44) suggesting prominent Complex I activity in these particular resistant models. Any reduced enzyme activity after metformin treatment was subsequently assessed as a weak (+), moderate (++), high (+++) or very high reduction (++++) in the staining signal (Table 4.17).

NADH dehydrogenase activity	0.5mM	1mM	1.5mM	2mM
MCF7	-------	+	++	+++
TamR	+	+	++	+++
TamRLT	-------	+	++	+++
FasR	-------	+	++	+++
FasRLT	-------	+	++	+++
MCF7(X)	+	++	+++	++++
MCF7(X)LT	+	+	+++	++++

Table 4.17. The effect of metformin after 24hrs treatment on staining for NADH dehydrogenase activity in the panel of resistant models. Metformin impact is indicated by + weak, ++ moderate, +++ high or ++++ very high reductions in staining, as compared to untreated control. No impact is indicated by ----.

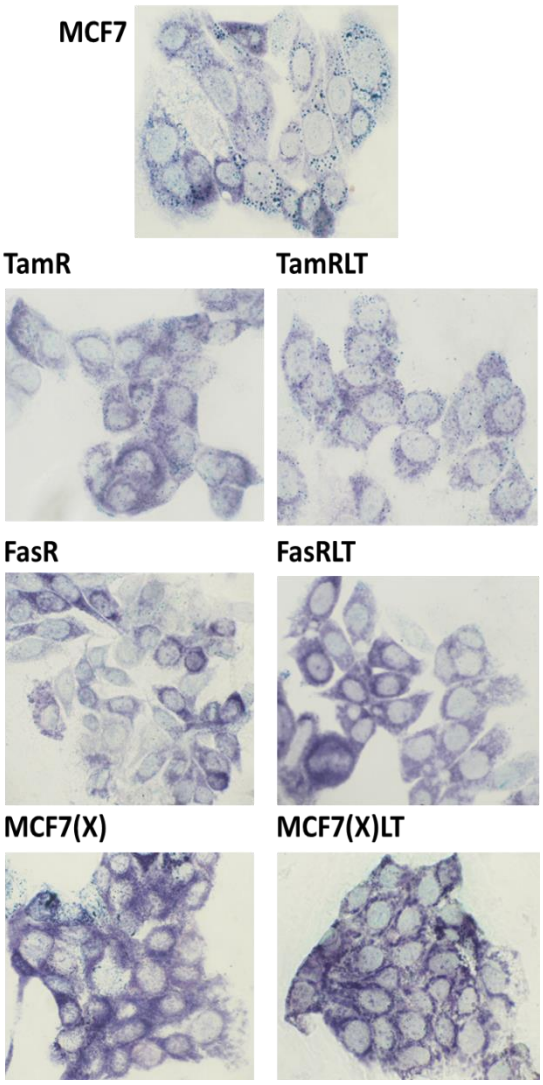

Fig 4.44. Staining for basal NADH dehydrogenase activity across the panel of resistant models & MCF7 cells. Original magnification 40X.

In MCF7, the enzyme activity was not robustly changed by 0.5mM metformin treatment, but it was reduced in a dose dependent manner after 1, 1.5 and 2mM metformin treatment as compared to the untreated control (Fig 4.45, Table 4.17). In TamR, the enzyme activity was diminished by 0.5 and 1mM metformin treatment but it was reduced more substantially after 1.5 and 2mM treatment as compared to untreated control (Fig 4.46, Table 4.17). In TamRLT, NADH dehydrogenase activity was not markedly changed after 0.5mM treatment, but it was reduced in a dose dependent manner by 1, 1.5 and 2mM metformin (Fig 4.47, Table 4.17). The enzyme activity was not robustly changed in FasR and FasRLT after 0.5mM metformin treatment but was reduced in a dose dependent manner after 1, 1.5 and 2mM metformin treatment as compared to untreated control (Fig 4.48-4.49, Table 4.17). Enzyme activity was reduced in a

dose dependent manner from 0.5mM to 2mM metformin treatment in MCF7(X) and MCF7(X)LT as compared to untreated control for each model (Fig 4.50-4.51, Table 4.17).

In summary, high specificity of the drug to target complex I of OxPhos was indicated by its ability to abolish NADH dehydrogenase activity (in a dose dependent manner) across the panel of endocrine resistant models and the MCF7 cells (Fig 4.45-4.51).

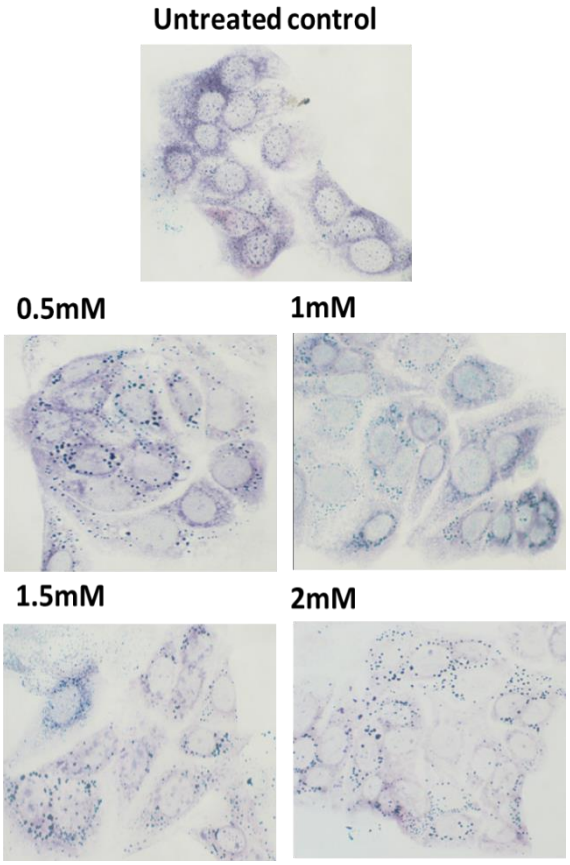

Fig 4.45. Staining for NADH dehydrogenase activity after 24hrs metformin treatment (0.5mM-2mM) in MCF7 cells. Original magnification 40X.

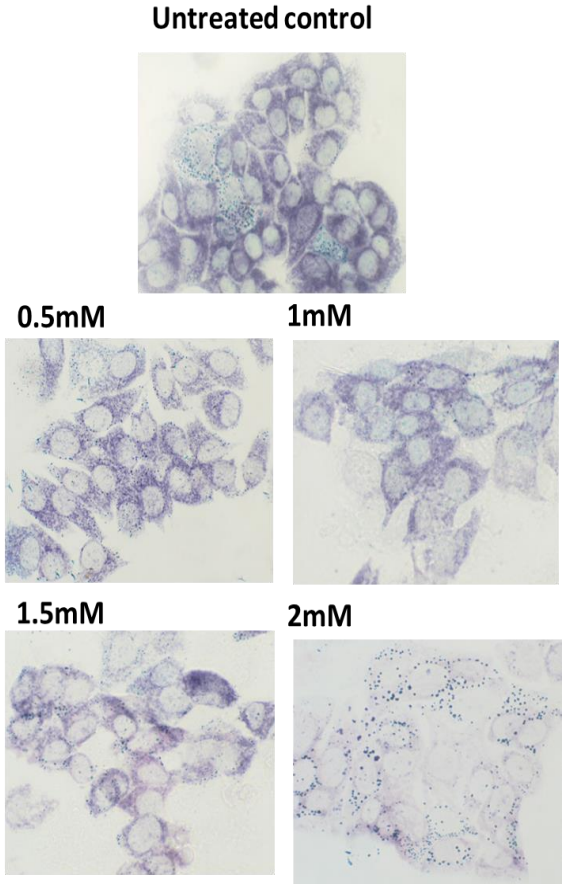

Fig 4.46. Staining for NADH dehydrogenase activity after 24hrs metformin treatment (0.5mM-2mM) in TamR cells. Original magnification 40X.

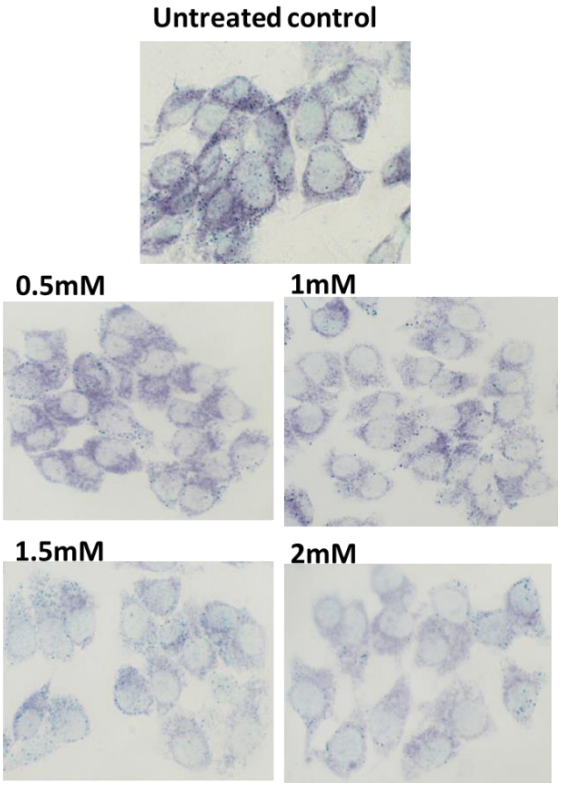

Fig 4.47. Staining for NADH dehydrogenase activity after 24hrs metformin treatment (0.5mM-2mM) in TamRLT cells. Original magnification 40X.

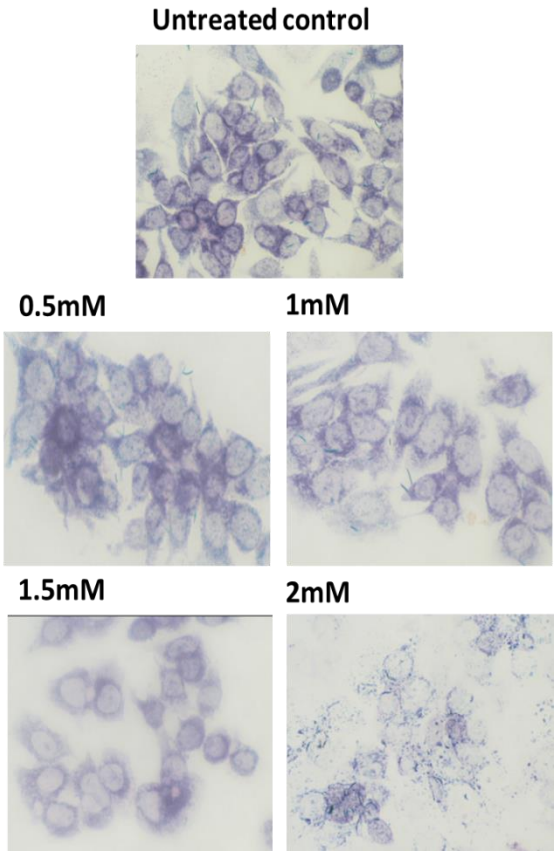

Fig 4.48. Staining for NADH dehydrogenase activity after 24hrs metformin treatment (0.5mM-2mM) in FasR cells. Original magnification 40X.

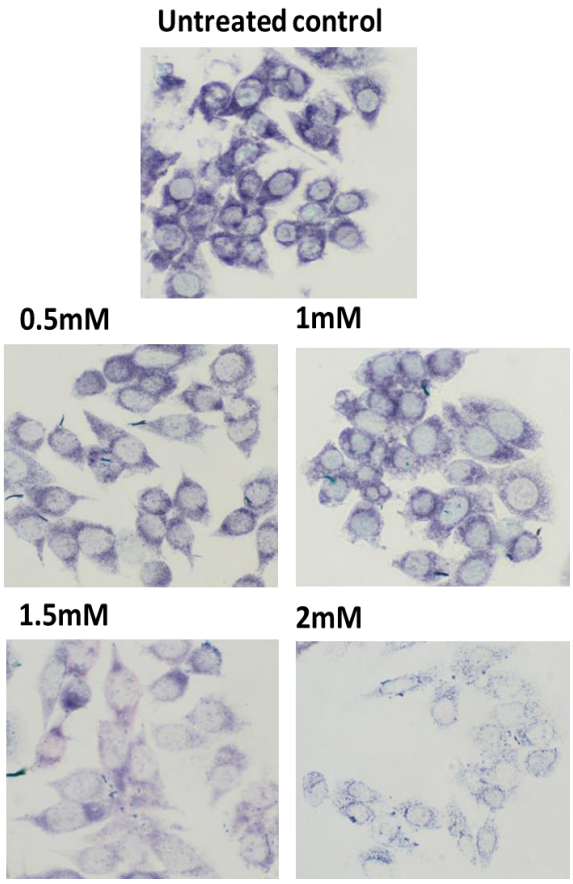

Fig 4.49. Staining for NADH dehydrogenase activity after 24hrs metformin treatment (0.5mM-2mM) in FasRLT cells. Original magnification 40X.

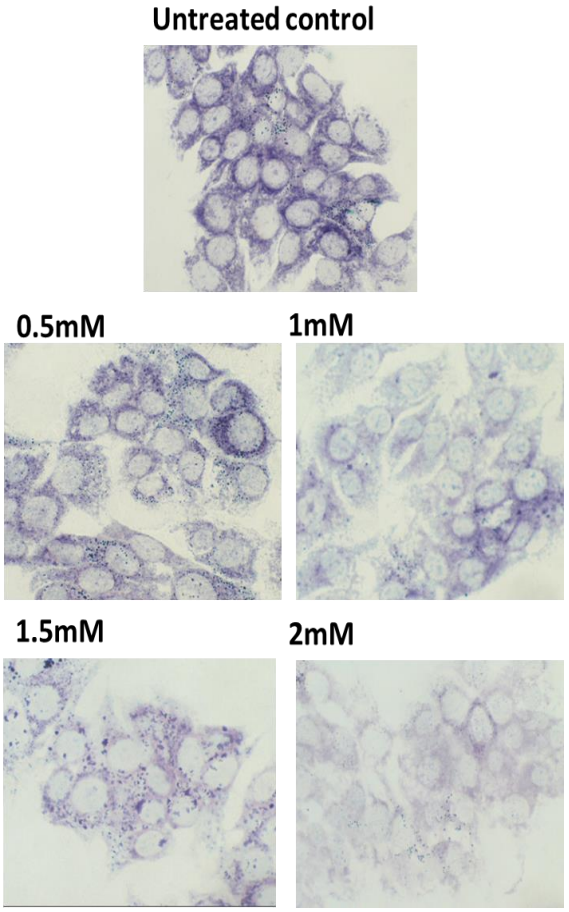

Fig 4.50. Staining for NADH dehydrogenase activity after 24hrs metformin treatment (0.5mM-2mM) in MCF7(X) cells. Original magnification 40X.

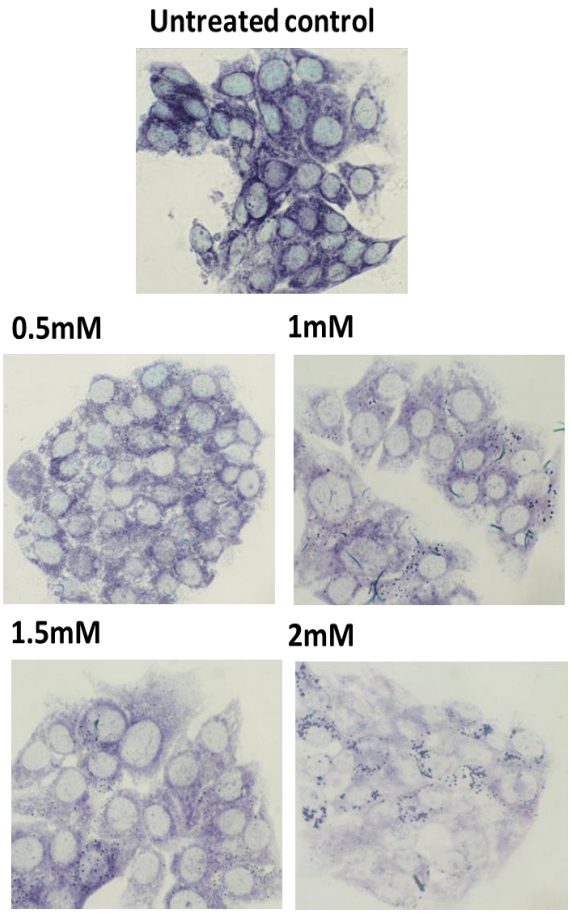

Fig 4.51. Staining for NADH dehydrogenase activity after 24hrs metformin treatment (0.5mM-2mM) in MCF7(X)LT cells. Original magnification 40X.

The inhibitory effect of metformin on electron transfer from complex I to the rest of the electron transport chain complexes was assessed by staining the models for cytochrome c oxidase (COX) activity. Cytochrome C oxidase (a Warburg respiratory enzyme) is the last enzyme complex (complex IV) in the electron transport chain and catalyses the transfer of reducing equivalents from cytochrome c to molecular oxygen. On the microarrays, expression of COX7B (Structural subunit of complex IV) was increased in all resistant models as compared to MCF7 control (Chapter 3, 3.2.2.5, Table 3.16) but no probe IDs were available to assess expression of catalytic subunits (mitochondrial encoded subunits: MT-CO1, MT-CO2 and MT-CO3) of cytochrome c oxidase in resistant models. The enzyme histochemistry method chosen in this study to visualize COX activity in the models was based on using diaminobenzidine (DAB) as the electron donor for cytochrome c (Seligman et al. 1968). The end product of the reaction after DAB oxidation is

brown cytoplasmic staining which also equates with mitochondrion distribution in the cells or tissue. Darker staining indicates more abundant mitochondria content in a tissue or cells, although (as for NADH dehydrogenase activity) the approach can only be semi-quantitative.

Cytoplasmic staining for cytochrome c oxidase activity was generally higher in tamoxifen resistant (TamR and TamRLT) and fulvestrant resistant (FasR and FasRLT) cells (suggestive of higher complex IV activity in all these antioestrogen resistant states), but in contrast was lower in the oestrogen deprived resistant models (MCF7(X) and MCF7(X)LT), as compared to MCF7 under untreated basal growth conditions (Fig 4.52, Table 4.18).

In MCF7, COX enzyme activity was reduced in a dose-dependent manner after metformin treatment (0.5-2mM) as compared to untreated control (Fig 4.53, Table 4.18). In TamR cells, while COX activity was only partially-reduced after 0.5 and 1mM metformin (Fig 4.54, Table 4.18), a larger fall in enzyme activity was observed after 1.5mM and 2mM treatment as compared to untreated control (Fig 4.54, Table 4.18). The enzyme activity in TamRLT was unchanged after 0.5mM treatment but reduced after 1, 1.5 and 2mM metformin (Fig 4.55, Table 4.18). The enzyme activity in FasR and FasRLT was not changed after 0.5mM and 1mM metformin, but slightly reduced after 1.5 and 2mM treatment as compared to the untreated control (Fig 4.56-4.57, Table 4.18). In MCF7(X), the low basal level of COX activity was further reduced in a dose dependent manner with metformin as compared to untreated control (Fig 4.58, Table 4.18). In MCF7(X)LT, the limited enzyme activity was unchanged after 0.5mM and 1mM metformin but slightly reduced after 1.5 and 2mM treatment (Fig 4.59, Table 4.18).

In summary, metformin treatment appeared able to reduce COX activity in all the models in the panel and indeed the reduction in cytochrome c oxidase invariably followed a similar pattern to that for reduced NADH dehydrogenase activity after metformin treatment (Table 4.17-4.18), with evidence of dose dependency. This suggests that metformin treatment reduced electron transfer from complex I to the rest of the complexes in the electron transport chain, which consequently reduced COX activity across the panel.

COX dehydrogenase activity	0.5mM	1mM	1.5mM	2mM
MCF7	+	+	++	+++
TamR	+	+	++	++
TamRLT	-------	+	++	++
FasR	-------	-------	+	+
FasRLT	-------	-------	+	+
MCF7(X)	+	+	++	+++
MCF7(X)LT	-------	-------	+	++

Table 4.18. The effect of metformin treatment after 24hrs treatment on staining for cytochrome c oxidase (COX) activity in the panel of resistant models. Metformin impact on enzyme activity is indicated by; + weak ++moderate, +++ high or ++++ very high reductions in staining, as compared to untreated control. No impact is indicated by ----.

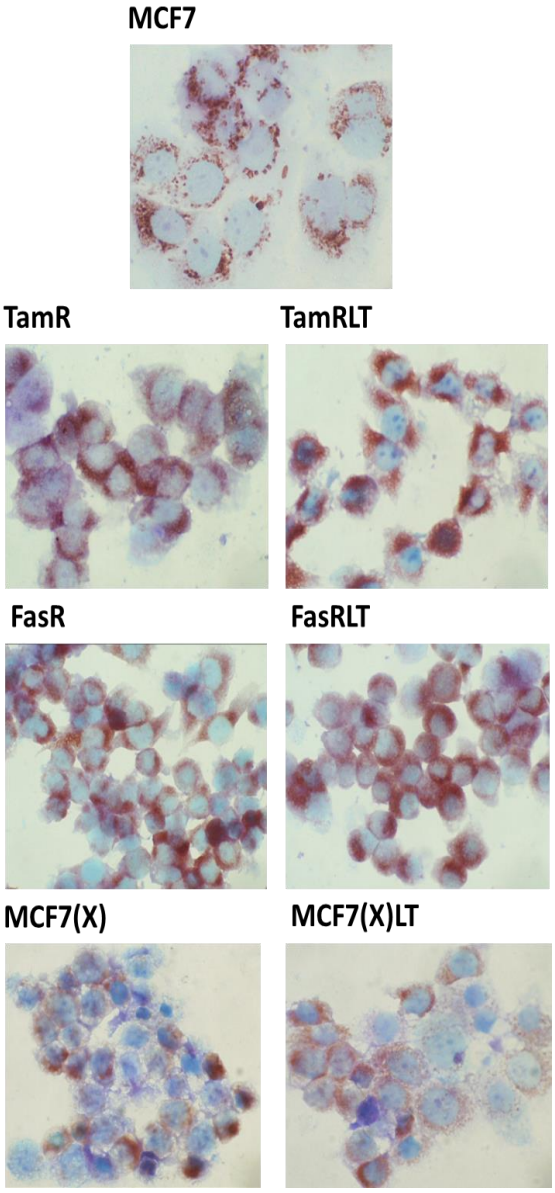

Fig 4.52. Staining for basal cytochrome c oxidase activity across the panel of resistant models and MCF7 cells. Original magnification 40X.

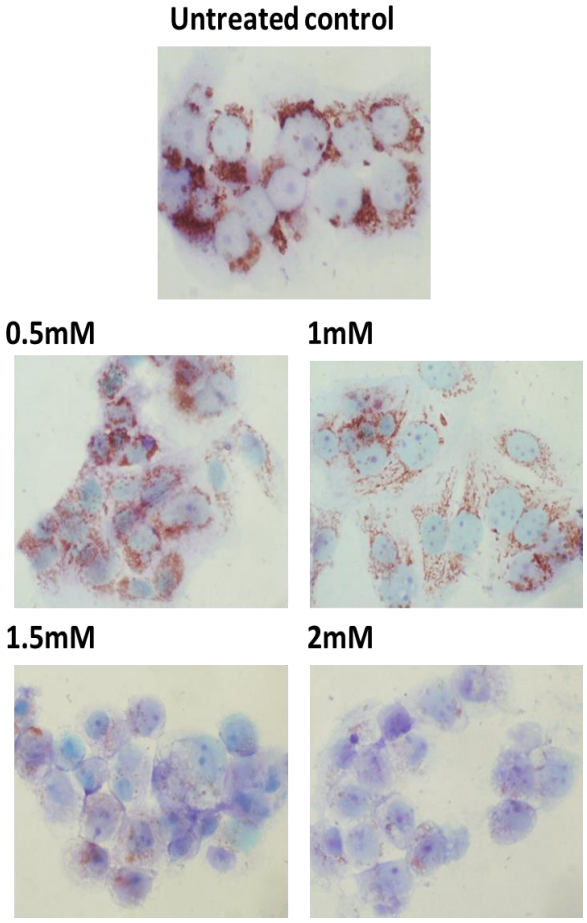

Fig 4.53. Staining for cytochrome c oxidase activity after 24hrs metformin treatment (0.5mM-2mM) in MCF7 cells. Original magnification 40X.

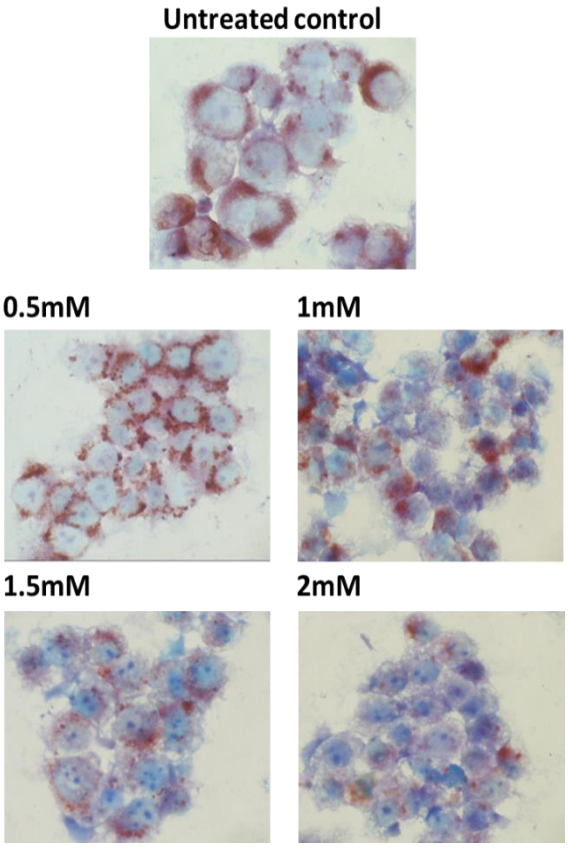

Fig 4.54. Staining for cytochrome c oxidase activity after 24hrs metformin treatment (0.5mM-2mM) in TamR cells. Original magnification 40X.

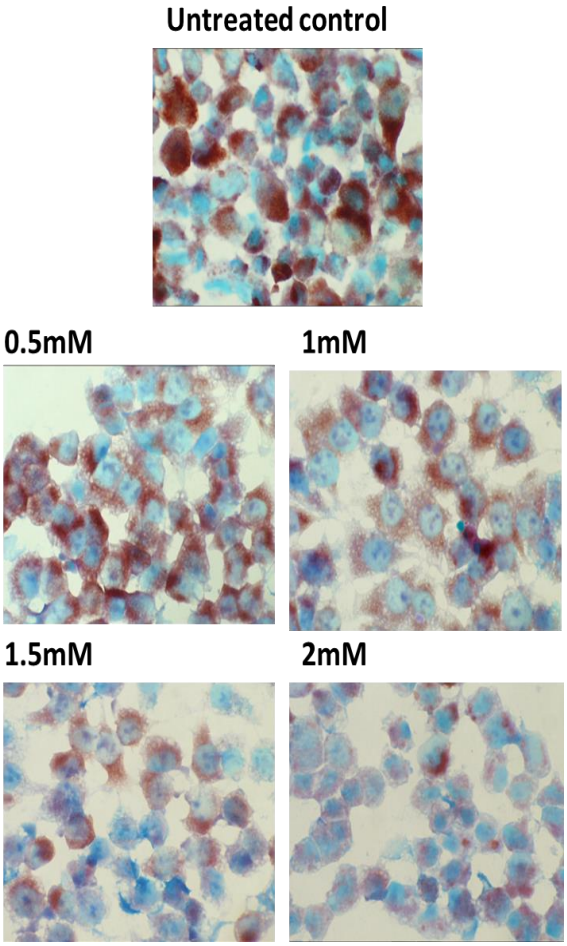

Fig 4.55. Staining for cytochrome c oxidase activity after 24hrs metformin treatment (0.5mM-2mM) in TamRLT cells. Original magnification 40X.

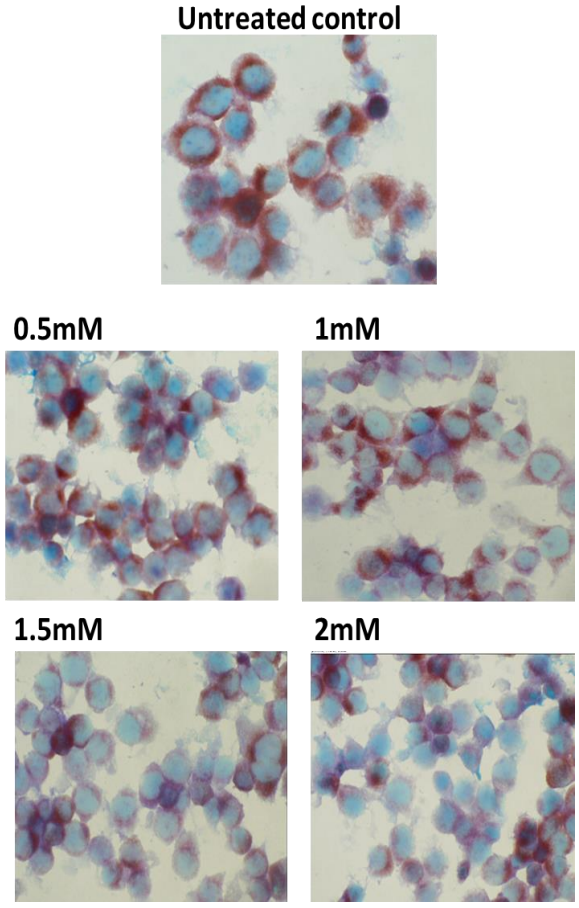

Fig 4.56. Staining for cytochrome c oxidase activity after 24hrs metformin treatment (0.5mM-2mM) in FasR cells. Original magnification 40X.

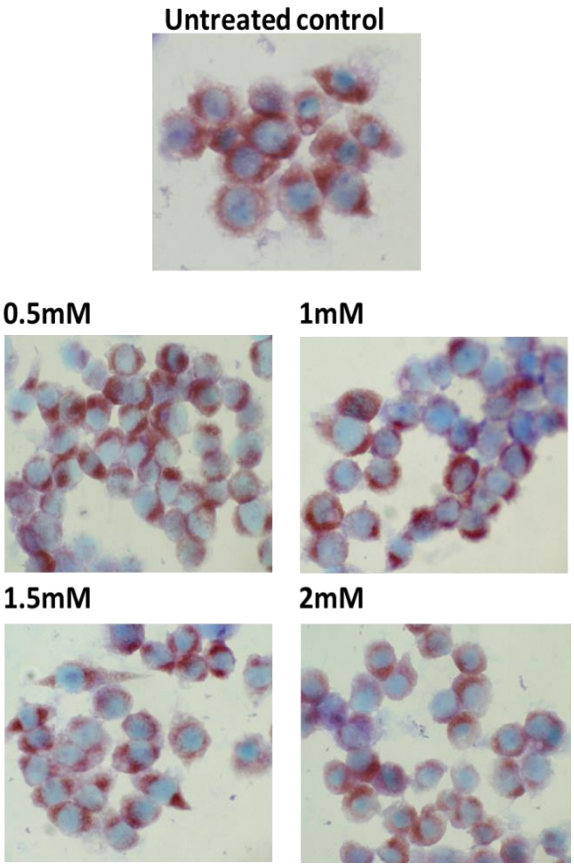

Fig 4.57. Staining for cytochrome c oxidase activity after 24hrs metformin treatment (0.5mM-2mM) in FasRLT cells. Original magnification 40X.

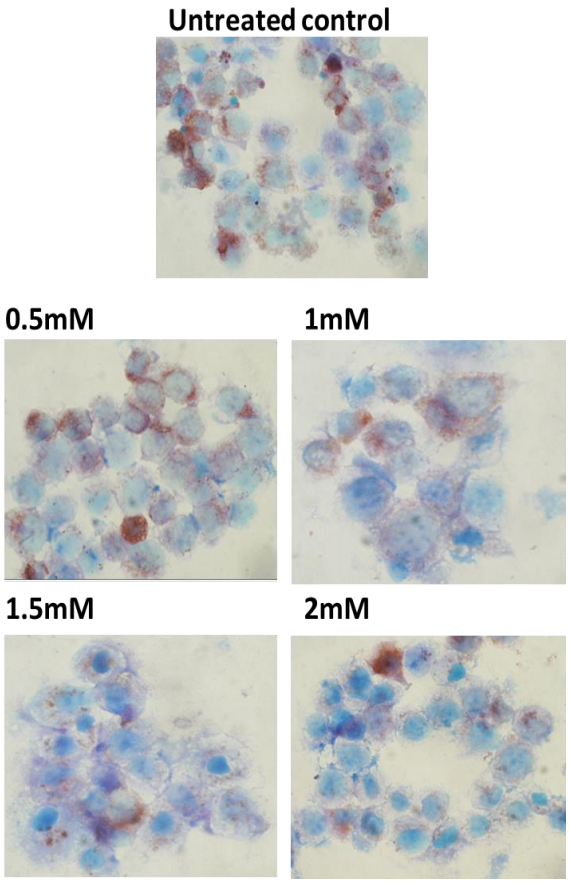

Fig 4.58. Staining for cytochrome c oxidase activity after 24hrs metformin treatment (0.5mM-2mM) in MCF7(X) cells. Original magnification 40X.

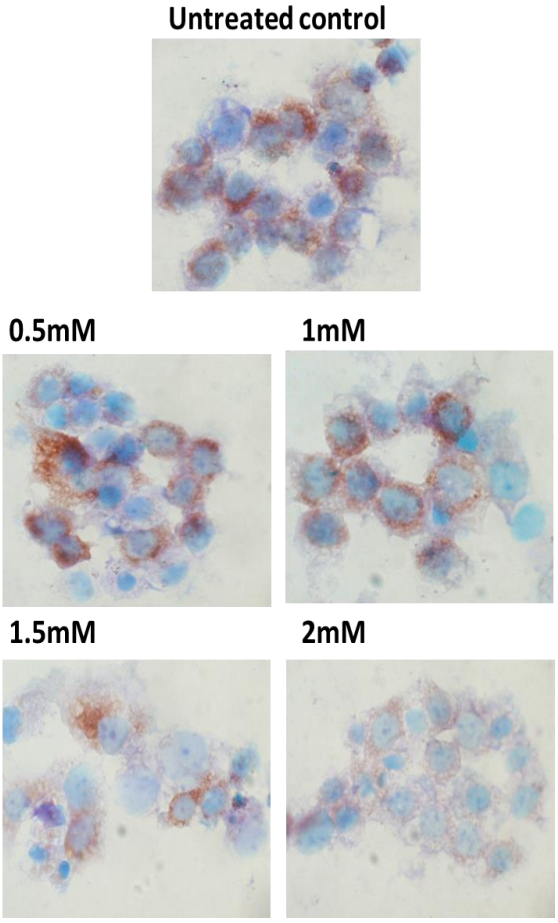

Fig 4.59. Staining for cytochrome c oxidase activity after 24hrs metformin treatment (0.5mM-2mM) in MCF7(X)LT cells. Original magnification 40X.

4.2.5.4 The inhibitory effect of metformin on oxygen consumption in endocrine resistant breast cancer cells

Oxidative phosphorylation in the mitochondria involves ATP generation by transferring electrons from TCA cycle-derived substrates to molecular oxygen. Metformin acts to inhibit electron transfer from complex I to the rest of electron transport chain (Wheaton et al. 2014) and in Section 4.2.5.3 above we have demonstrated the drug impacts on activity of Complex I through to Complex IV in the model panel. Therefore, we hypothesized that metformin treatment would also reduce oxygen consumption (as a surrogate for overall OxPhos activity) in breast cancer cells. OC was determined in breast cancer cells after metformin treatment for 24hrs (MitoXpress® Xtra probe; as described in section 4.2.4.1). Cells were seeded (80,000 cells/well) for 24hrs prior to metformin treatment (0.5mM-2mM) and the OC was then determined 24hrs after metformin administration.

In MCF7 cells, the OC was reduced by metformin treatment in a dose dependent manner (Fig 4.60A). Thus, OC was significantly reduced by 30% through to 65% after 1mM (P<0.05), 1.5mM (P<0.001) and 2mM (P<0.001) metformin as compared to untreated control (Fig 4.60A), with significant further reduction by 2mM compared to either 0.5mM (P<0.001) or 1mM (P<0.01) treatment (Fig 4.60A). In TamR cells, OC was again reduced in a dose dependent manner by metformin (from 23%-60% over 0.5mM-2mM) (Fig 4.60B). OC was significantly reduced by 1mM (P<0.01), 1.5mM (P<0.01) and 2mM (P<0.001) treatment versus untreated control, and further reduced by 2mM compared to 0.5mM (P<0.01) and 1mM (P<0.05) drug (Fig 4.60B). There was also evidence of a dose dependent impact in TamRLT cells (with OC reduced by 20%-55% over 0.5mM-2mM metformin) (Fig 4.60C). In these tamoxifen resistant cells, OC was significantly reduced by 1.5mM (P<0.01) and 2mM (P<0.001) metformin versus untreated control, and further reduced by 2mM compared to 0.5mM (P<0.01) and 1mM drug (P<0.05) (Fig 4.60C). In FasR, OC was also reduced in a dose dependent manner by 35% through to 70% with metformin treatment (0.5mM-2mM) (Fig 4.60D). OC was significantly reduced after 0.5mM (P<0.001), 1mM (P<0.001), 1.5mM (P<0.001) and 2mM (P<0.001) metformin compared with untreated control, and further reduced after 1.5mM (P<0.05) and 2mM (P<0.01) versus 0.5mM treatment (Fig 4.60D). Dose dependent reduction was also seen in FasRLT cells (30%-60% for 0.5mM-2mM metformin), with significant reductions for 1mM (P<0.01), 1.5mM (P<0.01) and 2mM (P<0.001) metformin versus untreated control (Fig 4.61A). Finally, in MCF7(X), OC was reduced in a dose dependent manner by 25%-60% with metformin (0.5mM-2mM) (Fig 4.61B), with the decline significant for 0.5mM (P<0.05), 1mM (P<0.01), 1.5mM (P<0.001) and 2mM (P<0.001) metformin compared to untreated control and further reduction by 2mM versus 0.5mM (P<0.01) and 1mM

(*P*<0.05) treatment (Fig 4.61B). OC was also reduced in MCF7(X)LT cells in a dose dependent manner (25%-75% over 0.5mM-2mM) (Fig 4.61C), with significant reduction by 1mM (*P*<0.05), 1.5mM (*P*<0.001) and 2mM (*P*<0.001) drug versus untreated control and further significant reduction by 2mM compared to 0.5mM (*P*<0.01) and 1mM (*P*<0.05) drug (Fig 4.61 C). In summary, therefore, all resistant models and also MCF7 cells showed evidence that metformin could reduce OC, reflecting the ability of metformin to impact on OxPhos and furthermore the importance of Complex I to this process in all models. Dose dependency was shown for metformin in all models; however, it was noted that ≥50% OC reduction was observed with 1.5mM metformin treatment in fulvestrant resistant and oestrogen deprived models (Fig 4.60-4.61), while such reduction required 2mM treatment in tamoxifen resistant models (Figs 4.60). This tentatively suggested somewhat higher importance for Complex I-driven OxPhos in fulvestrant or oestrogen deprivation resistant models.

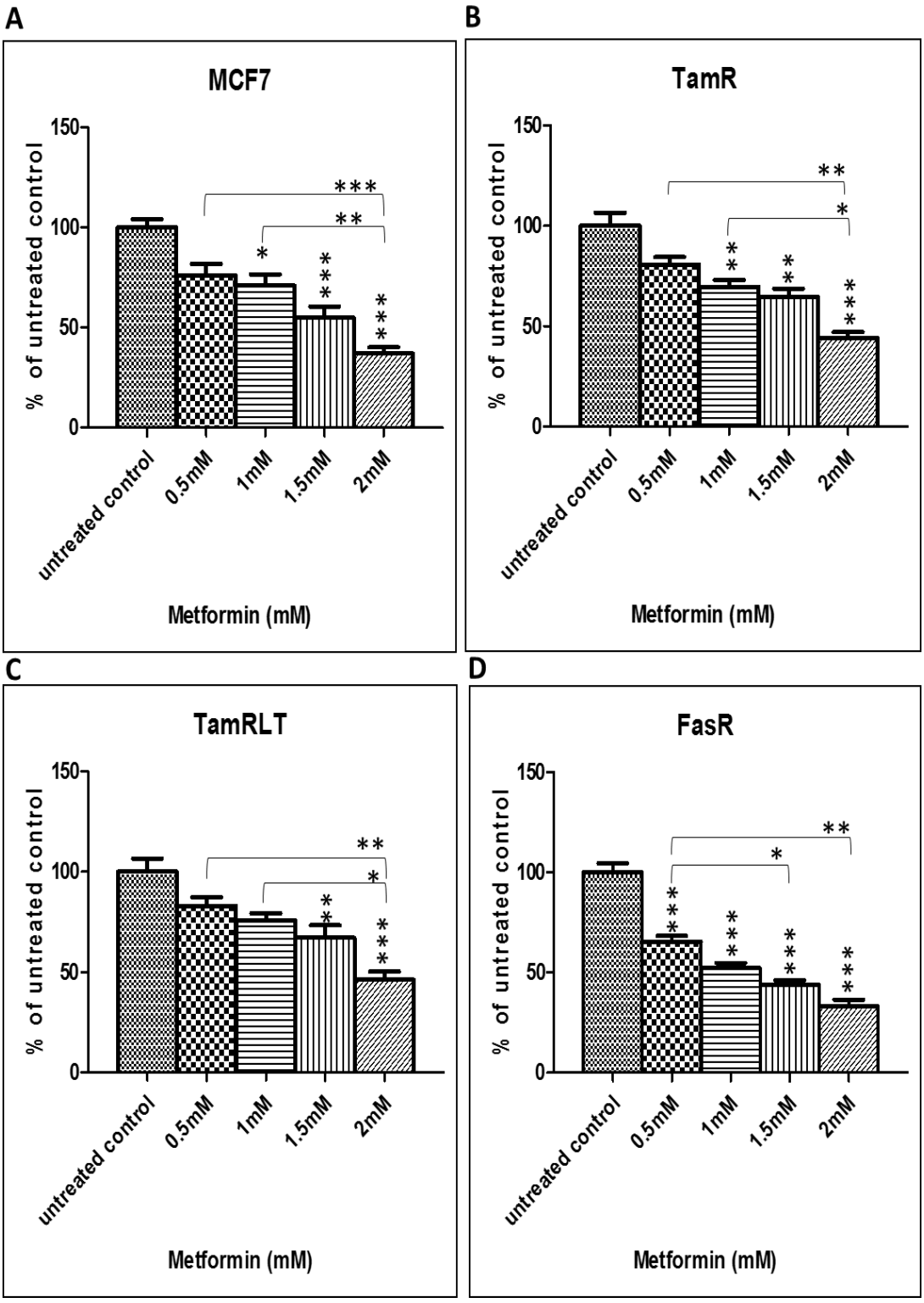

Fig 4.60 A-D. OC quantified in MCF7, TamR, TamRLT & FasR cells after 24hrs metformin treatment. Data are expressed as % of untreated control and comprise a mean of 3 independent experiments (N=3). The error bar indicates SEM. * (*P*<0.05), ** (*P*<0.01) & *** (*P*<0.001) following ANOVA with Bonferroni post hoc correction.

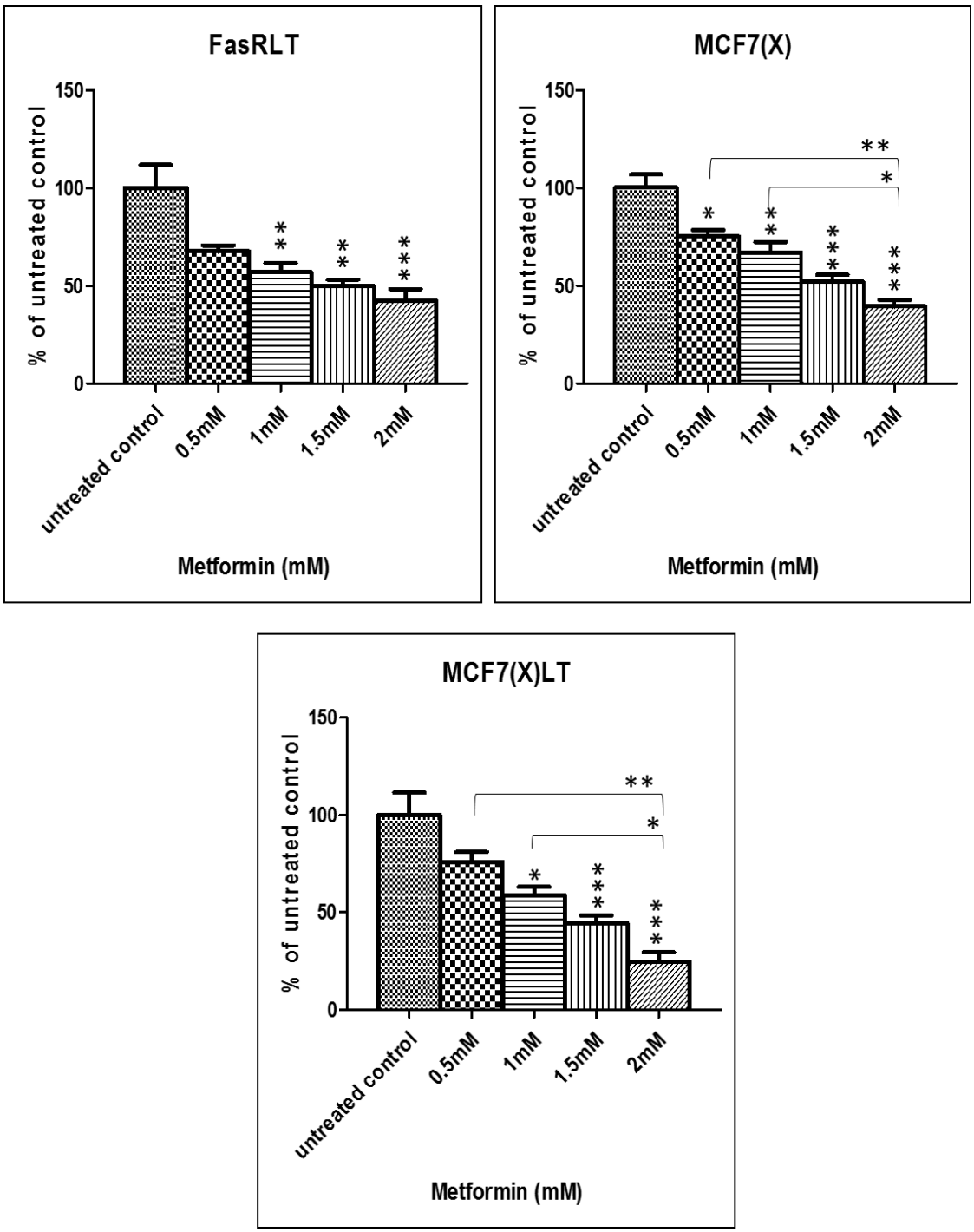

Fig 4.61 A-C. OC quantified in FasRLT, MCF7(X) & MCF7(X)LT cells after 24hrs metformin treatment. Data are expressed as % of untreated control and comprise a mean of 3 independent experiments (N=3). The error bar indicates SEM. * (*P*<0.05), ** (*P*<0.01) & *** (*P*<0.001) following ANOVA with Bonferroni post hoc correction.

4.2.5.5 The inhibitory effect of metformin on cell signalling pathways in endocrine resistant breast cancer cells

To explain growth inhibitory effects of metformin in cancer, two major hypotheses have been described:

- Systemic mechanism: Metformin reduces tumour growth via reducing plasma insulin/insulin like growth factor 1 (IGF1), thereby reducing tumour mitogenic IGF-1R signalling (Pollak et al. 2010).

- Direct mechanism: By impacting on OxPhos, metformin mediates a cytostatic effect by altering cellular ATP balance, activating the energy sensor adenosine monophosphate activated protein kinase (AMPK) which switches off anabolic processes such as lipid, ribosomal RNA and protein synthesis (Hardie et al. 2012).

In the present study, the focus for signalling studies with metformin was the direct mechanism. In detail, metformin inhibits the electron transport chain in OxPhos and is reported to increase ADP: ATP and AMP: ATP ratios (Hawley et al. 2010). AMP or ADP binding to AMPK causes conformational changes and promotes AMPK phosphorylation at Thr172 by upstream liver kinase B1 (LKB1, encoded by STK11) (Hawley et al. 2003). AMPK is a multi-subunit enzyme comprising α1 (PRKAA1), α2 (PRKAA2), β1 (PRKAB1), β2 (PRKAB2), γ1 (PRKAG1), γ2 (PRKAG2) and γ3 (PRKAG3) proteins (Hardie et al. 2015). There are three binding sites for AMP, ADP and ATP binding on the γ subunit of AMPK, where ADP and ATP compete with AMP for binding to AMPK. Activation of AMPK by AMP binding leads to a conformational change allowing increased AMPK phosphorylation at the active site (Thr172) in the α subunit by LKB1, inhibition of dephosphorylation at the same site by phosphatases, and also allosteric activation of AMPK by more than 10 fold (Gowans et al. 2013). AMPK activation subsequently inhibits anabolic processes and promotes catabolic processes to overcome energy stress. LKB1, together with two accessory subunits STRAD (STRADA/B) and MO25 (CAB 39), is an immediate upstream kinase that phosphorylates AMPK (Hawley et al. 2003). Heterozygous mutation of LKB1 (STK11) is associated with cancer susceptibility (Peutz–Jeghers syndrome) (Jenne et al. 1998). Therefore, LKB1 is known as a tumour suppressor which links AMPK phosphorylation with reduced tumour growth. Downstream mechanisms of AMPK include phosphorylation of acetyl co A carboxylase (ACC1 and ACC2) inhibiting fatty acid synthesis and promoting fatty acid oxidation in mitochondria (Steinberg et al. 2009). This inhibition of lipid synthesis is associated with reduced cell proliferation (Hadad et al. 2011). AMPK activation also inhibits the mammalian target of rapamycin (mTOR) pathway by phosphorylating both Tuberous Sclerosis 2 (TSC2) (Inoki et al.

2003) and Regulatory Associated Protein of MTOR (Raptor), reducing protein synthesis and thus inhibiting tumour growth (Gwinn et al. 2008). Interestingly, tumour cells with a downregulated LKB1-AMPK pathway are more sensitive to the decreased ATP levels mediated by metformin, confirming the pathway's critical role in energy homeostasis (Algire et al. 2011).

Having established the drug impacts on components of OxPhos, in this project the key signalling events associated with metformin's direct mechanism were studied in model panel. The impact of metformin on AMPK phosphorylation (Thr172) and on downstream pathways regulating fatty acid synthesis (gauged by monitoring ACC phosphorylation (Ser79)) and protein synthesis (by monitoring phosphorylation of mTORC1 (Ser2448) and Ribosomal Protein S6 Kinase (P70S6K, Thr389)) was examined by Western blotting after 2, 12 and 24 hrs metformin treatment (0.5mM-2mM) (Fig 4.62-4.83, Table 4.19) in each model.

Endocrine responsive MCF7 cells

After 2hrs metformin treatment in MCF7, while there was no change or even a decline up to 1.5mM, p-AMPK was significantly induced by 2mM metformin compared to the untreated control (P<0.05) and versus lower drug doses (1mM and 1.5mM, P<0.001) (Fig 4.62-4.63). Thereafter, all p-AMPK blots generally showed higher signal than at 2 hrs. While there was a transient induction of p-AMPK at 12 hrs by 0.5mM drug compared to the untreated control (P<0.05), the induction with 2mM metformin was lost (Fig 4.62-4.63). At 2 hrs, p-ACC was not significantly induced in MCF7 cells by metformin (Fig 4.62-4.63). At 12 and 24 hrs, some blots showed p-ACC induction with metformin treatment compared with untreated control (for example with 0.5mM and 1.5mM treatment by 24hrs, Fig. 4.62-4.63), but this did not prove significant across replicates (Fig.4.63). At 2 hrs, p-mTOR appeared slightly reduced on the blots after 1mM treatment compared to untreated control (p<0.05) (Fig 4.62 and 4.64). p-mTOR was unchanged at 12 hrs (Fig 4.62 and 4.64), while the reduction noted on the blots at 24 hrs by 2mM treatment versus untreated control (p<0.05) (Fig 4.62 and 4.64). However, significant changes in activity of the further mTOR signalling element, P70S6K, were observed with metformin (Fig 4.62 and 4.64). From 2 hrs, significant reduction of p-P70S6K was observed with 1 or 1.5 mM metformin as compared to both untreated control and 0.5mM (P<0.001). There was a dose dependent in p-P70S6 decline at 12 hrs versus untreated control (1, 1.5 and 2mM (P<0.001) and for 1mM (P<0.01), 1.5mM (P<0.001) and 2mM (P<0.001) treatment compared to 0.5mM metformin at this time point). At 24 hrs, p-P70S6K was again significantly reduced in a dose-dependent manner (1.5mM (P<0.05) and 2mM (P<0.001) compared to untreated control cells. (Fig 4.62 and 4.64).

In summary from 12hrs treatment, there was some evidence that metformin could reduce protein synthesis-regulating mTOR signalling (monitored using p-p70S6K) independent of any robust change in AMPK activity in MCF7 cells, and contrasting the lack of evidence for impact on fatty-acid synthesis regulation.

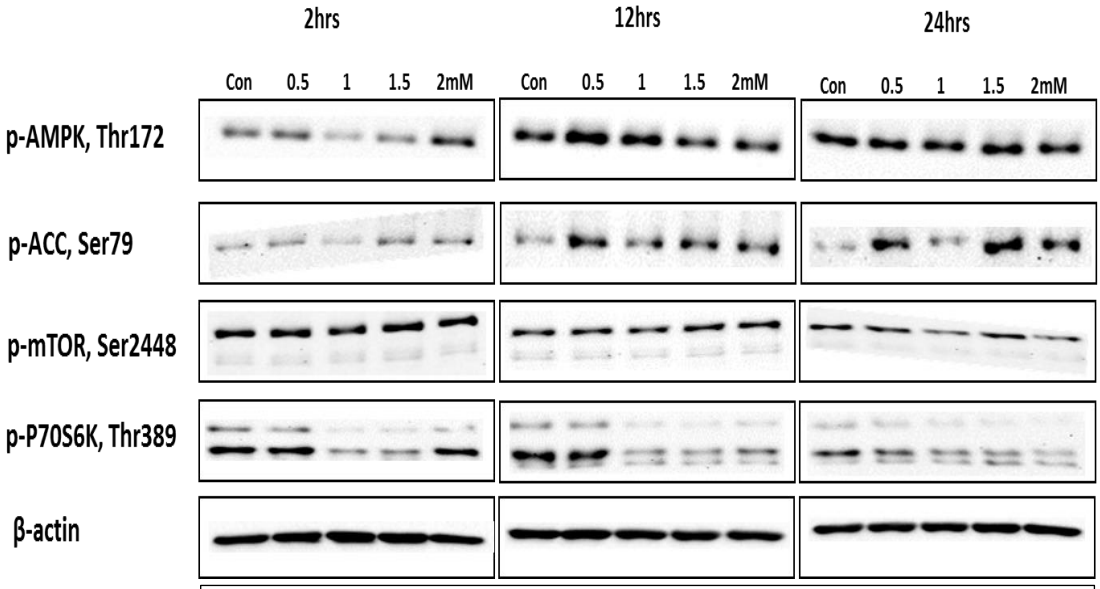

Fig 4.62. Western blots monitoring the effect of 2, 12 & 24hrs metformin treatment (0.5mM-2mM) on p-AMPK (Thr172), p-ACC (Ser79), p-mTOR (Ser2448) & p-P70S6K (Thr389) phosphorylation in MCF7 cells, using β-actin as a loading control.

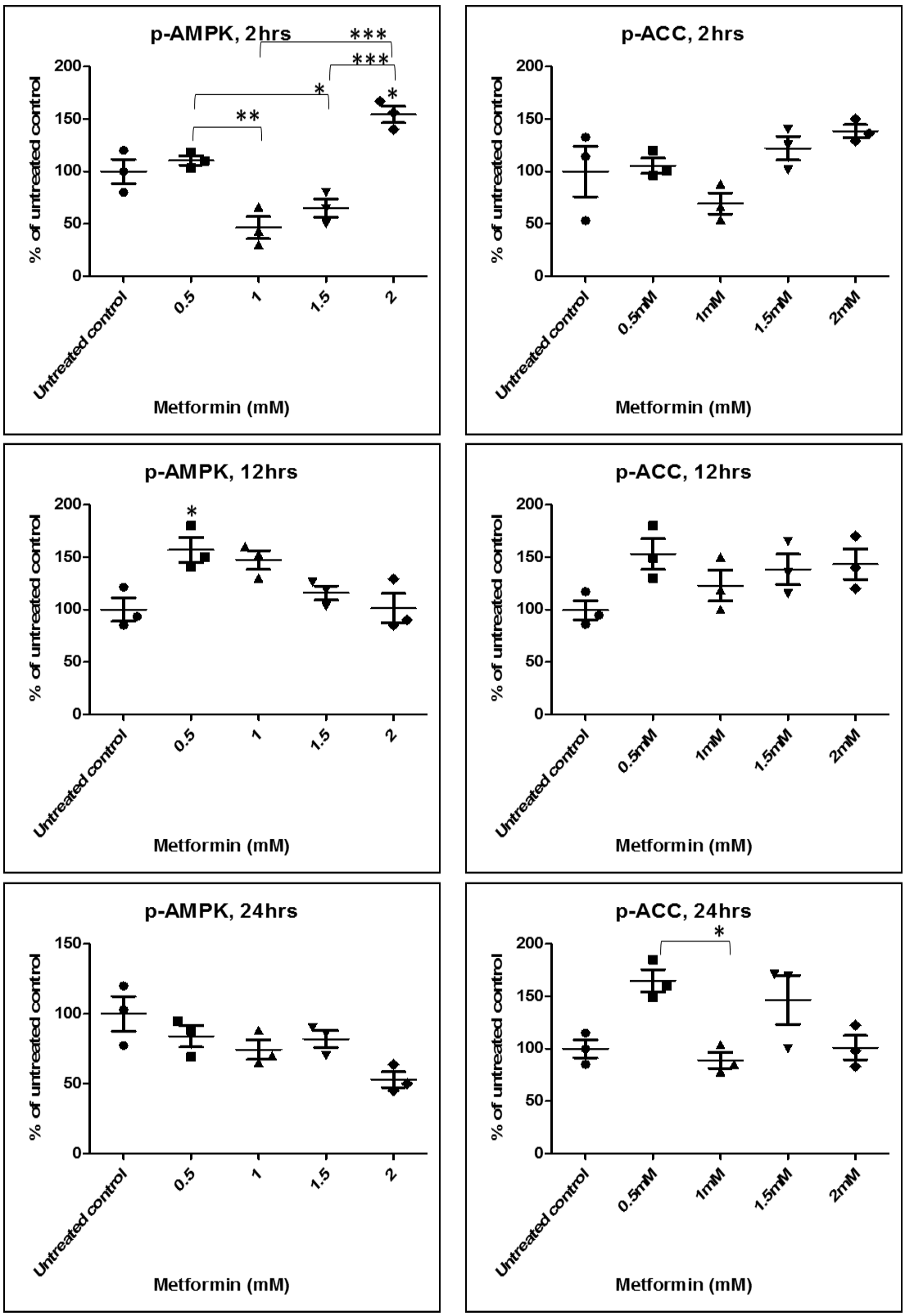

Fig 4.63. Data from scanned blots after actin normalisation showing the effect of 2, 12 & 24hrs metformin treatment (0.5mM-2mM) on p-AMPK & p-ACC phosphorylation by Western blotting in MCF7 cells. Data are represented as percentage of untreated control, and comprise the mean of three independent experiments (N=3). The error bar indicates SEM. * (P<0.05), ** (P<0.01) & *** (P<0.001) followed by ANOVA with Bonferroni post hoc correction.

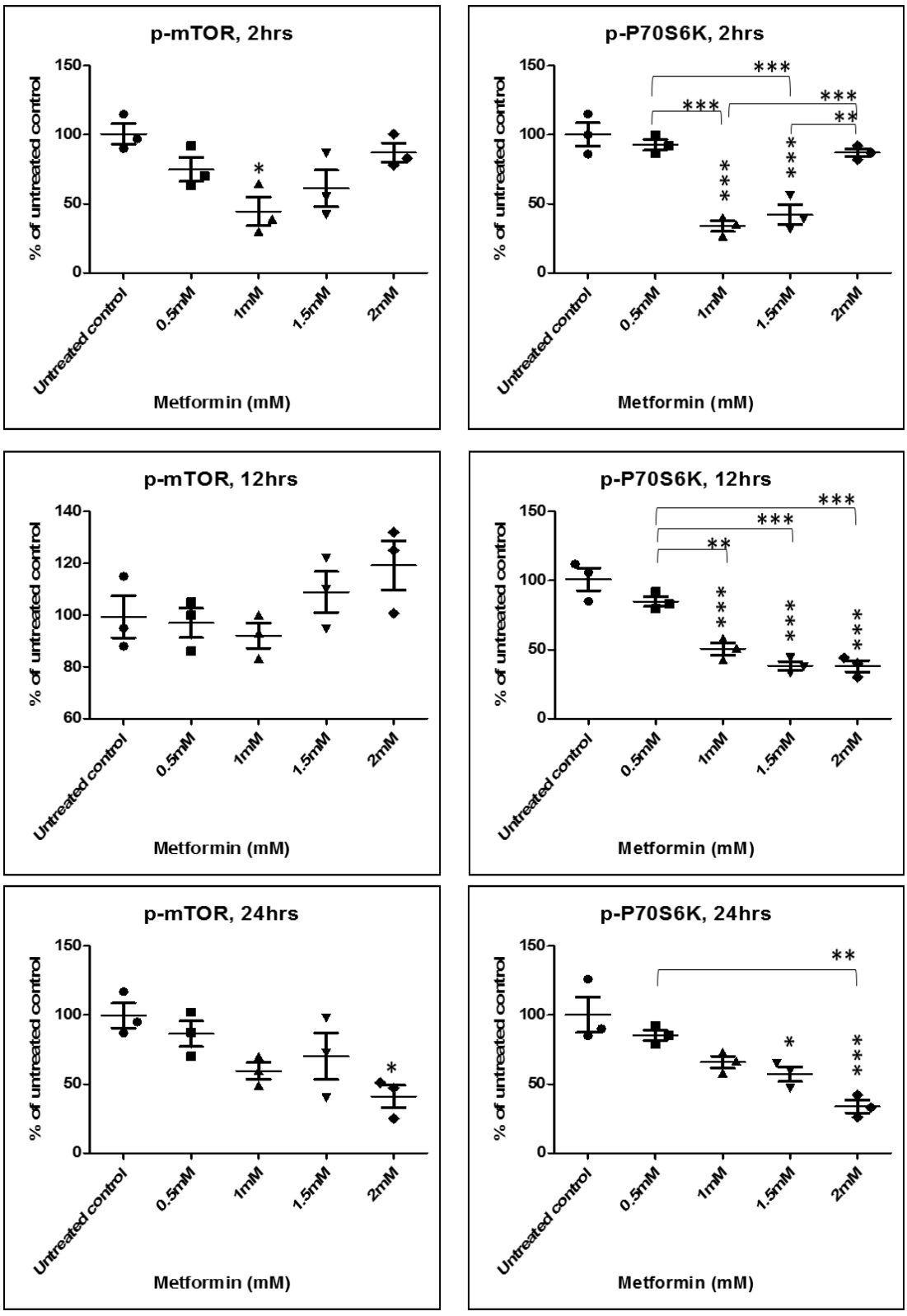

Fig 4.64. Data from scanned blots after actin normalisation showing the effect of 2, 12 & 24hrs metformin treatment (0.5mM-2mM) on p-mTOR & p-P70S6K phosphorylation by Western blotting in MCF7 cells. Data are represented as percentage of untreated control, and comprise the mean of three independent experiments (N=3). The error bar indicates SEM. * (P<0.05), ** (P<0.01) & *** (P<0.001) followed by ANOVA with Bonferroni post hoc correction.

Tamoxifen resistant cells: TamR

After 2hrs treatment in the TamR model, there was evidence for p-AMPK induction by metformin reaching significance with 1mM treatment compared to untreated control (P<0.05) (Fig 4.65 and 4.66). After 12hrs metformin, although changes were not detected at lower doses, p-AMPK was significantly induced by both 1.5mM and 2mM metformin (P<0.001) compared to the untreated control, 0.5mM (P<0.001) or 1mM treatment (P<0.001) (Fig 4.65 and 4.66). However, after 24hrs metformin treatment (where some increase in basal pAMPK was noted), p-AMPK signal was equivalent to the untreated control (Fig 4.65 and 4.66).

p-ACC level was largely unchanged by 2 hrs metformin treatment (Fig 4.65 and 4.66). However, by 12 hrs there was significant p-ACC induction with 1.5mM metformin as compared to untreated control (P<0.001) and versus lower doses of the drug (0.5mM P<0.001 and 1mM P<0.001) (Fig 4.65 and 4.66). p-ACC was also significantly induced by 2mM as compared to 1mM treatment at this time point (P<0.001). At 24 hrs there was some further evidence for p-ACC induction by metformin, reaching significance for 1mM treatment (P<0.05) (Fig 4.65 and 4.66).

At all time points, p-mTOR level remained largely unchanged with metformin treatment compared to untreated control (Fig 4.65 and 4.67). In contrast, by 2 hrs p-P70S6K was reduced by 2mM metformin, an effect also seen as a trend from some of the blots after 12 hrs treatment with 1mM or 2mM metformin (Fig 4.65 and 4.67). At 24 hrs, p-P70S6K was significantly reduced by 1.5mM (P<0.01) and 2mM (P<0.01) treatment as compared to untreated control and versus 0.5mM treatment (P<0.05 for both; Fig 4.65 and 4.67).

In summary, by 24hrs treatment, there was evidence that metformin could potentially inhibit protein synthesis in TamR cells since it reduced activity of the mTOR signalling element p-P70S6K, although this occurred independent of any parallel change in p-AMPK. Robust p-AMPK induction by the drug occurred at a somewhat earlier time point (12hrs) and this event was also associated with some reduction in the fatty acid regulatory pathway in the resistant model by 12hrs.

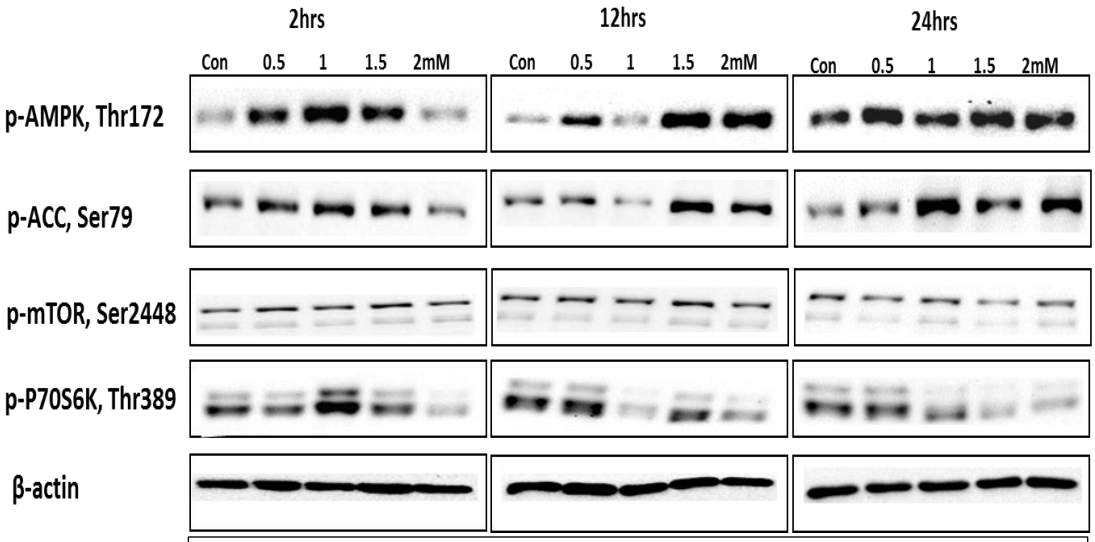

Fig 4.65. Western blots monitoring the effect of 2, 12 & 24hrs metformin treatment (0.5mM-2mM) on p-AMPK (Thr172), p-ACC (Ser79), p-mTOR (Ser2448) & p-P70S6K (Thr389) phosphorylation in TamR cells, using β-actin as a loading control.

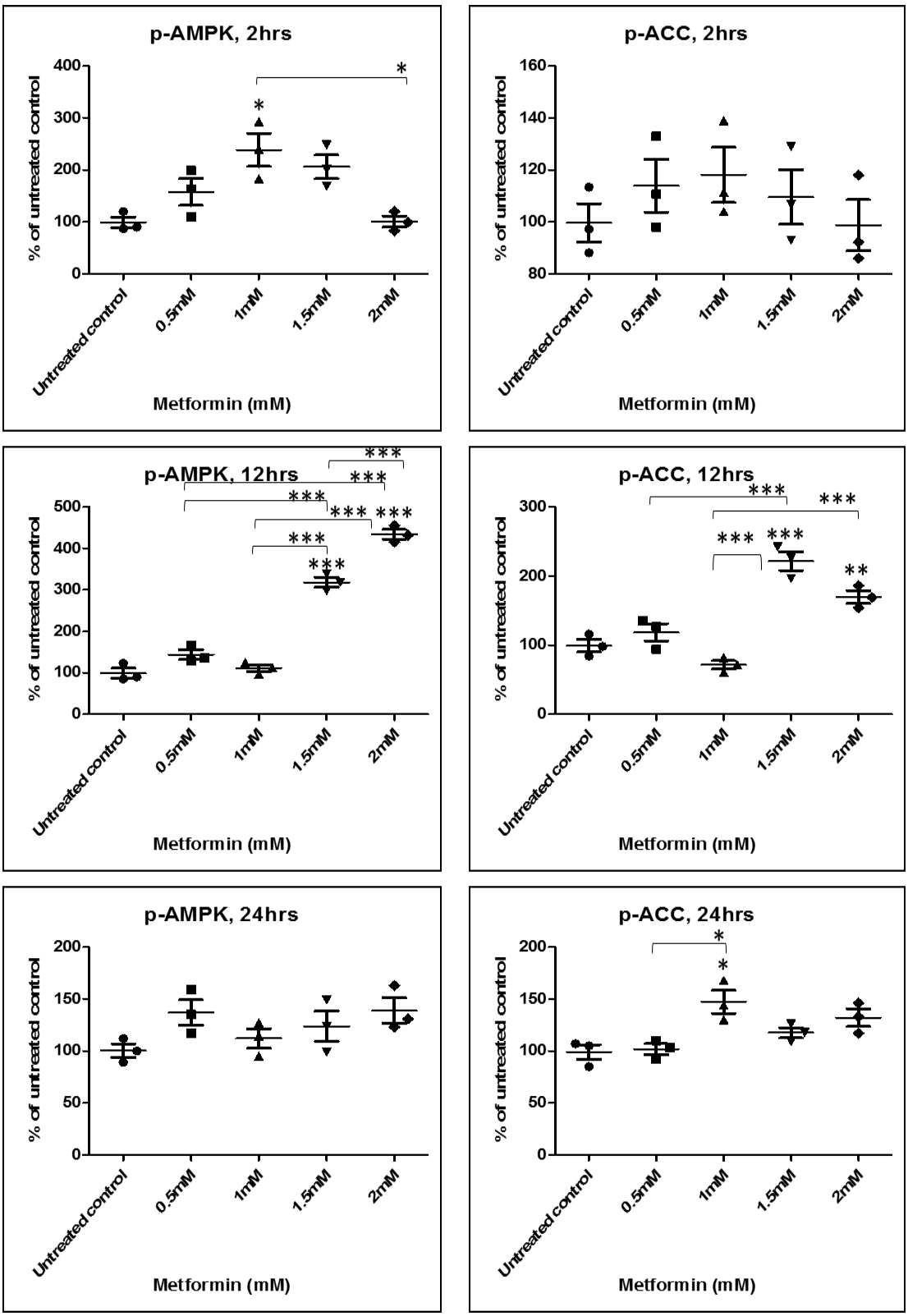

Fig 4.66. Data from scanned blots after actin normalisation showing the effect of 2, 12 & 24hrs metformin treatment (0.5mM-2mM) on p-AMPK & p-ACC phosphorylation by Western blotting in TamR cells. Data are represented as percentage of untreated control, and comprise the mean of three independent experiments (N=3). The error bar indicates SEM. * (P<0.05), ** (P<0.01) & *** (P<0.001) followed by ANOVA with Bonferroni post hoc correction.

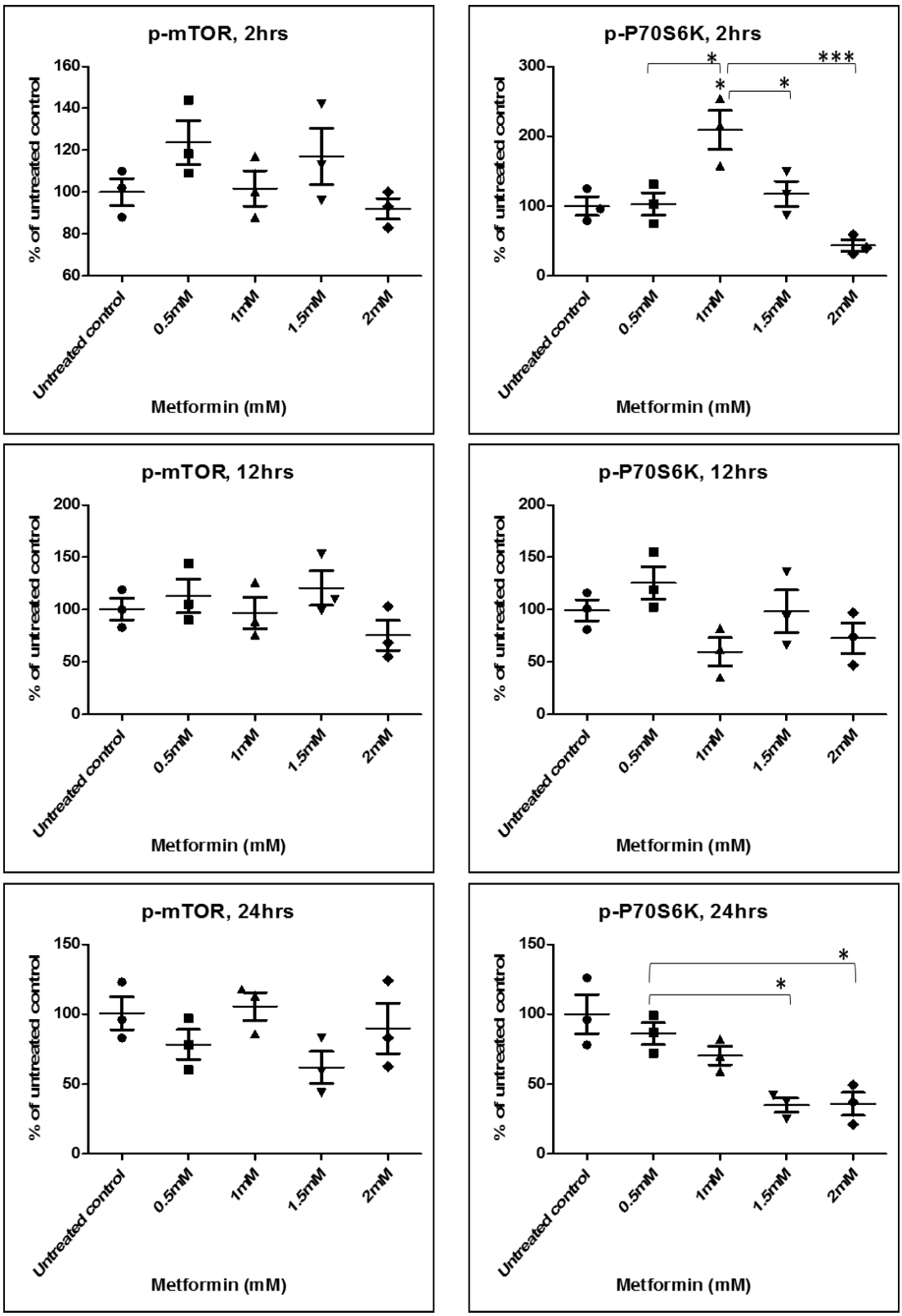

Fig 4.67. Data from scanned blots after actin normalisation showing the effect of 2, 12 & 24hrs metformin treatment (0.5mM-2mM) on p-mTOR & p-P70S6K phosphorylation by Western blotting in TamR cells. Data are represented as percentage of untreated control, and comprise the mean of three independent experiments (N=3). The error bar indicates SEM. * (P<0.05) & *** (P<0.001) followed by ANOVA with Bonferroni post hoc correction.

Tamoxifen resistant cells: TamRLT

After 2hrs treatment of TamRLT cells, p-AMPK was induced in a metformin dose dependent manner, reaching significance for 1.5mM (P<0.05) and 2mM (P<0.01) treatment versus untreated control (Fig 4.68 and 4.69). At 12hrs, there was evidence that p-AMPK remained elevated with 2mM metformin since it was significantly induced (P<0.05) versus 0.5mM treatment (Fig 4.68 and 4.69). pAMPK was also significantly induced by this metformin concentration at 24 hrs (P<0.05) as compared to 1.5mM treatment (Fig 4.68 and 4.69).

At 2 hrs, p-ACC was significantly induced in a dose dependent manner by 1mM (P<0.05), 1.5mM (P<0.01) and 2mM (P<0.01) metformin compared to untreated control (Fig 4.68 and 4.69). At 12 hrs, p-ACC remained significantly induced (P<0.05) for 2mM treatment only and the same effects was observed at 1.5mM (P<0.05) and 2mM (P<0.05) treatment as compared to untreated control by24 hrs (Fig 4.68 and 4.69).

Over the time course, p-mTOR levels remained largely unchanged with metformin compared to untreated control (Fig 4.68 and 4.70). In contrast, there was a modest decline in p-P70S6K with metformin in TamRLT cells. At all time points, p-P70S6K was significantly reduced by 2mM as compared to untreated control (Fig 4.69-4.70; all P<0.05).

Therefore, from 2 hrs onwards there was evidence in TAMRLT cells that metformin promoted AMPK activity, with an early impact on regulation of fatty acid synthesis, as well as a modest inhibitory effect over the full time course on mTOR signalling (based on the p-P70S6K findings) that can regulate protein synthesis.

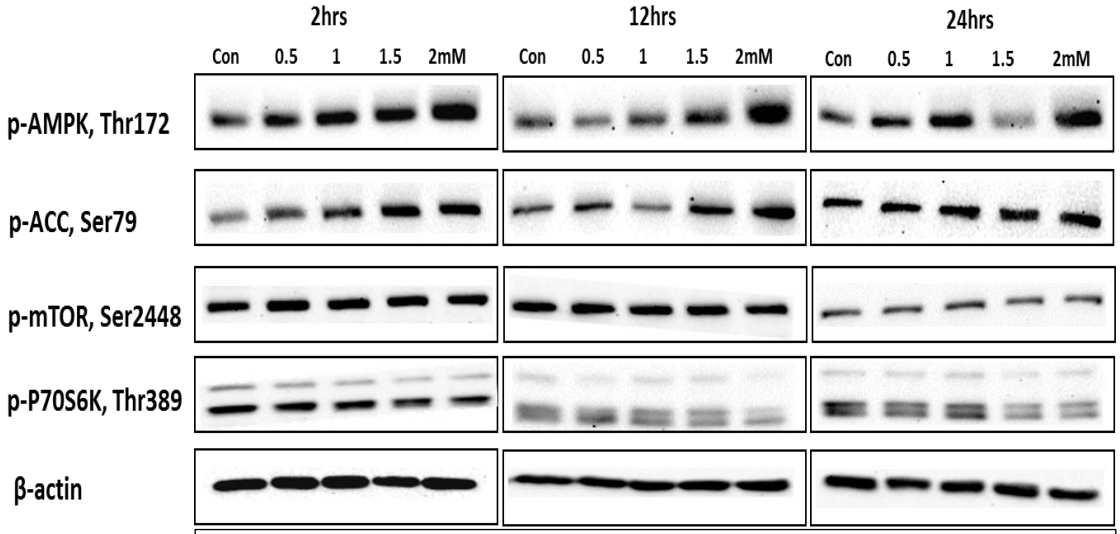

Fig 4.68. Western blots monitoring the effect of 2, 12 & 24hrs metformin treatment (0.5mM-2mM) on p-AMPK (Thr172), p-ACC (Ser79), p-mTOR (Ser2448) & p-P70S6K (Thr389) phosphorylation in TamRLT cells, using β-actin as a loading control.

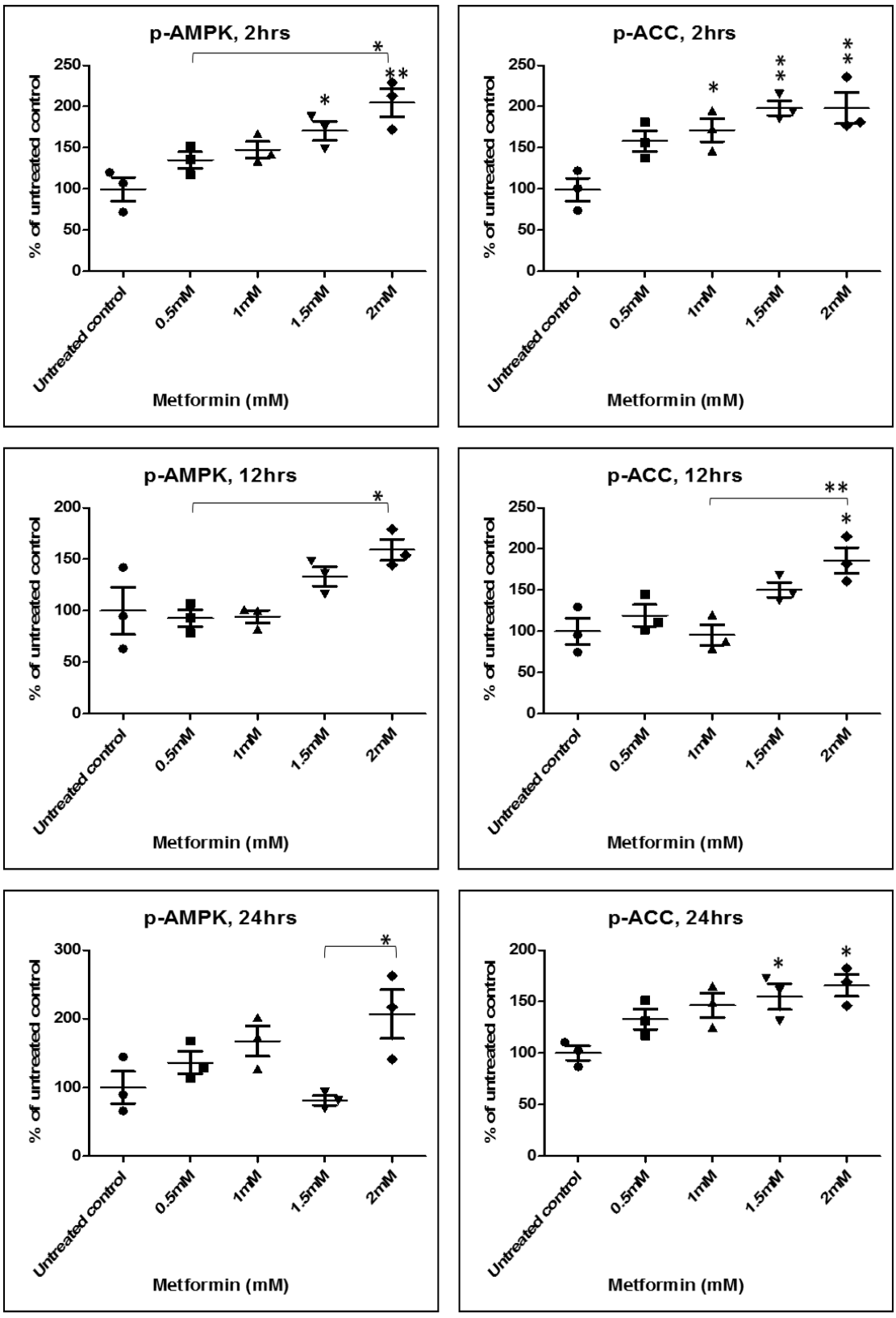

Fig 4.69. Data from scanned blots after actin normalisation showing the effect of 2, 12 & 24hrs metformin treatment (0.5mM-2mM) on p-AMPK & p-ACC phosphorylation by Western blotting in TamRLT cells. Data are represented as percentage of untreated control, and comprise the mean of three independent experiments (N=3). The error bar indicates SEM. * (P<0.05) & ** (P<0.01) followed by ANOVA with Bonferroni post hoc correction.

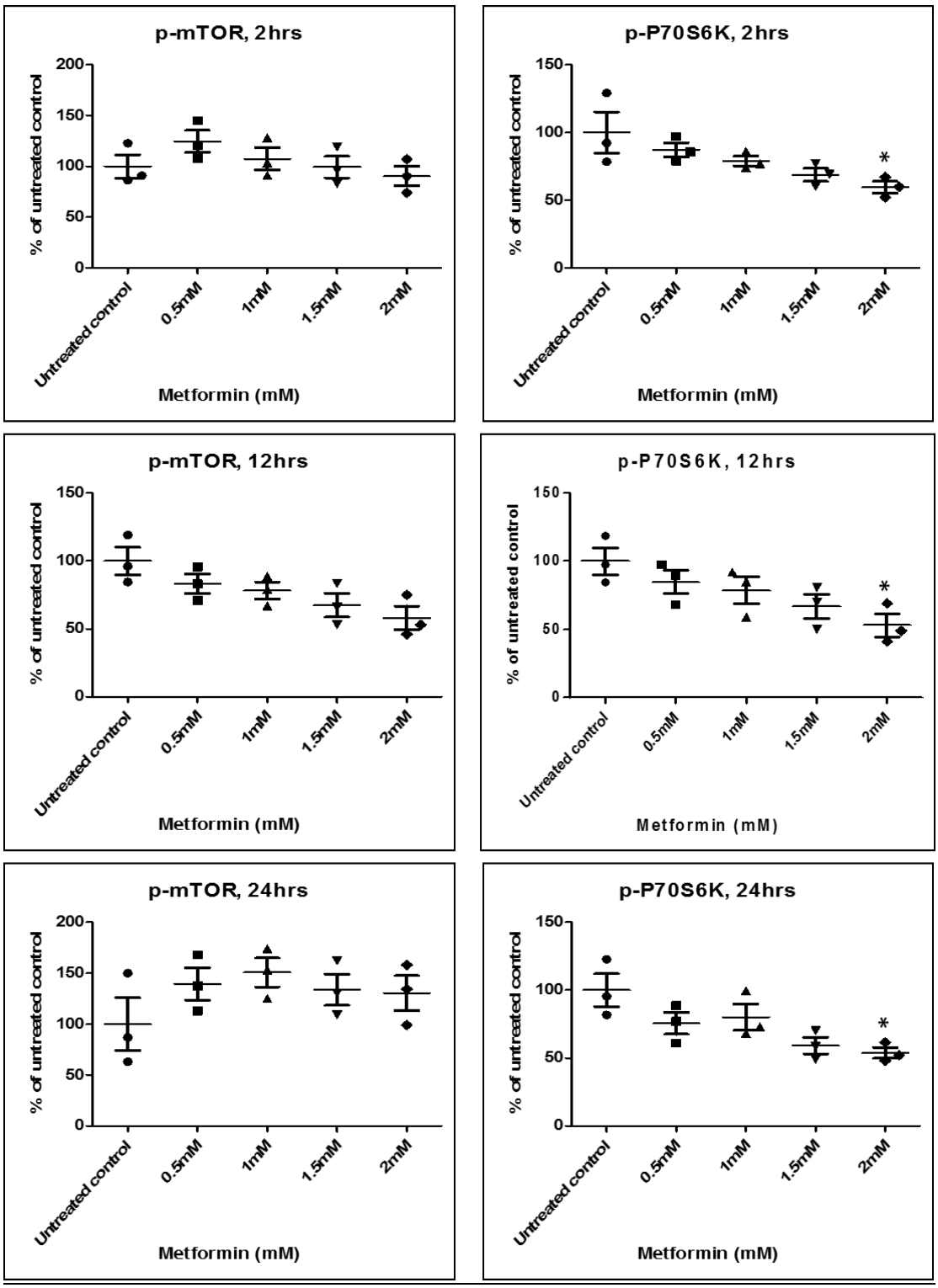

Fig 4.70. Data from scanned blots after actin normalisation showing the effect of 2, 12 & 24hrs metformin treatment (0.5mM-2mM) on p-mTOR & p-P70S6K phosphorylation by Western blotting in TamRLT cells. Data are represented as percentage of untreated control, and comprise the mean of three independent experiments (N=3). The error bar indicates SEM. * (P<0.05) followed by ANOVA with Bonferroni post hoc correction.

Fulvestrant resistant cells: FasR

After 2hrs treatment in FasR cells, p-AMPK was significantly induced by 1mM metformin (P<0.05) as compared to the untreated control (Fig 4.71 and 4.72). By 12 hrs, p-AMPK had been robustly induced by 1mM (P<0.05), 1.5mM (P<0.01) and 2mM (P<0.05) metformin versus the untreated control and versus 0.5mM drug (P<0.05, P<0.001, P<0.01 respectively (Fig 4.71 and 4.72). However, at 24hrs metformin treatment, p-AMPK was unchanged versus untreated control (although the basal pAMPK level was somewhat increased at this time point).

While not robustly changed at 2 hrs, by 12 hrs p-ACC was significantly induced by 1.5mM (P<0.01) and 2mM (P<0.01) metformin compared to untreated control and also versus 0.5mM and 1mM drug (Fig 4.71 and 4.72). There was also evidence for p-ACC induction following 24 hrs metformin, detected significantly for 0.5mM (P<0.01) and 1.5mM (P<0.01) treatment (Fig 4.71 and 4.72).

Surprisingly, p-mTOR was significantly induced by 1mM (P<0.01) and 1.5mM metformin at 2 hrs (P<0.001) and by 0.5mM (P<0.05) treatment at 12 hrs in this model compared to untreated control (Fig 4.72 and 4.73). At 24 hrs, p-mTOR was again slightly induced by 0.5mM treatment versus the control, and also significantly increased versus higher metformin doses (Fig 4.93 and 4.95).

Similarly, at 2 hrs, p-P70S6K was significantly induced (P<0.05) by 1.5mM treatment as compared to untreated control (Fig 74.2 and 4.73). Although basal level was somewhat elevated at 12 hrs, nevertheless, p-P70S6 level declined with metformin at this time point, reaching significance at 2mM (P<0.05). Some dose dependent decline was also detected after 24 hrs metformin, with the p-P70S6K fall reaching significance for 2mM treatment (P<0.05) (Fig 4.72 and 4.73).

Therefore, by 12 hrs metformin promoted AMPK activity in FasR cells. There was evidence for metformin impact on regulation of fatty acid synthesis at this and the subsequent 24hr time points. There was also some evidence from p-P70S6K for some inhibitory impact on mTOR signalling (and thereby protein synthesis) from 12 hrs in this model. However, at the longest time point the protein and fatty acid pathway events were not paralleled by p-AMPK induction.

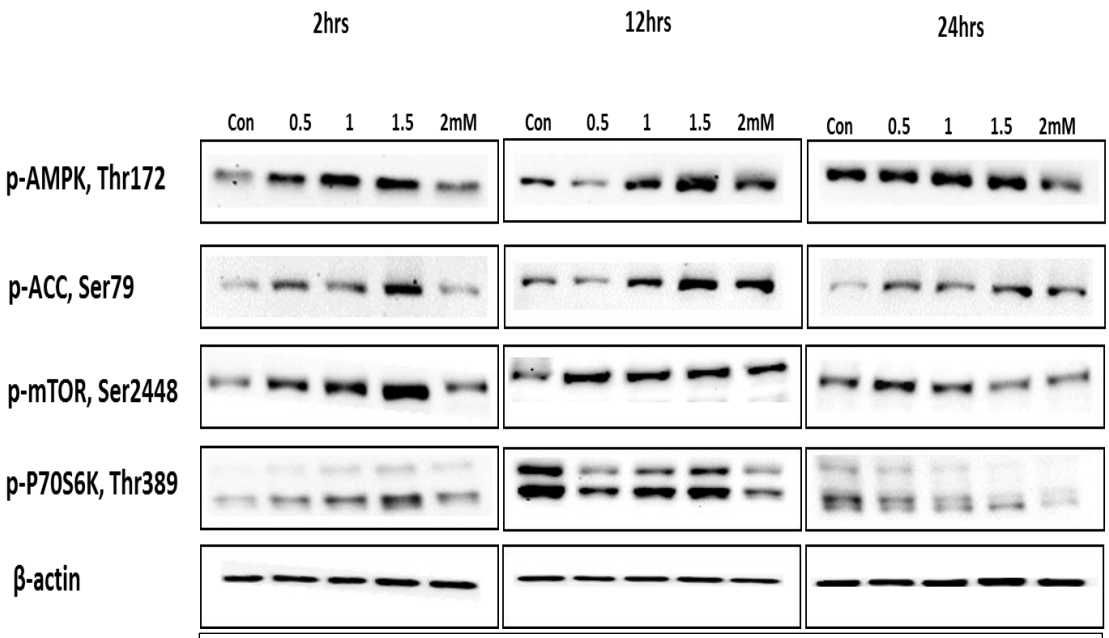

Fig 4.71. Western blots monitoring the effect of 2, 12 & 24hrs metformin treatment (0.5mM-2mM) on p-AMPK (Thr172), p-ACC (Ser79), p-mTOR (Ser2448) & p-P70S6K (Thr389) phosphorylation in FasR cells, using β-actin as a loading control.

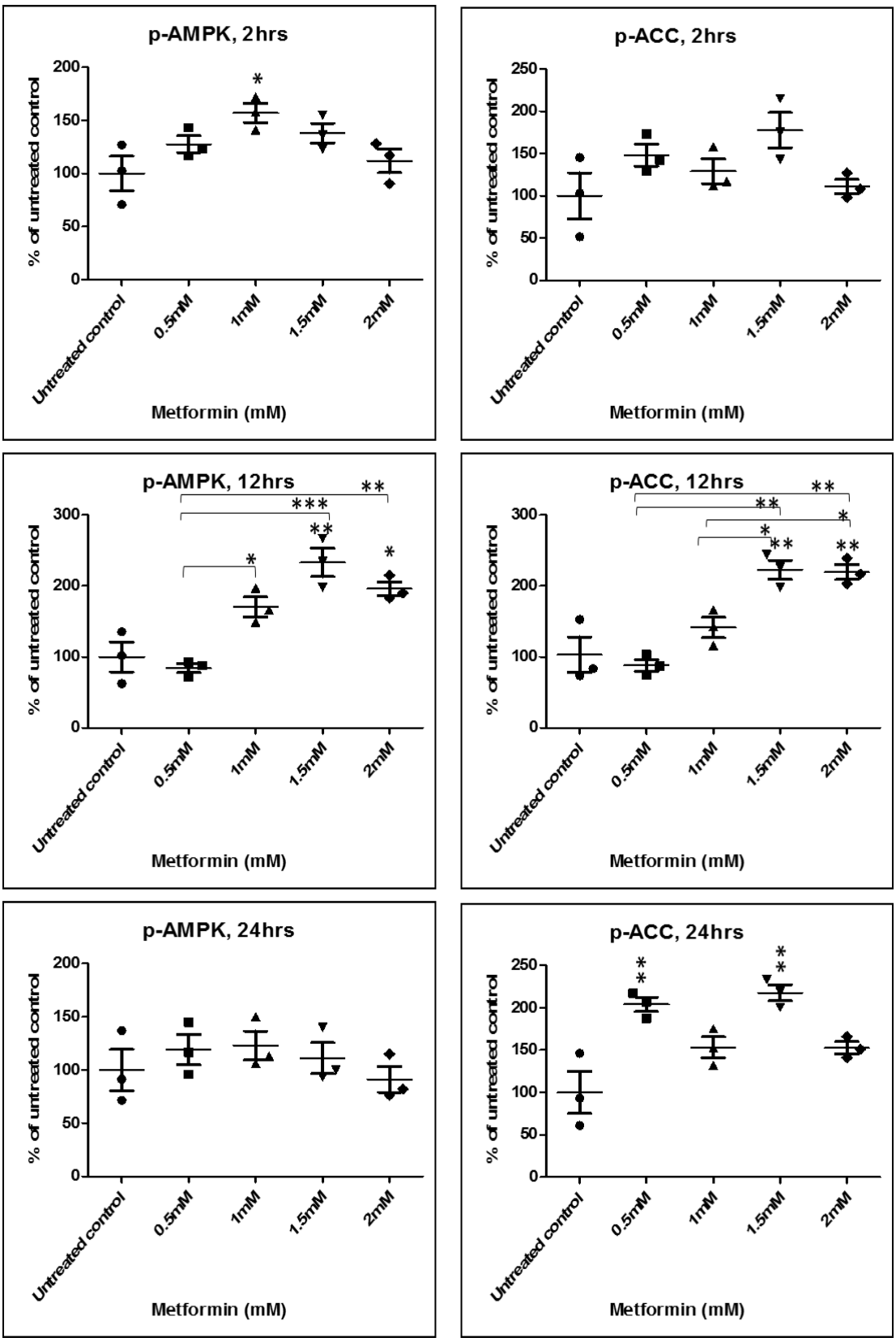

Fig 4.72. Data from scanned blots after actin normalisation showing the effect of 2, 12 & 24hrs metformin treatment (0.5mM-2mM) on p-AMPK & p-ACC phosphorylation by Western blotting in FasR cells. Data are represented as percentage of untreated control, and comprise the mean of three independent experiments (N=3). The error bar indicates SEM. * (P<0.05), ** (P<0.01) & *** (P<0.001) followed by ANOVA with Bonferroni post hoc correction.

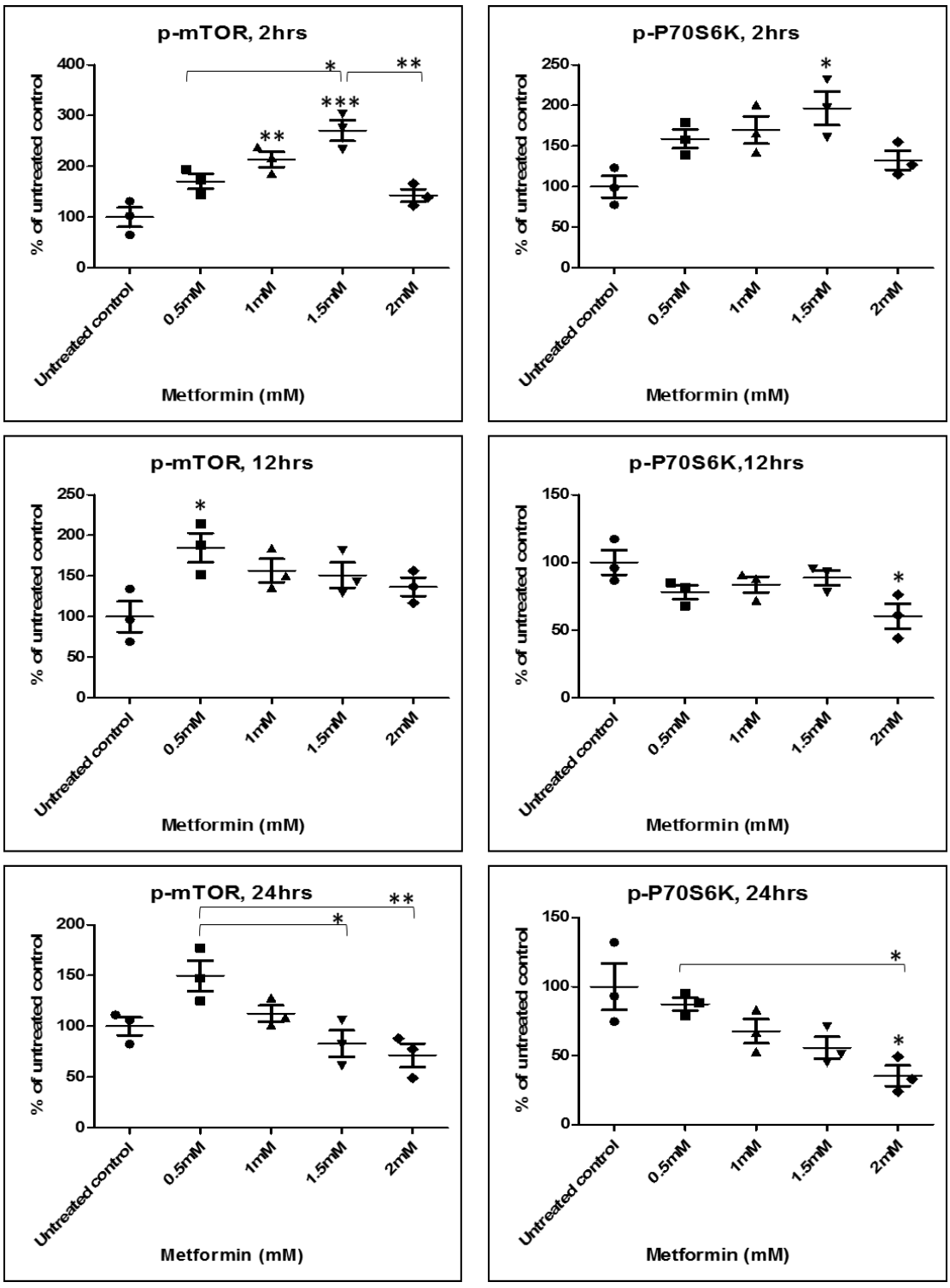

Fig 4.73. Data from scanned blots after actin normalisation showing the effect of 2, 12 & 24hrs metformin treatment (0.5mM-2mM) on p-mTOR & p-P70S6K phosphorylation by Western blotting in FasR cells. Data are represented as percentage of untreated control, and comprise the mean of three independent experiments (N=3). The error bar indicates SEM. * (P<0.05), ** (P<0.01) & *** (P<0.001) followed by ANOVA with Bonferroni post hoc correction.

Fulvestrant resistant cells: FasRLT

After 2hrs treatment of FasRLT cells, p-AMPK was significantly induced by 1.5mM (P<0.05) and 2mM metformin (P<0.01) compared to untreated control (Fig 4.74 and 4.75). Significant induction was also observed for 1mM-2mM drug (all P<0.01) compared to 0.5mM treatment at this time point. After 12hrs, p-AMPK was significantly induced by 1mM (P<0.05) and 1.5mM metformin (P<0.001) versus untreated control (Fig 4.74 and 4.75), and for the latter dose versus 0.5mM treatment (P<0.05; Fig 4.96 and 4.97). By 24hrs, p-AMPK induction was significance for 0.5mM (P<0.05), 1mM (P<0.01), 1.5mM (P<0.001) and 2mM (P<0.001) metformin versus untreated control (Fig 4.74 and 4.75).

While p-ACC was not significantly changed at the earliest time point, by 12 hrs it was induced with 1.5mM (P<0.05) and at 24hrs significantly with 1mM (P<0.001), 1.5mM (P<0.01) and 2mM (P<0.01) metformin versus untreated control (Fig 4.74 and 4.75).

At 2 hrs, p-mTOR was somewhat reduced after 0.5mM and 1.5mM treatment, and at 12 hours by most doses of metformin and changes reached significant by 1mM metformin (P<0.05) as compared to untreated control (Fig 4.74 and 4.76). By 24 hrs, these decreases reached significance for 2mM treatment (P<0.05) as compared to untreated control (Fig 4.74 and 4.76).

p-P70S6K was significantly reduced after 2mM treatment with metformin for 2 hrs (P<0.01) compared to untreated control, also versus 0.5mM (P<0.05) and 1mM (P<0.05) treatment (Fig 4.74 and 4.76). By 12 hrs, it was significantly reduced by both 1mM (P<0.01) and 2mM metformin (P<0.001) (Fig 4.74 and 4.76), the latter also versus 0.5mM drug (P<0.01). Reduction persisted to 24 hrs, with significant decline in p-70S6K for 1.5mM (P<0.01) and 2mM (P<0.01) metformin versus untreated control, for the latter dosage also versus 0.5mM drug (P<0.05) (Fig 4.74 and 4.76).

Therefore, for 2-12 hrs, metformin induced significant AMPK activity which potentially impacted on protein synthesis by reducing activity of the mTOR signalling element p-P70S6. At the later time points, metformin influenced regulators of both fatty acid and protein synthesis in FasRLT cells (Fig 4.74-4.76).but this was not paralleled by p-AMPK change at 24hrs

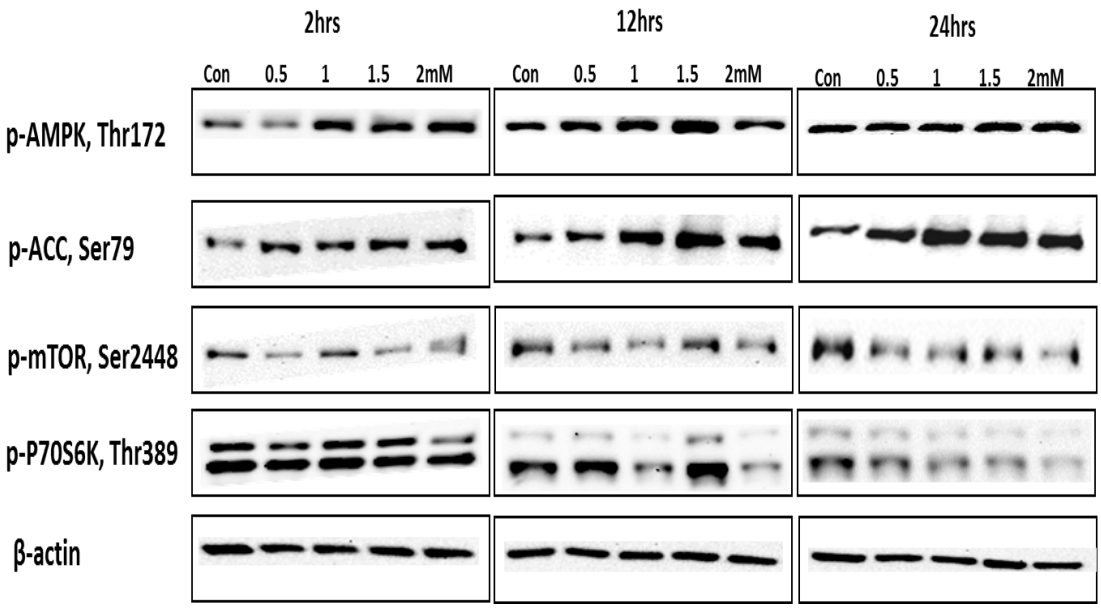

4.Fig 74. Western blots monitoring the effect of 2, 12 & 24hrs metformin treatment (0.5mM-2mM) on p-AMPK (Thr172), p-ACC (Ser79), p-mTOR (Ser2448) & p-P70S6K (Thr389) phosphorylation in FasRLT cells, using β-actin as a loading control.

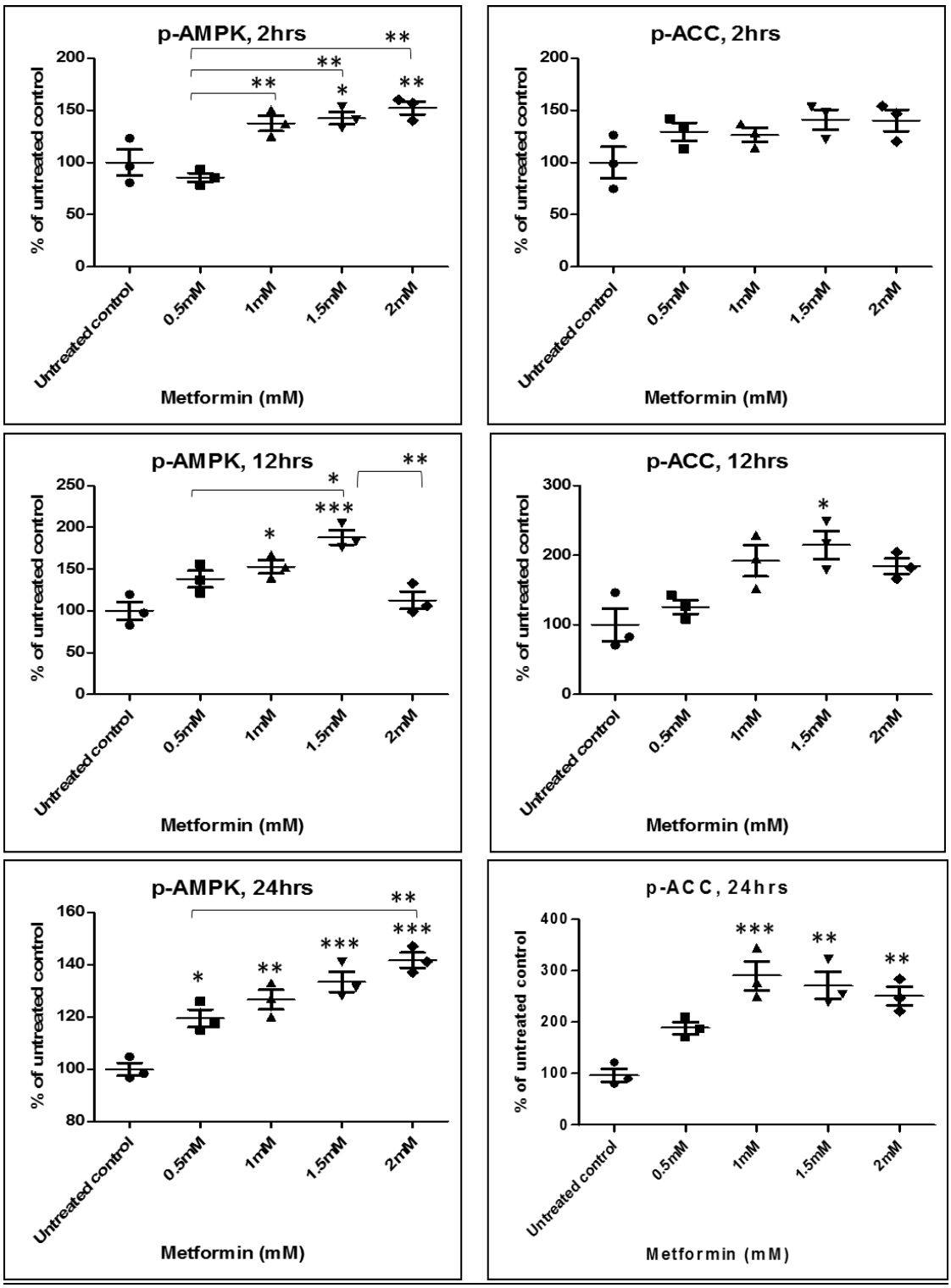

Fig 4.75. Data from scanned blots after actin normalisation showing the effect of 2, 12 & 24hrs metformin treatment (0.5mM-2mM) on p-AMPK & p-ACC phosphorylation by Western blotting in FasRLT cells. Data are represented as percentage of untreated control, and comprise the mean of three independent experiments (N=3). The error bar indicates SEM. * (P<0.05), ** (P<0.01) & *** (P<0.001) followed by ANOVA with Bonferroni post hoc correction.

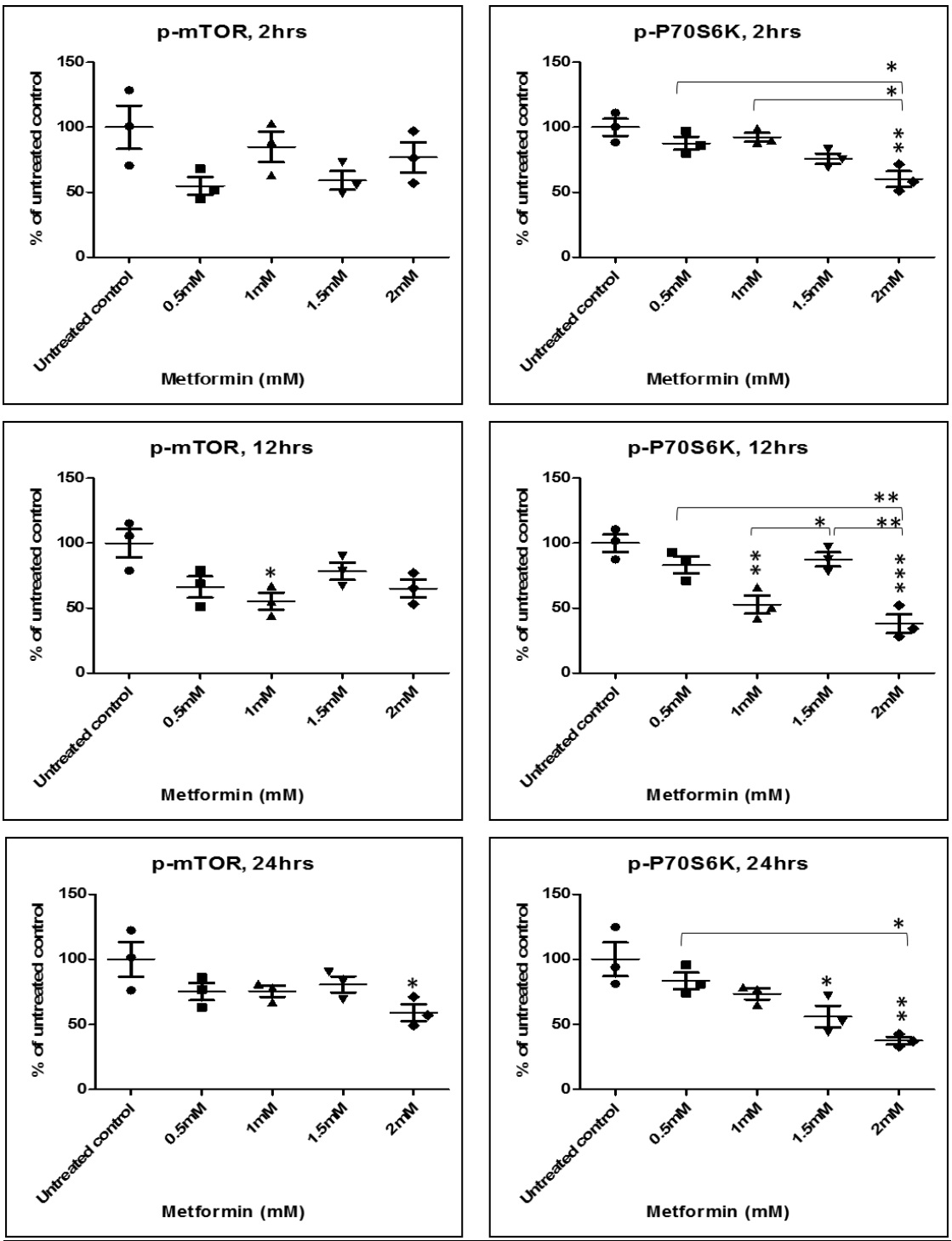

Fig 4.76. Data from scanned blots after actin normalisation showing the effect of 2, 12 & 24hrs metformin treatment (0.5mM-2mM) on p-mTOR & p-P70S6K phosphorylation by Western blotting in FasRT cells. Data are represented as percentage of untreated control, and comprise the mean of three independent experiments (N=3). The error bar indicates SEM. * (P<0.05), ** (P<0.01) & *** (P<0.001) followed by ANOVA with Bonferroni post hoc correction.

Oestrogen deprivation resistant cells: MCF7(X)

After 2hrs treatment of MCF7(X) cells, p-AMPK was significantly reduced by 0.5mM (P<0.05) and 1.5mM (P<0.05) metformin as compared to untreated control (Fig 4.77 and 4.78). By 12hrs treatment p-AMPK was significantly induced by 1.5mM drug only (P<0.05), as compared to untreated control and versus 0.5mM (P<0.01) and 1mM (P<0.01) treatment (Fig 4.77 and 4.78). After 24hrs metformin, p-AMPK was significantly induced by 1-2mM treatments (all P<0.001) compared to the untreated control and versus 0.5mM drug (for 1mM P<0.05; 1.5mM P<0.001; 2mM P≤0.001) (Fig 4.77 and 4.78).

p-ACC was significantly induced by treating MCF7(X) cells for 2 hrs with 2mM metformin, as compared to untreated control or versus 0.5-1.5mM drug (all P<0.001) (Fig 4.77 and 4.78). Significant p-ACC induction was also seen at 12 hrs for 1mM (P<0.05), 1.5mM (P<0.01) and 2mM (P<0.01) metformin versus untreated control or versus 0.5mM drug (for 1mM P<0.05; 1.5mM P<0.01 and 2mM (P<0.01) respectively) (Fig 4.77 and 4.78). p-ACC induction persisted at 24 hrs with 1.5mM (P<0.05) and 2mM (P<0.001) treatment versus the untreated control, and for the latter dosage versus 0.5mM (P<0.01), 1mM (P<0.001) and 1.5mM (P<0.05) treatment (Fig 4.77 and 4.78).

p-mTOR remained largely unchanged after 2 hrs treatment with metformin versus untreated control (Fig 4.77 and 4.79), and at 12 hrs there was a surprising increase with 1.5mM (P<0.01) and 2mM (P<0.001) treatment as compared to untreated control and also for the highest dose versus lower drug dosages (0.5mM P<0.01, 1mM P<0.05) (Fig 4.77 and 4.79). By 24 hrs, the induction was lost and p-mTOR was reduced significantly by 1.5-2mM (P<0.05) treatment (Fig 4.77 and 4.79) There was no marked change in p-P70S6K with 2 hrs metformin treatment, and by 12 hrs p-P70S6K was significantly reduced only by 0.5mM treatment (P<0.05) (Fig 4.77 and 4.79). However, by 24 hrs p-P70S6K was significantly reduced by 1mM (P<0.01), 1.5mM (P<0.001) and 2mM (P<0.001) metformin versus higher basal levels in the untreated control and also versus. 0.5mM treatment (1.5mM P<0.001; 2mM P<0.001) (Fig 4.77 and 4.79).

Therefore, along with some induction of p-AMPK from 12hrs metformin treatment potentially reduced fatty acid synthesis as it also increased p-ACC activity. After 24hrs metformin treatment, impact on regulatory mechanisms both for fatty acid and protein synthesis was observed in an AMPK-dependent manner in MCF7(X) cells (Fig 4.77-4.79).

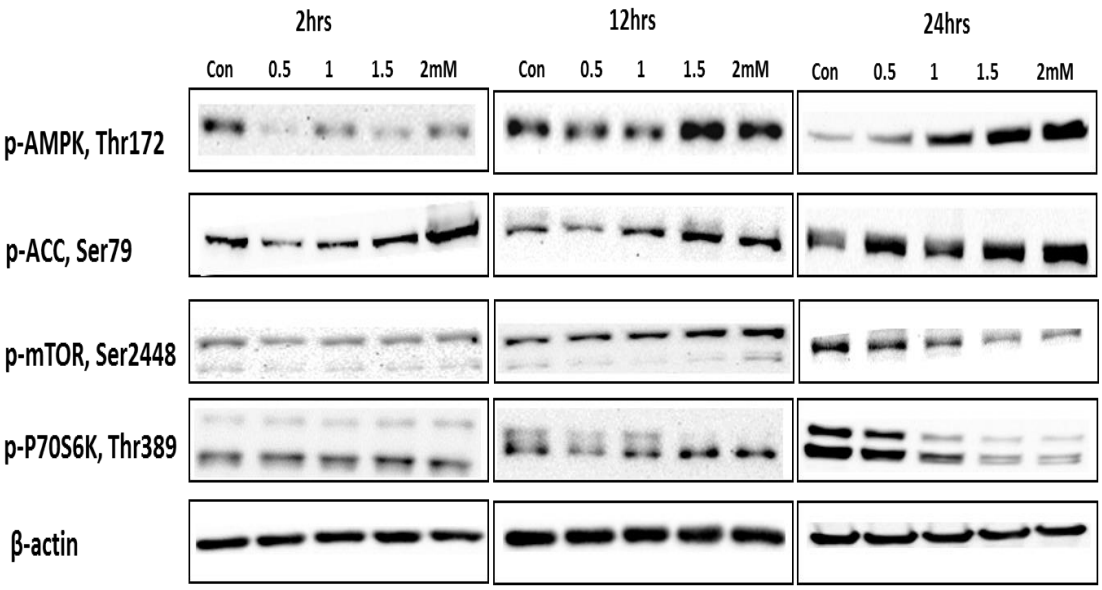

Fig 4.77. Western blots monitoring the effect of 2, 12 & 24hrs metformin treatment (0.5mM-2mM) on p-AMPK (Thr172), p-ACC (Ser79), p-mTOR (Ser2448) & p-P70S6K (Thr389) phosphorylation in MCF7(X) cells, using β-actin as a loading control.

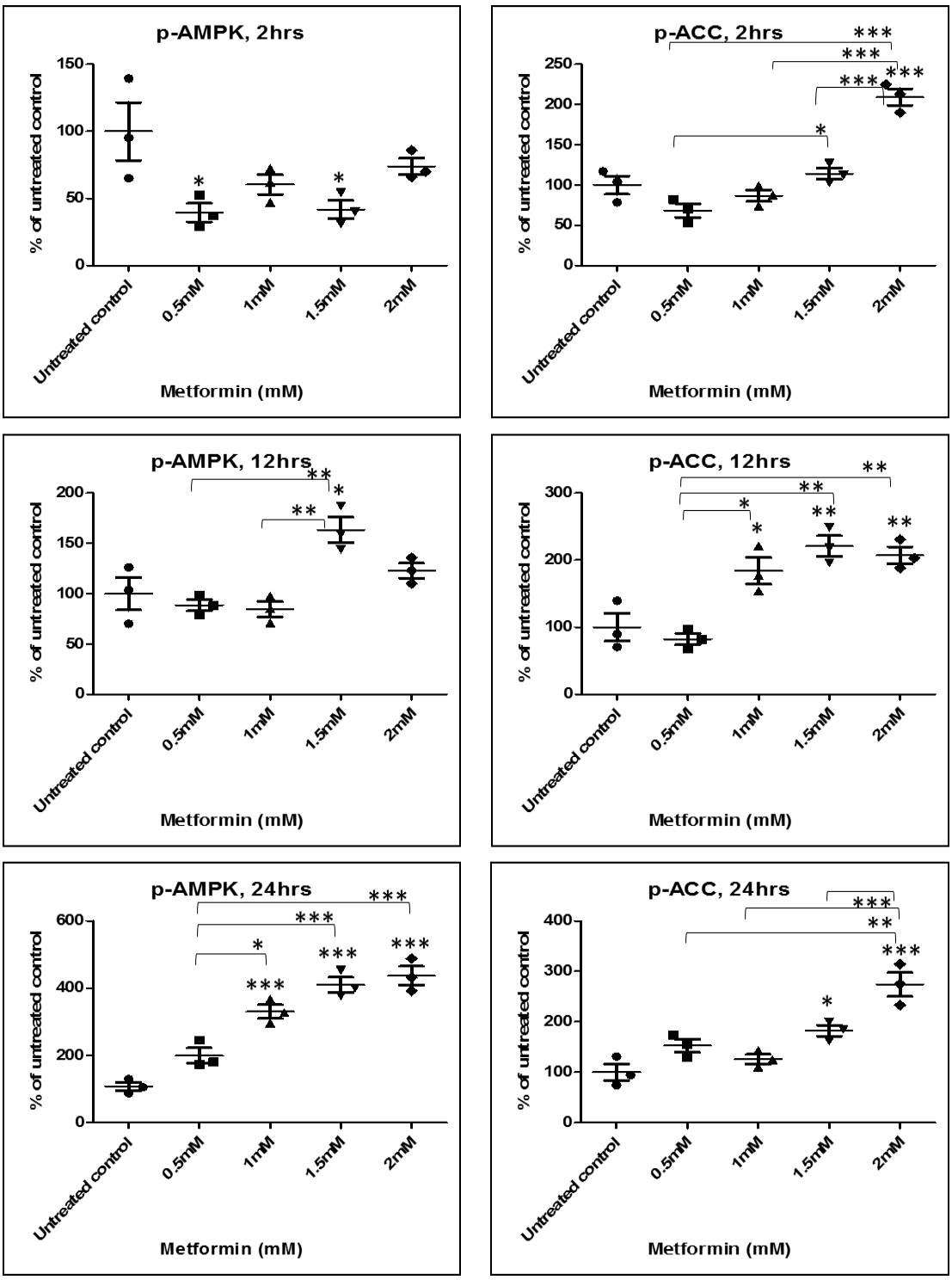

Fig 4.78. Data from scanned blots after actin normalisation showing the effect of 2, 12 & 24hrs metformin treatment (0.5mM-2mM) on p-AMPK & p-ACC phosphorylation by Western blotting in MCF7(X) cells. Data are represented as percentage of untreated control, and comprise the mean of three independent experiments (N=3). The error bar indicates SEM. * (P<0.05), ** (P<0.01) & *** (P<0.001) followed by ANOVA with Bonferroni post hoc correction.

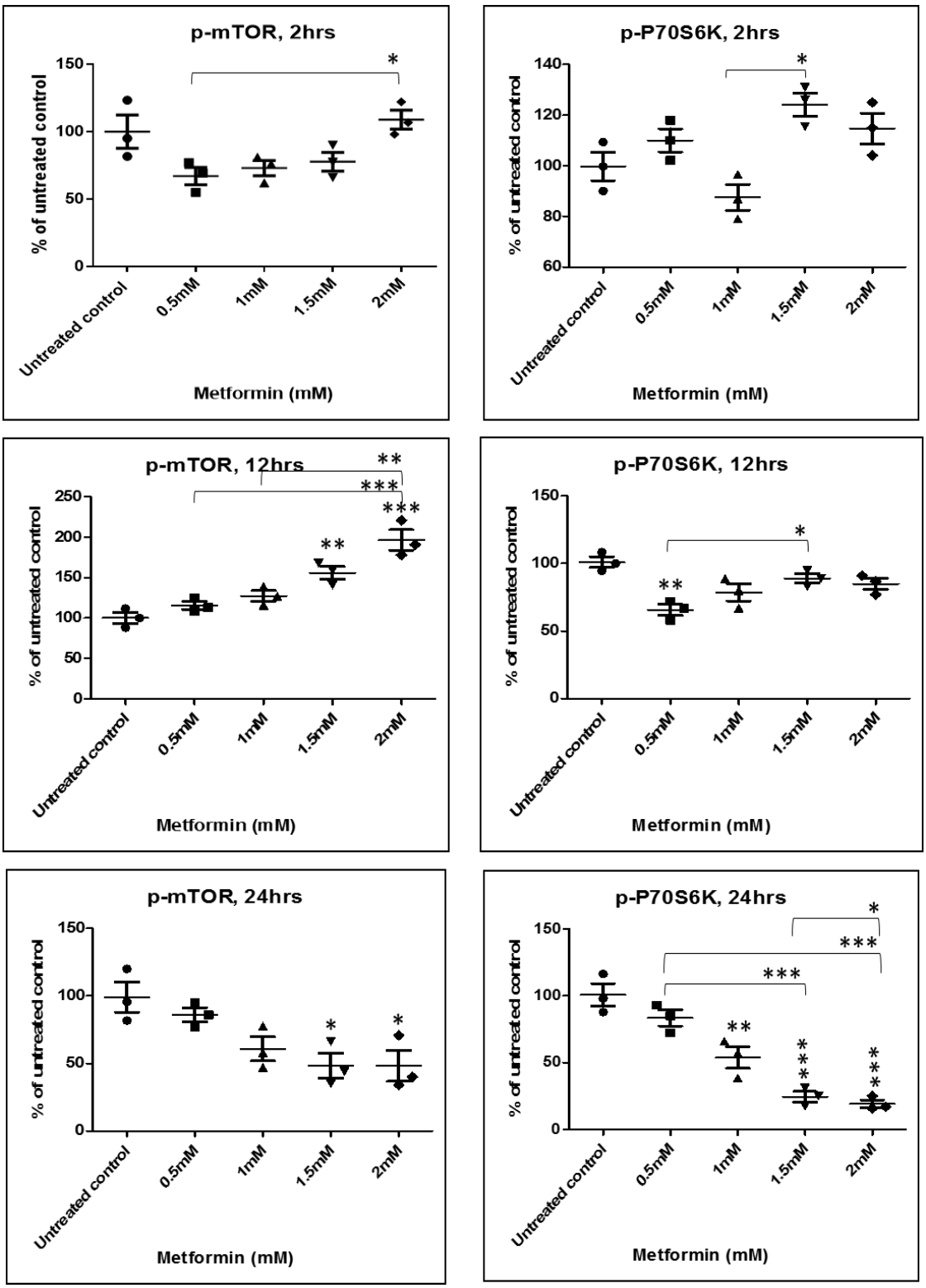

Fig 4.79. Data from scanned blots after actin normalisation showing the effect of 2, 12 & 24hrs metformin treatment (0.5mM-2mM) on p-mTOR & p-P70S6K phosphorylation by Western blotting in MCF7(X) cells. Data are represented as percentage of untreated control, and comprise the mean of three independent experiments (N=3). The error bar indicates SEM. * (P<0.05), ** (P<0.01) & *** (P<0.001) followed by ANOVA with Bonferroni post hoc correction.

Oestrogen deprivation resistant cells: MCF7(X)LT

After 2hrs treatment of MCF7(X)LT, p-AMPK was significantly induced by 0.5mM metformin (P<0.05) (Fig 4.80 and 4.81) versus very low basal activity. At 12hrs, p-AMPK induction was significant for 1mM (P<0.05) and 1.5mM (P<0.01) metformin compared to untreated control and versus 0.5mM treatment (P<0.01). Induction was also detected at 24hrs, reaching significance for 1mM metformin (P<0.05) (Fig 4.80 and 4.81).

While p-ACC levels at 2 hrs significantly induced by 1mM (P<0.05) and 2mM (P<0.05) as compared to untreated control (Fig 4.80 and 4.81), at 12 hrs p-ACC was significantly induced by 1.5mM and 2mM metformin versus untreated control (P<0.01) and versus 0.5mM drug (P<0.01) (Fig 4.80 and 4.81). p-ACC was significantly induced by all 0.5- 2mM dosages at 24 hrs treatment (P<0.001) (Fig 4.80 and 4.81).

There was also evidence for reduction of p-mTOR by metformin in this model. Thus at 2hrs p-mTOR fell significantly with 1.5mM (P<0.05) or 2mM (P<0.01) treatment as compared to untreated control and also versus 0.5mM treatment (P<0.05 and P<0.01 respectively) (Fig 4.80 and 4.82). Some reduction was also detected at 12 hrs for 2mM metformin (P<0.05), and at 24 hrs for both 1mM (P<0.05) and 2mM treatment (P<0.01) compared to untreated control and for 2mM versus 0.5mM drug (Fig 4.80 and 4.82).

Similarly, p-P70S6K fell with metformin treatment in MCF7(X)LT cells. At 2 hrs p-P70S6K was significantly reduced by 1.5mM and 2mM metformin versus untreated control or versus 0.5mM or 1mM drug (all P<0.001) (Fig 4.80 and 4.82). Furthermore, at 12 hrs p-P70S6K levels fell with 0.5mM (P<0.01), 1mM (P<0.01) or 2mM (P<0.001) treatment, while at 24 hrs there was a dose dependent decline in p-P70S6K with 1mM (P<0.01), 1.5mM (P<0.001) and 2mM (P<0.001) metformin compared to untreated control. This was also apparent for 1.5mM (P<0.01) and 2mM treatment (P<0.001) versus 0.5mM drug at this time point (Fig 4.80 and 4.82).

Therefore, from 2 hrs there was evidence that metformin reduced mTOR signalling in a sustained manner, which could potentially impact on protein synthesis in MCF7(X)LT. Induction of activity for the fatty acid synthesis pathway regulator ACC emerged after longer treatment times in this model. While p-AMPK was also metformin-induced by 12 hours, earlier or later profile changes for the protein and fatty acid regulatory elements were not always paralleled by p-AMPK change.

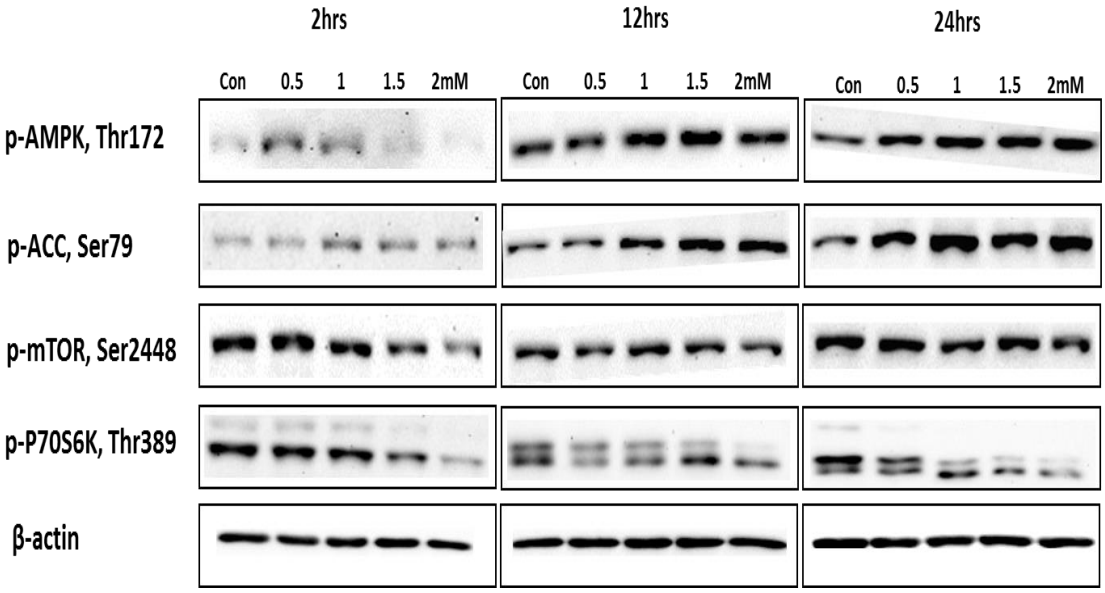

Fig 4.80. Western blots monitoring the effect of 2, 12 & 24hrs metformin treatment (0.5mM-2mM) on p-AMPK (Thr172), p-ACC (Ser79), p-mTOR (Ser2448) & p-P70S6K (Thr389) phosphorylation in MCF7(X)LT cells, using β-actin as a loading control.

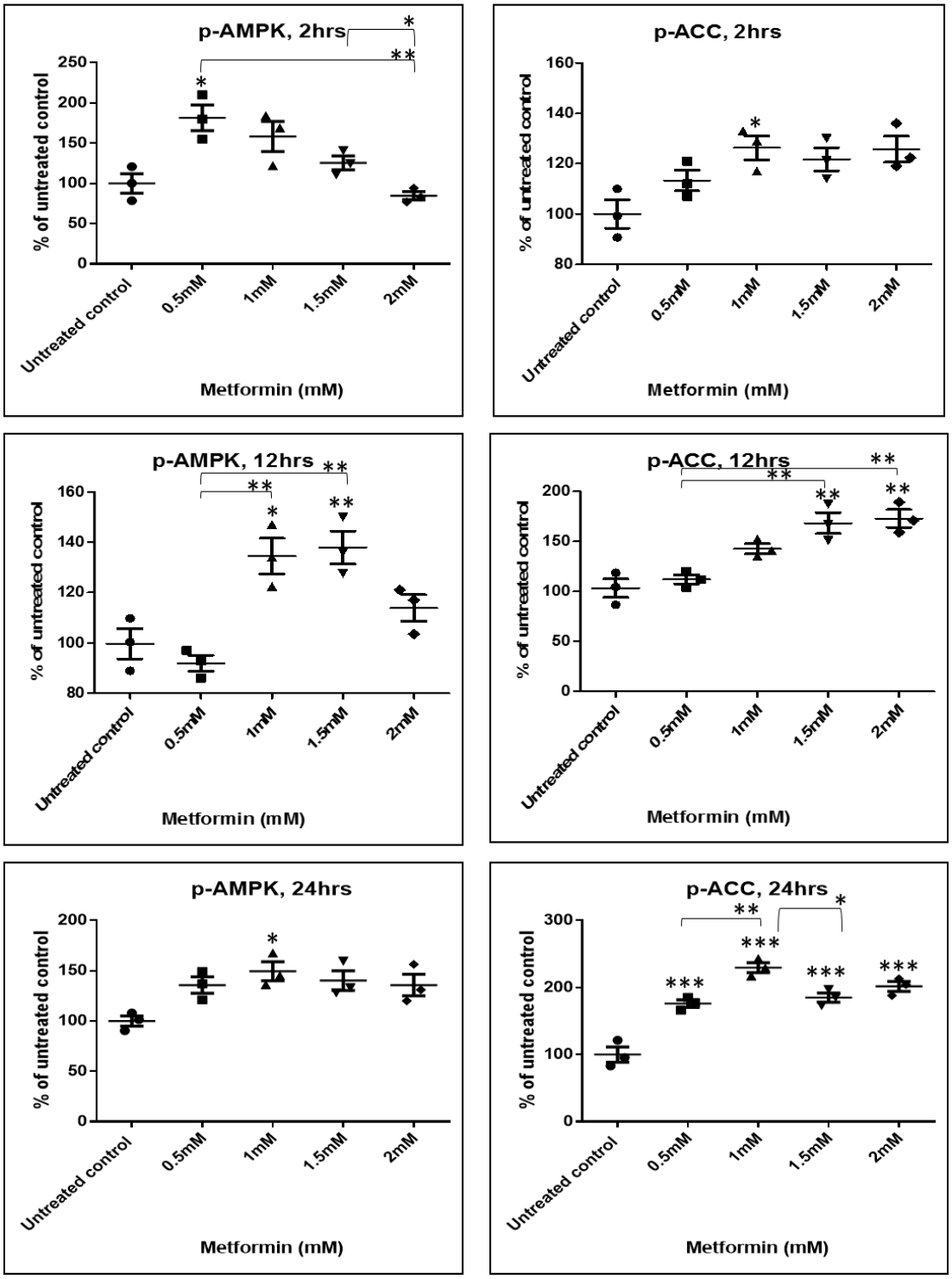

Fig 4.81. Data from scanned blots after actin normalisation showing the effect of 2, 12 & 24hrs metformin treatment (0.5mM-2mM) on p-AMPK & p-ACC phosphorylation by Western blotting in MCF7(X)LT cells. Data are represented as percentage of untreated control, and comprise the mean of three independent experiments (N=3). The error bar indicates SEM. * (P<0.05), ** (P<0.01) & *** (P<0.001) followed by ANOVA with Bonferroni post hoc correction.

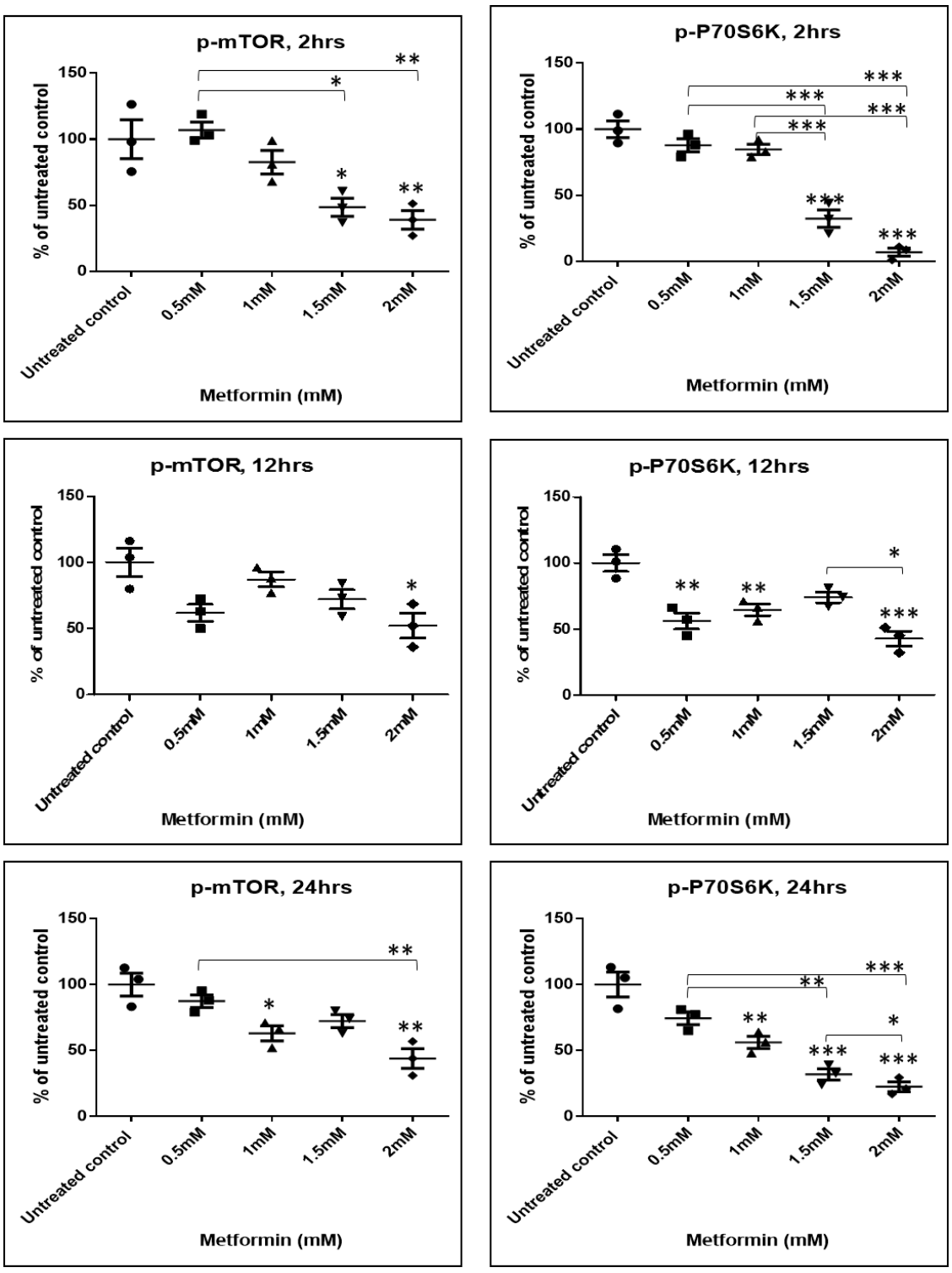

Fig 4.82. Data from scanned blots after actin normalisation showing the effect of 2, 12 & 24hrs metformin treatment (0.5mM-2mM) on p-mTOR & p-P70S6K phosphorylation by Western blotting in MCF7(X)LT cells. Data are represented as percentage of untreated control, and comprise the mean of three independent experiments (N=3). The error bar indicates SEM. * (*P*<0.05), ** (*P*<0.01) & *** (*P*<0.001) followed by ANOVA with Bonferroni post hoc correction.

In overall summary, the effect of metformin treatment (0.5-2mM) on either fatty acid or protein synthesis regulatory elements varied across the resistant panel with regards to dosage and time frame (Table 4.19). Variation between the onset of any fatty acid and protein synthesis reduction might potentially be associated with slower accumulation of metformin in some of the breast cancer cells. Nevertheless, most resistant models showed evidence for some impact of metformin on these pathways at some point during the time course. This contrasts the endocrine responsive MCF7 cells, where impact on mTOR signalling only was noted.

Similarly, all resistant models showed some evidence of induction of p-AMPK by metformin during the time course, contrasting MCF7. There is thus evidence for metformin's direct signalling mechanism on AMPK activation and also on anabolic pathway regulators in the resistant cells, but this mechanism is less convincing in the endocrine responsive MCF7 cells. Furthermore, in some cases it was seen that the profile for the anabolic-related processes could occur independently of changes in AMPK activity, again most notably for MCF7 cells, suggesting further mechanisms also contribute to regulating these downstream events which are additionally targeted by metformin.

Cell model	AMPK induction/time	Early events (2hrs treatment)	Late events (12hrs treatment)	Late events (24hrs treatment)
MCF7	N	P70S6K↓	P70S6K↓	mTOR↓ P70S6K↓
TamR	Y/12hrs	———	ACC↑	P70S6K↓
TamRLT	Y/2hrs	ACC↑ P70S6K↓	ACC↑ P70S6K↓	ACC↑ P70S6K↓
FasR	Y/12hrs	———	ACC↑	ACC↑ P70S6K↓
FasRLT	Y/2-24hrs	P70S6K↓	ACC↑ mTOR↓ P70S6K↓	ACC↑ mTOR↓ P70S6K↓
MCF7(X)	Y/12 & 24hrs	ACC↑	ACC↑	ACC↑ mTOR↓ P70S6K↓
MCF7(X)LT	Y/12 & 24hrs	ACC↑ mTOR↓ P70S6K↓	ACC↑ P70S6K↓	ACC↑ mTOR↓ P70S6K↓

Table 4.19. The effect of metformin treatment (0.5mM-2mM) on induction of p-AMPK and inhibition of fatty acid/protein synthesis after 2, 12 & 24hrs treatment across the panel of resistant models. N: no induction, Y: AMPK induction, ↓reduced phosphorylation & ↑indicates induced phosphorylation.

4.2.5.6 The inhibitory effect of metformin on cell growth of the model panel

To further explore the contribution of OxPhos (in particular complex I activity) to the models, the impact of metformin treatment (0.5mM-2mM) on growth of the endocrine resistant and responsive breast cancer cells was monitored for 7 days. Cells were seeded at 20,000 cells/well for 24hrs prior to metformin administration and growth was then determined by Coulter counting after day 3, 5 and 7. Growth curves were plotted and the mean of half-maximum response (EC_{50}) was calculated based on growth on day 7 for each model in the panel, as summarised in Table 4.20 (Appendix 21).

Cell models	EC50 (mM) metformin
MCF7	0.81±0.17
TamR	0.92±0.11
TamRLT	1.41±0.13
FasR	0.62±0.29
FasRLT	0.73±0.05
MCF7(X)	0.45±0.23
MCF7(X)LT	0.41±0.07

Table 4.20. EC_{50} calculated based on Coulter counter growth data on day 7 for the model panel. EC50 data are represented here as mean of 3 independent experiments (N=3). ± SD.

Growth curves revealed a dose dependent growth inhibitory effect of metformin in MCF7. By day 7 growth was significantly reduced after treating with 1.5mM (P<0.05) and 2mM (P<0.01) metformin compared to untreated control (Fig 4.83A-B). The mean of EC_{50} for metformin treatment in MCF7 was 0.81mM (Table 4.20). TamR cells were also inhibited by metformin in a dose-dependent manner, with growth significantly reduced at day 7 by more than 50% after 1.5mM (P<0.05) and substantially by approximately 75% for 2mM (P<0.01) treatment as compared to untreated control. Indeed, growth was also significantly reduced by 2mM (P<0.05) as compared to 0.5mM treatment (Fig 4.84A-B). The mean of EC_{50} for metformin treatment in TamR cells was 0.92mM (Table 4.20). Growth of the further tamoxifen resistant model TamRLT cells was also significantly reduced by day 7 treatment with metformin, but inhibitory effects were more modest in this tamoxifen resistant model, with 30% inhibition for 1.5mM (P<0.05) and 50% for 2mM (P<0.001) metformin compared to untreated control. Again, growth was significantly reduced versus 0.5mM drug for 2mM treatment (P<0.05) (Fig 4.85 A-B). The mean EC_{50} for metformin treatment in TamRLT was 1.41mM (Table 4.20). Growth of the FasR model was significantly reduced by day 7 treatment with metformin, by 50% after 1.5mM (P<0.05) and 60% for 2mM (P<0.05) treatment compared to untreated control (Fig 4.86 A-B). The mean of EC_{50} for metformin treatment in this model was 0.62mM (Table 20). Metformin impact in the further fulvestrant model FasRLT was comparable to FasR cells, with growth significantly reduced by 50% after 1.5mM (P<0.05) and by 55% for 2mM (P<0.001) treatment as compared to untreated control (Fig 4.87 A-B). The mean of EC_{50} for metformin treatment was also largely comparable, at 0.73mM (Table 4.20). In MCF7(X) cells, growth was significantly reduced by >50% after 1mM (P<0.05) and 1.5mM drug (P<0.05), reaching 70% inhibition for 2mM (P<0.01) metformin treatment compared to untreated control (Fig 4.88A-B). Mean of EC_{50} for metformin treatment in MCF7(X) was 0.45mM (Table 4.20). In MCF7(X)LT, growth was significantly reduced by over 70% after either 1mM (P<0.05), 1.5mM (P<0.05) or 2mM (P<0.05) metformin treatment compared to untreated control (Fig 4.89A-B). The EC_{50} for metformin treatment in MCF7(X)LT was comparable with the MCF7(X) model at 0.41mM (Table 4.20).

In conclusion, metformin growth inhibitory effects were observed in all the models, reflecting the importance of OxPhos in driving breast cancer cell growth. However, based on EC_{50} the oestrogen deprived resistant models (followed by FasR cells) were the most metformin-sensitive models, with lower EC50s when compared with the further resistant models or the endocrine responsive MCF7 cells, suggesting increased importance for Complex I-driven OxPhos in oestrogen deprived resistant cells. Tamoxifen resistant models were the least sensitive models in the panel with metformin treatment (Table 4.20).

[A]

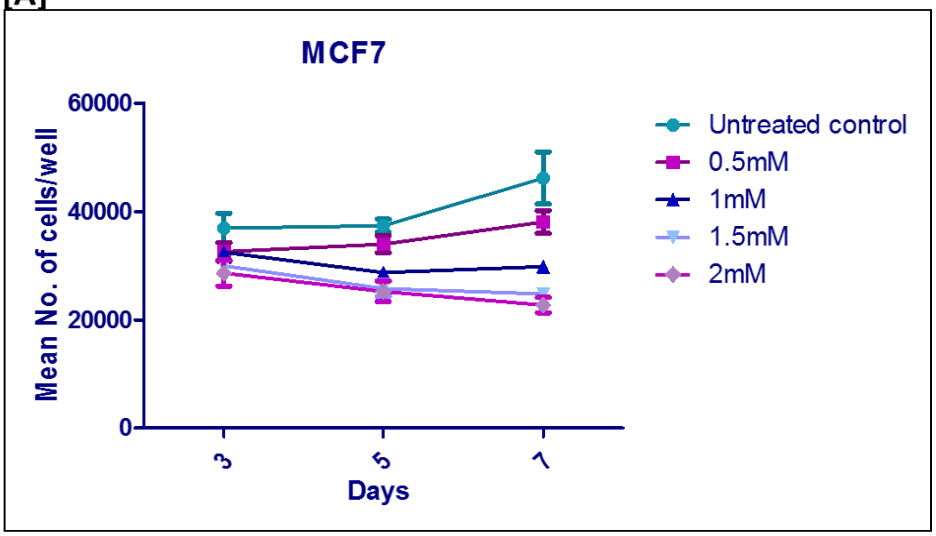

[B]

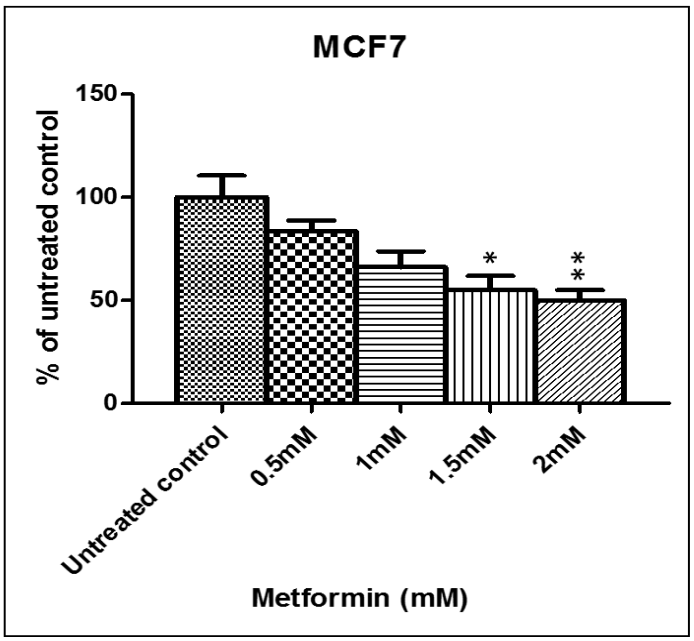

Fig 4.83. MCF7 were seeded at 20,000 cells/well and the growth rate was determined by Coulter counting after 0.5-2mM metformin treatment on day 3, 5 & 7. (A) Shows growth curve profiles and (B) % untreated control growth at day 7. Data are represented as mean of 3 independent experiments (N=3). The error bar indicates SEM. * (P<0.05) & ** (P<0.01) following ANOVA with Bonferroni post hoc correction.

[A]

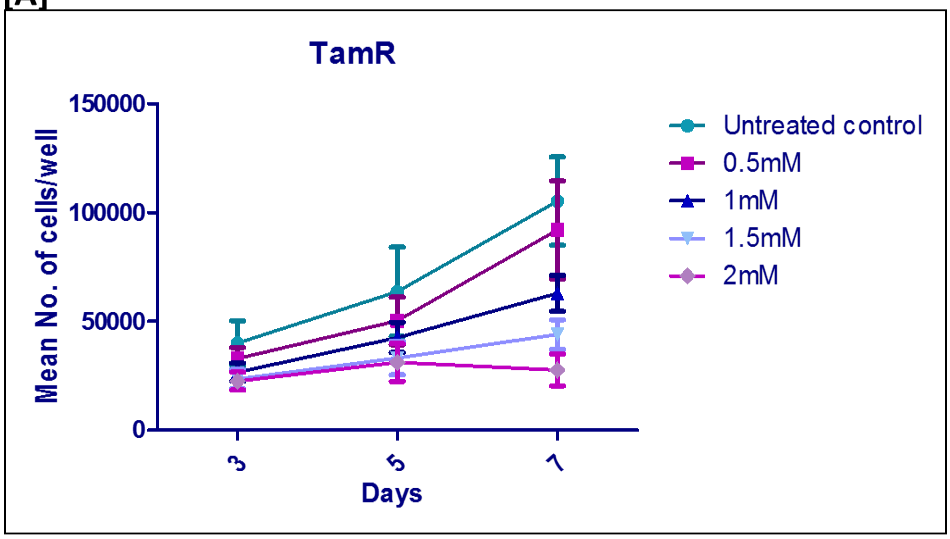

[B]

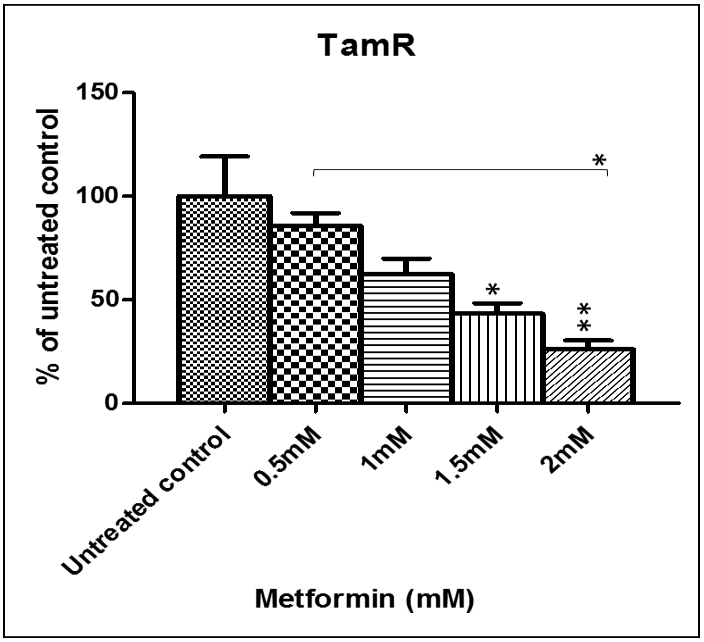

Fig 4.84. TamR were seeded at 20,000 cells/well and the growth rate was determined by Coulter counting after 0.5-2mM metformin treatment on day 3, 5 & 7. (A) Shows growth curve profiles and (B) % untreated control growth at day 7. Data are represented as mean of 3 independent experiments (N=3). The error bar indicates SEM. * (P<0.05) & ** (P<0.01) following ANOVA with Bonferroni post hoc correction.

[A]

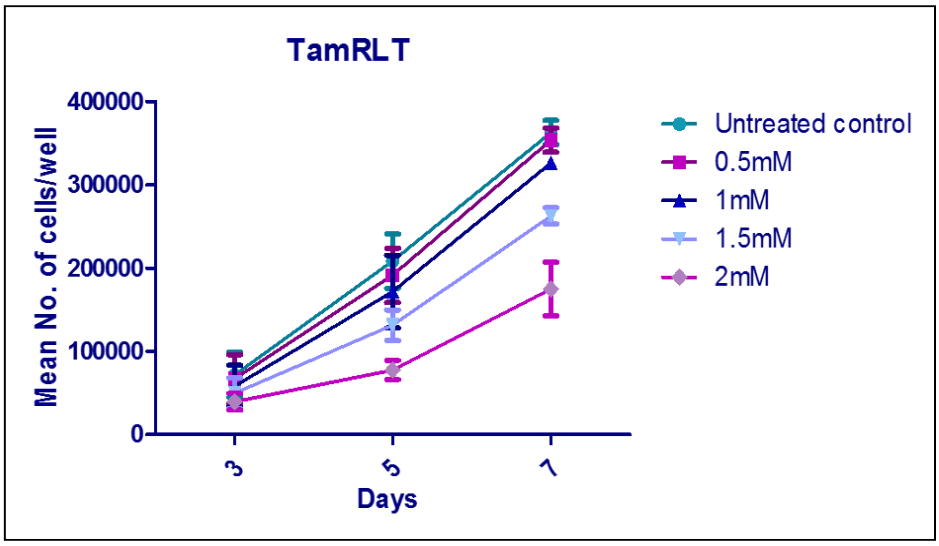

[B]

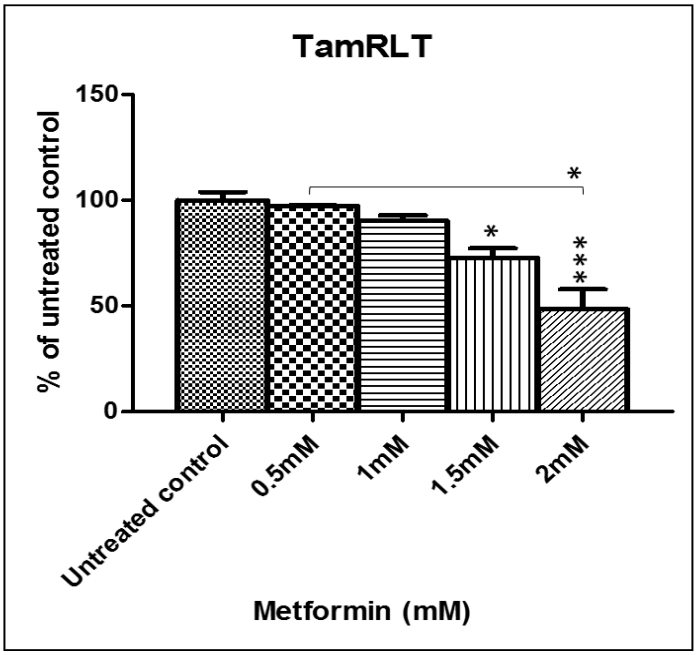

Fig 4.85. TamRLT were seeded at 20,000 cells/well and the growth rate was determined by Coulter counting after 0.5-2mM metformin treatment on day 3, 5 & 7. (A) Shows growth curve profiles and (B) % untreated control growth at day 7. Data are represented as mean of 3 independent experiments (N=3). The error bar indicates SEM. * (P<0.05) & *** (P<0.001) following ANOVA with Bonferroni post hoc correction.

[A]

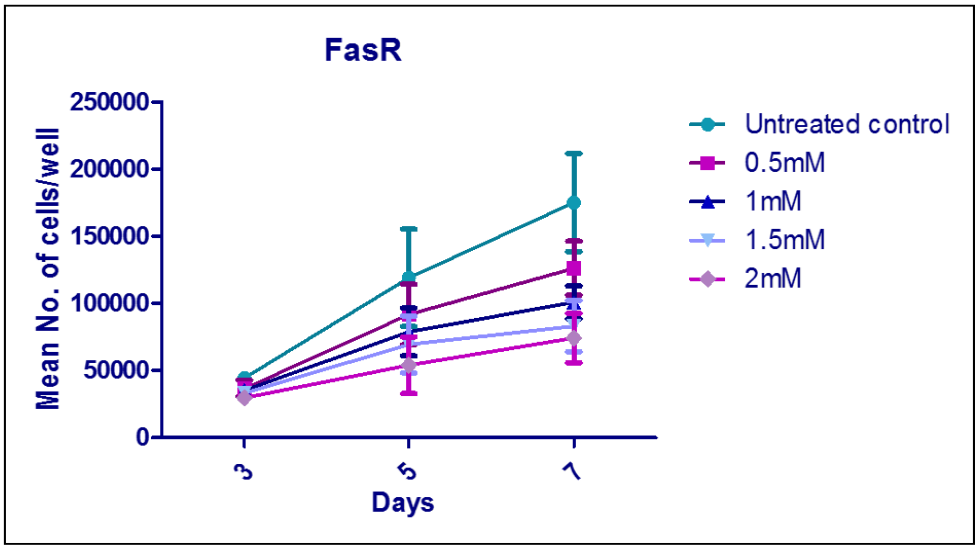

[B]

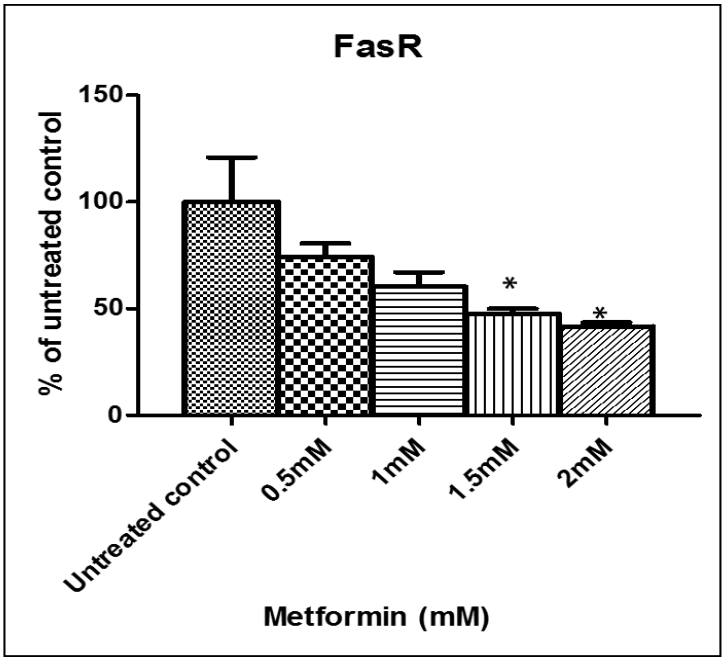

Fig 4.86. FasR were seeded at 20,000 cells/well and the growth rate was determined by Coulter counting after 0.5-2mM metformin treatment on day 3, 5 & 7. (A) Shows growth curve profiles and (B) % untreated control growth at day 7. Data are represented as mean of 3 independent experiments (N=3). The error bar indicates SEM. * (P<0.05) following ANOVA with Bonferroni post hoc correction.

[A]

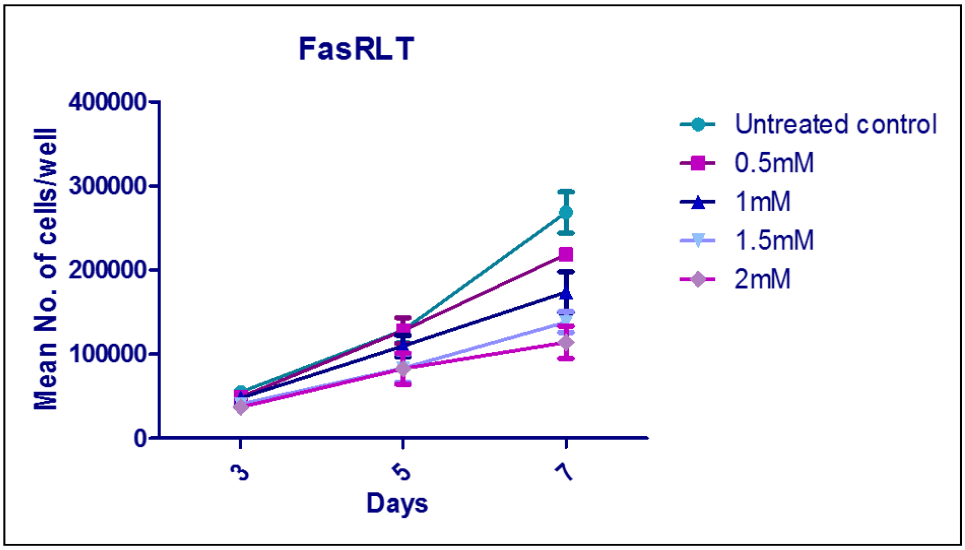

[B]

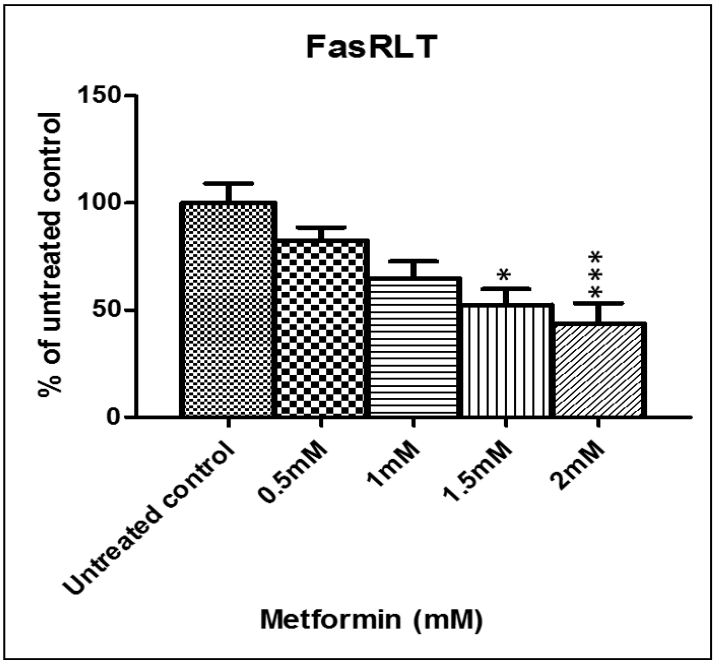

Fig 4.87. FasRLT were seeded at 20,000 cells/well and the growth rate was determined by Coulter counting after 0.5-2mM metformin treatment on day 3, 5 & 7. (A) Shows growth curve profiles and (B) % untreated control growth at day 7. Data are represented as mean of 3 independent experiments (N=3). The error bar indicates SEM. * (P<0.05) & *** (P<0.001) following ANOVA with Bonferroni post hoc correction.

[A]

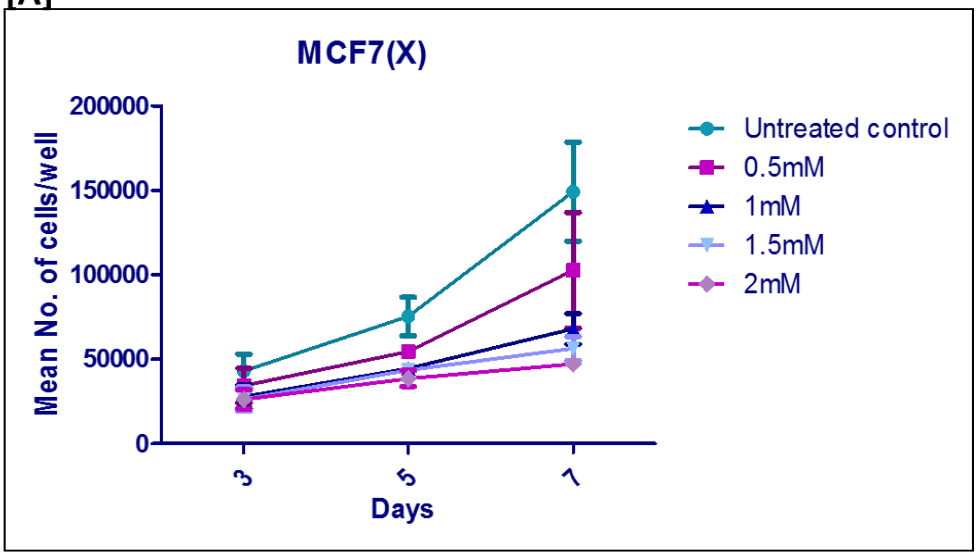

[B]

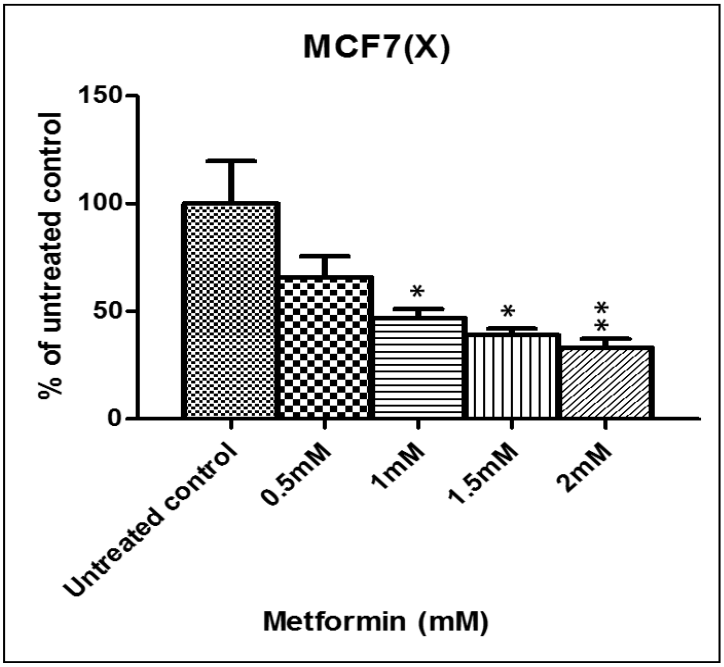

Fig 4.88. MCF7(X) were seeded at 20,000 cells/well and the growth rate was determined by Coulter counting after 0.5-2mM metformin treatment on day 3, 5 & 7. (A) Shows growth curve profiles and (B) % untreated control growth at day 7. Data are represented as mean of 3 independent experiments (N=3). The error bar indicates SEM. * (P<0.05) & ** (P<0.01) following ANOVA with Bonferroni post hoc correction.

[A]

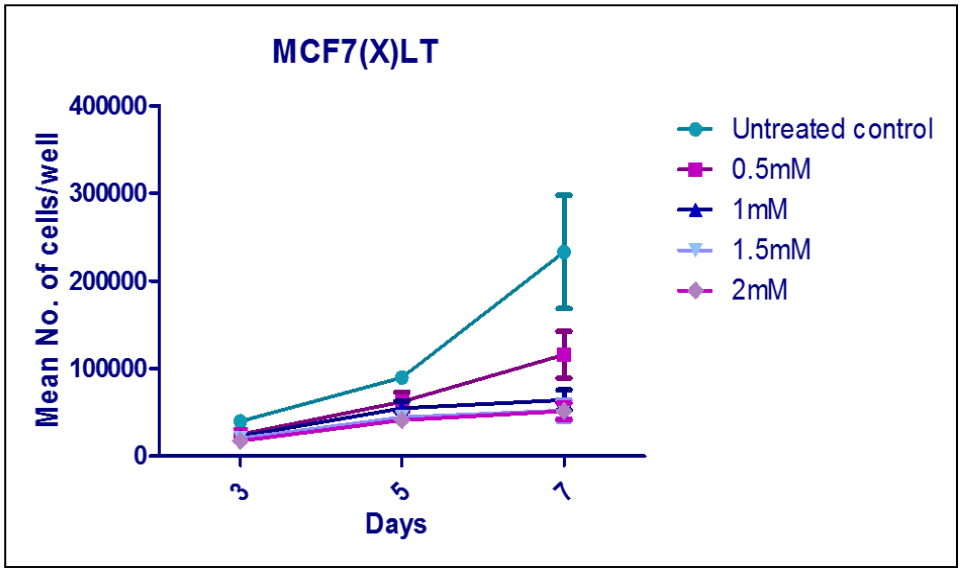

[B]

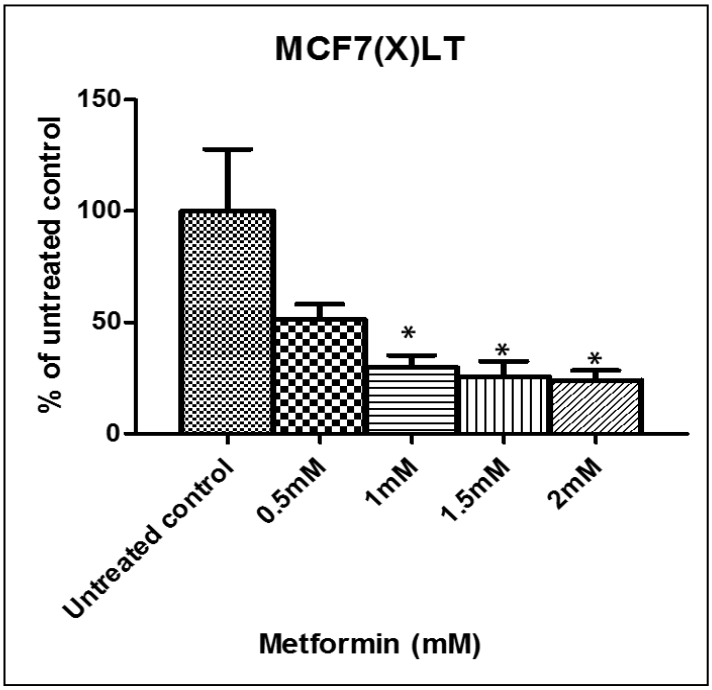

Fig 4.89. MCF7(X)LT were seeded at 20,000 cells/well and the growth rate was determined by Coulter counting after 0.5-2mM metformin treatment on day 3, 5 & 7. (A) Shows growth curve profiles and (B) % untreated control growth at day 7. Data are represented as mean of 3 independent experiments (N=3). The error bar indicates SEM. * (P<0.05) following ANOVA with Bonferroni post hoc correction.

Expression of LKB1-AMPK pathway components in the model panel and sensitivity to metformin treatment:

Induced energy stress (i.e. increased AMP: ATP ratio) by metformin treatment can be compensated by LKB1-AMPK activation in an attempt to minimize the energy consuming process by suppressing anabolic processes in the cell (Hardie et al. 2015). The ultimate impact on tumour growth by metformin would thus be envisaged to depend on the magnitude of this compensatory AMPK activation, and indeed enhanced anti-tumour sensitivity to metformin treatment has been associated with loss of LKB1 expression (Algire et al. 2011). To help interpret metformin growth studies in the model panel, the expression profiles for key LKB1-AMPK components was examined using the 1.0ST gene microarrays to identify significant expression changes (>1.2 fold) in the panel. LKB1 forms a heterotrimeric complex with STE20-related adaptor (STRADA/B) and Calcium binding protein 39 (CAB 39) (Boudeau et al. 2003). CAB39 stabilizes STRAD-LKB1 interaction and thus activates LKB1 when it is localised from the nucleus to the cytoplasm.

STK11 (LKB1) expression was reduced in the FasR and oestrogen deprived resistant models compared to MCF7 on the arrays (Fig.4.90, Table 4.21). While expression of STRADA was induced in FasR, FasRLT and MCF7(X) cells and STRADB expression was increased in all resistant models, CAB39 expression was reduced across most resistant models (Fig.4.90, Table 4.21) where CAB39 decline might serve to reduce stability of STRAD-LKB1 interaction and thus further modify LKB1-AMPK activation. Basal p-AMPK profiling of all the models by Western blotting revealed the reduced STK11 expression in FasR and oestrogen deprived models was associated with reduced basal AMPK activity in these models as compared to MCF7 (Fig.4.91). The reduced STK11 and associated diminished AMPK activity in FasR and oestrogen deprived models might potentially enhance growth sensitivity of these models to metformin treatment. In contrast, induced STK11 expression was seen in TAMRLT cells (Fig. 4.90, Table 4.21). This observation, coupled with unchanged STK11 expression in TamR and FasRLT cells, may account for the higher basal p-AMPK in tamoxifen resistant models and FasRLT cells relative to their oestrogen deprived resistant counterparts (Fig 4.91) and might potentially adversely influence metformin sensitivity profile in tamoxifen resistant and FASRLT cells.

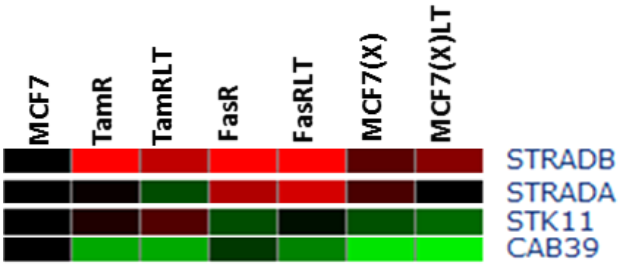

Fig 4.90. Gene expression of LKB1-AMPK pathway components STRADA/B, CAB39 & STK11 across the panel of resistant models. On the heatmap, red, green & black indicate increased, decreased or unchanged in gene expression respectively as compared to the endocrine responsive control line MCF7.

Gene symbols	TamR	TamRLT	FasR	FasRLT	MCF7(X)	MCF7(X)LT
STRADB	1.95	1.63	2.62	3	1.25	1.41
STRADA	1	1.21	1.56	1.71	1.20	1
STK11	1.08	1.22	1.21	1.04	1.22	1.30
CAB39	1.53	1.54	1.15	1.39	1.79	1.85

Table 4.21. Fold changes for STRADA/B, CAB39 & STK11 mRNA expression from gene microarray studies in endocrine resistant models vs. MCF7 cells. Reductions with significant fold changes (≥1.2) are indicated green & induced events (≥1.2) are indicated red.

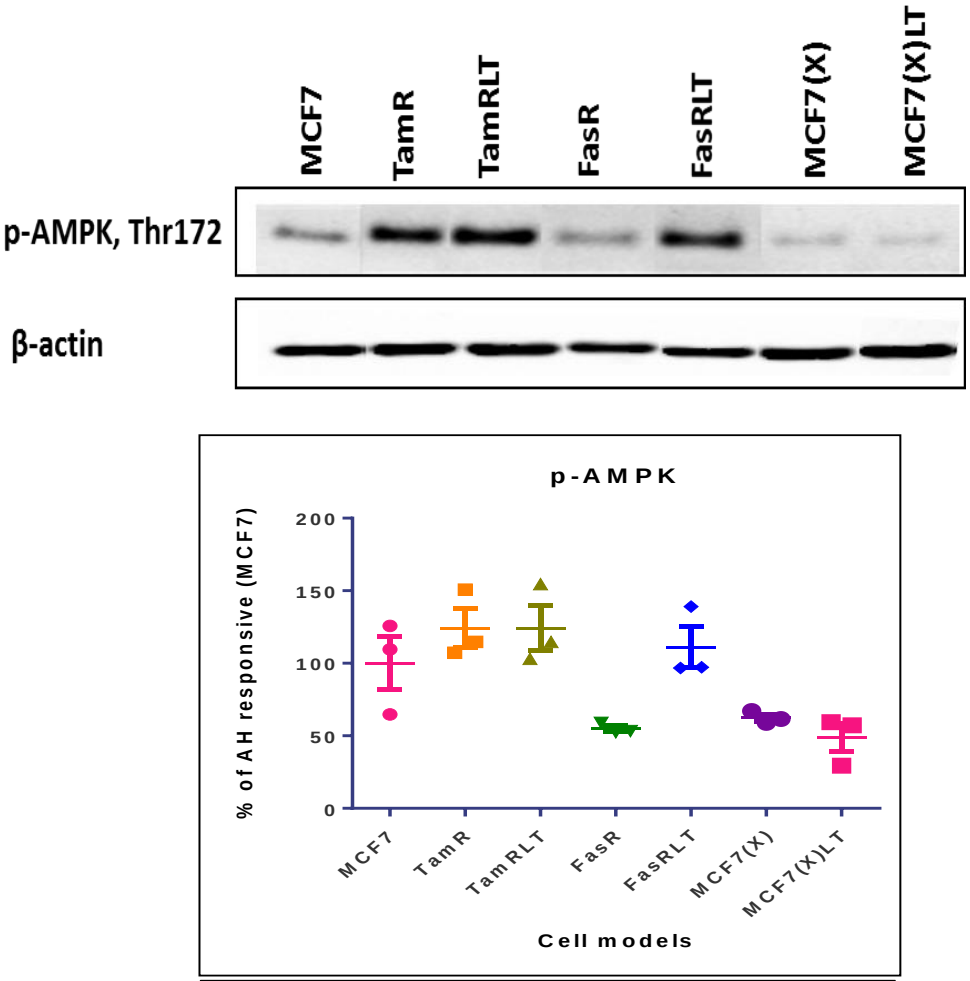

Fig 4.91. Basal AMPK activity in the model panel**.** **R**epresentative blot & graph determined by Western blotting after actin normalisation are presented as percentage of expression in antihormone (AH) responsive parental MCF7 cells. Data are represented as the mean of 3 independent experiments (N=3). The error bar indicates SEM.

4.2.5.7 The effect of metformin treatment on a proliferation marker (Ki-67) in the model panel

Ki-67 (a nuclear protein) is associated with cell proliferation and is expressed during the active phase of the cell cycle including interphase and mitosis, but is absent in quiescent cells in G0 (Gerdes et al. 1984). Moreover, lower Ki-67 expression was detected during the G1 and S phases and higher expression was detected in early mitosis followed by sharp decrease in late mitosis (Lopez et al. 1991). Ki-67 expression is thus commonly used as a marker (by staining using MIB1 antibody) to detect growth fraction, discriminating between proliferative and non-proliferative cells. Ki-67 staining which tend to show proliferative cells may be faint or undetectable at the onset of DNA synthesis but it generally accepted that Ki-67 is expressed during active phase of the cell cycle. However, cells with disrupted growth kinetics (e.g. due to drug administration) may remain Ki-67 positive if a drug acts to arrest in a particular active phase of the cell cycle if they pass G1/S or G2/M phases (Scholzen et al. 2000). Decreases in Ki-67 staining between pre-treatment biopsy and post-treatment surgical specimens are also emerging as a promising predictive marker of clinical response to neoadjuvant treatment in breast cancer patients (Yerushalmi et al. 2010), most recently demonstrated in the IMPACT study for anti-hormones in breast cancer (Dowsett et al. 2005).

In the current study, the effect of metformin treatment (0.5-2mM) on proliferation (Ki67) of the models was determined after 7 days to further gauge importance of Complex I-driven OxPhos to the panel. Cells were seeded at 100,000 cells/coverslip for 24hrs prior to metformin administration (0.5mM-2mM). To determine Ki-67 expression, cells were harvested and fixed at day 7 and immunostained with MIB1 antibody. The percentage of nuclear Ki67 (MIB1) positive cells for each metformin dose was determined by counting over 6 fields at 40X magnification, and data were represented as means of 3 independent experiments.

Under basal growth conditions, MCF7 cells were 81% positive for Ki-67 staining. Ki-67 staining was modestly reduced by 10% and 20% after 0.5mM and 1mM metformin treatment and more significantly by 40% with 1.5mM treatment (P<0.05). The highest dose of metformin treatment (2mM) gave only a 25% Ki-67 reduction (Fig 4.92). TamR was 87% positive for Ki-67 expression under basal conditions. While Ki-67 expression was modestly reduced by 30% after 1mM treatment (P<0.05) compared to untreated control, all other doses had little impact on Ki67 staining (10%-15% reduction) in TamR cells (Fig 4.93). TamRLT cells were 93% Ki-67 posiitive under basal conditions. Reduction of Ki-67 with metformin was statistically significant but modest in this model, 17% at 1mM (P<0.01), 15% at 1.5mM (P<0.05) and at the highest dose

(12%) versus untreated control (Fig 4.94). FasR cells was 89% positive for Ki-67 under basal conditions, with a modest 30% reduction in staining after 2mM treatment (P<0.01) versus untreated control (Fig 4.95). FasRLT were 91% positive and the marker was again only modestly reduced by 15-20% after either 1mM or 1.5mM (P<0.05 for both) or 2mM metformin treatment (Fig 4.96). MCF7(X) cells were 76% Ki67 positive under basal conditions, with a modest 35% reduction in Ki-67 staining after 2mM metformin treatment compared to untreated control and versus the 0.5mM dose (P<0.01) (Fig 4.97). MCF7(X)LT had comparable Ki67 positivity (78%) and there was a modest but significant reduction by 22%, 24% and 35% after 1mM (P<0.05), 1.5mM (P<0.05) and 2mM (P<0.001) metformin treatment respectively (Fig 4.98).

In summary, metformin inhibitory impact on Ki67 proliferation staining was relatively modest in MCF7 and all the resistant models, with many cells remaining Ki67 positive despite treatment. By 2mM metformin the least impact on Ki67 proliferation staining was noted in MCF7, the tamoxifen resistant and FASRLT cell lines.

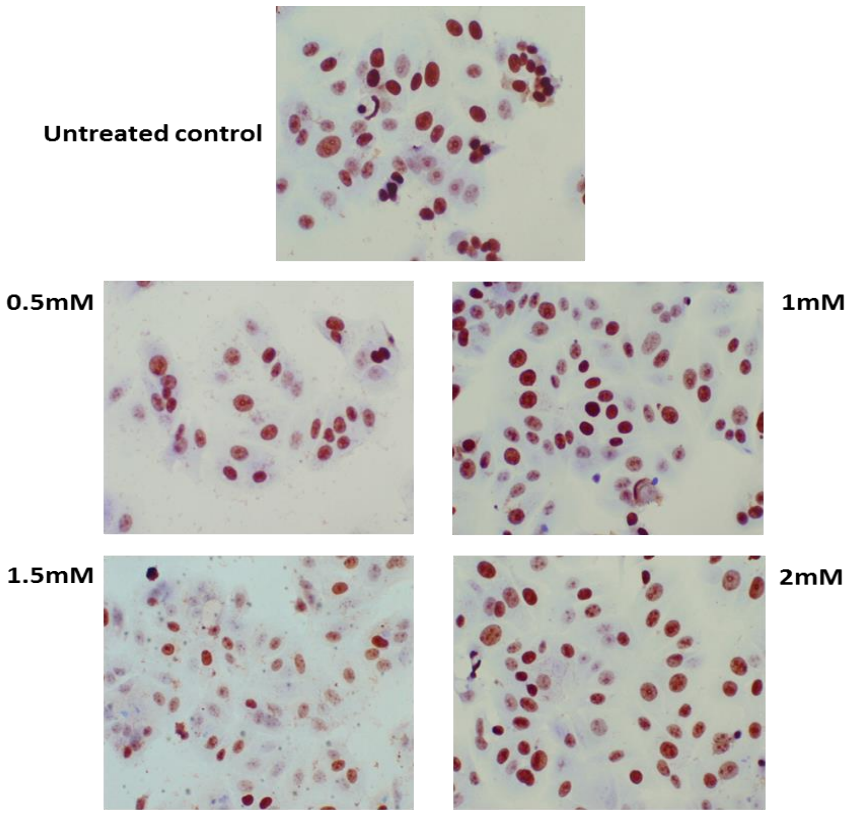

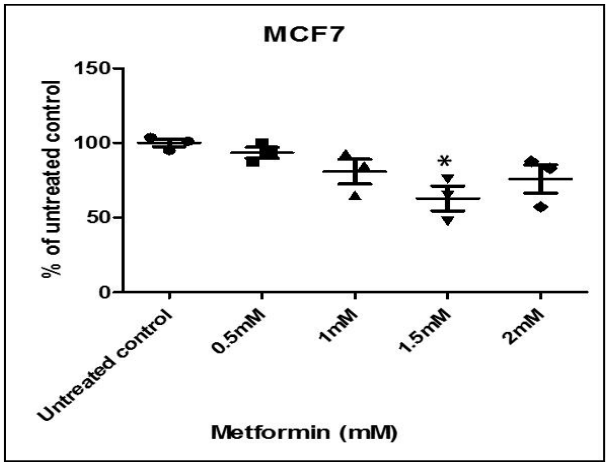

Fig 4.92. MCF7 cells were seeded at 100,000 cells/coverslip and Ki-67 staining was performed after fixation, staining assessment determined percentage Ki67 positivity after metformin treatment for 7d. Ki67 positivity data are presented here as % of untreated control, and represent the mean of 3 independent experiments (N=3). The error bar indicates SEM. * (P<0.05) following ANOVA with Bonferroni post hoc correction. Original magnification was 40X.

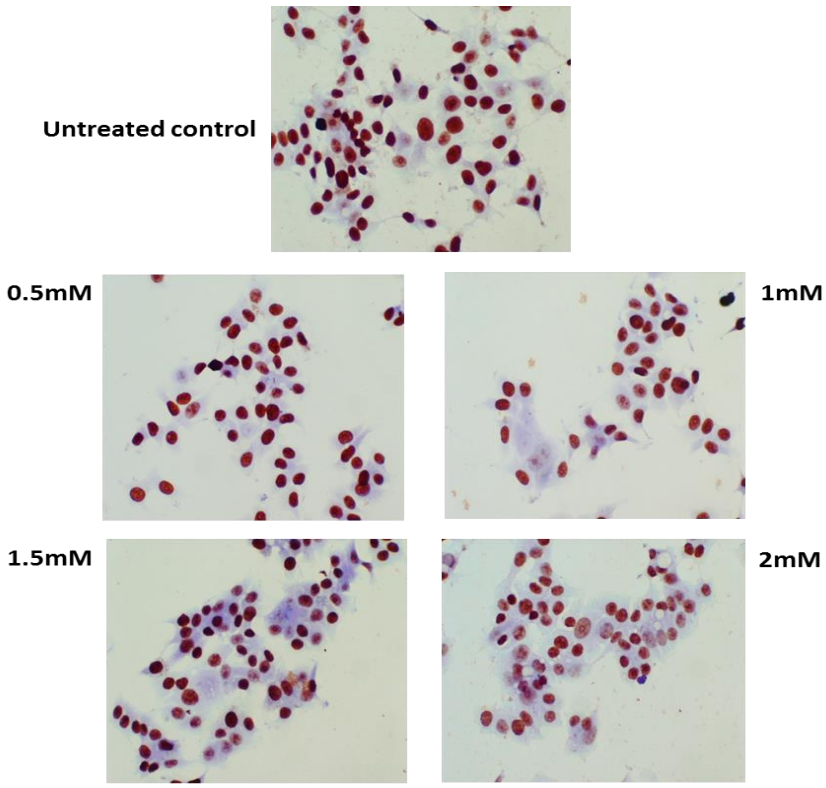

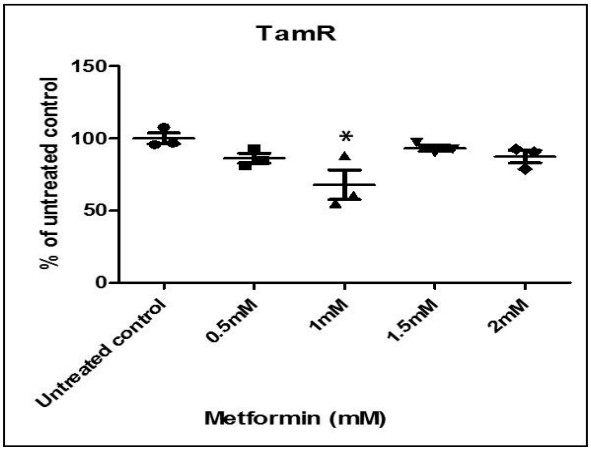

Fig 4.93. TamR cells were seeded at 100,000 cells/coverslip and Ki-67 staining was performed after fixation, staining assessment determined percentage Ki67 positivity after metformin treatment for 7d. Ki67 positivity data are presented here as % of untreated control, and represent the mean of 3 independent experiments (N=3). The error bar indicates SEM. * (P<0.05) following ANOVA with Bonferroni post hoc correction. Original magnification was 40X.

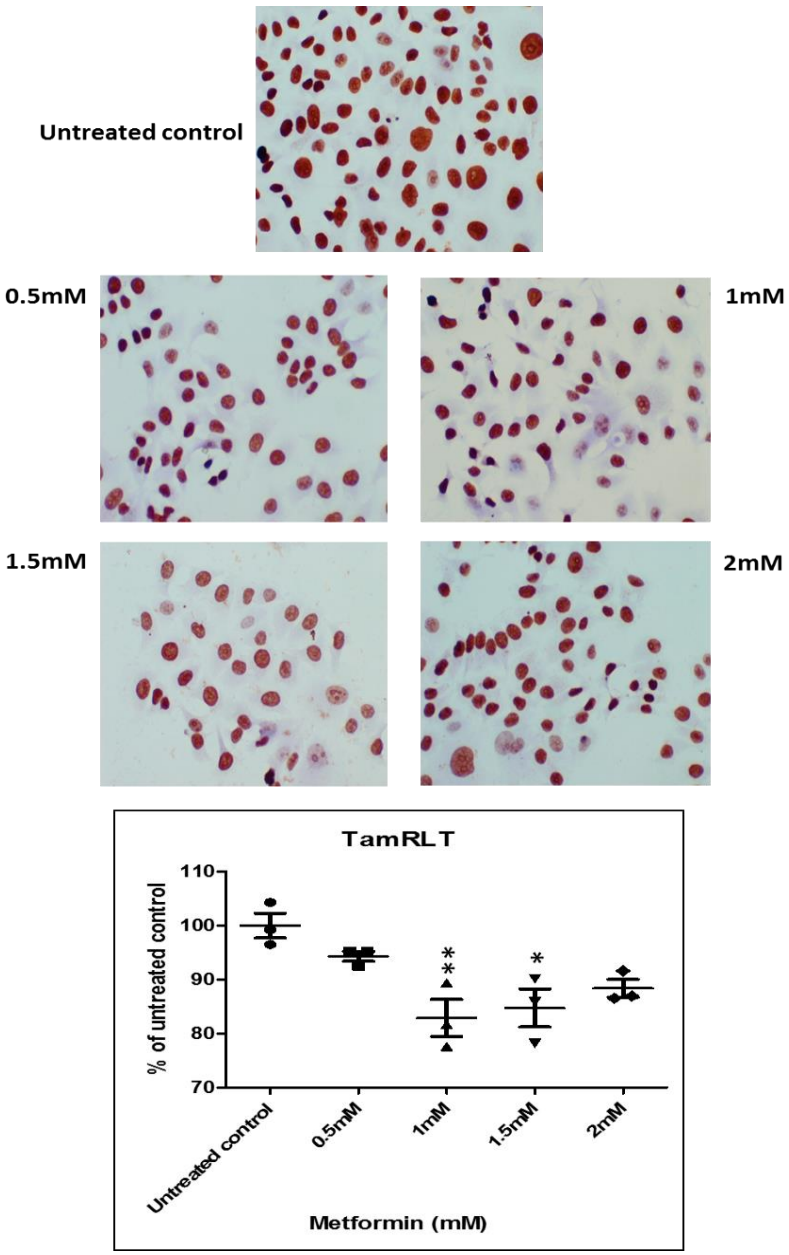

Fig 4.94. TamRLT cells were seeded at 100,000 cells/coverslip and Ki-67 staining was performed after fixation, staining assessment determined percentage Ki67 positivity after metformin treatment for 7d. Ki67 positivity data are presented here as % of untreated control, and represent the mean of 3 independent experiments (N=3). The error bar indicates SEM. * (P<0.05) & ** (P<0.01) following ANOVA with Bonferroni post hoc correction. Original magnification was 40X.

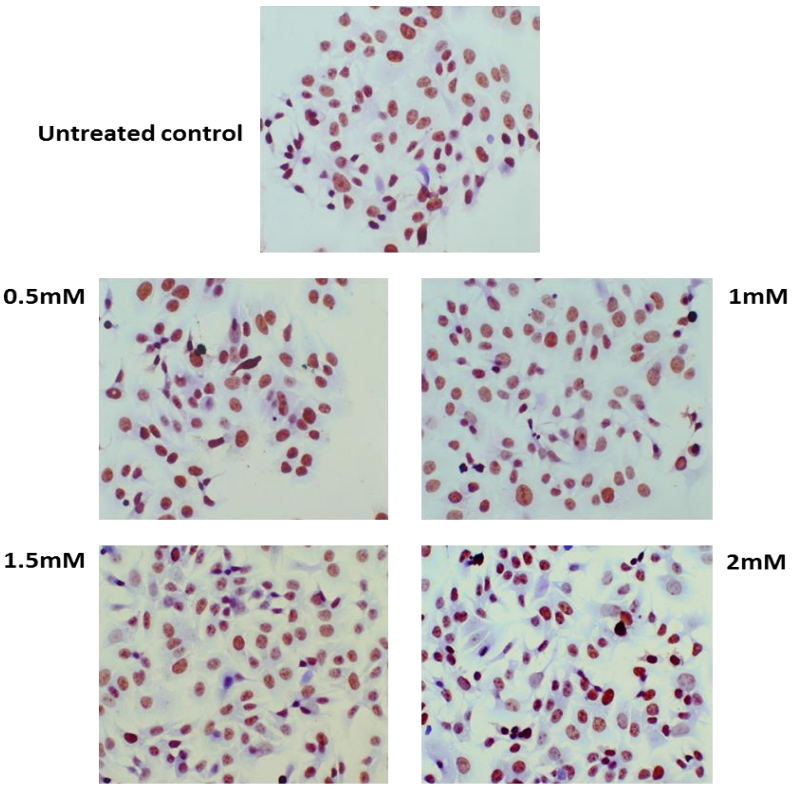

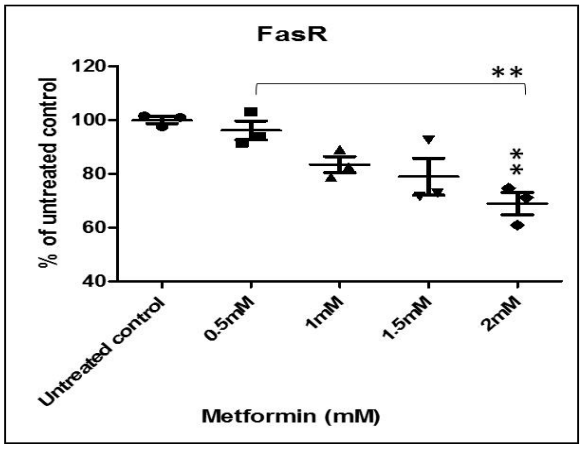

Fig 4.95. FasR cells were seeded at 100,000 cells/coverslip and Ki-67 staining was performed after fixation, staining assessment determined percentage Ki67 positivity after metformin treatment for 7d. Ki67 positivity data are presented here as % of untreated control, and represent the mean of 3 independent experiments (N=3). The error bar indicates SEM. * (P<0.05) & ** (P<0.01) following ANOVA with Bonferroni post hoc correction. Original magnification was 40X.

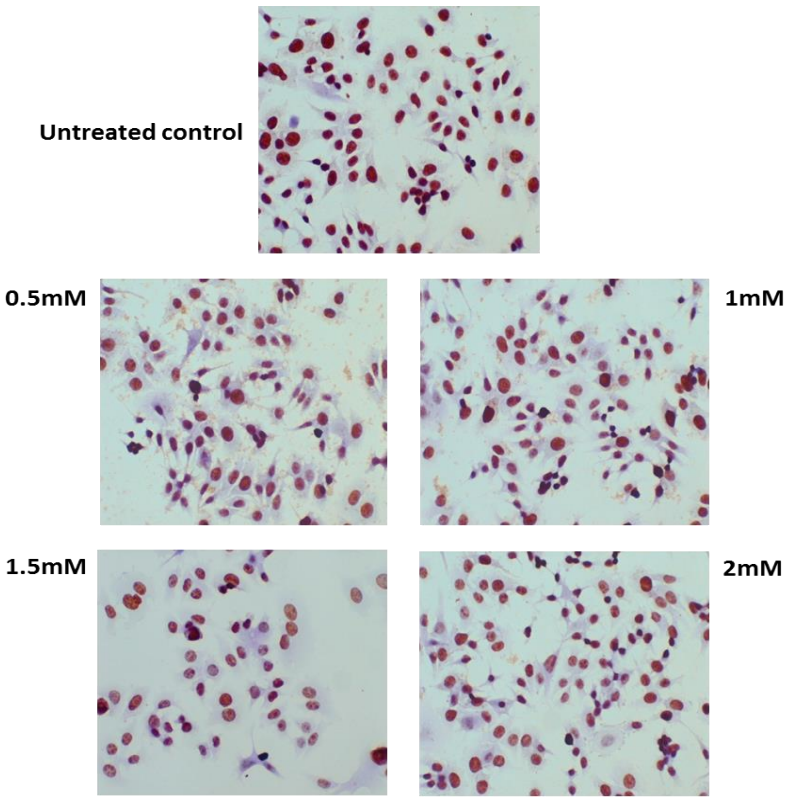

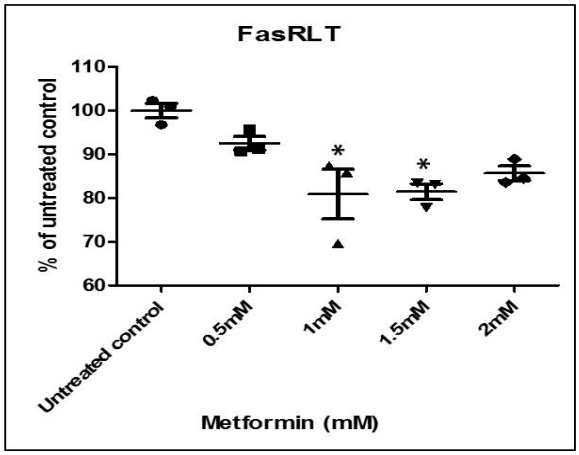

Fig 4.96. FasRLT cells were seeded at 100,000 cells/coverslip and Ki-67 staining was performed after fixation, staining assessment determined percentage Ki67 positivity after metformin treatment for 7d. Ki67 positivity data are presented here as % of untreated control, and represent the mean of 3 independent experiments (N=3). The error bar indicates SEM. * (P<0.05) following ANOVA with Bonferroni post hoc correction. Original magnification was 40X.

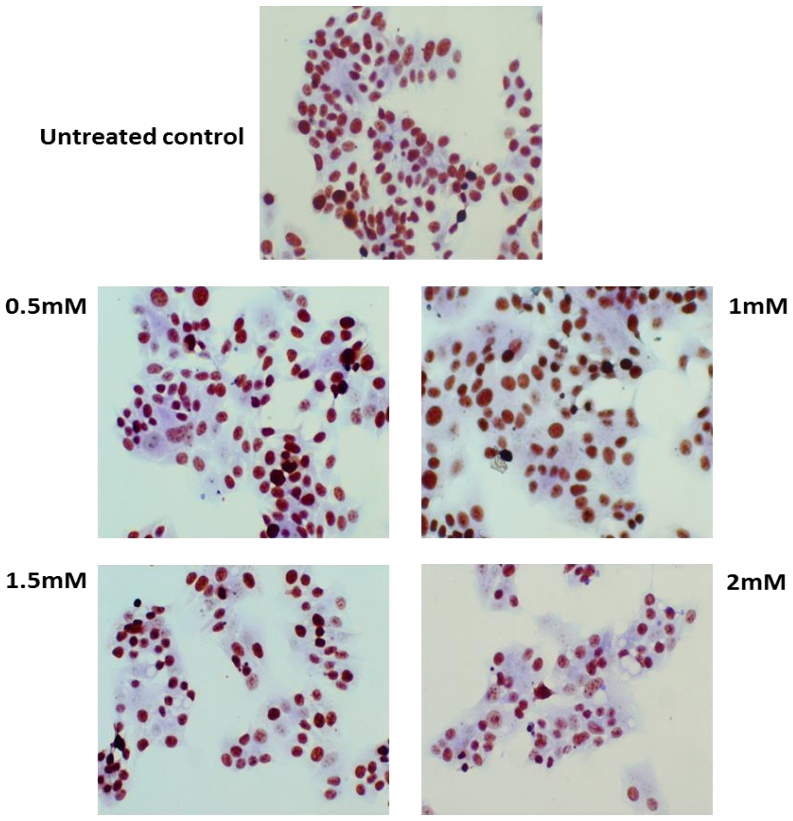

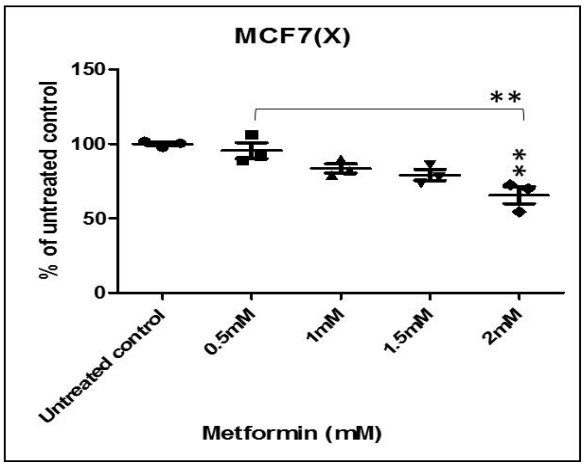

Fig 4.97. MCF7(X) cells were seeded at 100,000 cells/coverslip and Ki-67 staining was performed after fixation, staining assessment determined percentage Ki67 positivity after metformin treatment for 7d. Ki67 positivity data are presented here as % of untreated control, and represent the mean of 3 independent experiments (N=3). The error bar indicates SEM. ** (P<0.01) following ANOVA with Bonferroni post hoc correction. Original magnification was 40X.

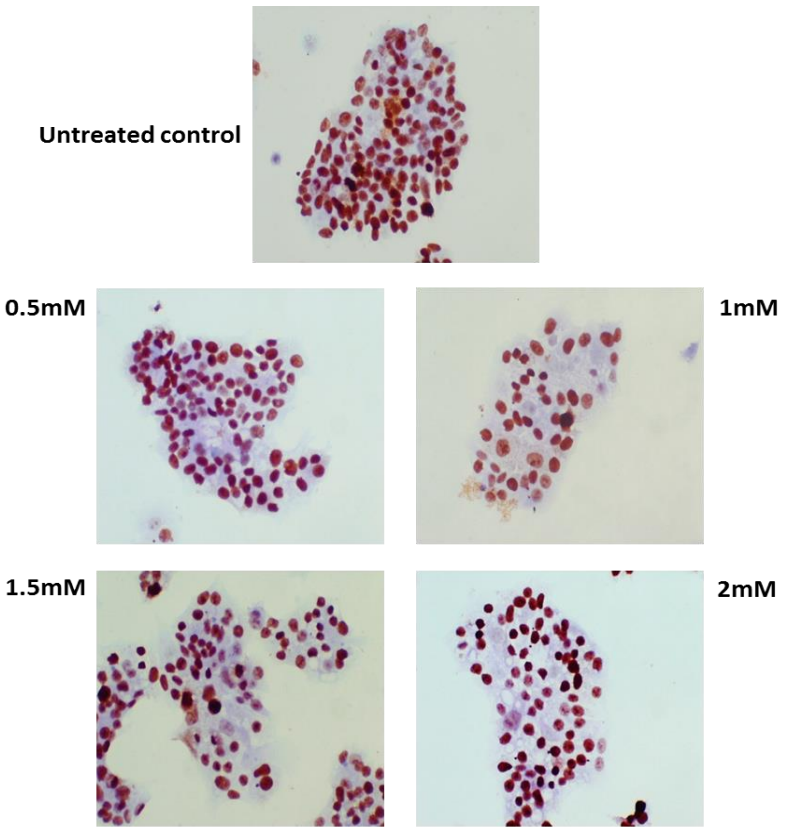

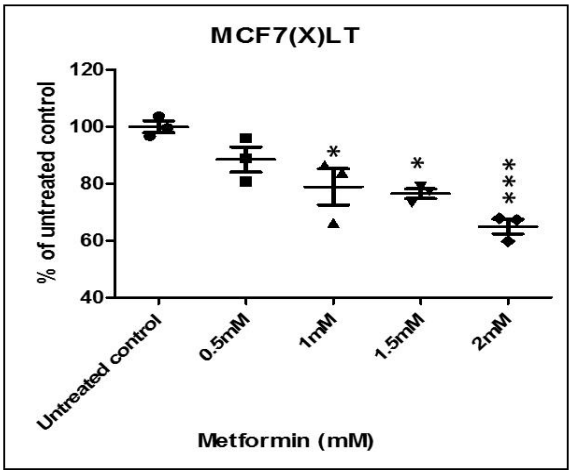

Fig 4.98. MCF7(X)LT cells were seeded at 100,000 cells/coverslip and Ki-67 staining was performed after fixation, staining assessment determined percentage Ki67 positivity after metformin treatment for 7d. Ki67 positivity data are presented here as % of untreated control, and represent the mean of 3 independent experiments (N=3). The error bar indicates SEM. * (P<0.05) & *** (P<0.001) following ANOVA with Bonferroni post hoc correction. Original magnification was 40X.

4.2.5.6 Expression evidence for hyperactive mitochondria that may impact on OxPhos or sensitivity to metformin in the model panel

Expression of Plasma membrane metformin transporters in endocrine resistant breast cancer cells using 1.0ST gene microarrays:

The NADH substrate derived from glycolysis (via Malate-Aspartate shuttle), β-oxidation of fatty acids and from the TCA cycle is oxidized by NADH dehydrogenase of complex I during OxPhos. Two electrons from this NADH oxidation reduce ubiquinone to ubiquinol, and so complex I supplies electrons through to complex III and IV to reduce O_2 to H_2O. The released energy from the reaction at complex I drives ATP synthesis by ATP synthase. The primary effect of metformin treatment in its direct mechanism is inhibition of complex I, which induces energy stress by reducing ATP synthesis. Metformin influx into the cell is facilitated by several organic cation transporters (OCTs: OCT1-3) (Pernikova et al. 2014) and also by plasma membrane monoamine transporters (PMAT) (Zhou et al. 2007). The positive charge on metformin then assists its reversible accumulation into the mitochondrial matrix in response to mitochondrial membrane potential (Bridges et al. 2014), while the hydrocarbon side chain of the drug aids binding into the complexes within the mitochondrial membranes. Metformin requires several hours to accumulate in the mitochondria (Bridges et al. 2014) and bind to the core subunits of complex I where it exerts its inhibitory effect (Hirst et al. 2013). Indeed, Bridges et al. (2014) reported reversibility of metformin accumulation after 6hrs in hepatocellular carcinoma.

To further evaluate whether such metformin delivery may impact on the growth sensitivity profile in the model panel, expression of metformin influx transporters (e.g. OCTs, PMAT) and also relevant drug efflux transporters (multidrug and toxin extrusion proteins, MATEs) were studied using 1.0ST gene microarray (Fig 4.99). While some of the metformin transporters across the plasma membrane OCT1-3 (SLC22A1-3) were not expressed in the model panel (log_2<7) (Fig 4.99, Table 4.22), PMAT (SLC29A4) was detected on the arrays. Its expression was reduced (>1.5 fold changes) in FasR, FasRLT, MCF7(X) and MCF7(X)LT cells as compared to MCF7 (Fig 4.99, Table 4.22), suggesting capacity for metformin influx may be reduced in fulvestrant resistant and oestrogen deprivation resistant models. However, the potential metformin efflux transporters MATE1 and MATE 2 (encoded by SLC47A1 and SLC47A2 genes respectively; Emami Riedmaier et al., 2013) were also determined across the model panel and while SLC47A2 were in general not expressed across the panel (favouring metformin accumulation in most models), SLC47A1 was expressed and increased in tamoxifen resistant models as compared to MCF7 but not expressed

in the rest of models (Fig 4.99, Table 4.22). Therefore, the reduced metformin growth sensitivity observed in tamoxifen resistant models might be associated with increased drug efflux.

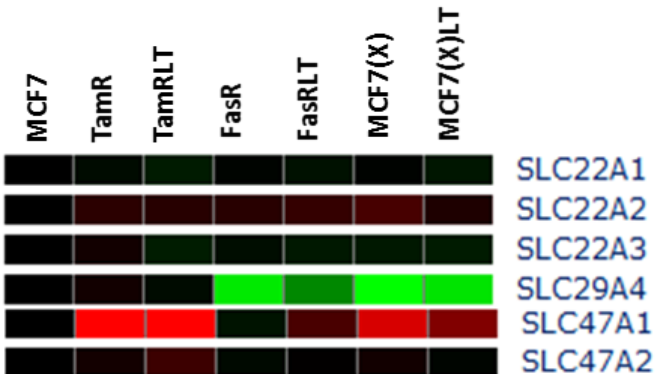

Fig 4.99. Microarray expression of metformin influx and efflux transporters across the panel of resistant models. On the heatmap, green, black & red indicate decreased, no change & increase in gene expression respectively as compared to MCF7 control.

Gene symbols	TamR	TamRLT	FasR	FasRLT	MCF7(X)	MCF7(X)LT
SLC29A4	1.05	1.03	1.89	1.45	2.04	1.86
SLC47A1	3.96	2.49	———	———	———	———

Table 4.22. Fold changes for microarray expression of metformin transporters in endocrine resistant models vs. MCF7. Fold decreases (≥1.2) are indicated in green and fold increases (≥1.2) indicated in red.

Mitochondrial Shuttles:

Efficiency of substrate transport across the mitochondrial membrane may also potentially influence metformin sensitivity, and so mitochondrial shuttle expression was also monitored on the arrays. Mitochondrial shuttles consist of enzymes and transporters to convert metabolites and deliver them from the cytoplasm into the mitochondrial matrix or vice versa. NADH which is synthesized in the cytoplasm cannot cross the mitochondrial membrane and thus the Glycerophosphate shuttle, Malate-Aspartate shuttle and Citrate-Pyruvate shuttle all aid the process.

For the glycerophosphate shuttle, glycerol-3- phosphate dehydrogenase 1 (GPD1, cytosolic) converts a glycolytic intermediate (dihydroxyacetone phosphate) into glycerol-3-phosphate by converting NADH to NAD^+. In the mitochondria, the enzyme flavoprotein dehydrogenase (which converts FADH2 to FAD) then assists conversion of this glycerol-3-phosphate to dihydroxyacetone phosphate via GPD2 (mitochondrial). The flavoprotein dehydrogenase thus can transfer electrons to reduce ubiquinone to ubiquinol (similar to the complex II activity, without pumping protons to mitochondrial inner membrane space (Fig 4.101). As the Glycerophosphate shuttle is an irreversible reaction, it is used only under essential conditions and the electron transport from this shuttle generates 2ATP molecules as compared to 3ATP molecules derived from NADH. Array profiling revealed that while the mitochondrial shuttle GPD1 was only expressed in fulvestrant resistant models (Fig 4.100, Table 4.23), GPD2 expression was induced in TamR, TamRLT and FasR while it reduced in MCF7(X) as compared to MCF7 cells (Fig 4.100, Table 4.23). Since high basal GPD2 expression may feasibly assist bypass mechanism of electron transport through to ubiquinone, this may contribute to the reduced growth-sensitivity of the fulvestrant resistant models to the complex I inhibitor metformin (Table 4.23). The induced GPD expression and thus increased electron transfer to the OxPhos complexes may also account for the modest reduced COX activity after metformin treatment (0.5mM-2mM) observed in fulvestrant resistant models (Fig 56-57).

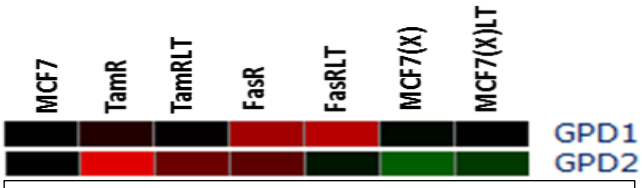

Fig 4.100. Microarray expression of glycerol-3-phosphate dehydrogenase (GPD1 & GPD2) for the panel of resistant models. On the heatmap, red, green & black indicate increased, decreased and no change in gene expression respectively as compared to MCF7 cells.

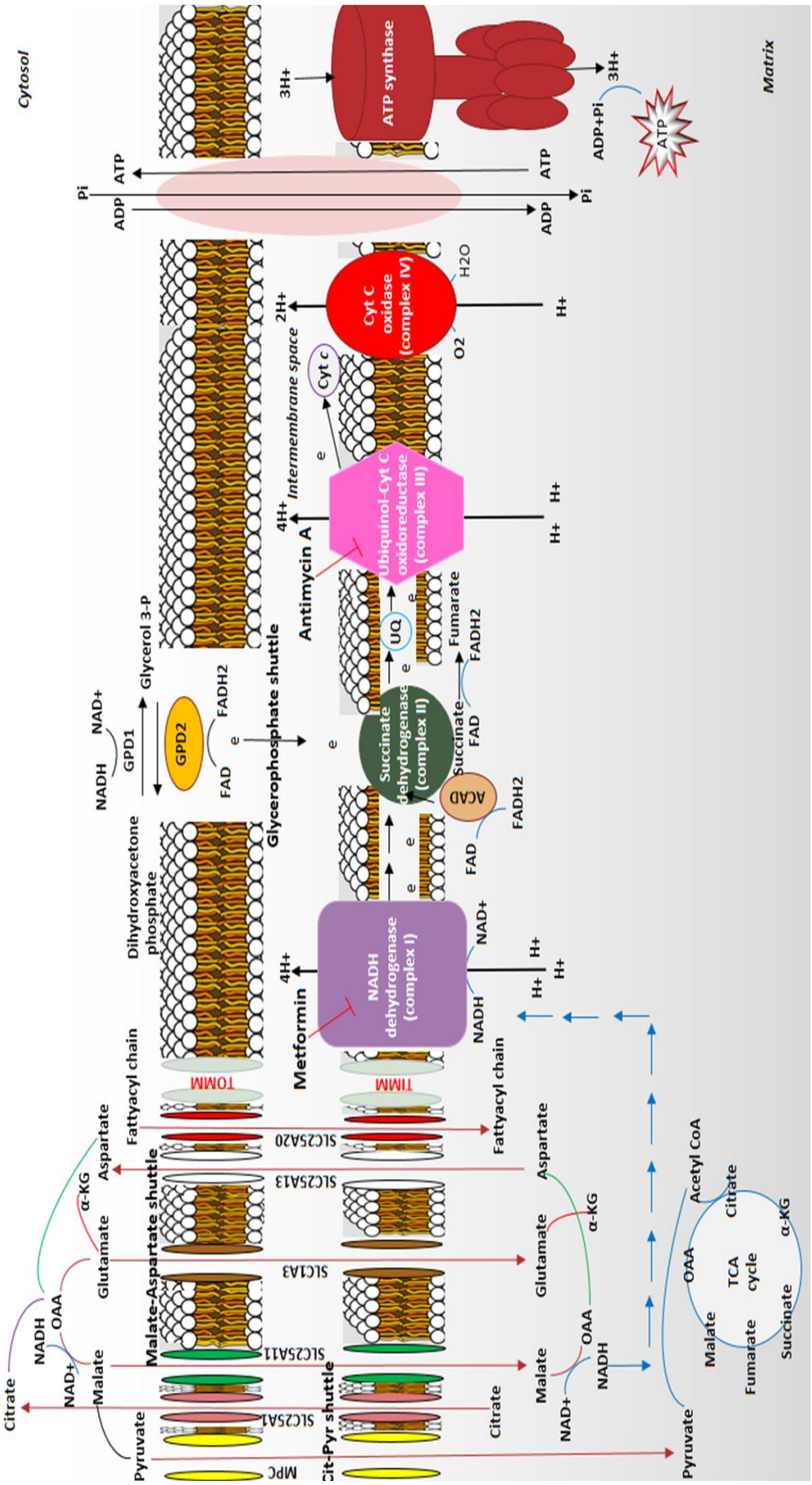

Fig 101. Schematic representation of mitochondrial shuttles and transporters.

Gene symbols	TamR	TamRLT	FasR	FasRLT	MCF7(X)	MCF7(X)LT
GPD1	———	———	1.56	1.65	———	———
GPD2	1.84	1.34	1.29	1.06	1.29	1.17

Table 4.23. Fold changes for microarray expression GPD1 & GPD2 in endocrine resistant models vs. MCF7. Fold decreases (≥1.2) are indicated in green and fold increases (≥1.2) indicated in red.

The malate-aspartate shuttle may also be of relevance. Oxaloactate (OAA) cannot pass through the mitochondrial membrane and thus cytoplasmic malate dehydrogenase converts OAA into malate by oxidizing NADH to NAD^+. Transfer of malate to the mitochondrial matrix is then facilitated via the malate/α-KG anti-porter (SLC25A11). For this, the mitochondrial malate dehydrogenase oxidizes malate to OAA via converting NAD^+ to NADH in the mitochondrial matrix. The NADH can then enter the OxPhos pathway to generate 3ATP molecules, while the OAA recycles to the cytoplasm via a mechanism which involves an aspartate/glutamate anti-porter (SLC25A13). In this process nitrogen in OAA and α-KG is a keto acid counterpart of aspartate and glutamate, respectively (Fig 4.101). Thus, metabolite exchange between cytoplasm and mitochondrial matrix via the Malate-Aspartate shuttle can supply electrons in the form of the substrate NADH to the OXPhos pathway. On the arrays, expression of the malate/α-KG transporter SLC25A11 was induced in FasRLT as compared to MCF7 (Fig 4.102, Table 4.24) and the anti-porter aspartate/glutamate transporter SLC25A13 was induced by >3 fold in FasR and FasRLT (and by >1.2 fold in TamR and MCF7(X) cells) as compared to MCF7 (Fig 4.102, Table 4.24). Therefore, an apparently efficient Malate-Aspartate shuttle may provide fulvestrant resistant models with high NADH substrate. High NADH supply may perhaps in turn contribute towards the higher basal NADH dehydrogenase activity detected in these models (Fig 4.44), the diminished effect of the lowest dose (0.5mM) of metformin on NADH dehydrogenase activity (Fig 4.48-4.49, Table 4.17) and the lack of impact of metformin treatment (up to 1mM) on COX activity in these cells (Fig 4.56-4.57, Table. 4.18).

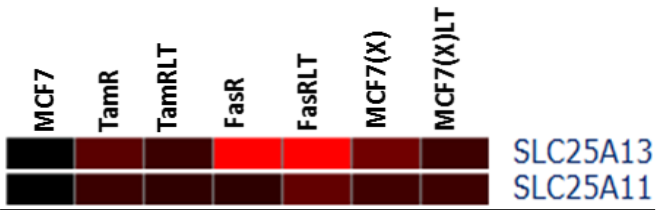

Fig 4.102. Microarray expression of malate-aspartate shuttle components SLC25A11 and SLC25A13 for the panel of resistant models. On the heatmap, red & black indicate increased and no change in gene expression respectively as compared to MCF7 cells.

Gene symbols	TamR	TamRLT	FasR	FasRLT	MCF7(X)	MCF7(X)LT
SLC25A11	1.17	1.14	1.13	1.31	1.19	1.18
SLC25A13	1.28	1.17	3.67	3.69	1.36	1.18

Table 4.24. Fold changes for microarray expression of SLC25A11 & SLC25A13 in endocrine resistant models vs. MCF7. Fold increases (≥1.2) indicated are red.

The Citrate-Pyruvate shuttle transfers pyruvate (a substrate for TCA and thereby driver of OxPhos) to the mitochondrial matrix. In this, ATP-citrate lyase (ACLY) uses ATP to convert citrate to OAA. Malate dehydrogenase (MDH1) then oxidizes NADH to convert OAA to malate, and the malic enzyme (ME1) reduces NADP to generate pyruvate which returns via a mitochondrial pyruvate carrier (BRP44L or MPC) to the mitochondrial matrix to complete the TCA cycle (Fig 4.101). On the microarrays, ACLY expression was induced in tamoxifen resistant models, oestrogen deprived models and FasRLT, while MDH1 expression was only induced in TamR as compared to MCF7 (Fig 4.103, Table 4.25). ME1 expression was also induced in tamoxifen resistant and oestrogen deprived models (Fig 4.103, Table 4.25) and BRP44L induced in the fulvestrant resistant and oestrogen deprived models as compared to MCF7 (Fig 4.103, Table 4.25). However, BRP44L was decreased in tamoxifen resistant cells. Therefore, increased expression of Citrate-Pyruvate shuttle components and the mitochondrial pyruvate carrier could increase pyruvate flux in fulvestrant resistant and oestrogen deprived resistant models (Fig 4.103, Table 4.25). Induced pyruvate entry into the TCA cycle could serve to induce OxPhos and basal OC (Fig 35) in fulvestrant resistant and oestrogen deprived models.

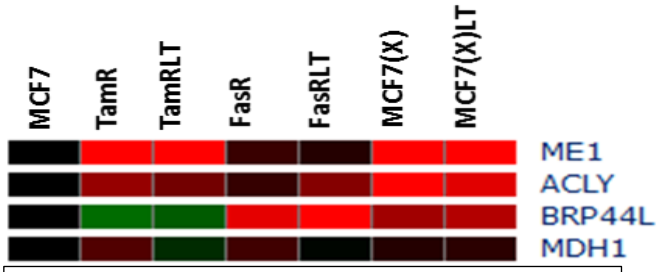

Fig 4.103. Microarray expression of citrate-pyruvate shuttle components ME1, MDH1, ACLY & BRP44L for the panel of resistant models. On the heatmap, red, green & black indicate induced, reduced & no change in gene expression respectively as compared to MCF7 cells.

Gene symbols	TamR	TamRLT	FasR	FasRLT	MCF7(X)	MCF7(X)LT
ME1	2	2.97	1.17	1.10	2	2
ACLY	1.50	1.37	1.16	1.44	2.23	1.84
BRP44L	1.34	1.28	1.86	2.17	1.55	1.63
MDH1	1.25	1.12	1.19	1.01	1.10	1.13

Table 4.25. Fold changes for microarray expression of ME1, MDH1, ACLY & BRP44L in endocrine resistant models vs. MCF7. Fold decreases (≥1.2) are indicated in green & increased fold changes (≥1.2) are indicated in red.

Substrate provision for TCA/OxPhos

Mitochondrial β-oxidation of fatty acids, which ultimately produces substrates for TCA cycle and OxPhos, is additionally worthy of consideration. This process involves successive removal of two-carbon units in the form of acetyl-CoA from the carboxyl end of fatty acyl chains. In the first reaction, acyl-CoA dehydrogenase (comprising ACADS, ACADM, ACADL and ACADVL) oxidizes the fatty acyl-CoA by reducing FAD to $FADH_2$, and the FADH2 donates an electron to an electron-transferring flavoprotein (ETFP) of the inner mitochondrial membrane. Then, reduced ubiquinone transfers a pair of electrons to form O_2 and generates 2ATP molecules (Fig 4.101). In the second reaction, enoyl-CoA hydratase (ECHS1) catalyses formation of β-hydroxyacyl-CoA. In the third reaction, β-hydroxyacyl-CoA dehydrogenase (HADH, HADHA and HADHB) reduces NAD^+ to convert β-hydroxyacyl-CoA into β-ketoacyl-CoA. The NADH formed by this reaction donates electrons to complex I of OxPhos and generates 3ATP molecules. In the fourth reaction, acyl-CoA acetyltransferase (ACAT1 and ACAT2) catalyses conversion of β-ketoacyl-CoA to acetyl CoA which further oxidizes in the TCA cycle. As a result 5ATP molecules are generated for each acetyl-CoA in successive oxidation of fatty acids. Transfer of the fatty acyl chain from cytosol to mitochondrial inner membrane during the process is mediated via the Carnitine/Acylcarnitine Translocase (SLC25A20) transporter (Fig 4.101).

Expression of the genes associated with fatty acid translocation and β-oxidation in the mitochondria was examined for the panel of resistant models using the 1.0ST gene microarrays (Fig 4.104, Table 4.26). Expression of SLC25A20 was induced in fulvestrant resistant and oestrogen deprived models as compared to MCF7. For the first reaction in β-oxidation of fatty acid involving acyl-CoA dehydrogenase, ACADS expression was induced in TamRLT and FasRLT cells and ACADM expression was induced across all resistant models (except TamR) compared to MCF7 (ACADL was not expressed and ACADVL expression unchanged across the panel). For the second reaction, ECHS1 expression was induced in fulvestrant resistant models but reduced in MCF7(X) as compared to MCF7 cells. For the third reaction involving β-hydroxyacyl-CoA

dehydrogenase, HADH expression was induced in all the resistant models and HADHA induced in FasRLT, although HADHB expression was reduced in TamR and MCF7(X) as compared to MCF7 cells. For the fourth reaction involving acyl-CoA acetyltransferase, ACAT1 was induced in all resistant models and ACAT2 induced in oestrogen deprived resistant models (but reduced in TamRLT) as compared to MCF7. Based on these various deregulated expression profiles, fatty acid flux to mitochondrial inner membrane was potentially induced in fulvestrant resistant and oestrogen deprived models while β -oxidation of fatty acids to increase supply of FADH2 and/or NADH was also potentially raised in all the antihormone resistant models. This could account for higher OxPhos in the resistant models versus MCF7, although further investigation would be required to gauge impact of fatty acid oxidation on metformin sensitivity in the panel.

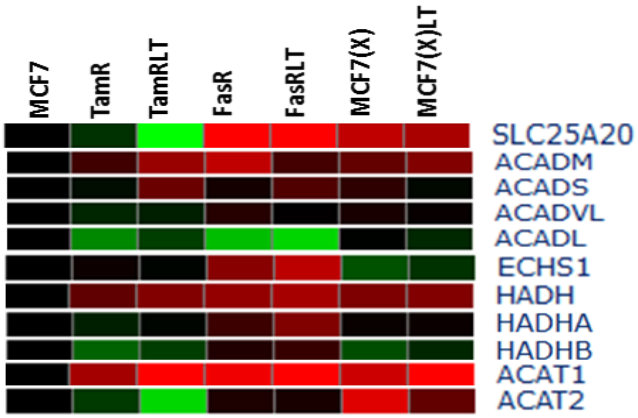

Fig 4.104. Microarray expression of genes for fatty acid translocation and β-oxidation in the mitochondria for the panel of resistant models. On the heatmap, red, green & black indicate induced, reduced & no change in gene expression respectively as compared to MCF7 cells.

Gene symbols	TamR	TamRLT	FasR	FasRLT	MCF7(X)	MCF7(X)LT
SLC25A20	1.14	———	2.08	2.83	1.69	1.59
ACADS	1.04	1.33	1.06	1.25	1.14	1.02
ACADM	1.19	1.52	1.69	1.21	1.31	1.43
ACADL	———	———	———	———	———	———
ACADVL	1.11	1.09	1.11	1.01	1.07	1.02
ECHS1	1.04	1.01	1.45	1.67	1.25	1.15
HADH	1.3	1.43	1.5	1.58	1.41	1.43
HADHA	1.09	1.01	1.18	1.42	1.03	1.03
HADHB	1.31	1.18	1.09	1.16	1.24	1.11
ACAT1	1.57	2.27	1.92	2.17	1.74	2.27
ACAT2	1.17	1.79	1.08	1.07	1.84	1.31

Table 4.26. Fold changes for microarray expression of fatty acid transporter and β-oxidation in the mitochondria in endocrine resistant models vs. MCF7. Fold decreases (≥1.2) are indicated in green & increased fold changes (≥1.2) are indicated in red

OxPhos complex I subunit expression

In this project, NADH dehydrogenase activity was found to be increased across the resistant panel as compared to MCF7 (Fig 4.44). The highest enzyme activity was detected in oestrogen deprived resistant models, and in keeping with this were the most growth-sensitive to metformin treatment (Table 4.20). Expression of core subunits for NADH dehydrogenase were assessed using 1.0ST gene microarray (Fig 4.105, Table 4.27). Core subunits of NADH dehydrogenase is composed of catalytic subunits (mitochondrial encoded genes: ND1, ND2, ND3, ND4, ND4L, ND5 and ND6) and subunits responsible for minimal assembly and catalysis (nuclear encoded genes; NDUFS1, NDUFS2, NDUFS3, NDUFS7, NDUFS8, NDUFV1 and NDUFV2). ND6 expression was induced in TamR and FasR as compared to MCF7 (Fig 4.105, Table 4.27), although ND4L and ND5 expression were unchanged (while further mitochondrial-encoded subunits were not represented on the 1.0ST gene microarray platform). For the nuclear encoded genes, NDUFS3, NDUFS1, NDUFS7 and NDUFV1 expression were induced in all the resistant panel (except TamRLT for NDUFS1, MCF7XLT for NDUFS7 and TamR for NDUFV1) as compared to MCF7. NDUFS2 expression was induced in TamRLT and NDUFS8 induced in FasRLT as compared to MCF7 cells. Expression of NDUFV2 alone was reduced and only in oestrogen deprived resistant models. Therefore, it seems likely that the induced expression of core subunits contribute in some way towards induced NADH dehydrogenase activity and impact on metformin sensitivity in resistant models.

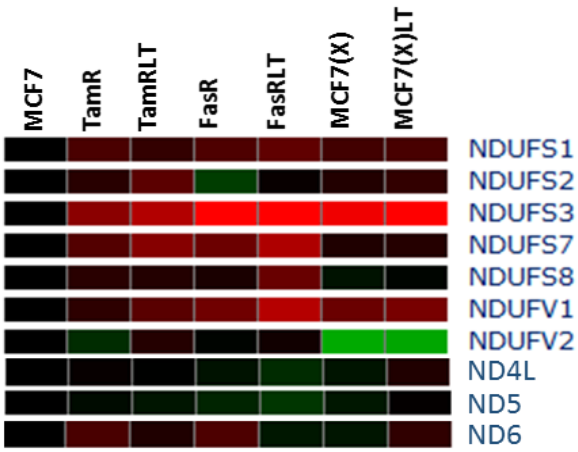

Fig 4.105. Microarray expression of NADH dehydrogenase core subunits for the panel of resistant models. On the heatmap, red, green & black indicate induced, reduced & no change in gene expression respectively as compared to MCF7 cells.

Gene symbols	TamR	TamRLT	FasR	FasRLT	MCF7(X)	MCF7(X)LT
ND4L	1.02	1	1.05	1.12	1.06	1.09
ND5	1.03	1.06	1.10	1.16	1.07	1
ND6	1.22	1.09	1.24	1.07	1.06	1.14
NDUFS1	1.23	1.15	1.24	1.30	1.20	1.22
NDUFS2	1.12	1.28	1.18	1.02	1.10	1.15
NDUFS3	1.46	1.63	2.20	2.31	1.92	2
NDUFS7	1.25	1.44	1.34	1.60	1.09	1.11
NDUFS8	1.12	1.10	1.07	1.33	1.05	1.02
NDUFV1	1.13	1.28	1.36	1.64	1.33	1.39
NDUFV2	1.13	1.10	1.01	1.05	1.59	1.57

Table 4.27. Fold changes for microarray expression of core subunits of NADH dehydrogenase in endocrine resistant models vs. MCF7. Fold decreases (≥1.2) are indicated in green & increased fold changes (≥1.2) are indicated in red.

Regulators of expression and localisation of key TCA/OxPhos components

TCA cycle enzyme isoforms and OxPhos component subunits in the mitochondria are encoded both by the nucleus and by the mitochondria itself. Transport of the nuclear-encoded TCA cycle enzyme isoforms and OxPhos subunits into the mitochondria is facilitated via translocase inner/outer mitochondrial membrane proteins (TIMMs/TOMMs). The mitochondrial ribosome machinery (including small and large ribosomal subunits) translates mitochondrial-encoded TCA cycle enzyme isoforms and OxPhos subunits (detailed in Table 4.28-4.29). Interestingly, induced expression of mitochondrial translation and biogenesis genes (including mitochondrial ribosome subunits and translocases) has been demonstrated in breast cancer compared to adjacent stromal tissue (Sotgio et al. 2012*a*).

Since they impact on the TCA and OxPhos machinery and mitochondrial biogenesis expression of the mitochondrial translation machinery genes (small and large mitochondrial ribosome subunits) and also the mitochondrial inner translocases were therefore assessed using the 1.0ST gene microarrays (Fig 4.106). Furthermore, ORA-O GO terms for induced genes were interrogated using the Innatedb database to determine if there was any enrichment of such mitochondrial translation and translocation genes in the resistant cells (Table 4.30). Heatmap profiling revealed expression of large ribosomal subunits (MRPL 2/15/17/20/21/34/37/ 40 and 47), small ribosomal subunits (MRPS5/15/18A/18B and 34) and translocase inner mitochondrial subunits (TIMM8A/9/17A and 44) were commonly induced (≥1.2 fold changes) in the resistant panel compared to MCF7 cells (Fig 4.106).

Enzyme	Isoform
Aconitase	1 nuclear encoded isoform 1 mitochondrial encoded isoform (ACO2)
Isocitrate dehydrogenase	4 nuclear encoded isoforms 1 mitochondrial encoded isoform (IDH2)
Dihydrolipoamide S-Succinyltransferase	1 mitochondrial encoded isoform (DLST)
Succinyl-CoA Synthetase	1 nuclear encoded isoform 2 mitochondrial encoded isoforms (SUCLG1 & SUCLG2)
Malate dehydrogenase	1 nuclear encoded isoform 1 mitochondrial encoded isoform (MDH2)

Table 4.28. Nuclear and mitochondrial encoded isoforms for key TCA cycle enzymes.

Enzyme	subunits
I: NADH-ubiquinone oxidoreductase	40 nuclear encoded subunits 7 mitochondrial encoded subunits (ND1, ND2, ND3, ND4, ND4L, ND5 & ND6)
II: succinate dehydrogenase	4 nuclear encoded subunits
III: cytochrome bc_1 complex	10 nuclear encoded subunits 1 mitochondrial encoded subunits (UQCRC2)
IV: cytochrome *c* oxidase	10 nuclear encoded subunits 3 mitochondrial encoded subunits (CO1, CO2 & CO3)

Table 4.29. Nuclear and mitochondrial encoded subunits of key OxPhos complex I-IV components.

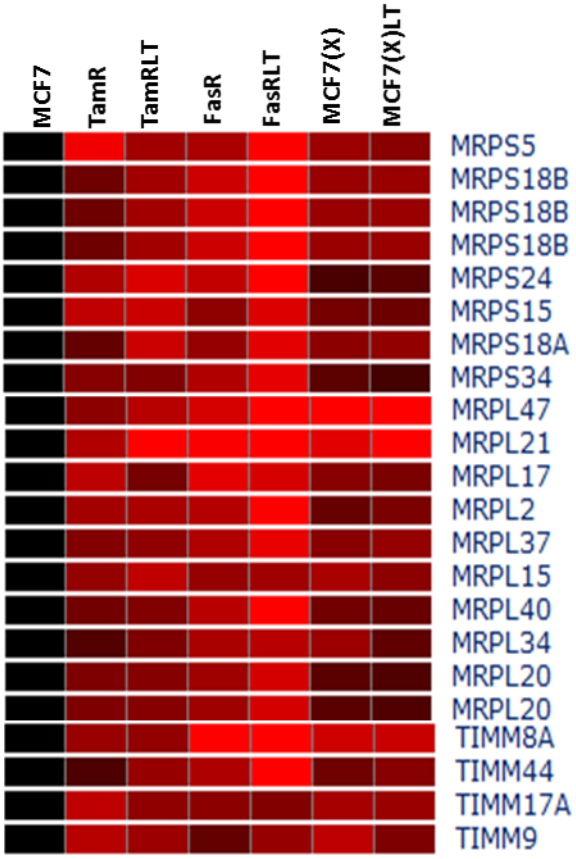

Fig 4.106. Microarray expression of small/large subunits of mitochondrial ribosomes and also Translocase Inner Mitochondrial Membrane (TIMMs) whose induction is shared across the resistant panel. Red indicates induced expression (≥1.2 fold change) as compared to MCF7 cells.

Mitochondrial biomarkers	ORA Cellular components	P value	ORA Molecular Function	P value	ORA Biological Process	P value
Mitochondrial ribosomal subunits	mitochondrion	1.53E-23	Structural constituent of ribosome	0.01666	translation	0.00014
Translocase inner mitochondrial membrane	mitochondrion	1.53E-23	Metal ion binding	0.00066	Protein targeting to mitochondrion	0.00062

Table 4.30. Significantly enriched ORA-O GO terms for small/large subunits of mitochondrial ribosome and Translocase Inner Mitochondrial Membrane (TIMMs) in the resistant models vs. MCF7 cells.

For the translocase outer mitochondrial membrane proteins (TOMM20) expression was of particular interest as it has been reported specifically as a marker of mitochondrial mass and biogenesis in lymph node positive breast cancer (Sotgio et al. 2012*b*). TOMM20 was evaluated across the resistant panel using the 1.0ST gene microarrays, and was induced by ≥1.2 fold changes in TamR, TamRLT and MCF7(X) cells versus MCF7 (Fig 4.107, Table 4.31). Further study using paraffin-embedded pellets of the resistant model panel and MCF7 cells immuno-stained for TOMM20 expression detected punctuated cytoplasmic staining in accordance with mitochondrial localisation. H-scoring of the staining determined TOMM20 protein expression was induced in TamR, TamRLT, FasRLT, MCF7(X) and MCF7(X)LT cells by 1.7, 1.4, 1.2, 1.5 and 1.3 fold changes as compared to MCF7 (Fig 4.108-4.109). This finding suggests more prominent mitochondria in these resistant states that may also contribute to increasing OxPhos capacity in antihromone resistant models.

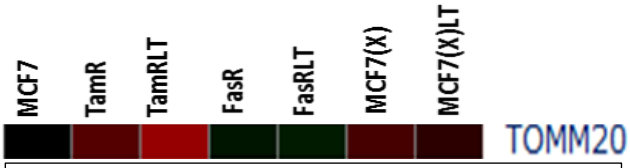

Fig 4.107. Microarray expression of TOMM20 in the panel of resistant models. On the heatmap, red & black indicate induced or no change in gene expression respectively as compared to MCF7 cells.

Fold change	TamR	TamRLT	FasR	FasRLT	MCF7(X)	MCF7(X)LT
MCF7	1.26	1.5	1.06	1.08	1.21	1.13

Table 4.31. Fold changes for microarray expression of TOMM20 in endocrine resistant models vs. MCF7. Fold increases (≥1.2) are indicated in red.

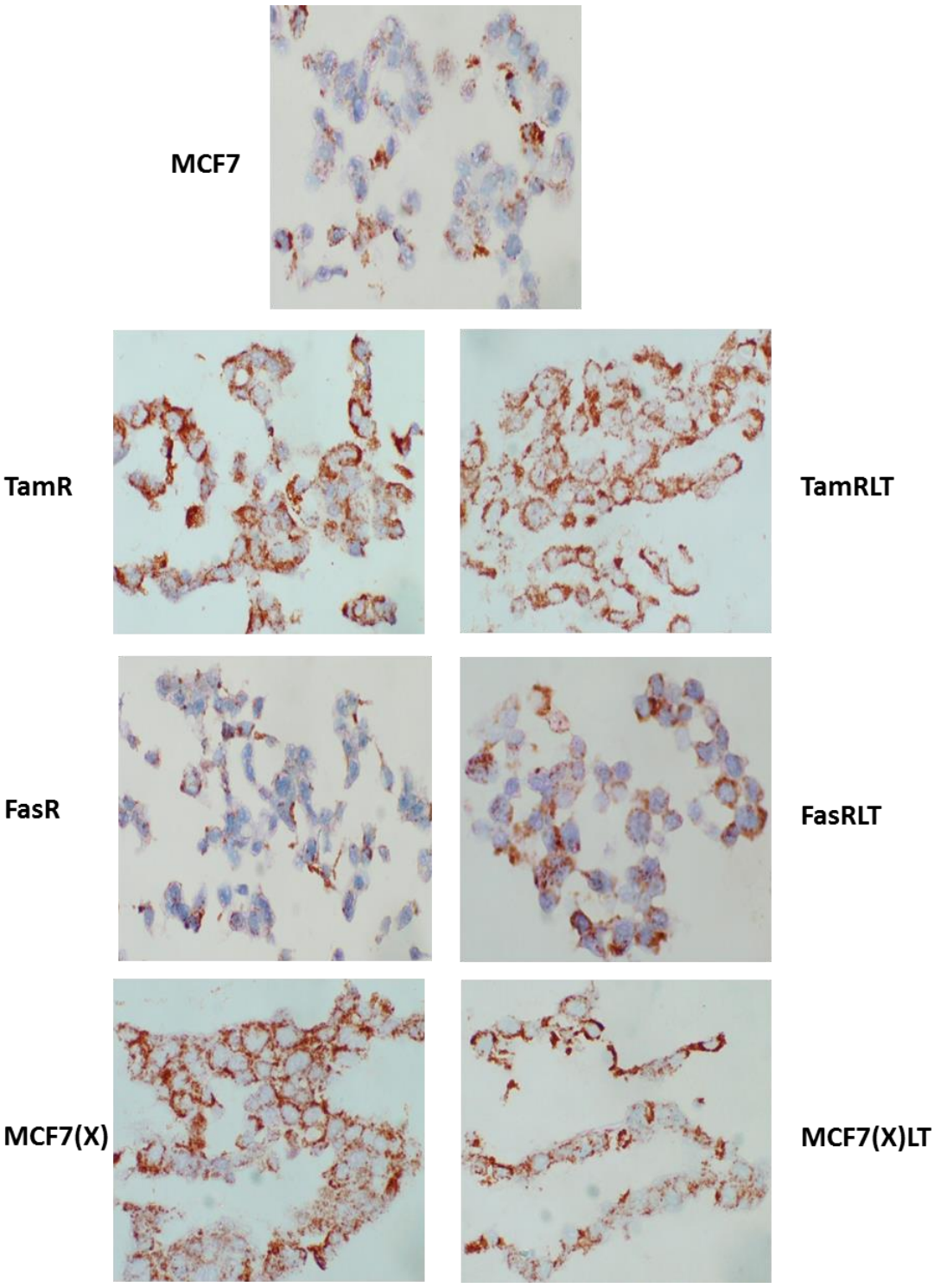

Fig 4.108. Paraffin-embedded section of endocrine resistant and responsive breast cancer cell pellets immuno-stained with TOMM20 antibody (1:500) and counterstained with methyl green. Original magnification was 40X.

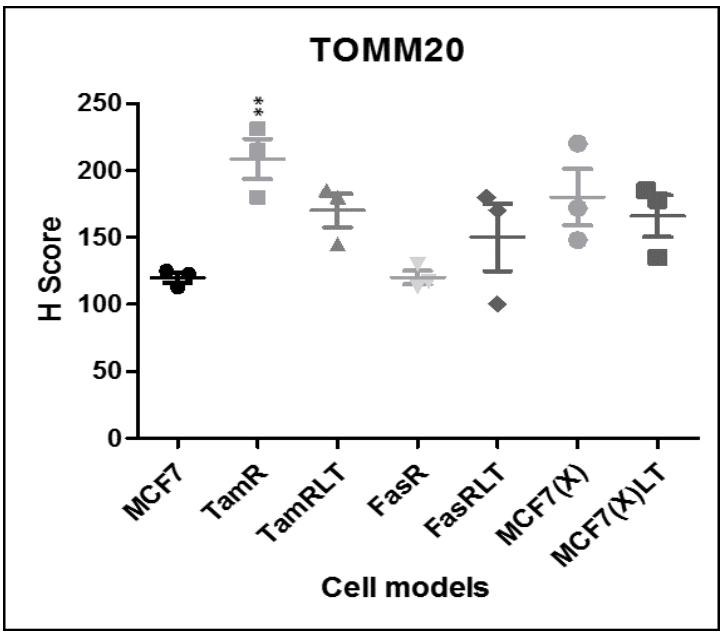

Fold change	TamR	TamRLT	FasR	FasRLT	MCF7(X)	MCF7(X)LT
MCF7	1.7	1.4	1	1.2	1.5	1.3

Fig 4.109. H-score for the TOMM20 staining in the panel. Data are represented as mean of 3 independent experiments (N=3). The error bar indicates SEM. ** (P<0.01) following ANOVA with Dunnett's post hoc correction. Fold changes for TOMM20 protein expression in endocrine resistant models vs. MCF7 is represented. Induced fold changes (>1.2) are indicated in red.

Phosphate and ADP/ATP carriers

Glycolysis, acetyl CoA formation and TCA cycle store energy in the form of $FADH_2$ and NADH that are subsequently oxidized in the electron transport chain. The energy of electron transfer generates a proton gradient which drives ATP synthase to form ATP molecules in the mitochondria. However, for OxPhos to be productive towards growth (most anabolic process), ATP needs to transport out to the cytoplasm via a phosphate carrier, since this is where most ATP-dependent processes occur. ADP/ATP carriers in turn are required to facilitate ADP/ATP transport in the opposite direction (Fig 4.101). Induced expression of the phosphate carrier and ADP/ATP carriers have been reported, alongside increased OxPhos, in breast cancer as compared to adjacent stroma, highlighting their importance (Sotgio et al. 2012*a*). Expression of the phosphate carrier SLC25A3 and also several ADP/ATP carriers (SLC25A4, SLC25A5, SLC25A6 and SLC25A31) were therefore assessed across the panel of resistant models using 1.0ST gene microarray (Fig 4.109, Table 4.32). While expressed in all models, the phosphate carrier SLC25A3 expression was only induced in FasR compared to MCF7 cells. For the ADP/ATP carriers, SLC25A5 expression was increased in all resistant cells, with SLC25A4 expression induced in fulvestrant

resistant models and MCF7(X) cells compared with MCF7 cells. SLC25A6 expression was unchanged and SLC25A31 not expressed in this panel. Therefore, increased expression of ADP/ATP transporter (SLC25A5) is accompanied with increased OxPhos in the resistant models compared to MCF7.

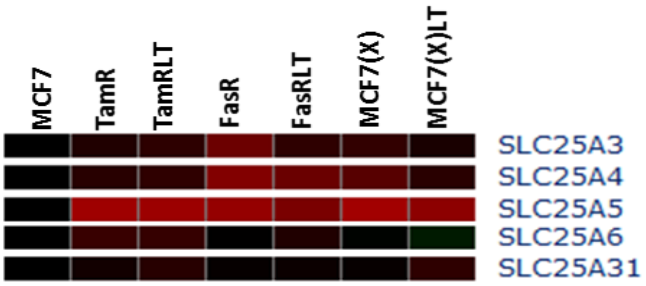

Fig 4.109. Microarray expression of the phosphate carrier SLC25A3 and several ADP/ATP transporters across the panel of resistant models. On the heatmap, red and black indicate induced or no change in gene expression respectively, as compared to the control MCF7 cells.

Gene symbols	TamR	TamRLT	FasR	FasRLT	MCF7(X)	MCF7(X)LT
SLC25A3	1.09	1.13	1.34	1.14	1.15	1.07
SLC25A4	1.12	1.14	1.43	1.34	1.27	1.12
SLC25A5	1.54	1.53	1.50	1.39	1.56	1.47
SLC25A6	1.16	1.16	1.00	1.09	1.01	1.07
SLC25A31	———	———	———	———	———	———

Table 4.32. Fold changes for the phosphate carrier and various ADP/ATP transporters in endocrine resistant models vs. MCF7. Induced fold changes (≥1.2) are indicated in red.

4.3 Discussion

Carbon metabolism and associated metabolic pathways, notably glycolysis, pyruvate metabolism and the TCA cycle, together with OxPhos that uses the resultant NADH and $FADH_2$ substrates to efficiently-generate ATP in the cell, have gained attention in cancer research since tumour cells require high levels of nutrients and energy for their uncontrolled growth. Indeed, reprograming of energy metabolism is a hallmark of cancer (Hanahan et al. 2011). Increased glycolysis (in the presence of O_2) and diminished oxidative phosphorylation were initially described as features of cancer by Warburg et al. (1956), and increased glycolysis has been reported as the main energy pathway in mammary adenocarcinoma (Eskey et al. 1993) and is prominent within breast cancer cells (Mazurek et al. 1997). One explanation for the elevated glycolysis in cancer was proposed by Pedersen et al. (2008), who noted that interaction between hexokinase-2 (HK2) and voltage dependent anionic channels (VDACs) within the outer mitochondrial membrane enabled the HK enzyme to efficiently-utilise mitochondrial ATP to convert glucose to glucose-6-phosphate. Therefore, it focused on intact mitochondrial function in the presence of induced glycolysis. On this basis, the glucose analog 2-(18F)-fluoro-2-deoxy-d-glucose (FDG) can be used clinically in positron emission tomography (PET) to detect tumour cells with induced glucose consumption in the clinic. Furthermore, in most hypoxic tumours with increased glycolysis O_2 concentration is about 8-57μM (Vaupel et al 1989). The Km value for cytochrome C oxidase in both normal and tumour cells is 0.1–0.8 μM (Mason et al.2006) and saturating concentration is 1-8 μM. Therefore, O_2 concentration in hypoxic areas of tumours cannot limit the enzyme activity and oxidative phosphorylation (Rodriguez-Enriquez et al. 2010). However, reduced gene expression of isoforms of NADH dehydrogenase, cytochrome C oxidase, ATP synthase and glutaminase occurs in cancer cells after prolonged hypoxia (Ebert et al. 1996; Kobayashi et al.2001). Moreover, hypoxia-inducible factor-1 (HIF-1) activation increases glucose transporter and glycolytic enzymes to induce metabolite flux into hypoxic regions of the tumour favouring glycolysis in tumours (Marin-Hernandez et al.2009). Furthermore, HIF-1α can inhibit pyruvate dehydrogenase activity via regulating pyruvate dehydrogenase kinase (PDK1), preventing pyruvate from fuelling the TCA cycle and thereby limiting substrates required for efficient OxPhos (Papandreou et al.2006).

Role for glycolysis in the model panel:

In this chapter, dependency of the endocrine resistant breast cancer cells (and of their parental endocrine responsive MCF7 line) on glycolysis and also glutaminolysis for their carbon source (glucose and glutamine) was demonstrated via challenge with 2DG and glutamine deprivation respectively. Successful ECA measurement in the models provided evidence for use of glycolysis in all the endocrine resistant and responsive cells in the panel, in keeping with the central role for this metabolic pathway in cancer (Hanahan et al. 2011). However, an increased basal glycolytic (measured using ECA which relates to lactate production as the endpoint of glycolysis) was detected in tamoxifen resistant (particularly TamRLT) and to some extent oestrogen deprived resistant models as compared to MCF7 cells, which was paralleled by induced LDHB expression in these models. Moreover, there was an increased sensitivity with regards to ECA reduction by 2DG in all endocrine resistant lines compared with the MCF7 cells, with TamRLT again the most sensitive model (requiring 0.5mM in TamRLT versus 5mM 2DG treatment in MCF7 cells for 24hrs to give 50% reduction). This in total suggests that all the endocrine resistant cells in the model panel are more dependent on glycolysis to supply carbon fuel and ATP versus their endocrine responsive counterpart. While glycolysis is reported to be reduced during response to tamoxifen in MCF7 for in vitro and in vivo models (Rivenzon-Segal et al., 2003), increased glycolysis has also been reported in an additional MCF7-derived tamoxifen resistant cell line which had increased LDH levels and increased glucose uptake (Farabegoli et al., 2012).

All the resistant and responsive models in the panel were growth inhibited by 2DG treatment. These observations confirm that all endocrine resistant cells are dependent to some degree on glycolysis to drive their growth which could potentially have therapeutic interest given that 2DG has also been studied in advanced clinical cancer trials. Efficacy of docetaxel in combination with 2DG was studied in locally-advanced or metastatic solid tumours, where 2DG was administered orally once daily for 7 days every other week starting at a dose of 2 mg/kg and docetaxel was administered intravenously at 30 mg/m^2 for 3 of every 4 weeks. The study found 2DG at 63 mg/kg in combination with weekly docetaxel was well-tolerated and the most common side effects were sweating, fatigue and dizziness which mimic hypoglycemic symptoms, with stable disease in 32% of patients (Raez et al. 2013). Based on the findings here, 2DG anti-tumour impact might be worthy of exploration in breast cancers including endocrine resistant disease.

Interestingly, while the tamoxifen resistant, oestrogen deprived resistant models, and MCF7 cells were all growth inhibited by 2DG (with up to 90% inhibition achieved for higher doses in

TamRLT cells), EC_{50} studies indicated that it was the fulvestrant resistant models that were the most sensitive cells (EC_{50}: 0.4mM) for growth inhibition by 2DG treatment (after 7 days), as compared to MCF7 and the further resistant models (EC_{50} ~1mM).However, gene microarray interrogation suggested this high growth-sensitivity of fulvestrant resistant models to the growth inhibitory effect of 2DG may have been explained by their induced glucose transporter SLC2A3, which would act to increase 2DG flux into the cell and also by their increased HK (HK1 and HK2) which would potentially accelerate glycolytic inhibition by 2DG (via efficient conversion to 2DG phosphate). In contrast, lysine, valine, leucine and isoleucine degradation (associated with increased ACAA2, OGDHL, ALDH3A2 and DLST expression) replenishes the TCA cycle with acetyl CoA and succinyl CoA in tamoxifen resistant and oestrogen deprived and thus accounts for reduced sensitivity of these models to growth inhibition of 2-DG treatment.

It has also been shown in MCF7 cells that 2DG reduces ATP levels and activates AMPK, which further phosphorylates cAMP response element-binding protein (CREB) and activates oestrogen-related receptor α protein (ERR) leading to induced mitochondrial biogenesis and β-oxidation of fatty acids (Wu et al. 2015). Hence, prevalence of "compensatory metabolic mechanisms" recruited during 2DG treatment might also contribute towards the growth profile with 2DG in the panel and explain discordance for the growth versus ECA findings. Nevertheless, the reduced growth inhibitory effect of 2DG in tamoxifen resistant models may also reflect that alternative carbon sources alongside their prominent glycolysis contribute to generate building blocks, ATP and thereby growth of these models, while fulvestrant resistant cells are highly growth-dependent on their more modest glycolytic activity.

Role for glutaminolysis in the model panel:

In this chapter sensitivity of the breast cancer models to glutamine deprivation was monitored after day 7. All the endocrine resistant models showed increased sensitivity to such deprivation compared with the endocrine responsive MCF7 cells, but of these the tamoxifen resistant models were the most sensitive. These differential effects are compatible with further studies, in lung cancer, showing glutamine dependency ("glutamine addiction") can vary among tumour cells (van den Heuvel et al,. 2012), while study of breast cancer has also revealed differential sensitivity to glutamine deprivation according to tumour subtype (Kung et al., 2011). Cancer cells more dependent on glutamine availability for their proliferation are also reported to have a higher glutaminolysis rate (van den Heuvel et al.2012). In total, the glutamine deprivation findings suggest an increased dependency in the endocrine resistant cells, but particularly those resistant to tamoxifen, on increased glutaminolysis as a further source of fuel. The lower impact of glutamine deprivation in fulvestrant versus tamoxifen resistant cells is in keeping with the

2DG findings above that imply enhanced growth dependency on glycolysis in the fulvestrant resistant cells for their fuel supply. The observation of apparent increased dependency on available glutamine in tamoxifen resistance, coupled with the 2DG growth findings in such cells, also seem compatible with the "third wave" of metabolic change reported during malignant transformation which results in prominent glutaminolysis to support the substantial metabolism of highly-proliferative tumours (Smolkova et al. 2010). The induced expression profile of transporters SLC1A5 and SLC7A6 suggests an increased capacity for glutamine influx into the endocrine resistant models, in keeping with findings from Nicklin et al. (2009) that glutamine influx and exchange with essential amino acids is important in regulating cell proliferation. However, this profile cannot easily explain the increased sensitivity of the resistant models to glutamine deprivation versus MCF7. Interestingly, the reduced sensitivity to glutamine deprivation for fulvestrant and oestrogen deprived resistance compared with tamoxifen resistant models was paralleled by reduced glutaminase (GLS and GLS2) enzyme expression, implying somewhat diminished capacity for glutaminolysis in these models versus tamoxifen resistance which may underpin the growth profile with glutamine deprivation in the panel. Nevertheless, it should be remembered that the induced transaminase enzyme (GLUD1) detected in FasRLT and oestrogen deprived models may also allow their use of L-glutamic acid in the growth media (0.13mM in RPMI1640) as an alternative carbon source to generate α-KG and ultimately promote some growth despite glutamine deprivation in these models. As GLUL was also induced in MCF7(X) cells, de novo glutamine synthesis may provide an additional explanation for the reduced sensitivity of this model to glutamine deprivation versus tamoxifen resistant cells. While this observation in ER+ MCF7(X) cells is not in accordance with Kung et al. (2011) findings for glutamine synthase (GS: encoded by the GLUL gene), which primarily sustained the growth and proliferation of the basal subtype rather than luminal breast cancer cells, such GLUL induction in MCF7(X) cells may reflect further deregulation of this pathway in acquired endocrine resistance emerging from ER+ cells.

Interestingly, glutamine restriction is perceived to be a potentially-attractive means of inhibiting growth of tumours. γ-L-glutamyl p-nitroanilide (GPNA) is an inhibitor of a glutamine transporter (SLC1A5), and this reduces growth of lung cancer cells via impacting on downstream mTOR signalling (Hassanein et al. 2013). A further agent, Compound 968, is able to inhibit GLS activity and this blocks downstream Rho GTPases to inhibit the growth of breast cancer cells, B lymphoma and fibroblasts (Wang et al. 2010). The findings in this Chapter imply that pharmacological restriction of glutamine might also be worthy of further exploration in the context of endocrine resistance, particularly tamoxifen resistant states.

Role for TCA cycle and OxPhos in the model panel:

Along with evidence supportive of increased glycolysis and glutaminolysis contributing towards fuel and ATP production and thereby acquired endocrine resistant cell growth, microarray profiling in chapter 3 had revealed a shift in gene expression towards induced pyruvate metabolism, TCA cycle and OxPhos pathways in the endocrine resistant models. Further expression studies here also suggest prominent mitochondrial transport of nuclear-encoded TCA/OxPhos elements via several increased translocase inner mitochondrial membrane proteins (TIMM8A/9/17A and 44), enhanced translation of mitochondrial-encoded TCA/OxPhos elements by increases in 14 mitochondrial ribosome machinery subunits, and also increased TOMM20, in total suggesting increases in TCA/OxPhos machinery and mitochondrial biogenesis in resistant versus MCF7 cells. Comparison of the TamR and MCF7 cells by mass spectrometry analysis of both phospho- and non-phosphorylated peptides also confirmed that induced expression of TCA/OxPhos enzymes persists at the protein level in endocrine resistant cell models.

Further exploring OxPhos (ETC) components in this chapter by staining for basal NADH dehydrogenase activity revealed Complex I was induced in the FasRLT, MCF7(X) and MCF7(X)LT cells, while basal complex IV activity (COX) was elevated in tamoxifen and fulvestrant resistant lines. In keeping with these various findings, evaluation of oxygen consumption by the models further re-enforced that OxPhos was commonly increased in the endocrine resistant models compared with MCF7 cells, particularly for fulvestrant and oestrogen deprived resistant cells. While studies have to date been confined to tamoxifen resistance, there is a little supportive literature for the concept of increased OxPhos in endocrine resistance from reactive oxygen species studies in two MCF7-derived TAM resistant lines TAMC3 and TAMR3 (Leung et al. 2014) and from RNA-seq observations of increased NADH dehydrogenase subunits and cytochrome oxidases in a further MCF7 derived tamoxifen resistant line, MTR-3 (Huber-Keener et al. 2012). Induced respiration and upregulation of OxPhos components has also been reported in several further types of cancer cells (Moreno-Sanchez et al. 2007; Jose et al. 2011).

Clinical breast cancer survival analysis performed using publically-available mRNA array datasets in this chapter through the KMPlotter tool also identified that the induced genes associated with pyruvate metabolism (PCK2), TCA cycle (FH) and OxPhos pathways (NDUFA3, NDUFA7, NDUFA8, NDUFA9, NDUFB5, NDUFS3, UQCRFS1, and ATP5J2) are all associated with earlier relapse in ER+ and tamoxifen-treated breast cancer patients, implying there may also be an increased OxPhos contribution towards endocrine resistance in vivo. Such a concept of altered energy metabolic pathways during progression seems in keeping with in situ metabolic and flux analysis clinical

studies from Kaambre et al. (2012) that have revealed induced respiration and higher sensitivity to OxPhos inhibitors in advanced breast tumours as compared to normal tissues. In the Kaambre study, complex IV, ATP synthase and ADP/ATP transporters were recognized as particular deregulated components in the breast cancer models.

A hypothesis reconciling the apparent increase in OxPhos in cancer and glycolysis in fibroblast associated cancer in vivo has been recently proposed by the Lisanti group, termed the "Reverse Warburg" effect. In this mechanism, tumour epithelial cells promote loss of caveolin (CAV1) from the associated stroma (Witkiewicz et al. 2009). This results in tumour-associated fibroblasts undergoing extensive aerobic glycolysis, oxidative stress and autophagy (Pavlides et al., 2010), with the lactate and ketones in turn "feeding" TCA and thereby OxPhos within the cancer epithelial cells (Whitaker-Menezes et al. 2011). In accordance with this concept, Bonuccelli et al. (2010) reported that induced gene expression of oxidative energy metabolism occurs in breast tumour epithelial cells as compared to the adjacent stroma following laser-captured micro-dissection in >2000 breast cancer patients, while Sotgio et al. (2012a) have reported increases in mitochondrial biogenesis genes in breast cancer relative to adjacent stromal tissue. Interestingly, co-culture of MCF7 with fibroblasts or provision of potential fuels (lactate or ketone bodies or glutamine) can also promote mitochondrial OxPhos and endocrine insensitivity in such cells, and this can be overcome with inhibitors of OxPhos, metformin or arsenic trioxide (Ko et al. 2011, Martinez-Outschoorn et al. 2011). This in total suggests that the "Reverse Warburg" effect, mediated by stroma and tumour epithelial interplay, can contribute to endocrine resistance in vivo. However, the mRNA and protein expression (including multiple deregulated complex I and III elements), NADH dehydrogenase activity, COX activity, and oxygen consumption observations made in this chapter are novel in that they reveal that intrinsic capacity for OxPhos is commonly increased in breast cancer cells when they acquire endocrine resistance.

Building on these considerable mRNA and protein expression, enzyme activity, and oxygen consumption findings for the model panel that all implicate deregulation of OxPhos in endocrine resistance, dependency of such cells on OxPhos as an alternative energy pathway to generate ATP was further evaluated in this chapter. To achieve this, the effects of antimycin A (AA) and metformin as complex III and I inhibitors respectively were studied in the panel of resistant models.

Impact of Antimycin A (AA) in the model panel:

AA binds to the Q_i site of cytochrome b in complex III and it partially reduces oxidation of cytochrome b and thus reduction of cytochrome c, so disrupting Q cycle function of Complex III (Muller et al. 2002). The oxygen consumption of all resistant models (except MCF7(X) cells) showed increased sensitivity to AA (at 24 hrs) compared with MCF7 cells, where the most sensitive models were TamRLT followed by FasR and FasRLT cells. Similarly, all resistant models were more growth-sensitive to AA (7 days treatment), with TamRLT (EC50: 0.72nM) and (to a lesser extent) FasRLT (EC50: 1.3nM) again being the most sensitive to this inhibitor compared with MCF7 cells (EC50: 10.5nM). These findings strongly suggest an increased role for Complex III-driven OxPhos in endocrine resistant models, particularly TamRLT and fulvestrant resistance. It is also known that in the presence of AA at the Q_i site, 4 mechanisms can potentially bypass AA inhibition and thus minimize sensitivity to such treatment; a) transfer of two sequential electrons from UQH2 oxidation at Q_0 site to ISP releases 2 protons into the inner membrane space. b) semiquinone oxidizes b_L which reduces quinone to $UBQH_2$. c) semiquinone directly reduces cytochrome c. d) semiquinone directly reduces a molecule of O_2 and forms superoxide (Muller et al. 2002). Therefore, one or a combination of bypass mechanisms can explain reduced sensitivity of endocrine resistant breast cancer cells to AA treatment which needs further investigation. In contrast, stigmatellin and myxothiazol which bind to the Q_0 site of cytochrome b in complex III are more potent to inhibit cytochrome b oxidation and proton pump into the inner membrane space.

Impact of metformin in the model panel:

Metformin reduced NADH dehydrogenase activity in the model panel, confirming the ability of this drug to inhibit complex I activity of the ETC (Wheaton et al. 2014) in endocrine resistant and responsive breast cancer cells. Such metformin impact was particularly striking in oestrogen-deprived resistant and FasRLT cells. The drug also substantially reduced cytochrome c oxidase activity, in keeping with the inhibitor also affecting subsequent electron transfer from complex I through to complex IV (Whitaker-Menezes et al. 2011), although effects were less marked in the fulvestrant resistant lines. Moreover, oxygen consumption was reduced in all models by metformin confirming this drug is able to inhibit OxPhos (Wheaton et al. 2014), with fulvestrant and oestrogen deprived resistant cells again proving the most sensitive and tamoxifen resistant and MCF7 cells the least sensitive. On balance, these findings suggest somewhat increased importance for Complex I-driven OxPhos in fulvestrant and oestrogen deprived resistant cells.

In keeping with this concept, these models that were most metformin-sensitive also had the highest basal NADH dehydrogenase (complex I) activity and basal oxygen consumption in the panel. Gene expression interrogation suggested that enhanced NADH supply via increased fatty

acid flux through SLC25A20 to the mitochondrial inner member (coupled with increases in further components for β-oxidation of fatty acids apparent for all resistant lines) may occur in oestrogen deprived and fulvestrant resistant models, while further substrate may be derived from the Malate-Aspartate shuttle via increased transporter expression in the latter. This could potentially fuel more prominent basal NADH dehydrogenase activity in such models that in turn may equate with their increased OxPhos sensitivity (oxygen consumption) to complex I blockade with metformin. Increased expression of the mitochondrial pyruvate carrier BRP44L which feeds pyruvate into the TCA cycle (schell et al. 2014) and thereby further substrates for OxPhos may also contribute.

However, it is important to note that other than NADH dehydrogenase activity there may be additional contributory factors towards the profile of metformin impact on oxygen consumption in the model panel. Wheaton et al. (2014) reported significant reduction of OCR with a low metformin concentration (0.25-1mM) in saponin-permeabilized cells as compared to intact cells, inferring the plasma membrane acts as a barrier to metformin action on complex I. Influx and efflux transporters for this drug have also been described (Pernicova et al. 2014). While magnitude of metformin treatment impact in the model panel was not correlated with expression profile on the microarrays for organic cation transporters OCT1-3 or the plasma membrane monoamine transporter responsible for metformin influx (Pernikova et al. 2014), interestingly the metformin efflux transporter MATE1 (SLC47A1) was induced in tamoxifen resistant models which may contribute to their somewhat lower sensitivity to metformin impact on oxygen consumption. Furthermore, it is known that metformin slowly permeates across the mitochondrial inner membrane where it inhibits complex I activity and its positive charge assists reversible accumulation of the drug into the mitochondrial matrix in response to mitochondrial membrane potential (MMP) (Bridges et al. 2014). A study by Appleby et al. (1999) suggested ATP synthase could function in reverse in response to any inhibition of electron transfer, pumping protons across the mitochondrial membrane to maintain MMP and Wheaton et al. (2014) have shown reverse ATP synthesis occurs after metformin treatment to maintain MMP in colon cancer cells. In the same study association of MMP with magnitude of metformin-dependent inhibition of complex I was demonstrated. Therefore, sensitivity to metformin treatment across the resistant panel might also be associated with differential MMP in these cells.

Metformin exerted a growth inhibitory effect in all the endocrine resistant and responsive models, reflecting the important contribution of OxPhos as a driver for breast cancer cell growth (Zakikhani et al. 2006). Higher growth sensitivity to metformin (as measured by EC_{50} at 7days)

compared to MCF7 cells was seen in the oestrogen deprived resistant models (with the lowest sensitivity for the panel exhibited by tamoxifen resistant cells). The cell model findings are compatible with their NADH dehydrogenase activity and oxygen consumption sensitivity to such treatment. Interestingly, the oestrogen deprived resistant models also had reduced LKB1 expression and reduced basal AMPK activity, while higher levels were detected in TamRLT cells which were less growth-sensitive to metformin. The oestrogen-deprived resistant models thus may have decreased capacity to compensate for the energy crisis promoted by metformin, and interestingly in clinical breast cancer reduced AMPK phosphorylation has also been reported in biopsies from breast tumours with evidence of disease progression (i.e. high histological grade and associated axillary node metastasis) as compared to normal tissue (Hadad et al. 2009).The findings are complemented by studies from Algire et al. (2011) who reported higher sensitivity in colon cancer cells to metformin as a consequence of a downregulated LKB1-AMPK pathway. Signalling studies in this chapter revealed that complex I blockade with metformin was able to promote AMPK activity in the oestrogen deprived resistant models, and after 12hrs such treatment had reduced their protein and fatty acid anabolic regulatory pathways, as monitored by p-p70S6K in the mTOR pathway and p-ACC respectively. Inhibition of such pathways has been implicated as an important contributor to the anti-tumour effects of metformin (Hadad et al. 2008). Fulvestrant resistant models were the next most sensitive to the growth inhibitory effect of metformin, and in these models AMPK activation as well as inhibition of the pathways underpinning fatty acid and protein synthesis again occurred with such treatment (from 12 hrs). Microarrays revealed there was increased expression of elements in the glycerophosphate shuttle in the fulvestrant resistant cells, where this shuttle may feed OxPhos via complex II and so help bypass the metformin inhibitory mechanism (potentially evidenced by their reduced COX sensitivity to metformin). Such expression may perhaps account for their slightly reduced growth-sensitivity to metformin treatment as compared to the oestrogen deprived resistant models. The growth studies with this inhibitor in total re-enforce the concept that complex I-driven OxPhos is of particular importance to oestrogen deprived and fulvestrant resistant cells, and although the signalling studies revealed a substantial inhibitory impact on anabolic pathways in such models it seems probable that these events were unable to overcome the energy crisis instigated following targeting of critical complex I-driven OxPhos by metformin, so adversely impacting on growth (Zakikhani et al. 2006).

Tamoxifen resistant cells were the least growth-sensitive of the endocrine resistant models to metformin, as was their NADH dehydrogenase activity and oxygen consumption, inferring some diminished dependency on complex I-driven OxPhos as compared with other resistant lines in

the panel. TamRLT also only showed a 15% reduction in Ki67 proliferative capacity after metformin. Berstein et al. 2010 have similarly shown that a further tamoxifen resistant cell line was less sensitive to the growth inhibitory effect of metformin treatment compared with a long-term oestrogen deprived model (LTED). In TamR and TamRLT cells, AMPK activation occurred with such treatment (after 12hrs and 2 hrs respectively) and there was also reduction in p-70S6K by 24 hrs. However, no sustained impact on fatty acid regulation was observed by this time, contrasting the fulvestrant and oestrogen deprived resistant lines. This implies that there may be less of an adverse impact of complex I-driven OxPhos blockade on energy balance in tamoxifen resistant cells. In this regard, increased basal ECA and its reduction by 2-DG treatment in TamRLT, as well as some 2-DG growth impact in this model, evidences glycolysis can provide an alternative source of ATP in this model. The somewhat reduced sensitivity of MCF7 to the growth inhibitory effects of metformin suggested that complex I-driven OxPhos may not be as critical to energy supply in these endocrine sensitive cells as compared with oestrogen deprived and fulvestrant resistant lines, This was further re-enforced by an absence of p-AMPK induction with metformin, at least over the examined dose range and time course, and its apparent lack of inhibitory impact on one of the anabolic pathways (fatty acid synthesis). While, glycolysis might remain the main energy producing pathway during metformin treatment to maintain growth of MCF7 cells. Furthermore, the apparent decrease in protein synthesis (implied by reduced p-P70S6K) after 12hrs metformin treatment seemed independent of an obvious AMPK impact, implying mechanisms other than those mediated by complex I can be targeted by metformin upstream of, or within, the mTOR signalling pathway to influence growth. “Uncoupling” of the inhibitory impact on anabolic pathways and p-AMPK induction that was also apparent at some time points in the resistant lines perhaps further evidenced alternative metformin mechanisms. A study by Hadada et al. (2014), increased AMPK and reduced fatty acid synthesis was reported in MCF7 cells after 2hrs metformin treatment. However, DMEM was used as the basal growth media in this study (normoglycemic condition). In contrast, hyperglycemic condition (RPMI 1640) which used in this thesis might be the reason for lack of AMPK induction in MCF7. Moreover, alternative compensatory mechanism such as glycolysis acts to maintain some cell growth after exposure to metformin treatment for 7days in both MCF7 cells and the tamoxifen resistant lines (Zhuang et al. 2014).

As described above from the gene expression profiles, there may be further contributory mechanisms underpinning metformin’s differential growth inhibitory impact across the panel, for example involving drug transporters (e.g. increased metformin efflux via MATE1 in tamoxifen resistant models (Pernicova et al. 2014), the effect of MMP on metformin accumulation and

thereby reversible inhibition of complex I activity (Bridges et al. 2014; Wheaton et al., 2014), alternative shuttles (e.g. induced electron entry at complex II via the glycerophosphate shuttle in fulvestrant resistant and alternative substrate provision (e.g. from β-oxidation of fatty acids) could all feasibly play a part. Furthermore, it is apparent that the metformin concentration range used for such in vitro cancer studies is somewhat higher than used for in vivo studies (max 2000mg/day). Increased metformin may be required in vitro because of the high glucose level invariably found in cell culture media (in this instance, glucose in RPMI 1640 media was 11.11mM, with extra glucose from added serum). Menendez et al. (2012) showed that increased breast cancer cell death could be achieved by metformin treatment under conditions of glucose deprivation. In turn, study on colon cancer cells by Wheaton et al (2014) suggested reduced cell growth after metformin treatment in the presence of a high glucose concentration in culture media, but cell death under glucose-deprived conditions. Zhuang et al. (2014) also revealed improved sensitivity to metformin treatment by lowering the glucose level to physiological concentrations (5-7mM), with reduced 4EBP1 and mTOR phosphorylation observed after metformin treatment independent of AMPK activation under low glucose conditions. Therefore, supraphysiological glucose concentration may also account for inconsistency of signalling events across the resistant panel after metformin treatment. This may also explain why anti-proliferative effects at 7 days in the model panel measured by Ki-67 staining were in general only minor. It is interesting that efficacy of metformin treatment on breast cancer proliferation (Ki-67 staining) has been successfully studied in non-diabetic women with operable invasive breast cancer. Patients received metformin prior to surgery (500-2000mg/d) and such treatment reduced Ki-67 in the post-treatment surgical specimen (Hadad et al. 2011). Furthermore, the effect of metformin as a neoadjuvant treatment (window of opportunity; 500-1500mg/d) was studied by Niraula et al. (2012) in newly diagnosed, untreated, early stage breast cancer patients where patients with fasting glucose ≥7 mmol/L were ineligible for this study. Significant reduction of Ki-67 was observed in tumours after metformin treatment.

Anti-proliferative activity of metformin (850-1700mg/d) was also examined in a window-of-opportunity study in non-diabetic breast cancer patients. Ki-67 was not significantly changed overall in tumour samples as compared to matched untreated controls; however, differential effects on Ki67 were observed based on insulin resistance status (HOMA index) in the post-surgical specimens. It was reduced non-significantly in the insulin resistant patient cohort (HOMA>2.8) and increased non-significantly in patients with HOMA<2.8 (Bonanni 2012). A further window of opportunity trial studied non-diabetic patients who received pre-surgical metformin (850mg/d) and these again showed no significant changes in tumour proliferation.

However, differential effect on Ki-67 expression was observed based on insulin resistance status (HOMA index) in post-surgical specimen. Reduced Ki-67 was observed in the insulin resistant, overweight patients (HOMA>2.8, BMI≥27kg/m^{-2}) whereas increased Ki-67 was detected in patients with HOMA<2.8, BMI≤27kg/m^{-2} (Cazzaniga 2013). Metformin (850-1700mg/d) in non-diabetic breast cancer patients has also been examined in a phase II placebo-controlled trial by DeCensi et al. (2014). Compared to placebo, metformin reduced Ki-67 in insulin resistant (HOMA index>2.8) or HER2+ tumours. Moreover, association of higher serum drug level with reduced Ki-67 was observed in women with HOMA index>2.8 (insulin resistant) but no effect was determined in women with HOMA<2.8.

In conclusion, the induced mitochondrial biogenesis and bioenergetics detected in these acquired endocrine resistant models build further on studies from the Lisanti's group (including studies by Bonuccelli et al. (2010) and Whitaker-Menezes et al. (2011) in clinical breast cancer epithelium), since the models have revealed there is an intrinsic capacity for all endocrine treatments to ultimately promote increased OxPhos in breast cancer cells. The chapter has shown endocrine resistant breast cancer cells use two carbon sources (glucose and glutamine) towards this increased oxidative respiration, with evidence suggesting enhanced glycolytic and glutaminolytic activity in endocrine resistant versus responsive cells. Targeting OxPhos via AA and metformin respectively demonstrates differential dependency of the resistant breast cancer cells on complex I (oestrogen deprived models), complex III (tamoxifen resistant models) or both complexes (fulvestrant resistant models) for their increased respiration. AA was also more potent in acquired resistant cells with evidence of ER loss (i.e. TamRLT, FasR and FasRLT). However, as there was a more prominent direct mechanism for metformin (i.e. AMPK activation and inhibition of multiple anabolic pathways) in ER+ oestrogen deprived and ER- fulvestrant resistant models, metformin appeared effective in endocrine resistant cells regardless of ER status. This observation is compatible with results from a study by Zhuang et al. (2008) examining effect of metformin treatment in further breast cancer cells.

Importantly, therefore, clinic trials are examining metformin in early breast cancer, including alongside endocrine agents (for example, the METEOR trial in the neoadjuvant setting with the aromatase inhibitor letrozole (Kim et al. 2014)). Others are exploring whether metformin can modulate hormonal response in advanced disease. Indeed, there may also be unperceived benefits to such metformin use: for example, Brown et al. (2010) have revealed inhibitory effects of this treatment on aromatase enzyme expression in breast stromal adipose cells (via AMPK activation). Encouragingly, exemestane (25mg/d) in combination with metformin (2000mg/d) in non-diabetic obese postmenopausal women who had previously had chemotherapy and

endocrine therapy appeared well tolerated (Esteva et al. 2013). The NCIC CTG MA.32 clinical trial enrolled 3582 breast cancer patients to examine metformin efficacy (for 5years) after complete resection in addition to standard chemotherapy/radiotherapy completion and endocrine treatment. This trial suggests metformin (1700mg/d) as compared to placebo improves survival in endocrine-treated breast cancer patients (Goodwin et al. 2011). Kim et al. have also recently reported that metformin improves survival of diabetic breast cancer patients when used alongside chemotherapy and endocrine treatment (Kim et al., 2015). Therefore, repurposing metformin has potential to improve survival in breast cancer, particularly under conditions where there are gains in the mitochondrial energy pathway promoted in endocrine resistance.

Chapter 5

Identification of deregulated kinases and associated genes in endocrine resistant breast cancer cells

5.1 Introduction

Protein kinases mediate many important cellular processes including cell cycle and proliferation, gene transcription, metabolism, cell survival and apoptosis, and differentiation (Bononi et al. 2011). Furthermore, deregulated kinases play an important role in cancer progression (Blume-Jensen & Hunter, 2001) and thus many drugs have been developed to inhibit the activity of protein kinases in cancer cells (Cohen et al. 2002). The human kinome comprises 518 genes and includes enzymes that drive protein phosphorylation and diverse signal transduction pathways (Manning et al. 2002). Protein kinases can be divided into two categories: receptor protein kinases and non-receptor protein kinases. Receptor kinases are transmembrane proteins with a cytoplasmic catalytic domain and an extracellular ligand binding domain. Non-receptor protein kinases are soluble proteins in the cytoplasm. Protein kinases can be further classified based on their phosphorylating their target proteins at either the serine/threonine residue (serine/threonine kinases) or tyrosine residue (tyrosine kinases) (Manning et al. 2002).

Protein kinases have attracted considerable attention as therapeutic targets to inhibit growth of breast cancer cells. In ER+ breast tumours, increased expression of the membrane receptor kinases EGFR and HER2 has been associated with development of resistance to endocrine treatment (Meha et al. 2014). Targeting EGFR (e.g. via gefitinib) and HER2 (e.g. via trastuzumab) or inhibiting downstream kinase cascades (including PI3K/AKT/mTOR) alongside endocrine therapy has improved progression free survival in some clinical trials (Osborne et al. 2011, Kaufman et al. 2009 and Baselga et al. 2012) Unfortunately, however, resistance again develops (Ferrer-Soler et al. 2007, Yardley et al. 2013), and so continued discovery of new, improved targets remains essential to better treat endocrine resistance and improve overall survival.

In this regard, identification of new kinases potentially relevant to multiple endocrine resistant states comprises an important goal. This chapter aims to exploit the gene microarray resource prepared for the panel of endocrine resistant cells (versus MCF7) as a new tool to discover shared induced kinases. Since resistance can involve activation of several signalling pathways (Viedma-Rodriguez et al. 2014). The Chapter will interrogate the genes in publically-available clinical breast cancer resources (using KMplotter; in ER+ disease and tamoxifen treated patients) and will investigate their associated ontological information using the DAVID bioinformatics and Innatedb online databases. Attempts will also be made to verify the

expression profile of promising identified elements via RT-PCR. This in total will ascertain whether the identified genes contribute to multiple endocrine resistant states, and so might ultimately yield new therapeutic approaches for resistance.

5.2 Results

5.2.1 Identification of shared induced kinases in the endocrine resistant cells

A list of shared induced genes across the resistant models versus MCF7 (n=572) was interrogated for protein kinases by comparison with the Human kinome list (518 genes: Manning et al. 2002; www.kinase.com/human/kinome). While there was some differential expression in individual lines, 14 kinases (PCK2, MARK1, PRKAA2, XYLB, ALDH18A1, PFKFB2, ICK, PRKD3, ADCK3, VRK3, COASY, RIOK1, STK35 and TEC) were significantly induced (≥1.2 fold changes, $p \leq 0.05$) in all endocrine resistant models versus MCF7 cells (Fig 5.1, Table 5.1).

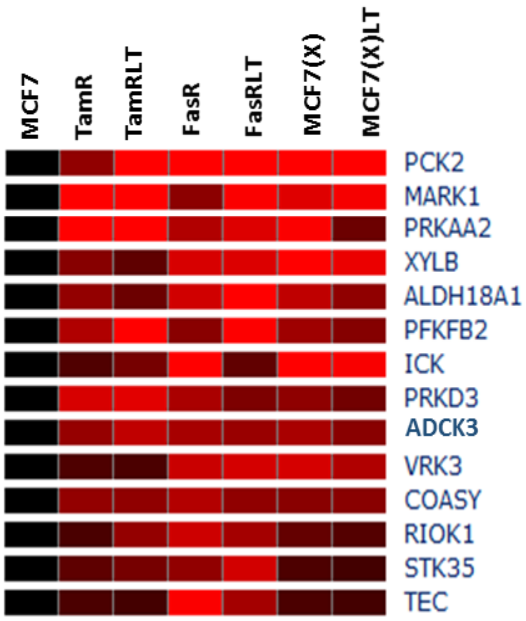

Fig 5.1. Heatmap displays 14 shared and significantly induced kinase genes (≥1.2 fold changes) in endocrine resistant models. Expression of these genes in resistant models vs. MCF7 was statistically tested using ANOVA with *Benjamini and Hochberg post hoc* correction ($p \leq 0.05$).

Gene symbols	TamR	TamRLT	FasR	FasRLT	MCF7(X)	MCF7(X)LT
PCK2	1.48	3.5	2.98	4.22	5	5.89
MARK1	2.52	5.46	1.46	1.98	1.84	1.95
PRKAA2	2.18	3.20	1.62	1.83	1.98	1.34
XYLB	1.45	1.30	1.80	1.82	2	1.90
ALDH18A1	1.49	1.34	1.76	2.59	1.68	1.48
PFKFB2	1.62	2.19	1.45	1.99	1.54	1.44
ICK	1.24	1.38	2.17	1.30	2.28	1.97
PRKD3	1.80	1.85	1.59	1.41	1.48	1.36
ADCK3	1.51	1.69	1.58	1.52	1.59	1.45
VRK3	1.24	1.23	1.73	1.78	1.79	1.61
COASY	1.49	1.48	1.63	1.48	1.45	1.45
RIOK1	1.22	1.50	1.75	1.56	1.32	1.26
STK35	1.29	1.38	1.49	1.77	1.23	1.20
TEC	1.23	1.21	1.98	1.56	1.23	1.21

Table 5.1. Fold changes of the shared induced kinases in resistant models vs. MCF7 (all ≥1.2 fold).

5.2.2 Ontology analysis of shared induced kinases (n=14) identified from the endocrine resistant breast cancer cells

Gene microarray probe IDs of induced kinase genes were converted to ENSEMBL gene IDs and then analysed for ontology in the Innatedb database. Not surprisingly given that kinases had been specifically selected for in the project, the most significant known molecular function for the induced kinases was ATP binding (*p*=5.62E-11) followed by transferring phosphorus containing groups for 9 of the kinases (ADCK3, ICK, MARK1, PRKAA2, PRKD3, RIOK1, STK35, TEC and VRK3, *p*=4.19E-09), and then protein kinase activity for 8 (ICK, MARK1, PRKAA2, PRKD3, RIOK1, STK35, TEC and VRK3, *p*=7.30E-08) (Table 5.2). This analysis also revealed that 6 had known serine/threonine kinase activity, while 6 had tyrosine kinase activity (with some overlapping: ICK, MARK1, PRKAA2 and STK35). The most significant biological process for the induced shared kinases was protein phosphorylation (ADCK3, ICK, MARK1, PRKAA2, PRKD3, RIOK1, STK35, TEC and VRK3, *p*=9.5E-09), followed by phosphorylation (ALDH18A1, COASY, PCK2 and XYLB, *p*=1.29E-04) and also carbohydrate phosphorylation (PFKFB2 & XYLB, *p*=0.002671) (Table 5.3). Several of the kinases were also implicated in signal transduction (e.g. ICK, MARK1, PRKD3 and TEC; Table 5.3).

GO term name (Molecular –Function)	GO term p-value (corrected)	Gene Symbols
ATP binding	5.62E-11	ADCK3; ALDH18A1; COASY; ICK; MARK1; PFKFB2; PRKAA2; PRKD3; RIOK1; STK35; TEC; VRK3; XYLB;
transferase activity, transferring phosphorus-containing groups	4.19E-09	ADCK3; ICK; MARK1; PRKAA2; PRKD3; RIOK1; STK35; TEC; VRK3;
protein kinase activity	7.30E-08	ICK; MARK1; PRKAA2; PRKD3; RIOK1; STK35; TEC; VRK3;
protein serine/threonine kinase activity	7.46E-06	ADCK3; ICK; MARK1; PRKAA2; RIOK1; STK35;
protein tyrosine kinase activity	2.32E-05	ICK; MARK1; PRKAA2; PRKD3; STK35; TEC;
glutamate 5-kinase activity	0.006794	ALDH18A1;
glutamate-5-semialdehyde dehydrogenase activity	0.006794	ALDH18A1;
pantetheine-phosphate adenylyltransferase activity	0.006794	COASY;
xylulokinase activity	0.006794	XYLB;
[acetyl-CoA carboxylase] kinase activity	0.010039	PRKAA2;
[hydroxymethylglutaryl-CoA reductase (NADPH)] kinase activity	0.010039	PRKAA2;
phosphoenolpyruvate carboxykinase (GTP) activity	0.010039	PCK2;
phosphoenolpyruvate carboxykinase activity	0.010039	PCK2;
phosphotransferase activity, alcohol group as acceptor	0.012213	PRKD3; XYLB;
6-phosphofructo-2-kinase activity	0.014785	PFKFB2;
fructose-2,6-bisphosphate 2-phosphatase activity	0.014785	PFKFB2;
histone serine kinase activity	0.014785	PRKAA2;
dephospho-CoA kinase activity	0.014886	COASY;
kinase activity	0.016204	PCK2; XYLB;
AMP-activated protein kinase activity	0.016806	PRKAA2;
phosphatidic acid binding	0.016806	MARK1;
purine nucleotide binding	0.016806	PCK2;
tau-protein kinase activity	0.022628	MARK1;
magnesium ion binding	0.023339	ICK; MARK1;
catalytic activity	0.025475	ALDH18A1; COASY; RIOK1;
protein kinase C activity	0.026113	PRKD3;
phosphatidylserine binding	0.034071	MARK1;
protein serine/threonine/tyrosine kinase activity	0.044199	PRKAA2;
cyclin-dependent protein serine/threonine kinase activity	0.046844	ICK;

Table 5.2. Molecular function of shared induced kinases across the resistant models obtained using Innatedb database interrogation (the p value was generated after hypergeometric statistical analysis for significant molecular function).

GO term name (Biological-Process)	GO term p-value (corrected)	Gene Symbols
protein phosphorylation	9.50E-09	ADCK3; ICK; MARK1; PRKAA2; PRKD3; RIOK1; STK35; TEC; VRK3;
phosphorylation	1.29E-04	ALDH18A1; COASY; PCK2; XYLB;
carbohydrate phosphorylation	0.002671	PFKFB2; XYLB;
pyruvate metabolic process	0.003288	PCK2; PFKFB2;
intracellular signal transduction	0.003895	ICK; MARK1; PRKD3; TEC;
positive regulation of insulin secretion	0.005648	PCK2; PFKFB2;
ornithine biosynthetic process	0.006794	ALDH18A1;
xylulose catabolic process	0.006794	XYLB;
D-xylose metabolic process	0.010039	XYLB;
xylulose metabolic process	0.010039	XYLB;
NADH oxidation	0.013316	PCK2;
citrulline biosynthetic process	0.013316	ALDH18A1;
glucose metabolic process	0.014659	PCK2; PFKFB2;
L-proline biosynthetic process	0.014785	ALDH18A1;
fructose 2,6-bisphosphate metabolic process	0.014785	PFKFB2;
positive regulation of glucokinase activity	0.014785	PFKFB2;
glucose catabolic process	0.014886	PFKFB2;
histone-serine phosphorylation	0.014886	PRKAA2;
lactate metabolic process	0.014886	PFKFB2;
regulation of platelet activation	0.014886	TEC;
carbohydrate metabolic process	0.016241	PCK2; PFKFB2; XYLB;
coenzyme biosynthetic process	0.016469	COASY;
small molecule metabolic process	0.0165	ALDH18A1; COASY; PCK2; PFKFB2; PRKAA2;
proline biosynthetic process	0.016806	ALDH18A1;
regulation of energy homeostasis	0.016806	PRKAA2;
regulation of fatty acid biosynthetic process	0.016806	PRKAA2;
carnitine shuttle	0.020321	PRKAA2;
cellular response to nutrient levels	0.020321	PRKAA2;
cullin deneddylation	0.020321	COPS6;
fructose metabolic process	0.021719	PFKFB2;
Wnt signaling pathway	0.021818	MARK1; PRKAA2;
coenzyme A biosynthetic process	0.021823	COASY;
fatty acid homeostasis	0.021823	PRKAA2;
oxaloacetate metabolic process	0.021823	PCK2;

Table 5.3 Continue …

GO term name (Biological-Process)	GO term p-value (corrected)	Gene Symbols
positive regulation of phosphoprotein phosphatase activity	0.021823	VRK3;
ubiquinone biosynthetic process	0.021823	ADCK3;
pantothenate metabolic process	0.022628	COASY;
positive regulation of glycolytic process	0.02411	PRKAA2;
glutamate metabolic process	0.024757	ALDH18A1;
lipid biosynthetic process	0.024757	PRKAA2;
cell death	0.026333	ADCK3; COASY;
cellular response to glucose starvation	0.028704	PRKAA2;
tissue regeneration	0.029941	TEC;
cellular amino acid biosynthetic process	0.031141	ALDH18A1;
negative regulation of TOR signaling	0.032306	PRKAA2;
positive regulation of autophagy	0.034071	PRKAA2;
B cell receptor signaling pathway	0.045105	TEC;
negative regulation of ERK1 and ERK2 cascade	0.045986	VRK3;
rhythmic process	0.047678	PRKAA2;
cholesterol biosynthetic process	0.048491	PRKAA2;
regulation of circadian rhythm	0.048682	PRKAA2;

Table 5.3 Biological processes for the shared induced kinases across the resistant models obtained using the Innatedb database (p value was generated after hypergeometric statistical analysis for significant biological processes).

5.2.3 Relation to outcome of ER+ and tamoxifen treated breast cancer patients in publicly-available datasets and ontology studies of the induced kinases

The induced kinases from the resistant models were studied for their mRNA expression association with relapse free survival (RFS) in both the tamoxifen treated and all ER+ breast cancer patient cohorts using KMPlotter (Table 5.4). Since the probe ID for some kinases was only available on the HGU133 plus 2.0 array platform, patient number could differ (tamoxifen treated: 111 and ER+: 695 patients) compared with the remainder of the induced kinases that were represented on the HGU133A platform in KMplotter (tamoxifen treated: 712 and ER+: 1802 patients). Associations of the induced kinases with cellular pathways and also identification of possible substrates for their enzyme activity were then determined using the KEGG database (Table 5.4), although some kinases such as ADCK3, VRK3, MARK1, STK35 and ICK were not indicated as participating in any particular pathway.

Unfortunately, several of the kinases failed to show a significant relation with adverse clinical outcome in the breast cancer datasets examined, although some had interesting ontology implying they may feasibly contribute to regulation of growth and aggressiveness of the resistant models in vitro. For example, MARK1 (MAP/microtubule affinity-regulating kinase 1) is reported to be a serine/threonine-protein kinase implicated in neural migration that can regulate cell polarity and microtubule dynamics. There was also expression deregulation of PRKAA2 in the models, which encodes one of several subunits of AMPK and is involved in pathways including AMPK-mTOR (Table 5.4). Two kinases showed significant adverse associations with outcome in the clinical breast cancer datasets (Table 5.4): STK35 in the ER+ ($p=0.00042$) and tamoxifen treated cohorts ($p=0.014$), and COASY in ER+ patients only ($p=0.042$). While STK35 (serine/threonine kinase 35) is as yet only a very poorly-described kinase, COASY (Coenzyme A synthase) is reported to catalyse the two last steps of CoA synthesis from its substrate pantothenic acid (vitamin B5; Table 5.4) by dephospho-CoA kinase activity and so may contribute to fatty acid biosynthesis and further metabolic pathways.

5.2.3.1 Shared induced metabolic pathway kinases

Based on this ontological analysis, three further kinases PCK2, ALDH18A1 and PFKFB2 were associated with metabolic pathways. PCK2 (phosphoenolpyruvate carboxykinase 2) catalyses conversion of substrates oxaloacetate with GTP (Table 5.4) to phosphoenolpyruvate. As detailed in Chapter 4 (4.2.2). Its mRNA expression significantly related to shortened RFS in ER+ clinical disease and tamoxifen treated patients (Table 5.4).

ALDH18A1 (Aldehyde Dehydrogenase 18 Family, Member A1) gene encodes a mitochondrial enzyme catalyses reduction of its substrate glutamate to delta1-pyrroline-5-carboxylate as a key step during de novo biosynthesis of amino acids proline, ornithine and arginine (Table 5.4).

ATP + L-glutamate → ADP + L-glutamate 5-phosphate

It seems likely that induced glutamine uptake in resistant models (via SLC1A5 and SLC7A5, Chapter 4) will supply the substrate for ALDH18A1 activity. Higher expression of ALDH18A1 was significantly associated with shortened relapse free survival and increased risk of relapse in the tamoxifen treated ER+ cohort ($n=111$ patients, $HR=4.58$, $P=0.0017$). There was also significance in all ER+ ($n=695$ patients, $HR=1.53$, $P=0.016$) breast cancer patients, although this adverse association seemed only apparent over the first 120 months when examining the associated Kaplan Meier survival curves (Table 5.4; Figure 5.2).

Finally, the PFKFB2 (6-Phosphofructo-2-Kinase/Fructose-2,6-Biphosphatase 2) gene encodes a cytosolic protein which is involved in both the synthesis and degradation of its substrate

fructose-2,6-bisphosphate (Table 5.4). PFKFB2 has 6-phosphofructo-2-kinase activity that catalyses the synthesis of fructose-2,6-bisphosphate, and also fructose-2,6-biphosphatase activity that catalyses the degradation of fructose-2,6-bisphosphate. Therefore, it regulates levels of fructose-2,6-bisphosphate in the cell.

ATP + beta-D-fructose 6-phosphate → ADP + beta-D-fructose 2,6-bisphosphate

This generates fructose which contributes to amino sugar and nucleotide sugar metabolism. In turn, the reverse reaction of PFKFB2 can generate fructose-6-phosphate which is involved in the glycolysis pathway. Therefore, induced expression of this enzyme might again be able to contribute to growth of the endocrine resistant cancer cells, regulating their elevated glycolytic capacity or amino sugar and nucleotide sugar metabolism (Chapter 4). Although hazard ratios were >1 suggesting an adverse association, this gene was not significantly related to RFS in either clinical sample cohort in KMPlotter (Table 5.4, Figure 5.2). Hence, PFKFB2 deregulation may be specific to acquired rather than intrinsic endocrine resistance.

Gene symbols	RFS, Tamoxifen treated N=712 (Kmplotter.com)	RFS, ER+ N=1802 (Kmplotter.com)	Pathways (KEGG database)	Substrates (KEGG)
PCK2	HR=1.59, P=0.007	HR=1.46, P=2.5E-05	Gluconeogenesis, pyruvate metabolism & TCA cycle	GTP & OAA
MARK1	HR=0.49, P=0.15 (n=111)	HR=1.32 ,P=0.085 (n=695)		ATP & protein
PRKAA2	HR=2.06 ,P=0.13 (n=111)	HR=0.85 ,P=0.32 (n=695)	FoxO signaling pathway, Regulation of autophagy, mTOR signaling pathway, PI3K-Akt signaling pathway, AMPK signaling pathway, Insulin signaling pathway, Adipocytokine signaling pathway	ATP & protein
XYLB	HR=0.88 ,P=0.4	HR=0.84 ,P=0.045	Pentose and glucuronate interconversions	ATP & xylulose
ALDH18A1	HR=4.58 ,P=0.0017 (n=111)	HR=1.53 ,P=0.016 (n=695)	Arginine and proline metabolism	ATP & L-glutamate
PFKFB2	HR=1.64 ,P=0.3 (n=111)	HR=1.21 ,P=0.26 (n=695)	Fructose and mannose metabolism	ATP & beta-D-fructose 6-phosphate
ICK	HR=0.73, P=0.086	HR=0.88, P=0.19	———	———
PRKD3	HR=0.78, P=0.12	HR=0.89, P=0.19	Rap1 signaling pathway, Aldosterone synthesis and secretion	ATP & protein
ADCK3	HR=2.05, P=0.14	HR=1.27, P=0.13	———	———
VRK3	HR=1.28, P=0.11	HR=1.18, P=0.09	———	———
COASY	HR=1.23, P=0.17	HR=1.2, P=0.042	COASY Pantothenate and CoA biosynthesis	ATP & pantetheine 4'-phosphate
RIOK1	HR= 2, P=0.22 (n=111)	HR=1.33, P=0.072 (n=695)	Ribosome biogenesis in eukaryotes	ATP & protein
STK35	HR=3.73, P=0.014 (n=111)	HR=1.95, P=0.00042 (n=695)	———	ATP & protein
TEC	HR=0.7, P=0.058	HR=0.87, P=0.11	Osteoclast differentiation, T cell receptor signaling pathway	ATP & [protein]-L-tyrosine

Table 5.4. Summary of Relapse Free Survival (RFS) analysis using KMplotter for the induced kinase genes in tamoxifen treated ER+ and all ER+ breast cancer patient cohorts. A Hazard ratio (HR) >1 is associated with increased risk of relapse & logrank *P* ≤0.05 was considered to be significant. Any associated pathways and substrates for the induced kinases were also discovered using the KEGG database.

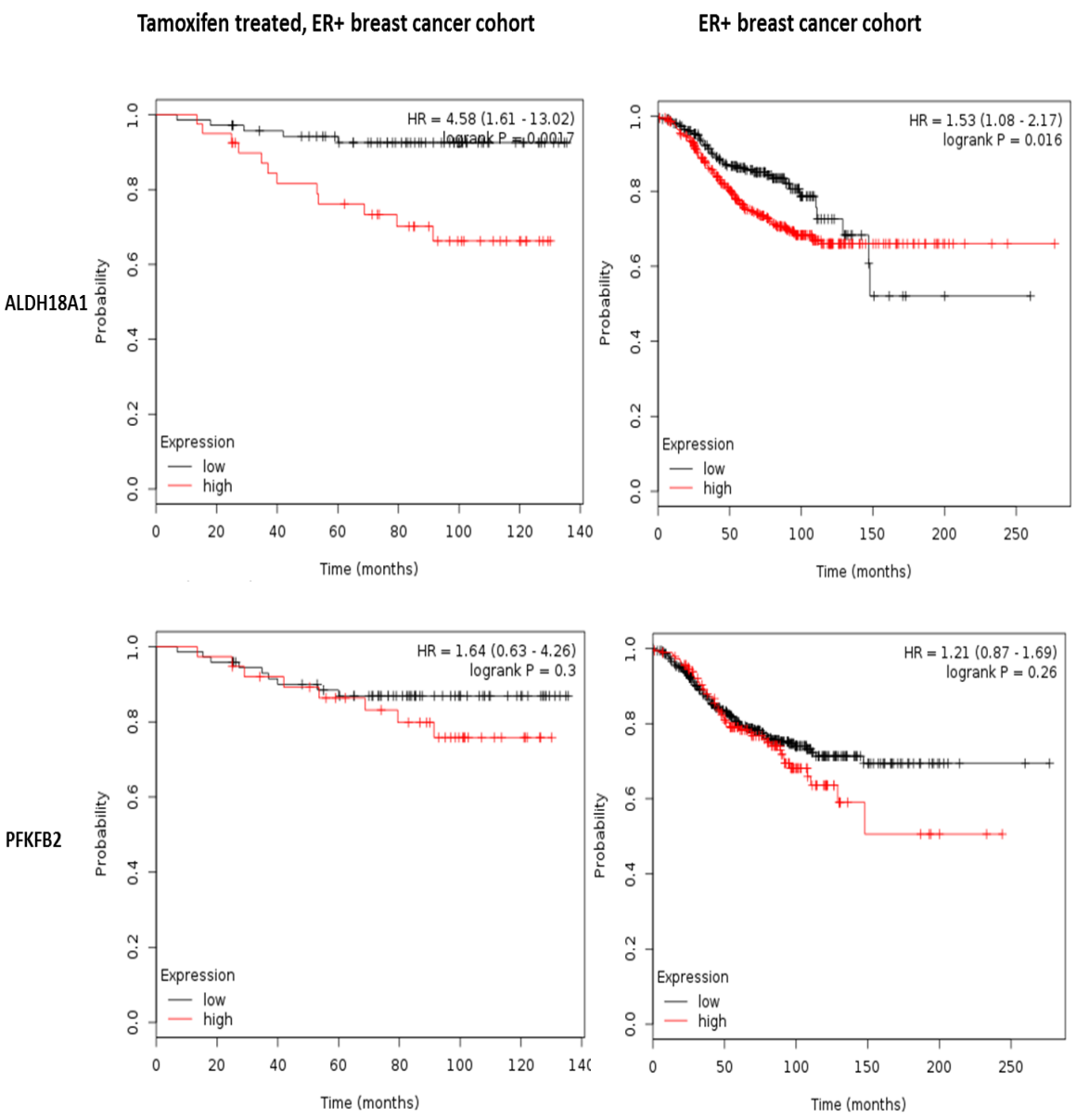

Fig 5.2. Kaplan Meier survival curves generated using KM plotter showing higher ALDH18A1 mRNA expression was significantly associated with relapse free survival in both tamoxifen treated ER+ (left graph) and all ER+ patient cohorts (right graph). No significant associations were obtained for the further kinase gene PFKFB2.

5.2.4 mRNA expression of shared induced genes PCK2, ALDH18A1 and PFKFB2 in the panel of endocrine resistant models using RT-PCR

Based on their shared induced profile, metabolic pathway kinase ontology and in some instances association of higher levels of the kinases with shortened RFS using the virtual clinical datasets, mRNA expression of ALDH18A1, PCK2 and PFKFB2 were prioritised for verification across the model panel via RT-PCR.

PCK2 expression was significantly increased in TamRLT (p<0.05), FasRLT (p<0.001), MCF7(X) (p<0.001) and MCF7(X)LT (p<0.001) cells by 1.70, 1.97, 2.17 and 2.24 fold as compared to MCF7 respectively, PCK2 expression was also modestly induced in FasR by 1.4 fold as compared to MCF7 cells (Fig 5.3). It was maintained at the MCF7 expression level in TamR cells (which also showed the lowest expression change on the microarrays for this gene, Fig 5.1, Table 5.1)

ALDH18A1 expression was significantly induced in FasR (p<0.05), FasRLT (p<0.001) and MCF7(X) (p<0.05) by 1.35, 1.54 and 1.32 fold as compared to MCF7 cells. The expression of this gene was also modestly increased in TamR, TamRLT and MCF7(X)LT by 1.2 fold as compared to MCF7 cells but these increases did not reach significance (Fig 5.3). Lower fold changes were also recorded in these three models on the arrays (Fig 5.1, Table 5.1)

PFKFB2 expression was significantly induced in TamR (p<0.01), TamRLT (p<0.001), FasRLT (p<0.001), MCF7(X) (p<0.01) and MCF7(X)LT cells (p<0.05) by 1.87, 2.20, 2, 1.78, 1.65 fold as compared to MCF7 respectively. Expression of this gene was modestly increased by 1.25 fold in FasR as compared to MCF7 cells but this did not reach significance (Fig 5.3). Expression increases were also seen on the arrays in all models (Fig 5.1, Table 5.1).

In general, the RT-PCR profile verified the microarray expression profile of the kinases (PCK2, ALDH18A1 and PFKFB2) across the panel (Fig 5.3), with some increased expression detected in most resistant models.

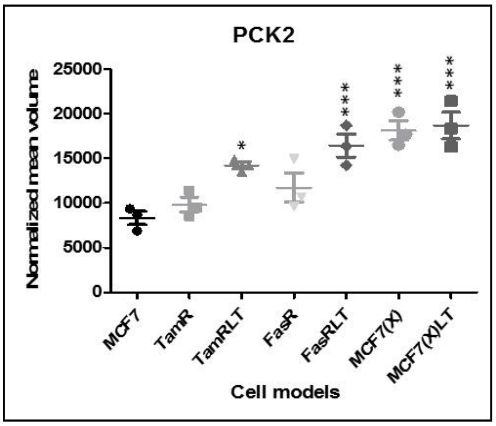

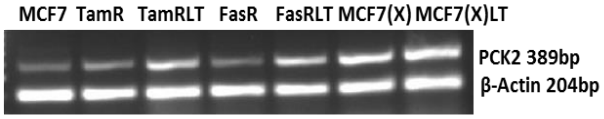

Fold change	TamR	TamRLT	FasR	FasRLT	MCF7(X)	MCF7(X)LT
MCF7	1.18	1.70	1.41	1.97	2.17	2.24

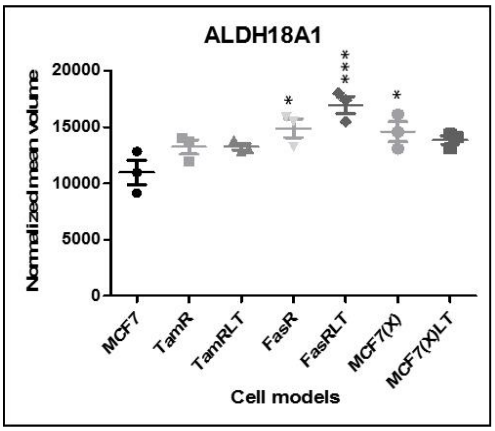

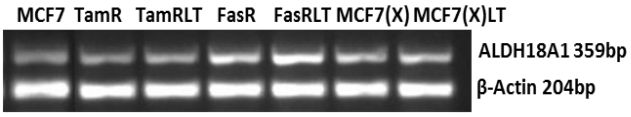

Fold change	TamR	TamRLT	FasR	FasRLT	MCF7(X)	MCF7(X)LT
MCF7	1.20	1.20	1.35	1.54	1.32	1.26

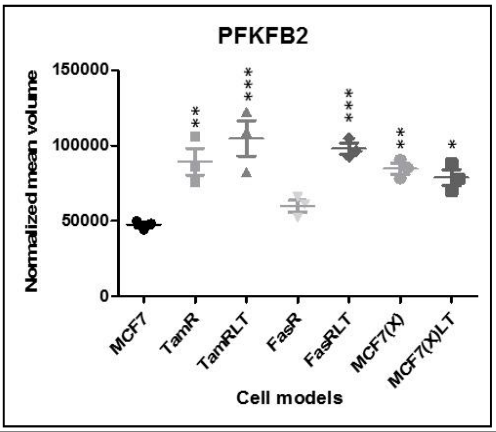

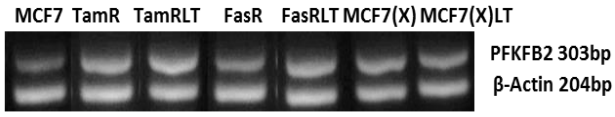

Fold change	TamR	TamRLT	FasR	FasRLT	MCF7(X)	MCF7(X)LT
MCF7	1.87	2.20	1.25	2.06	1.78	1.65

Fig 5.3. Representative gels following RT-PCR and graphs display actin-normalized mean volume of PCK2, ALDH18A1 and PFKFB2 for the model panel (comprising the mean of three independent experiments, +/-SEM for each cell line). Statistical analysis (using ANOVA with Dunnett *post hoc* correction) was performed to compare gene expression in each model vs. MCF7 (* $p<0.05$, ** $p<0.01$ &*** $p<0.001$). Mean fold change in gene expression for each resistant model vs. MCF7

5.2.5 Shared induced SLC39A transporter and metallothionein genes in resistant models

Zinc (Zn) acts as an antioxidant and protects cells from mechanisms which are involved in oxidative stress, and so the antioxidant activity of Zn can maintain genomic stability by reducing reactive oxygen species (ROS) in the cell (Eide et al. 2011). Zn flux is controlled by two Zn transporter families. The SLC30 family transport Zn either out of the cytosol or into the cellular organelles. In contrast the SLC39 family transport Zn either into the cytosol or out of the cellular organelles (Lichten and Cousins 2009). Induced metallothioneins (MTs) expression in response to Zn administration was reported in astrocytes to protect cells against cytotoxicity (Aschner et al. 1998). MTs expression was detected in proliferative epithelial cells of breast tumours (Cherian et al. 2003).

There is emerging evidence for deregulation of Zn in breast cancer. A study by Tinoco-Veras et al. (2011) showed there is a lower Zn level in erythrocytes of breast cancer patients as compared to healthy premenopausal women, with no significant difference observed in plasma Zn level in both groups. However, a study by Cui et al. (2007) found an association between high Zn levels within benign breast tissue and modest increase in risk of subsequent breast cancer (with Zn measured using X-ray fluorescence spectroscopy). MT expression has also been detected in proliferative epithelial cells of breast tumours (Cherian et al. 2003). Furthermore, Zn has previously been shown to activate the receptor tyrosine kinases EGFR and IGF-1R in the TamR cell line that has been used in this thesis. The mechanism was dependent in the TamR model on increased levels of a Zn influx transporter, SLC39A7 (Taylor et al 2008).

To begin to shed light on this, the microarray profile of this influx transporter was studied, alongside expression of Zn-regulated MTs, using the gene microarrays.

The expression of the SLC39A7 Zn influx transporter was significantly induced (≥1.2 fold) in the TamR model and furthermore in all endocrine resistant models in the panel versus MCF7 (Fig 5.4, Table 5.5). Expression of 6 metallothioneins MT1E, MT1F, MT1G, MT1H, MT1X and MT2A were also significantly induced in all resistant models versus MCF7 (Fig 5.4, Table 5.5). The Zn influx transporter and MT2A, MT1G, MT1H and MT1E expression were induced with somewhat higher fold change in the ER+ TamR cells and oestrogen deprived resistant models. MT1F and MT1X were higher particularly in fulvestrant and oestrogen deprived resistance (Fig 5.4, Table 5.5).

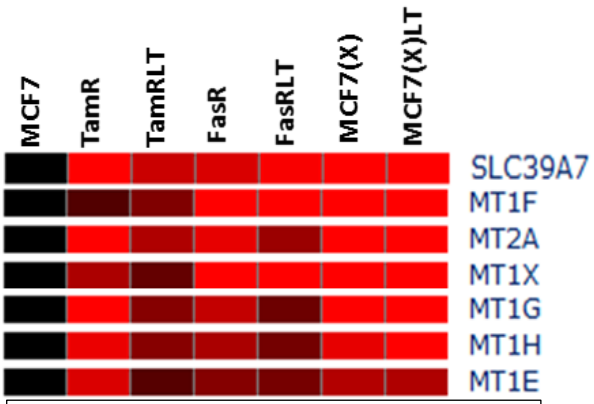

Fig 5.4. Heatmap displays SLC39A7 and several metallothionein genes (≥1.2 fold change) were increased in expression in all endocrine resistant models vs. MCF7 cells.

Gene symbols	TamR	TamRLT	FasR	FasRLT	MCF7(X)	MCF7(X)LT
SLC39A7	2.56	1.74	1.81	1.97	2.29	2.12
MT1F	1.25	1.42	4	2.4	2.13	2.16
MT2A	2.33	1.61	1.88	1.53	2.38	2.41
MT1X	1.60	1.31	2.28	2.50	2	2.39
MT1G	2	1.44	1.70	1.35	2	2
MT1H	1.9	1.44	1.59	1.37	1.88	2
MT1E	1.81	1.27	1.44	1.38	1.63	1.61

Table 5.5. Fold changes for SLC39A7 and MTs that are increased in all resistant models vs. MCF7.

5.2.6 Ontology analysis for SLC39A7 and the induced MTs and expression interrogation versus outcome of breast cancer patients using publicly-available datasets

The SLC39A7 gene encodes a protein which transports Zn from the endoplasmic reticulum and Golgi apparatus to the cytoplasm. Expression of this transporter has been associated with tyrosine kinase activation and tamoxifen resistant cells in vitro (Taylor et al. 2008). Using KMplotter, higher expression of SLC39A7 was significantly associated with shortened relapse free survival and increased risk of relapse in the tamoxifen treated ER+ (n=712 patients, HR=1.59, P=0.0023) and the all ER+ (n=1802 patients, HR=1.36, P=0.0013) breast cancer patient cohorts (Fig 5.5A, Table 5.6).

MT genes including MT1E, MT1F, MT1G, MT1H, MT1X and MT2A encode cysteine-rich proteins which bind heavy metals (Zn and Cu). Expression of these proteins has been reported to be regulated by heavy metals and also by glucocorticoids (Martinho et al. 2013) High expression of MT1E, MT1F, MT1G, MT1H and MT2A was significantly associated with shortened relapse free survival and increased risk of relapse in tamoxifen treated ER+ (n=712) and all ER+ (n=1802) breast cancer patients, while MT1X significantly associated with shortened RFS in the tamoxifen treated ER+ cohort only (Fig 5.5A-5.5C, Table 5.6).

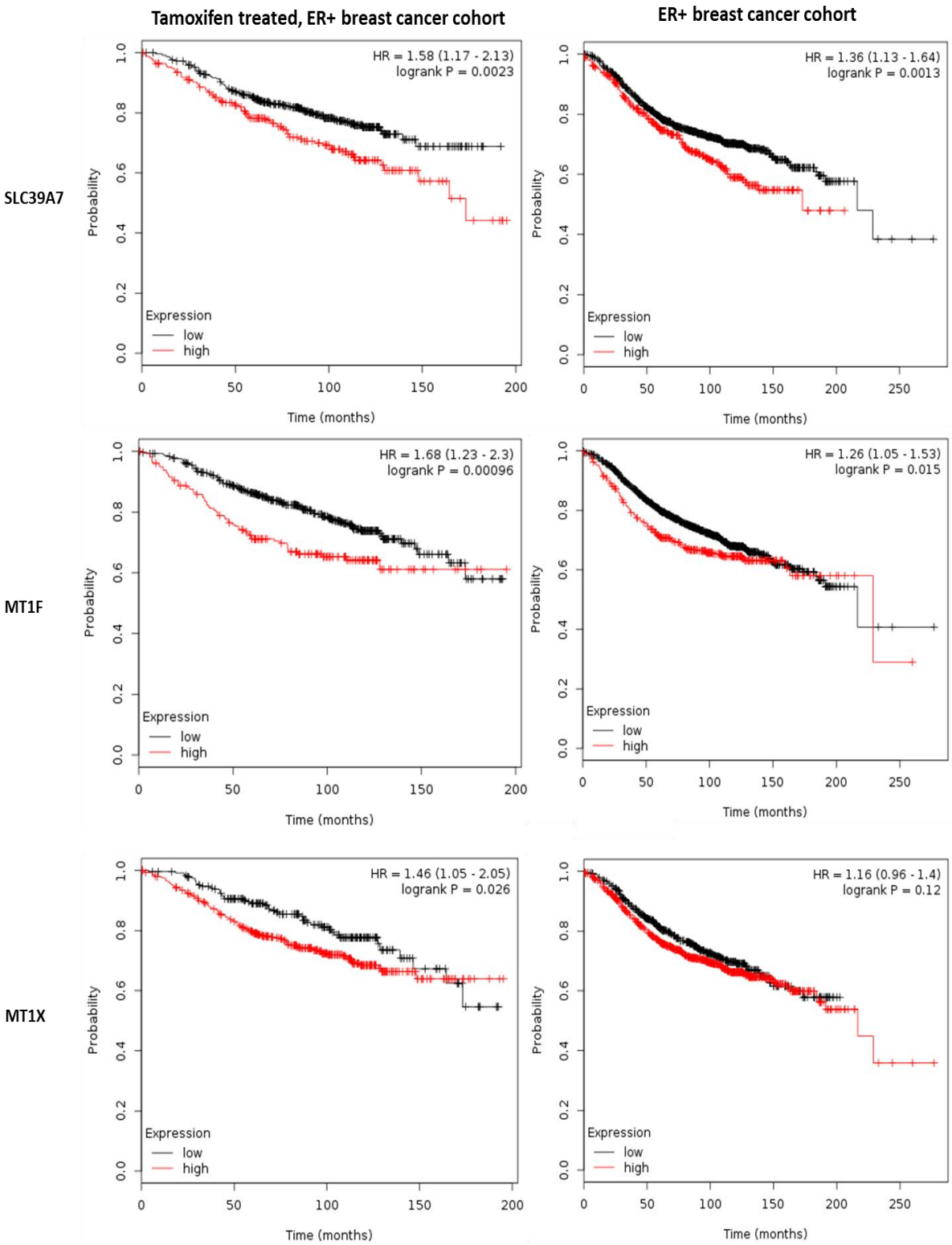

Fig 5.5A. Kaplan Meier survival curves generated using KM plotter showing higher mRNA expression of SLC39A7 & MT1F was significantly associated with shortened relapse free survival in both the tamoxifen treated ER+ (left graph) and the all ER+ breast cancer patient cohorts (right graph). Higher expression of MT1X expression was only significantly related to shortened RFS in tamoxifen treated ER+ breast cancer patients.

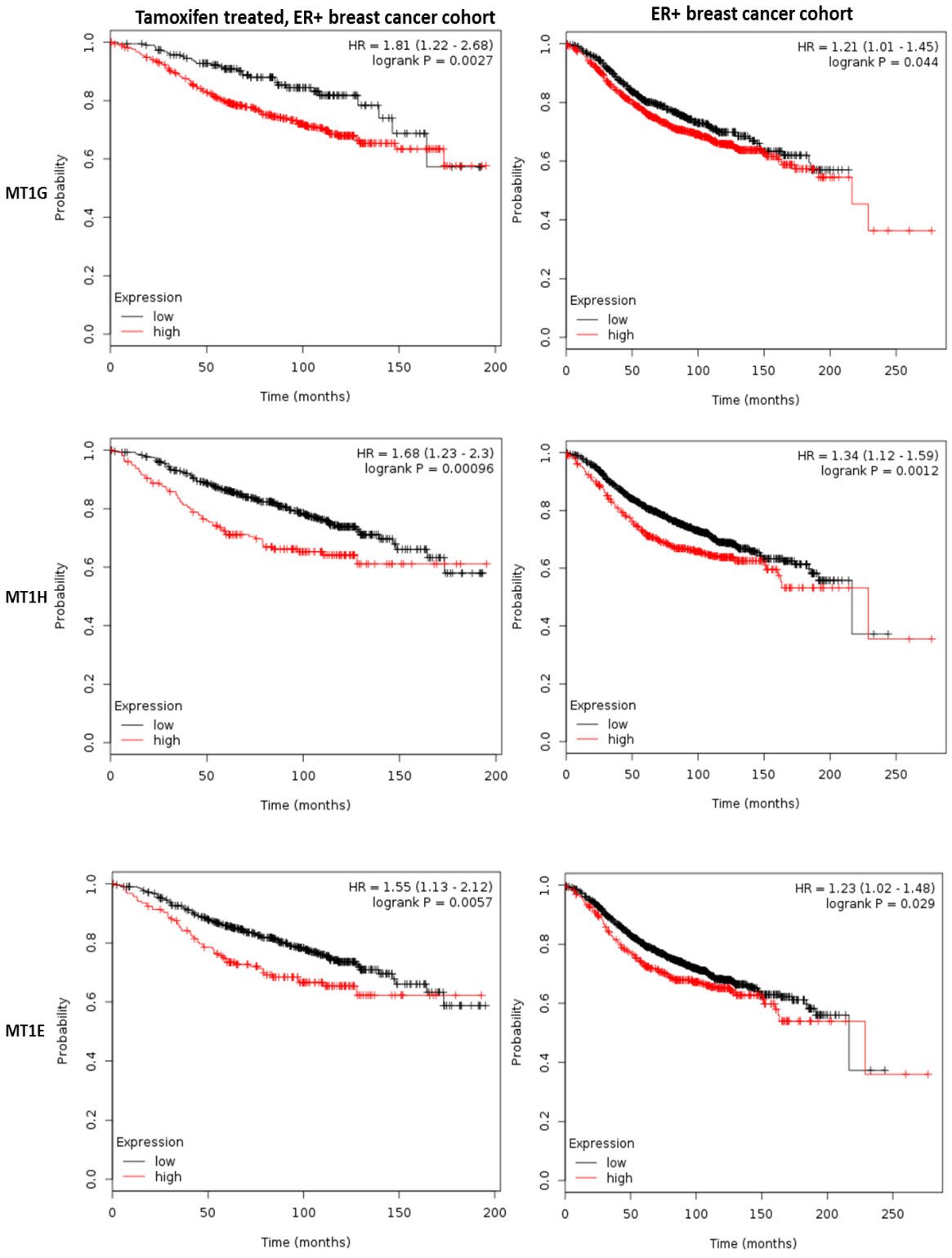

Fig 5.5B. Kaplan Meier survival curves generated using KM plotter showing higher mRNA expression of MT1G, MT1H & MT1E was significantly associated with shortened relapse free survival in both the tamoxifen treated ER+ (left graph) and the all ER+ breast cancer patient cohorts (right graph).

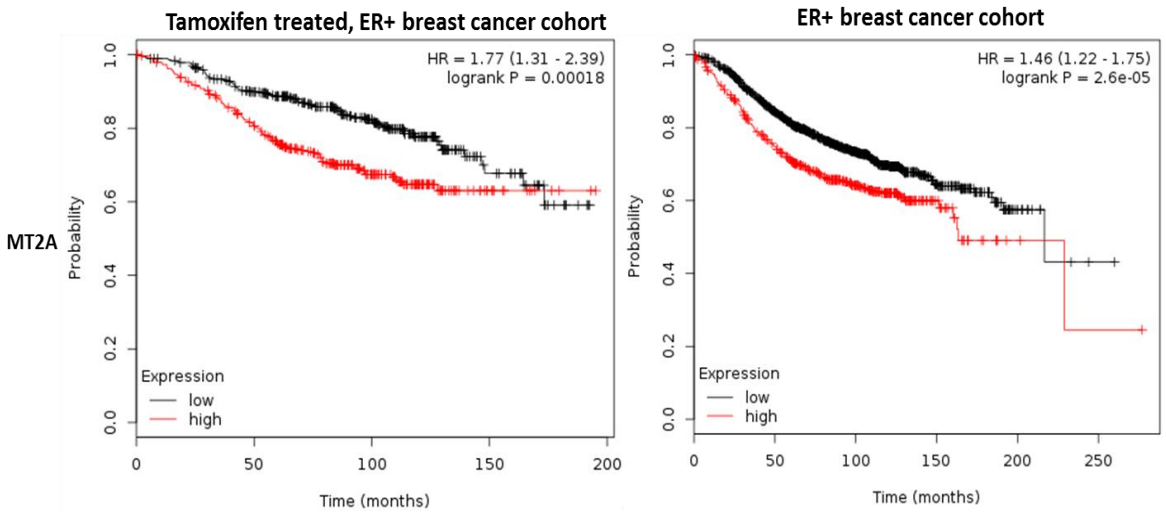

Fig 5.5C. Kaplan Meier survival curves generated using KM plotter showing higher mRNA expression of MT2A was significantly associated with shortened relapse free survival in both the tamoxifen treated ER+ (left graph) and the all ER+ breast cancer patient cohorts (right graph).

Gene symbols	RFS, Tamoxifen treated N=712	RFS, ER+ N=1802
SLC39A7	HR=1.59, P=0.0023	HR=1.36, P=0.0013
MT1F	HR=1.68, P=0.00096	HR=1.26, P=0.015
MT1X	HR=1.46, P=0.026	HR=1.16, P=0.12
MT1G	HR=1.81, P=0.0027	HR=1.21, P=0.044
MT1H	HR=1.68, P=0.00096	HR=1.34, P=0.0012
MT1E	HR=1.55, P=0.0057	HR=1.23, P=0.029
MT2A	HR=1.77, P=0.00018	HR=1.46, P=2.6E-5

Table 5.6. Summary of RFS analysis using KMplotter for SLC39A7 and MTs genes in the tamoxifen treated ER+ and the all ER+ breast cancer patient cohorts. Hazard ratio (HR) >1 indicates higher expression is associated with increased risk of relapse & logrank *P* ≤0.05 was considered to be significant.

5.2.7 mRNA expression of shared induced genes SLC39A7 and MT2A in the panel of endocrine resistant models using RT-PCR

SLC39A7 expression was most significantly increased in TamR (p<0.001), FasRLT (p<0.05), MCF7(X) and MCF7(X)LT cells (p<0.001) by 1.79, 1.42, 1.81 and 1.68 fold as compared to MCF7 cells (Fig 5.6). The expression was more modestly increased in TamRLT and FasR by 1.2 and 1.3 fold changes respectively as compared to MCF7 cells (Fig 5.6).

As an example of the MTs increased in all resistant cells on the arrays, PCR profiling of MT2A revealed expression in all the models. MT2A was significantly increased in the ER+ TamR (p<0.01), MCF7(X) (p<0.001) and MCF7(X)LT cells (p<0.01) by 2.29, 2.61 and 2.34 fold changes as compared to MCF7 (Fig 5.6). Expression of this gene was more modestly increased in TamRLT, FasR and FasRLT by 1.5-1.8 fold as compared to MCF7 (Fig 5.6). In general, therefore, RT-PCR broadly verified the array profile of expression for both SLC39A7 and MT2A across the resistant panel (Fig 5.4, Table 5.5)

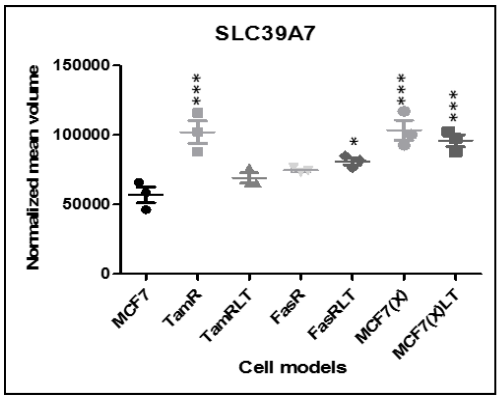

Fold change	TamR	TamRLT	FasR	FasRLT	MCF7(X)	MCF7(X)LT
MCF7	1.79	1.21	1.31	1.42	1.81	1.68

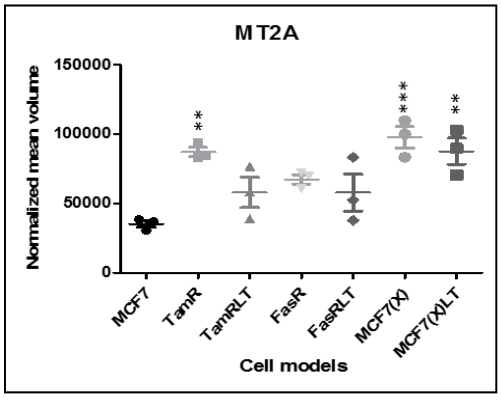

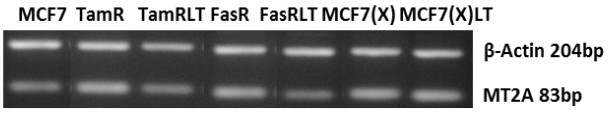

Fold change	TamR	TamRLT	FasR	FasRLT	MCF7(X)	MCF7(X)LT
MCF7	2.29	1.55	1.88	1.54	2.61	2.34

Fig 5.6. Representative gels following RT-PCR and graphs display actin normalized mean volume of SLC39A7 & MT2A signal for the model panel (comprising the mean of three independent experiments, +/-SEM for each cell line). Statistical analysis (using ANOVA with Dunnett *post hoc* correction) was performed to compare gene expression in each model vs. MCF7 (* p<0.05, ** p<0.01 &*** p<0.001). Mean fold change in gene expression for each resistant model vs. MCF7 cells is also tabulated.

5.2.8 Protein expression of shared induced gene SLC39A7 in the panel of endocrine resistant models using Western blotting

Building on the promising mRNA profile findings that increases occurred for SLC39A7 expression in multiple endocrine resistant models, further profile verification at a protein level was performed by Western blotting. Protein expression of SLC39A7 was most significantly induced in TamR (p<0.05), MCF7(X) (p<0.01) and MCF7(X)LT cells (p<0.05) by 2.5, 2.6 and 2.5 fold respectively, as compared to MCF7 (Fig 5.7). Expression of this protein was also increased in TamRLT, FasR and FasRLT cells, as compared to MCF7, but these increases were more modest (1.5, 1.3 and 1.7 fold respectively) (Fig 5.7). In general, the SLC39A7 protein expression profile verified the mRNA profile (Fig 5.4 and 5.6), in that some expression increase occurred in all resistant models, but particularly in those retaining ER.

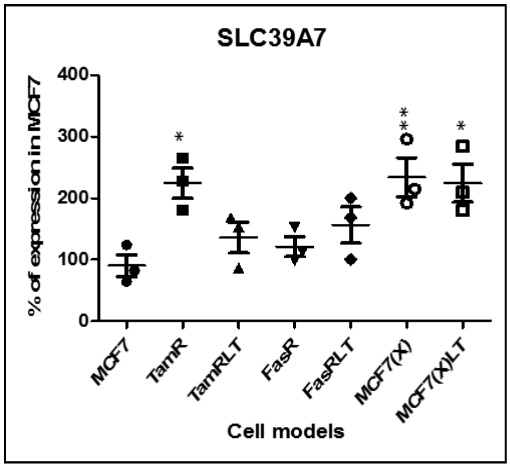

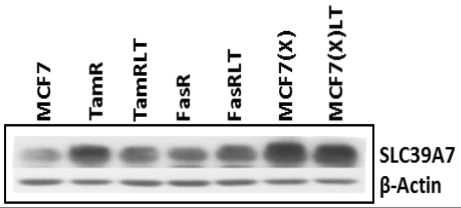

Fold change	TamR	TamRLT	FasR	FasRLT	MCF7(X)	MCF7(X)LT
MCF7	2.49	1.51	1.34	1.73	2.60	2.49

Fig 5.7. Representative blot following protein detection and graph displaying actin-normalized mean volume of SLC39A7 signal for the model panel (comprising the mean of three independent experiments, +/-SEM for each cell line). Statistical analysis (using ANOVA with Dunnett *post hoc* correction) was performed to compare protein expression in each model vs. MCF7 (* p<0.05 & ** p<0.01). Mean fold change in gene expression for each resistant model vs. MCF7 is also tabulated.

5.3 Discussion

The human protein kinome comprises the largest protein family which is highly interactive with diverse, complex cellular signalling networks (Verkhivker et al. 2015). As a consequence deregulated kinases are prominent in cancer and can play an important role in its progression (Tsai et al. 2013). Protein kinases are the most tractable target for cancer therapy and over 130 kinase inhibitors are being evaluated in clinical trials (Walker and Newell 2009). Candidate targets including receptor tyrosine kinases (e.g. EGFR, HER2, IGF-1R) and, most recently, downstream kinases mTOR (targeted by everolimus), AKT, and CDK4/6 (targeted by palbociclib) has studied in endocrine-treated breast cancer (Cristofanilli et al. 2010, Huober et al. 2011, Robertson et al. 2013, Bachelot et al. 2012 and Finn et al. 2015)

Pharmacological targeting of kinases is challenging since the kinase networks are complex and interrelated. Development of resistance to kinase targeted therapies is common due to bypass mechanisms and activation of other kinases (Bagrodia et al. 2012). To uncover new kinases in endocrine resistance in this chapter, microarrays from the endocrine resistant models were compared to endocrine responsive MCF7 cells to discriminate kinase genes commonly increased in resistance. In total, 14 shared induced kinases were identified in resistant models (Fig 5.1, Table 5.1). Most of these kinases (ADCK3, ICK, MARK1, PRKAA2, PRKD3, RIOK1, STK35, TEC and VRK3) participate in protein phosphorylation via ATP molecules, but two (PFKFB2 and XYLB) are involved in carbohydrate phosphorylation.

Ontology analysis and exploration of their associated cellular pathways revealed the shared induced kinases included several metabolic genes (e.g. PCK2, XYLB, ALDH18A1, PFKFB2 and COASY). The mRNA expression of some of these also related to shortened RFS in breast cancer patients (ER+ and tamoxifen treated cohorts: PCK2 and ALDH18A1). Induced PCK2 expression may serve to provide resistant cells with higher levels of precursor (phosphoenol pyruvate: PEP) for gluconeogenesis or pyruvate metabolism (Leithner et al. 2015). Induced ALDH18A1 alongside enhanced glutamine uptake might also contribute to de novo synthesis of proline and arginine and enhanced growth of the resistant models. Finally, induced PFKFB2 may supply precursors for either amino sugar/nucleotide sugar metabolism or glycolysis (Ros and Schulze 2013). PCR was able to verify the expression increase of these metabolic genes in all the resistant models. In total, these findings are supportive of a contribution for these metabolic kinases and their associated pathways to sustain endocrine resistant growth, irrespective of endocrine treatment type or duration. They serve to re-enforce observations in Chapter 4 that deregulation of metabolic pathways hallmarks endocrine resistance and could potentially yield new therapeutic avenues to overcome this state.

In this Chapter the Zn transporter SLC39A7 and several MTs (MT1E, MT1F, MT1G, MT1H, MT1X and MT2A) were also found to be elevated on the microarrays from all acquired endocrine resistant models (particularly in those models retaining ER). Induced expression of SLC39A7 at both the transcriptional and translational level was verified in resistant models using RT-PCR and protein blotting respectively. Furthermore, the transporter and MTs appear to have clinical relevance since increased expression of SLC39A7 and various MTs (MT1E, MT1F, MT1G, MT1H and MT2A) was associated with shortened RFS in both the tamoxifen treated ER+ and all ER+ cohorts. The latter findings are compatible with the observation of induced MT expression and association with shortened overall survival in tamoxifen treated breast cancer patients made by Surowiak et al. (2005).

Elevated SLC39A7 has previously been implicated in a non-genomic mechanism whereby this transporter releases Zn from the endoplasmic reticulum to trigger activation of several receptor tyrosine kinases in TamR cells (Taylor et al 2008). The induction of SLC39A7 expression seen across all endocrine resistant models here suggests SLC39A7 may have a dominant role in increasing their cellular Zn (also suggested by the common increases in MTs), which again may perhaps activate multiple signalling pathways to drive resistant growth and progression. The clinical profiling is further supportive of the transporter having relevance to endocrine resistance. Additionally, the antioxidant activity of such Zn signalling may be of importance in protecting these resistant cells against free-radicals (ROS) that are likely to arise from the increased mitochondrial respiration identified in Chapter 4. Transfer of electrons from complex I and II to a molecule of O_2 can allow electrons to escape and participate in single-electron reduction of oxygen to generate superoxide as a progenitor of ROS (Starkov et al. 2008). Induced MT expression has previously been reported in response to mitochondrial-derived ROS (Kadota et al. 2010), in keeping with the observations of increased MTs in all the endocrine resistant models which have elevated OxPhos. Therefore, induced Zn transporter and MTs may also be predictive markers of resistance to endocrine treatment in breast cancer patients as a response to ROS generated from their hyperactive mitochondria.

Chapter 6

General discussion

Endocrine therapy is beneficial in luminal breast cancer and can be achieved by either competitively inhibiting ER activity (with tamoxifen/fulvestrant treatment) or by suppressing oestrogen production (by aromatase inhibitor or zoladex treatment). However, many ER+ patients eventually relapse on endocrine treatment which can result in more aggressive disease and poorer prognosis. For many patients, the value of targeting particular growth factor signalling pathways to hinder endocrine resistance can be limited. Therefore, continued deciphering of resistance to antihormone therapy remains critical in breast cancer to reveal new therapeutic strategies (Johnston et al. 2015).

The work presented in this thesis focused on discovery of key shared mechanisms of resistance to endocrine treatment, using whole genome microarray profiling of MCF7 derived acquired resistant breast cancer models. This new panel encompassed breast cancer cells treated with either antioestrogens or oestrogen deprivation for up to 3 years to try to better-mimic prolonged clinical antihormone exposure, and so has potential to reveal important mechanisms of resistance. A particular importance was placed on identifying shared induced events likely to contribute to resistant growth, since these may be targetable to inhibit resistance. Initial basal characterization in the thesis revealed significant growth and proliferative capacity gained in the antihormone resistant cells compared to the endocrine responsive MCF7 control cells, confirming alternative mechanisms had been acquired in such models that were able to drive growth under antihormone-treated conditions. The gene microarray expression profiling successfully-revealed that 572 gene probes were upregulated in all resistant models versus MCF7 cells.

The thesis met its first objective since through ontological analysis, pathway analysis and functional classification of these upregulated gene probes, it discovered that enrichment of many TCA cycle and oxidative phosphorylation enzymes occurred in all resistant models. There was furthermore common induction of additional mitochondrial elements including translocase inner mitochondrial membrane proteins (TIMMs), mitochondrial ribosomal machinery subunits and mitochondrial ADP/ATP carriers that may support increased mitochondrial biogenesis and bioenergetics in the resistant cells. Mass spectrometry further confirmed that TCA/OxPhos enzymes were also elevated at the protein level in resistant models (exemplified by TamR cells).

Gains in such mechanisms are reported to convert mitochondria into a biosynthetic and bioenergetics factory able to support rapidly dividing cancer cells (Ahn and Metalo, 2015), in this instance endocrine resistant models. This clearly contrasted enrichment of lysosome pathway, lipid and amino acid biosynthesis gene expression in MCF7 cells during the early endocrine responsive phase. The regulatory mechanisms resulting in the increased expression of TCA cycle and OxPhos enzymes in the resistant models have not been examined in detail in this thesis, but many of the genes were oestrogen-suppressed elements since they were partially-induced in microarrays from oestrogen-deprived MCF7 cells. This finding adds further to the concept that antihormone induction of oestrogen-suppressed elements is likely to contribute to resistance, as previously reported for EGFR and HER2 (Gee et al. 2011). An increase in the total upregulated probe number occurred for fulvestrant resistant and oestrogen deprived resistant models, which may be because such antihormonal approaches lack the partial-oestrogenicity exhibited by tamoxifen (Ariazi et al. 2006). However, the observations that the metabolic genes were not induced by initial antioestrogen treatment in MCF7 cells, and were only maximised for oestrogen deprivation in the MCF7(X) and MCF(X)LT resistant models, implies there may also be further mechanisms underpinning the OxPhos and TCA gene expression increases in resistance. Considerable further supportive evidence was accumulated in the thesis for the concept that OxPhos was more prominent in acquired endocrine resistant cells. There was elevated oxygen consumption (an indicator of OxPhos function) by the resistant lines compared with MCF7 cells, particularly in fulvestrant (FasRLT) and oestrogen deprived resistant models that also showed increased staining for NADH dehydrogenase activity (complex I). Further microarray interrogation suggested increased NADH supply via enhanced pyruvate carrier and fatty acid carrier expression may underpin the particular prominence of complex I-driven OxPhos in the fulvestrant and oestrogen deprived resistant cells. Staining for cytochrome C oxidase activity (complex IV) was also increased in the tamoxifen and fulvestrant resistant cells compared with MCF7. Glycolytic adjacent stromal cells are reported to comprise a major driver for the increased OxPhos detected in breast tumour epithelium in vivo (Whitaker-Menezes et al. 2011). However, the observations made here for the first time in acquired endocrine resistance show that elevated OxPhos can also arise as a consequence of prolonged antihormone treatment.

The thesis also met a further objective in that it was able to use pharmacological intervention with ETC inhibitors to reveal substantial growth dependency in all the resistant cells on their increased OxPhos, providing new potential therapeutic avenues for endocrine resistance. Thus, the complex III inhibitor antimycin A suppressed the oxygen consumption and growth of most resistant models more substantially versus MCF7, particularly for the fulvestrant resistant and

TAMRLT cells. In turn, the complex I inhibitor metformin decreased NADH dehydrogenase activity and oxygen consumption in all models, particularly in oestrogen deprived and fulvestrant resistant cells, as well as inhibiting complex IV activity. Again, metformin inhibited growth of all the models confirming their dependence on OxPhos, in this instance with the highest impact in the oestrogen deprived resistant cells and moderate sensitivity in fulvestrant resistance, but with lower sensitivity in tamoxifen resistant cells. Gene profiling and Western blotting suggested factors likely to underpin this differential metformin profile in the resistant model panel including (i) a downregulated basal LKB1/AMPK, and/or metformin-induced AMPK activity with substantial depletion of anabolic processes (protein, fatty acid synthesis) in the more growth-sensitive models and (ii) a lack of AMPK induction by metformin and no apparent impact on fatty acid synthesis, increased expression of a metformin efflux transporter (MATE1), and increased glycerophosphate shuttle components (a potential complex II bypass mechanism) in the less-sensitive tamoxifen resistant cells.

A third objective of the thesis was met in that the use of publicly-available clinical expression databases revealed TCA/OxPhos gene increases also had a potential adverse function in promoting clinical relapse. Several of the genes associated with earlier relapse in ER+ and/or tamoxifen treated breast cancer patients when explored using KMplotter. Coupled with the observation that increased OxPhos comprises an important growth-promoting mechanism in many resistant models irrespective of type or duration of endocrine treatment, these clinical profiles are supportive of targeting OxPhos to control antihormone resistance. In this regard, the thesis findings indicate that the OxPhos inhibitor metformin could exert superior activity in acquired endocrine resistant patients, particularly for oestrogen deprivation and fulvestrant resistant disease

Excitingly, therefore, clinical trials are ongoing for “re-purposing” of metformin in breast cancer, currently with some focus on obesity and diabetic versus non-diabetic patient cohorts since this agent is also used as an anti-diabetic agent in type 2 disease, is weight-reducing, and has been reported to reduce cancer risk (Leon et al. 2014). Host metabolism is known to play an important role in the development and prognosis of breast cancer (Goodwin et al 2008), with a link between breast cancer risk and metabolic syndrome including high blood pressure (Largent et al. 2006), obesity (Harvie et al. 2003), high blood glucose (Michels et al. 2003) and type 2 diabetes (16% increased risk after adjustment for the BMI; Boyle et al. (2012)). Obesity is furthermore associated with poorer prognosis in ER+ breast cancer patients (Barnett et al. 2008). Encouragingly, several Window of Opportunity (WOP) studies of metformin have shown the drug can impact on proliferation in early stage breast cancer in non-diabetic patients (Hadad

et al. 2015, Dowling et al. 2015), where some trials have also detected complex I inhibition, hallmarked by increased pAMPK with metformin (Hadad et al. 2015). Although there are as yet little data on metformin in clinical endocrine resistant disease, a further study in non-diabetic patients reported Ki67 changes after neoadjuvant metformin in luminal B patients (Bonanni et al 2012), a patient cohort more likely to show poor endocrine responses. In vivo it is notable that there are also significant indirect effects of metformin on host metabolism that are likely to contribute towards the drug's anti-tumour impact, via changes in pathways such as mTOR, PI3K/AKT and ERK1/2 MAPK. Thus, metformin as a monotherapy in early stage breast cancer (1500mg/d for 6 months) improved insulin sensitivity and reduced fasting insulin in non-diabetic patients (Goodwin et al. 2008), which may decrease mitogenic input to breast tumours via the insulin receptor. Neoadjuvant metformin can also reduce PDE3B expression, TNFR and the mTOR pathway (Hadad et al. 2011), as well as reducing insulin receptor, phosphorylation of Akt and ERK1/2 MAPK (Dowling et al. 2015). Many of these signalling elements contribute in endocrine resistance (Jordan et al. 2014) and so, along with direct tumour complex 1 inhibition, their blockade with metformin could be of further value. However, impact of metfomin monotherapy on proliferation remains controversial and complex in clinical breast cancer, and this thesis also showed only very limited impact of metformin on Ki-67 in the endocrine resistant models. A study reported no effect on Ki-67 in non-diabetic patients after WOP metformin (850mg twice per day) compared to the control arm. However, there were trends according to insulin resistance with reductions in Ki-67 staining only in those patients with HOMA>2.8 (Bonanni et al 2012). Similarly, reduced Ki-67 after metformin has been reported in HER2+ DCIS in women who had abdominal obesity and were insulin resistant (HOMA>2.8).

The mixed results regarding Ki-67 impact after metformin beg the question whether this drug would prove more effective if used alongside other treatments, including antihormones, a concept that needs to be addressed in the future in the endocrine resistant models that retain ER. Indeed, metformin in combination with fulvestrant was able to stimulate Cyclin G2 expression and growth arrest in MCF7-derived tumours (Horne et al. 2015). Interestingly, therefore, prospective clinical trials have been designed to test metformin efficacy in combination with endocrine agents in breast cancer patients and promising findings are emerging. A phase I combination study of metformin (doses up to 2000mg/day) with exemestane recruited 20 ER+ postmenopausal women with metastatic breast cancer who had received prior endocrine treatment. In this study, 30% stable disease was reported for the combination arm (Esteva et al. 2013). A summary of some of the ongoing endocrine combination trials with metformin is provided in Table 6.1. These focus on oestrogen deprivation, a direction

which is supported by the observations here of particular metformin sensitivity in oestrogen deprivation resistant models.

Study ID	Patient Characteristics	Combination treatment	Current primary outcome	Current secondary outcome
NCT01589367	ER-positive postmenopausal breast cancer	Letrozole (2.5mg/d) Everolimus (10mg/d) Metformin (500-1000mg/d)	Clinical Benefit Rate (8 weeks)	Progression Free Survival (6 months)
NCT01627067	Postmenopausal Women With ER-Positive Metastatic Breast Cancer and BMI >/= 25	Exemestane (10mg/d) Everolimus (10mg/d) Metformin (start from 500mg/d for three days, increased by 500mg/d every three days to reach 1000mg twice/d)	Progression Free Survival (2 months)	———

Table 6.1. Ongoing clinical trials using metformin in combination with endocrine treatment in ER+ postmenopausal breast cancer patients.

However, the reduced metformin sensitivity noted in this thesis in tamoxifen resistant models suggests an alternative energy mechanism also contributes to antihormone resistant breast cancer cells. Monitoring of extracellular lactate and sensitivity to the inhibitor 2DG revealed that, in addition to OxPhos, all the endocrine resistant models were dependent on glycolysis. Fulvestrant resistant cells were the most growth-sensitive to 2DG, utilising glycolysis alongside prominent OxPhos. Thus, co-targeting of energy metabolism using glycolysis and OxPhos inhibitors may prove a more effective therapeutic option to overcome fulvestrant resistance. Encouragingly, 2DG is well-tolerated in cancer patients (Raez et al. 2013) and pre-clinically co-targeting of OxPhos and glycolysis using metformin and 2DG respectively was achievable in MCF7 cells and able to improve efficacy of radioiodine treatment (De et al. 2015). In this thesis, basal glycolysis was found to be highest in the tamoxifen resistant cells. Surprisingly, however, these cells were less sensitive to 2DG, which may have been related to their increased dependency on glutaminolysis as an alternative energy fuel source. Pharmacological glutamine restriction might therefore be an alternative means to inhibit growth in such endocrine resistant breast cancer, using an antimetabolite to mediate cell death via nutrient deprivation. Inhibitors of glutaminase (e.g. compound-968) have been developed that may have potential (Shajahan-Haq et al. 2014).

The final thesis objective was to investigate from the arrays if further shared induced genes with kinase activity, or their potential regulators, could be identified in the endocrine resistant models. This revealed increased mRNA expression of several metabolic kinases (PCK2,

ALDH18A1 and PFKFB2) in resistant models compared to MCF7. Such kinases (which were PCR verified) have been implicated in gluconeogenesis or pyruvate metabolisn (PCK2), de novo biosynthesis of proline and arginine (ALDH18A1) and glycolysis or aminosugar/nucleotide sugar metabolism (PFKFB2), and so may be growth contributory in resistance. However, it remains to be explored whether their genetic or pharmacological targeting alongside further antihormone treatment can reduce growth in endocrine resistant breast cancer cells, suggesting further therapeutic avenues. Similarly, the increased expression of metallothioneins alongside Zn transporter SCL39A7 in all endocrine resistant cells (again associated with adverse clinical outcome) may protect against ROS generated during increased OxPhos in such cells.

6.1 Study limitations and future work

Although this thesis has provided evidence for hyperactivation of mitochondria with enhanced energy pathways in endocrine resistant cells, additional studies are required in the future to address some limitations of the current study.

Firstly, further detail is needed regarding the metabolic pathways that can confer resistance in breast cancer cells. Metabolite profiling could be used to monitor more than 30 different metabolites in resistant cells compared to MCF7 through analytical techniques such as nuclear magnetic resonance (NMR) spectroscopy and mass spectrometry (MS).For example, the detail underpinning an increased glycine biosynthetic pathway (Jain et al. 2012), induced fatty acid synthesis, glycolysis and TCA cycle has been successfully determined in breast cancer cells via 13C NMR spectroscopy and GC–MS techniques (Yang et al. 2007). Furthermore, intracellular metabolite flux analysis (metabolite amount converted/cell/time) using heavy isotope (13C) labelled nutrients (e.g. glucose/glutamine) can help track flow of carbon through metabolic pathways, and thus potentially determine the interplay between glycolysis and OxPhos and monitor any metabolic plasticity following OxPhos blockade with metformin in resistant cells. Bioenergetic pathway dependency and capacity of resistant cells to oxidize the three key mitochondrial fuels (glucose, glutamine and fatty acids) can also be determined using the XF Seahorse Analyser. This technique can be used to explore whether resistant cells can use alternative fuel for mitochondrial respiration in the presence and absence of inhibitors and hence flexibility of such cells to overcome energy crisis, for example following metformin treatment. Furthermore, the Seahorse XF Cell Mito Stress test enables measurement of basal respiration, ATP-linked respiration, proton leak, maximal respiration, spare respiratory capacity, and non-mitochondrial respiration after metformin treatment which may better explain the growth sensitivity profile to such treatment in the model panel. Energy phenotyping via measuring glycolysis and mitochondrial respiration using the XF analyser under basal conditions

and after an energy crisis (stressed phenotype) can also further help categorize breast cancer cells as quiescent, energetic, aerobic or glycolytic to better-understand the role of energy metabolism in such cells and thus sensitivity to glycolysis and OxPhos inhibitors.

Secondly, the thesis has focussed primarily on studying an acquired endocrine resistant model panel derived from luminal A MCF7 cells in vitro to obtain promising data supportive of targeting bioenergetic pathways in endocrine resistance. However, there remains a need to profile dependency on OxPhos and glycolysis, and critically metformin and 2DG sensitivity, in further acquired endocrine resistant models since a single model panel is unlikely to represent the full spectrum of luminal A (and luminal B) derived antihormone resistance. This should be possible in the future since the BCMP group have very recently developed further long-term acquired antihormone resistant cell models from the additional luminal A line T47D as well as from luminal B BT474 and MDA-MB-361 cells.

Finally, although KMplotter encouragingly suggested that the induced genes also relate to poorer outcome in breast cancer patients, this in silico clinical dataset does not include tumour samples taken at the time of relapse to be able to profile expression in clinical acquired resistance. Such study remains a challenging future goal, since relapse samples can be inaccessible to biopsy. Furthermore, given the findings from the Lisanti group showing stromal cells can influence bioenergetic pathways in tumour epithelium (Whitaker-Menezes et al. 2011, Martinez-Outschoorn et al. 2011), it also remains important to use orthotopic xenografts of the acquired endocrine resistant lines, or co-culture with stromal fibroblasts, to gauge how the microenvironment further influences the intrinsic gain of OxPhos in acquired endocrine resistance and impacts on the apparent metformin sensitivity of this state. Embracing such approaches in the future should further help interpret the emerging clinical trials with this agent alongside endocrine treatment in breast cancer.

References

(EBCTCG), E.B.C.T.C.G., 2005. Effects of chemotherapy and hormonal therapy for early breast cancer on recurrence and 15-year survival: an overview of the randomised trials. The Lancet 365, 1687–1717. doi:10.1016/S0140-6736(05)66544-0

Abdulkareem, I.H., 2013. Aetio-pathogenesis of breast cancer. Niger Med J 54, 371–375. doi:10.4103/0300-1652.126284

Aguas, F., Martins, A., Gomes, T.P., de Sousa, M., Silva, D.P., Portuguese Menopause Society and Portuguese Gynaecology Society, 2005. Prophylaxis approach to a-symptomatic post-menopausal women: breast cancer. Maturitas 52 Suppl 1, S23–31. doi:10.1016/j.maturitas.2005.06.015

Ahn, C.S., Metallo, C.M., 2015. Mitochondria as biosynthetic factories for cancer proliferation. Cancer & Metabolism 3, 1. doi:10.1186/s40170-015-0128-2

Algire, C., Amrein, L., Bazile, M., David, S., Zakikhani, M., Pollak, M., 2011. Diet and tumor LKB1 expression interact to determine sensitivity to anti-neoplastic effects of metformin in vivo. Oncogene 30, 1174–1182. doi:10.1038/onc.2010.483

Ali, S., Coombes, R.C., 2002. Endocrine-responsive breast cancer and strategies for combating resistance. Nat Rev Cancer 2, 101–112. doi:10.1038/nrc721

Anbalagan, M., Rowan, B.G., 2015. Estrogen receptor alpha phosphorylation and its functional impact in human breast cancer. Molecular and Cellular Endocrinology, Estrogen action: receptors, transcripts, cell signaling, and non-coding RNAs in normal physiology and disease 418, Part 3, 264–272. doi:10.1016/j.mce.2015.01.016

Appleby, R.D., Porteous, W.K., Hughes, G., James, A.M., Shannon, D., Wei, Y.H., Murphy, M.P., 1999. Quantitation and origin of the mitochondrial membrane potential in human cells lacking mitochondrial DNA. Eur. J. Biochem. 262, 108–116.

Ariazi, E.A., Lewis-Wambi, J.S., Gill, S.D., Pyle, J.R., Ariazi, J.L., Kim, H.R., Sharma, C.G.N., Cordera, F., Shupp, H.A., Li, T., Jordan, V.C., 2006. Emerging principles for the development of resistance to antihormonal therapy: Implications for the clinical utility of fulvestrant. J Steroid Biochem Mol Biol 102, 128–138. doi:10.1016/j.jsbmb.2006.09.003

Aschner, M., Conklin, D.R., Yao, C.P., Allen, J.W., Tan, K.H., 1998. Induction of astrocyte metallothioneins (MTs) by zinc confers resistance against the acute cytotoxic effects of methylmercury on cell swelling, Na+ uptake, and K+ release. Brain Research 813, 254–261. doi:10.1016/S0006-8993(98)00947-0

Bachelot, T., Bourgier, C., Cropet, C., Ray-Coquard, I., Ferrero, J.-M., Freyer, G., Abadie-Lacourtoisie, S., Eymard, J.-C., Debled, M., Spaëth, D., Legouffe, E., Allouache, D., Kouri, C.E., Pujade-Lauraine, E., 2012. Randomized Phase II Trial of Everolimus in Combination With Tamoxifen in Patients With Hormone Receptor–Positive, Human Epidermal Growth Factor Receptor 2–Negative Metastatic Breast Cancer With Prior Exposure to Aromatase Inhibitors: A GINECO Study. JCO 30, 2718–2724. doi:10.1200/JCO.2011.39.0708

Bagrodia, S., Smeal, T., Abraham, R.T., 2012. Mechanisms of intrinsic and acquired resistance to kinase-targeted therapies. Pigment Cell Melanoma Res 25, 819–831. doi:10.1111/pcmr.12007

Balan, I.S., Fiskum, G., Kristian, T., 2010. Visualization and quantification of NAD(H) in brain sections by a novel histo-enzymatic nitrotetrazolium blue staining technique. Brain Res 1316C, 112. doi:10.1016/j.brainres.2009.12.042

Barnett, G.C., Shah, M., Redman, K., Easton, D.F., Ponder, B.A.J., Pharoah, P.D.P., 2008. Risk Factors for the Incidence of Breast Cancer: Do They Affect Survival From the Disease? JCO 26, 3310–3316. doi:10.1200/JCO.2006.10.3168

Barton, V.N., D'Amato, N.C., Gordon, M.A., Christenson, J.L., Elias, A., Richer, J.K., 2015*a*. Androgen Receptor Biology in Triple Negative Breast Cancer: a Case for Classification as AR+ or Quadruple Negative Disease. Horm Cancer 6, 206–213. doi:10.1007/s12672-015-0232-3

Barton, V.N., D'Amato, N.C., Gordon, M.A., Lind, H.T., Spoelstra, N.S., Babbs, B.L., Heinz, R.E., Elias, A., Jedlicka, P., Jacobsen, B.M., Richer, J.K., 2015*b*. Multiple molecular subtypes of triple-negative breast cancer critically rely on androgen receptor and respond to enzalutamide in vivo. Mol. Cancer Ther. 14, 769–778. doi:10.1158/1535-7163.MCT-14-0926

Bartsch, R., Bago-Horvath, Z., Berghoff, A., DeVries, C., Pluschnig, U., Dubsky, P., Rudas, M., Mader, R.M., Rottenfusser, A., Fitzal, F., Gnant, M., Zielinski, C.C., Steger, G.G., 2012. Ovarian function suppression and fulvestrant as endocrine therapy in premenopausal women with metastatic breast cancer. European Journal of Cancer 48, 1932–1938. doi:10.1016/j.ejca.2012.03.002

Bartsch, R., Wenzel, C., Steger, G.G., 2007. Trastuzumab in the management of early and advanced stage breast cancer. Biologics 1, 19–31.

Baselga, J., Campone, M., Piccart, M., Burris, H.A.I., Rugo, H.S., Sahmoud, T., Noguchi, S., Gnant, M., Pritchard, K.I., Lebrun, F., Beck, J.T., Ito, Y., Yardley, D., Deleu, I., Perez, A., Bachelot, T., Vittori, L., Xu, Z., Mukhopadhyay, P., Lebwohl, D., Hortobagyi, G.N., 2012. Everolimus in Postmenopausal Hormone-Receptor–Positive Advanced Breast Cancer. New England Journal of Medicine 366, 520–529. doi:10.1056/NEJMoa1109653

Beatson, G., 1896. On treatment of inoperable cases of carcinoma of the mamma: suggestions for a new method of treatment with illustrative cases. The Lancet 148, 162–165. doi:10.1016/S0140-6736(01)72384-7

Bénit, P., Slama, A., Cartault, F., Giurgea, I., Chretien, D., Lebon, S., Marsac, C., Munnich, A., Rötig, A., Rustin, P., 2004. Mutant NDUFS3 subunit of mitochondrial complex I causes Leigh syndrome. J. Med. Genet. 41, 14–17.

Bensmail, A., Hutcheson, I., Giles, M., Gee, J., Nicholson, R., 2008. Loss of oestrogen receptor alpha in long-term antioestrogen-resistant cells: reversal by a c-src inhibitor. Breast Cancer Res 10, O3. doi:10.1186/bcr1883

Berg, J.M., Tymoczko, J.L., Stryer, L., Berg, J.M., Tymoczko, J.L., Stryer, L., 2002. Biochemistry, 5th ed. W H Freeman.

Bergqvist, J., Elmberger, G., Ohd, J., Linderholm, B., Bjohle, J., Hellborg, H., Nordgren, H., Borg, A.-L., Skoog, L., Bergh, J., 2006. Activated ERK1/2 and phosphorylated oestrogen receptor α are associated with improved breast cancer survival in women treated with tamoxifen. European Journal of Cancer 42, 1104–1112. doi:10.1016/j.ejca.2006.01.028

Berstein, L.M., Yue, W., Wang, J.-P., Santen, R.J., 2010. Isolated and combined action of tamoxifen and metformin in wild-type, tamoxifen-resistant, and estrogen-deprived MCF-7 cells. Breast Cancer Res Treat 128, 109–117. doi:10.1007/s10549-010-1072-z

Birsoy, K., Possemato, R., Lorbeer, F.K., Bayraktar, E.C., Thiru, P., Yucel, B., Wang, T., Chen, W.W., Clish, C.B., Sabatini, D.M., 2014. Metabolic determinants of cancer cell sensitivity to glucose limitation and biguanides. Nature advance online publication. doi:10.1038/nature13110

Blume-Jensen, P., Hunter, T., 2001. Oncogenic kinase signalling. Nature 411, 355–365. doi:10.1038/35077225

Bonanni, B., Puntoni, M., Cazzaniga, M., Pruneri, G., Serrano, D., Guerrieri-Gonzaga, A., Gennari, A., Trabacca, M.S., Galimberti, V., Veronesi, P., Johansson, H., Aristarco, V., Bassi, F., Luini, A., Lazzeroni, M., Varricchio, C., Viale, G., Bruzzi, P., DeCensi, A., 2012. Dual Effect of Metformin on Breast Cancer Proliferation in a Randomized Presurgical Trial. JCO 30, 2593–2600. doi:10.1200/JCO.2011.39.3769

Bononi, A., Agnoletto, C., De Marchi, E., Marchi, S., Patergnani, S., Bonora, M., Giorgi, C., Missiroli, S., Poletti, F., Rimessi, A., Pinton, P., Bononi, A., Agnoletto, C., De Marchi, E., Marchi, S., Patergnani, S., Bonora, M., Giorgi, C., Missiroli, S., Poletti, F., Rimessi, A., Pinton, P., 2011. Protein Kinases and Phosphatases in the Control of Cell Fate, Protein Kinases and Phosphatases in the Control of Cell Fate. Enzyme Research, Enzyme Research 2011, 2011, e329098. doi:10.4061/2011/329098, 10.4061/2011/329098

Bonuccelli, G., Tsirigos, A., Whitaker-Menezes, D., Pavlides, S., Pestell, R.G., Chiavarina, B., Frank, P.G., Flomenberg, N., Howell, A., Martinez-Outschoorn, U.E., Sotgia, F., Lisanti, M.P., 2010. Ketones and lactate "fuel" tumor growth and metastasis. Cell Cycle 9, 3506–3514. doi:10.4161/cc.9.17.12731

Boyle, P., Boniol, M., Koechlin, A., Robertson, C., Valentini, F., Coppens, K., Fairley, L.-L., Boniol, M., Zheng, T., Zhang, Y., Pasterk, M., Smans, M., Curado, M.P., Mullie, P., Gandini, S., Bota, M., Bolli, G.B., Rosenstock, J., Autier, P., 2012. Diabetes and breast cancer risk: a meta-analysis. Br J Cancer 107, 1608–1617. doi:10.1038/bjc.2012.414

Bradford, M.M., 1976. A rapid and sensitive method for the quantitation of microgram quantities of protein utilizing the principle of protein-dye binding. Anal. Biochem. 72, 248–254.

Brentani, H., Caballero, O.L., Camargo, A.A., da Silva, A.M., da Silva, W.A., Dias Neto, E., Grivet, M., Gruber, A., Guimaraes, P.E.M., Hide, W., Iseli, C., Jongeneel, C.V., Kelso, J., Nagai, M.A., Ojopi, E.P.B., Osorio, E.C., Reis, E.M.R., Riggins, G.J., Simpson, A.J.G., de Souza, S., Stevenson, B.J., Strausberg, R.L., Tajara, E.H., Verjovski-Almeida, S., Acencio, M.L., Bengtson, M.H., Bettoni, F., Bodmer, W.F., Briones, M.R.S., Camargo, L.P., Cavenee, W., Cerutti, J.M., Coelho Andrade, L.E., Costa dos Santos, P.C., Ramos Costa, M.C., da Silva, I.T., Estécio, M.R.H., Sa Ferreira, K., Furnari, F.B., Faria, M., Galante, P.A.F., Guimaraes, G.S., Holanda, A.J., Kimura, E.T., Leerkes, M.R., Lu, X., Maciel, R.M.B., Martins, E.A.L., Massirer, K.B., Melo, A.S.A., Mestriner, C.A., Miracca, E.C.,

Miranda, L.L., Nobrega, F.G., Oliveira, P.S., Paquola, A.C.M., Pandolfi, J.R.C., Campos Pardini, M.I. de M., Passetti, F., Quackenbush, J., Schnabel, B., Sogayar, M.C., Souza, J.E., Valentini, S.R., Zaiats, A.C., Amaral, E.J., Arnaldi, L.A.T., de Araújo, A.G., de Bessa, S.A., Bicknell, D.C., Ribeiro de Camaro, M.E., Carraro, D.M., Carrer, H., Carvalho, A.F., Colin, C., Costa, F., Curcio, C., Guerreiro da Silva, I.D.C., Pereira da Silva, N., Dellamano, M., El-Dorry, H., Espreafico, E.M., Scattone Ferreira, A.J., Ayres Ferreira, C., Fortes, M.A.H.Z., Gama, A.H., Giannella-Neto, D., Giannella, M.L.C.C., Giorgi, R.R., Goldman, G.H., Goldman, M.H.S., Hackel, C., Ho, P.L., Kimura, E.M., Kowalski, L.P., Krieger, J.E., Leite, L.C.C., Lopes, A., Luna, A.M.S.C., Mackay, A., Mari, S.K.N., Marques, A.A., Martins, W.K., Montagnini, A., Mourão Neto, M., Nascimento, A.L.T.O., Neville, A.M., Nobrega, M.P., O'Hare, M.J., Otsuka, A.Y., Ruas de Melo, A.I., Paco-Larson, M.L., Guimarães Pereira, G., Pereira da Silva, N., Pesquero, J.B., Pessoa, J.G., Rahal, P., Rainho, C.A., Rodrigues, V., Rogatto, S.R., Romano, C.M., Romeiro, J.G., Rossi, B.M., Rusticci, M., Guerra de Sá, R., Sant' Anna, S.C., Sarmazo, M.L., Silva, T.C. de L.E., Soares, F.A., Sonati, M. de F., de Freitas Sousa, J., Queiroz, D., Valente, V., Vettore, A.L., Villanova, F.E., Zago, M.A., Zalcberg, H., Human Cancer Genome Project/Cancer Genome Anatomy Project Annotation Consortium, Human Cancer Genome Project Sequencing Consortium, 2003. The generation and utilization of a cancer-oriented representation of the human transcriptome by using expressed sequence tags. Proc. Natl. Acad. Sci. U.S.A. 100, 13418–13423. doi:10.1073/pnas.1233632100

Breuer, K., Foroushani, A.K., Laird, M.R., Chen, C., Sribnaia, A., Lo, R., Winsor, G.L., Hancock, R.E.W., Brinkman, F.S.L., Lynn, D.J., 2013. InnateDB: systems biology of innate immunity and beyond—recent updates and continuing curation. Nucl. Acids Res. 41, D1228–D1233. doi:10.1093/nar/gks1147

Bridges, H.R., Jones, A.J.Y., Pollak, M.N., Hirst, J., 2014. Effects of metformin and other biguanides on oxidative phosphorylation in mitochondria. Biochem. J. 462, 475–487. doi:10.1042/BJ20140620

Brinkman, J.A., El-Ashry, D., 2009. ER re-expression and re-sensitization to endocrine therapies in ER-negative breast cancers. J Mammary Gland Biol Neoplasia 14, 67–78. doi:10.1007/s10911-009-9113-0

Britton, D.J., Hutcheson, I.R., Knowlden, J.M., Barrow, D., Giles, M., McClelland, R.A., Gee, J.M.W., Nicholson, R.I., 2006. Bidirectional cross talk between ERalpha and EGFR signalling pathways regulates tamoxifen-resistant growth. Breast Cancer Res. Treat. 96, 131–146. doi:10.1007/s10549-005-9070-2

Britton, D., Zen, Y., Quaglia, A., Selzer, S., Mitra, V., Lößner, C., Jung, S., Böhm, G., Schmid, P., Prefot, P., Hoehle, C., Koncarevic, S., Gee, J., Nicholson, R., Ward, M., Castellano, L., Stebbing, J., Zucht, H.D., Sarker, D., Heaton, N., Pike, I., 2014. Quantification of Pancreatic Cancer Proteome and Phosphorylome: Indicates Molecular Events Likely Contributing to Cancer and Activity of Drug Targets. PLoS One 9. doi:10.1371/journal.pone.0090948

Brodie, A., Macedo, L., Sabnis, G., 2010. Aromatase resistance mechanisms in model systems in vivo. The Journal of Steroid Biochemistry and Molecular Biology, Proceedings of the IX International Aromatase Conference "Aromatase 2008" (Shanghai, China, on October 13–16th, 2008) 118, 283–287. doi:10.1016/j.jsbmb.2009.09.004

Brouckaert, O., Paridaens, R., Floris, G., Rakha, E., Osborne, K., Neven, P., 2013. A critical review why assessment of steroid hormone receptors in breast cancer should be quantitative. Ann Oncol 24, 46–53. doi:10.1093/annonc/mds238

Brown, K.A., Hunger, N.I., Docanto, M., Simpson, E.R., 2010. Metformin inhibits aromatase expression in human breast adipose stromal cells via stimulation of AMP-activated protein kinase. Breast Cancer Res. Treat. 123, 591–596. doi:10.1007/s10549-010-0834-y

Brünner, N., Boulay, V., Fojo, A., Freter, C.E., Lippman, M.E., Clarke, R., 1993*a*. Acquisition of hormone-independent growth in MCF-7 cells is accompanied by increased expression of estrogen-regulated genes but without detectable DNA amplifications. Cancer Res. 53, 283–290.

Brünner, N., Boysen, B., Jirus, S., Skaar, T.C., Holst-Hansen, C., Lippman, J., Frandsen, T., Spang-Thomsen, M., Fuqua, S.A., Clarke, R., 1997. MCF7/LCC9: an antiestrogen-resistant MCF-7 variant in which acquired resistance to the steroidal antiestrogen ICI 182,780 confers an early cross-resistance to the nonsteroidal antiestrogen tamoxifen. Cancer Res. 57, 3486–3493.

Brünner, N., Frandsen, T.L., Holst-Hansen, C., Bei, M., Thompson, E.W., Wakeling, A.E., Lippman, M.E., Clarke, R., 1993*b*. MCF7/LCC2: A 4-Hydroxytamoxifen Resistant Human Breast Cancer Variant That Retains Sensitivity to the Steroidal Antiestrogen ICI 182,780. Cancer Res 53, 3229–3232.

Bugiani, M., Invernizzi, F., Alberio, S., Briem, E., Lamantea, E., Carrara, F., Moroni, I., Farina, L., Spada, M., Donati, M.A., Uziel, G., Zeviani, M., 2004. Clinical and molecular findings in children with complex I deficiency. Biochim. Biophys. Acta 1659, 136–147. doi:10.1016/j.bbabio.2004.09.006

Carlson, R.W., Henderson, I.C., 2003. Sequential hormonal therapy for metastatic breast cancer after adjuvant tamoxifen or anastrozole. Breast Cancer Research and Treatment 80, S19–S26. cc.8.23.10238, n.d.

Carlson, R.W., O'Neill, A., Vidaurre, T., Gomez, H.L., Badve, S.S., Sledge, G.W., 2012. A randomized trial of combination anastrozole plus gefitinib and of combination fulvestrant plus gefitinib in the treatment of postmenopausal women with hormone receptor positive metastatic breast cancer. Breast Cancer Res. Treat. 133, 1049–1056. doi:10.1007/s10549-012-1997-5

Cascón, A., Comino-Méndez, I., Currás-Freixes, M., de Cubas, A.A., Contreras, L., Richter, S., Peitzsch, M., Mancikova, V., Inglada-Pérez, L., Pérez-Barrios, A., Calatayud, M., Azriel, S., Villar-Vicente, R., Aller, J., Setién, F., Moran, S., Garcia, J.F., Río-Machín, A., Letón, R., Gómez-Graña, Á., Apellániz-Ruiz, M., Roncador, G., Esteller, M., Rodríguez-Antona, C., Satrústegui, J., Eisenhofer, G., Urioste, M., Robledo, M., 2015. Whole-exome sequencing identifies MDH2 as a new familial paraganglioma gene. J. Natl. Cancer Inst. 107. doi:10.1093/jnci/djv053

Cazzaniga, M., DeCensi, A., Pruneri, G., Puntoni, M., Bottiglieri, L., Varricchio, C., Guerrieri-Gonzaga, A., Gentilini, O.D., Pagani, G., Dell'Orto, P., Lazzeroni, M., Serrano, D., Viale, G., Bonanni, B., 2013. The effect of metformin on apoptosis in a breast cancer presurgical trial. Br. J. Cancer 109, 2792–2797. doi:10.1038/bjc.2013.657

Chakraborty, A.K., Welsh, A., DiGiovanna, M.P., 2009. Co-targeting the insulin-like growth factor I receptor enhances growth-inhibitory and pro-apoptotic effects of anti-estrogens in human breast cancer cell lines. Breast Cancer Res Treat 120, 327–335. doi:10.1007/s10549-009-0382-5

Chan, C.M.W., Martin, L.-A., Johnston, S.R.D., Ali, S., Dowsett, M., 2002. Molecular changes associated with the acquisition of oestrogen hypersensitivity in MCF-7 breast cancer cells on long-term oestrogen deprivation. The Journal of Steroid Biochemistry and Molecular Biology 81, 333–341. doi:10.1016/S0960-0760(02)00074-2

Chen, D., Washbrook, E., Sarwar, N., Bates, G.J., Pace, P.E., Thirunuvakkarasu, V., Taylor, J., Epstein, R.J., Fuller-Pace, F.V., Egly, J.-M., Coombes, R.C., Ali, S., 2002. Phosphorylation of human estrogen receptor alpha at serine 118 by two distinct signal transduction pathways revealed by phosphorylation-specific antisera. Oncogene 21, 4921–4931. doi:10.1038/sj.onc.1205420

Cheng, T., Sudderth, J., Yang, C., Mullen, A.R., Jin, E.S., Matés, J.M., DeBerardinis, R.J., 2011. Pyruvate carboxylase is required for glutamine-independent growth of tumor cells. Proc Natl Acad Sci U S A 108, 8674–8679. doi:10.1073/pnas.1016627108

Cherian, M.G., Jayasurya, A., Bay, B.-H., 2003. Metallothioneins in human tumors and potential roles in carcinogenesis. Mutation Research/Fundamental and Molecular Mechanisms of Mutagenesis, Metals and Human Cancer 533, 201–209. doi:10.1016/j.mrfmmm.2003.07.013

Choe, M., Brusgard, J.L., Chumsri, S., Bhandary, L., Zhao, X.F., Lu, S., Goloubeva, O.G., Polster, B.M., Fiskum, G.M., Girnun, G.D., Kim, M.S., Passaniti, A., 2015. The RUNX2 Transcription Factor Negatively Regulates SIRT6 Expression to Alter Glucose Metabolism in Breast Cancer Cells. J. Cell. Biochem. 116, 2210–2226. doi:10.1002/jcb.25171

Choi, D.-S., Choi, D.-Y., Hong, B.S., Jang, S.C., Kim, D.-K., Lee, J., Kim, Y.-K., Kim, K.P., Gho, Y.S., 2012. Quantitative proteomics of extracellular vesicles derived from human primary and metastatic colorectal cancer cells. J Extracell Vesicles 1. doi:10.3402/jev.v1i0.18704

Clarke, R., Brünner, N., Katzenellenbogen, B.S., Thompson, E.W., Norman, M.J., Koppi, C., Paik, S., Lippman, M.E., Dickson, R.B., 1989. Progression of human breast cancer cells from hormone-dependent to hormone-independent growth both in vitro and in vivo. Proc Natl Acad Sci U S A 86, 3649–3653.

Clarke, R., Leonessa, F., Welch, J.N., Skaar, T.C., 2001. Cellular and Molecular Pharmacology of Antiestrogen Action and Resistance. Pharmacol Rev 53, 25–72.

Clarke, R., Tyson, J.J., Dixon, J.M., 2015. Endocrine resistance in breast cancer – An overview and update. Molecular and Cellular Endocrinology, Estrogen action: receptors, transcripts, cell signaling, and non-coding RNAs in normal physiology and disease 418, Part 3, 220–234. doi:10.1016/j.mce.2015.09.035

Cohen, P., 2002. Protein kinases — the major drug targets of the twenty-first century? Nat Rev Drug Discov 1, 309–315. doi:10.1038/nrd773

Colleoni, M., Montagna, E., 2012. Neoadjuvant therapy for ER-positive breast cancers. Ann Oncol 23, x243–x248. doi:10.1093/annonc/mds305

Coller, J.K., Krebsfaenger, N., Klein, K., Endrizzi, K., Wolbold, R., Lang, T., Nüssler, A., Neuhaus, P., Zanger, U.M., Eichelbaum, M., Mürdter, T.E., 2002. The influence of CYP2B6, CYP2C9 and CYP2D6 genotypes on the formation of the potent antioestrogen Z-4-hydroxy-tamoxifen in human liver. British Journal of Clinical Pharmacology 54, 157–167. doi:10.1046/j.1365-2125.2002.01614.x

Cristofanilli, M., Valero, V., Mangalik, A., Royce, M., Rabinowitz, I., Arena, F.P., Kroener, J.F., Curcio, E., Watkins, C., Bacus, S., Cora, E.M., Anderson, E., Magill, P.J., 2010. Phase II, Randomized Trial to Compare Anastrozole Combined with Gefitinib or Placebo in Postmenopausal Women with Hormone Receptor–Positive Metastatic Breast Cancer. Clin Cancer Res 16, 1904–1914. doi:10.1158/1078-0432.CCR-09-2282

Cui, Y., Vogt, S., Olson, N., Glass, A.G., Rohan, T.E., 2007b. Levels of Zinc, Selenium, Calcium, and Iron in Benign Breast Tissue and Risk of Subsequent Breast Cancer. Cancer Epidemiol Biomarkers Prev 16, 1682–1685. doi:10.1158/1055-9965.EPI-07-0187

Dasatinib–Letrozole Gets Split Verdict, 2014. . Cancer Discovery 4, 138–139. doi:10.1158/2159-8290.CD-NB2013-181

De, A., Chatterjee, S., Thaker, N., 2015. Combined 2-deoxy glucose and metformin improves therapeutic efficacy of sodium-iodide symporter-mediated targeted radioiodine therapy in breast cancer cells. Breast Cancer: Targets and Therapy 251. doi:10.2147/BCTT.S84648

DeCensi, A., Puntoni, M., Gandini, S., Guerrieri-Gonzaga, A., Johansson, H.A., Cazzaniga, M., Pruneri, G., Serrano, D., Schwab, M., Hofmann, U., Mora, S., Aristarco, V., Macis, D., Bassi, F., Luini, A., Lazzeroni, M., Bonanni, B., Pollak, M.N., 2014. Differential effects of metformin on breast cancer proliferation according to markers of insulin resistance and tumor subtype in a randomized presurgical trial. Breast Cancer Res. Treat. 148, 81–90. doi:10.1007/s10549-014-3141-1

DeCensi, A., Puntoni, M., Guerrieri-Gonzaga, A., Cazzaniga, M., Serrano, D., Lazzeroni, M., Vingiani, A., Gentilini, O., Petrera, M., Viale, G., Cuzick, J., Bonanni, B., Pruneri, G., 2015. Effect of Metformin on Breast Ductal Carcinoma In Situ Proliferation in a Randomized Presurgical Trial. Cancer Prev Res (Phila) 8, 888–894. doi:10.1158/1940-6207.CAPR-15-0048

Dent, R., Trudeau, M., Pritchard, K.I., Hanna, W.M., Kahn, H.K., Sawka, C.A., Lickley, L.A., Rawlinson, E., Sun, P., Narod, S.A., 2007. Triple-Negative Breast Cancer: Clinical Features and Patterns of Recurrence. Clin Cancer Res 13, 4429–4434. doi:10.1158/1078-0432.CCR-06-3045

Di Leo, A., Jerusalem, G., Petruzelka, L., Torres, R., Bondarenko, I.N., Khasanov, R., Verhoeven, D., Pedrini, J.L., Smirnova, I., Lichinitser, M.R., Pendergrass, K., Malorni, L., Garnett, S., Rukazenkov, Y., Martin, M., 2014. Final overall survival: fulvestrant 500 mg vs 250 mg in the randomized CONFIRM trial. J. Natl. Cancer Inst. 106, djt337. doi:10.1093/jnci/djt337

Dixon, J.M., Dixon, J.M., 2014. Endocrine Resistance in Breast Cancer, Endocrine Resistance in Breast Cancer. New Journal of Science, New Journal of Science 2014, 2014, e390618. doi:10.1155/2014/390618, 10.1155/2014/390618

Doisneau-Sixou, S.F., Sergio, C.M., Carroll, J.S., Hui, R., Musgrove, E.A., Sutherland, R.L., 2003. Estrogen and antiestrogen regulation of cell cycle progression in breast cancer cells. Endocr. Relat. Cancer 10, 179–186.

Doughty, J.C., 2011. When to start an aromatase inhibitor: Now or later? J. Surg. Oncol. 103, 730–738. doi:10.1002/jso.21801

Dowling, R.J., Niraula, S., Chang, M.C., Done, S.J., Ennis, M., McCready, D.R., Leong, W.L., Escallon, J.M., Reedijk, M., Goodwin, P.J., Stambolic, V., 2015. Changes in insulin receptor signaling underlie neoadjuvant metformin administration in breast cancer: a prospective window of opportunity neoadjuvant study. Breast Cancer Res 17. doi:10.1186/s13058-015-0540-0

Dowling, R.J.O., Zakikhani, M., Fantus, I.G., Pollak, M., Sonenberg, N., 2007. Metformin Inhibits Mammalian Target of Rapamycin–Dependent Translation Initiation in Breast Cancer Cells. Cancer Res 67, 10804–10812. doi:10.1158/0008-5472.CAN-07-2310

Dowsett, M., Smith, I.E., Ebbs, S.R., Dixon, J.M., Skene, A., Griffith, C., Boeddinghaus, I., Salter, J., Detre, S., Hills, M., Ashley, S., Francis, S., Walsh, G., 2005. Short-Term Changes in Ki-67 during Neoadjuvant Treatment of Primary Breast Cancer with Anastrozole or Tamoxifen Alone or Combined Correlate with Recurrence-Free Survival. Clin Cancer Res 11, 951s–958s.

Dowsett, M., Cuzick, J., Ingle, J., Coates, A., Forbes, J., Bliss, J., Buyse, M., Baum, M., Buzdar, A., Colleoni, M., Coombes, C., Snowdon, C., Gnant, M., Jakesz, R., Kaufmann, M., Boccardo, F., Godwin, J., Davies, C., Peto, R., 2010. Meta-analysis of breast cancer outcomes in adjuvant trials of aromatase inhibitors versus tamoxifen. J. Clin. Oncol. 28, 509–518. doi:10.1200/JCO.2009.23.1274

Drury, S.C., Detre, S., Leary, A., Salter, J., Reis-Filho, J., Barbashina, V., Marchio, C., Lopez-Knowles, E., Ghazoui, Z., Habben, K., Arbogast, S., Johnston, S., Dowsett, M., 2011. Changes in breast cancer biomarkers in the IGF1R/PI3K pathway in recurrent breast cancer after tamoxifen treatment. Endocr Relat Cancer 18, 565–577. doi:10.1530/ERC-10-0046

Dumitrescu, R.G., Cotarla, I., 2005. Understanding breast cancer risk - where do we stand in 2005? Journal of Cellular and Molecular Medicine 9, 208–221. doi:10.1111/j.1582-4934.2005.tb00350.x

Dupont, J., Le Roith, D., 2001. Insulin-like growth factor 1 and oestradiol promote cell proliferation of MCF-7 breast cancer cells: new insights into their synergistic effects. Mol Pathol 54, 149–154.

Dutertre, M., Smith, C.L., 2003. Ligand-Independent Interactions of p160/Steroid Receptor Coactivators and CREB-Binding Protein (CBP) with Estrogen Receptor-α: Regulation by Phosphorylation Sites in the A/B Region Depends on Other Receptor Domains. Molecular Endocrinology 17, 1296–1314. doi:10.1210/me.2001-0316

Early Breast Cancer Trialists' Collaborative Group, 1988. Effects of adjuvant tamoxifen and of cytotoxic therapy on mortality in early breast cancer. An overview of 61 randomized trials among 28,896 women. N. Engl. J. Med. 319, 1681–1692. doi:10.1056/NEJM198812293192601

Early Breast Cancer Trialists' Collaborative Group (EBCTCG), 2005. Effects of chemotherapy and hormonal therapy for early breast cancer on recurrence and 15-year survival: an overview of the randomised trials. Lancet 365, 1687–1717. doi:10.1016/S0140-6736(05)66544-0

Early Breast Cancer Trialists' Collaborative Group (EBCTCG), 2011. Relevance of breast cancer hormone receptors and other factors to the efficacy of adjuvant tamoxifen: patient-level meta-analysis of randomised trials. The Lancet 378, 771–784. doi:10.1016/S0140-6736(11)60993-8

Ebert, B.L., Gleadle, J.M., O'Rourke, J.F., Bartlett, S.M., Poulton, J., Ratcliffe, P.J., 1996. Isoenzyme-specific regulation of genes involved in energy metabolism by hypoxia: similarities with the regulation of erythropoietin. Biochem. J. 313 (Pt 3), 809–814.

Eide, D.J., 2011. The oxidative stress of zinc deficiency. Metallomics 3, 1124–1129. doi:10.1039/C1MT00064K

Ellis, M.J., Tao, Y., Luo, J., A'Hern, R., Evans, D.B., Bhatnagar, A.S., Ross, H.A.C., Kameke, A. von, Miller, W.R., Smith, I., Eiermann, W., Dowsett, M., 2008. Outcome Prediction for Estrogen Receptor–Positive Breast Cancer Based on Postneoadjuvant Endocrine Therapy Tumor Characteristics. JNCI J Natl Cancer Inst 100, 1380–1388. doi:10.1093/jnci/djn309

Emami Riedmaier, A., Fisel, P., Nies, A.T., Schaeffeler, E., Schwab, M., 2013. Metformin and cancer: from the old medicine cabinet to pharmacological pitfalls and prospects. Trends Pharmacol. Sci. 34, 126–135. doi:10.1016/j.tips.2012.11.005

Eskey, C.J., Koretsky, A.P., Domach, M.M., Jain, R.K., 1993. Role of oxygen vs. glucose in energy metabolism in a mammary carcinoma perfused ex vivo: direct measurement by 31P NMR. Proc Natl Acad Sci U S A 90, 2646–2650.

Esteva, F.J., Moulder, S.L., Gonzalez-Angulo, A.M., Ensor, J., Murray, J.L., Green, M.C., Koenig, K.B., Lee, M.-H., Hortobagyi, G.N., Yeung, S.-C., 2013. Phase I trial of exemestane in combination with metformin and rosiglitazone in nondiabetic obese postmenopausal women with hormone receptor-positive metastatic breast cancer. Cancer Chemother. Pharmacol. 71, 63–72. doi:10.1007/s00280-012-1977-9

Fan, J., Kamphorst, J.J., Mathew, R., Chung, M.K., White, E., Shlomi, T., Rabinowitz, J.D., 2013. Glutamine-driven oxidative phosphorylation is a major ATP source in transformed mammalian cells in both normoxia and hypoxia. Mol. Syst. Biol. 9, 712. doi:10.1038/msb.2013.65

Farabegoli, F., Vettraino, M., Manerba, M., Fiume, L., Roberti, M., Di Stefano, G., 2012. Galloflavin, a new lactate dehydrogenase inhibitor, induces the death of human breast cancer cells with different glycolytic attitude by affecting distinct signaling pathways. European Journal of Pharmaceutical Sciences 47, 729–738. doi:10.1016/j.ejps.2012.08.012

Fathi, A.T., Sadrzadeh, H., Comander, A.H., Higgins, M.J., Bardia, A., Perry, A., Burke, M., Silver, R., Matulis, C.R., Straley, K.S., Yen, K.E., Agresta, S., Kim, H., Schenkein, D.P., Borger, D.R., 2014. Isocitrate dehydrogenase 1 (IDH1) mutation in breast adenocarcinoma is associated with elevated levels of serum and urine 2-hydroxyglutarate. Oncologist 19, 602–607. doi:10.1634/theoncologist.2013-0417

Ferrer-Soler, L., Vazquez-Martin, A., Brunet, J., Menendez, J.A., De Llorens, R., Colomer, R., 2007. An update of the mechanisms of resistance to EGFR-tyrosine kinase inhibitors in breast cancer: Gefitinib (Iressa) -induced changes in the expression and nucleo-cytoplasmic trafficking of HER-ligands (Review). Int. J. Mol. Med. 20, 3–10.

Finn R. S, n.d., 2013 A randomized, multicenter, double-blind phase III study of palbociclib (PD-0332991), an oral CDK 4/6 inhibitor, plus letrozole versus placebo plus letrozole for the treatment of postmenopausal women with ER(+), HER2(–) breast cancer who have not received any prior systemic anticancer treatment for advanced disease. J. Clin. Oncol.

Finn, R.S., Crown, J.P., Lang, I., Boer, K., Bondarenko, I.M., Kulyk, S.O., Ettl, J., Patel, R., Pinter, T., Schmidt, M., Shparyk, Y., Thummala, A.R., Voytko, N.L., Fowst, C., Huang, X., Kim, S.T., Randolph, S., Slamon, D.J., 2015. The cyclin-dependent kinase 4/6 inhibitor palbociclib in combination with letrozole versus letrozole alone as first-line treatment of oestrogen receptor-positive, HER2-negative, advanced breast cancer (PALOMA-1/TRIO-18): a randomised phase 2 study. The Lancet Oncology 16, 25–35. doi:10.1016/S1470-2045(14)71159-3

Frasor, J., Danes, J.M., Komm, B., Chang, K.C.N., Lyttle, C.R., Katzenellenbogen, B.S., 2003. Profiling of estrogen up- and down-regulated gene expression in human breast cancer cells: insights into gene networks and pathways underlying estrogenic control of proliferation and cell phenotype. Endocrinology 144, 4562–4574. doi:10.1210/en.2003-0567

Fuqua, S.A.W., Gu, G., Rechoum, Y., 2014. Estrogen receptor (ER) α mutations in breast cancer: hidden in plain sight. Breast Cancer Res Treat 144, 11–19. doi:10.1007/s10549-014-2847-4

Gee, J.M.W., Harper, M.E., Hutcheson, I.R., Madden, T.A., Barrow, D., Knowlden, J.M., McClelland, R.A., Jordan, N., Wakeling, A.E., Nicholson, R.I., 2003. The antiepidermal growth factor receptor agent gefitinib (ZD1839/Iressa) improves antihormone response and prevents development of resistance in breast cancer in vitro. Endocrinology 144, 5105–5117. doi:10.1210/en.2003-0705

Gee, J.M.W., Nicholson, R.I., Barrow, D., Dutkowski, C.M., Goddard, L., Jordan, N.J., McClelland, R.A., Knowlden, J.M., Francies, H.E., Hiscox, S.E., Hutcheson, I.R., 2011. Antihormone induced compensatory signalling in breast cancer: an adverse event in the development of endocrine resistance. Hormone Molecular Biology and Clinical Investigation 5, 67–77. doi:10.1515/HMBCI.2011.009

Gennari, A., Nanni, O., DeCensi, A., Sarti, S., Freschi, A., Bologna, A., Gianni, L., Amaducci, L., Rosetti, F., Giovanardi, F., Fedeli, A., Ambroggi, M., Bruzzi, P., Amadori, D., 2015. Abstract P3-13-02: Phase II randomised clinical study of first line chemotherapy plus metformin versus first line chemotherapy alone in HER2 negative, non diabetic, metastatic breast cancer patients: Final results of the MYME study. Cancer Res 75, P3–13–02–P3–13–02. doi:10.1158/1538-7445.SABCS14-P3-13-02

Gerdes, J., Lemke, H., Baisch, H., Wacker, H.H., Schwab, U., Stein, H., 1984. Cell cycle analysis of a cell proliferation-associated human nuclear antigen defined by the monoclonal antibody Ki-67. J. Immunol. 133, 1710–1715.

Goodwin, P.J., Pritchard, K.I., Ennis, M., Clemons, M., Graham, M., Fantus, I.G., 2008. Insulin-lowering effects of metformin in women with early breast cancer. Clin. Breast Cancer 8, 501–505. doi:10.3816/CBC.2008.n.060

Goodwin, P.J., Stambolic, V., 2011. Obesity and insulin resistance in breast cancer – Chemoprevention strategies with a focus on metformin. The Breast, Proceedings of the 12th International Conference on Primary Therapy of Early Breast Cancer 20, Supplement 3, S31–S35. doi:10.1016/S0960-9776(11)70291-0

Gowans, G.J., Hawley, S.A., Ross, F.A., Hardie, D.G., 2013. AMP is a true physiological regulator of AMP-activated protein kinase by both allosteric activation and enhancing net phosphorylation. Cell Metab. 18, 556–566. doi:10.1016/j.cmet.2013.08.019

Griffin, J.L., Shockcor, J.P., 2004. Metabolic profiles of cancer cells. Nat Rev Cancer 4, 551–561. doi:10.1038/nrc1390

Group, E.B.C.T.C., 1988. Effects of Adjuvant Tamoxifen and of Cytotoxic Therapy on Mortality in Early Breast Cancer. New England Journal of Medicine 319, 1681–1692. doi:10.1056/NEJM198812293192601

Guarneri, V., Conte, P., 2009. Metastatic breast cancer: therapeutic options according to molecular subtypes and prior adjuvant therapy. Oncologist 14, 645–656. doi:10.1634/theoncologist.2009-0078

Gutierrez, M.C., Detre, S., Johnston, S., Mohsin, S.K., Shou, J., Allred, D.C., Schiff, R., Osborne, C.K., Dowsett, M., 2005. Molecular changes in tamoxifen-resistant breast cancer: relationship between estrogen receptor, HER-2, and p38 mitogen-activated protein kinase. J. Clin. Oncol. 23, 2469–2476. doi:10.1200/JCO.2005.01.172

Gwinn, D.M., Shackelford, D.B., Egan, D.F., Mihaylova, M.M., Mery, A., Vasquez, D.S., Turk, B.E., Shaw, R.J., 2008. AMPK phosphorylation of raptor mediates a metabolic checkpoint. Mol. Cell 30, 214–226. doi:10.1016/j.molcel.2008.03.003

Győrffy, B., Lanczky, A., Eklund, A.C., Denkert, C., Budczies, J., Li, Q., Szallasi, Z., 2010. An online survival analysis tool to rapidly assess the effect of 22,277 genes on breast cancer prognosis using microarray data of 1,809 patients. Breast Cancer Res. Treat. 123, 725–731. doi:10.1007/s10549-009-0674-9

Haack, T.B., Madignier, F., Herzer, M., Lamantea, E., Danhauser, K., Invernizzi, F., Koch, J., Freitag, M., Drost, R., Hillier, I., Haberberger, B., Mayr, J.A., Ahting, U., Tiranti, V., Rötig, A., Iuso, A., Horvath, R., Tesarova, M., Baric, I., Uziel, G., Rolinski, B., Sperl, W., Meitinger, T., Zeviani, M., Freisinger, P., Prokisch, H., 2012. Mutation screening of 75 candidate genes in 152 complex I deficiency cases identifies pathogenic variants in 16 genes including NDUFB9. J. Med. Genet. 49, 83–89. doi:10.1136/jmedgenet-2011-100577

Hadad, S., Iwamoto, T., Jordan, L., Purdie, C., Bray, S., Baker, L., Jellema, G., Deharo, S., Hardie, D.G., Pusztai, L., Moulder-Thompson, S., Dewar, J.A., Thompson, A.M., 2011. Evidence for biological effects of metformin in operable breast cancer: a pre-operative, window-of-opportunity, randomized trial. Breast Cancer Res. Treat. 128, 783–794. doi:10.1007/s10549-011-1612-1

Hadad, S.M., Baker, L., Quinlan, P.R., Robertson, K.E., Bray, S.E., Thomson, G., Kellock, D., Jordan, L.B., Purdie, C.A., Hardie, D.G., Fleming, S., Thompson, A.M., 2009. Histological evaluation of AMPK signalling in primary breast cancer. BMC Cancer 9, 307. doi:10.1186/1471-2407-9-307

Hadad, S.M., Coates, P., Jordan, L.B., Dowling, R.J.O., Chang, M.C., Done, S.J., Purdie, C.A., Goodwin, P.J., Stambolic, V., Moulder-Thompson, S., Thompson, A.M., 2015. Evidence for biological effects of metformin in operable breast cancer: biomarker analysis in a pre-operative window of opportunity randomized trial. Breast Cancer Res. Treat. 150, 149–155. doi:10.1007/s10549-015-3307-5

Hadad, S.M., Fleming, S., Thompson, A.M., 2008. Targeting AMPK: A new therapeutic opportunity in breast cancer. Critical Reviews in Oncology/Hematology 67, 1–7. doi:10.1016/j.critrevonc.2008.01.007

Hadad, S.M., Hardie, D.G., Appleyard, V., Thompson, A.M., 2014. Effects of metformin on breast cancer cell proliferation, the AMPK pathway and the cell cycle. Clin Transl Oncol 16, 746–752. doi:10.1007/s12094-013-1144-8

Hanahan, D., Weinberg, R.A., 2011. Hallmarks of Cancer: The Next Generation. Cell 144, 646–674. doi:10.1016/j.cell.2011.02.013

Hardie, D.G., 2015. Molecular Pathways: Is AMPK a Friend or a Foe in Cancer? Clin Cancer Res 21, 3836–3840. doi:10.1158/1078-0432.CCR-14-3300

Hardie, D.G., Ross, F.A., Hawley, S.A., 2012. AMPK: a nutrient and energy sensor that maintains energy homeostasis. Nat Rev Mol Cell Biol 13, 251–262. doi:10.1038/nrm3311

Hartong, D.T., Dange, M., McGee, T.L., Berson, E.L., Dryja, T.P., Colman, R.F., 2008. Insights from retinitis pigmentosa into the roles of isocitrate dehydrogenases in the Krebs cycle. Nat. Genet. 40, 1230–1234. doi:10.1038/ng.223

Hartwell, L., Mankoff, D., Paulovich, A., Ramsey, S., Swisher, E., 2006. Cancer biomarkers: a systems approach. Nat Biotech 24, 905–908. doi:10.1038/nbt0806-905

Harvie, M., Hooper, L., Howell, A. h., 2003. Central obesity and breast cancer risk: a systematic review. Obesity Reviews 4, 157–173. doi:10.1046/j.1467-789X.2003.00108.x

Hassanein, M., Hoeksema, M.D., Shiota, M., Qian, J., Harris, B.K., Chen, H., Clark, J.E., Alborn, W.E., Eisenberg, R., Massion, P.P., 2013. SLC1A5 Mediates Glutamine Transport Required for Lung Cancer Cell Growth and Survival. Clin Cancer Res 19, 560–570. doi:10.1158/1078-0432.CCR-12-2334

Hawley, S.A., Boudeau, J., Reid, J.L., Mustard, K.J., Udd, L., Mäkelä, T.P., Alessi, D.R., Hardie, D.G., 2003. Complexes between the LKB1 tumor suppressor, STRAD alpha/beta and MO25 alpha/beta are upstream kinases in the AMP-activated protein kinase cascade. J. Biol. 2, 28. doi:10.1186/1475-4924-2-28

Hawley, S.A., Ross, F.A., Chevtzoff, C., Green, K.A., Evans, A., Fogarty, S., Towler, M.C., Brown, L.J., Ogunbayo, O.A., Evans, A.M., Hardie, D.G., 2010. Use of cells expressing gamma subunit variants to identify diverse mechanisms of AMPK activation. Cell Metab. 11, 554–565. doi:10.1016/j.cmet.2010.04.001

Heldring, N., Pike, A., Andersson, S., Matthews, J., Cheng, G., Hartman, J., Tujague, M., Ström, A., Treuter, E., Warner, M., Gustafsson, J.-Å., 2007. Estrogen Receptors: How Do They Signal and What Are Their Targets. Physiological Reviews 87, 905–931. doi:10.1152/physrev.00026.2006

Hirst, J., 2013. Mitochondrial complex I. Annu. Rev. Biochem. 82, 551–575. doi:10.1146/annurev-biochem-070511-103700

Hiscox, S., Jiang, W.G., Obermeier, K., Taylor, K., Morgan, L., Burmi, R., Barrow, D., Nicholson, R.I., 2006a. Tamoxifen resistance in MCF7 cells promotes EMT-like behaviour and involves modulation of β-catenin phosphorylation (a). Int. J. Cancer 118, 290–301. doi:10.1002/ijc.21355

Hiscox, S., Jordan, N.J., Jiang, W., Harper, M., McClelland, R., Smith, C., Nicholson, R.I., 2006b. Chronic exposure to fulvestrant promotes overexpression of the c-Met receptor in breast cancer cells: implications for tumour–stroma interactions (b). Endocr Relat Cancer 13, 1085–1099. doi:10.1677/erc.1.01270

Horne, M., Zimmermann, M., Don, A.A., Donaldson, M., Patriarchi, T., 2015. Cyclin G2 Contributes to the Cell Cycle Arrest Response of Breast Cancer Cells to Estrogen Signaling-Antagonists and the AMPK Agonist, Metformin. FASEB J 29, 576.10.

Howell, A., 2008. The endocrine prevention of breast cancer. Best Practice & Research Clinical Endocrinology & Metabolism, Endocrine and Metabolic Determinants of Cancer Risk 22, 615–623. doi:10.1016/j.beem.2008.09.002

Howell, A., Dowsett, M., 2004. Endocrinology and hormone therapy in breast cancer: Aromatase inhibitors versus antioestrogens. Breast Cancer Research 6, 269. doi:10.1186/bcr945

Hu, R., Hilakivi-Clarke, L., Clarke, R., 2015. Molecular mechanisms of tamoxifen-associated endometrial cancer (Review). Oncol Lett 9, 1495–1501. doi:10.3892/ol.2015.2962

Huber-Keener, K.J., Liu, X., Wang, Z., Wang, Y., Freeman, W., Wu, S., Planas-Silva, M.D., Ren, X., Cheng, Y., Zhang, Y., Vrana, K., Liu, C.-G., Yang, J.-M., Wu, R., 2012. Differential Gene Expression in Tamoxifen-Resistant Breast Cancer Cells Revealed by a New Analytical Model of RNA-Seq Data. PLOS ONE 7, e41333. doi:10.1371/journal.pone.0041333

Huober, J., Fasching, P.A., Barsoum, M., Petruzelka, L., Wallwiener, D., Thomssen, C., Reimer, T., Paepke, S., Azim, H.A., Ragosch, V., Kubista, E., Baumgärtner, A.K., Beckmann, M.W., May, C., Nimmrich, I., Harbeck, N., 2012. Higher efficacy of letrozole in combination with trastuzumab compared to letrozole monotherapy as first-line treatment in patients with HER2-positive, hormone-receptor-positive metastatic breast cancer – Results of the eLEcTRA trial. The Breast 21, 27–33. doi:10.1016/j.breast.2011.07.006

Hutcheson, I.R., Knowlden, J.M., Jones, H.E., Burmi, R.S., McClelland, R.A., Barrow, D., Gee, J.M.W., Nicholson, R.I., 2006. Inductive mechanisms limiting response to anti-epidermal growth factor receptor therapy. Endocr Relat Cancer 13, S89–S97. doi:10.1677/erc.1.01279

Icard, P., Lincet, H., 2012. A global view of the biochemical pathways involved in the regulation of the metabolism of cancer cells. Biochimica et Biophysica Acta (BBA) - Reviews on Cancer 1826, 423–433. doi:10.1016/j.bbcan.2012.07.001

Inoki, K., Zhu, T., Guan, K.-L., 2003. TSC2 mediates cellular energy response to control cell growth and survival. Cell 115, 577–590.

Iwata, S., Lee, J.W., Okada, K., Lee, J.K., Iwata, M., Rasmussen, B., Link, T.A., Ramaswamy, S., Jap, B.K., 1998. Complete structure of the 11-subunit bovine mitochondrial cytochrome bc1 complex. Science 281, 64–71.

Jain, M., Nilsson, R., Sharma, S., Madhusudhan, N., Kitami, T., Souza, A.L., Kafri, R., Kirschner, M.W., Clish, C.B., Mootha, V.K., 2012. Metabolite Profiling Identifies a Key Role for Glycine in Rapid Cancer Cell Proliferation. Science 336, 1040–1044. doi:10.1126/science.1218595

Jang, M., Kim, S.S., Lee, J., 2013. Cancer cell metabolism: implications for therapeutic targets. Exp Mol Med 45, e45. doi:10.1038/emm.2013.85

Jansen, M.P.H.M., Foekens, J.A., Staveren, I.L. van, Dirkzwager-Kiel, M.M., Ritstier, K., Look, M.P., Gelder, M.E.M., Sieuwerts, A.M., Portengen, H., Dorssers, L.C.J., Klijn, J.G.M., Berns, E.M.J.J., 2005. Molecular Classification of Tamoxifen-Resistant Breast Carcinomas by Gene Expression Profiling. JCO 23, 732–740. doi:10.1200/JCO.2005.05.145

Jenne, D.E., Reimann, H., Nezu, J., Friedel, W., Loff, S., Jeschke, R., Müller, O., Back, W., Zimmer, M., 1998. Peutz-Jeghers syndrome is caused by mutations in a novel serine threonine kinase. Nat. Genet. 18, 38–43. doi:10.1038/ng0198-38

Jeselsohn, R., Yelensky, R., Buchwalter, G., Frampton, G., Meric-Bernstam, F., Gonzalez-Angulo, A.M., Ferrer-Lozano, J., Perez-Fidalgo, J.A., Cristofanilli, M., Gómez, H., Arteaga, C.L., Giltnane, J., Balko, J.M., Cronin, M.T., Jarosz, M., Sun, J., Hawryluk, M., Lipson, D., Otto, G., Ross, J.S., Dvir, A., Soussan-Gutman, L., Wolf, I., Rubinek, T., Gilmore, L., Schnitt, S., Come, S.E., Pusztai, L., Stephens, P., Brown, M., Miller, V.A., 2014. Emergence of Constitutively Active Estrogen Receptor-α Mutations in Pretreated Advanced Estrogen Receptor–Positive Breast Cancer. Clin Cancer Res 20, 1757–1767. doi:10.1158/1078-0432.CCR-13-2332

Jiang, J., Sarwar, N., Peston, D., Kulinskaya, E., Shousha, S., Coombes, R.C., Ali, S., 2007. Phosphorylation of Estrogen Receptor-α at Ser167 Is Indicative of Longer Disease-Free and Overall Survival in Breast Cancer Patients. Clin Cancer Res 13, 5769–5776. doi:10.1158/1078-0432.CCR-07-0822

Jiao, X., Sherman, B.T., Huang, D.W., Stephens, R., Baseler, M.W., Lane, H.C., Lempicki, R.A., 2012. DAVID-WS: a stateful web service to facilitate gene/protein list analysis. Bioinformatics 28, 1805–1806. doi:10.1093/bioinformatics/bts251

Jirström, K., Stendahl, M., Rydén, L., Kronblad, A., Bendahl, P.-O., Stål, O., Landberg, G., 2005. Adverse effect of adjuvant tamoxifen in premenopausal breast cancer with cyclin D1 gene amplification. Cancer Res. 65, 8009–8016. doi:10.1158/0008-5472.CAN-05-0746

Jochmanová, I., Zhuang, Z., Pacak, K., 2015. Pheochromocytoma: Gasping for Air. Horm Cancer 6, 191–205. doi:10.1007/s12672-015-0231-4

Johnston, S., Pippen, J., Pivot, X., Lichinitser, M., Sadeghi, S., Dieras, V., Gomez, H.L., Romieu, G., Manikhas, A., Kennedy, M.J., Press, M.F., Maltzman, J., Florance, A., O'Rourke, L., Oliva, C., Stein, S., Pegram, M., 2009. Lapatinib Combined With Letrozole Versus Letrozole and Placebo As First-Line Therapy for Postmenopausal Hormone Receptor–Positive Metastatic Breast Cancer. JCO 27, 5538–5546. doi:10.1200/JCO.2009.23.3734

Johnston, S.R.D., 2015. Enhancing Endocrine Therapy for Hormone Receptor–Positive Advanced Breast Cancer: Cotargeting Signaling Pathways. JNCI J Natl Cancer Inst 107, djv212. doi:10.1093/jnci/djv212

Johnston, S.R.D., Dowsett, M., 2003. Aromatase inhibitors for breast cancer: lessons from the laboratory. Nat Rev Cancer 3, 821–831. doi:10.1038/nrc1211

Jordan, V.C., Robinson, S.P., 1987. Species-specific pharmacology of antiestrogens: role of metabolism. Fed. Proc. 46, 1870–1874.

Jordan, N.J., Dutkowski, C.M., Barrow, D., Mottram, H.J., Hutcheson, I.R., Nicholson, R.I., Guichard, S.M., Gee, J.M.W., 2014. Impact of dual mTORC1/2 mTOR kinase inhibitor AZD8055 on acquired endocrine resistance in breast cancer in vitro. Breast Cancer Res. 16, R12. doi:10.1186/bcr3604

Jose, C., Bellance, N., Rossignol, R., 2011. Choosing between glycolysis and oxidative phosphorylation: a tumor's dilemma? Biochim. Biophys. Acta 1807, 552–561. doi:10.1016/j.bbabio.2010.10.012

Kaambre, T., Chekulayev, V., Shevchuk, I., Tepp, K., Timohhina, N., Varikmaa, M., Bagur, R., Klepinin, A., Anmann, T., Koit, A., Kaldma, A., Guzun, R., Valvere, V., Saks, V., 2013. Metabolic control analysis of respiration in human cancer tissue. Front Physiol 4. doi:10.3389/fphys.2013.00151

Kadota, Y., Suzuki, S., Ideta, S., Fukinbara, Y., Kawakami, T., Imai, H., Nakagawa, Y., Sato, M., 2010. Enhanced metallothionein gene expression induced by mitochondrial oxidative stress is reduced in phospholipid hydroperoxide glutathione peroxidase-overexpressed cells. European Journal of Pharmacology 626, 166–170. doi:10.1016/j.ejphar.2009.09.060

Kalinsky, K., Crew, K.D., Refice, S., Xiao, T., Wang, A., Feldman, S.M., Taback, B., Ahmad, A., Cremers, S., Hibshoosh, H., Maurer, M., Hershman, D.L., 2014. Presurgical trial of metformin in overweight and obese patients with newly diagnosed breast cancer. Cancer Invest. 32, 150–157. doi:10.3109/07357907.2014.889706

Kaneko, S.J., Gerasimova, T., Smith, S.T., Lloyd, K.O., Suzumori, K., Young, S.R., 2003. CA125 and UQCRFS1 FISH studies of ovarian carcinoma. Gynecologic Oncology 90, 29–36. doi:10.1016/S0090-8258(03)00144-6

Kaplon, J., Zheng, L., Meissl, K., Chaneton, B., Selivanov, V.A., Mackay, G., van der Burg, S.H., Verdegaal, E.M.E., Cascante, M., Shlomi, T., Gottlieb, E., Peeper, D.S., 2013. A key role for mitochondrial gatekeeper pyruvate dehydrogenase in oncogene-induced senescence. Nature 498, 109–112. doi:10.1038/nature12154

Kato, S., Endoh, H., Masuhiro, Y., Kitamoto, T., Uchiyama, S., Sasaki, H., Masushige, S., Gotoh, Y., Nishida, E., Kawashima, H., Metzger, D., Chambon, P., 1995. Activation of the estrogen receptor through phosphorylation by mitogen-activated protein kinase. Science 270, 1491–1494.

Kaufman, B., Mackey, J.R., Clemens, M.R., Bapsy, P.P., Vaid, A., Wardley, A., Tjulandin, S., Jahn, M., Lehle, M., Feyereislova, A., Révil, C., Jones, A., 2009. Trastuzumab Plus Anastrozole Versus Anastrozole Alone for the Treatment of Postmenopausal Women With Human Epidermal Growth Factor Receptor 2–Positive, Hormone Receptor–Positive Metastatic Breast Cancer: Results From the Randomized Phase III TAnDEM Study. JCO 27, 5529–5537. doi:10.1200/JCO.2008.20.6847

Kennecke, H., Yerushalmi, R., Woods, R., Cheang, M.C.U., Voduc, D., Speers, C.H., Nielsen, T.O., Gelmon, K., 2010. Metastatic behaviour of breast cancer subtypes. J. Clin. Oncol. 28, 3271–3277. doi:10.1200/JCO.2009.25.9820

Kim, C.W., Lee, H.M., Lee, T.H., Kang, C., Kleinman, H.K., Gho, Y.S., 2002. Extracellular Membrane Vesicles from Tumor Cells Promote Angiogenesis via Sphingomyelin. Cancer Res 62, 6312–6317.

Kim, H.J., Kwon, H., Lee, J.W., Kim, H.J., Lee, S.B., Park, H.S., Sohn, G., Lee, Y., Koh, B.S., Yu, J.H., Son, B.H., Ahn, S.H., 2015. Metformin increases survival in hormone receptor-positive, HER2-positive breast cancer patients with diabetes. Breast Cancer Research 17, 64. doi:10.1186/s13058-015-0574-3

Kim, J., Lim, W., Kim, E.-K., Kim, M.-K., Paik, N.-S., Jeong, S.-S., Yoon, J., Park, C.H., Ahn, S.H., Kim, L.S., Han, S., Nam, S.J., Kang, H.-S., Kim, S.I., Yoo, Y.B., Jeong, J., Kim, T.H., Kang, T., Kim, S.-W., Jung, Y., Lee, J.E., Kim, K.S., Yu, J.-H., Chae, B.J., Jung, S.-Y., Kang, E., Choi, S.Y., Moon, H.-G., Noh, D.-Y., Han, W., 2014. Phase II randomized trial of neoadjuvant metformin plus letrozole versus placebo plus letrozole for estrogen receptor positive postmenopausal breast cancer (METEOR). BMC Cancer 14, 170. doi:10.1186/1471-2407-14-170

Kim, S., Kim, D.H., Jung, W.-H., Koo, J.S., 2013. Succinate dehydrogenase expression in breast cancer. Springerplus 2. doi:10.1186/2193-1801-2-299

Kim, S.-Y., 2015. Cancer Metabolism: Strategic Diversion from Targeting Cancer Drivers to Targeting Cancer Suppliers. Biomol Ther (Seoul) 23, 99–109. doi:10.4062/biomolther.2015.013

Kim, Y.-W., Kwon, C., Liu, J.-L., Kim, S.H., Kim, S., 2012. Cancer Association Study of Aminoacyl-tRNA Synthetase Signaling Network in Glioblastoma. PLOS ONE 7, e40960. doi:10.1371/journal.pone.0040960

Kirkegaard, T., Witton, C.J., McGlynn, L.M., Tovey, S.M., Dunne, B., Lyon, A., Bartlett, J.M., 2005. AKT activation predicts outcome in breast cancer patients treated with tamoxifen. J. Pathol. 207, 139–146. doi:10.1002/path.1829

Klinge, C.M., 2000. Estrogen receptor interaction with co-activators and co-repressors☆. Steroids 65, 227–251. doi:10.1016/S0039-128X(99)00107-5

Klinge, C.M., Jernigan, S.C., Smith, S.L., Tyulmenkov, V.V., Kulakosky, P.C., 2001. Estrogen response element sequence impacts the conformation and transcriptional activity of estrogen receptor α1. Molecular and Cellular Endocrinology 174, 151–166. doi:10.1016/S0303-7207(01)00382-3

Knowlden, J.M., Hutcheson, I.R., Jones, H.E., Madden, T., Gee, J.M.W., Harper, M.E., Barrow, D., Wakeling, A.E., Nicholson, R.I., 2003. Elevated Levels of Epidermal Growth Factor Receptor/c-erbB2 Heterodimers Mediate an Autocrine Growth Regulatory Pathway in Tamoxifen-Resistant MCF-7 Cells. Endocrinology 144, 1032–1044. doi:10.1210/en.2002-220620

Knowlden, J.M., Hutcheson, I.R., Barrow, D., Gee, J.M.W., Nicholson, R.I., 2005. Insulin-like growth factor-I receptor signaling in tamoxifen-resistant breast cancer: a supporting role to the epidermal growth factor receptor. Endocrinology 146, 4609–4618. doi:10.1210/en.2005-0247

Ko, Y.-H., Lin, Z., Flomenberg, N., Pestell, R.G., Howell, A., Sotgia, F., Lisanti, M.P., Martinez-Outschoorn, U.E., 2011. Glutamine fuels a vicious cycle of autophagy in the tumor stroma and oxidative mitochondrial metabolism in epithelial cancer cells. Cancer Biology & Therapy 12, 1085–1097. doi:10.4161/cbt.12.12.18671

Kobayashi, S., Millhorn, D.E., 2001. Hypoxia regulates glutamate metabolism and membrane transport in rat PC12 cells. J. Neurochem. 76, 1935–1948.

Kok, M., Holm-Wigerup, C., Hauptmann, M., Michalides, R., Stål, O., Linn, S., Landberg, G., 2009. Estrogen Receptor-α Phosphorylation at Serine-118 and Tamoxifen Response in Breast Cancer. JNCI J Natl Cancer Inst 101, 1725–1729. doi:10.1093/jnci/djp412

Kumar, V., Green, S., Stack, G., Berry, M., Jin, J.R., Chambon, P., 1987. Functional domains of the human estrogen receptor. Cell 51, 941–951.

Kung, H.-N., Marks, J.R., Chi, J.-T., 2011. Glutamine Synthetase Is a Genetic Determinant of Cell Type–Specific Glutamine Independence in Breast Epithelia. PLOS Genet 7, e1002229. doi:10.1371/journal.pgen.1002229

L'Espérance, S., Popa, I., Bachvarova, M., Plante, M., Patten, N., Wu, L., Têtu, B., Bachvarov, D., 2006. Gene expression profiling of paired ovarian tumors obtained prior to and following adjuvant chemotherapy: molecular signatures of chemoresistant tumors. Int. J. Oncol. 29, 5–24.

Laemmli, U.K., 1970. Cleavage of Structural Proteins during the Assembly of the Head of Bacteriophage T4. Nature 227, 680–685. doi:10.1038/227680a0

Lander, E.S., Linton, L.M., Birren, B., Nusbaum, C., Zody, M.C., Baldwin, J., Devon, K., Dewar, K., Doyle, M., FitzHugh, W., Funke, R., Gage, D., Harris, K., Heaford, A., Howland, J., Kann, L., Lehoczky, J., LeVine, R., McEwan, P., McKernan, K., Meldrim, J., Mesirov, J.P., Miranda, C., Morris, W., Naylor, J., Raymond, C., Rosetti, M., Santos, R., Sheridan, A., Sougnez, C., Stange-Thomann, N., Stojanovic, N., Subramanian, A., Wyman, D., Rogers, J., Sulston, J., Ainscough, R., Beck, S., Bentley, D., Burton, J., Clee, C., Carter, N., Coulson, A., Deadman, R., Deloukas, P., Dunham, A., Dunham, I., Durbin, R., French, L., Grafham, D., Gregory, S., Hubbard, T., Humphray, S., Hunt, A., Jones, M., Lloyd, C., McMurray, A., Matthews, L., Mercer, S., Milne, S., Mullikin, J.C., Mungall, A., Plumb, R., Ross, M., Shownkeen, R., Sims, S., Waterston, R.H., Wilson, R.K., Hillier, L.W., McPherson, J.D., Marra, M.A., Mardis, E.R., Fulton, L.A., Chinwalla, A.T., Pepin, K.H., Gish,

W.R., Chissoe, S.L., Wendl, M.C., Delehaunty, K.D., Miner, T.L., Delehaunty, A., Kramer, J.B., Cook, L.L., Fulton, R.S., Johnson, D.L., Minx, P.J., Clifton, S.W., Hawkins, T., Branscomb, E., Predki, P., Richardson, P., Wenning, S., Slezak, T., Doggett, N., Cheng, J.-F., Olsen, A., Lucas, S., Elkin, C., Uberbacher, E., Frazier, M., Gibbs, R.A., Muzny, D.M., Scherer, S.E., Bouck, J.B., Sodergren, E.J., Worley, K.C., Rives, C.M., Gorrell, J.H., Metzker, M.L., Naylor, S.L., Kucherlapati, R.S., Nelson, D.L., Weinstock, G.M., Sakaki, Y., Fujiyama, A., Hattori, M., Yada, T., Toyoda, A., Itoh, T., Kawagoe, C., Watanabe, H., Totoki, Y., Taylor, T., Weissenbach, J., Heilig, R., Saurin, W., Artiguenave, F., Brottier, P., Bruls, T., Pelletier, E., Robert, C., Wincker, P., Rosenthal, A., Platzer, M., Nyakatura, G., Taudien, S., Rump, A., Smith, D.R., Doucette-Stamm, L., Rubenfield, M., Weinstock, K., Lee, H.M., Dubois, J., Yang, H., Yu, J., Wang, J., Huang, G., Gu, J., Hood, L., Rowen, L., Madan, A., Qin, S., Davis, R.W., Federspiel, N.A., Abola, A.P., Proctor, M.J., Roe, B.A., Chen, F., Pan, H., Ramser, J., Lehrach, H., Reinhardt, R., McCombie, W.R., Bastide, M. de la, Dedhia, N., Blöcker, H., Hornischer, K., Nordsiek, G., Agarwala, R., Aravind, L., Bailey, J.A., Bateman, A., Batzoglou, S., Birney, E., Bork, P., Brown, D.G., Burge, C.B., Cerutti, L., Chen, H.-C., Church, D., Clamp, M., Copley, R.R., Doerks, T., Eddy, S.R., Eichler, E.E., Furey, T.S., Galagan, J., Gilbert, J.G.R., Harmon, C., Hayashizaki, Y., Haussler, D., Hermjakob, H., Hokamp, K., Jang, W., Johnson, L.S., Jones, T.A., Kasif, S., Kaspryzk, A., Kennedy, S., Kent, W.J., Kitts, P., Koonin, E.V., Korf, I., Kulp, D., Lancet, D., Lowe, T.M., McLysaght, A., Mikkelsen, T., Moran, J.V., Mulder, N., Pollara, V.J., Ponting, C.P., Schuler, G., Schultz, J., Slater, G., Smit, A.F.A., Stupka, E., Szustakowki, J., Thierry-Mieg, D., Thierry-Mieg, J., Wagner, L., Wallis, J., Wheeler, R., Williams, A., Wolf, Y.I., Wolfe, K.H., Yang, S.-P., Yeh, R.-F., Collins, F., Guyer, M.S., Peterson, J., Felsenfeld, A., Wetterstrand, K.A., Myers, R.M., Schmutz, J., Dickson, M., Grimwood, J., Cox, D.R., Olson, M.V., Kaul, R., Raymond, C., Shimizu, N., Kawasaki, K., Minoshima, S., Evans, G.A., Athanasiou, M., Schultz, R., Patrinos, A., Morgan, M.J., 2001. Initial sequencing and analysis of the human genome. Nature 409, 860–921. doi:10.1038/35057062

Largent, J.A., McEligot, A.J., Ziogas, A., Reid, C., Hess, J., Leighton, N., Peel, D., Anton-Culver, H., 2006. Hypertension, diuretics and breast cancer risk. J Hum Hypertens 20, 727–732. doi:10.1038/sj.jhh.1002075

Larionov, A.A., Miller, W.R., 2009. Challenges in defining predictive markers for response to endocrine therapy in breast cancer. Future Oncology 5, 1415–1428. doi:10.2217/fon.09.113

Larsen, S.L., Laenkholm, A.-V., Duun-Henriksen, A.K., Bak, M., Lykkesfeldt, A.E., Kirkegaard, T., 2015. Src Drives Growth of Antiestrogen Resistant Breast Cancer Cell Lines and Is a Marker for Reduced Benefit of Tamoxifen Treatment. PLoS One 10. doi:10.1371/journal.pone.0118346

Lavinsky, R.M., Jepsen, K., Heinzel, T., Torchia, J., Mullen, T.-M., Schiff, R., Del-Rio, A.L., Ricote, M., Ngo, S., Gemsch, J., Hilsenbeck, S.G., Osborne, C.K., Glass, C.K., Rosenfeld, M.G., Rose, D.W., 1998. Diverse signaling pathways modulate nuclear receptor recruitment of N-CoR and SMRT complexes. PNAS 95, 2920–2925.

Lehtonen, H.J., Kiuru, M., Ylisaukko-Oja, S.K., Salovaara, R., Herva, R., Koivisto, P.A., Vierimaa, O., Aittomäki, K., Pukkala, E., Launonen, V., Aaltonen, L.A., 2006. Increased risk of cancer in patients with fumarate hydratase germline mutation. J. Med. Genet. 43, 523–526. doi:10.1136/jmg.2005.036400

Leithner, K., Hrzenjak, A., Trötzmüller, M., Moustafa, T., Köfeler, H.C., Wohlkoenig, C., Stacher, E., Lindenmann, J., Harris, A.L., Olschewski, A., Olschewski, H., 2015. PCK2 activation mediates an adaptive response to glucose depletion in lung cancer. Oncogene 34, 1044–1050. doi:10.1038/onc.2014.47

Leone, A., Di Gennaro, E., Bruzzese, F., Avallone, A., Budillon, A., 2014. New perspective for an old antidiabetic drug: metformin as anticancer agent. Cancer Treat. Res. 159, 355–376. doi:10.1007/978-3-642-38007-5_21

Leung, E.Y., Kim, J.E., Askarian-Amiri, M., Joseph, W.R., McKeage, M.J., Baguley, B.C., 2014. Hormone Resistance in Two MCF-7 Breast Cancer Cell Lines is Associated with Reduced mTOR Signaling, Decreased Glycolysis, and Increased Sensitivity to Cytotoxic Drugs. Front Oncol 4. doi:10.3389/fonc.2014.00221

Levenson, A.S., Jordan, V.C., 1997. MCF-7: the first hormone-responsive breast cancer cell line. Cancer Res. 57, 3071–3078.

Levin, E.R., 2009. G Protein-Coupled Receptor 30: Estrogen Receptor or Collaborator? Endocrinology 150, 1563–1565. doi:10.1210/en.2008-1759

Li, Q., Birkbak, N.J., Gyorffy, B., Szallasi, Z., Eklund, A.C., 2011. Jetset: selecting the optimal microarray probe set to represent a gene. BMC Bioinformatics 12, 474. doi:10.1186/1471-2105-12-474

Lichten, L.A., Cousins, R.J., 2009. Mammalian Zinc Transporters: Nutritional and Physiologic Regulation. Annual Review of Nutrition 29, 153–176. doi:10.1146/annurev-nutr-033009-083312

Lieberman, B.P., Ploessl, K., Wang, L., Qu, W., Zha, Z., Wise, D.R., Chodosh, L.A., Belka, G., Thompson, C.B., Kung, H.F., 2011. PET imaging of glutaminolysis in tumors by 18F-(2S,4R)4-fluoroglutamine. J. Nucl. Med. 52, 1947–1955. doi:10.2967/jnumed.111.093815

Lieberman, B.P., Ploessl, K., Wang, L., Qu, W., Zha, Z., Wise, D.R., Chodosh, L.A., Belka, G., Thompson, C.B., Kung, H.F., 2011. PET imaging of glutaminolysis in tumors by 18F-(2S,4R)4-fluoroglutamine. J. Nucl. Med. 52, 1947–1955. doi:10.2967/jnumed.111.093815

Liu, J., Zhan, X., Li, M., Li, G., Zhang, P., Xiao, Z., Shao, M., Peng, F., Hu, R., Chen, Z., 2012. Mitochondrial proteomics of nasopharyngeal carcinoma metastasis. BMC Med Genomics 5, 62. doi:10.1186/1755-8794-5-62

Locke, D., 1998. Gap junctions in normal and neoplastic mammary gland. J. Pathol. 186, 343–349. doi:10.1002/(SICI)1096-9896(199812)186:4<343::AID-PATH189>3.0.CO;2-X

Lopez, F., Belloc, F., Lacombe, F., Dumain, P., Reiffers, J., Bernard, P., Boisseau, M.R., 1991. Modalities of synthesis of Ki67 antigen during the stimulation of lymphocytes. Cytometry 12, 42–49. doi:10.1002/cyto.990120107

Ma, C.X., Sanchez, C.G., Ellis, M.J., 2009. Predicting endocrine therapy responsiveness in breast cancer. ONCOLOGY 23, 133–142.

Mackay, A., Weigelt, B., Grigoriadis, A., Kreike, B., Natrajan, R., A'Hern, R., Tan, D.S.P., Dowsett, M., Ashworth, A., Reis-Filho, J.S., 2011. Microarray-based class discovery for molecular classification of breast cancer: analysis of interobserver agreement. J. Natl. Cancer Inst. 103, 662–673. doi:10.1093/jnci/djr071

Manning, G., Whyte, D.B., Martinez, R., Hunter, T., Sudarsanam, S., 2002. The Protein Kinase Complement of the Human Genome. Science 298, 1912–1934. doi:10.1126/science.1075762

Marín-Hernández, A., Gallardo-Pérez, J.C., Ralph, S.J., Rodríguez-Enríquez, S., Moreno-Sánchez, R., 2009. HIF-1alpha modulates energy metabolism in cancer cells by inducing over-expression of specific glycolytic isoforms. Mini Rev Med Chem 9, 1084–1101.

Martin, L.-A., Ghazoui, Z., Weigel, M.T., Pancholi, S., Dunbier, A., Johnston, S., Dowsett, M., 2011. An in vitro model showing adaptation to long-term oestrogen deprivation highlights the clinical potential for targeting kinase pathways in combination with aromatase inhibition. Steroids, 10th International Aromatase Conference Proceedings, September 2010 76, 772–776. doi:10.1016/j.steroids.2011.02.035

Martinez-Outschoorn, U.E., Lin, Z., Ko, Y.-H., Goldberg, A.F., Flomenberg, N., Wang, C., Pavlides, S., Pestell, R.G., Howell, A., Sotgia, F., Lisanti, M.P., 2011. Understanding the metabolic basis of drug resistance. Cell Cycle 10, 2521–2528. doi:10.4161/cc.10.15.16584

Martinez-Outschoorn, U.E., Pavlides, S., Sotgia, F., Lisanti, M.P., 2011. Mitochondrial Biogenesis Drives Tumor Cell Proliferation. Am J Pathol 178, 1949–1952. doi:10.1016/j.ajpath.2011.03.002

Martinho, A., Gonçalves, I., Santos, C.R., 2013. Glucocorticoids regulate metallothionein-1/2 expression in rat choroid plexus: effects on apoptosis. Mol Cell Biochem 376, 41–51. doi:10.1007/s11010-012-1547-9

Mason, M.G., Nicholls, P., Wilson, M.T., Cooper, C.E., 2006. Nitric oxide inhibition of respiration involves both competitive (heme) and noncompetitive (copper) binding to cytochrome c oxidase. Proc. Natl. Acad. Sci. U.S.A. 103, 708–713. doi:10.1073/pnas.0506562103

Masri, S., Phung, S., Wang, X., Wu, X., Yuan, Y.-C., Wagman, L., Chen, S., 2008. Genome-Wide Analysis of Aromatase Inhibitor-Resistant, Tamoxifen-Resistant, and Long-Term Estrogen-Deprived Cells Reveals a Role for Estrogen Receptor. Cancer Res 68, 4910–4918. doi:10.1158/0008-5472.CAN-08-0303

Massarweh, S., Osborne, C.K., Jiang, S., Wakeling, A.E., Rimawi, M., Mohsin, S.K., Hilsenbeck, S., Schiff, R., 2006. Mechanisms of Tumor Regression and Resistance to Estrogen Deprivation and Fulvestrant in a Model of Estrogen Receptor–Positive, HER-2/neu-Positive Breast Cancer. Cancer Res 66, 8266–8273. doi:10.1158/0008-5472.CAN-05-4045

Massarweh, S., Schiff, R., 2006. Resistance to endocrine therapy in breast cancer: exploiting estrogen receptor/growth factor signaling crosstalk. Endocr. Relat. Cancer 13 Suppl 1, S15–24. doi:10.1677/erc.1.01273

Mayer, I.A., Abramson, V.G., Isakoff, S.J., Forero, A., Balko, J.M., Kuba, M.G., Sanders, M.E., Yap, J.T., Abbeele, A.D.V. den, Li, Y., Cantley, L.C., Winer, E., Arteaga, C.L., 2014. Stand Up to Cancer Phase Ib Study of Pan-Phosphoinositide-3-Kinase Inhibitor Buparlisib With Letrozole in Estrogen Receptor-Positive/Human Epidermal Growth Factor Receptor 2-Negative Metastatic Breast Cancer. JCO 32, 1202–1209. doi:10.1200/JCO.2013.54.0518

Mazurek, S., Michel, A., Eigenbrodt, E., 1997. Effect of Extracellular AMP on Cell Proliferation and Metabolism of Breast Cancer Cell Lines with High and Low Glycolytic Rates. J. Biol. Chem. 272, 4941–4952. doi:10.1074/jbc.272.8.4941

McClelland, R.A., Barrow, D., Madden, T.-A., Dutkowski, C.M., Pamment, J., Knowlden, J.M., Gee, J.M.W., Nicholson, R.I., 2001. Enhanced Epidermal Growth Factor Receptor Signaling in MCF7 Breast Cancer Cells after Long-Term Culture in the Presence of the Pure Antiestrogen ICI 182,780 (Fulvestrant). Endocrinology 142, 2776–2788. doi:10.1210/endo.142.7.8259

Mehta, A., Tripathy, D., 2014. Co-targeting estrogen receptor and HER2 pathways in breast cancer. The Breast 23, 2–9. doi:10.1016/j.breast.2013.09.006

Meier-Ruge, W.A., Bruder, E., 2008. Current concepts of enzyme histochemistry in modern pathology. Pathobiology 75, 233–243. doi:10.1159/000132384

Menendez, J.A., Oliveras-Ferraros, C., Cufí, S., Corominas-Faja, B., Joven, J., Martin-Castillo, B., Vazquez-Martin, A., 2012. Metformin is synthetically lethal with glucose withdrawal in cancer cells. Cell Cycle 11, 2782–2792. doi:10.4161/cc.20948

Meng, M., Chen, S., Lao, T., Liang, D., Sang, N., 2010. Nitrogen anabolism underlies the importance of glutaminolysis in proliferating cells. Cell Cycle 9, 3921–3932. doi:10.4161/cc.9.19.13139

Michels, K.B., Solomon, C.G., Hu, F.B., Rosner, B.A., Hankinson, S.E., Colditz, G.A., Manson, J.E., 2003. Type 2 Diabetes and Subsequent Incidence of Breast Cancer in the Nurses' Health Study. Dia Care 26, 1752–1758. doi:10.2337/diacare.26.6.1752

Miller, W.R., Bartlett, J.M.S., Canney, P., Verrill, M., 2007. Hormonal therapy for postmenopausal breast cancer: the science of sequencing. Breast Cancer Res. Treat. 103, 149–160. doi:10.1007/s10549-006-9369-7

Miller, W.R., Larionov, A., Renshaw, L., Anderson, T.J., Walker, J.R., Krause, A., Sing, T., Evans, D.B., Dixon, J.M., 2009. Gene Expression Profiles Differentiating Between Breast Cancers Clinically Responsive or Resistant to Letrozole. JCO 27, 1382–1387. doi:10.1200/JCO.2008.16.8849

Miller, W.R., Larionov, A., Renshaw, L., Anderson, T.J., White, S., Hampton, G., Walker, J.R., Ho, S., Krause, A., Evans, D.B., Dixon, J.M., 2007. Aromatase inhibitors—Gene discovery. The Journal of Steroid Biochemistry and Molecular Biology, Proceedings of the VIII International Aromatase Conference "Aromastase 2006" (Baltimore, Maryland, USA, 18-20 September, 2006) 106, 130–142. doi:10.1016/j.jsbmb.2007.05.013

Miller, W.R., O'Neill, J.S., 1989. The relevance of local oestrogen metabolism within the breast. Proceedings of the Royal Society of Edinburgh Section B: Biological Sciences 95, 203–217. doi:10.1017/S026972700001068X

Millour, M., Charbonnel, C., Magrangeas, F., Minvielle, S., Campion, L., Gouraud, W., Campone, M., Déporte-Féty, R., Bignon, Y.-J., Penault-Llorca, F., Jézéquel, P., 2006. Gene Expression Profiles Discriminate between Pathological Complete Response and Resistance to Neoadjuvant FEC100 in Breast Cancer. Cancer Genomics Proteomics 3, 89–95.

Mohammed, H., Russell, I.A., Stark, R., Rueda, O.M., Hickey, T.E., Tarulli, G.A., Serandour, A.A., Birrell, S.N., Bruna, A., Saadi, A., Menon, S., Hadfield, J., Pugh, M., Raj, G.V., Brown, G.D., D'Santos, C., Robinson, J.L.L., Silva, G., Launchbury, R., Perou, C.M., Stingl, J., Caldas, C., Tilley, W.D., Carroll, J.S., 2015. Progesterone receptor modulates ERα action in breast cancer. Nature 523, 313–317. doi:10.1038/nature14583

Moreno-Sánchez, R., Rodríguez-Enríquez, S., Marín-Hernández, A., Saavedra, E., 2007. Energy metabolism in tumor cells. FEBS J. 274, 1393–1418. doi:10.1111/j.1742-4658.2007.05686.x

Moy, B., Neven, P., Lebrun, F., Bellet, M., Xu, B., Sarosiek, T., Chow, L., Goss, P., Zacharchuk, C., Leip, E., Turnbull, K., Bardy-Bouxin, N., Duvillié, L., Láng, I., 2014a. Bosutinib in Combination With the Aromatase Inhibitor Exemestane: A Phase II Trial in Postmenopausal Women With Previously Treated Locally Advanced or Metastatic Hormone Receptor-Positive/HER2-Negative Breast Cancer. The Oncologist 19, 346–347. doi:10.1634/theoncologist.2014-0022

Moy, B., Neven, P., Lebrun, F., Bellet, M., Xu, B., Sarosiek, T., Chow, L., Goss, P., Zacharchuk, C., Leip, E., Turnbull, K., Bardy-Bouxin, N., Duvillié, L., Láng, I., 2014b. Bosutinib in Combination With the Aromatase Inhibitor Letrozole: A Phase II Trial in Postmenopausal Women Evaluating First-Line Endocrine Therapy in Locally Advanced or Metastatic Hormone Receptor-Positive/HER2-Negative Breast Cancer. The Oncologist 19, 348–349. doi:10.1634/theoncologist.2014-0021

Muller, F., Crofts, A.R., Kramer, D.M., 2002. Multiple Q-cycle bypass reactions at the Qo site of the cytochrome bc1 complex. Biochemistry 41, 7866–7874.

Munster, P.N., Thurn, K.T., Thomas, S., Raha, P., Lacevic, M., Miller, A., Melisko, M., Ismail-Khan, R., Rugo, H., Moasser, M., Minton, S.E., 2011. A phase II study of the histone deacetylase inhibitor vorinostat combined with tamoxifen for the treatment of patients with hormone therapy-resistant breast cancer. Br J Cancer 104, 1828–1835. doi:10.1038/bjc.2011.156

Murphy, C.E., Carder, P.J., Lansdown, M.R.J., Speirs, V., 2006. Steroid hormone receptor expression in male breast cancer. European Journal of Surgical Oncology (EJSO) 32, 44–47. doi:10.1016/j.ejso.2005.09.013

Nakayama, K., Okamoto, F., Harada, Y., 1956. Antimycin A: isolation from a new Streptomyces and activity against rice plant blast fungi. J. Antibiot. 9, 63–66.

Naughton, C., MacLeod, K., Kuske, B., Clarke, R., Cameron, D.A., Langdon, S.P., 2007. Progressive Loss of Estrogen Receptor α Cofactor Recruitment in Endocrine Resistance. Molecular Endocrinology 21, 2615–2626. doi:10.1210/me.2007-0110

Neve, R.M., Chin, K., Fridlyand, J., Yeh, J., Baehner, F.L., Fevr, T., Clark, L., Bayani, N., Coppe, J.-P., Tong, F., Speed, T., Spellman, P.T., DeVries, S., Lapuk, A., Wang, N.J., Kuo, W.-L., Stilwell, J.L., Pinkel, D., Albertson, D.G., Waldman, F.M., McCormick, F., Dickson, R.B., Johnson, M.D., Lippman, M., Ethier, S., Gazdar, A., Gray, J.W., 2006. A collection of breast cancer cell lines for the study of functionally distinct cancer subtypes. Cancer Cell 10, 515–527. doi:10.1016/j.ccr.2006.10.008

Nicholson, R.I., Hutcheson, I.R., Hiscox, S.E., Knowlden, J.M., Giles, M., Barrow, D., Gee, J.M.W., 2005. Growth factor signalling and resistance to selective oestrogen receptor modulators and pure anti-oestrogens: the use of anti-growth factor therapies to treat or delay endocrine resistance in breast cancer. Endocr Relat Cancer 12, S29–S36. doi:10.1677/erc.1.00991

Nicholson, R.I., Hutcheson, I.R., Jones, H.E., Hiscox, S.E., Giles, M., Taylor, K.M., Gee, J.M.W., 2007. Growth factor signalling in endocrine and anti-growth factor resistant breast cancer. Rev Endocr Metab Disord 8, 241–253. doi:10.1007/s11154-007-9033-5

Nicklin, P., Bergman, P., Zhang, B., Triantafellow, E., Wang, H., Nyfeler, B., Yang, H., Hild, M., Kung, C., Wilson, C., Myer, V.E., MacKeigan, J.P., Porter, J.A., Wang, Y.K., Cantley, L.C., Finan, P.M., Murphy, L.O., 2009. Bidirectional transport of amino acids regulates mTOR and autophagy. Cell 136, 521–534. doi:10.1016/j.cell.2008.11.044

Nieman, K.M., Kenny, H.A., Penicka, C.V., Ladanyi, A., Buell-Gutbrod, R., Zillhardt, M.R., Romero, I.L., Carey, M.S., Mills, G.B., Hotamisligil, G.S., Yamada, S.D., Peter, M.E., Gwin, K., Lengyel, E., 2011. Adipocytes promote ovarian cancer metastasis and provide energy for rapid tumor growth. Nat Med 17, 1498–1503. doi:10.1038/nm.2492

Niraula, S., Dowling, R.J.O., Ennis, M., Chang, M.C., Done, S.J., Hood, N., Escallon, J., Leong, W.L., McCready, D.R., Reedijk, M., Stambolic, V., Goodwin, P.J., 2012. Metformin in early breast cancer: a prospective window of opportunity neoadjuvant study. Breast Cancer Res. Treat. 135, 821–830. doi:10.1007/s10549-012-2223-1

Office for National Statistics Cancer Registration Statistics, England. URL http://www.ons.gov.uk/peoplepopulationandcommunity/healthandsocialcare/conditionsanddiseases/bulletins/cancerregistrationstatisticsengland/firstrelease2014 (accessed 3.24.16).

Ohashi, Y., Kaneko, S.J., Cupples, T.E., Young, S.R., 2004. Ubiquinol cytochrome c reductase (UQCRFS1) gene amplification in primary breast cancer core biopsy samples. Gynecologic Oncology 93, 54–58. doi:10.1016/j.ygyno.2004.01.019

Osborne, C.K., Bardou, V., Hopp, T.A., Chamness, G.C., Hilsenbeck, S.G., Fuqua, S.A.W., Wong, J., Allred, D.C., Clark, G.M., Schiff, R., 2003. Role of the estrogen receptor coactivator AIB1 (SRC-3) and HER-2/neu in tamoxifen resistance in breast cancer. J. Natl. Cancer Inst. 95, 353–361.

Osborne, C.K., Neven, P., Dirix, L.Y., Mackey, J.R., Robert, J., Underhill, C., Schiff, R., Gutierrez, C., Migliaccio, I., Anagnostou, V.K., Rimm, D.L., Magill, P., Sellers, M., 2011. Gefitinib or Placebo in Combination with Tamoxifen in Patients with Hormone Receptor–Positive Metastatic Breast Cancer: A Randomized Phase II Study. Clin Cancer Res 17, 1147–1159. doi:10.1158/1078-0432.CCR-10-1869

Osborne, C.K., Wakeling, A., Nicholson, R.I., 2004. Fulvestrant: an oestrogen receptor antagonist with a novel mechanism of action. Br J Cancer 90, S2–S6. doi:10.1038/sj.bjc.6601629

Osipo, C., Gajdos, C., Liu, H., Chen, B., Jordan, V.C., 2003. Paradoxical action of fulvestrant in estradiol-induced regression of tamoxifen-stimulated breast cancer. J. Natl. Cancer Inst. 95, 1597–1608.

Paik, S., Shak, S., Tang, G., Kim, C., Baker, J., Cronin, M., Baehner, F.L., Walker, M.G., Watson, D., Park, T., Hiller, W., Fisher, E.R., Wickerham, D.L., Bryant, J., Wolmark, N., 2004. A multigene assay to predict recurrence of tamoxifen-treated, node-negative breast cancer. N. Engl. J. Med. 351, 2817–2826. doi:10.1056/NEJMoa041588

Papandreou, I., Cairns, R.A., Fontana, L., Lim, A.L., Denko, N.C., 2006. HIF-1 mediates adaptation to hypoxia by actively downregulating mitochondrial oxygen consumption. Cell Metab. 3, 187–197. doi:10.1016/j.cmet.2006.01.012

Parker, J., Prat, A., Cheang, M., Lenburg, M., Paik, S., Perou, C., 2009. Breast Cancer Molecular Subtypes Predict Response to Anthracycline/Taxane-Based Chemotherapy. Cancer Res 69, 2019–2019. doi:10.1158/0008-5472.SABCS-09-2019

Pavlides, S., Whitaker-Menezes, D., Castello-Cros, R., Flomenberg, N., Witkiewicz, A.K., Frank, P.G., Casimiro, M.C., Wang, C., Fortina, P., Addya, S., Pestell, R.G., Martinez-Outschoorn, U.E., Sotgia, F., Lisanti, M.P., 2009. The reverse Warburg effect: aerobic glycolysis in cancer associated fibroblasts and the tumor stroma. Cell Cycle 8, 3984–4001.

Pavon-Eternod, M., Gomes, S., Geslain, R., Dai, Q., Rosner, M.R., Pan, T., 2009. tRNA over-expression in breast cancer and functional consequences. Nucleic Acids Res 37, 7268–7280. doi:10.1093/nar/gkp787

Pawitan, Y., Bjöhle, J., Amler, L., Borg, A.-L., Egyhazi, S., Hall, P., Han, X., Holmberg, L., Huang, F., Klaar, S., Liu, E.T., Miller, L., Nordgren, H., Ploner, A., Sandelin, K., Shaw, P.M., Smeds, J., Skoog, L., Wedrén, S., Bergh, J., 2005. Gene expression profiling spares early breast cancer patients from adjuvant therapy: derived and validated in two population-based cohorts. Breast Cancer Research 7, R953. doi:10.1186/bcr1325

Pedersen, P.L., 2008. Voltage dependent anion channels (VDACs): a brief introduction with a focus on the outer mitochondrial compartment's roles together with hexokinase-2 in the "Warburg effect" in cancer. J. Bioenerg. Biomembr. 40, 123–126. doi:10.1007/s10863-008-9165-7

Pelicano, H., Martin, D.S., Xu, R.-H., Huang, P., 2006. Glycolysis inhibition for anticancer treatment. Oncogene 25, 4633–4646. doi:10.1038/sj.onc.1209597

Pelicano, H., Zhang, W., Liu, J., Hammoudi, N., Dai, J., Xu, R.-H., Pusztai, L., Huang, P., 2014. Mitochondrial dysfunction in some triple-negative breast cancer cell lines: role of mTOR pathway and therapeutic potential. Breast Cancer Research 16, 434. doi:10.1186/s13058-014-0434-6

Pernicova, I., Korbonits, M., 2014. Metformin--mode of action and clinical implications for diabetes and cancer. Nat Rev Endocrinol 10, 143–156. doi:10.1038/nrendo.2013.256

Perou, C.M., Sørlie, T., Eisen, M.B., van de Rijn, M., Jeffrey, S.S., Rees, C.A., Pollack, J.R., Ross, D.T., Johnsen, H., Akslen, L.A., Fluge, Ø., Pergamenschikov, A., Williams, C., Zhu, S.X., Lønning, P.E., Børresen-Dale, A.-L., Brown, P.O., Botstein, D., 2000. Molecular portraits of human breast tumours. Nature 406, 747–752. doi:10.1038/35021093

Poliakov, E., Managadze, D., Rogozin, I.B., Poliakov, E., Managadze, D., Rogozin, I.B., 2014. Generalized Portrait of Cancer Metabolic Pathways Inferred from a List of Genes Overexpressed in Cancer, Generalized Portrait of Cancer Metabolic Pathways Inferred from a List of Genes Overexpressed in Cancer. Genetics Research International, Genetics Research International 2014, 2014, e646193. doi:10.1155/2014/646193, 10.1155/2014/646193

Pollak, M., 2010. Metformin and other biguanides in oncology: advancing the research agenda. Cancer Prev Res (Phila) 3, 1060–1065. doi:10.1158/1940-6207.CAPR-10-0175

Pollard, P.J., Brière, J.J., Alam, N.A., Barwell, J., Barclay, E., Wortham, N.C., Hunt, T., Mitchell, M., Olpin, S., Moat, S.J., Hargreaves, I.P., Heales, S.J., Chung, Y.L., Griffiths, J.R., Dalgleish, A., McGrath, J.A., Gleeson, M.J., Hodgson, S.V., Poulsom, R., Rustin, P., Tomlinson, I.P.M., 2005. Accumulation of Krebs cycle intermediates and over-expression of HIF1alpha in tumours which result from germline FH and SDH mutations. Hum. Mol. Genet. 14, 2231–2239. doi:10.1093/hmg/ddi227

Province, M.A., Goetz, M.P., Brauch, H., Flockhart, D.A., Hebert, J.M., Whaley, R., Suman, V.J., Schroth, W., Winter, S., Zembutsu, H., Mushiroda, T., Newman, W.G., Lee, M.-T.M., Ambrosone, C.B., Beckmann, M.W., Choi, J.-Y., Dieudonné, A.-S., Fasching, P.A., Ferraldeschi, R., Gong, L., Haschke-Becher, E., Howell, A., Jordan, L.B., Hamann, U., Kiyotani, K., Krippl, P., Lambrechts, D., Latif, A., Langsenlehner, U., Lorizio, W., Neven, P., Nguyen, A.T., Park, B.-W., Purdie, C.A., Quinlan, P., Renner, W., Schmidt, M., Schwab, M., Shin, J.-G., Stingl, J.C., Wegman, P., Wingren, S., Wu, A.H.B., Ziv, E., Zirpoli, G., Thompson, A.M., Jordan, V.C., Nakamura, Y., Altman, R.B., Ames, M.M., Weinshilboum, R.M., Eichelbaum, M., Ingle, J.N., Klein, T.E., 2014. CYP2D6 Genotype and Adjuvant Tamoxifen: Meta-Analysis of Heterogeneous Study Populations. Clin Pharmacol Ther 95, 216–227. doi:10.1038/clpt.2013.186

Putti, T.C., El-Rehim, D.M.A., Rakha, E.A., Paish, C.E., Lee, A.H., Pinder, S.E., Ellis, I.O., 2004. Estrogen receptor-negative breast carcinomas: a review of morphology and immunophenotypical analysis. Mod Pathol 18, 26–35. doi:10.1038/modpathol.3800255

Raez, L.E., Papadopoulos, K., Ricart, A.D., Chiorean, E.G., DiPaola, R.S., Stein, M.N., Lima, C.M.R., Schlesselman, J.J., Tolba, K., Langmuir, V.K., Kroll, S., Jung, D.T., Kurtoglu, M., Rosenblatt, J., Lampidis, T.J., 2012. A phase I dose-escalation trial of 2-deoxy-d-glucose alone or combined with docetaxel in patients with advanced solid tumors. Cancer Chemother Pharmacol 71, 523–530. doi:10.1007/s00280-012-2045-1

Ralph, S.J., Rodríguez-Enríquez, S., Neuzil, J., Moreno-Sánchez, R., 2010. Bioenergetic pathways in tumor mitochondria as targets for cancer therapy and the importance of the ROS-induced apoptotic trigger. Molecular Aspects of Medicine, Mitochondria, Apoptosis and Cancer 31, 29–59. doi:10.1016/j.mam.2009.12.006

Recouvreux, S., Sampayo, R., Bessone, M.I.D., Simian, M., 2015. Microenvironment and endocrine resistance in breast cancer: Friend or foe? World J Clin Oncol 6, 207–211. doi:10.5306/wjco.v6.i6.207

Riggins, R.B., Schrecengost, R.S., Guerrero, M.S., Bouton, A.H., 2007. Pathways to tamoxifen resistance. Cancer Letters 256, 1–24. doi:10.1016/j.canlet.2007.03.016

Rivenzon-Segal, D., Boldin-Adamsky, S., Seger, D., Seger, R., Degani, H., 2003. Glycolysis and glucose transporter 1 as markers of response to hormonal therapy in breast cancer. Int. J. Cancer 107, 177–182. doi:10.1002/ijc.11387

Robertson, J.F., Ferrero, J.-M., Bourgeois, H., Kennecke, H., de Boer, R.H., Jacot, W., McGreivy, J., Suzuki, S., Zhu, M., McCaffery, I., Loh, E., Gansert, J.L., Kaufman, P.A., 2013. Ganitumab with either exemestane or fulvestrant for postmenopausal women with advanced, hormone-receptor-positive breast cancer: a randomised, controlled, double-blind, phase 2 trial. The Lancet Oncology 14, 228–235. doi:10.1016/S1470-2045(13)70026-3

Rodríguez-Enríquez, S., Carreño-Fuentes, L., Gallardo-Pérez, J.C., Saavedra, E., Quezada, H., Vega, A., Marín-Hernández, A., Olín-Sandoval, V., Torres-Márquez, M.E., Moreno-Sánchez, R., 2010. Oxidative phosphorylation is impaired by prolonged hypoxia in breast and possibly in cervix carcinoma. Int. J. Biochem. Cell Biol. 42, 1744–1751. doi:10.1016/j.biocel.2010.07.010

Ros, S., Schulze, A., 2013a. Balancing glycolytic flux: the role of 6-phosphofructo-2-kinase/fructose 2,6-bisphosphatases in cancer metabolism. Cancer & Metabolism 1, 8. doi:10.1186/2049-3002-1-8

Rouzier, R., Perou, C.M., Symmans, W.F., Ibrahim, N., Cristofanilli, M., Anderson, K., Hess, K.R., Stec, J., Ayers, M., Wagner, P., Morandi, P., Fan, C., Rabiul, I., Ross, J.S., Hortobagyi, G.N., Pusztai, L., 2005. Breast Cancer Molecular Subtypes Respond Differently to Preoperative Chemotherapy. Clin Cancer Res 11, 5678–5685. doi:10.1158/1078-0432.CCR-04-2421

SATO-KUWABARA, Y., MELO, S.A., SOARES, F.A., CALIN, G.A., 2014. The fusion of two worlds: Non-coding RNAs and extracellular vesicles - diagnostic and therapeutic implications (Review). Int J Oncol 46, 17–27. doi:10.3892/ijo.2014.2712

Schell, J.C., Olson, K.A., Jiang, L., Hawkins, A.J., Van Vranken, J.G., Xie, J., Egnatchik, R.A., Earl, E.G., DeBerardinis, R.J., Rutter, J., 2014. A Role for the Mitochondrial Pyruvate Carrier as a Repressor of the Warburg Effect and Colon Cancer Cell Growth. Molecular Cell 56, 400–413. doi:10.1016/j.molcel.2014.09.026

Scholzen, T., Gerdes, J., 2000. The Ki-67 protein: from the known and the unknown. J. Cell. Physiol. 182, 311–322. doi:10.1002/(SICI)1097-4652(200003)182:3<311::AID-JCP1>3.0.CO;2-9

Segars, J.H., Driggers, P.H., 2002. Estrogen action and cytoplasmic signaling cascades. Part I: membrane-associated signaling complexes. Trends Endocrinol. Metab. 13, 349–354.

Seligman, A.M., Karnovsky, M.J., Wasserkrug, H.L., Hanker, J.S., 1968. NONDROPLET ULTRASTRUCTURAL DEMONSTRATION OF CYTOCHROME OXIDASE ACTIVITY WITH A POLYMERIZING OSMIOPHILIC REAGENT, DIAMINOBENZIDINE (DAB). J Cell Biol 38, 1–14.

Shajahan-Haq, A.N., Cook, K.L., Schwartz-Roberts, J.L., Eltayeb, A.E., Demas, D.M., Warri, A.M., Facey, C.O.B., Hilakivi-Clarke, L.A., Clarke, R., 2014. MYC regulates the unfolded protein response and glucose and glutamine uptake in endocrine resistant breast cancer. Molecular Cancer 13, 239. doi:10.1186/1476-4598-13-239

Shou, J., Massarweh, S., Osborne, C.K., Wakeling, A.E., Ali, S., Weiss, H., Schiff, R., 2004. Mechanisms of Tamoxifen Resistance: Increased Estrogen Receptor-HER2/neu Cross-Talk in ER/HER2–Positive Breast Cancer. JNCI J Natl Cancer Inst 96, 926–935. doi:10.1093/jnci/djh166

Soule, H.D., Vazguez, J., Long, A., Albert, S., Brennan, M., 1973. A human cell line from a pleural effusion derived from a breast carcinoma. J. Natl. Cancer Inst. 51, 1409–1416.

Soule, H.D., McGrath, C.M., 1980. Estrogen responsive proliferation of clonal human breast carcinoma cells in athymic mice. Cancer Lett. 10, 177–189.

Simpson, E.R., 2003. Sources of estrogen and their importance. The Journal of Steroid Biochemistry and Molecular Biology, Proceedings of the VI International Aromatase Conference "AROMATASE 200" 86, 225–230. doi:10.1016/S0960-0760(03)00360-1

Smid, M., Wang, Y., Zhang, Y., Sieuwerts, A.M., Yu, J., Klijn, J.G.M., Foekens, J.A., Martens, J.W.M., 2008. Subtypes of breast cancer show preferential site of relapse. Cancer Res. 68, 3108–3114. doi:10.1158/0008-5472.CAN-07-5644

Smolková, K., Plecitá-Hlavatá, L., Bellance, N., Benard, G., Rossignol, R., Ježek, P., 2011. Waves of gene regulation suppress and then restore oxidative phosphorylation in cancer cells. Int. J. Biochem. Cell Biol. 43, 950–968. doi:10.1016/j.biocel.2010.05.003

Song, R.X.-D., Mor, G., Naftolin, F., McPherson, R.A., Song, J., Zhang, Z., Yue, W., Wang, J., Santen, R.J., 2001. Effect of Long-Term Estrogen Deprivation on Apoptotic Responses of Breast Cancer Cells to 17β-Estradiol. JNCI J Natl Cancer Inst 93, 1714–1723. doi:10.1093/jnci/93.22.1714

Sørlie, T., Perou, C.M., Tibshirani, R., Aas, T., Geisler, S., Johnsen, H., Hastie, T., Eisen, M.B., van de Rijn, M., Jeffrey, S.S., Thorsen, T., Quist, H., Matese, J.C., Brown, P.O., Botstein, D., Lønning, P.E., Børresen-Dale, A.-L., 2001. Gene expression patterns of breast carcinomas distinguish tumor subclasses with clinical implications. Proc Natl Acad Sci U S A 98, 10869–10874. doi:10.1073/pnas.191367098

Sotgia, F., Whitaker-Menezes, D., Martinez-Outschoorn, U.E., Salem, A.F., Tsirigos, A., Lamb, R., Sneddon, S., Hulit, J., Howell, A., Lisanti, M.P., 2012a. Mitochondria "fuel" breast cancer metabolism: Fifteen markers of mitochondrial biogenesis label epithelial cancer cells, but are excluded from adjacent stromal cells. Cell Cycle 11, 4390–4401. doi:10.4161/cc.22777

Sotgia, F., Whitaker-Menezes, D., Martinez-Outschoorn, U.E., Flomenberg, N., Birbe, R., Witkiewicz, A.K., Howell, A., Philp, N.J., Pestell, R.G., Lisanti, M.P., 2012b. Mitochondrial metabolism in cancer metastasis: visualizing tumor cell mitochondria and the "reverse Warburg effect" in positive lymph node tissue. Cell Cycle 11, 1445–1454. doi:10.4161/cc.19841

Soule, H.D., McGrath, C.M., 1980. Estrogen responsive proliferation of clonal human breast carcinoma cells in athymic mice. Cancer Lett. 10, 177–189.

Soule, H.D., Vazquez, J., Long, A., Albert, S., Brennan, M., 1973. A Human Cell Line From a Pleural Effusion Derived From a Breast Carcinoma. JNCI J Natl Cancer Inst 51, 1409–1416. doi:10.1093/jnci/51.5.1409

Sparano, J.A., Gray, R.J., Makower, D.F., Pritchard, K.I., Albain, K.S., Hayes, D.F., Geyer, C.E.J., Dees, E.C., Perez, E.A., Olson, J.A.J., Zujewski, J., Lively, T., Badve, S.S., Saphner, T.J., Wagner, L.I., Whelan, T.J., Ellis, M.J., Paik, S., Wood, W.C., Ravdin, P., Keane, M.M., Gomez Moreno, H.L., Reddy, P.S., Goggins, T.F., Mayer, I.A., Brufsky, A.M., Toppmeyer, D.L., Kaklamani, V.G., Atkins, J.N., Berenberg, J.L., Sledge, G.W., 2015. Prospective Validation of a 21-Gene Expression Assay in Breast Cancer. New England Journal of Medicine 373, 2005–2014. doi:10.1056/NEJMoa1510764

Spiegel, R., Pines, O., Ta-Shma, A., Burak, E., Shaag, A., Halvardson, J., Edvardson, S., Mahajna, M., Zenvirt, S., Saada, A., Shalev, S., Feuk, L., Elpeleg, O., 2012. Infantile cerebellar-retinal degeneration associated with a mutation in mitochondrial aconitase, ACO2. Am. J. Hum. Genet. 90, 518–523. doi:10.1016/j.ajhg.2012.01.009

Staka, C.M., Nicholson, R.I., Gee, J.M.W., 2005. Acquired resistance to oestrogen deprivation: role for growth factor signalling kinases/oestrogen receptor cross-talk revealed in new MCF-7X model. Endocr Relat Cancer 12, S85–S97. doi:10.1677/erc.1.01006

Starkov, A.A., 2008. The Role of Mitochondria in Reactive Oxygen Species Metabolism and Signaling. Ann N Y Acad Sci 1147, 37–52. doi:10.1196/annals.1427.015

Steinberg, G.R., Kemp, B.E., 2009. AMPK in Health and Disease. Physiol. Rev. 89, 1025–1078. doi:10.1152/physrev.00011.2008

Stephenne, X., Foretz, M., Taleux, N., van der Zon, G.C., Sokal, E., Hue, L., Viollet, B., Guigas, B., 2011. Metformin activates AMP-activated protein kinase in primary human hepatocytes by decreasing cellular energy status. Diabetologia 54, 3101–3110. doi:10.1007/s00125-011-2311-5

Strickland, P., Shin, G.C., Plump, A., Tessier-Lavigne, M., Hinck, L., 2006. Slit2 and netrin 1 act synergistically as adhesive cues to generate tubular bi-layers during ductal morphogenesis. Development 133, 823–832. doi:10.1242/dev.02261

Surowiak, P., Matkowski, R., Materna, V., Györffy, B., Wojnar, A., Pudelko, M., Dziegiel, P., Kornafel, J., Zabel, M., 2005. Elevated metallothionein (MT) expression in invasive ductal breast cancers predicts tamoxifen resistance. Histol. Histopathol. 20, 1037–1044.

Taylor, K.M., Vichova, P., Jordan, N., Hiscox, S., Hendley, R., Nicholson, R.I., 2008. ZIP7-Mediated Intracellular Zinc Transport Contributes to Aberrant Growth Factor Signaling in Antihormone-Resistant Breast Cancer Cells. Endocrinology 149, 4912–4920. doi:10.1210/en.2008-0351

Thompson, E.W., Katz, D., Shima, T.B., Wakeling, A.E., Lippman, M.E., Dickson, R.B., 1989. ICI 164,384, a pure antagonist of estrogen-stimulated MCF-7 cell proliferation and invasiveness. Cancer Research 49, 6929–6934.

Tinoco-Veras, C.M., Bezerra Sousa, M.S., Borges da Silva, B., Franciscato Cozzolino, S.M.ª., Viana Pires, L., Coelho Pimentel, J.A., do Nascimento-Nogueira, N., do Nascimento-Marreiro, D., 2011. Analysis of plasma and erythrocyte zinc levels in premenopausal women with breast cancer. Nutrición Hospitalaria 26, 293–297.

Tsai, C.-J., Nussinov, R., 2013. The molecular basis of targeting protein kinases in cancer therapeutics. Seminars in Cancer Biology, Cancer-related networks: A help to understand, predict and change malignant transformation 23, 235–242. doi:10.1016/j.semcancer.2013.04.001

Tuncal, A., Aydin, H.H., Askar, N., Ozkaya, A.B., Ergenoglu, A.M., Yeniel, A.O., Akdemir, A., Ak, H., 2014. Increased expression of electron transport chain genes in uterine leiomyoma. Ann. Clin. Lab. Sci. 44, 466–468.

Uchikado, Y., Inoue, H., Haraguchi, N., Mimori, K., Natsugoe, S., Okumura, H., Aikou, T., Mori, M., 2006. Gene expression profiling of lymph node metastasis by oligomicroarray analysis using laser microdissection in esophageal squamous cell carcinoma. Int. J. Oncol. 29, 1337–1347.

Valadi, H., Ekström, K., Bossios, A., Sjöstrand, M., Lee, J.J., Lötvall, J.O., 2007. Exosome-mediated transfer of mRNAs and microRNAs is a novel mechanism of genetic exchange between cells. Nat Cell Biol 9, 654–659. doi:10.1038/ncb1596

van de Vijver, M.J., He, Y.D., van ’t Veer, L.J., Dai, H., Hart, A.A.M., Voskuil, D.W., Schreiber, G.J., Peterse, J.L., Roberts, C., Marton, M.J., Parrish, M., Atsma, D., Witteveen, A., Glas, A., Delahaye, L., van der Velde, T., Bartelink, H., Rodenhuis, S., Rutgers, E.T., Friend, S.H., Bernards, R., 2002. A Gene-Expression Signature as a Predictor of Survival in Breast Cancer. New England Journal of Medicine 347, 1999–2009. doi:10.1056/NEJMoa021967

van den Bosch, B.J.C., Gerards, M., Sluiter, W., Stegmann, A.P.A., Jongen, E.L.C., Hellebrekers, D.M.E.I., Oegema, R., Lambrichs, E.H., Prokisch, H., Danhauser, K., Schoonderwoerd, K., de Coo, I.F.M., Smeets, H.J.M., 2012. Defective NDUFA9 as a novel cause of neonatally fatal complex I disease. J. Med. Genet. 49, 10–15. doi:10.1136/jmedgenet-2011-100466

van den Heuvel, A.P.J., Jing, J., Wooster, R.F., Bachman, K.E., 2012. Analysis of glutamine dependency in non-small cell lung cancer. Cancer Biol Ther 13, 1185–1194. doi:10.4161/cbt.21348

Vaupel, P., Kallinowski, F., Okunieff, P., 1989. Blood Flow, Oxygen and Nutrient Supply, and Metabolic Microenvironment of Human Tumors: A Review. Cancer Res 49, 6449–6465.

Verkhivker, Gennady M., 2015. Integrating genetic and structural data on human protein kinome in network-based modeling of kinase sensitivities and resistance to targeted and personalized anticancer drugs, in: Biocomputing 2016. WORLD SCIENTIFIC, pp. 45–56.

Viedma-Rodrïguez, R., Baiza-Gutman, L., Salamanca-Gï¿½mez, F., Diaz-Zaragoza, M., Martï¿½nez-Hernï¿½ndez, G., Ruiz Esparza-Garrido, R., Velï¿½zquez-Flores, M., Arenas-Aranda, D., 2014. Mechanisms associated with resistance to tamoxifen in estrogen receptor-positive breast cancer (Review). Oncology Reports. doi:10.3892/or.2014.3190

Viollet, B., Guigas, B., Sanz Garcia, N., Leclerc, J., Foretz, M., Andreelli, F., 2012. Cellular and molecular mechanisms of metformin: an overview. Clin. Sci. 122, 253–270. doi:10.1042/CS20110386

Vrieling, A., Buck, K., Kaaks, R., Chang-Claude, J., 2010. Adult weight gain in relation to breast cancer risk by estrogen and progesterone receptor status: a meta-analysis. Breast Cancer Res Treat 123, 641–649. doi:10.1007/s10549-010-1116-4

Wakeling, A.E., 2000. Similarities and distinctions in the mode of action of different classes of antioestrogens. Endocr Relat Cancer 7, 17–28. doi:10.1677/erc.0.0070017

Walker, I., Newell, H., 2009. Do molecularly targeted agents in oncology have reduced attrition rates? Nat Rev Drug Discov 8, 15–16. doi:10.1038/nrd2758

Warburg, O., 1956. On the origin of cancer cells. Science 123, 309–314.

Ward, P.S., Thompson, C.B., 2012. Signaling in Control of Cell Growth and Metabolism. Cold Spring Harb Perspect Biol 4, a006783. doi:10.1101/cshperspect.a006783

Wheaton, W.W., Weinberg, S.E., Hamanaka, R.B., Soberanes, S., Sullivan, L.B., Anso, E., Glasauer, A., Dufour, E., Mutlu, G.M., Budigner, G.S., Chandel, N.S., 2014. Metformin inhibits mitochondrial complex I of cancer cells to reduce tumorigenesis. eLife 3. doi:10.7554/eLife.02242

Whitaker-Menezes, D., Martinez-Outschoorn, U.E., Flomenberg, N., Birbe, R., Witkiewicz, A.K., Howell, A., Pavlides, S., Tsirigos, A., Ertel, A., Pestell, R.G., Broda, P., Minetti, C., Lisanti, M.P., Sotgia, F., 2011. Hyperactivation of oxidative mitochondrial metabolism in epithelial cancer cells in situ. Cell Cycle 10, 4047–4064. doi:10.4161/cc.10.23.18151

Wieser, W., Krumschnabel, G., 2001. Hierarchies of ATP-consuming processes: direct compared with indirect measurements, and comparative aspects. Biochem J 355, 389–395.

Williams, C.C., Basu, A., El-Gharbawy, A., Carrier, L.M., Smith, C.L., Rowan, B.G., 2009. Identification of four novel phosphorylation sites in estrogen receptor α: impact on receptor-dependent gene expression and phosphorylation by protein kinase CK2. BMC Biochemistry 10, 36. doi:10.1186/1471-2091-10-36

Witkiewicz, A.K., Dasgupta, A., Sotgia, F., Mercier, I., Pestell, R.G., Sabel, M., Kleer, C.G., Brody, J.R., Lisanti, M.P., 2009. An Absence of Stromal Caveolin-1 Expression Predicts Early Tumor Recurrence and Poor Clinical Outcome in Human Breast Cancers. The American Journal of Pathology 174, 2023–2034. doi:10.2353/ajpath.2009.080873

Wolff, A.C., Lazar, A.A., Bondarenko, I., Garin, A.M., Brincat, S., Chow, L., Sun, Y., Neskovic-Konstantinovic, Z., Guimaraes, R.C., Fumoleau, P., Chan, A., Hachemi, S., Strahs, A., Cincotta, M., Berkenblit, A., Krygowski, M., Kang, L.L., Moore, L., Hayes, D.F., 2013. Randomized Phase III Placebo-Controlled Trial of Letrozole Plus Oral Temsirolimus As First-Line Endocrine Therapy in Postmenopausal Women With Locally Advanced or Metastatic Breast Cancer. JCO 31, 195–202. doi:10.1200/JCO.2011.38.3331

Wu, Y., Sarkissyan, M., Mcghee, E., Lee, S., Vadgama, J.V., 2015. Combined inhibition of glycolysis and AMPK induces synergistic breast cancer cell killing. Breast Cancer Res. Treat. 151, 529–539. doi:10.1007/s10549-015-3386-3

Yamashita, H., Nishio, M., Kobayashi, S., Ando, Y., Sugiura, H., Zhang, Z., Hamaguchi, M., Mita, K., Fujii, Y., Iwase, H., 2005. Phosphorylation of estrogen receptor α serine 167 is predictive of response to endocrine therapy and increases postrelapse survival in metastatic breast cancer. Breast Cancer Research 7, R753. doi:10.1186/bcr1285

Yamashita, H., Nishio, M., Toyama, T., Sugiura, H., Kondo, N., Kobayashi, S., Fujii, Y., Iwase, H., 2008. Low phosphorylation of estrogen receptor α (ERα) serine 118 and high phosphorylation of ERα serine 167 improve survival in ER-positive breast cancer. Endocr Relat Cancer 15, 755–763. doi:10.1677/ERC-08-0078

Yang, C., Richardson, A.D., Smith, J.W., Osterman, A., 2007. Comparative metabolomics of breast cancer. Pac Symp Biocomput 181–192.

Yardley, D.A., Ismail-Khan, R.R., Melichar, B., Lichinitser, M., Munster, P.N., Klein, P.M., Cruickshank, S., Miller, K.D., Lee, M.J., Trepel, J.B., 2013. Randomized Phase II, Double-Blind, Placebo-Controlled Study of Exemestane With or Without Entinostat in Postmenopausal Women With Locally Recurrent or Metastatic Estrogen Receptor-Positive Breast Cancer Progressing on Treatment With a Nonsteroidal Aromatase Inhibitor. JCO 31, 2128–2135. doi:10.1200/JCO.2012.43.7251

Yardley, D.A., Ismail-Khan, R.R., Melichar, B., Lichinitser, M., Munster, P.N., Klein, P.M., Cruickshank, S., Miller, K.D., Lee, M.J., Trepel, J.B., 2013. Randomized phase II, double-blind, placebo-controlled study of exemestane with or without entinostat in postmenopausal women with locally recurrent or metastatic estrogen receptor-positive breast cancer progressing on treatment with a nonsteroidal aromatase inhibitor. J. Clin. Oncol. 31, 2128–2135. doi:10.1200/JCO.2012.43.7251

Yerushalmi, R., Woods, R., Ravdin, P.M., Hayes, M.M., Gelmon, K.A., 2010. Ki67 in breast cancer: prognostic and predictive potential. The Lancet Oncology 11, 174–183. doi:10.1016/S1470-2045(09)70262-1

Yin, C., Qie, S., Sang, N., 2012. Carbon Source Metabolism and Its Regulation in Cancer Cells. Crit Rev Eukaryot Gene Expr 22, 17–35.

Zakikhani, M., Dowling, R., Fantus, I.G., Sonenberg, N., Pollak, M., 2006. Metformin Is an AMP Kinase–Dependent Growth Inhibitor for Breast Cancer Cells. Cancer Res 66, 10269–10273. doi:10.1158/0008-5472.CAN-06-1500

Zhou, M., Xia, L., Wang, J., 2007. Metformin transport by a newly cloned proton-stimulated organic cation transporter (plasma membrane monoamine transporter) expressed in human intestine. Drug Metab. Dispos. 35, 1956–1962. doi:10.1124/dmd.107.015495

Zhuang, Y., Chan, D.K., Haugrud, A.B., Miskimins, W.K., 2014. Mechanisms by Which Low Glucose Enhances the Cytotoxicity of Metformin to Cancer Cells Both In Vitro and In Vivo. PLoS One 9. doi:10.1371/journal.pone.0108444

Zhuang, Y., Miskimins, W.K., 2008. Cell cycle arrest in Metformin treated breast cancer cells involves activation of AMPK, downregulation of cyclin D1, and requires p27Kip1 or p21Cip1. J Mol Signal 3, 18. doi:10.1186/1750-2187-3-18

Appendices

Fig A Glycolysis

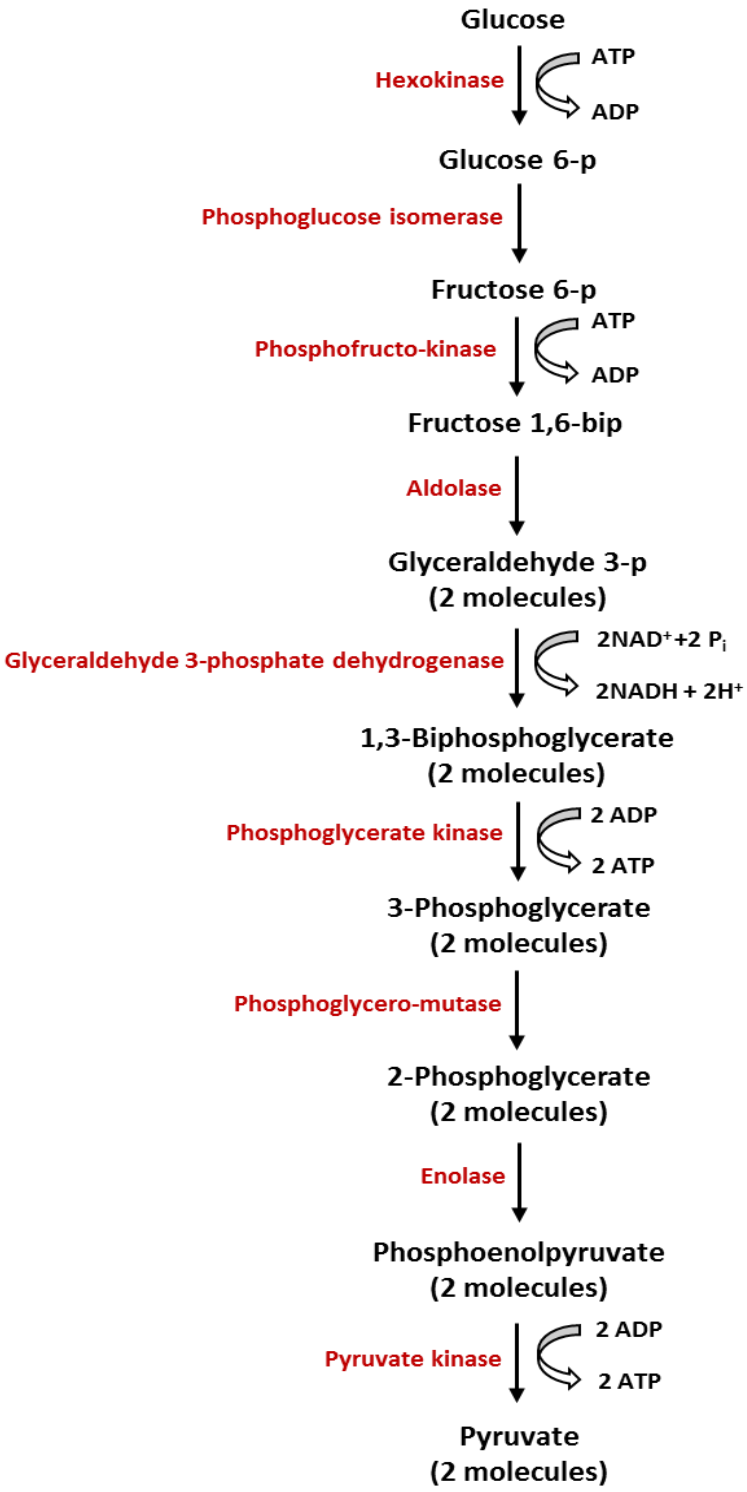

Fig B Citric acid cycle

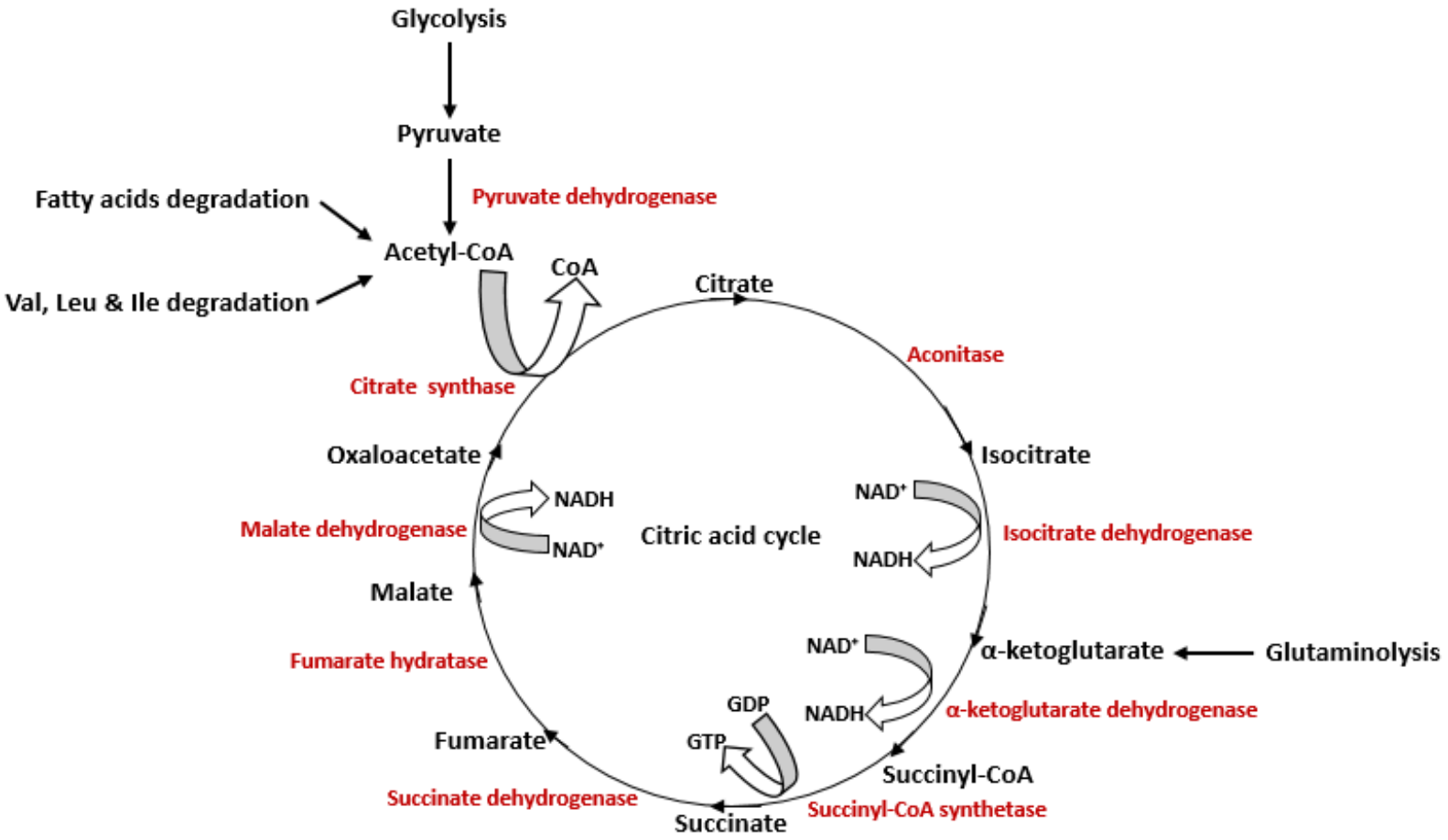

Appendix 1-19 involves following information:

Sheet 1

Significantly deregulated probe IDs, gene symbol, gene title and corresponding *P* value after ANOVA with Benjamini and Hochberg post hoc correction in resistant model(s) compared to MCF7.

Sheet 2

ID conversion from probe IDs to ENSEMBL IDs using DAVID bioinformatics database

Sheet3

Over-represented ontology (molecular function, biological process and cellular component) of deregulated genes after hypergeometric algorithm with Benjamini and Hochberg correction were investigated using Innatedb database. Bold GO terms and gene symbols were significantly ($p \leq 0.05$) over-represented in resistant model(s) compared to MCF7. Number of uploaded genes and total number of genes for each GO term was indicated.

Sheet 4

Over-represented pathways of deregulated genes after hypergeometric algorithm with Benjamini and Hochberg correction were investigated using Innatedb database. Bold Pathway names and gene symbols were significantly ($p \leq 0.05$) over-represented in resistant model(s) compared to MCF7). Number of uploaded genes and total number of genes for each pathway was indicated.

Appendix 1

Downregulated probe IDs in tamoxifen resistant models (TamR and TamRLT) compared to MCF7.

Appendix 2

Downregulated probe IDs in fulvestrant resistant models (FasR and FasRLT) compared to MCF7.

Appendix 3

Downregulated probe IDs in oestrogen-deprived resistant models (MCF7(X) and MCF7(X)LT) compared to MCF7.

Appendix 4

Downregulated probe IDs in short-term resistant models (TamR, FasR and MCF7(X)) compared to MCF7.

Appendix 5

Downregulated probe IDs in long-term resistant models (TamRLT, FasRLT and MCF7(X)LT) compared to MCF7.

Appendix 6

Downregulated probe IDs in all resistant models (TamR, TamRLT, FasR, FasRLT, MCF7(X) and MCF7(X)LT) compared to MCF7.

Appendix 7

Upregulated probe IDs in tamoxifen resistant model (TamR) compared to MCF7.

Appendix 8

Upregulated probe IDs in tamoxifen resistant model (TamRLT) compared to MCF7.

Appendix 9

Upregulated probe IDs in fulvestrant resistant model (FasR) compared to MCF7.

Appendix 10

Upregulated probe IDs in fulvestrant resistant model (FasRLT) compared to MCF7.

Appendix 11

Upregulated probe IDs in oestrogen-deprived resistant model (MCF7(X)) compared to MCF7.

Appendix 12

Upregulated probe IDs in oestrogen-deprived resistant model (MCF7(X)LT) compared to MCF7.

Appendix 13

Upregulated probe IDs in tamoxifen resistant models (TamR and TamRLT) compared to MCF7.

Appendix 14

Upregulated probe IDs in fulvestrant resistant models (FasR and FasRLT) compared to MCF7.

Appendix 15

Upregulated probe IDs in oestrogen-deprived resistant models (MCF7(X) and MCF7(X)LT) compared to MCF7.

Appendix 16

Upregulated probe IDs in short-term resistant models (TamR, FasR and MCF7(X)) compared to MCF7.

Appendix 17

Upregulated probe IDs in long-term resistant models (TamRLT, FasRLT and MCF7(X)LT) compared to MCF7.

Appendix 18

Upregulated probe IDs in all resistant models (TamR, TamRLT, FasR, FasRLT, MCF7(X) and MCF7(X)LT) compared to MCF7.

Appendix 19

Upregulated probe IDs in AH treated cells (MCF7[-E2], MCF7[HSFCS], MCF7[+tamoxifen] and MCF7[+fulvestrant]) compared to oestradiol treated control.

Appendix 20

Sheet 1

Significantly upregulated Uniprot IDs, protein name, phosphorylation status and corresponding *P* value in TamR compared to MCF7.

Sheet 2

ID conversion from Uniprot IDs to ENSEMBL IDs using DAVID bioinformatics database

Sheet3

Over-represented ontology (molecular function, biological process and cellular component) of upregulated genes (corresponding proteins) after hypergeometric algorithm with Benjamini and Hochberg correction were investigated using Innatedb database. Bold GO terms and gene symbols were significantly ($p \leq 0.05$) over-represented in TamR compared to MCF7. Number of uploaded genes and total number of genes for each GO term was indicated.

Sheet 4

Over-represented pathways of upregulated genes (proteins) after hypergeometric algorithm with Benjamini and Hochberg correction were investigated using Innatedb database. Bold Pathway names and gene symbols (corresponding genes) were significantly ($p \leq 0.05$) over-represented in TamR compared to MCF7). Number of uploaded genes and total number of genes for each pathway was indicated.

Appendix 21

Sigmoid curve, log transformed EC50 graphs after 2DG, antimycin A and metformin treatment for 7 days was demonstrated in all breast cancer models including MCF7, TamR, TamRLT, FasR, FasRLT, MCF7(X) and MCF7(X)LT (three independent experiments for each model).